
Port of Otago Dredging Project: Harbour and Offshore Modelling



Source: Port of Otago Ltd

**NIWA Client Report: HAM2008-179
February 2009—revised August 2009**

NIWA Projects: POL08203/POL09201

Port of Otago Dredging Project: Harbour and Offshore Modelling

R.G. Bell
J.W. Oldman
B. Beamsley (MetOcean Solutions Ltd)
M.O. Green
M. Pritchard
D. Johnson (MetOcean Solutions Ltd)
P. McComb (MetOcean Solutions Ltd)
N. Hancock
D. Grant (Hydraulic Modelling Services Ltd)
R. Zyngfogel (MetOcean Solutions Ltd)

NIWA contact/Corresponding author

R.G. Bell

Prepared for

Port Otago Ltd

NIWA Client Report: HAM2008–179
February 2009—revised August 2009

NIWA Projects: POL08203/POL09201

National Institute of Water & Atmospheric Research Ltd
Gate 10, Silverdale Road, Hamilton
P O Box 11115, Hamilton, New Zealand
Phone +64-7-856 7026, Fax +64-7-856 0151
www.niwa.co.nz

Contents

1.	Introduction	1
1.1	Project Next Generation	1
1.2	Summary of Brief for Numerical Modelling	2
1.2.1	NIWA modelling	2
1.2.2	MetOcean Solutions modelling	3
1.3	Main purposes for numerical modelling	4
1.4	Scope of technical report	4
1.5	Geographic context	5
1.5.1	Otago Harbour	5
1.5.2	Otago Heads shelf	6
2.	Hydrodynamic and wave observations	9
2.1	Tidal wave propagation in Otago Harbour and phase changes	9
2.2	Harbour hydrodynamics from previous and supporting 2008 studies	12
2.3	Offshore shelf hydrodynamics	13
2.4	Waves	17
3.	Bathymetry and Otago Harbour model grids	19
3.1	Introduction	19
3.2	Bathymetry datasets	19
3.3	Hydrodynamic model grid (existing channel)	24
3.4	Deepened shipping channel configuration	26
3.5	Harbour wave model grid	28
4.	Harbour hydrodynamic modelling: set-up, calibration and verification	30
4.1	Hydrodynamic model setup	30
4.2	Calibration of Harbour model on 1988 field measurements	31
4.2.1	Tide Data	31
4.2.2	Braystoke current meter	31
4.3	Harbour model validation	40
4.3.1	Model verification with S4 measurements	40
4.3.2	Verification with boat-mounted ADCP surveys (1998–2000)	52
4.4	Overall assessment of the calibrated Harbour Model	56
5.	Potential changes in hydrodynamics of Otago Harbour	57
5.1	Simulation for assessing hydrodynamic changes	57
5.2	Hydrodynamic changes to tidal ranges and currents	57
5.2.1	Tide-height differences	58
5.2.2	Tidal-current differences	60
5.3	Spring-neap velocity differences at specific Harbour locations	65
5.4	Comparison of fluxes through the Entrance and ebb-tide sand bar	67
5.4.1	Ebb, flood and net water fluxes	68
5.4.2	Differences in net volumes due to dredging	73
5.5	Synthesis and summary of hydrodynamic changes	74
6.	Set-up and sensitivity testing of the Harbour plume-dispersal model	77
6.1	Dispersion model justification and set-up	77
6.2	Sensitivity testing	78

6.3	Winds	79
6.4	Dispersion coefficients	81
6.5	Sediment fall velocity	81
6.6	Dredger source fluxes	83
6.7	Dredged site	84
6.8	Results from plume-model sensitivity testing	84
6.9	Overall results from sensitivity testing	96
6.10	Decisions on Harbour plume model parameters	97
7.	Modelling results for turbidity and deposition of Harbour dredging operations	99
7.1	Types of dredgers to be used	99
7.2	Trailing Suction Hopper Dredger operations	99
7.3	Dredging parameters for Harbour plume modelling	102
7.3.1	Dredging predominantly sand areas	103
7.3.2	Dredging predominantly silt areas	104
7.3.3	Dredging cycles including disposal trips	104
7.4	Harbour plume modelling approach	108
7.5	Predicted results for SSC and deposition from Harbour dredging	110
7.5.1	Average SSC over a 14-day spring/neap cycle	110
7.5.2	Statistics of 14-day plume model results for SSC	118
7.5.3	Accumulated seabed deposition over a 14-day spring/neap cycle	118
7.5.4	Statistics of 14-day plume model results for accumulated deposition	126
7.5.5	Deposition accumulated over the entire dredging programme	126
7.6	Summary of Harbour sediment-plume modelling results	130
8.	Offshore wave modelling	160
8.1	Wave model	160
8.2	Model grid domains	160
8.3	Model set-up	162
8.3.1	Boundary conditions	162
8.3.2	Winds	162
8.3.3	Currents	162
8.3.4	Model output	162
8.4	Wave hindcast validation	164
8.5	Offshore and coastal wave climate	168
8.6	Effects of dredging on the offshore wave climate	175
9.	Harbour wind-wave modelling	186
9.1	Introduction	186
9.2	Lower Harbour wave model set-up	186
9.3	Lower Harbour wind-generated waves	187
9.4	Summary	192
10.	Offshore hydrodynamic model	193
10.1	Offshore hydrodynamic model set-up	193
10.2	Offshore model calibration and verification	195
10.3	Residual (net) circulation on the Otago shelf	198
10.4	Appraisal of the offshore hydrodynamic model performance	199
11.	Offshore plume dispersal and deposition	201
11.1	Plume model set-up	201

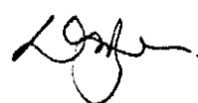
11.1.1	PT plume model parameters	202
11.2	Offshore disposal ground options	204
11.3	Plume modelling approach	206
11.3.1	Hydrodynamic model scenarios	206
11.3.2	Plume model scenarios	209
11.4	Suspended-sediment concentrations predicted using disposal site A0	212
11.4.1	Results for different wind scenarios	212
11.4.2	Differences between size classes and surface vs. bottom layer	226
11.4.3	Predicted plume concentrations for predominantly-silt hopper loads	244
11.4.4	Predicted upper-bound deposition patterns	252
12.	Long-term sediment transport from the disposal site	261
12.1	Disposal mound	261
12.2	Approach to long-term sand transport from a disposal mound	261
12.3	Sand transport through disposal site A1	262
12.3.1	2008 field period assessment	263
12.3.2	10-year wave hindcast estimates of active sand transport occurrences at A1	282
12.4	Sand transport through the preferred disposal site A0	287
12.4.1	Four-month 2008 field period	287
12.4.2	10-year wave hindcast estimates of active sand transport occurrences at A0	299
12.5	Comments on long-term sand transport from the disposal mound	303
12.5.1	Direction of sediment movement	303
12.5.2	Transport rates and deflation of the disposal mound	306
12.6	Comments on long-term silt transport	309
13.	Summary and Conclusions	311
14.	Acknowledgements	316
15.	References	317
16.	Appendix I – Wave statistics from full directional wave spectra	321
17.	Appendix II – Offshore sediment transport methodology	323
17.1	Estimation of sand transport using wave and current field data at site A1	323
17.2	Estimation of sand transport using wave and current field data at site A0	327

Reviewed by:



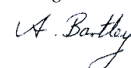
Mark Hadfield

Approved for release by:



David Roper

Formatting checked



1. Introduction

1.1 Project Next Generation

Project Next Generation is an initiative by Port Otago Ltd (POL) to expand the capability of Port Chalmers to handle larger container vessels of up to 8000 TEU capacity¹ through a substantial channel deepening capital works project. The main Harbour channel from Port Chalmers to Harington Bend would need to be dredged to 15 m below Chart Datum to accommodate such vessels, but would need to be deepened to 17.5 m below Chart Datum in the offshore approach channel to accommodate vessel motions arising from a combination of waves, swell and currents.

As part of assessing environmental effects for Project Next Generation, Port Otago Ltd. commissioned NIWA to carry out hydrodynamic, dispersion and sediment transport modelling investigations. The modelling provides quantitative or comparative before-and-after information to underpin the assessments of the possible effects of dredging and disposal operations on both Otago Harbour and offshore-shelf environments.

Wave modelling in the Harbour and offshore was undertaken by MetOcean Solutions through a separate contract with POL, but their wave modelling results are presented here in this combined report on all the numerical modelling investigations. Wave climate model results were also supplied by MetOcean Solutions to NIWA for input to sediment transport modelling.

Two oceanographic measurement programmes were also run within the period from March to August 2008 to support calibration and verification of the numerical models and to provide insights into the flow patterns that were relevant to assessing environmental effects. Within Otago Harbour, current-meter measurements were undertaken in Portobello Bay and Eastern Channel by Marine Sciences Dept, University of Otago (Bowman, 2008a, b). Offshore on the inner shelf, NIWA deployed two current/wave meters for about four months and measured water properties (Bell & Hart, 2008).

A geophysical field programme carried out by Opus International Consultants (2008), provided data on sediment grain sizes that were converted to sediment settling velocities. The geophysical data were analysed by Stuart Hughes & Associates

¹ Twenty-foot Equivalent Unit (or TEU) is an inexact unit of cargo capacity often used to describe the capacity of container vessels. It is based on the volume of a standard-size 20-foot (~6 m) long shipping container.

(consultant to POL) and combined with the initial channel design² (15 m below Chart Datum up-harbour from Harington Bend) to derive a typical dredge operations schedule, from which realistic sediment discharge rates, dredged volumes and round-trip dredging/disposal sequences were derived. These parameters were used as input to sediment plume dispersion models for both the Harbour dredging and the offshore disposal.

The initial channel design, which was used as the basis for the numerical modelling simulations in this Report, would have generated around 7.5 Mm³ of dredged sediments (excluding rock). The final channel design (adopted by POL in March 2009 after detailed ship-handling studies and navigational requirements) would yield a slightly lower volume of dredged sediments at around 7.06 Mm³ to be disposed³ (which is 6% less than for the initial channel design). The slight modification in channel design only affects some of the model simulations already undertaken, namely for assessing changes in the tidal characteristics of Otago Harbour and sediment deposition over the dredging programme. Accordingly, only these simulations and analyses were re-run for the final channel design to update the assessments discussed in this Report.

1.2 Summary of Brief for Numerical Modelling

1.2.1 NIWA modelling

The main components for NIWA's Brief were to provide modelling services to support the environmental impact assessment of a dredged 15 m deep channel and effects of the associated dredging operations as follows:

Otago Harbour:

- Hydrodynamic modelling (currents, tides and winds) in addition to supplying output from these models to external contractors for ship-handling simulations and wave modelling.
- Dispersion modelling of suspended-sediment plumes generated during the dredging operation.

² Currently channel depths from Port Chalmers to Harington Bend are maintained at a channel bed level of 13 m below Chart Datum (but deeper in the offshore approach channel).

³ In reality, this volume will be somewhat lower due to sediment losses from plumes generated during the actual dredging operation.

Offshore shelf region:

- Hydrodynamic modelling (currents, tides, winds) for the shelf region centred on the Otago Heads.
- Dispersion modelling of the short-term behaviour of suspended-sediment plumes generated following disposal of material from the dredge hopper at regular intervals.
- Sediment transport modelling of the long-term movement of material from the mound deposited on the disposal area.

NIWA applied DHI MIKE-21 and MIKE-3 models respectively to Otago Harbour and the shelf area offshore to simulate hydrodynamic flows and plume dispersion modelling. The sediment transport model was developed in-house by a world-recognised sediment transport expert at NIWA and is based on well-respected sediment-transport formulae. Outputs from NIWA's hydrodynamic modelling studies are either discussed in this Report or were passed on to other external consultants to provide input to ship-simulation studies or to the wave modellers (MetOcean Solutions) in the form of total current velocities or their tidal components.

1.2.2 MetOcean Solutions modelling

The main components for the Brief to MetOcean Solutions were to provide wave modelling services to support ship-handling investigations and the environmental impact assessment of a dredged 15 m deep channel option and associated disposal as follows:

Otago Harbour:

- Wave modelling of the existing channel that included the influences of fetch from different wind directions, wind speed and tidal currents (sourced from NIWA modelling) for the purposes of characterising the wave climate within the Lower Harbour. This wave information was also used as input to ship-handling simulations and to underpin an assessment of the likely effects of a deepened channel on shorelines and channel margins in and around the Harbour (Single et al. 2009).

Offshore shelf region:

- Wave hindcast modelling focused on the shelf region centred on the Otago Heads covering at least 5 years, which compares the wave characteristics before and after the offshore disposal mound has been fully formed. As above this information also provides information to

underpin an assessment of the likely effects of the disposal mound on coastal shorelines and margins.

MetOcean Solutions applied the SWAN (Simulating Waves Nearshore) model separately to Otago Harbour and the shelf area offshore to simulate wave spectra. Wave hindcast results for the shelf region, including disposal mound options, were passed to NIWA to undertake sediment transport modelling.

1.3 Main purposes for numerical modelling

The contribution of the different numerical models to the assessment of the main environmental impacts can be mapped as follows:

Numerical model type	Range of environmental impact assessments supported
Hydrodynamic (flow) models	<p>Changes to currents and tide ranges before and after dredging.</p> <p>Provides flow fields as input to all the remaining models below.</p>
Particle-tracking dispersion models	<p>Tracking sweep zones, concentrations and seabed deposition in the Harbour from suspended-sediment plumes generated at the seabed and near surface during dredging.</p> <p>Tracking sweep zones, concentrations and seabed deposition from suspended-sediment plumes generated at the offshore disposal site (i.e., short-term effects).</p>
Wave/swell models (MetOcean Solutions)	<p>Provide wave characteristics (height, period, direction) inside the Harbour or offshore for:</p> <ol style="list-style-type: none"> 1. assessing changes to coastal and harbour shorelines and margins from differences in waves due to a deepened channel and/or disposal mound; 2. assessing ship-handling characteristics to ensure safe navigation; 3. quantifying changes in wave height arising from the physical size and shape of the offshore disposal mound; 4. long-term sediment transport from the disposal mound.
Sediment-transport models	<p>Predict how often, at what rate and where fine sand from the disposal mound moves in the long term.</p>

1.4 Scope of technical report

This technical report summarises the methodology, model calibration and verification processes and provides the key results in tabular or plot format for a 15-m Harbour channel option (which terminates with a channel bed level of 17.5 m relative to Chart

Datum in the offshore approach channel). The report details the main findings from the modelling investigations that are relevant to both the environmental and navigational/ship-handling outcomes of Project Next Generation. Interpretations of the modelling results in terms of likely levels of environmental impact or ship-handling performance were undertaken separately in companion technical reports or investigations.

To place the hydrodynamic and wave model results in context, the report outlines observed hydrodynamic features of Otago Harbour and the shelf region offshore in its present configuration, before discussing the predicted changes following deepening of the shipping channel and offshore disposal of the associated dredged sediment. This newer, higher-resolution information on the tides and flows for the Harbour supersedes preliminary findings presented in an earlier feasibility investigation by Oldman et al. (2008) using a coarser, uncalibrated 100-m grid model of the Harbour.

Sediment plume concentrations and sediment deposition values extracted from the modelling results are the direct increases due to the discharge of sediment over and above the background concentration or seabed deposition from natural processes or other discharges. Setting the background concentrations to zero in the plume models allows a direct comparison of the additional effects due to dredging operations and can be more easily applied to setting consent monitoring conditions as an allowable excess concentration relative to background concentrations. The context for actual background concentrations of suspended sediment in the Harbour is discussed by James et al. (2009).

1.5 Geographic context

This Report conveniently divides the modelling description, results and analysis into the two receiving environments, which are: 1) the environs of Otago Harbour including the approach channel and; 2) the wider shelf area offshore from the Harbour Entrance.

1.5.1 Otago Harbour

Otago Harbour is 21 km long along a SW/NE orientation. The Harbour occupies an area of approximately 46 km² with a spring tidal prism (volume that flows out over an ebb spring tide) of 66×10^6 m³ (Old & Vennell, 2001). The tidal range varies from approximately 1.2 m on a mean neap-tide to around 2.0 m on a spring tide at Port Chalmers, with approximately an additional 0.1 m increase in range at Dunedin

Wharf.⁴ Currents are dominated by the tides, with some variability due to forcing from the prevailing south-west and north-east winds.

Geographic sites referred to in this Report are shown in Figure 1.1. The main Harbour channels referred to are: shipping channel (Entrance to Port Chalmers); Victoria Channel (shallower navigation channel in the Upper Harbour from Port Chalmers to Dunedin bounded by half-tide training walls in Fig. 1.1); and Eastern Channel (side channel from Kilgours Point to Grassy Point (Fig. 1.1).

1.5.2 Otago Heads shelf

The inner shelf area of interest, centred on Otago Harbour Entrance, extends from Cape Saunders in the south up to Green Point at the northern end of Blueskin Bay and out to the 30 m depth contour. This area is shown in Figure 1.2.

Two key sandbars are referred to in the Report: a) the northerly-oriented ebb-tide sand bar at 6–7 m depth on the eastern side of the approach channel that terminates near Landfall Tower (see Fig. 1.2); and, b) the northerly-oriented submergent sand deposit offshore in 25–29 m water depth, that extends for 25 km from Cape Saunders to gradually thin out on the middle shelf opposite Karitane (see Fig. 1.2). Carter (1986) and Carter et al. (1985) refer to this offshore sand feature as the Peninsula Spit. The options assessed for dredged-sediment disposal sites are on the landward side of the Peninsula Spit or on the Spit itself up to the northern terminus at the 30 m contour (Fig. 1.2).

The ebb-tide jet emanating from the Harbour Entrance channel off Landfall Tower is directed to the NNE, with flood-tide flows entering from both sides based on a current meter deployment during the 1988 Otago Harbour Board channel deepening investigation (Barnett, 1988). Measurements during the supporting 2008 field programme (Bell & Hart, 2008) show the tidal currents rapidly dissipate from the approach channel to become a minor contributor to currents on the inner shelf, while wind-generated currents and the Southland Current dominate.

⁴ <http://www.linz.govt.nz/hydro/tidal-info/tide-tables/tidal-levels/index.aspx>

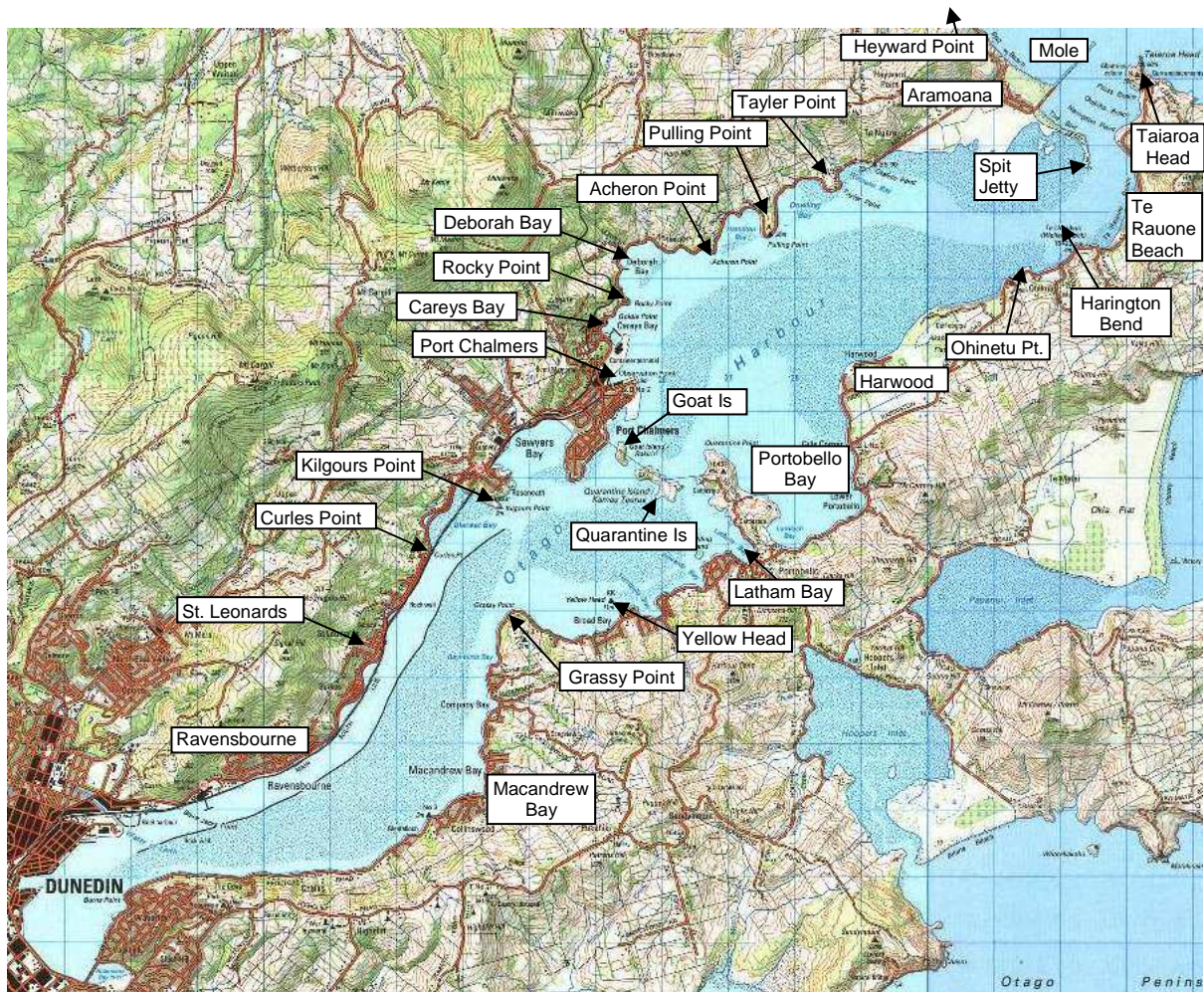


Figure 1.1: Geographical sites in Otago Harbour [Source: ©LINZ 1:50,000 topographic maps].

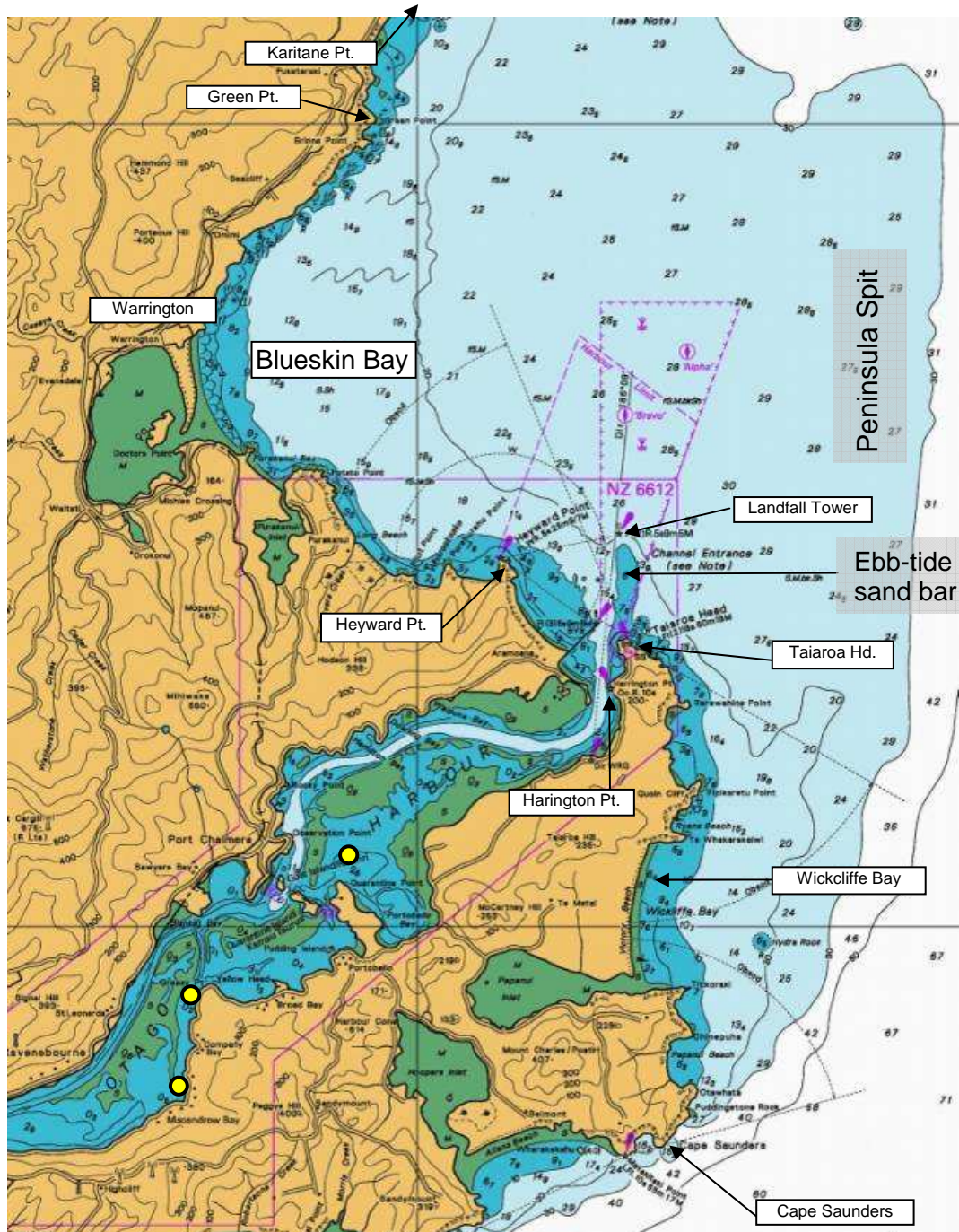


Figure 1.2: Geographical features and bathymetry of the inner shelf off Otago Harbour Entrance and Harbour S4 current-meter sites (yellow circles) during the 2008 field investigations. [Source: Chart NZ661, ©LINZ].

2. Hydrodynamic and wave observations

This chapter provides more details on relevant aspects of the hydrodynamic regime of both the Harbour and offshore shelf and the wave climate to provide some background understanding before changes likely to occur from the dredging project are modelled and discussed.

2.1 Tidal wave propagation in Otago Harbour and phase changes

Figure 2.1 shows a time history of measured tide levels from POL gauges at Dunedin, Port Chalmers and the Spit Jetty (near Taiaroa Head) for one tidal cycle of a larger spring tide recorded in January 2007. The combined plot illustrates the tide-wave form as it propagates up Otago Harbour. There are two key features.

Firstly, the tide range increases with distance from the harbour entrance due to friction, shallow-water effects and reflection of the tidal wave. For example, in Figure 2.1 the high water level at Dunedin of 2.25 m compares with a lower high-water level of 2.03 m at the Spit Jetty, and the tide range on this day was 2.04 m at Dunedin versus 1.73 m at the Spit Jetty (an 18% increase in range up the Harbour).

Secondly there is a phase (time) lag between the high or low tides with distance up the Harbour. On this particular day (22-Jan-2007), the high tide at Port Chalmers lags the Spit Jetty by around 18 minutes, with a further lag of around 15 minutes up to Dunedin Wharf (a total lag of 35 minutes). However low tide at Port Chalmers lags the Spit Jetty by around 45 minutes, with a further lag of around 50 minutes up to Dunedin Wharf (a total lag of 95 minutes). Vennell & Old (1999) show that the time lags for high and low tides at Port Chalmers, relative to the Spit Jetty, varied considerably over a 105-day period, with the lag for high tide in the range 5–20 minutes and for low tide from 35–60 minutes. The reason for the longer phase (time) lags during low tide is the tidal wave propagates at a speed proportional to the square-root of the depth h (i.e., \sqrt{h}), so as the average water depth in the Harbour reduces considerably towards low tide, the tide wave slows down, lengthening the ebb tide and shortening the flood tide. Also, the lag or delay times for low tide are shorter for the stretch from the Spit Jetty to Port Chalmers, compared with the Upper Harbour, because the Lower Harbour is deeper, allowing the tide wave to propagate slightly faster.

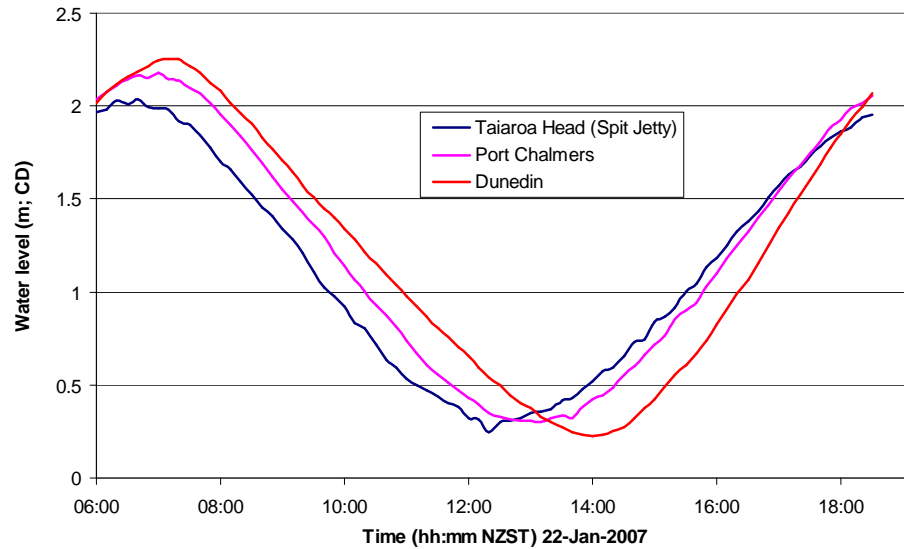


Figure 2.1: Measured spring tide levels (22-Jan-2007) at Spit Jetty, Port Chalmers and Dunedin showing the tidal phase lags at high and low tide moving up Otago Harbour and differences in tidal range.

This leads on to the implications for deepening the navigation channel—a deeper channel will generally cause a small **advance** in the time (i.e., phasing) of the low and high tides within the Harbour (considering calm wind conditions). The effect of such a change in phase on water levels (and similar for tidal currents), which needs to be considered in the results in Chapter 5, is illustrated in Figure 2.2. Here a schematic tide curve, that has been advanced by a nominal 5 minutes (e.g., simulating the effect of a deeper channel), is plotted against the present tide curve for a particular location. At high water the effect of the phase advance is relatively small because the slope of the tide curve is quite flat (at this location anyway). Therefore, model predictions at a fixed or clock time (e.g., 7.10 hours in Fig. 2.2) would indicate only a small change in predicted high water due to dredging. However during the mid ebb and flood tides (when the slope of the tide curve is at its maximum), a small phase advance can show an apparent change in water level (for a given date/time)—for this example between 0.03 and 0.05 m. So much of the “apparent” change in water level may be due to the phase (timing) shift in the whole tidal curve rather than changes in peak speeds or tide range.

Therefore, in terms of hydrodynamic and ecological effects on the Harbour, the key changes to watch for are actual changes in the magnitudes of tide range, high and low tide levels and peak ebb and flood-tide currents irrespective of timing (phase) changes. These actual differences arising from a deepened channel are quantified in Chapter 5.

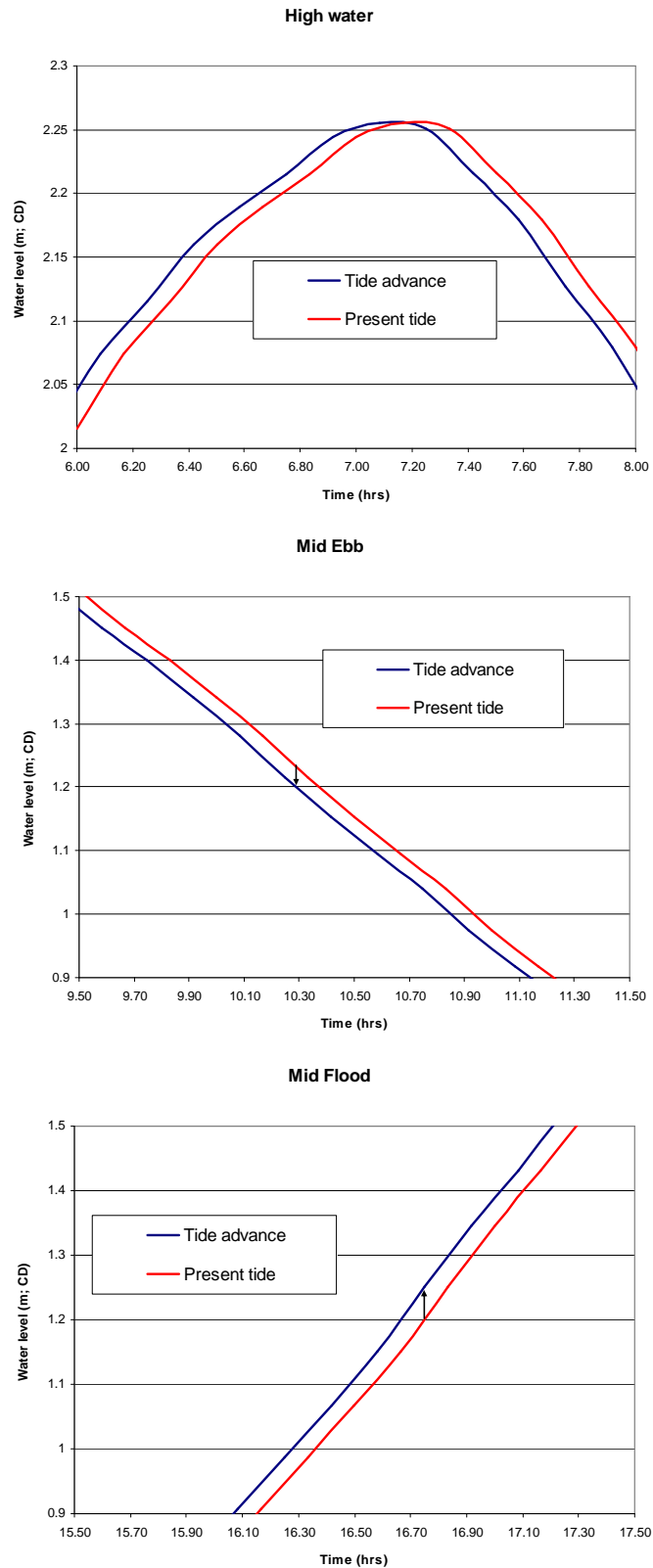


Figure 2.2: Schematic tide curve illustrating the effect of a 5-minute tidal phase advance on tide levels at any fixed (or clock) time.

2.2 Harbour hydrodynamics from previous and supporting 2008 studies

Previous hydrodynamic model and field programmes conducted in Otago Harbour provide an extensive set of data and modelling results on which to build the present model study. Barnett (1988), Wilson & Sutherland (1991), Old (1998) and Old & Vennell (2001), along with a series booklets of tidal current patterns such as Vennell & Old (1999) produced by Dept. of Marine Science (University of Otago) for POL from May 1998 to June 2000, provided useful datasets relevant to the main shipping channel for the calibrating and verifying the hydrodynamic model of the Harbour. Utilising these datasets also meant that the 2008 field programme could concentrate on measurements from the eastern side of the Harbour where few measurements exist, but are nevertheless important in assessing potential effects arising from dispersing suspended-sediment plumes.

Wilson & Sutherland (1991) summarised the tidal propagation process within the Harbour using the tidal amplification and average phase lag between the Harbour Entrance and Dunedin. They found that for larger spring tides, the amplification of the tidal range between the open coast and Dunedin was 1.178 (or ~18%) and the tidal phase lag (averaging low and high tides) was 1.08 hours (65 minutes). These values are in good agreement with the values extracted from the tide curve data in Section 2.1.

Velocity measurements from the Victoria Channel beacon marker #4 just south-west of Goat Island⁵ indicate spring tide currents peak around 0.8 m/s on flood tide and 0.6 m/s on the ebb tide (Barnett, 1988). At Harington Bend (Fig. 1.1) in the Lower Harbour, recorded neap currents are around 70% of spring currents and the maximum spring ebb currents of up 0.8 m/s were recorded during a tidal gauging (Barnett, 1988). However, using an Acoustic Doppler Current Profiler to provide much more extensive measurements, Vennell & Old (1999) found spring ebb currents on a 2 m tidal range in Harington Bend peaked at 1.3 m/s or 2.6 knots just to the north of No. 6 Beacon (NZ Chart 6612) around 2.5 hrs after high water (HW) at Port Chalmers.

Within the constricted tidal flow in the entrance to the Harbour, peak spring-tide currents of 1–1.55 m/s or 2–3 knots⁶ have been recorded on the flood tide between Harington Point and the Spit Jetty (Old, 1998; Vennell & Old, 1999), whereas the maximum ebb-tide current in the same area only reached 1.2 m/s. This means the entrance flows are flood dominant. The strong convergence and strengthening of the

⁵ upper-harbour channel beacon #4 on Chart NZ6612, and referred to as #4UH in Barnett et al. (1988)

⁶ also the same speed range mentioned in the 1944 NZ Nautical Almanac, Part II, indicating the peak speeds off Harington Point appear to have changed little with subsequent dredging.

incoming flood-tide flow occurs between the tip of the Mole and Taiaroa Head (locations in Fig. 1.2).

Higher currents on the flood compared with the ebb tide in the Entrance channel means Otago Harbour is flood-dominant in terms of potential sediment transport with a net influx to the Harbour occurring because of the non-linear increase in sediment transport at the peak of the flood tide relative to the differential between peak flood and peak-ebb current velocities. However to maintain equilibrium of the volume flowing in and out of the Entrance, the ebb tide duration is longer at 6.48 hours than the flood tide that occurs over a somewhat shorter 5.94 hours (Old, 1998). The velocity measurements from beacon #4 in the Victoria Channel (referred to above) also indicate a flood dominance of the Upper Harbour.

The tidal prism passing through the entrance on a Spring tide, based on current velocity measurements using an ADCP, was $68 \times 10^6 \text{ m}^3$ going out on the ebb tide and $65 \times 10^6 \text{ m}^3$ coming in on the subsequent flood tide (Old, 1998), with an average spring tidal prism volume of $66 \times 10^6 \text{ m}^3$ (Old & Vennell, 2001). [Note: apart from measurement tolerances, differences in tidal prism on flood versus ebb tides will occur as the high tide seldom returns to the exact level reached on the previous high tide].

Due to the extensive datasets available on currents in the main shipping channels of Otago Harbour from previous studies, current-meter measurements for the 2008 field investigations (Bowman, 2008a, b) were focused on the eastern side of the Harbour in Portobello Bay and two sites in the Eastern Channel (Fig. 1.2). A 1-month deployment of an S4 current meter in Portobello Bay showed ebb-tide currents flowing to the NE dominate, peaking at 0.3–0.37 m/s, with SW flood-tide currents seldom recorded (Bowman, 2008a). At the northern site in Eastern Channel, the flood and ebb currents were symmetrically directed along the axis of the channel, with a higher peak flood-tide speed (average) of 0.44 m/s compared with 0.3 m/s on the ebb tide (Bowman, 2008b). At the southern end of Eastern Channel in Macandrew Bay, tidal flows were dominated by southward currents on the flood tide averaging 0.33 m/s with only 0.09 m/s on the ebb tide (Bowman, 2008b).

2.3 Offshore shelf hydrodynamics

Once out of the ebb-tide jet or the influence of the flood-tide inflow off the Harbour Entrance, the tidal component of the current flows is quite weak on the Otago shelf, as shown in Figure 2.3 for the peak ebb and flood-tide currents on a mean tide range extracted from the NZ tidal model of Walters et al. (2001). South of Cape Saunders, the tidal-current component is parallel with the coast, but north of Otago Harbour

Entrance, the tidal-current component is relatively weak and is directed in an offshore/onshore orientation—onshore during the flood tide. These to and fro weak tidal components on the shelf would seldom be observed directly (other than by a current meter), as they are only a small contributor to the overall currents that are present.

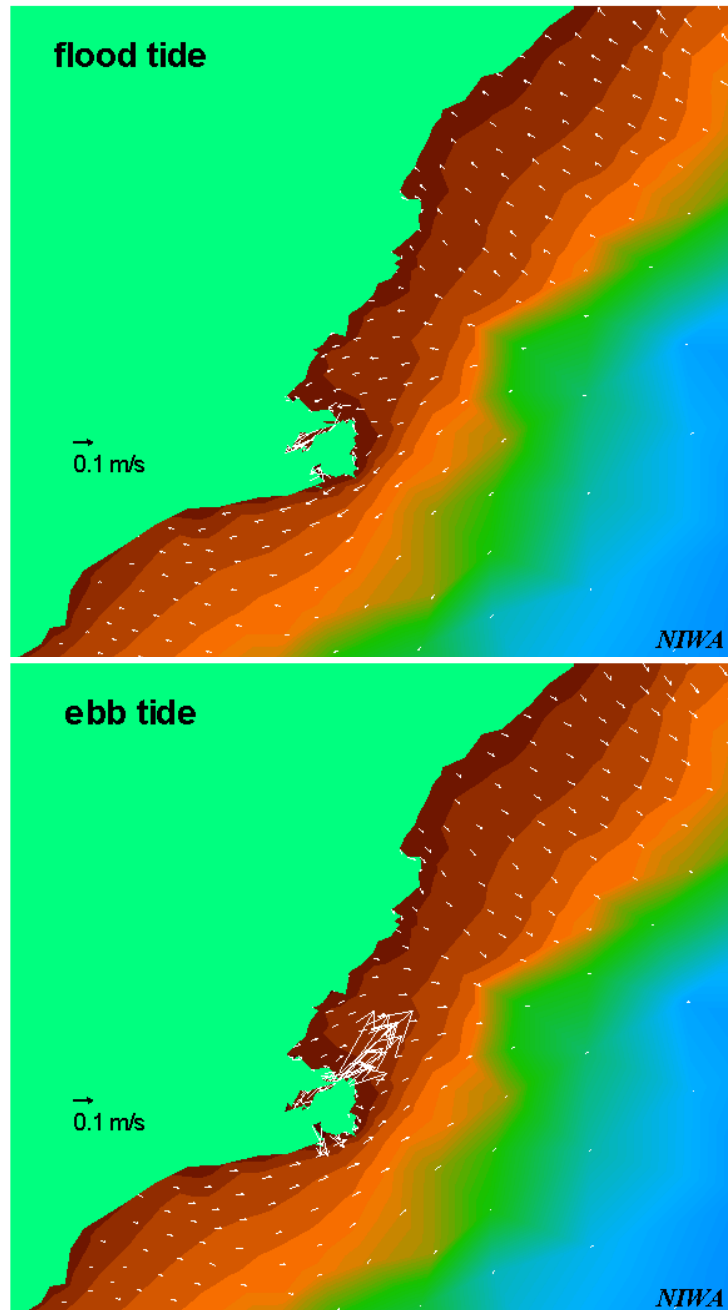


Figure 2.3: Tide-only current velocities at peak flood tide (top) and peak ebb tide (bottom) for an average tide range on the Otago shelf [Source: based on NZ tidal model of Walters et al. (2001)].

During the supporting 2008 field programme offshore (see Fig. 2.4 for sites), current and wave measurements were persistently made at one of the potential dredged-material disposal sites at A1 (4 km NE of Taiaroa Head) over a nominal 4 month period from March to early August 2008 (excluding gaps between deployments). For all but one of these deployments, a concurrent ADCP mooring site was also occupied at either B1 (Blueskin Bay) or B2 (Heyward Point). Inshore, waves were only measured at B2, due to a malfunction in the ADCP at site B1. The range of winds experienced during the field programme was not too dissimilar to the long-term average distribution from the long-term record at Taiaroa Head. But there were slightly more west to south-west winds offset mainly by slightly less winds from the north-east quadrant. Strong winds from the south-east are infrequent, but one event was measured in the last deployment, which provides insight into residual (net) current flows that coincide with large waves, with the potential for high sediment transport rates.

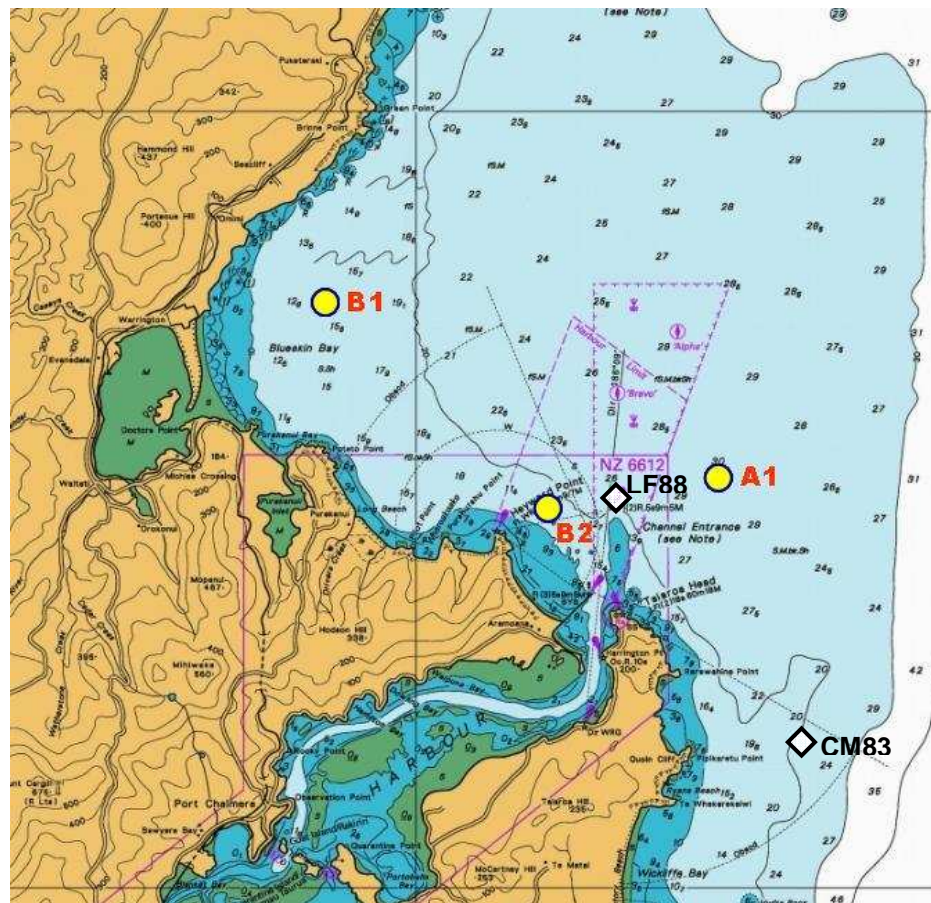


Figure 2.4: Location map of the three ADCP mooring sites (circles) occupied during the 2008 offshore field programme (Bell & Hart, 2008) plus two historic current-meter mooring sites (diamonds) at LF88 and CM83. [Source of map: extracted from Chart NZ661, *Approaches to Otago Harbour*, ©Land Information NZ, 2006].

The offshore field report (Bell & Hart, 2008) presents a detailed synthesis of the field measurements and draws out the key oceanographic and meteorological factors that explain the variability and extremes in the ADCP datasets.

The current velocity measurements provide a useful dataset in their own right showing the prevailing patterns of coastal and shelf circulation in the area of Otago Heads. Tidal currents at all three ADCP sites were a small proportion of the measured currents. At A1, the prevailing residual current drift in most cases is to the SE, with a slight deviation to the south in the last deployment (July 2008). This prevailing current drift is altered at times when moderate to strong south to SE winds are able to reverse the net drift, but otherwise the more frequent winds from the SW and NE quadrants appear to sustain the south-easterly drift. Sometimes winds from a more northerly direction cause this current drift to deviate slightly more towards the south at A1.

These results have implications for the hydrodynamic and sediment modelling for a disposal ground offshore (Bell & Hart, 2008), with tides being negligible, the Southland Current providing the regional context for mean flows (including the hint of an eddy off Otago Heads), and the winds being the predominant cause of variability in net current drift in the area of A1 (deviations from the SE drift), and shear between the near-surface and near-bed layers, which can result in currents in opposite directions.

In Blueskin Bay (B1), the net current drift was quite variable. For the first deployment in March/April 2008, the current drift exhibited slow cyclic meanders at the seabed arising from a succession of alternate NE and SW winds. This contrasts with the June 2008 deployment, where the current drift was more consistently towards the northerly quarter, due to more frequent and stronger winds from the SW and weaker less frequent winds from the NE.

Off Heyward Point (B2), the prevailing net current drift is generally eastwards at 1 km/day near the seabed. In a similar manner to site A1, south to SE winds can reverse the net drift at B2 to be in a more NW direction towards Blueskin Bay.

Consequently, the current velocity measurements at various depths from the 2008 field programme provide a reliable and consistent dataset for calibrating and verifying hydrodynamic, sediment transport and plume models used to assess environmental effects of the proposed dredging activities.

A previous deployment of an InterOcean S4 current meter at Landfall Tower (location LF88 in Fig. 2.4), at the northern end of the ebb-tide sand bar during the 1988 model study by the Otago Harbour Board (Barnett, 1988), showed a consistent northerly residual current. The average residual (or drift) velocity was 4.5 km per day to the

north based on the S4 current-meter record for a 78-day period from the 18-March to 7-June 1988. The only other known current-meter record from the offshore area is a short 4-day deployment by the Royal New Zealand Navy and the former NZ Oceanographic Institute of an Aanderaa current meter in 21 m water depth from 5–9 February 1983 off Otago Heads (location CM83 in Fig. 2.4). The currents from this short deployment were consistently flowing in a NE direction (mean of 40° True North) at a mean speed of 0.2 m/s peaking at 0.52 m/s.

Further offshore, the flow pattern is dominated by the Southland Current, which sets persistently towards the north-east, although it does vary in strength with changes in regional winds through Foveaux Strait (Chiswell, 1996). The Southland Current coalesces two main water masses, with a band of relatively warm, salty Subtropical Water on the continental shelf (sourced from the Tasman Sea) and colder, fresh Subantarctic Water offshore to the east, with the shelf Subtropical Water contributing only 10% of the flow within the overall Southland Current (Sutton, 2003). Previous inner shelf studies such as Murdoch et al. (1990), who combined analyses of satellite imagery, water properties and simple flow modelling, indicated the existence of an anti-clockwise eddy in the wider Blueskin Bay in the lee of Otago Peninsula, juxtaposed against the Southland Current. They surmised that the eddy feature, while persistent, could be disrupted by strong northerly or southerly winds.

2.4 Waves

Otago Harbour is orientated along the same alignment as the prevailing winds from either the SW or NE quadrants. This means that local wave heights within the Harbour are maximised due to the larger wind fetch along this orientation. However, the effective fetch is broken at the half-way point by Goat Island and Quarantine Island (collectively known as the Halfway Islands) and Portobello Peninsula which form a barrier to local wave growth throughout the Harbour. Few wave measurements have been made inside the Harbour, except for short deployments in the vicinity of Te Rauone Beach by the Otago Regional Council in 2006/07 (Lincoln Coe, POL, pers comm.).

Offshore, the only known wave measurements were recorded routinely in 2007 by a Triaxys waverider buoy during construction of the Tahuna outfall on the southern side of Otago Heads (Lawyers Head). The wave record from Jan–May 2007 (summer to early winter) is of a reasonable quality, and was used as validation of the wave hindcast modelling (Section 8.4). During this 5-month period, the highest significant wave height reached 4.5 m on 16 April 2007.

The three highest wave events recorded at site A1 (Figure 2.4) during the 2008 offshore field programme all occurred during the last deployment (Bell & Hart, 2008). The highest significant wave height of 4.7 m was reached at 1800 h on 31 July 2008, with peak spectral periods of 11–13 seconds (swell) arriving from an easterly direction. Local winds at Taiaroa Head preceding this wave peak were from the SE. The second highest significant wave height of 4.5 m was reached a week earlier at 0600 h on 24 July 2008, with peak spectral periods of 10–12 seconds (swell) arriving from a SE direction, with local winds blowing from the south.

Further inshore in 15 m water depth off Heyward Point at site B2 (Figure 2.4), the significant wave height was substantially lower (compared to the deeper site at A1), due mainly to sheltering by the Otago Heads. However, the highest wave event on 31 July with waves arriving directly onshore from the east shows the reduction in peak wave height was only 16% (4.0 m at B2 compared to 4.7 m at A1). Inshore at B2, the spectral peak wave direction arrived from a much narrower band of 60–100° True North, compared to the exposed offshore site at A1. This feature arises from the refraction of waves from both the south and north into more onshore-directed wave trains closer to the coast.

3. Bathymetry and Otago Harbour model grids

3.1 Introduction

A critical step in building a hydrodynamic flow or wave model is to develop a coherent and accurate set of soundings to a common datum that describe the bathymetry of both Otago Harbour and the offshore region. Within the Harbour, this needs to include the topography of the intertidal flats as well as the sub-tidal channels.

For the Harbour, all available soundings were averaged over square cells of the model grid to schematize the seabed of the entire Harbour and approach channel, initially on a grid of 10×10 m cells for input to the Lower Harbour wave model and then resolved to a grid of 30×30 m cells⁷ for the hydrodynamic flow model of the existing Harbour bathymetry. The bathymetries of these two grids were subsequently modified to include the initial dredged channel design, in order to compare wave and hydrodynamic conditions before and after dredging. Modifications arising from the final channel design were subsequently applied to the 30×30 m model grid and used to update the differences in tidal characteristics of the Harbour following dredging.

The set-up of the offshore wave and hydrodynamic models is described later in Sections 9 and 10.

3.2 Bathymetry datasets

Data from a number of sources were collated to provide raw bathymetry for the development of the Harbour model grid and offshore shelf model grids, with an overlap between model grids in the inner shelf area off the Harbour Entrance.

The main sources of bathymetry data or information were:

- Port Otago Ltd: fairsheets and digital soundings from POL holdings that included updated 2008 surveys commissioned in: a) areas of the Harbour not well covered by past surveys e.g., embayments adjacent to the main shipping channel and side channels, and b) extensive coverage of the inner shelf from Taiaaroa Head to Waikouaiti Bay north of Karitane Point (see Fig. 3.1).
- University of Otago (Surveying School): digital soundings data undertaken for various areas of the Harbour and supplied by POL.

⁷ 30×30 m is an area almost the size of a quarter-acre section.

- Otago Regional Council: supplied LiDAR⁸ data for “tiles” around the Otago Harbour shoreline and adjacent intertidal flats. This aerial laser scanning dataset was a subset of the Otago-wide survey of the coastal topography. This data was used to fill gaps in the upper parts of intertidal flats around the Harbour perimeter, although unfortunately was too noisy and intermittent to use on the large tidal flat opposite Aramoana (location in Fig. 1.1).
- NIWA: extracted gridded seabed depths and contours for the offshore shelf area from the ocean bathymetry archive maintained by NIWA, particularly for depths >200 m.
- LINZ Charts: digitised contours from LINZ Hydrographic Chart NZ661 for areas not covered by POL or NIWA bathymetry datasets.

All bathymetry data sources (except the deeper NIWA contours) were converted to Chart Datum as the vertical datum (if not already in that depth datum) and to North Taieri Meridional Circuit Grid (1949) for the horizontal coordinate system, which is used by POL.

⁸ A laser scanning technique referred to as Light Detection And Ranging (LiDAR)

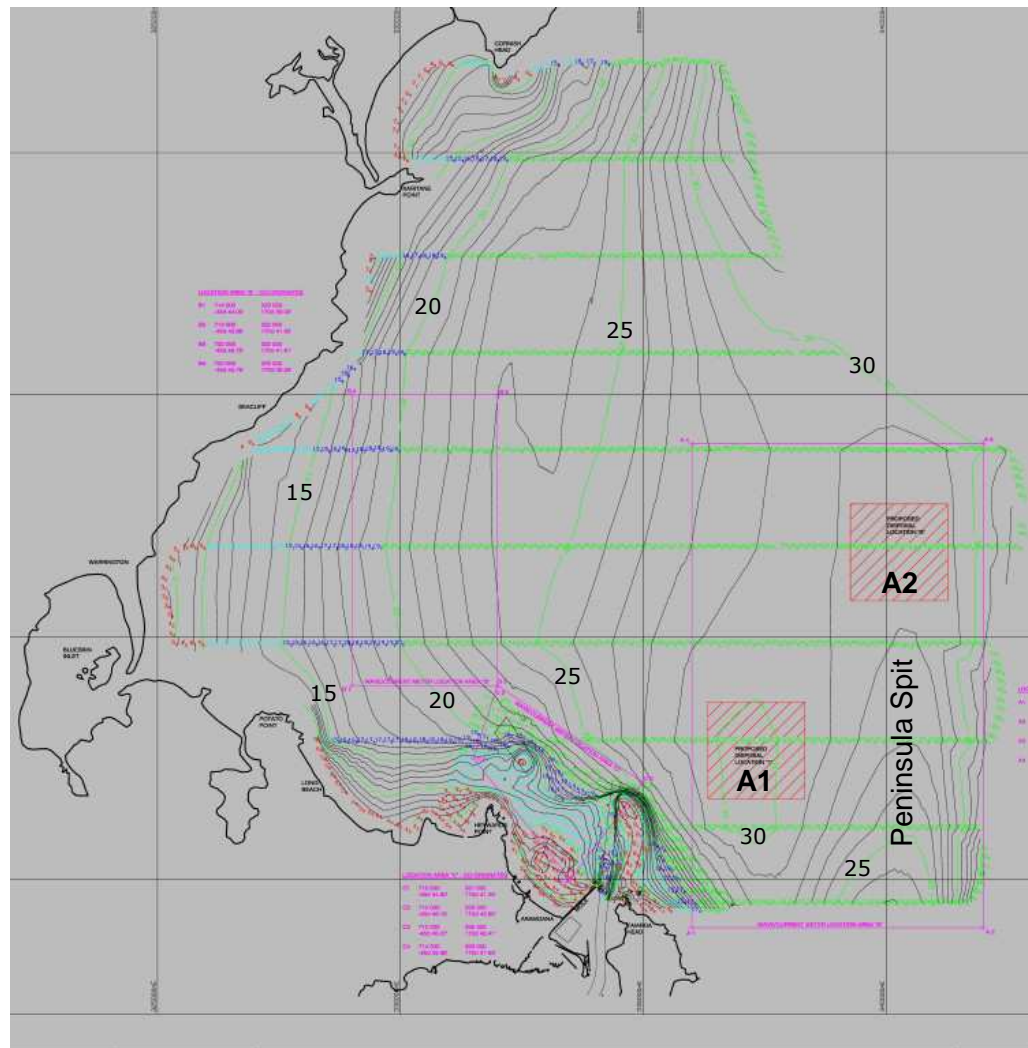


Figure 3.1: POL seabed sounding lines (2 km spacing offshore) and contours at 1 m increments and annotated every 5 m increments (m; Chart Datum), illustrating the bathymetry coverage within Blueskin Bay and the inner shelf. The hatched squares (A1, A2) indicate initial options for the disposal site which coincided with the offshore areas consented for deployment of oceanographic instruments.

The coverage of this sounding and depth contour data is shown in Figure 3.2.

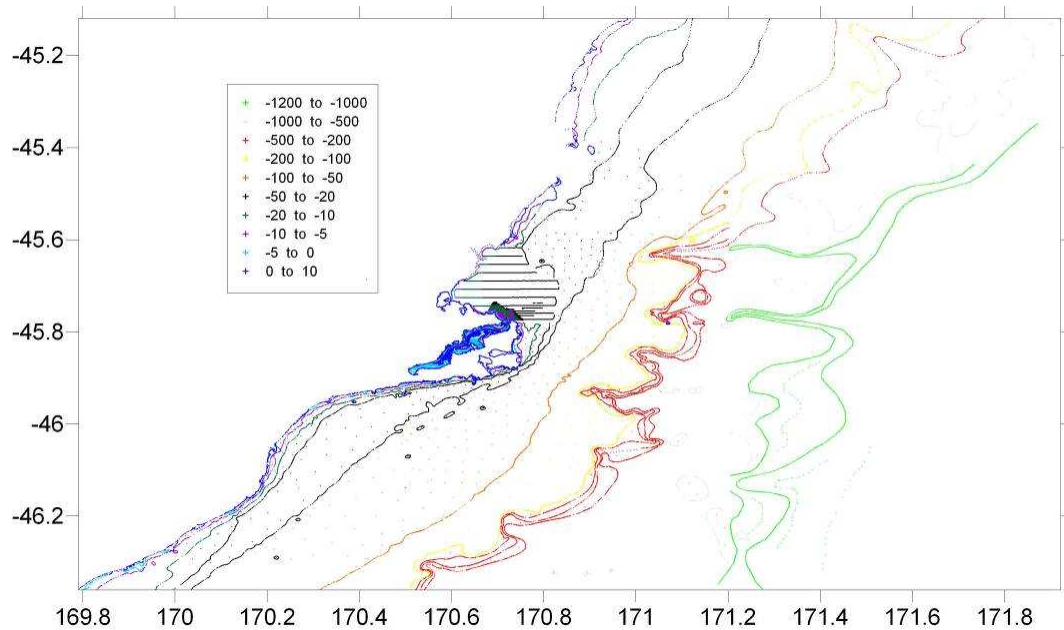


Figure 3.2: Amalgamated bathymetry dataset used for the development of Harbour and offshore model grids, plotted in a WGS-84 latitude/longitude coordinate system.

Subsequent quality assurance of the two Harbour grids using aerial photos at different stage of the tide highlighted some areas requiring fine tuning of the bathymetry. The following improvements to the Harbour model grids were made:

- elevation above Chart Datum for the major groynes in the Harington Bend area off Te Rauone Beach (Fig. 3.3);
- channels or culverts through embankments were sized by POL and positioned from aerial photos (e.g., see Fig. 3.4) and incorporated into the model grid to provide a realistic flow connection into partially impounded areas for sediment plume dispersal modelling. Embayment connections were inserted in the model grid for: a) Andersons Bay at the top of the Upper Harbour in Dunedin; b) two embayments behind the railway embankment in the Saint Leonards area; c) connections to Blanket Bay through the railway embankment;
- averaged cell depths for the intertidal flats in the centre of the Lower Harbour (adjacent to the port side of the shipping channel) were corrected by using photographs at various states of the tide to obtain the present-day shape and area of the emergent sand banks (Fig. 3.5);
- seabed levels on the Aramoana intertidal bank were estimated from a few available cross sections and aerial photos of drainage and waterline at different

stages of the tide (see example in Fig 3.6). The levels are only approximate for small-scale drainage patterns, but this shouldn't affect the use of the model for larger scale plume dispersion and changes in hydrodynamic flows arising from the deeper channel.



Figure 3.3: Example of an aerial photo used to determine the exposure of groynes in the Harington Bend area at Beacon Nos. 8 & 10 at different stages of the tide. [Source: Port Otago Ltd].



Figure 3.4: Aerial photo showing bridged gaps in the railway embankment between the Victoria Channel and embayments in the area of Saint Leonards (see Fig 1.1) in the Upper Harbour. [Source: Port Otago Ltd].



Figure 3.5: Examples of aerial photos showing the shapes and extent of the intertidal banks on the port side of the shipping channel in the Lower Harbour during different stages of the tides. Arrow marks the high-tide subsidiary channel through to Portobello Bay. [Source: Port Otago Ltd].



Figure 3.6: Drainage patterns and waterline on the Aramoana intertidal bank. [Source: Port Otago Ltd].

3.3 Hydrodynamic model grid (existing channel)

The amalgamated bathymetry dataset was used to generate a 10×10 m and a 30×30 m grid of cells for the Harbour wave and flow models respectively and a flexible

triangular mesh for the offshore model. The Harbour model grids also included the area outside the Entrance from southern Blueskin Bay and Heyward Point to south of Taiaroa Head as shown in Figure 3.7 for the 30-m grid.

The grid is orientated to True North in the vertical axis with the grid origin at 170.504317°E and -45.895668°N (or 1406392 m Easting and 4914516 m Northing in NZ Transverse Mercator projection). The numbers of 30×30 m cells in the model grid are 537 in the vertical (north-south) and 621 in the horizontal (east-west).

The grid generation was undertaken in Surfer® (Golden Software), where individual model cells are assigned a flat seabed level across the cell representing the average height of seabed soundings within that cell (relative to Chart Datum), and taking into account bed slopes from neighbouring cells. The seabed levels relative to Chart Datum within each cell of the 30-m grid are contoured in Figure 3.7.

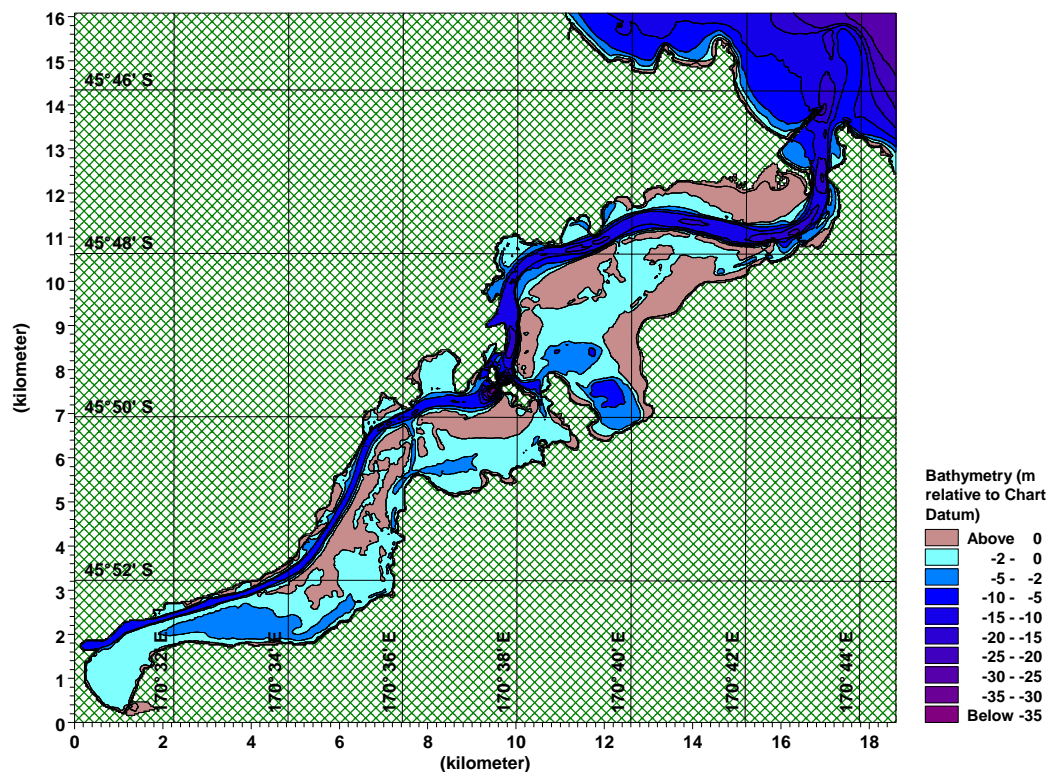


Figure 3.7: The 30-metre model grid used for hydrodynamic modelling scenarios on the existing Harbour bathymetry. Grid includes groynes off Harington Bend and culverts within the bays enclosed by causeways in the Upper Harbour. [See text for grid origin].

3.4 Deepened shipping channel configuration

The initial dredged channel design was for a minimum seabed level of 15 m below Chart Datum from Port Chalmers to Harington Bend, thereafter progressively deepening to reach a seabed level of 17.5 m (below Chart Datum) in the offshore approach channel between the Mole and Landfall Tower. The deeper channel sections from Harington Bend out to Landfall Tower allow for greater heave, roll and squat of vessels arising from combinations of waves, wind and tidal currents and the turning manoeuvre around Harington Bend.

An initial dredged channel design was developed by POL and its maritime advisers after preliminary ship-handling studies and used for most of the modelling results discussed in this report. After further ship-handling simulator trials and design work, a final channel design was adopted by POL in March 2009. The modifications to the initial channel design were mainly: i) a narrower width in the offshore approach channel, but the depth remained the same at 17.5 m below Chart Datum (hence less dredging volume from this source); ii) a reduction of 0.5 m depth to a 16 m–Chart Datum seabed level in the Entrance channel section from the Mole through to Harington Bend (was 16.5 m in the initial channel design) and also means less dredging volume from this source; iii) more gently-sloping batters on the channel flanks in some places (slightly more dredging volume from this source); iv) a slight straightening of the channel between Pulling Point and Acheron Head. Overall, these modifications to the final channel design require around 440,000 m³ less sediment volume to dredge than for the initial channel design. In the rest of the report, the proposed dredged channel design will be referred to as the “15-m Harbour channel” and relates to the final channel design unless otherwise stated. Table 3.1 summarises the design seabed levels and range of batter slopes used to modify the existing bathymetry grid for the final 15-m Harbour channel configuration.

Additional 10×10 m and 30×30 m Harbour model grids were reproduced from model grids of the existing Harbour bathymetry, and proposed changes to the bathymetry for the initial 15-m channel design inserted. These were used to run wave and tidal hydrodynamic models respectively. Subsequently, the 30×30 m Harbour model grid was modified to include the final design channel. This grid was used to re-run the tidal model to compare with results from the 30×30 m Harbour grid of the existing situation, thereby quantifying any changes in tides and currents solely due to channel dredging required for the final design. The contoured seabed levels in the 30×30 m grid in the Lower Harbour are shown in Figure 3.8 for the proposed 15-m Harbour channel (final design).

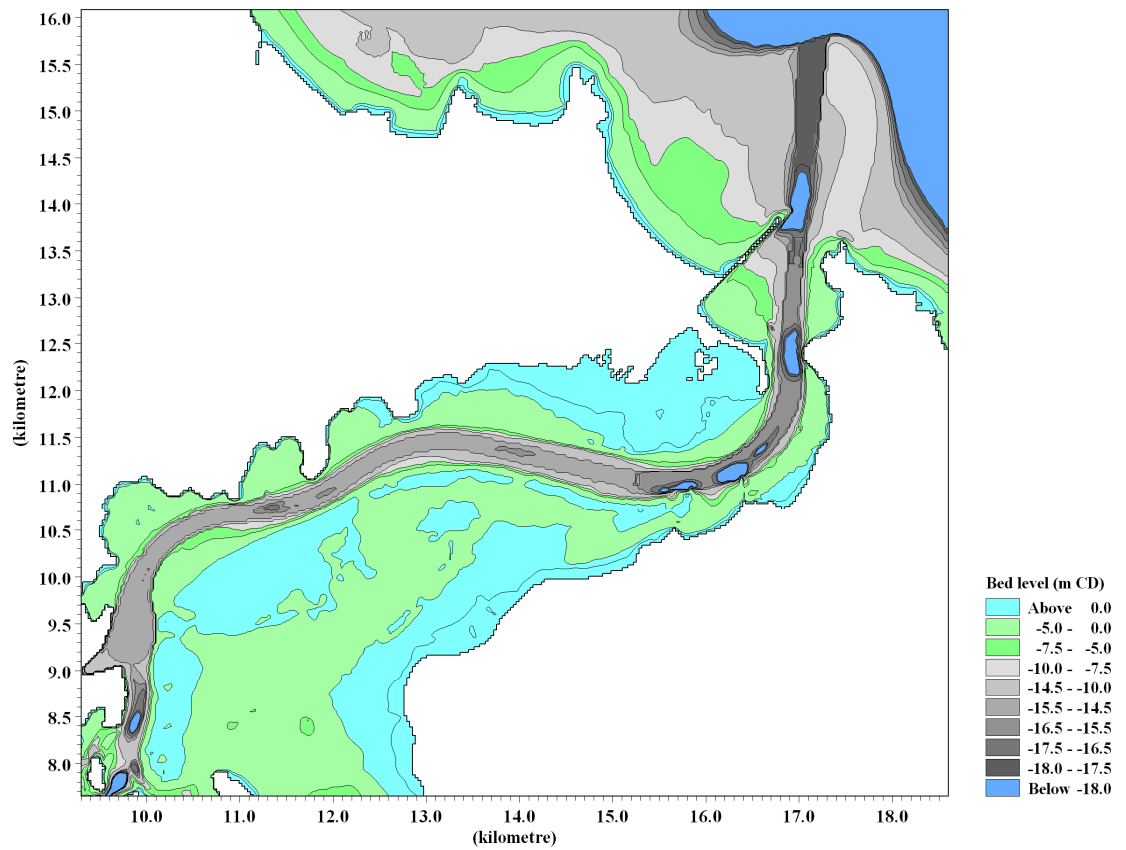


Figure 3.8: Contoured seabed levels (relative to Chart Datum) in the 30×30 m grid of the Lower Harbour for the 15-m Harbour channel design (final design) with areas outside the channel footprint showing the existing bathymetry. [See text for grid origin].

Table 3.1: Summary of design depths and batter slopes for adopted 15-m dredged channel configuration (final design), where the Entrance approach channel would be deeper to allow for greater wave heave and squat of vessels and progressively approaches a 15 m depth past Harington Bend at Beacon 12. Note: Beacon Nos. can be located on LINZ Hydrographic Chart NZ 6612.

Channel section	Description	Design seabed level for 15-m channel (m below Chart Datum)	Side batter slopes
Entrance Channel	Landfall Beacon to Mole	17.5	1:12
The Mole	(Depth transition)	17.5 to 16.0	N/A
Howletts Claim	Mole to Harington Point	16.0	1:7–1:10
Harington	Harington Pt - Beacon 10	16.0	1:5–1:8
Beacon 10–12	(Depth transition)	16.0 to 15.0	1:8
Cross Channel	Beacon 12 - Beacon 14	15.0	1:8
Taylers	Beacon 14 - Beacon 18	15.0	1:5–1:8
Pulling Point	150 m each side of Beacon 17	15.0	1:6–1:7
Hamilton	Beacon 18 - Beacon 20	15.0	1:3–1:8
Acheron Head	150 m each side of Beacon 19	15.0	1:1–1:6
Deborah Bay	Beacon 20 - Beacon 24	15.0	1:3
Rocky Point	100 m each side of Beacon 17	15.0	1:3
Turning Basin	Beacon 24 - Beacon 28	15.0	1:3

3.5 Harbour wave model grid

A 10×10 m grid of cells for the existing bathymetry was developed into a SWAN wave model grid for wind-generated waves in the Lower Harbour by MetOcean Solutions. The extent of the Lower Harbour wave model is shown in Figure 3.9.

A second wave model grid was developed with the proposed 15-m deepened channel inserted as discussed in the previous Section.

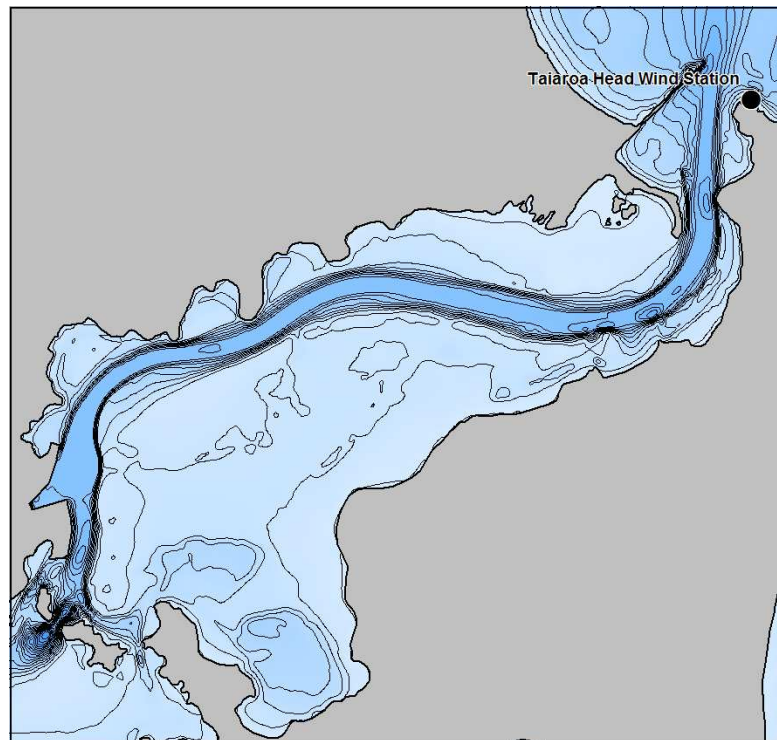


Figure 3.9: Area used to model wind-generated waves in the Lower Harbour including relative shading to represent the bathymetry (for the existing channel) and the location of the Taiaroa Head wind station. [Source: *MetOcean Solutions*].

4. Harbour hydrodynamic modelling: set-up, calibration and verification

4.1 Hydrodynamic model setup

For the Harbour modelling, the depth-averaged DHI MIKE-21⁹ modelling package was selected as the most appropriate model to use for assessing changes in hydrodynamics and providing flow fields for the suspended-sediment plume modelling. DHI is based in Denmark, and have a world-wide reputation for producing industry-standard modelling software, that has been well tested by numerous applications around the world, including dredging projects such as Next Generation.

MIKE-21 is a 2-dimensional hydrodynamic model that solves the depth-integrated St. Venant equations that describe continuity of mass and momentum on a regular grid of square cells (in this case 30×30 m cells).

Data from the Spit Jetty tide gauge from 2000–2007 were used to derive tidal height constituents as shown in Table 4.1. These constituents were used to define the offshore tidal boundary conditions for all the Harbour model simulations.

Wind forcing, when used in scenarios or hindcast simulations of previous field measurement campaigns, was obtained from wind velocities measured at Taiaoroa Head weather station. Wind stress is applied to the water surface of the water cells within the Harbour model grid.

Some simulations of the Harbour hydrodynamic model (existing channel and the 15-m deep channel option) were undertaken with just tidal forcing (i.e., no winds) and used to extract tidal current and tide height constituents from the Lower Harbour for: a) input to the Harbour wave modelling to include wave-current interactions; b) tidal input to the ship-handling investigations; c) to provide tidal height and current constituents before and after dredging the channel, to ascertain the magnitude of changes in the hydrodynamics of the Harbour.

Initially, calibration of the hydrodynamic model was undertaken using the field measurements available from the 1988 model study of the Harbour by the then Otago Harbour Board. Seabed roughness, which is the main tuning parameter in the calibration phase, required only minor adjustments, in order to get a good overall match with tide heights and currents.

⁹ <http://www.dhigroup.com/Software/Marine/MIKE21.aspx>

Verification of the hydrodynamic model, where all parameters determined during the calibration are fixed (unaltered), was undertaken for S4 and tide measurements obtained during the 2008 field programme.

Table 4.1: Main tide-height constituents and their amplitude (half-range) and phasing of high tide (°NZST) derived from the POL Spit Jetty tide gauge record.

Constituent	Amplitude (m)	Phase (°NZST)
Z ₀ (mean)	1.047	0
O ₁	0.028	59
K ₁	0.022	105
N ₂	0.175	71
M ₂	0.676	107
S ₂	0.089	118
M ₄	0.022	263

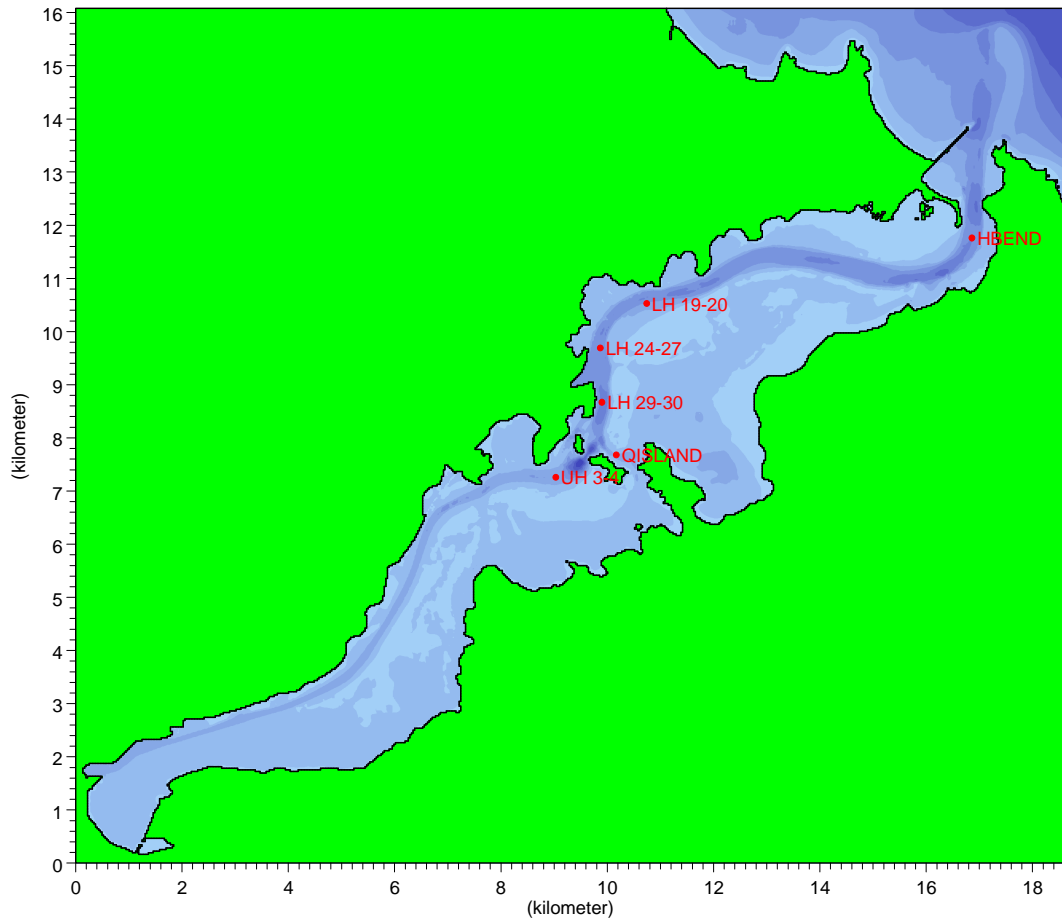
4.2 Calibration of Harbour model on 1988 field measurements

4.2.1 Tide Data

Tide data recorded in the Harbour was available for the period 19:00 14 April to 16:00 15 April 1988. This included measurements at three sites being Pilots Beach, Port Chalmers and Dunedin. Table 4.2 shows the tide sampling period compared to available Braystoke current meter data.

4.2.2 Braystoke current meter

Current speed and direction data in the Harbour was available from Braystoke current meter deployments between 20 March and 19 April 1988. The deployment cross-sections were typically in the Lower Harbour main channels as shown in Figure 4.1. At each cross section, 3–6 sampling sites were measured across the channel, giving a total of 29 sampling sites.



O:\POL08203\RawData\BATHYMETRY\HARBOUR\Otago_30m_001.dfs2

Figure 4.1: Brastoke current-meter deployment cross-sections from the previous 1988 field programme (Barnett, 1988).

Depth-averaged current speed and direction data were extracted from a printed hardcopy of the 1988 Brastoke measurements and converted to u (E–W) and v (N–S) velocity components. The data from each of the 29 sampling sites was loaded into a separate input files, detailing current speed, direction, u and v components, for comparison with the model predictions.

Table 4.2 provides details of each of the sites with sampling times, geographic co-ordinates (North Taieri Circuit Grid, 1949), relative model cell i - j coordinates, and the calibration data set number (different tidal cycles) for modelling calibration purposes.

Table 4.2: Tide and Braystone current meter sampling dates, locations (North Taieri Circuit Grid 1949), model grid coordinates i, j , and calibration datasets.

Location and Site	Sampling Date	Calibration Data Set	E	N	Model i	Model j
LH24-27 Site A	20 March 88	Calibration Data Set 1	327330	705680	338	323
LH24-27 Site B	20 March 88		327230	705680	334	323
LH24-27 Site C	20 March 88		327130	705680	331	323
LH24-27 Site D	20 March 88		327030	705680	328	323
LH24-27 Site E	20 March 88		326930	705680	324	323
LH24-27 Site F	20 March 88		326830	705680	321	323
LH29-30 Site A	21 March 88		327230	704675	334	289
LH29-30 Site B	21 March 88		327127	704650	331	288
LH29-30 Site C	21 March 88		327033	704636	328	288
LH29-30 Site D	21 March 88		326950	704675	325	289
LH19-20 Site A	13 April 88	Calibration Data Set 2	327330	706310	360	344
LH19-20 Site B	13 April 88		327980	706410	359	347
LH19-20 Site C	13 April 88		327950	706500	358	350
LH19-20 Site D	13 April 88		327910	706575	357	353
LH19-20 Site E	13 April 88		327905	706655	357	355
LH19-20 Site F	13 April 88		327870	706782	356	359
TIDE Pilot Beach	14-15 April 88		-	-	556	424
TIDE Port Chalmers	14-15 April 88		-	-	326	302
TIDE Dunedin	14-15 April 88		-	-	16	56
HBEND Site A	17 April 88	Calibration Data Set 3	327330	707750	569	392
HBEND Site B	17 April 88		334170	707728	566	391
HBEND Site C	17 April 88		334084	707755	563	392
HBEND Site D	17 April 88		333978	707705	559	390
HBEND Site E	17 April 88		333930	707755	558	392
HBEND Site F	17 April 88		333872	707847	556	395
UH3-4 Site A	19 April 88	Calibration Data Set 4	327330	703115	302	237
UH3-4 Site B	19 April 88		326250	703210	302	240
UH3-4 Site C	19 April 88		326235	703300	301	243
UH3-4 Site D	19 April 88		326215	703395	301	247
QISLAND Site A	19 April 88		327395	703710	340	257
QISLAND Site B	19 April 88		327365	703670	339	256
QISLAND Site C	19 April 88		327335	703640	338	255

Initial calibration of the DHI MIKE-21 simulations was conducted to check the tidal amplitude and phase predicted by the model with that recorded at the three sites at Pilots Beach, Port Chalmers and Dunedin. Figures 4.2 to 4.4 show the predicted and recorded tide for Pilots Beach, Port Chalmers and Dunedin respectively. Tide phasing was considered acceptable although amplitude was over-predicted at the tidal peak by approximately 0.1 m. In order to improve the amplitude prediction, bed roughness was increased within reasonable limits to a constant inverse Manning's n of 32 over the model grid. No significant improvement resulted, so the original inverse Manning's n values were reinstated for the velocity calibration simulations using the Braystoke current-meter data.

Four model simulations were run for each of the calibration data sets detailed in Table 4.2. Result files for the above model simulations are configured to produce surface elevation and current u and v velocity components at locations corresponding to the Braystoke and tide sites every 5 minutes. Figures 4.5 and 4.6 provide an example of the measured and predicted u and v velocity components respectively at location LH19-20 Site A (see Fig. 4.1 for cross-section location). In this case, the u -velocity component in the E-W direction is more closely aligned to the axis of the channel, and therefore more likely to achieve a good match with the modelled u -component, than the cross-channel v -velocity component.

The calibration simulation result files were compared with the corresponding individual Braystoke site measurements. A regression analysis was undertaken on the modelled results from the relevant 30 m \times 30 m cell and Braystoke "point" measurements for u and v depth-averaged velocity components and a correlation coefficient r^2 determined¹⁰ as shown by way of example in Figure 4.7. While this example shows a very high correlation, the slope of the line (0.7657) in Figure 4.7 is lower, indicating a somewhat lower prediction of velocity relative to the measured velocity.

The full set of correlation coefficients for the two velocity components are listed in Table 4.3. On average the correlation between the measured versus model-cell predictions for the velocity component that is closest to the channel-axis alignment (E-W or N-S at the cross-sections in Fig. 4.1), show consistently high values of the correlation coefficient (r^2) in the range 0.70 to 0.98, leaving aside some of the measurements from the channel sides where the local depth changes quickly, affecting the relativity between the Braystoke current-meter "point" measurement and an averaged current over a wider 30 m \times 30 m model cell. For the central channel sites, the correlation coefficient is above 0.86, which indicates a good calibration on

¹⁰ Ranges from 0 to 1, where 1 means there is a perfect match between the two variables

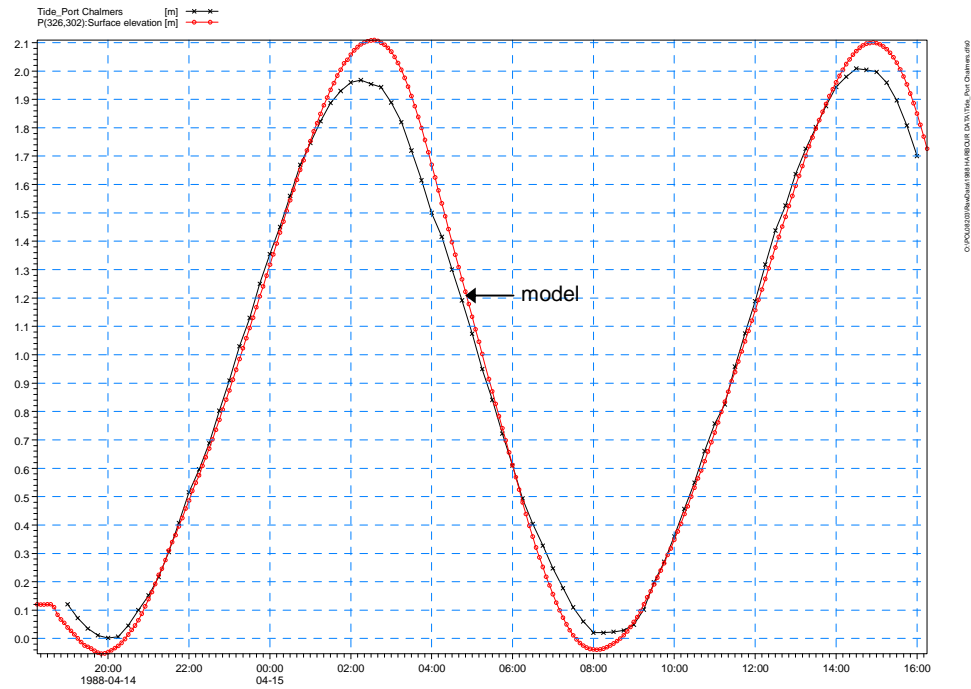


Figure 4.3: Modelled and recorded tide at Port Chalmers for 14 and 15 April 1988.

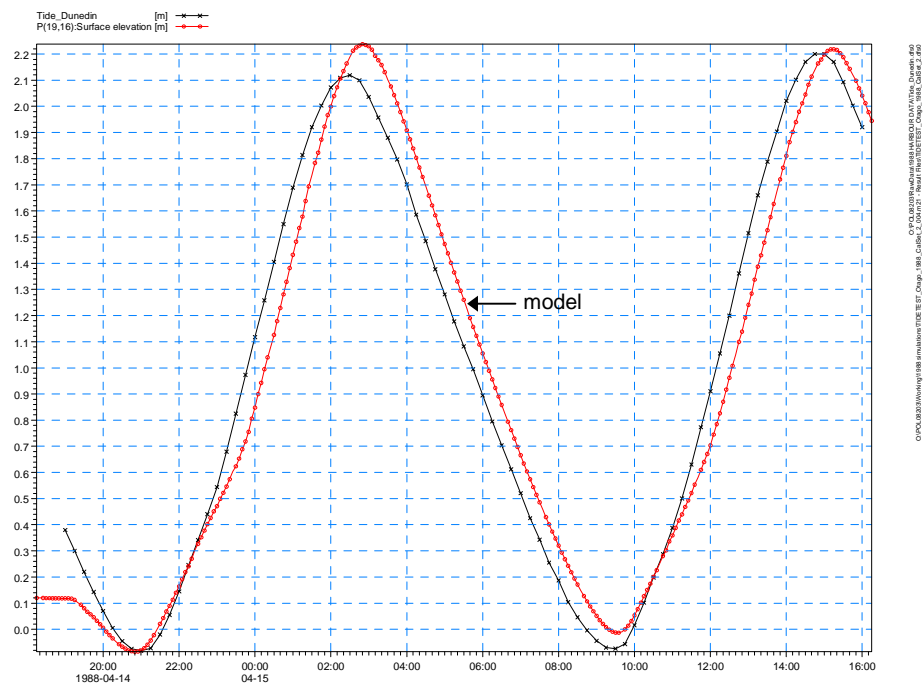


Figure 4.4: Modelled and recorded tide at Dunedin for 14 and 15 April 1988.

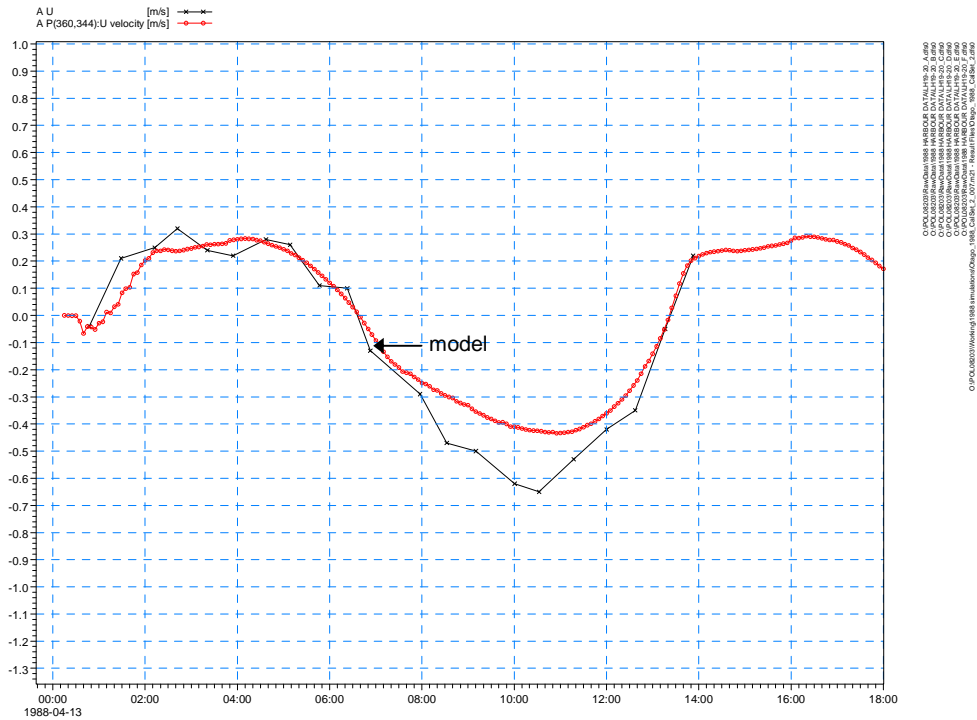


Figure 4.5: Modelled and recorded u -velocity at LH19-20 Site A for 13 April 1988. Note: measured currents were only recorded at 0.5 to 1 hour intervals.

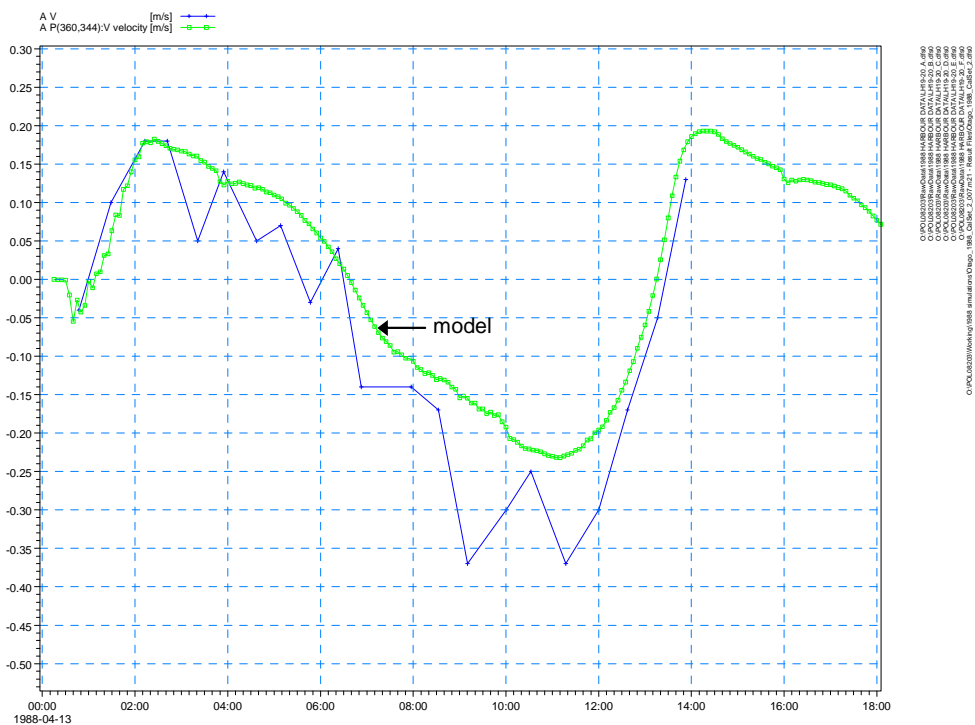


Figure 4.6: Modelled and recorded v -velocity at LH19-20 Site A for 13 April 1988. Note: measured currents were only recorded at 0.5 to 1 hour intervals.

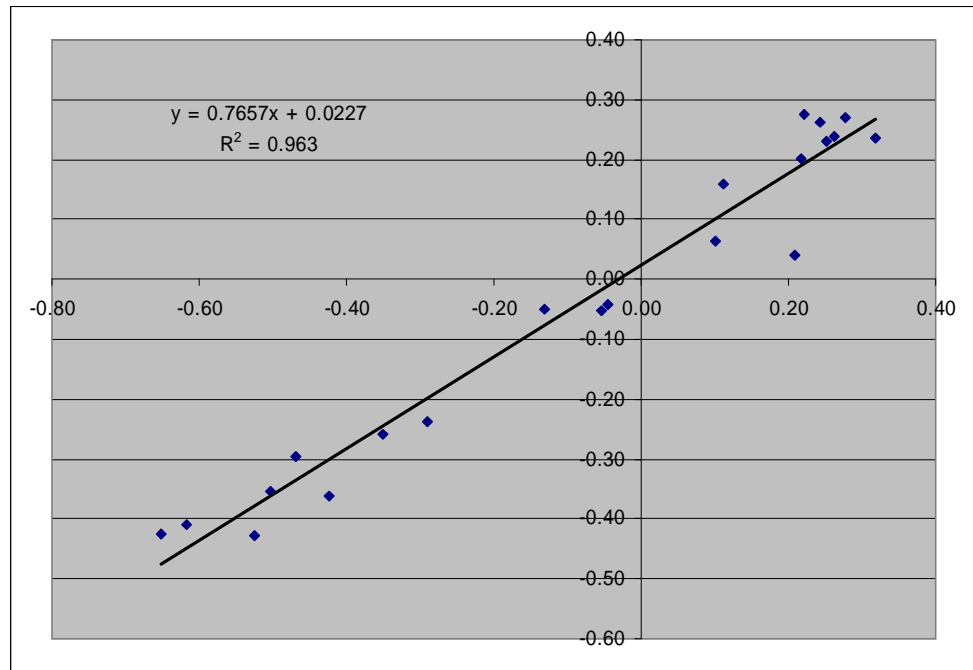


Figure 4.7: Regression analysis between modelled and recorded u -velocity at LH19-20 Site A for 13 April 1988.

Table 4.3: Correlation coefficient r^2 values between predicted and recorded u and v velocity components.

Braystoke site & model cell site	r^2 value for u velocity component	r^2 value for v velocity component
LH24-27_Site A _	0.66	0.94
LH24-27_Site B _	0.67	0.64
LH24-27_Site C _	0.38	0.96
LH24-27_Site D _	0.62	0.97
LH24-27_Site E _	0.58	0.97
LH24-27_Site F _	0.12	0.63
LH29-30_Site A _	0.06	0.79
LH29-30_Site B _	0.37	0.98
LH29-30_Site C _	0.68	0.97
LH29-30_Site D _	0.88	0.71
LH19-20_Site A _	0.96	0.90
LH19-20_Site B _	0.97	0.85
LH19-20_Site C _	0.97	0.71
LH19-20_Site D _	0.98	0.79
LH19-20_Site E _	0.92	0.43
LH19-20_Site F _	0.33	0.51
HBEND_Site A _	0.01	0.65
HBEND_Site B _	0.64	0.94
HBEND_Site C _	0.70	0.95
HBEND_Site D _	0.84	0.91
HBEND_Site E _	0.76	0.94
HBEND_Site F _	0.21	0.76
UH3-4_Site A _	0.84	0.32
UH3-4_Site B _	0.86	0.75
UH3-4_Site C _	0.89	0.42
UH3-4_Site D _	0.90	0.70
QISLAND_Site A _	0.92	0.65
QISLAND_Site B _	0.91	0.56
QISLAND_Site C _	0.59	0.52

4.3 Harbour model validation

Having achieved a reasonable calibration of the Harbour hydrodynamic model by tuning the resistance parameter to best match field measurements, the next stage in the modelling process is to validate the model against an independent set of measurements by keeping the model parameters fixed. The validation was performed using a set of InterOcean S4 current meter deployments carried out in 2008 (Bowman, 2008a, b) in the shallower, eastern parts of the Harbour. This provides measurements from areas of the Harbour that are distinctly different in their hydraulic regime than the main shipping channel, where the previous 1988 velocity measurements were recorded.

4.3.1 Model verification with S4 measurements

An S4 current meter was deployed consecutively at three Harbour locations, one in Portobello Bay and two within the Eastern Channel (Fig. 1.2). Table 4.4 below details the S4 current meter deployment locations and sampling periods. The S4 was mounted at 0.5 m above the bed in each case. Full details regarding deployment and available in the two deployment reports by Department of Marine Science, Otago University (Bowman 2008a, b).

Table 4.4: S4 current meter sampling locations and periods (NZST).

S4 Location	WGS84	NZTM (m)	Sampling Start	Sampling End
Portobello Bay	170°38.738	1417101.26	15:00	16:50
	−45°49.093	4923453.98	21 Apr 2008	31 May 2008
Eastern Channel–Site 1 (Grassy Pt.)	170°35.971	1413615.02	11:00	16:10
	−45°50.822	4920145.76	6 Jun 2008	21 Jun 2008
Eastern Channel–Site 2 (Macandrew Bay)	170°35.742	1413383.85	16:30	16:00
	−45°51.99	4917974.06	21 Jun 2008	12 Jul 2008

Current speed and direction and depth were extracted from the supplied S4 data files, and directions converted from magnetic (24.6°E) to True North for the current direction and computation of u and v velocity components. The dataset was cropped at the start and end to remove data recorded whilst the instrument was being deployed and retrieved.

Port Otago Ltd provided tide heights and wind velocities (Dunedin, Port Chalmers and the Spit Jetty gauges) and winds from Taiaroa Head to provide input data to the verification model runs for the relevant 2008 field periods. Tides recorded at the Spit were applied at the seaward model boundary and winds recorded at Taiaroa Head applied across the model.

The MIKE-21 model simulations were performed for the duration of the S4 deployment period (21 April to 12 July 2008) and the output results from the appropriate model grid cell were compared with the S4 field measurements and the three tide-gauge records.

Following the model runs, the MIKE-21 results were further processed to extract the water depth from the relevant model cell to compare with the local depth measured by the S4 current meter. An adjustment was needed to convert model output of water surface elevation to a water depth to enable a comparison with the S4 depth measurements. A depth output from the model does not necessarily match the actual S4 depth, because the relevant model grid cell for the deployment site represents the average depth over an area $30\text{ m} \times 30\text{ m}$ rather than the depth at the actual deployment site. There are also likely to be uncertainties in the S4 depth measurements as no updated instrument calibration was undertaken on matching total pressure (what the S4 measures) to water depth. Consequently, the model cell outputs for surface elevation at the three S4 deployment sites were adjusted upward by 3.08 m, 2.02 m and 1.62 m respectively in chronological order of deployments. The comparisons of this adjusted depth with the measured local depth by the S4 current meter are shown in Figures 4.8, 4.9 and 4.10. The local phasing of the tides has been simulated well and on average the tidal ranges have been replicated, but with some over- and under-estimates of the low and high tides of up to 0.1–0.2 m at times.

Modelled tides were also compared with the actual tide heights recorded at Dunedin, Port Chalmers and the Spit Jetty during the S4 deployment in Portobello Bay as shown in Figures 4.11, 4.12 and 4.13 respectively. Leaving aside the Harbour model start-up transition, which is most evident in the modelled tides at the site furthest from the Entrance (Dunedin; Fig. 4.11), there is a good match of modelled and measured tides.

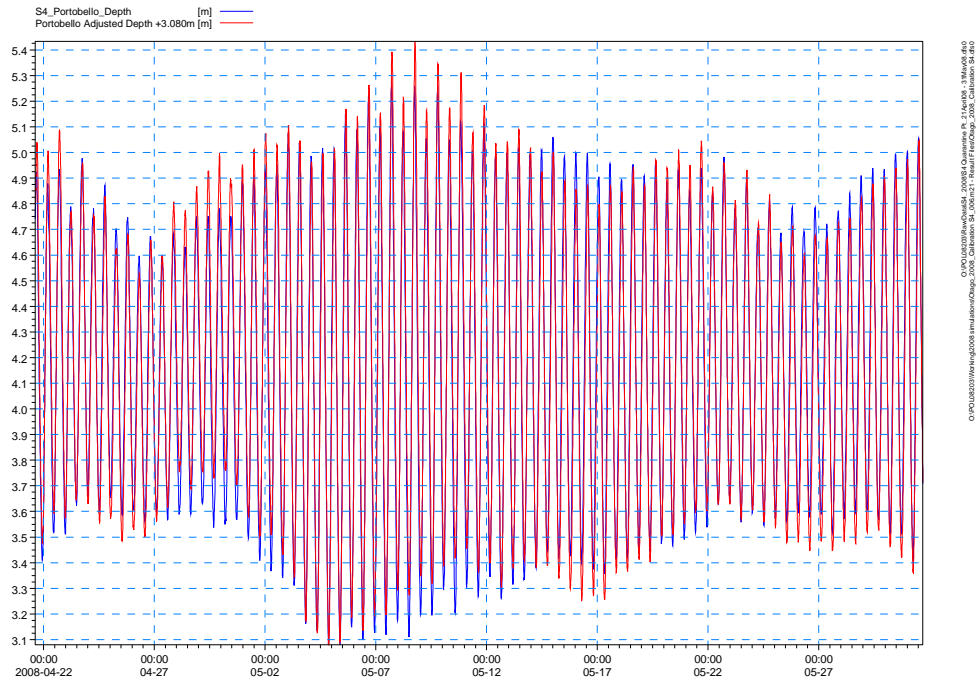


Figure 4.8: Comparison of recorded and predicted water depth at Portobello Bay S4 site (21 April to 31 May 2008).

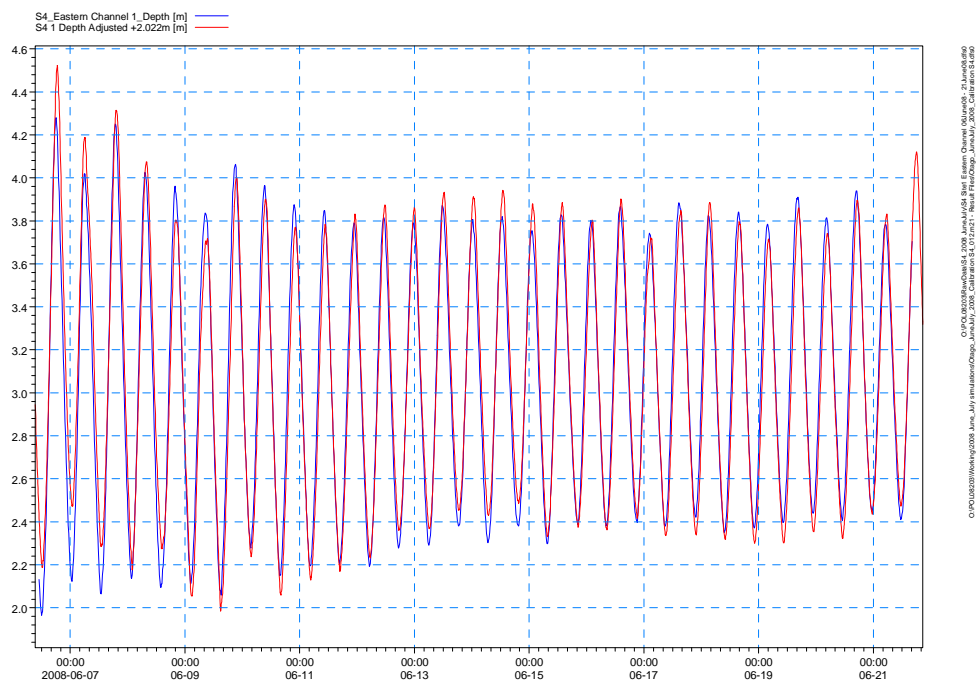


Figure 4.9: Comparison of recorded and predicted water depth at Eastern Channel S4 site 1 (North end) for 6–21 June 2008.

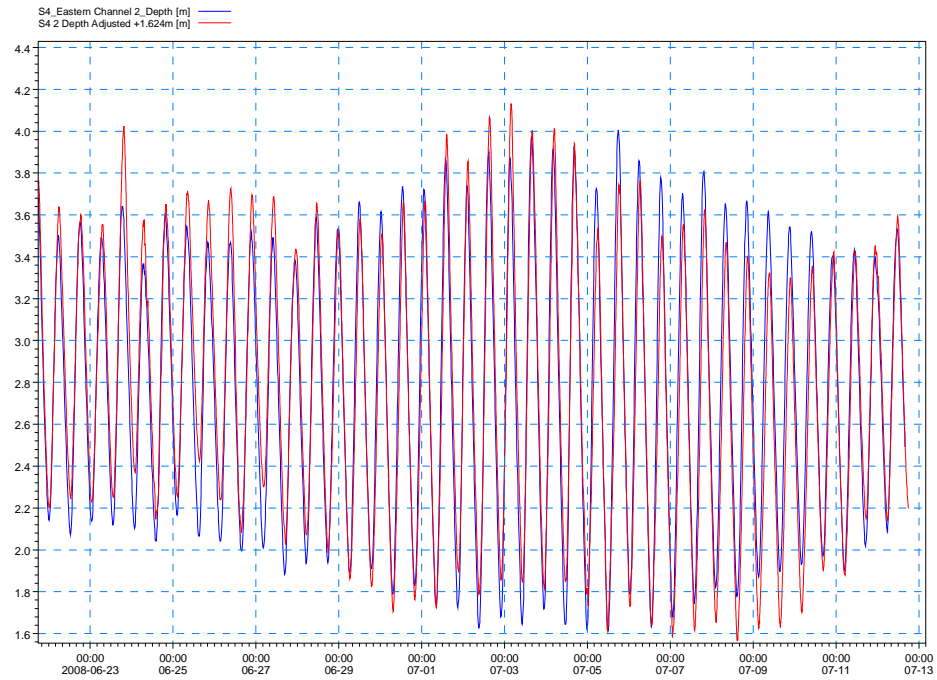


Figure 4.10: Comparison of recorded and predicted water depth at Eastern Channel S4 site 2 (South end) for 21 June to 12 July 2008.

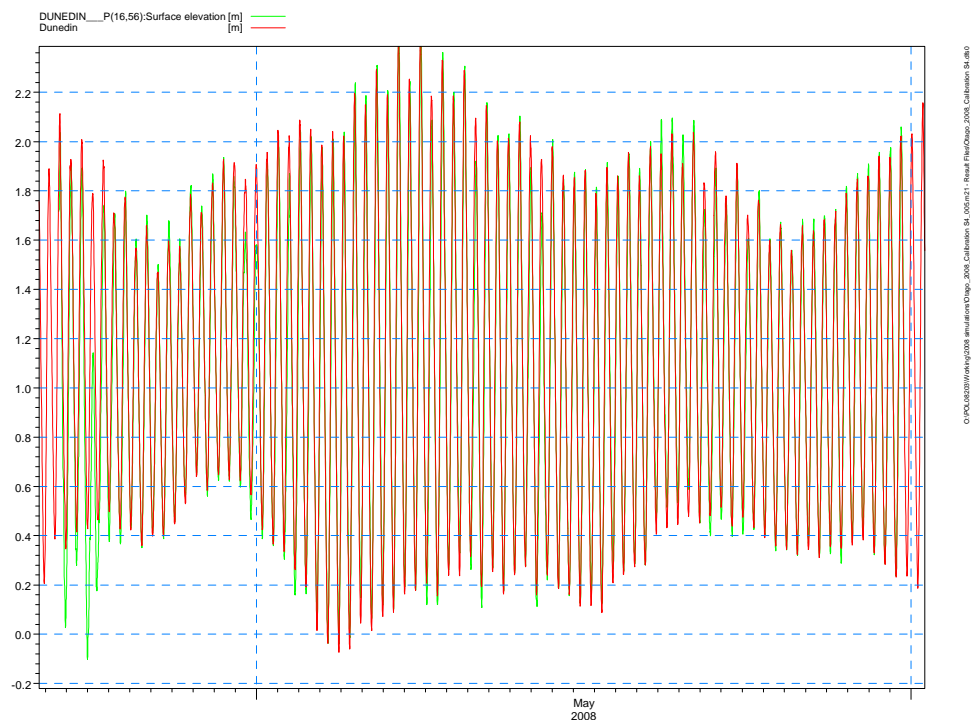


Figure 4.11: Comparison of recorded and predicted tides at Dunedin during Portobello S4 deployment (21 April to 1 June 2008).

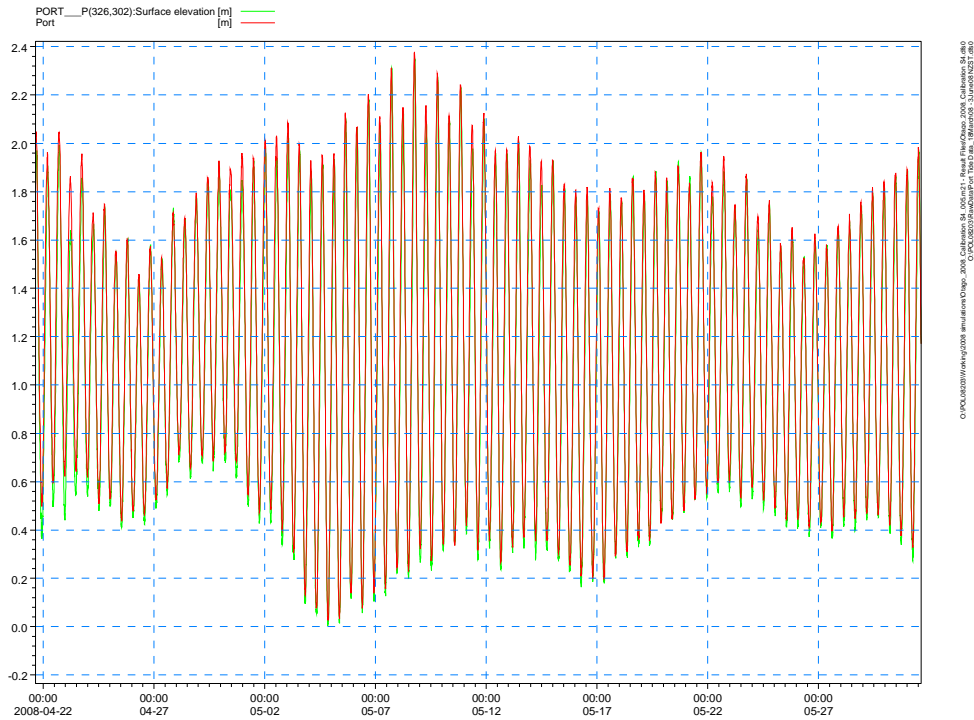


Figure 4.12: Comparison of recorded and predicted tides at Port Chalmers during Portobello Bay S4 deployment (21 April to 31 May 2008).

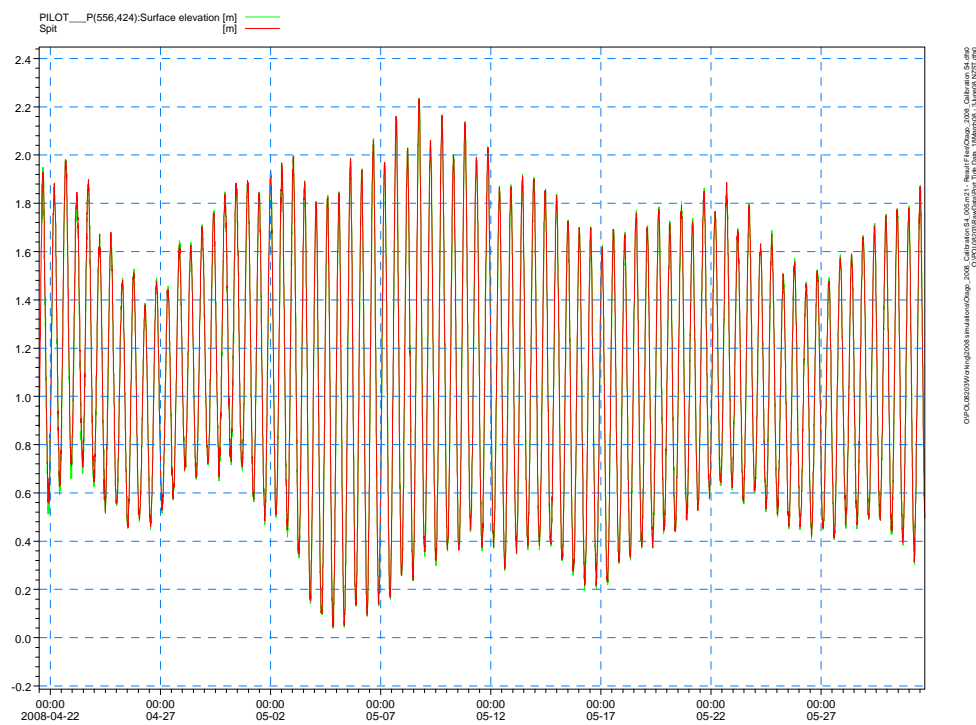


Figure 4.13: Comparison of recorded and predicted tides at Spit/Pilots Beach during Portobello Bay S4 deployment (21 April to 31 May 2008).

The u and v velocity components (E-W and N-S) that were modelled and recorded at the Portobello Bay S4 deployment site have been compared in Figure 4.14 to 4.15. The ebb-tide currents to the north-east dominate at this site with only weak currents recorded on the flood tide to the south-west. The match between the model predictions and the local current measurements is quite variable, especially with the model producing higher westerly (Fig. 4.14) and southerly (Fig. 4.15) current speeds to over-predict the weaker flood tide flow recorded by the S4 current meter. Regression analyses for both velocity components between the measured and modelled values are shown in Figures 4.16 and 4.17. There is a better match for the N-S velocity component (Fig. 4.17) than the E-W component (Fig. 4.16), with a correlation coefficient (r^2) of 0.64 between the modelled and measured E-W velocity components.

Overall, the bias shown in the measured data in Portobello Bay towards a dominant ebb-tide current to the north-east is also replicated in the modelled results. The scatter between the measured and modelled results will be partly due to the inevitable differences that arise when comparing a “point” velocity measurement with not only a depth-averaged model prediction, but also one that is spatially-averaged over a $30\text{ m} \times 30\text{ m}$ cell. These differences will be more pronounced in shallow areas of the Harbour compared with the closer match of currents that can be achieved in the stronger flows of the main shipping channel (Section 4.2).

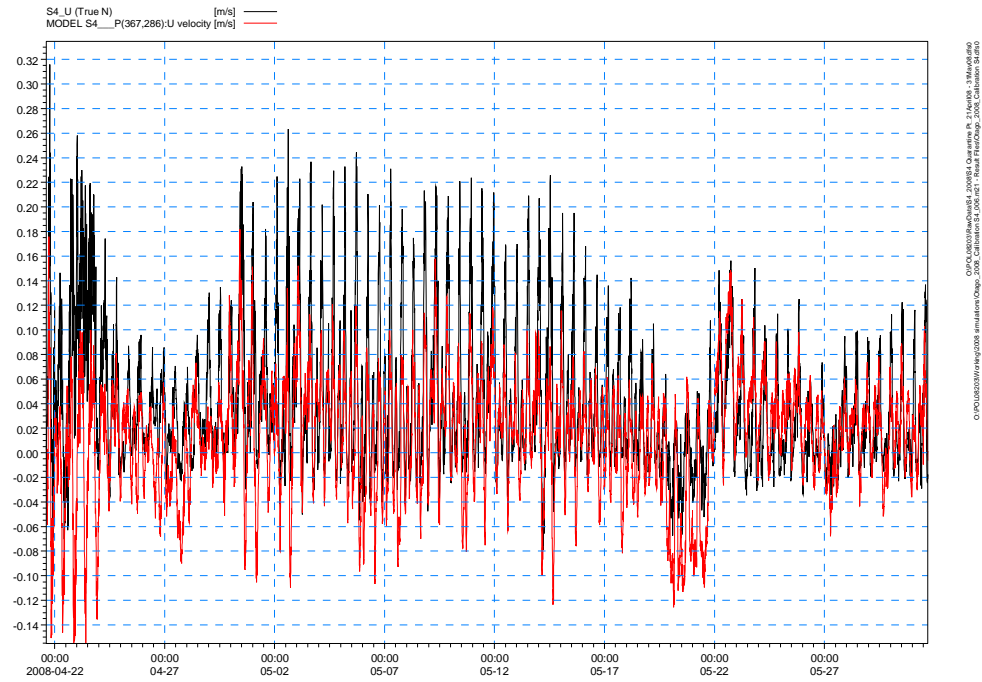


Figure 4.14: Comparison of E-W velocity component for measured (black) and model predictions (red) for Portobello Bay S4 site.

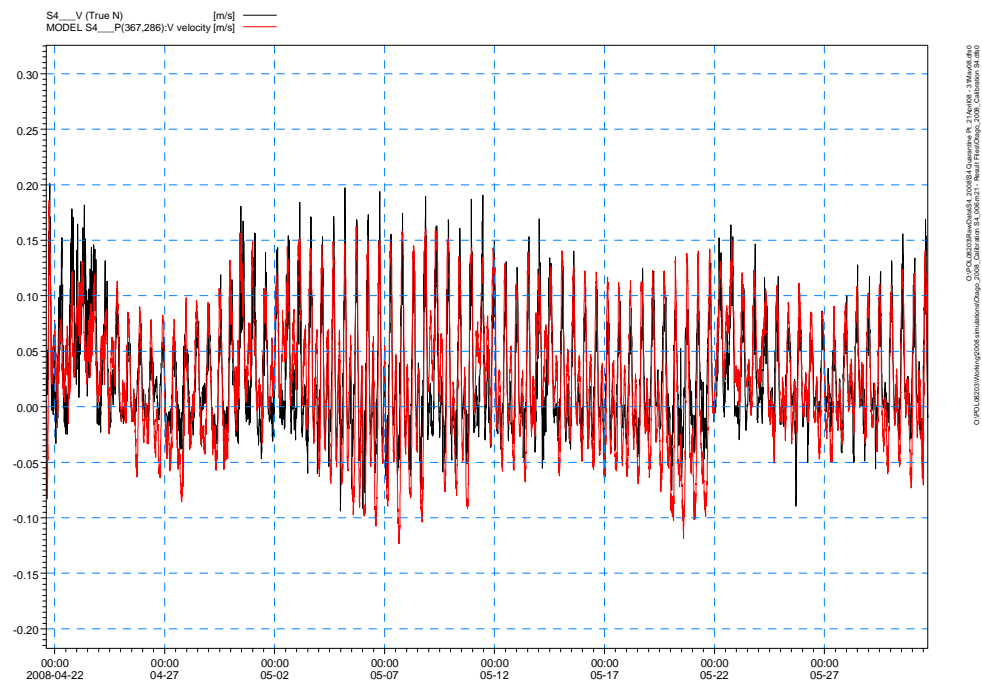


Figure 4.15: Comparison of N-S velocity component for measured (black) and model predictions (red) for Portobello Bay S4 site.

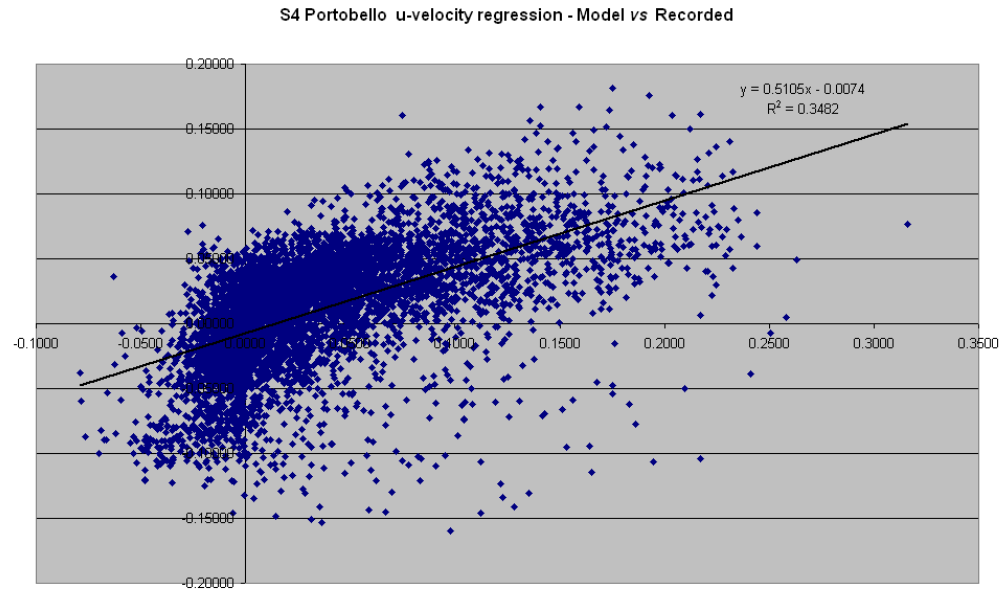


Figure 4.16: Regression analysis of recorded u (E-W) velocity component (x-axis) and model predictions (y-axis) for Portobello Bay S4 site.

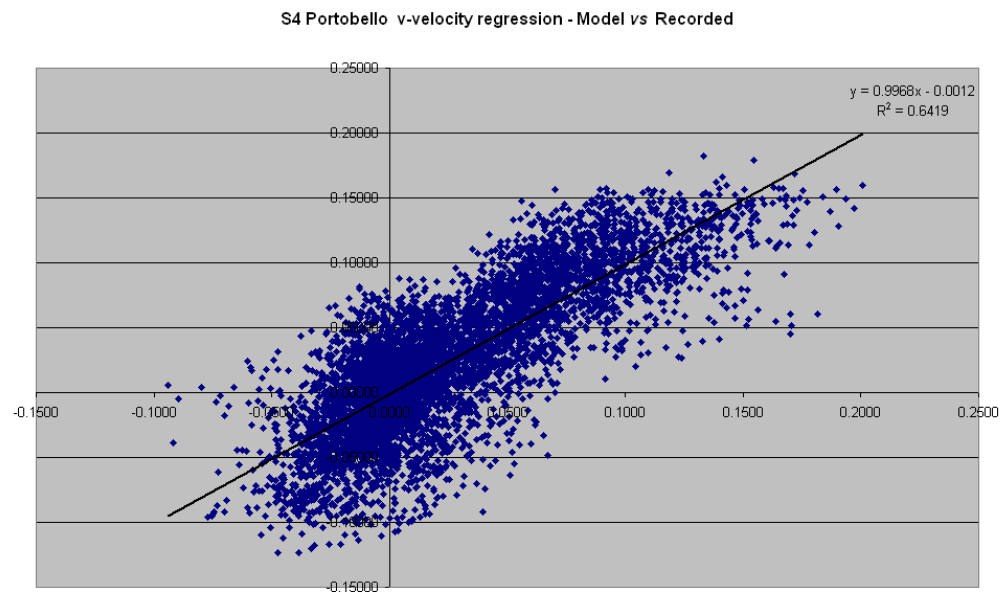


Figure 4.17: Regression analysis of recorded v (N-S) velocity component (x-axis) and model predictions (y-axis) for Portobello Bay S4 site.

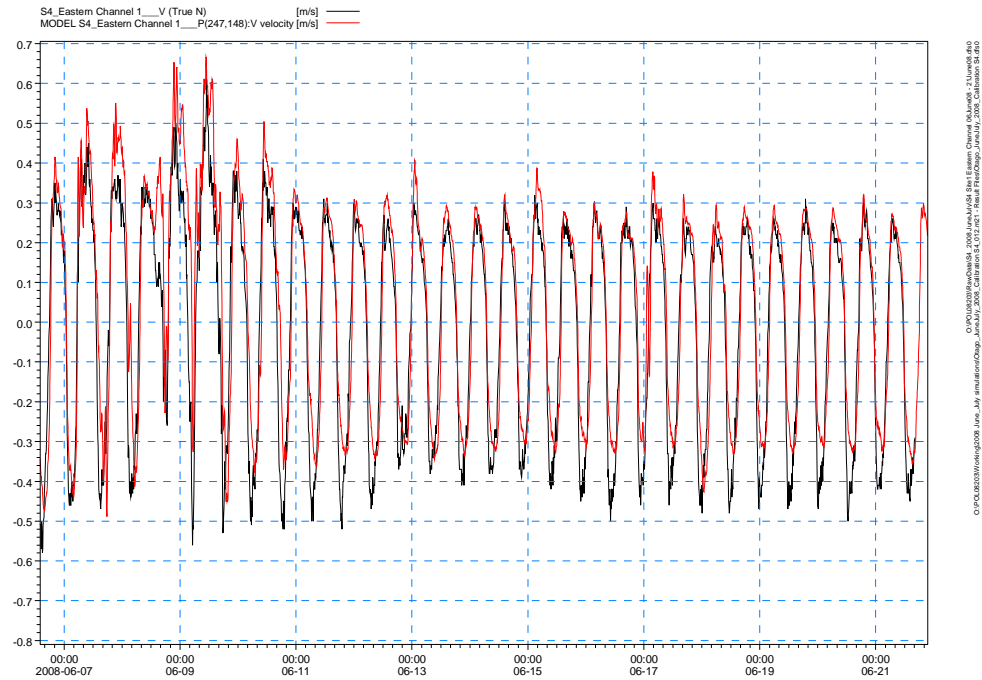


Figure 4.19: Comparison of the v (N-S) velocity component for the measured (black) and modelled predictions (red) for S4 site 1 in Eastern Channel to the south-west of Grassy Point.

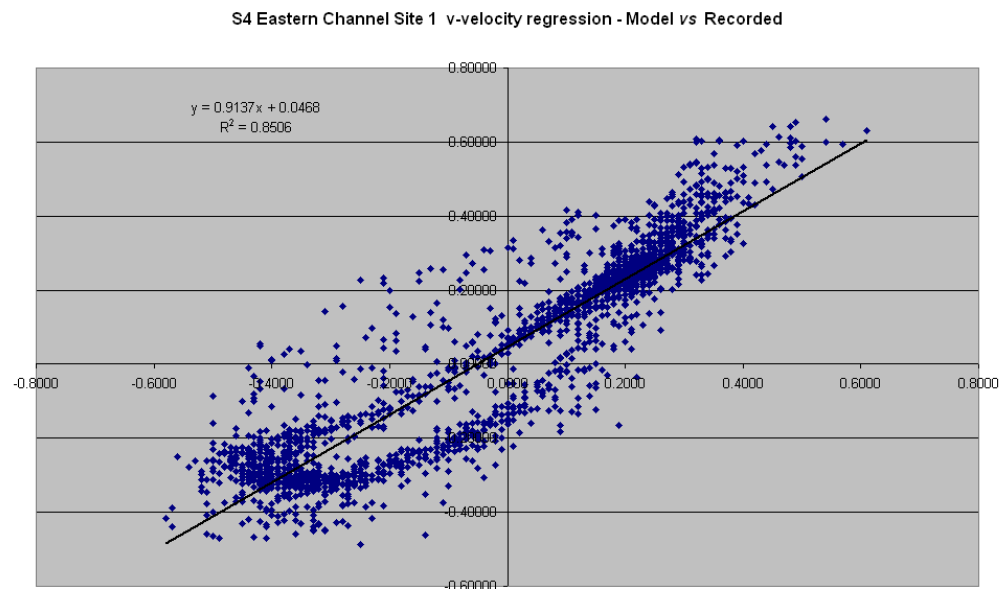


Figure 4.20: Regression analysis of recorded v (N-S) velocity component (x -axis) and model predictions (y -axis) for S4 site 1 in Eastern Channel (west of Grassy Point).

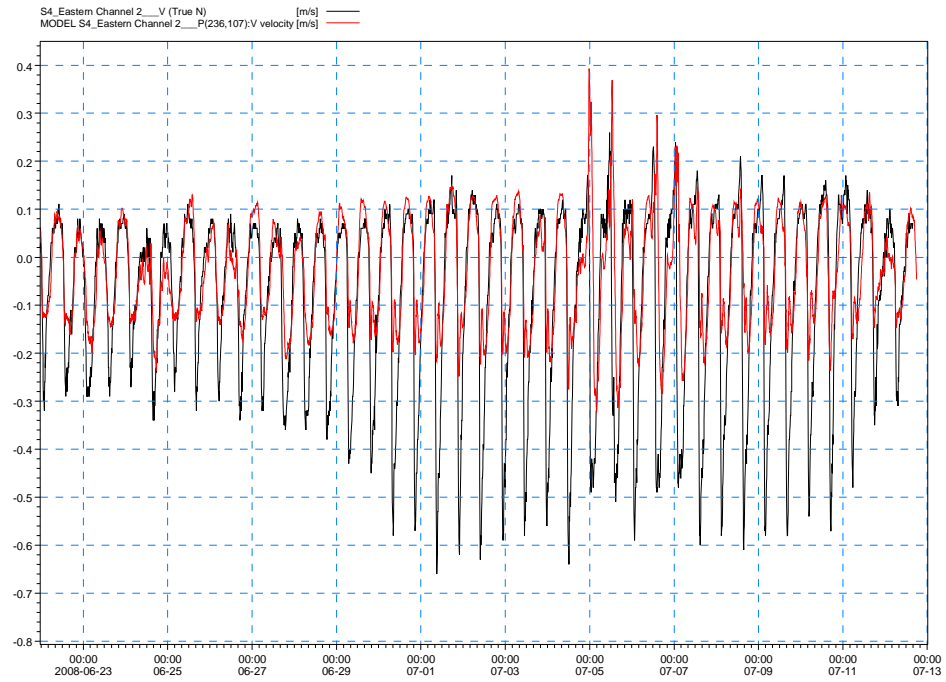


Figure 4.22: Comparison of v (N-S) velocity component for measured (black) and model predictions (red) for S4 site 2 in Eastern Channel off Macandrew Bay.

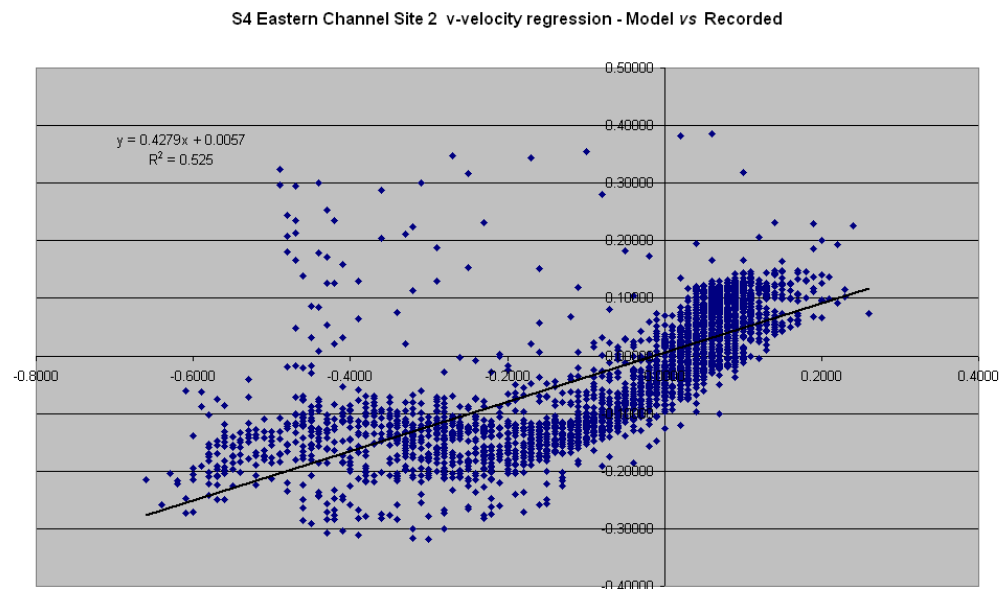


Figure 4.23: Regression analysis of recorded v (N-S) velocity component (x -axis) versus model prediction (y -axis) for S4 site 2 in Eastern Channel (Macandrew Bay).

4.3.2 Verification with boat-mounted ADCP surveys (1998–2000)

Boat-mounted ADCP current flow surveys recorded within the main shipping channel reach from Landfall Tower to Harington Bend in 1998 (Vennell & Old, 1999), and further up the Harbour in 1999–2000 (Vennell, 1999; Vennell & Old, 2000) were also available for comparison with Harbour hydrodynamic model output. This data is focused only within the main channel. Depth-averaged currents in the water column (either 8 or 10 m below the surface) from the ADCP surveys and modelled depth-averaged currents (entire water column) were considered for every hour of a tidal cycle, 6 hours before and 6 hours after the high tide at Port Chalmers.

Figures 4.24 to 4.27 show an overlay of velocity vectors from the boat-mounted ADCP surveys compared to depth-averaged currents from hydrodynamic model for the reach from the Mole to Harington Bend area and the reach from Acheron Head to Kilgours Point centred on the Port Chalmers area. Two sets of comparisons are presented for High Water + 3 hours and High Water – 3 hours relative to Port Chalmers when currents are approximately at their peak for the ebb and flood tides respectively. The comparison shows a good visual match between the modelled and measured boat-mounted ADCP current vectors—both in the magnitude and direction of the vectors and also the overall pattern of flows within the channels.

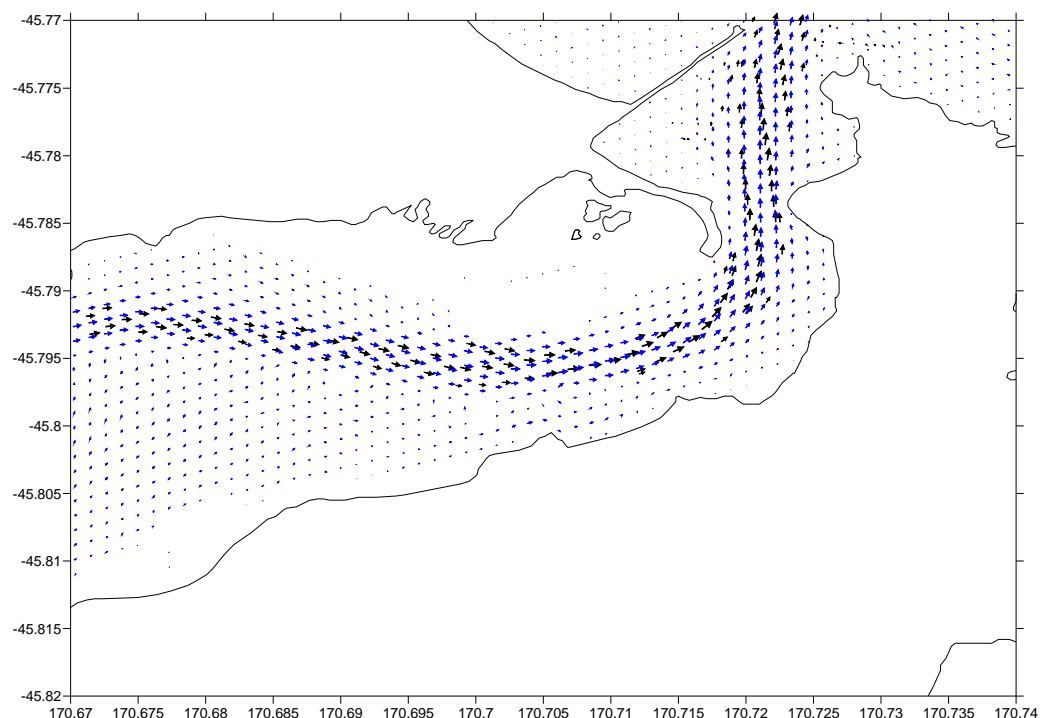


Figure 4.24: Comparison of 1998 boat-mounted ADCP current vectors (black) with the hydrodynamic model currents (blue) for the reach from The Mole–Harington Bend (peak ebb: High Water +3 hours at Port Chalmers).

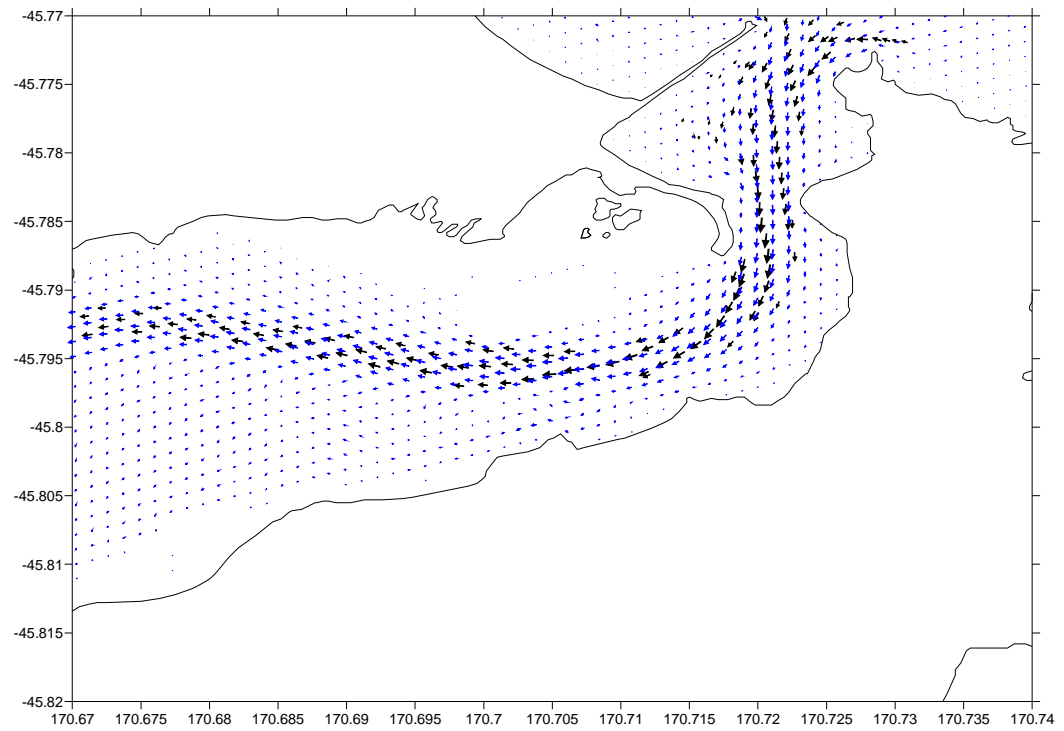


Figure 4.25: Comparison of 1998 boat-mounted ADCP current vectors (black) with the hydrodynamic model currents (blue) for the reach from The Mole–Harington Bend (peak flood: High Water –3 hours at Port Chalmers).

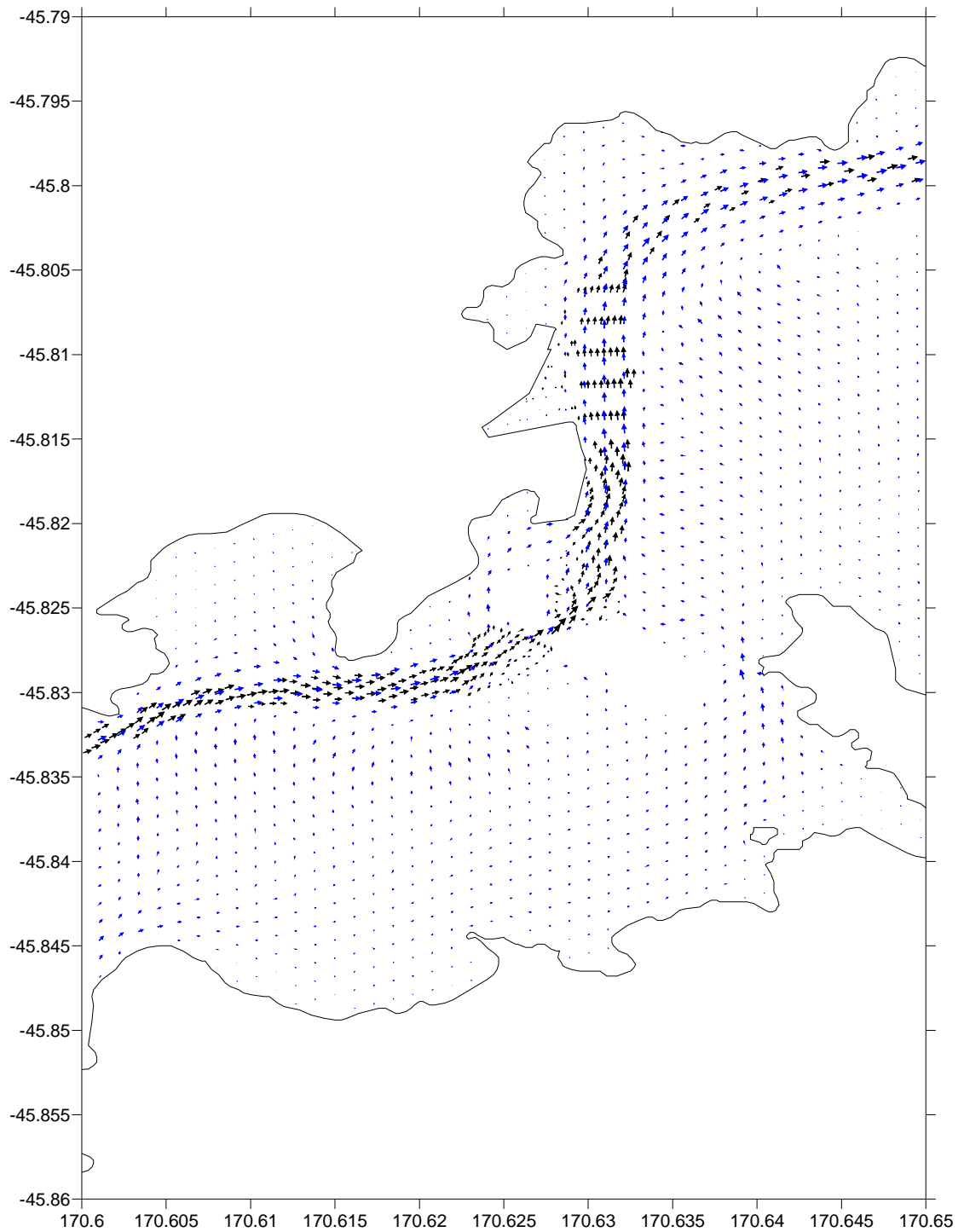


Figure 4.26: Comparison of 1999–2000 boat-mounted ADCP current vectors (black) with the hydrodynamic model currents (blue) for the reach from Acheron Head–Kilgours Point (peak ebb: High Water +3 hours at Port Chalmers). Note: outlines of Goat and Quarantine Islands not included for clarity.

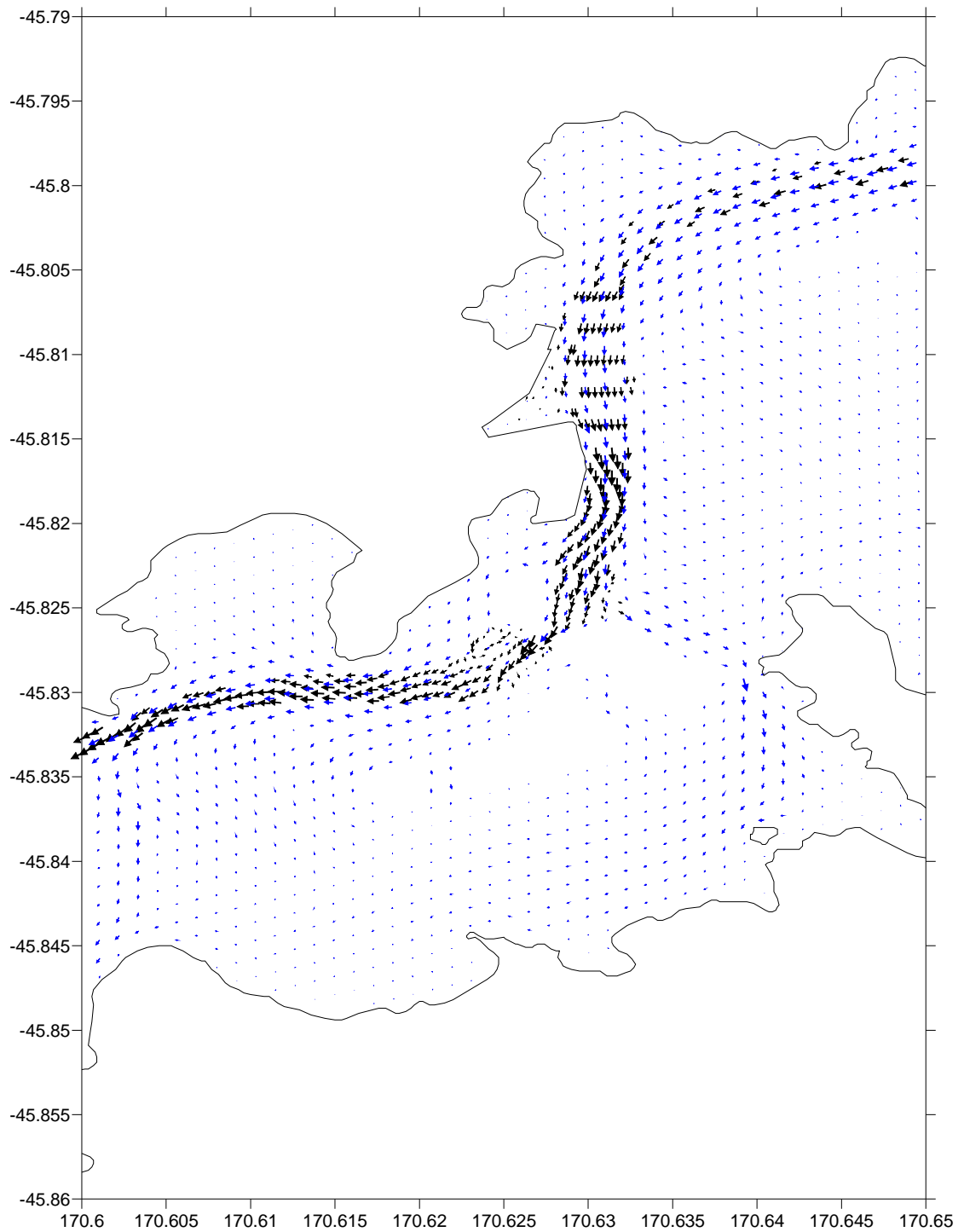


Figure 4.27: Comparison of 1999–2000 boat-mounted ADCP current vectors (black) with the hydrodynamic model currents (blue) for the reach from Acheron Head–Kilgours Point (peak flood: High Water –3 hours at Port Chalmers). Note: outlines of Goat and Quarantine Islands not included for clarity.

4.4 Overall assessment of the calibrated Harbour Model

A reasonable calibration of the Harbour hydrodynamic model was achieved using tides and currents from a previous field investigation carried out for the Otago Harbour Board in 1988 (Barnett, 1988). In this process, the model tuning parameters, principally the bed resistance coefficient, are altered to achieve the optimal match with the field data. The match with tide heights was satisfactory (with differences between measurements and the model predictions of up to 0.1 m). But the fit on tide heights is less critical in this case, as the relative differences in tide heights before and after dredging are more important to know than whether the absolute tide heights are accurately modelled. A reasonably good match was obtained between modelled and measured currents in the main channels, particularly in the central core of the channel flow. Normally, a good match on currents is harder to achieve than on tide heights. This good calibration leads to a dependable modelling platform to undertake the assessment of suspended-sediment plume transport, where the absolute values of the current velocity are important to simulate well as velocities strongly govern the transport processes that affect plume dispersion.

The Harbour model was also validated on two different sets of data: a) S4 current-meter measurements during the 2008 field programme from the eastern side of the Harbour; b) vessel-mounted ADCP survey currents measured by the University of Otago in the period 1998–2000. There was a reasonable fit to the overall pattern of flows and balance between of ebb and flood currents, particularly in the Eastern Channel (south-west of Grassy Point), but at the other two sites there were some differences between the model results and the field measurements, especially for the flood tide. These mismatches can mostly be explained by a situation comparing “apples with oranges”. Localised effects on currents, including wind or rapid changes in seabed bathymetry, are picked by a current meter at a “point”, but the current velocities in the model are depth-averaged and spatially averaged over a 30 m × 30 m model cell. Validation of the model using the boat-mounted ADCP currents from the main channel shows a good visual match between the modelled and measured boat-mounted ADCP current vectors - both in the magnitude and direction of the vectors and also the overall pattern of flows within the channels.

Overall, the Harbour hydrodynamic model is performing well in predicting the tide height and more-importantly, tidal currents. Therefore simulating relative hydrodynamic changes before and after dredging and providing supporting current flow fields for plume dispersion modelling can be achieved with reasonable confidence.

5. Potential changes in hydrodynamics of Otago Harbour

This section provides the relative comparison of the hydrodynamic characteristics of the Harbour between the existing channel bathymetry (with the main shipping channel currently dredged to a minimum depth of 13 m below Chart Datum with localised holes that are naturally deeper) and the dredged configuration of the final channel design.

5.1 Simulation for assessing hydrodynamic changes

A simulation of the calibrated MIKE-21 Harbour model was carried out for a period of 35 days (selected to be 1 January to 5 February 2007) with no winds, for both the existing bathymetry and a bathymetry with the 15-m deep dredged channel configuration inserted. From the results of both model runs, tidal constituents were calculated at every sub-tidal cell within the Harbour model grid¹¹ to provide comparable sets of tidal parameters before and after dredging. Time series of the differences in tide heights and currents before and after dredging were also generated for specific locations within the Harbour

5.2 Hydrodynamic changes to tidal ranges and currents

The focus in the comparison between the existing and proposed channels was on the changes in the average semi-diurnal (twice-daily) tide, which is represented by the lunar tide constituent M_2 . A tidal constituent analysis extracts the various lunar and solar tidal constituents that make up the observed or modelled tide at any location (and are used in predicting tide tables), but the overall observed tide is dominated by the lunar M_2 constituent (12.42 hour cycles). By taking the differences before and after dredging between the parameters that define the M_2 tide constituent, we can separate out any apparent changes, that occur due to the changes in the phasing or timing of high/low tides or peak flow and slack tides, from the absolute changes in tide range or peak velocities, as discussed previously in Section 2.1.

¹¹ The tidal analysis for intertidal cells which flood and dry during the 35-day run were excluded as a tidal constituent analysis is not meaningful for cells that partially dry. The plots however still show some isolated cells which almost dried out at low tide and should be ignored.

Plots were produced to show:

- tide height differences between the existing M_2 tide height amplitude (half-range) and high-tide phase and the corresponding set of results for the 15-m channel configuration;
- tidal current differences between the existing M_2 tidal-current ellipse parameters—the major and minor velocity amplitudes, the phase of the peak current, and the inclination of the peak current—and the corresponding set of results for the 15-m channel configuration.

5.2.1 Tide-height differences

Figure 5.1 shows the differences in M_2 tide amplitude (or half-range) between the existing channel and 15-m dredged channel configuration. Note: isolated high cells (with changes >0.005 m) are artefacts which should be ignored as they arise from the tidal analysis of shallow intertidal cells in the model.

The differences in Figure 5.1 are positive, (i.e., greater than zero), showing that the deepening of the channel would lead to a slight increase in tidal amplitude within the Harbour. This is expected, as a deeper channel means the tide wave would travel with less damping from seabed friction, as discussed in Section 2.1. In the Harbour Entrance, the increase in tide amplitude would be negligible (0.001–0.002 m) and only 0.002–0.003 m higher in amplitude between Harington Bend and Tayler Point (blue zone in Fig. 5.1). Over most of the Harbour, the increase would be in the range 0.003–0.004 m, which in practical terms would be imperceptible. In the vicinity of Port Chalmers and on the eastern side of the Lower Harbour in the Harwood area, the amplitude would increase slightly more to between 0.004–0.005 m, but again changes of this magnitude are imperceptible.

For differences to the full tidal range for an average tide (between spring and neap), these amplitude values should be doubled. For example, over most of the Harbour, the increase in amplitude of 0.003–0.004 m converts to an increase in 0.006–0.008 m in the average tide range.

Overall, changes to the tide range due to the 15-m dredged channel would be very small at no more than 0.01 m or 0.6% of the average 1.6-m tide range.

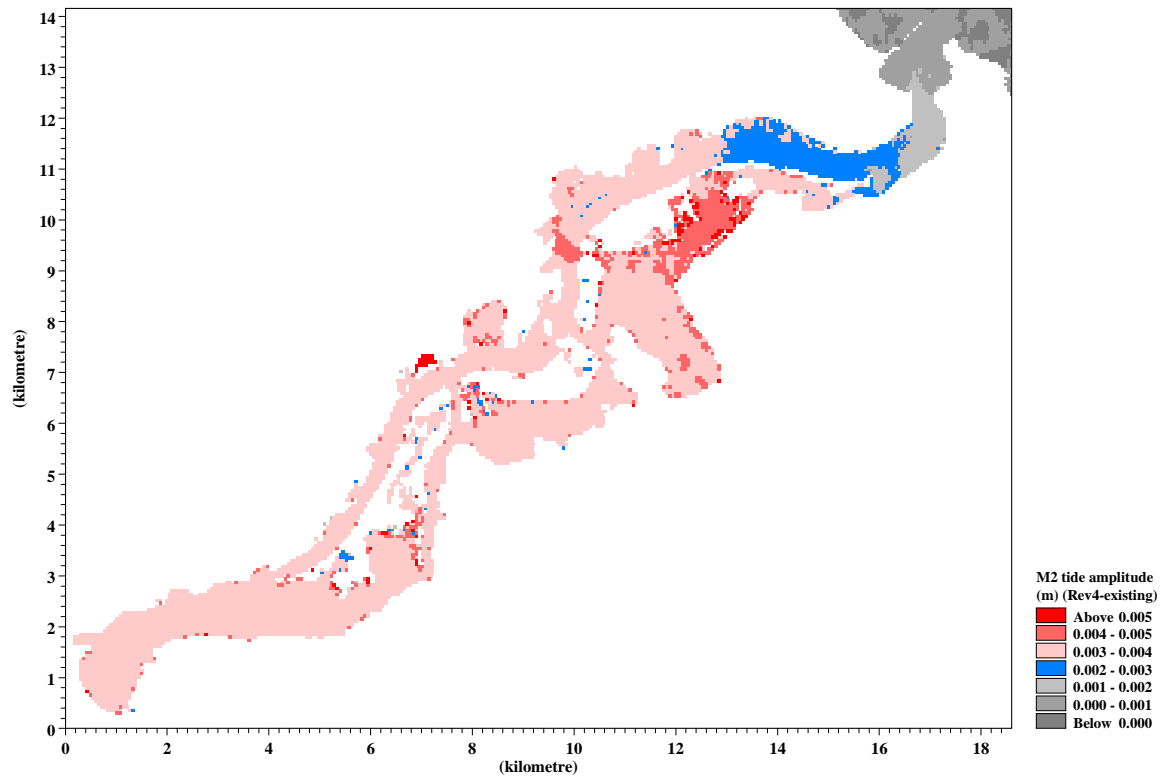


Figure 5.1: Differences in M_2 tide amplitude (half-range) between the existing bathymetry and 15 m dredged channel configuration. Positive values imply that the tidal amplitude is greater with the 15 m channel configuration than with the existing bathymetry.

Figure 5.2 shows the differences in the M_2 tidal phase (expressed as the change in timing of high or low water¹², in clock minutes) between the 15-m channel configuration and the existing bathymetry. Changes in tidal phase shows up as negative values, indicating that high and low water arrive slightly earlier due to the channel deepening (see Section 2.1 for an explanation). The largest shift in the timing of high and low water would occur from Deborah Bay and Harwood through to the Dunedin basin (see blue zone in Fig. 5.2), with an advance of between 3 and 4 minutes on the present high and low tide timing. Between the Harbour Entrance and Harington Bend the shift in the timing of the tide would be less than a 1 minute advance.

¹² The change in high-water time will generally be slightly more than the change in low-water time, owing to the greater influence of seabed friction at low tide. This effect will generally be very small, and is ignored by the present analysis of the average phase change for a mean tide.

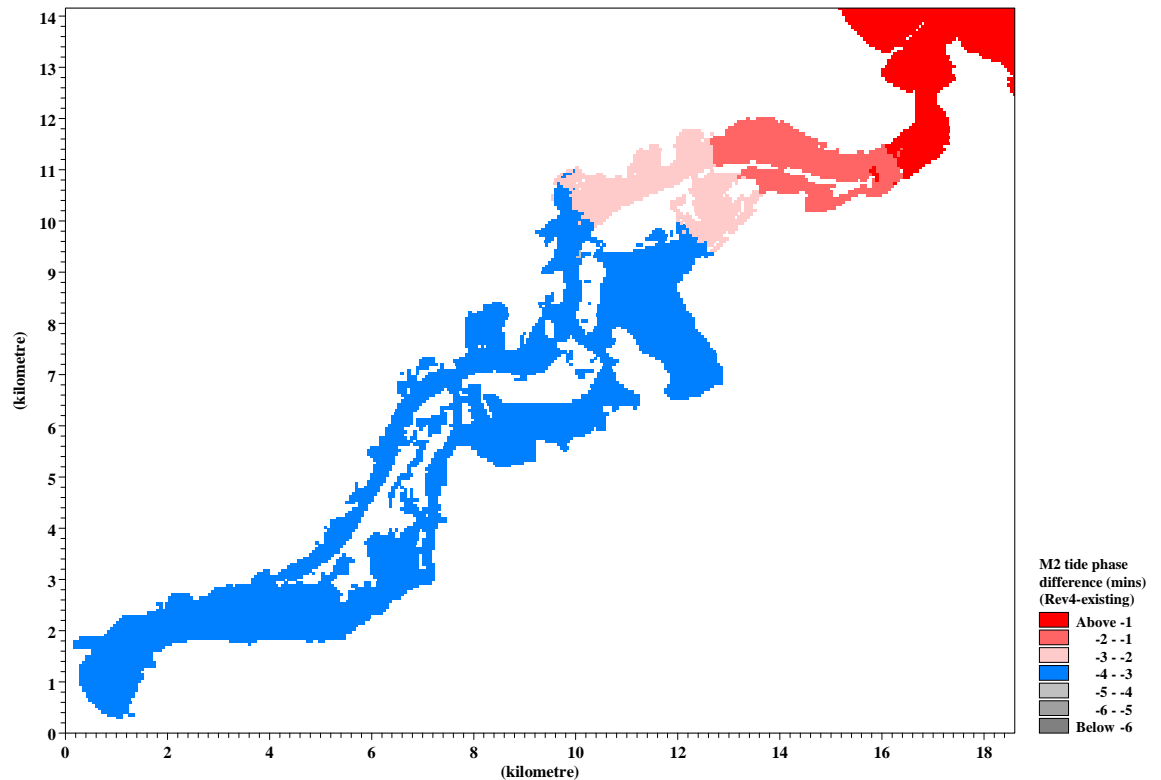


Figure 5.2: Differences in M₂ tidal phase between the existing bathymetry and 15-m channel configuration. Negative values indicate that high water occurs earlier under the 15-m channel configuration than with the existing bathymetry.

5.2.2 Tidal-current differences

Results from a tidal analysis of currents are more complex to represent than tide heights, as the analysis involves current vectors that vary in speed and direction.

Tidal currents are normally represented with an ellipse that traces out the tip of the current vector as it changes through a tidal cycle (Figure 5.3). The peak current (U), averaged over the flood and ebb tide, defines the major semi-axis of the tidal ellipse, while the minor semi-axis (u) represents the average of the minimum current speeds at the tide reversals around high and low tide periods. In confined channels, such as the main shipping channel, tidal current ellipses are usually very elongated with a small minor semi-axis (u), sometimes approaching a rectilinear to and fro track for flood and ebb currents, with minimum currents of near zero around a brief changeover at slack tide.

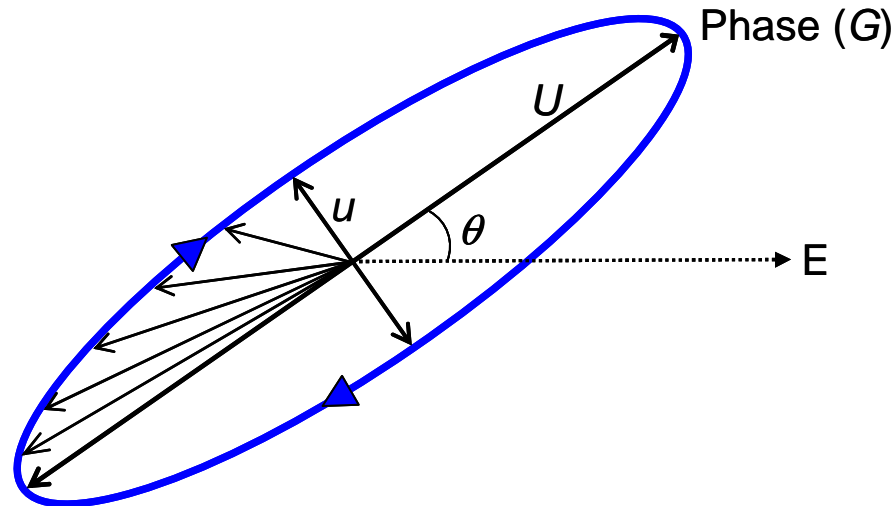


Figure 5.3: Ellipse representation for tidal current constituents, where the ellipse traces out the tips of the tidal current vector heads during a tidal cycle (e.g., for clarity diagram only shows a sequence of current vectors in north-west quadrant, moving clockwise in time for this case). U and u are the peak and minimum current speeds along the major and minor semi-axes of the ellipse, respectively. θ is the inclination angle for the peak current speed (U), measured in degrees ($^{\circ}$) counter-clockwise from East, and G is the phase ($^{\circ}$ through a tidal cycle) of the north-going peak current which relates to the timing of the peak current.

Figures 5.4a & b show the likely changes in magnitude of the major (peak) and minor (minimum) M_2 current speeds of the tidal current ellipse (Fig. 5.3) in each model cell.

Overall, changes of any more than ± 0.01 m/s (± 0.02 knot) to peak current speeds (averaging ebb and flood-tide peaks on a mean tide) would be limited to the Lower Harbour (i.e., non-blue areas of Fig. 5.4a).

Firstly, considering the dredged shipping channel, the peak velocity will mostly decrease due to the larger depth available for conveying the tidal flow. The largest decrease in the average major (peak) current would be a localised reduction of up to 0.1 m/s in the channel off Careys Bay (immediately to the north of Port Chalmers) arising from more of the flow being channelled through the eastern extension of the Port Chalmers Turning Basin and approach (where the peak velocity would increase by 0.02–0.05 m/s). Minor increases of up to 0.02–0.05 m/s in peak speeds would occur on the inside (northern side) of Harington Bend, where the existing shallow flanks will be dredged, thereby increasing the depth of channel flow through this area. No noticeable changes in peak tidal currents would occur in the narrow Entrance channel around Harington Point (shaded blue in Fig. 5.4a).

Secondly, away from the main shipping channel, there would only be a few localised areas where small changes in peak velocities could occur: a) small increases of 0.01–0.02 m/s (0.02–0.04 knot) in the subsidiary channel north of Quarantine Island and off the tip of Portobello Peninsula; b) a small decrease of 0.01 to 0.02 m/s (0.02–0.04 knot) in peak velocities on the eastern side of the Lower Harbour between Harwood and Ohinetu Point. These peak-velocity differences after dredging of no more than 0.02 m/s on a mean tide would be indistinguishable from the natural variability experienced in these areas (including wind effects) and would barely be detectable by conventional current meters (which are usually only accurate to between 0.01 to 0.02 m/s).

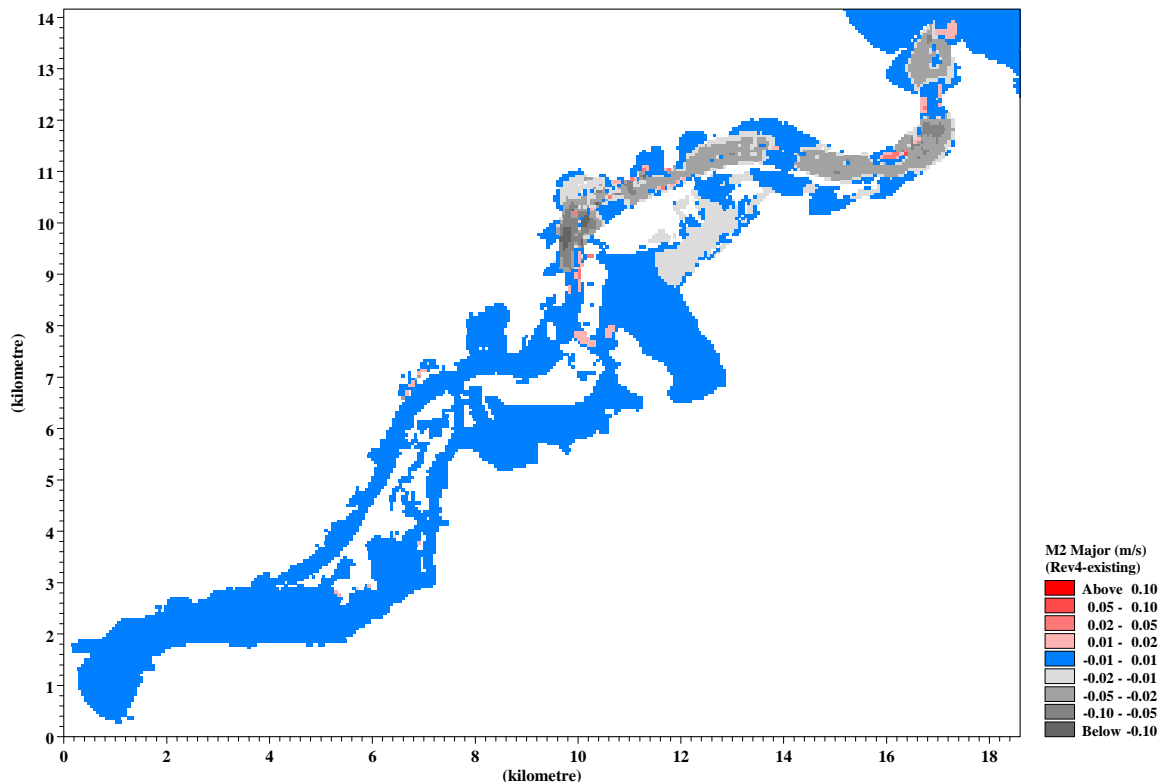


Figure 5.4a: Differences in M_2 major (peak) currents (m/s) between the existing bathymetry and 15-m channel configuration. Positive values indicate that tidal currents would be stronger after dredging and negative values indicate tidal currents would be slower. Blue areas show small changes between –0.01 and +0.01 m/s.

For minimum or lateral current speeds, there would be no noticeable change over much of the Harbour (Fig. 5.4b). The only exceptions would be the subsidiary channel, opposite Port Chalmers, through to Portobello Bay, where the shallow eastern flank of the existing channel and Turning Basin is to be dredged. Here the average minimum current speed (around low and high tide) would increase by small amount by just over 0.01 m/s (0.02 knot), with adjacent areas showing smaller increases of

0.002–0.01 m/s in the minimum current speed. There would be a similar, but localised, shift in the lateral or minimum tidal currents between Pulling Point and Acheron Head where a slight straightening of the channel is planned.

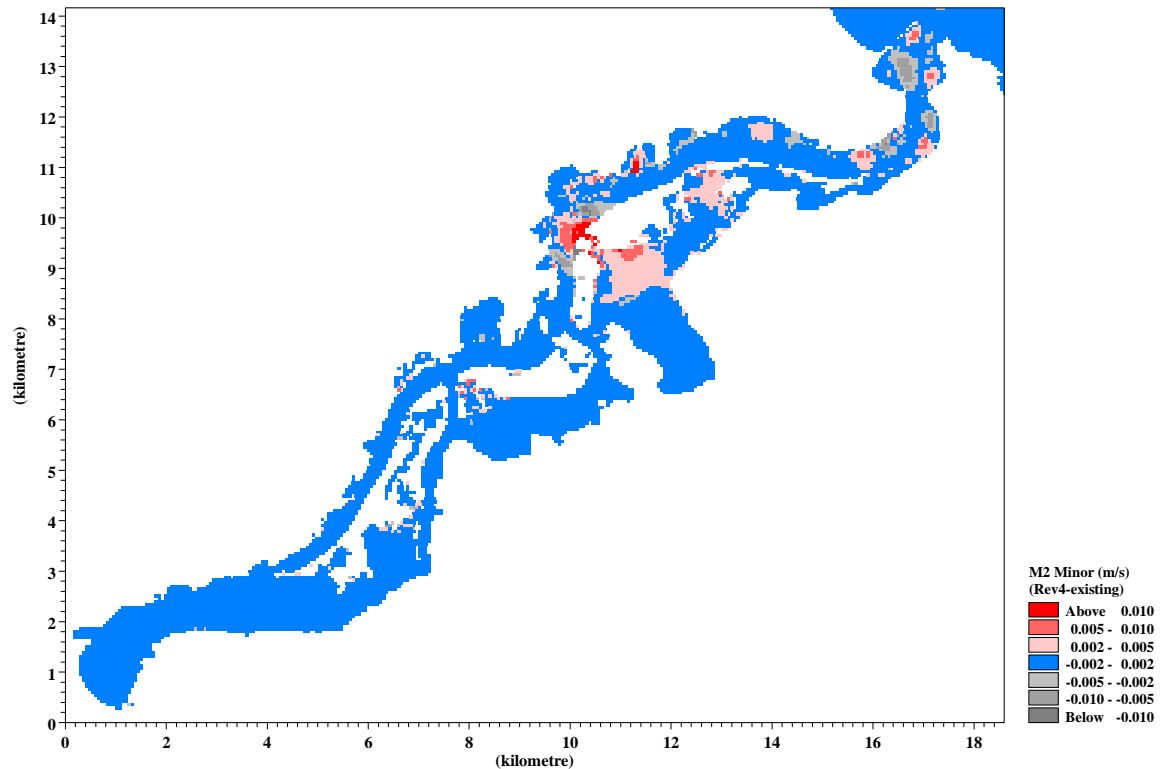


Figure 5.4b: Differences in M_2 minor (minimum or lateral) currents between the existing bathymetry and 15-m channel configuration. Positive values indicate tidal currents would be stronger after dredging and negative values indicate tidal currents would be slower. Blue areas show small changes between -0.002 and $+0.002$ m/s.

Figure 5.5 shows the difference in phasing of the M_2 peak tidal current before and after dredging the 15 m channel option. While discrimination at 1 minute time intervals is provided in the plot, patchiness in the plotted results arises partly from interpolating the model output of velocities (which are only at 10-minute intervals). Therefore the focus needs to be on the overall patterns of change rather than clumps of a few individual cells. Within most of the Harbour, the peak tidal current would occur between 2 and 4 minutes earlier (red colours in Fig. 5.5) with the deepened channel compared to the existing bathymetry. This matches closely with the 1–4 minute advance predicted for the high and low tides (Fig. 5.2). In the Lower Harbour, the advance of the peak current shows a more complex pattern than for the high and low tide phases. In this regard, the timing advance on the peak velocity would be slightly greater than the corresponding change in timing advance of high water, especially in Deborah Bay, Portobello Peninsula and the Harwood area, where the peak current

would be advanced by up to 7 to 9 minutes from the existing situation (and relative to an advance of only 3 to 4 minutes for high tides).

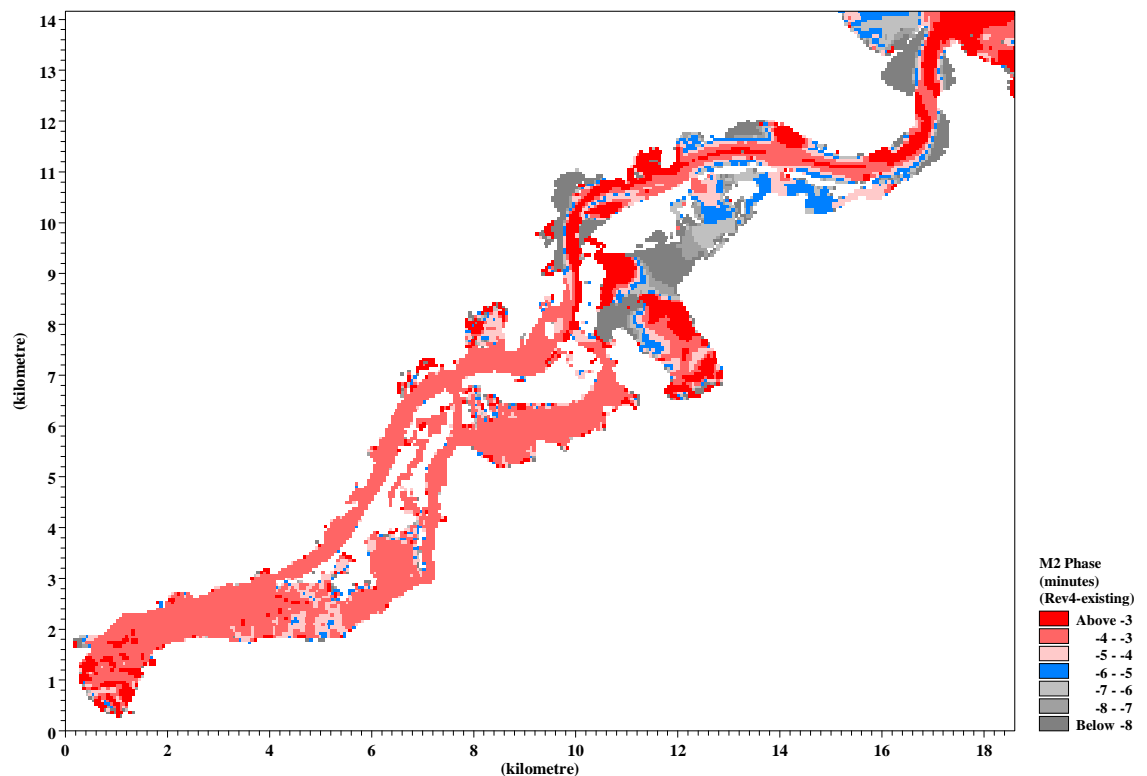


Figure 5.5: Differences in M_2 peak tidal current phases (expressed in minutes of time) between the existing bathymetry and 15-m channel configuration. Negative values indicate that the timing of the peak M_2 tidal current after dredging is advanced compared to the existing bathymetry.

Figure 5.6 shows the differences in the average inclination (direction) of the M_2 tidal current due to the 15-m Harbour channel configuration. This value refers to the principal flow direction of the peak current. As would be expected the deepening of the channel has little effect on the orientation of the tidal current within the majority of the Harbour, lying in the range between -2° and 2° (blue areas in Fig. 5.6). The only change in inclination would be to very minor extents in outer Portobello Bay, and the connecting shallow subsidiary channel through the intertidal bank to the main shipping channel (see left photo in Fig. 3.5). This arises from dredging required to widen and deepen the transition to the Port Chalmers Turning Basin on the eastern side of the channel. The change in peak M_2 current inclination in this area would be up $\pm 7-8^\circ$ (see small areas of red and dark grey in Fig. 5.6), with red areas showing an anti-clockwise rotation of the peak tidal current after dredging and darker grey clockwise rotation. These rotations arise from changes in eddies. They form in northern Portobello Bay later on the flooding tide as a result of deepening and

shortening of the entrance to the subsidiary channel that leads through the intertidal flats between port channel markers 24 and 24a into northern Portobello Bay (Fig. 3.5). There are similar localised shifts in orientation of the tidal currents off Pulling Point where a slight straightening of the channel is planned and on the northern-side of Harington Bend. Most of the other isolated patches are in shallow, almost intertidal, areas where the tidal analysis creates occasional artefacts in the differencing (e.g., southern Portobello Bay and Sawyers Bay).

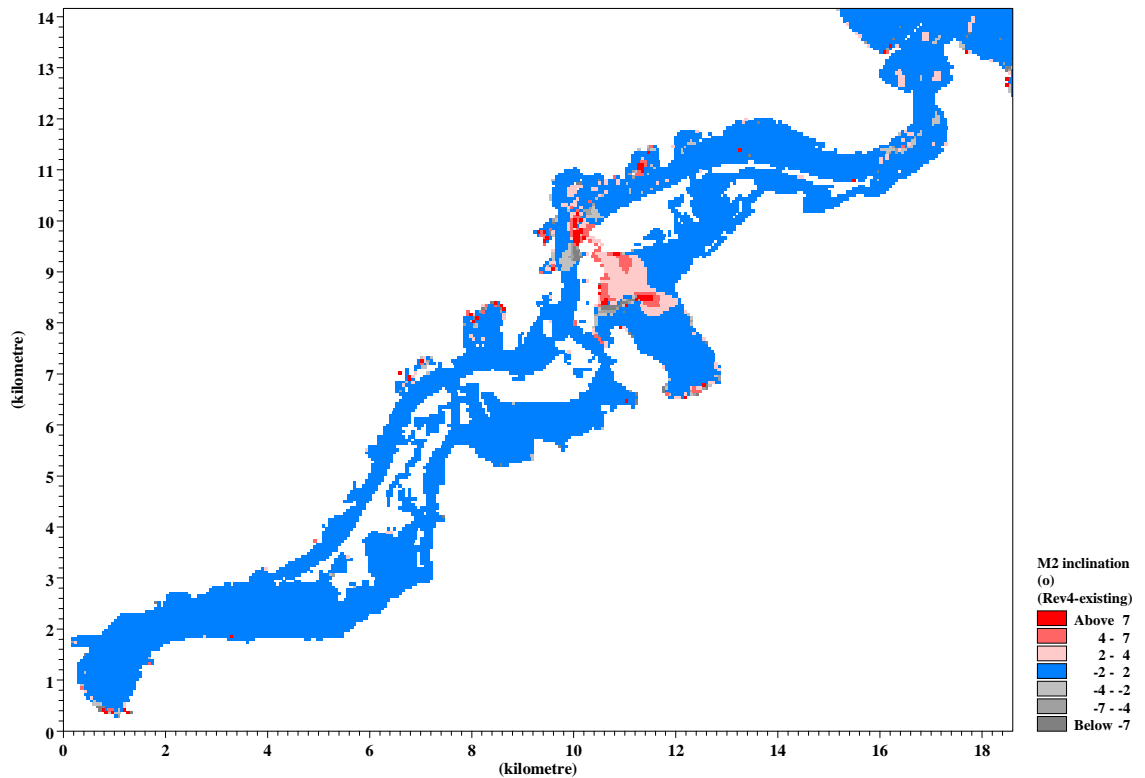


Figure 5.6: Differences in the inclination of the M_2 peak-current ($^\circ$) between the existing bathymetry and 15-m channel configuration. Positive values indicate that the direction of the peak M_2 tidal current with the 15 m channel would be rotated anti-clockwise relative to the tidal inclination that occurs with the existing bathymetry.

5.3 Spring-neap velocity differences at specific Harbour locations

In addition to the spatial plots of the differences in the mean tide (M_2 constituent) shown above in Section 5.2, time series of velocities were analysed from 12 specific sites in hydrodynamic model (Figure 5.7) within the main channel of the Harbour and in Portobello Bay. Predicted current speeds cover a 35-day period in 2007 simulation (see Section 5.1), which covered two spring/neap cycles.

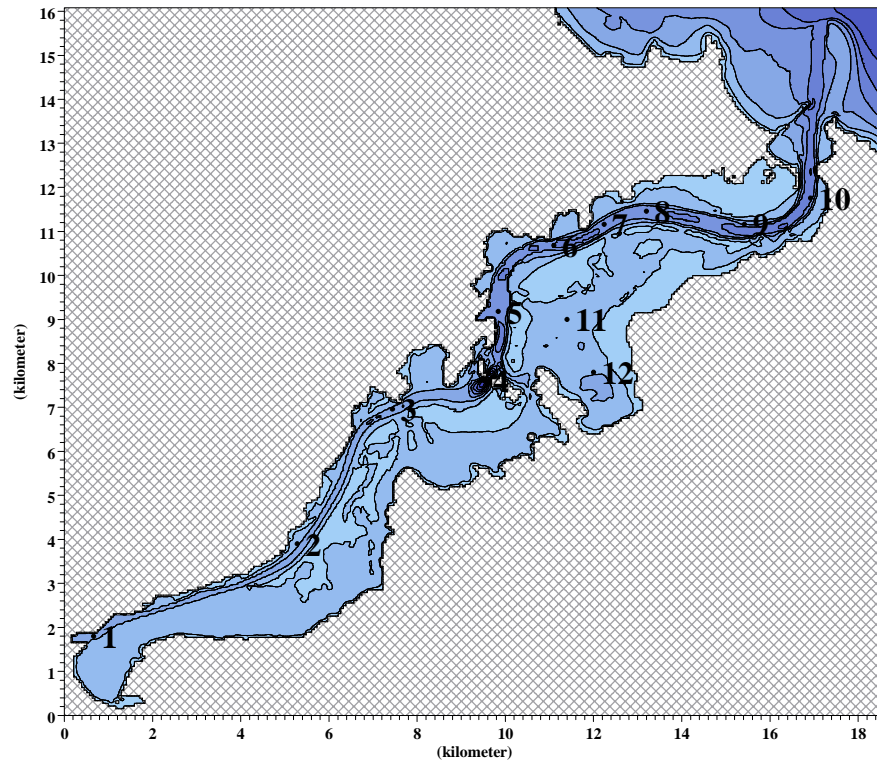


Figure 5.7: Sites selected to compare modelled current velocities before and after dredging over a 1-month period of spring/neap tide sequences.

Overall, the pattern was for no more than a 0.01–0.015 m/s variation over a neap to spring tide sequence in the differences between the 15-m Harbour channel and the existing bathymetry. For sites in some parts of the Harbour such as Dunedin, Ravensbourne and Portobello Bay (sites #1, 2, 11, 12 in Fig. 5.7), the spring/neap variation in differences would be very small (i.e., the differences in current speeds between the 15-m Harbour channel and the existing bathymetry would be fairly consistent for all tide ranges).

The mean or average tide used in the previous section lies in the middle between a spring and neap tide, so a spring-neap variation of 0.01–0.015 m/s translates into an approximate ± 0.0075 m/s spring/neap variation in differences to those shown by the peak average-tide current in Figure 5.4a. Such a spring/neap variation is a second order effect relative to the modest overall shift in peak tidal current speeds on an average tide arising from the deepened channel (Fig. 5.4a). This is because the overall difference in tide range between spring and neap tides, which is around 0.7 m, is substantially smaller than the overall change in depth of the main Harbour channel by about 2 m due to dredging (i.e., from 13 m presently to 15 m below Chart Datum).

5.4 Comparison of fluxes through the Entrance and ebb-tide sand bar

Another critical check on the hydrodynamic behaviour of Otago Harbour before and after dredging is a comparison of the water flux through the Entrance, which multiplied by a cross-section width, becomes a discharge in cumecs, and when summed over an ebb or flood tide, becomes the tidal prism volume in cubic metres. A comparison of these characteristics simulated by the model between the existing channel and the 15-m dredged channel provides a good overall indication of how much change there would be in terms of flows in and out of Otago Harbour and across the ebb-tide sand bar.

The comparison was undertaken on a mean tide of 1.45 m range (7–8 January 2007) and a spring tide with a range of 1.70 m (20 January 2007). The simulated water levels for both these tidal cycles for the dredged channel, adjacent to the Spit Jetty, are shown in Figure 5.8, along with circles marking the start and end of each tidal flow phase (ebb and flood).

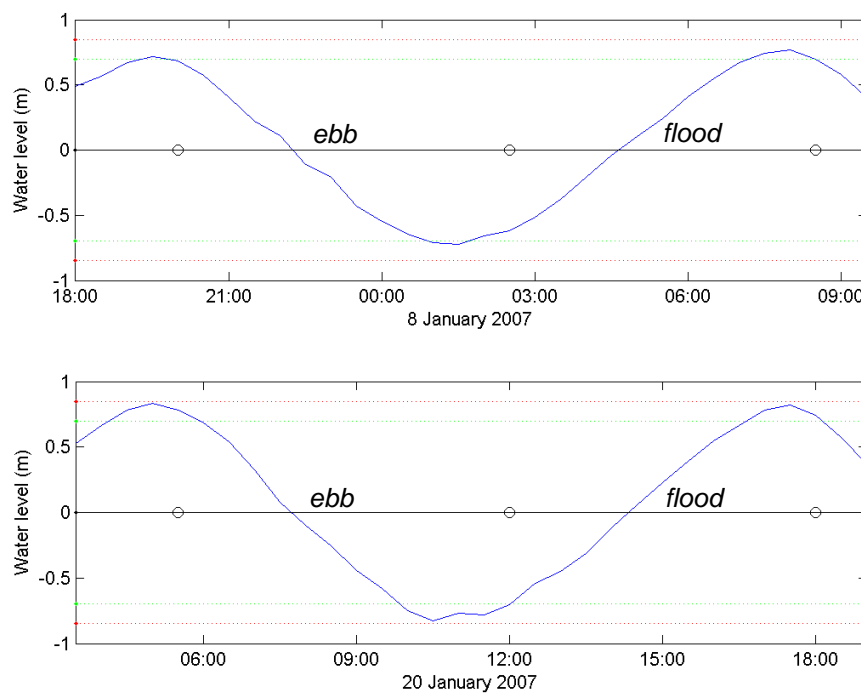


Figure 5.8: Simulated tidal cycles for the dredged channel, adjacent to the Spit Jetty, for a mean tide (TOP); and a spring tide (BOTTOM), using specific tides from January 2007. Circles mark the slack-tide times that approximately define the ebb and flood tide periods.

Fluxes were compared at the three transects shown in Figure 5.9, covering the flux in and out of Otago Harbour (Transect 1) and the fluxes across and up-and-down the ebb-tide sand bar (Transects 2 & 3).

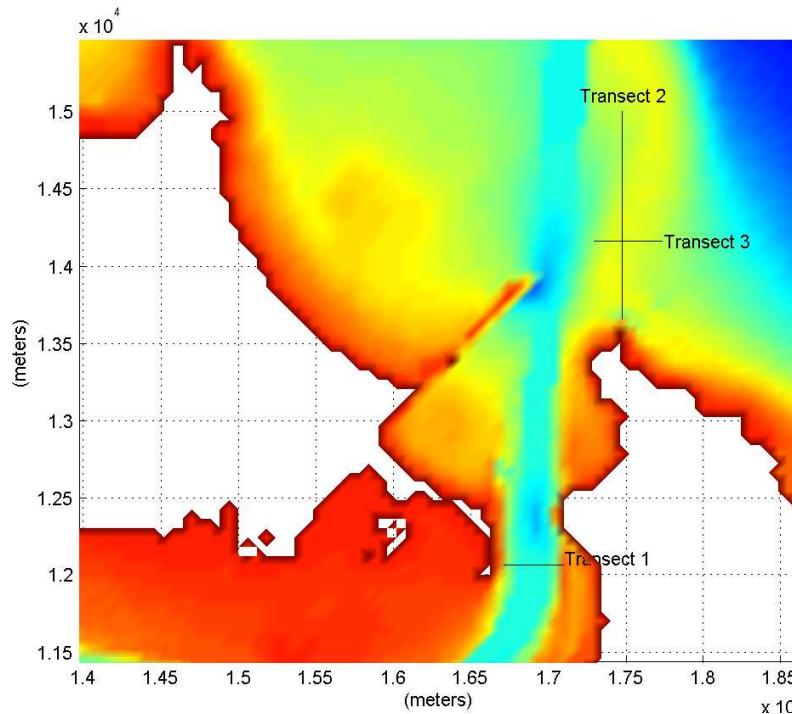


Figure 5.9: Transects used to compare fluxes simulated by the hydrodynamic model before and after dredging. Only the fluxes perpendicular to each transect were considered.

5.4.1 Ebb, flood and net water fluxes

The total ebb, flood and net water fluxes (or discharges) are considered through each of the three transects on the particular spring and mean tides modelled (Fig. 5.8).

The scalar current speeds (m/s) derived from the east-west and north-south velocity components near the centre of each transect are shown in Figure 5.10 (ebb tide first, then flood tide). For comparison, the threshold depth-averaged current speed for mobilising fine sand on the sea-bed by tidal currents alone is shown for each Transect by the dotted line in each plot (0.46 m/s threshold for Transect 1 near the Spit Jetty and 0.41 m/s threshold for Transect 2 & 3 on the shallower ebb-tide sand bar). These thresholds were calculated by the method of Soulsby (1997) using a median grain size (D_{50}) of 0.2 mm, an upper range grain size (D_{90}) of 0.3 mm, water temperature of 10°C, sediment grain to seawater density ratio (s) of 2.58, and depths below MSL of 17 m (Transect 1) and 7.5 m (Transects 2 & 3).

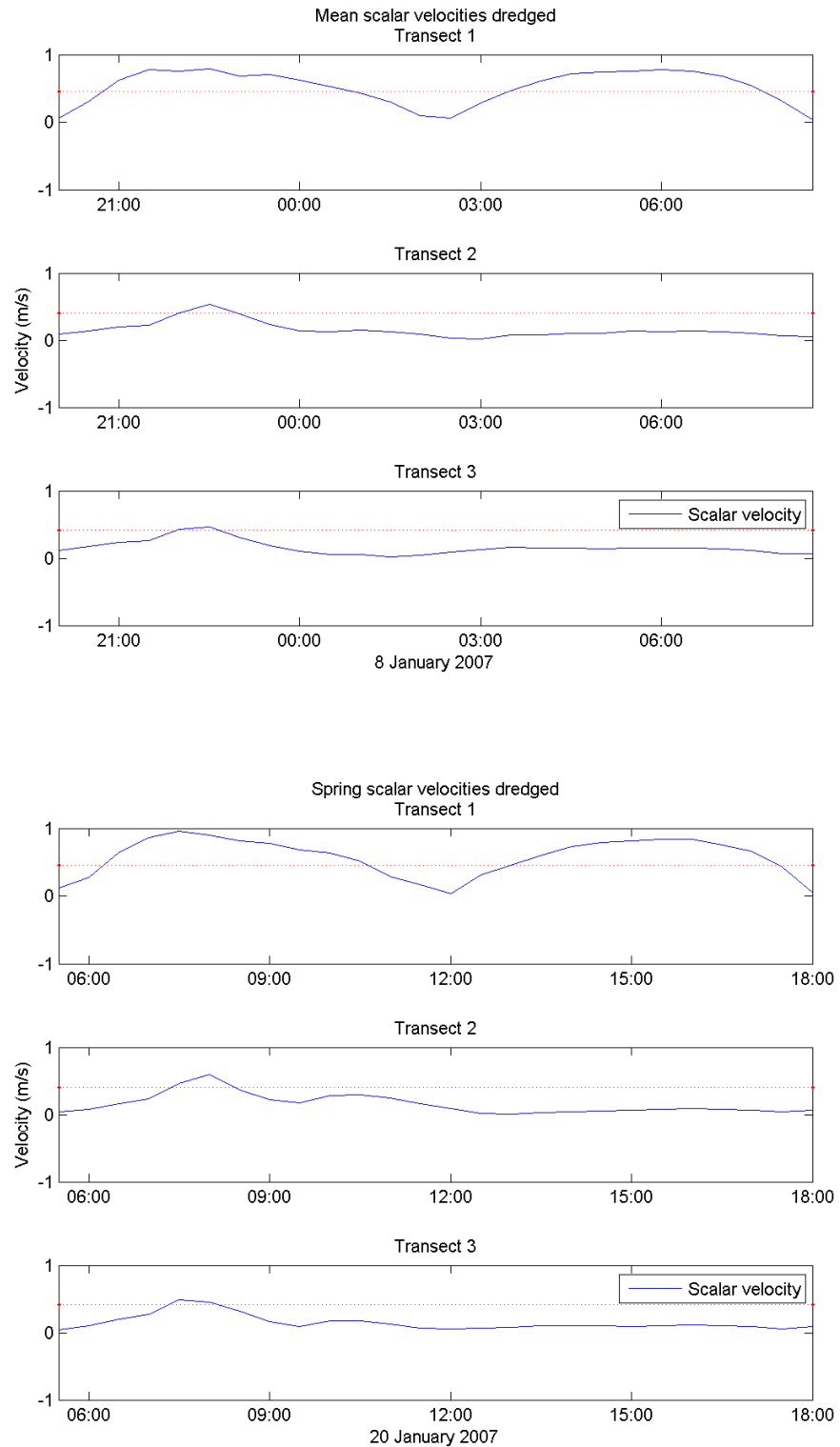


Figure 5.10: Scalar current speeds through Transects 1–3 for ebb followed by the flood tide after dredging for: (TOP three panels) the mean-tide simulation and, (BOTTOM three panels) spring tide simulation. The dotted line marks the threshold current speed for moving 0.2 mm fine sand on the seabed by tidal currents alone.

While Fig. 5.10 shows only the current speeds after dredging, the results for the existing situation are very similar, with a very slight phase lead of a few minutes in the dredged channel simulation as discussed above in Section 5.2.2. At Transect 1, the current speed is below the sediment threshold for about a third of a tidal cycle for both the mean and spring tides shown, but on spring tides the peak velocities are higher. However, on the ebb-tide sand bar, the peak ebb-tide current barely reaches the threshold speed for sand movement at Transect 3, and slightly above the threshold in the centre of Transect 2 further to the north, but only for a short time when the peak ebb-tidal jet spreads across the outer bar. Incidentally, we can infer from this result that most of the sediment transport on the sand bar must be initiated by wave stirring (followed by northwards transport by the ebb-tide currents—Fig. 5.10), as tidal currents acting alone are insufficient to enable mobilisation of fine sands on at least the inner half of the sand bar, and for only short periods during peak ebb-tide flows on the outer part of the bar.

After summing the model-derived depth-averaged fluxes (in $\text{m}^3/\text{s}/\text{m}$ width) along each transect and multiplying by the width of a model cell (60 m in this case), the total discharge (m^3/s) through each transect at 30-minute time steps was calculated, as shown in Figures 5.11–5.13 (for both mean and spring tides).

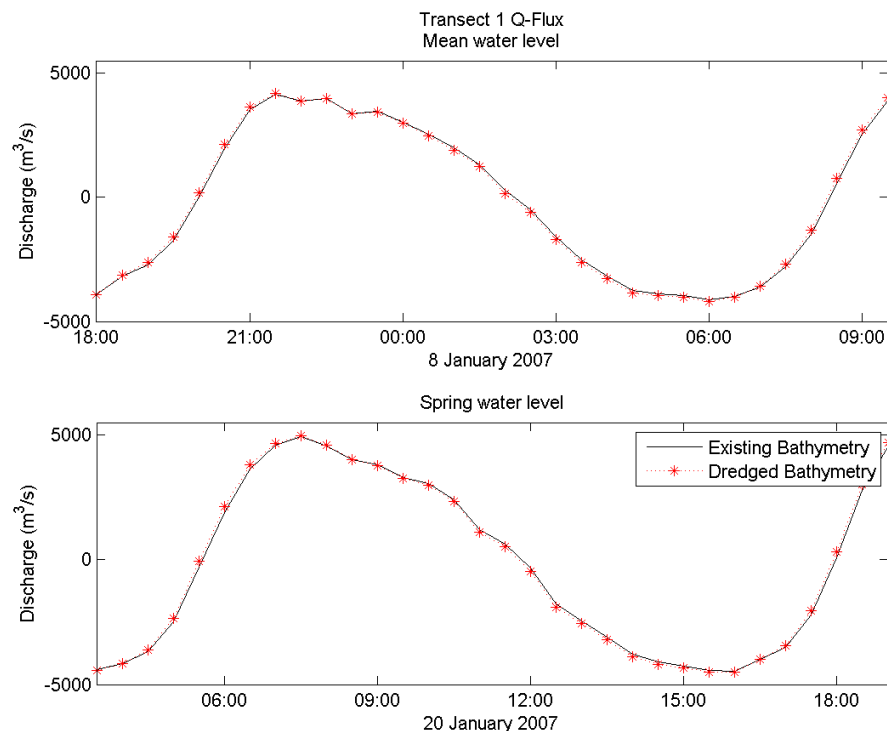


Figure 5.11: Comparison of discharge (m^3/s) through Transect 1 (off Spit Jetty) between existing channel bathymetry (line) and the proposed dredged channel (dotted line and asterisks) for: (TOP) 7/8 January 2007 mean tide; (BOTTOM) 20 January 2007 spring tide. Positive values are for an ebb tide, negative a flood tide.

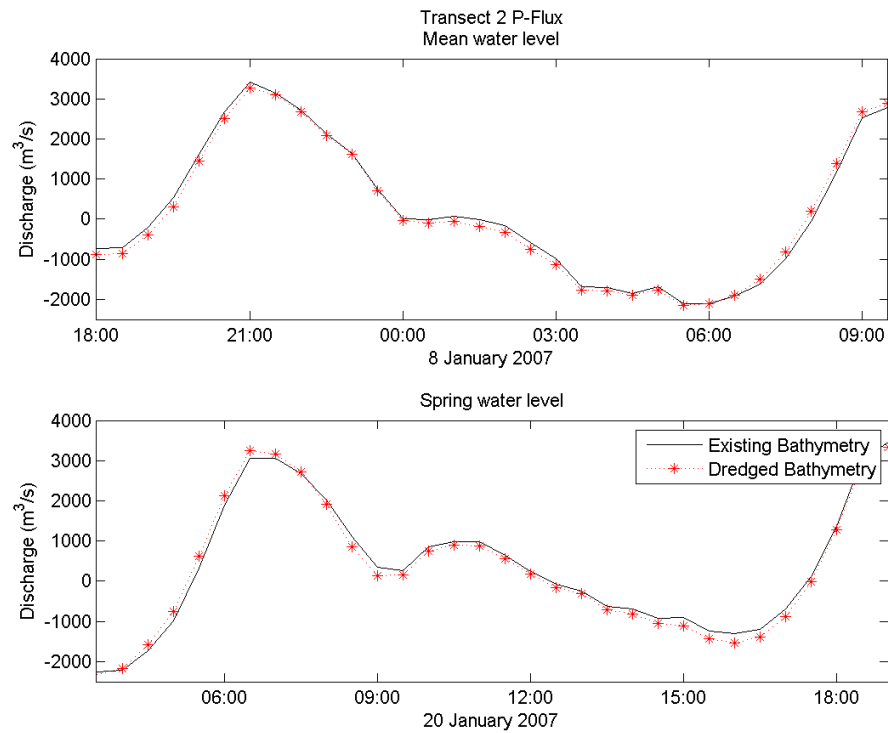


Figure 5.12: Similar to Fig. 5.11 but for discharge across Transect 2 (east-west discharge). Positive values for an easterly flow (ebb tide), negative for westerly flow (flood tide).

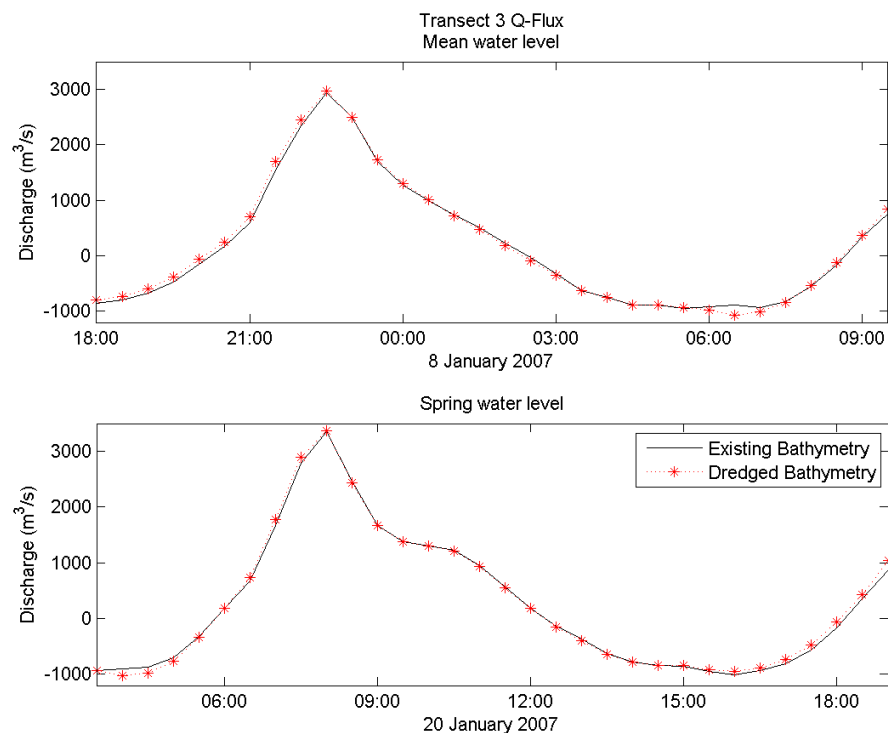


Figure 5.13: Similar to Fig. 5.11 but for discharge across Transect 3 (north-south discharge). Positive values for a northerly flow (ebb tide), negative for southerly flow (flood tide).

Figs. 5.11–5.13 compare directly the total discharge time series through each transect for the existing channel with the predicted 15-m dredged channel situation. The key result from these comparisons is that the differences in total discharges through these three transects as a result of the dredging would be relatively small.

Figures 5.12–5.13 show also that most of the flow across the ebb-tide sand bar mainly occurs on the ebb tide, with substantially weaker fluxes through those transects during a flood tide (also indicated by the current speed plots in Fig. 5.10. This pattern of stronger ebb-tide flows and weak flood tide flows over the sand bar is also confirmed by the ADCP vector plots in Vennell & Old (1999).

Integrating the area under the curves in Figs 5.11–5.13 for the modelled discharges over the ebb (+ve) and flood tide (–ve) phases provides the flow volumes through each transect on each tide phase. Table 5.1 lists the ebb and flood tidal volumes through these three transects before and after dredging for the tides selected in Figure 5.8.

Table 5.1: Ebb and flood tidal flow volumes (10^6 m^3) summed over successive ebb and flood tides through Transects 1–3 before and after dredging for the specific tides shown in Figure 5.8.

Transect	Tide range	Ebb-flow [existing] (10^6 m^3)	Ebb-flow [dredged] (10^6 m^3)	% change ebb-flow volume	Flood-flow [existing] (10^6 m^3)	Flood-flow [dredged] (10^6 m^3)	% change flood-flow volume
1	mean	60.09	60.11	0.03	63.22	63.95	1.16
	spring	68.25	68.46	0.31	68.91	69.79	1.28
2	mean	33.39	31.76	-4.9	31.29	32.73	4.6
	spring	32.96	32.33	-1.9	14.06	16.85	19.9
3	mean	27.90	28.70	2.9	15.60	16.17	3.6
	spring	32.95	33.38	1.3	14.28	13.68	-4.2

Further, summing the ebb (+ve) and flood (–ve) tide volumes generates the much smaller net total volume that passed in and out of each transect for the particular mean and spring tide. These net volumes are listed in Table 5.2. Also Table 5.2 lists the net “threshold” volumes for Transect 1 for the subset of the tidal cycle when the depth-averaged velocity reached the threshold of 0.46 m/s required to mobilise fine sand of median grain diameter of 0.2 mm. Changes in the net “threshold” flux before and after dredging is an approximate indicator of possible changes to the influx or efflux of

sand material as a result of the channel deepening. The net “threshold” volume was not calculated for Transect 2 & 3 on the ebb-tide sand bar as the tidal current speed only exceeded the sediment-transport threshold for a brief period around peak ebb flows and never exceeded the threshold on the flood tide (Fig. 5.10)

Table 5.2: Net total volumes (summed over a successive ebb and flood tide) through Transects 1–3 before and after dredging for the tides shown in Figure 5.8. The net “threshold” volumes are also shown for Transect 1, for the subset of flow periods when the velocity exceeds the threshold (0.46 m/s) for mobilising fine sand.

Transect	Tide range	Net total volume [existing] (10^6 m^3)	Net total volume [dredged] (10^6 m^3)	Net threshold volume [existing] (10^6 m^3)	Net threshold volume [dredged] (10^6 m^3)	Direction of net volume flux after dredging
1	mean	–3.13	–3.84	–3.34	–4.11	S (flood)
	spring	–0.66	–1.33	–0.64	–1.18	S (flood)
2	mean	2.09	–0.96	–	–	W (flood)
	spring	18.90	15.49	–	–	E (ebb)
3	mean	12.30	12.53	–	–	N (ebb)
	spring	18.67	19.70	–	–	N (ebb)

5.4.2 Differences in net volumes due to dredging

To provide context to the net changes in water volumes through Transects 1–3, Figs. 5.11–5.13 show that only small differences would occur in total discharges through these transects as a result of the dredging, and Table 5.1 shows that the changes to the total ebb and the flood volumes flowing through the transects would be quite small, especially for the critical Entrance area (<1.3% change).

Firstly, let’s look at the net changes in water flow volumes for Transect 1 near the Entrance adjacent to the Spit Jetty (Table 5.2). Small changes in ebb and flood fluxes following deepening of the channel would result in a slight enhancement of the flood volumes, based on the extra incoming flux $0.7 \times 10^6 \text{ m}^3$ for both these particular mean and spring tides (approximately 1% of the tidal prism volume going in and out on these particular days). A similar change is also evident in the net “threshold” volumes for ebb and flood-tide flows that exceed the threshold for mobilising fine sand (right-hand columns of Table 5.2). However, this doesn’t mean that the Harbour fills up with water over time. Taking many tide cycles over a longer period of time, the Harbour

would have a balanced inflow and outflow, with some tide cycles having a net ebb volume—all depending on successive tide heights, storm surge and winds.

Secondly, the changes in net flows over the ebb-tide sand bar are somewhat more complex and are partly affected by the open-sea boundaries of the Harbour model which are just offshore from Landfall Tower. From Table 5.1, the westerly flood-tide flow volume through Transect 2 is much lower on the spring tide than the mean tide for both the existing and dredged channels. This shows up in Table 5.2 as a much higher net ebb volume flowing east on the spring tide compared to the mean tide. This could be due to a tighter flood-tide stream close in around Taiaroa Head on a spring tide (which is not fully included in Transect 2 as it begins further offshore from Taiaroa Head), but also may be influenced by the balance of the model boundary between the north and east open-sea boundaries. What is more important are the differences between the existing and dredged channel situations, which for Transect 2 are mainly a small enhancement of the westerly flood flow volume through the transect relative to the ebb flow volume (Table 5.2). For the shorter east-west Transect 3 across the ebb-tide sand bar, the net volumes are strongly biased towards an ebb (northerly) residual flow up the sand bar, which would be slightly enhanced after dredging (Table 5.2). It is this net residual flow to the north (from dominant the ebb-tide jet and weak flood-tide currents) in combination with wave processes that has fashioned the geomorphic shape and orientation of the sand bar

5.5 Synthesis and summary of hydrodynamic changes

By comparing calibrated hydrodynamic model runs for both the existing situation and the final 15-m Harbour channel design, the relative changes in tide heights and current speeds from the dredging can be determined. The main focus in the comparison between before and after dredging was on spatial differences for a mean (average) tide. The mean tide is represented by the dominant twice-daily lunar tide (M_2) which was generated from a tidal analysis of the respective model results. Changes in velocity were also undertaken for some specific sites in the Harbour, comparing before and after dredging velocity time series over a 35-day period comprising spring and neap tides.

Tidal range—Deepening of the shipping channel leads to a slightly larger tidal range within the Harbour itself. This is expected, as a deeper channel means the tide wave travels with less dampening from seabed friction. Along the deepened part of the channel, the increase in average tide range (twice the half-range) would be almost negligible around the Harbour Entrance (up to 0.004 m) and a very small increase of between 0.004–0.006 m (relative to the existing situation) from Harington Bend down to Tayler Point. Over the rest of the Harbour, there would only be a small increase in

average tidal range of 0.006–0.008 m. Overall, these tidal-range differences due to the 15-m dredged channel would be very small (i.e., no more than 0.6% of the average 1.6-m tide range).

High-water phase—the timing (or phase) of high-water for a mean tide after dredging, would progressively change up the Harbour from less than a 1 minute advance on the existing high tides, between the Entrance and Harington Bend, up to a 3 to 4 minute advance for the Upper Harbour, Portobello Bay and the Port Chalmers area. This would occur as the tide wave travels faster in deeper water, then levels off as it propagates up the Victoria Channel of the Upper Harbour, which will not be subject to the capital dredging programme. Similar, but slightly smaller advances in the timing of low water would also occur.

Tidal currents—Over much of the Harbour (excluding the arterial channels in the Lower Harbour and the eastern area around Harwood) the changes in peak current speeds for an average tide range would be no more than ± 0.01 m/s (± 0.02 knot). This change would be imperceptible.

In the dredged shipping channel, the peak speeds will generally decrease due to the larger depth available for conveying the tidal flow. The largest decrease in peak speed in the channel would be a localised reduction of up to 0.1 m/s (0.2 knot) off Careys Bay (just north of Port Chalmers). This would arise from more of the flow being channelled through the eastern extension of the channel that transitions into the wider Turning Basin. Modest increases in peak velocities of up to 0.02–0.05 m/s (0.04–0.1 knot) would occur on the inside (northern side) of the extended Harington Bend where the shallow flanks of the present channel would be dredged.

Outside of the dredged shipping channel, a small decrease in peak speeds of 0.01–0.02 m/s (0.02–0.04 knot) would occur on the eastern side in the Harwood area, while a small increase would occur in the subsidiary channel north of Quarantine Island and off the tip of Portobello Peninsula (up to 0.01–0.02 m/s higher than present). These peak-velocity differences after dredging of no more than 0.02 m/s on a mean tide would be indistinguishable from the natural variability experienced in these areas (including wind effects) and would barely be detectable by conventional current meters (which are usually only accurate to between 0.01 to 0.02 m/s).

An analysis of the spring/neap tide current speed sequences shows that changes in current speeds for neap and spring tides would be up to ± 0.0075 m/s variation for spring and neap tides about the change on an average tide. Such a variation is mostly a second order effect relative to the modest overall change in the average peak tidal speeds from the deepened channel.

The advance in phasing (timing) of the peak mean-tide current would be between 2 and 4 minutes in most of the Harbour with the deepened channel compared to the existing bathymetry, matching similar advances for high and low tides. There would be some areas of the Lower Harbour where the peak velocity would be advanced by up to 7 to 9 minutes earlier, specifically in Deborah Bay, Portobello Peninsula and the Harwood area.

Mostly the inclination or direction of the peak-tide currents would be similar to the existing situation (within $\pm 2^\circ$). A small change in inclination would occur in outer Portobello Bay, and the connecting shallow subsidiary channel through the intertidal bank to the main shipping channel. This arises from dredging required to widen and deepen the Port Chalmers Turning Basin and lead-in transition on the eastern side of the shipping channel. The changes in peak-current inclination would be up to $\pm 7-8^\circ$ in magnitude. These would arise from changes in eddies that form later in the flooding tide in northern Portobello Bay as a result of deepening and shortening of the entrance way to the subsidiary channel.

Net current flows—Current flow volumes were extracted from the Harbour model for a specific mean and spring tide for flows through three transects (one across the Entrance channel at the Spit Jetty, and the others north-south and east-west across the ebb-tide sand bar offshore from Taiaroa Head). Following dredging, only small changes would occur in total ebb and flood flow volumes, especially at critical Spit Jetty transect in the Entrance, where changes would be less than 1.3%. These small changes in ebb and flood fluxes following deepening of the channel would result in a slight enhancement of the flood-tide volumes, for both the particular mean and spring tide cycles extracted, of approximately 1% of the tidal prism volume going in and out on these particular days. A similar change is also evident in the net “threshold” volumes for ebb and flood-tide flows that exceed the threshold for mobilising fine sand. On the ebb-tide sand bar, the existing bias of a dominant ebb-tide flow to the north up the axis of the sand bar would be slightly enhanced by the deepened channel. Tidal currents acting alone are insufficient to mobilise fine sands on the inner half of the sand bar, so wave processes obviously play the dominant role in mobilising and transporting sediment on the bar in tandem with the net northerly tidal-flow residual.

Wind effects—Hydrodynamic changes before and after dredging were also considered for 20-knot south-west and north-east wind scenarios in an earlier feasibility report (Oldman et al. 2008). Similar high-water phase changes and differences in velocities and tide ranges to the tide-only situation (with no winds) were obtained for a deepened channel option, indicating the tide dominates the Harbour hydrodynamics. Consequently, no further analysis was undertaken for this Report on extending the analysis of changes after dredging for different wind and tide combinations.

6. Set-up and sensitivity testing of the Harbour plume-dispersal model

6.1 Dispersion model justification and set-up

The next stage, having available current velocity flow fields from the calibrated hydrodynamic model, was to set-up and test a dispersion model to simulate suspended-sediment plumes generated during dredging of the shipping channel. The MIKE-21 Particle tracking model (PA) is a module that simulates the transport and dispersion processes that govern the spreading, mixing and dilution of particulates or contaminants discharged into a water body. It relies on the input of flow fields from previously-run simulations of the MIKE-21 hydrodynamic model.

The PA module is a particle tracking model where the mass from one or more discharges is apportioned to a finite number of “particles” (usually limited to 100,000 particles by the end of a simulation to keep the model run times manageable). Each numerical particle is assigned various characteristics such as sediment grain size class and the corresponding settling velocity (i.e., finer particles settle more slowly). Particles are subject to varying flows, dispersed according to a dispersion (or spreading) coefficient, and settle at a rate governed by the settling velocity. Particles are tracked in 3-dimensional space (x , y , and depth z) until they settle on the seabed and average concentrations are computed for each model-grid cell (in this case a 30 m \times 30 m cell).

For this project, a conservative approach was taken to estimate sediment deposition on the seabed from plumes produced by a dredger, by not allowing particles to be resuspended by waves and currents once they come into contact with the seabed in the model grid. This approach will produce an overestimate on sediment deposition depths arising from the dredging programme, but provides an upper-bound on the likely effects of sediment deposition on benthic communities. For water-column suspended-sediment concentrations, this approach is somewhat less conservative, as it neglects sediments resuspended during subsequent wave/storm events or by larger tidal currents. However, undertaking long-period modelling of erosion and deposition of fine silts would involve lengthy wave and current model simulations to be combined in realistic sequences, and would require seabed field experiments to calibrate sediment erosion and sediment pick-up parameters. Given the dredged sediments are natural materials and are not contaminated¹³, the approach of excluding resuspension of previously-settled sediments is reasonable, for areas outside the main channel, and is discussed later in the next Chapter after the results are presented.

¹³ Tests for contaminants in seabed sediment samples were undertaken by Opus International Consultants (2008).

The MIKE-21 PA model is classified as a “passive plume” model (CIRIA, 2000), compared to a class of “dynamic plume” models where the sediment/fluid mixture discharged dynamically interacts with the surrounding channel flow. Passive plume models treat the discharged sediments as being disaggregated once they enter the receiving waters, and their subsequent movements are only dictated by the surrounding flow and a sediment settling velocity. Dynamic plume models are more relevant for mud/silt discharges, where the discharged slurry remains intact for longer as a dense fluid/sediment mixture until it is progressively diluted and blended with the receiving waters, thereafter behaving as a passive plume. For Project Next Generation, it is intended that in predominantly-silt areas of the channel, that dredging will cease shortly after overflow commences, while in sandy areas, the silt content of the sand substrate is small (mostly <10%). Consequently, the use of a passive plume model for simulating discharges during dredging is justified.

The MIKE-21 PA model runs on the same 30-m grid as the hydrodynamic model, but requires input files that quantify the flow fields for various tide/wind combinations. The PA model also requires input values for several parameters that characterize the discharge (where, how much, staged in time or continuous?) and govern the behaviour of particles released into the water column. These model parameters can either be determined by:

- specific measurements using *in-situ* field instrumentation and laboratory analysis of samples e.g., dye tracing investigations to establish dispersion coefficients and deploying underwater suspended-sediment analysers;
- or, undertaking a sensitivity analysis of the sediment-dispersion model results to a range of parameter values that can be reasonably bounded by previous measurements or experience from other similar Harbour sites.

For this project the latter approach was adopted, because in-situ sediment analysers are still in a development stage (NIWA has been testing the LISST laser instrument with mixed success) and NIWA has gained extensive experience and knowledge from previous coastal dispersion and sediment field studies.

6.2 Sensitivity testing

The following sections outline the input forcing or parameters for sensitivity testing using the MIKE-21 PA model for the proposed Otago Harbour dredging programme.

Several PA model runs were considered to examine the sensitivity of the results to the effects of winds, a range of dispersion (plume-spreading) coefficients, sediment fall velocity and seabed-material type (e.g., predominantly silt or sand sites). Results were considered for both the predicted suspended sediment plume concentration (averaged over the 5 days) and the accumulated 5-day deposition on the seabed.

The sediment discharge for the sensitivity model runs was limited to a 5-day dredging period in the Port Chalmers Turning Basin, from where the effects on the Upper Harbour are likely to be worst. Dredging cycles for the Turning Basin were taken from an analysis of the in-situ volumes to be dredged, dredger performance, and unloading turn-around times that are described in detail in Section 7.2.

6.3 Winds

Three different wind sequences from different times of the Taiaroa Head wind record were used in conjunction with tides for the 5-day period 7–13 January 2007 to cover most of the range of likely winds. The first wind sequence was a five-day period from the record of virtually no winds (i.e., calm), the second a strong north-easterly event substituted towards the end of the 5-day simulation (Figure 6.1), and the third sequence, a strong south-west wind substituted towards the end of simulation (Figure 6.2). Note: These different wind sequences were extracted from the long-term wind record at Taiaroa Head, and each artificially substituted over the period 7–13 January 2007, but each time using the actual tides for that period. The mean wind speeds for the two sequences in Figures 6.1 and 6.2 are similar to that derived from the long-term wind record and the strong wind events towards the ends represent similar percentile wind speeds for winds from the north-east and south-west (with higher wind speeds for the latter).

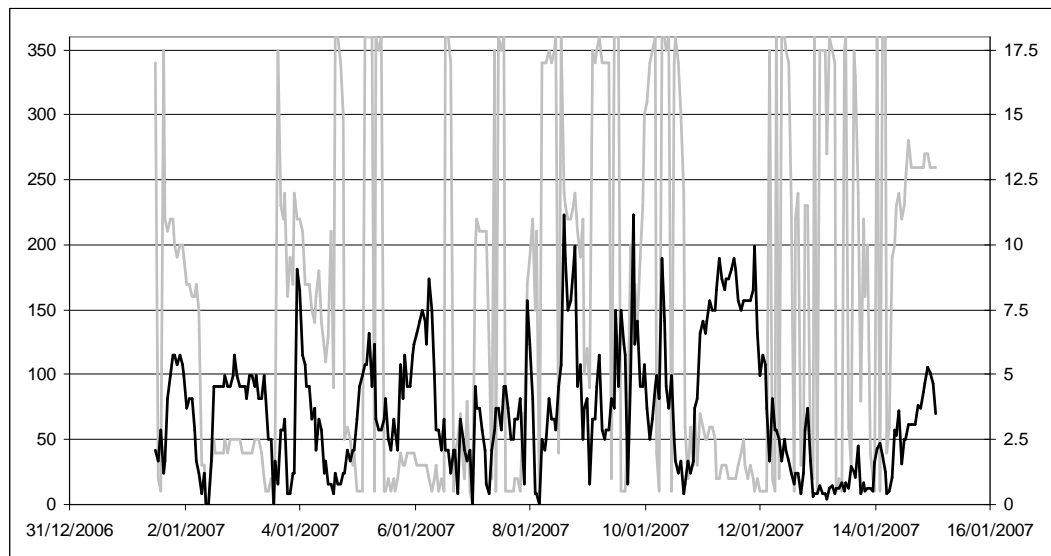


Figure 6.1: Substituted wind time series of speed (black) and direction (gray) used for the strong north-east wind scenario [direction °True N on left axis and wind speed (m/s) on right axis].

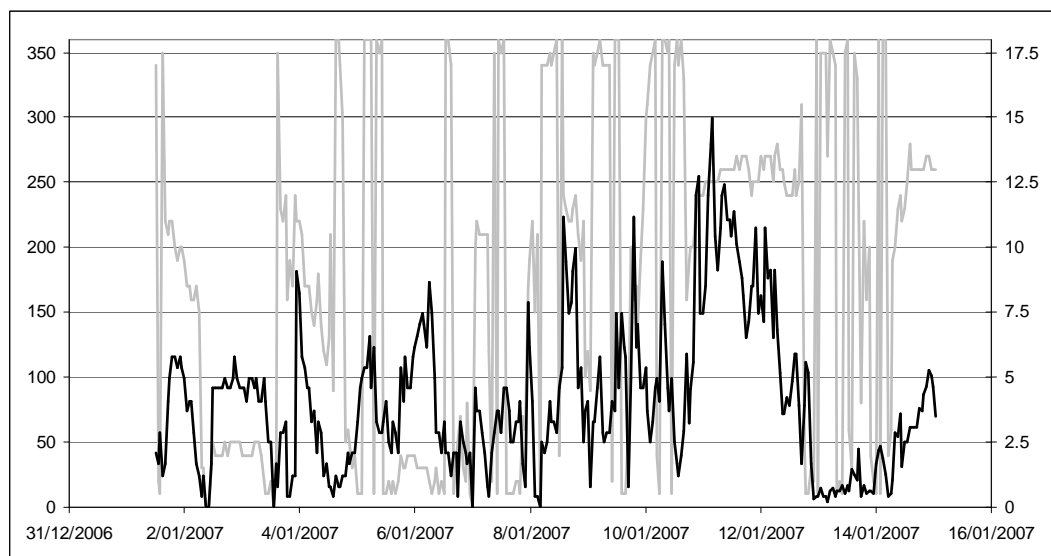


Figure 6.2: Substituted wind time-series of speed (black) and direction (gray) used for the strong south-west wind scenario [direction °True N on left axis and wind speed (m/s) on right axis].

6.4 Dispersion coefficients

Three values of horizontal dispersion coefficients were used corresponding to lower and upper limits of literature values for longitudinal dispersion (0.5 and 5 m²/s respectively) and a mid-range value of 1.5 m²/s (which is commonly used). Values for the more important lateral dispersion coefficient (side-ways spreading) obtained from the literature would suggest that the lateral dispersion is generally between half and one-tenth the longitudinal dispersion rate. The vertical transport of sediment is dominated by the fall or settling velocity, rather than by upwards and downwards dispersion, so the value of vertical dispersion coefficient will not substantially alter the results. For consistency the values of the vertical dispersion coefficients were set to 0.005, 0.015 and 0.05 m²/s (i.e., one-tenth of the lateral dispersion).

6.5 Sediment fall velocity

Geotechnical information on sediment size distributions was provided by Opus International Consultants (2008). Three grain size distributions were used (lower quartile, median and upper-quartile range) to represent the predominantly-silt seabed deposits as shown in Figure 6.3. The upper-quartile range means the silt grain sizes are higher e.g., for the same 60-percentile finer (see arrow on Fig. 6.3), the matching grain size is coarser for the upper-quartile line, while the lower-quartile grading curve represents a finer grain-size distribution and therefore slower settling velocities.

The relationship between grain size and fall velocity was developed from a combination of Stokes law (see Raudkivi, 1990) for silt particles and van Rijn (1984) for sands, which has been tested in the field with settling measurements of silts/sands in the Waitemata Harbour. An example composite settling velocity relationship with grain size is shown in Figure 6.4 for a summer water temperature of 13°C and a salinity of 33. The effect of salinity variations in the Harbour on settling rates is negligible, while seasonal temperature was found to have a minor influence on the predicted fall velocity. Therefore, an average of the winter (7°C sea temperature) and summer (13°C sea temperature) fall velocities were used to derive an average year-round fall velocity/grain size relationship. A typical specific gravity of 2.65 was used for the grain density in compiling the fall velocity curves. No allowance was made for flocculation of cohesive fine silts, which would enhance settling rates.

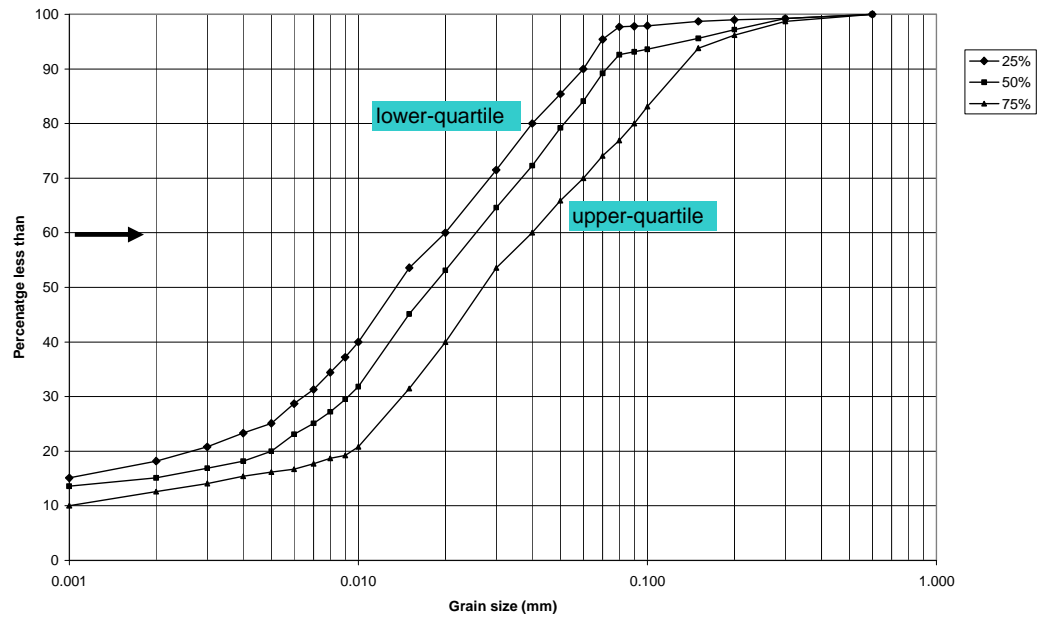


Figure 6.3: Grain size distributions derived for three silt grading curves that represent the upper quartile, median (middle line) and lower quartile distributions of silt composition from several boreholes [extracted from grading curves in Opus International Consultants (2008)].

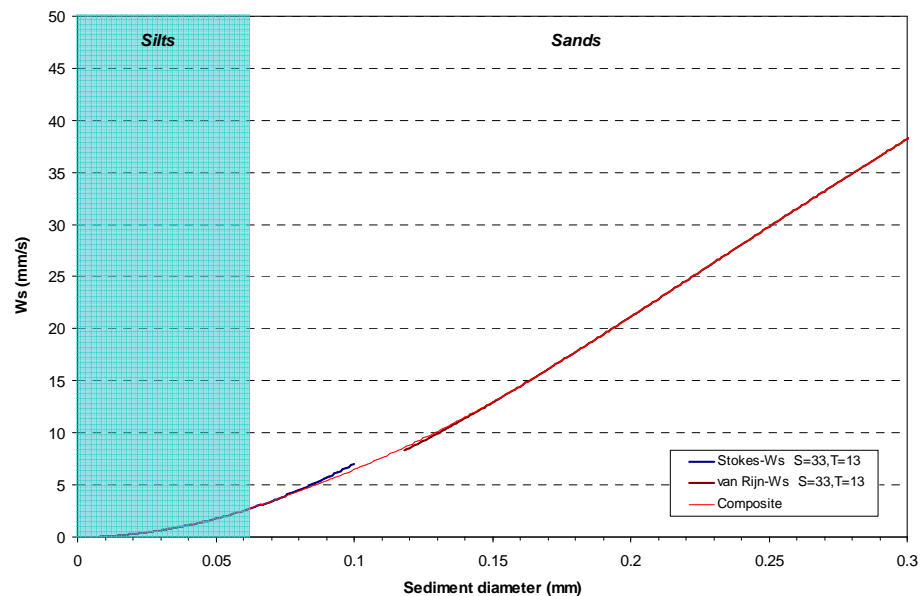


Figure 6.4: Fall velocity W_s (mm/s) and sediment size relationships combining Stokes law (finer particles) with a van Rijn (1984) formula into a composite curve (thin red line), which for this example is for a summer water temperature of 13°C and a salinity of 33. Silt sizes range up to 0.0625 mm diameter grains (shaded area).

6.6 Dredger source fluxes

The rate of release of sediment into the water column per unit time or flux (kg/s) is required as a source term in sediment plume modelling. Given that the in-situ and dredging volumes are in wet bulk densities, the modelling will be in terms of saturated-weight of sediment in the source discharge. The model results translate easily to sediment deposition thicknesses (if a recently-settled wet bulk density is used) which is fine for sediment deposition but means the suspended-sediment concentrations (normally expressed in dry weight for monitoring) will be overestimated but conservative. The detailed analysis of the likely dredging operation, including sediment fluxes and their timing, is presented in Section 7.1 (see Table 7.1). A trailing suction hopper dredger produces two types of sediment discharges: a) a discharge near the seabed of sediments disturbed by the trailing suction head (nominally set to discharge at 1 m above the bed); and, b) a discharge of sediment-laden supernatant water that commences when the storage hopper overflows. Modern trailing suction hopper dredgers have an overflow weir and pipe system that discharges the overflow well beneath the water surface (set to 5 m for a typical mid-range capacity dredger). For this sensitivity modelling exercise two types of dredging-claim scenarios were modelled:

- a predominantly “sand source” was modelled because even though the silt component is a small fraction (<10% and usually <4%), a discharge rate of silt-sized material at 60 kg/s for a 60 minutes overflow until the sands fill the hopper would discharge 216 tonnes of silts per dredging load. The suction-head disturbance was assigned a source flux of 30 kg/s;
- a predominantly “silt source”, where a short 4-minute overflow with a much higher silt discharge rate of 1000 kg/s was modelled to allow for shut-down of the plant. This would contribute about 240 tonnes of silts per dredging load in an overflow (somewhat more than the “sand source”). Normally pumping would cease just before overflows occur, but this scenario covers contingencies when dredging mixed sediments or seabed layering of lenses of silt within sands. The suction-head and propeller disturbance was assigned a source flux of 30 kg/s.

The time away from the dredging claim in the Turning Basin to complete a round trip to and from the offshore disposal site was set to 109 minutes for this sensitivity testing. These cyclic discharges separated by this disposal turn-around gap were set up in the plume model for a period of 5 days operating continuously.

6.7 Dredged site

Rather than model discharges from the dredging vessel at different sites in the shipping channel to check the sensitivity of the input parameters, the suite of model runs is applied only for the claim site in the Port Chalmers Turning Basin. This site will lead to the highest suspended-sediment concentrations in the Upper Harbour and give an indication of the level of deposition that may occur over 5 days in the vicinity of the adjacent intertidal banks to the east of the main channel (both Upper and Lower Harbour).

6.8 Results from plume-model sensitivity testing

This section provides an outline of the differences that can be observed in the plume model results arising from the variability due to winds, choice of dispersion coefficients and different silt grain size distributions.

Figures 6.5 to 6.7 show the predicted seabed deposition accumulated at the end of the 5-day test simulation for a dredging claim in the Port Chalmers Turning Basin. The deposition values are plotted in terms of sediment mass per unit area (kg/m^2) which is the mass flux onto the seabed. To convert to the thickness of deposition (mm) a settled wet bulk density has to be assumed. If this is assumed to be around 1500 kg/m^3 (at the higher end) then a deposition of 4 kg/m^2 equates to 2.7 mm (over the 5-day period) which converts to a value of 0.5 mm/day. If this is assumed very conservatively to be around 1000 kg/m^3 (i.e., a watery slurry), then a deposition of 4 kg/m^2 equates to 4 mm (over the 5-day period) which converts to a value of 0.8 mm/day.

Note: bed deposition in the plume model simulations occurs when sediment “particles” reach within a few cm of the bed, and are not subsequently resuspended by waves or currents (i.e., a “sticky-bed” approach).

Figures 6.5a–c show the effect of using different silt-size distributions (Fig. 6.3) and their associated fall velocities on bed deposition. In general the pattern of deposition is very similar. For the simulation using an upper-quartile silt distribution (Fig. 6.5c) the area of higher deposition (e.g., light blue ranging from $2\text{--}4 \text{ kg/m}^2$ over the five-day period) is greater due to the quicker fall velocity. However, the spatial extent of the deposition is subtly greater for the lower-quartile silt distribution (Fig. 6.5a) e.g., compare Eastern Channel shown by arrows in Figures 6.5a–c.

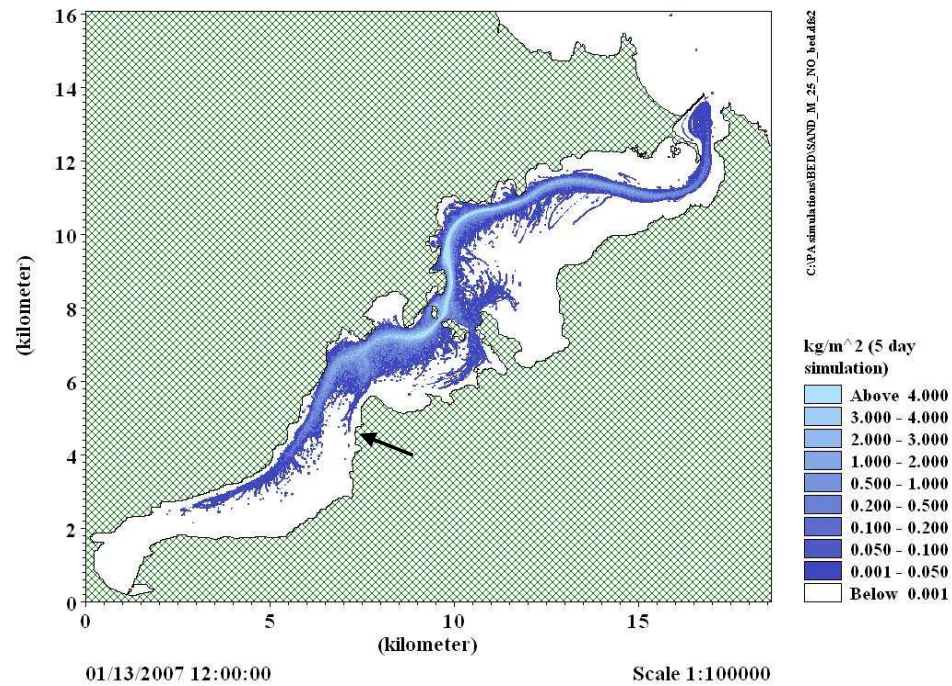


Figure 6.5a: 5-day deposition (kg/m²) for a "sand source" using mid-range dispersion coefficients, low-quartile silt distribution and calm wind conditions.

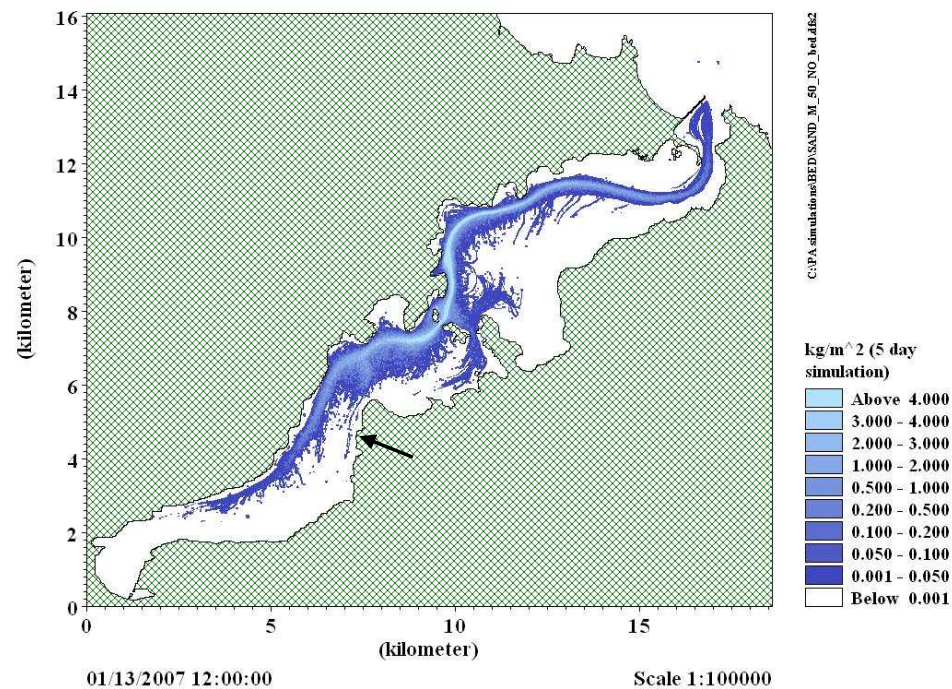


Figure 6.5b: 5-day deposition (kg/m²) for a "sand source" using mid-range dispersion coefficients, median silt distribution and calm wind conditions.

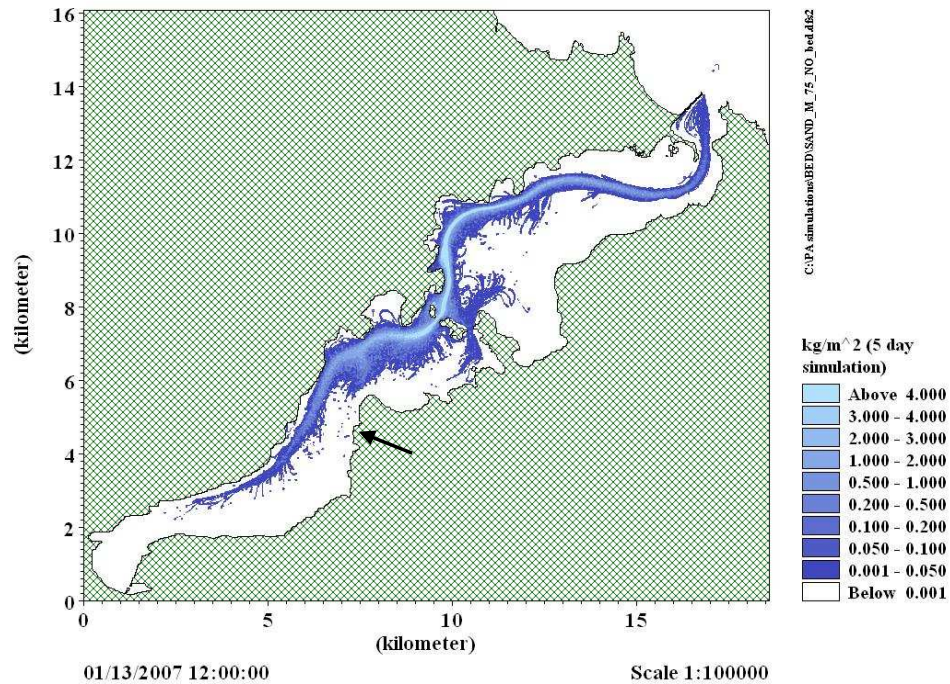


Figure 6.5c: 5-day deposition (kg/m²) for a “sand source” using mid-range dispersion coefficients, upper-quartile silt distribution and calm wind conditions.

Figures 6.6a–c show the effect of the different ranges of dispersion coefficients on the predicted sediment deposition. The results show that the predicted seabed deposition is quite insensitive to the choice of dispersion coefficients. Comparing the deposition in Eastern Channel again (see arrows in Figures 6.6a–c) emphasizes the low sensitivity to dispersion coefficients.

This illustrates the dominance of the hydraulic control of the deep channel and its advection which contrasts with the situation of a spreading plume in the ocean, which is unbounded and not depth limited, where dispersion processes are important.

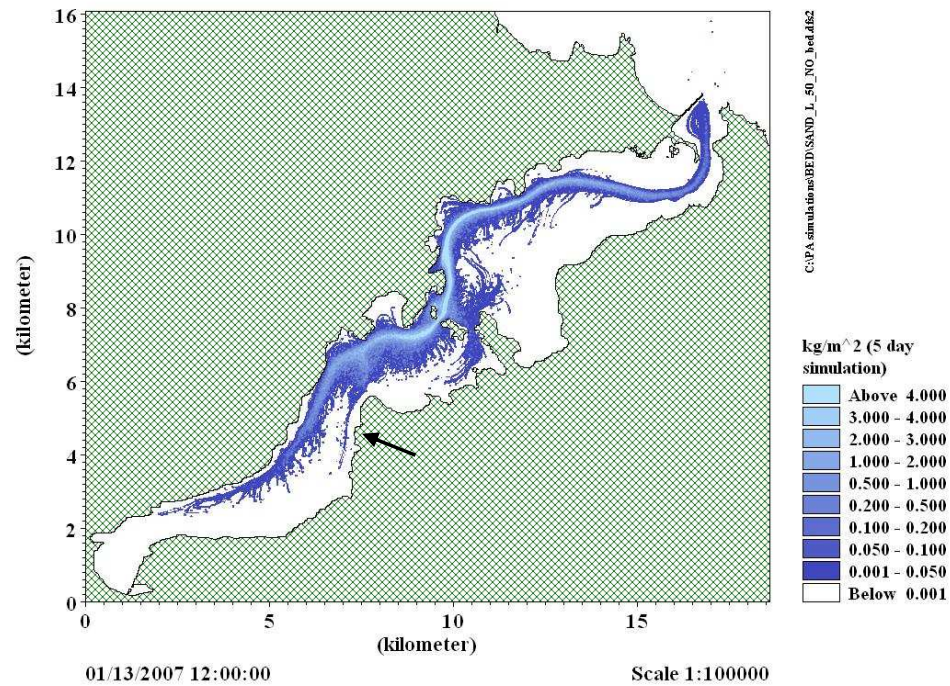


Figure 6.6a: 5-day deposition (kg/m²) for a "sand source" using low dispersion coefficients, median-range silt distribution and calm wind conditions.

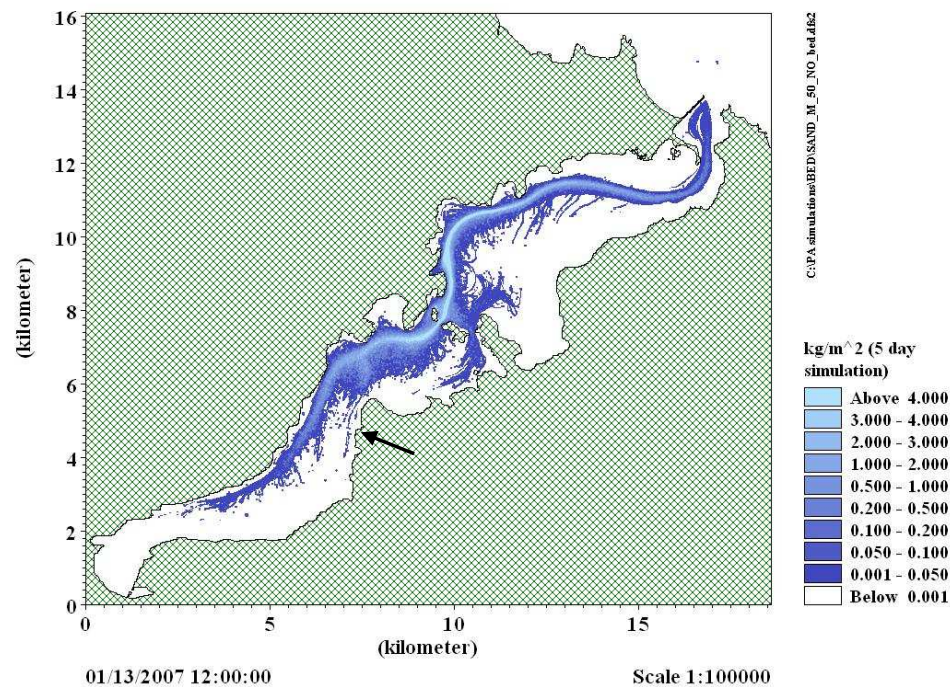


Figure 6.6b: 5-day deposition (kg/m²) for a "sand source" using mid-range dispersion coefficients, median-range silt distribution and calm wind conditions.

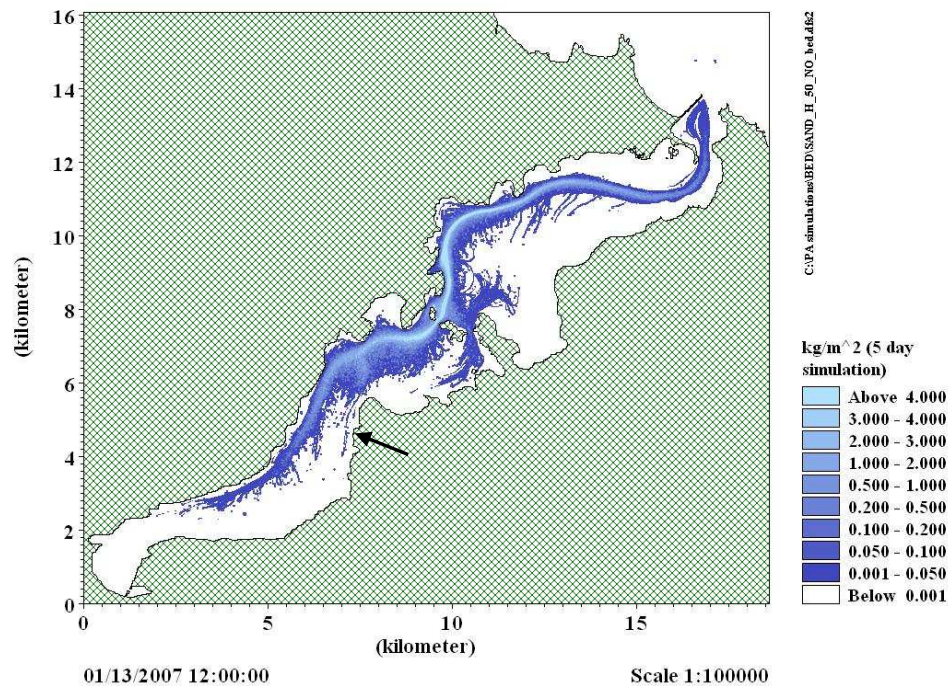


Figure 6.6c: 5-day deposition (kg/m^2) for a “sand source” using high dispersion coefficients, median-range silt distribution and calm wind conditions.

Figures 6.7a–c show the predicted bed deposition under calm winds and the two strong NE and SW wind-event sequences (Figs 6.1 and 6.2). It can be seen that under the north-east wind event (Fig. 6.7b) the predicted pattern of deposition is only slightly “nudged” towards the Upper Harbour compared to the deposition that would occur under calm wind conditions. Similarly, under the south west wind event (Fig. 6.7c) there is slightly more low-level deposition (i.e., less than 0.1 kg/m^2) occurring towards Portobello Bay and slightly higher deposition within the channel landward of the mid-harbour Islands compared to the deposition that would occur under calm wind conditions. Overall though, the pattern is reasonably similar given the differences in wind strength and direction (although excludes the effect of wind-wave processes).

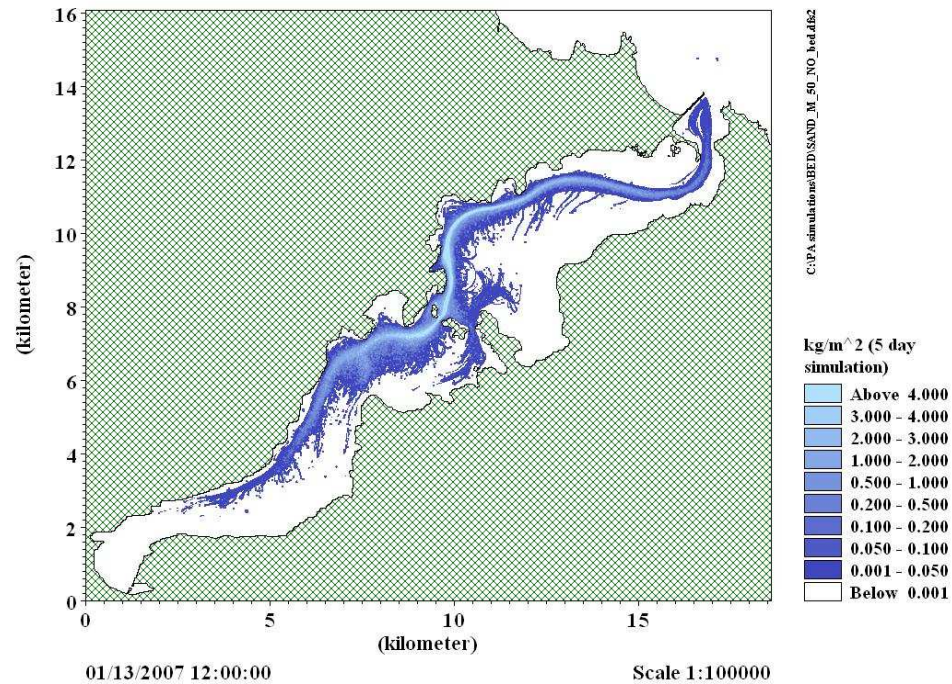


Figure 6.7a: 5-day deposition (kg/m^2) for a “sand source” using mid-range dispersion coefficients, median-range silt distribution and relatively calm wind conditions.

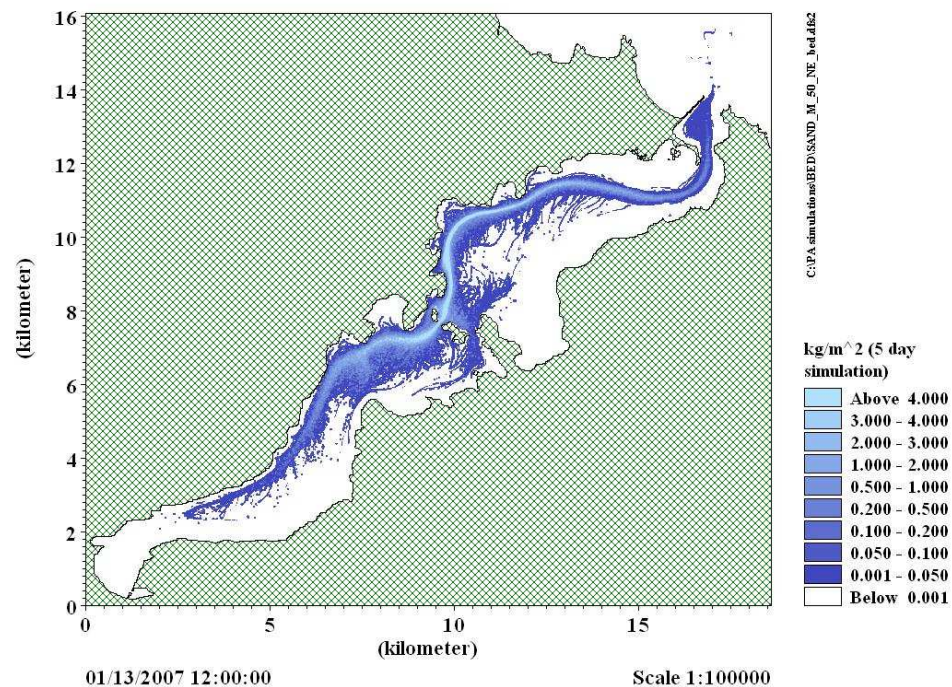


Figure 6.7b: 5-day deposition (kg/m^2) for a “sand source” using mid-range dispersion coefficients, median-range silt distribution and north-east wind event.

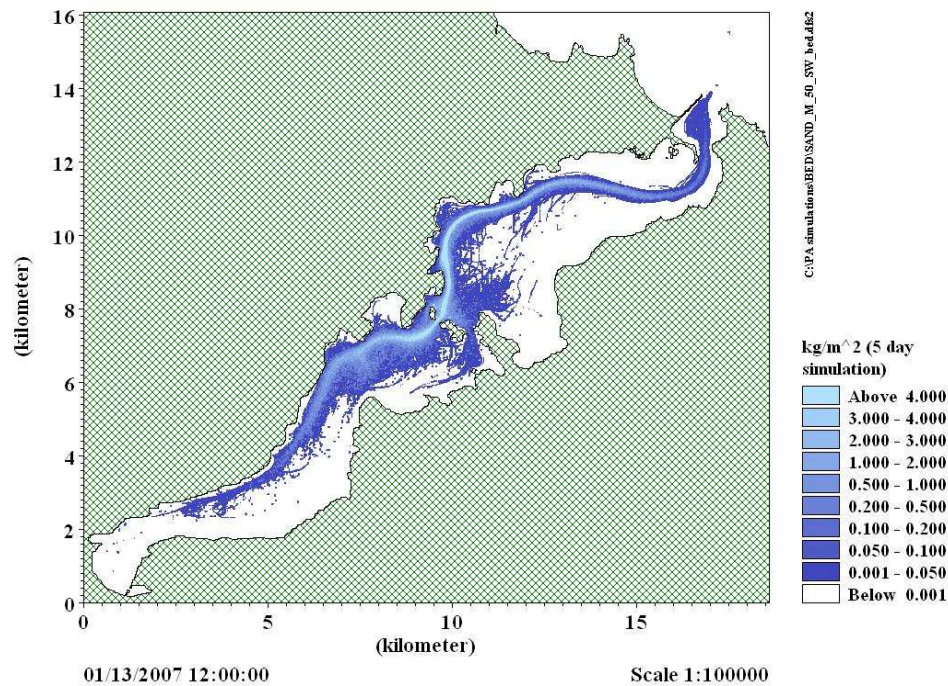


Figure 6.7c: 5-day deposition (kg/m^2) for a “sand source” using mid-range dispersion coefficients, median-range silt distribution and south-west wind event.

Figures 6.8–6.10 correspond to Figures 6.5–6.8, respectively, but show the predicted 5-day average suspended sediment concentration (kg/m^3) rather than the 5-day accumulated deposition. Note 1 kg/m^3 is equivalent to 1000 mg/L and 0.1 kg/m^3 is equivalent to 100 mg/L . The results are averaged over the 5-day period and through the water column and give an indication of the increase in suspended-sediment concentration (SSC) from the discharges, over and above background levels, that may occur while dredging the Port Chalmers Turning Basin claim. At times, the dredging operation and its synchrony with the tides, will give higher values of SSC but for the purposes of sensitivity testing the time-averaged SSC gives the best indication of the effects of sediment fall velocity, dispersion coefficients and winds on predicted SSC levels. The statistics of SSC at various specific locations, including the maximum predicted, are analysed in Chapter 7, where the various simulations using the base set of plume model parameters.

Figures 6.8a–c show the effect of fall velocity via the three different silt-size distributions, on predicted average SSC. In general the pattern of SSC is very similar. A patch of relatively high SSC occurs in the immediate vicinity of the dredged site with the predicted SSC reducing with increases silt grain size distribution. Away from the dredged site the low-range grain size material results in slightly higher SSC values than the high-range sediment (e.g., areas of $0.2\text{--}0.5 \text{ kg/m}^3$ is slightly increased near entrance to Eastern Channel).

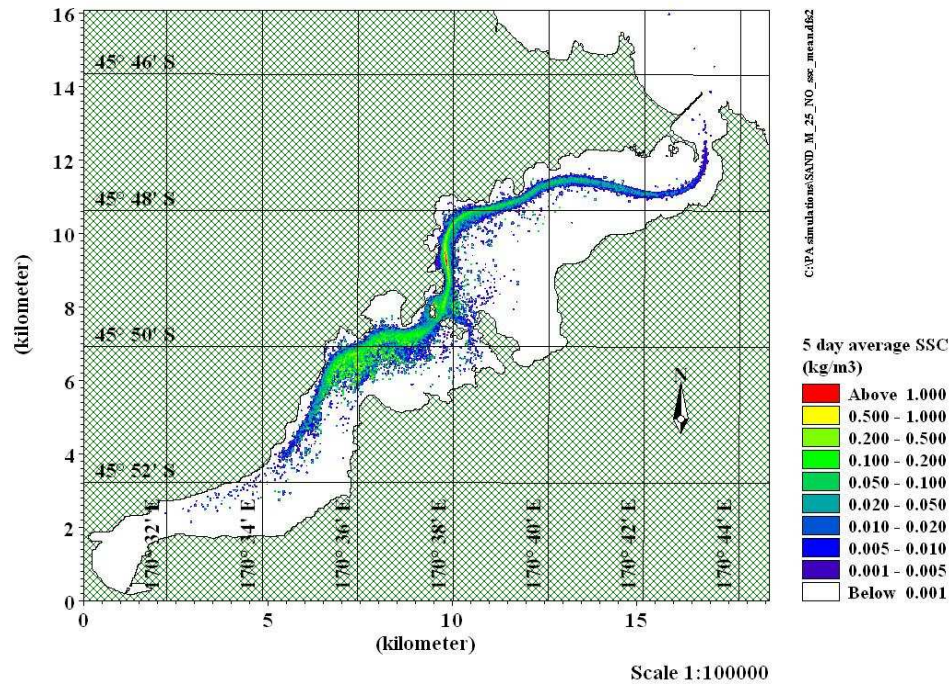


Figure 6.8a: 5-day average suspended sediment concentration (kg/m^3) for mid-range dispersion coefficients, lower-quartile silt distribution and calm wind conditions.

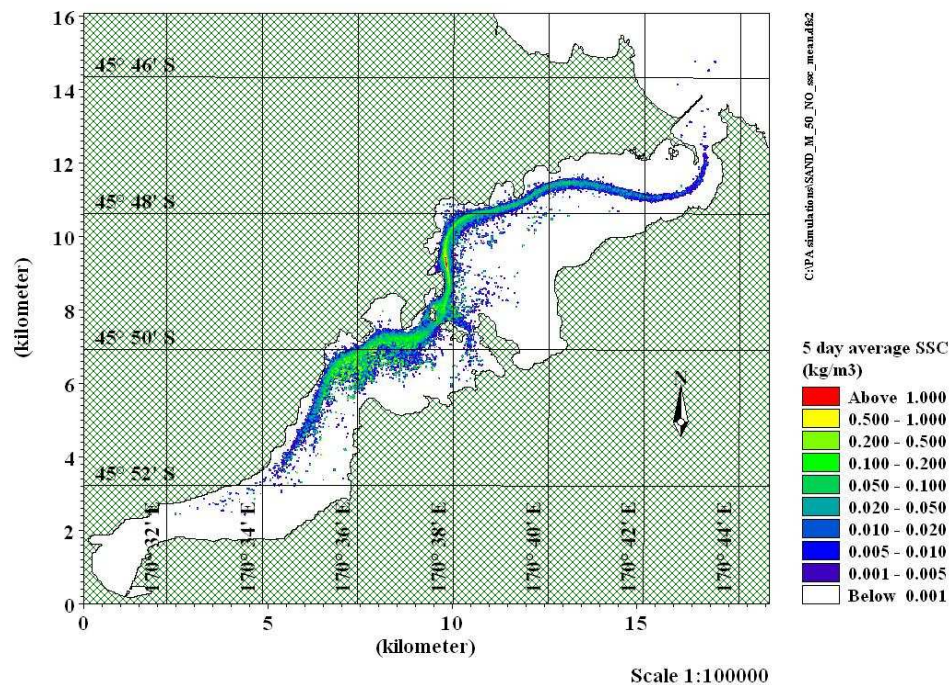


Figure 6.8b: 5-day average suspended sediment concentration (kg/m^3) for mid-range dispersion coefficients, median silt distribution and calm wind conditions.

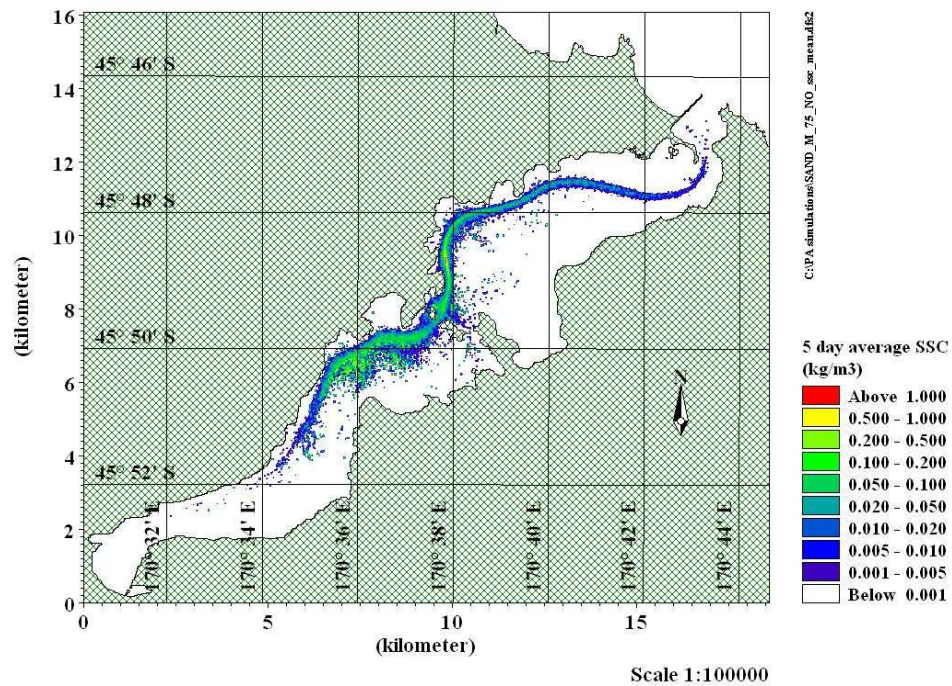


Figure 6.8c: 5-day average suspended sediment concentration (kg/m^3) for mid-range dispersion coefficients, upper-quartile silt distribution and calm wind conditions.

Figures 6.9a–c show the effect of varying the dispersion coefficients on the predicted average SSC. The results show that the predicted SSC levels are quite insensitive to the choice of dispersion coefficients, as also shown in the results for seabed deposition above.

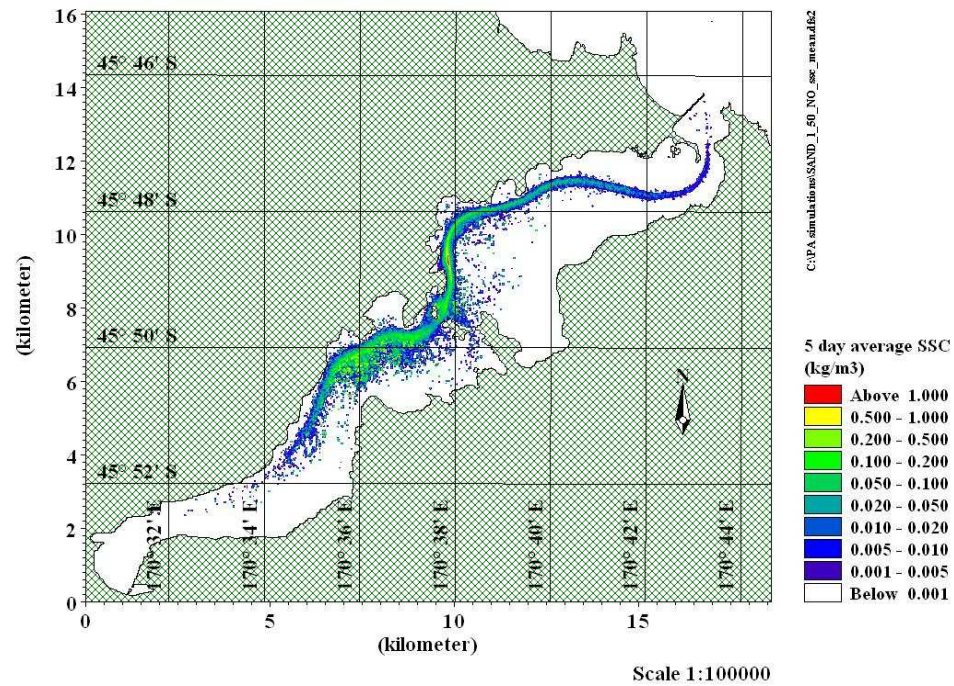


Figure 6.9a: 5-day average suspended sediment concentration (kg/m^3) for low dispersion coefficients, median silt distribution and calm wind conditions.

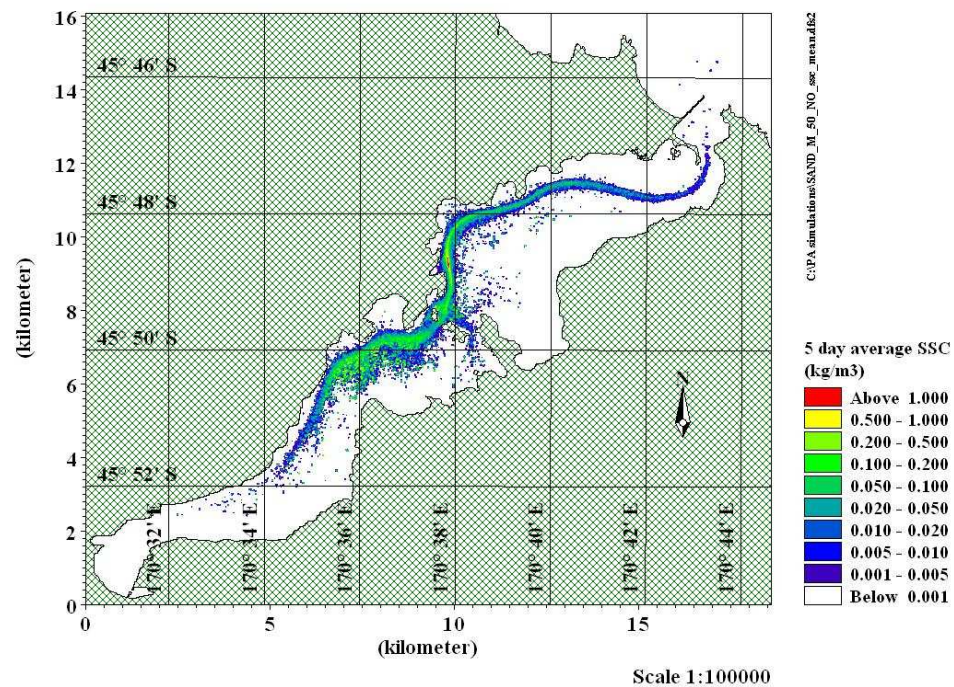


Figure 6.9b: 5-day average suspended sediment concentration (kg/m^3) for mid-range dispersion coefficients, median silt distribution and calm wind conditions.

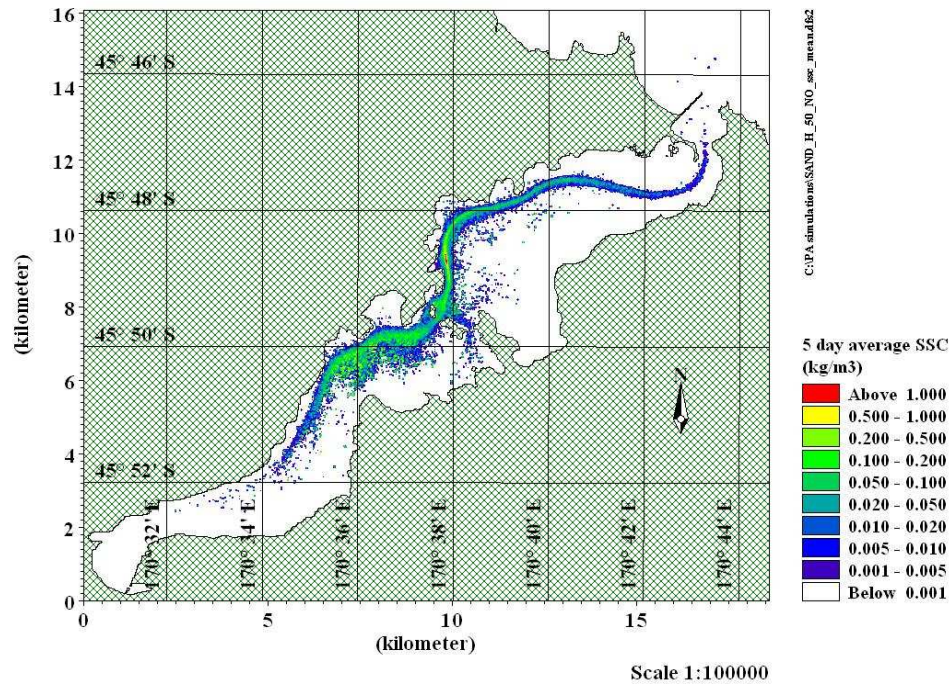


Figure 6.9c: 5-day average suspended sediment concentration (kg/m³) for high dispersion coefficients, median silt distribution and calm wind conditions.

Figures 6.10a–c show the predicted SSC under calm winds and the two strong wind events (Figs. 6.1 and 6.2). The results show the effects of quite different 5-day wind sequences are minimal in terms of the predicted average SSC within the Harbour. During any individual wind event and at certain states of the tide there will be minor differences in the suspended-sediment plume trajectory under calm conditions compared to strong winds.

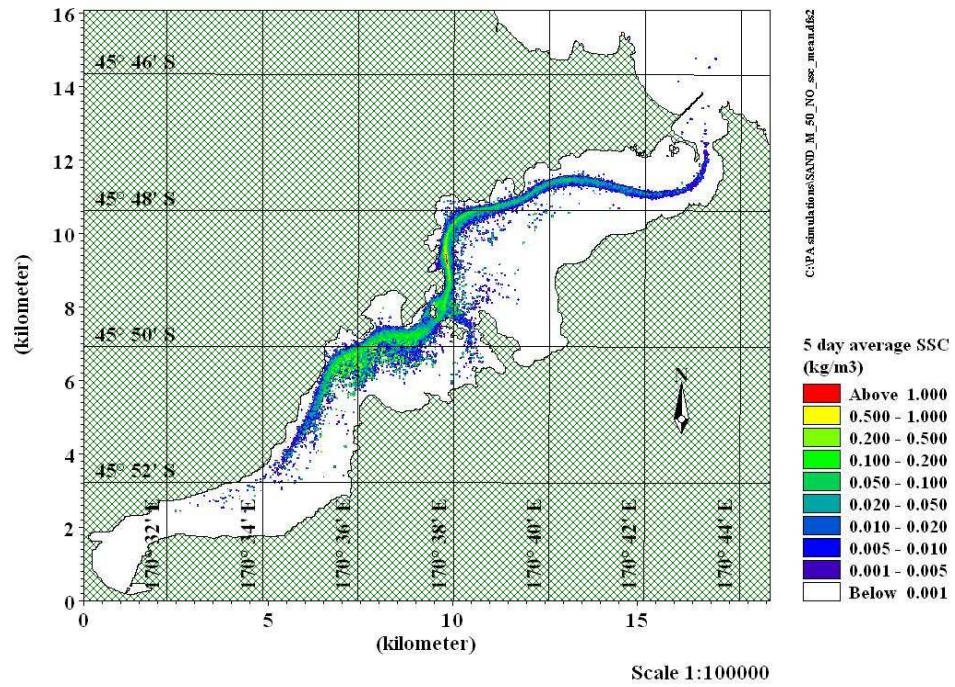


Figure 6.10a: 5-day average suspended sediment concentration (kg/m^3) for mid-range dispersion coefficients, median silt distribution and calm wind conditions.

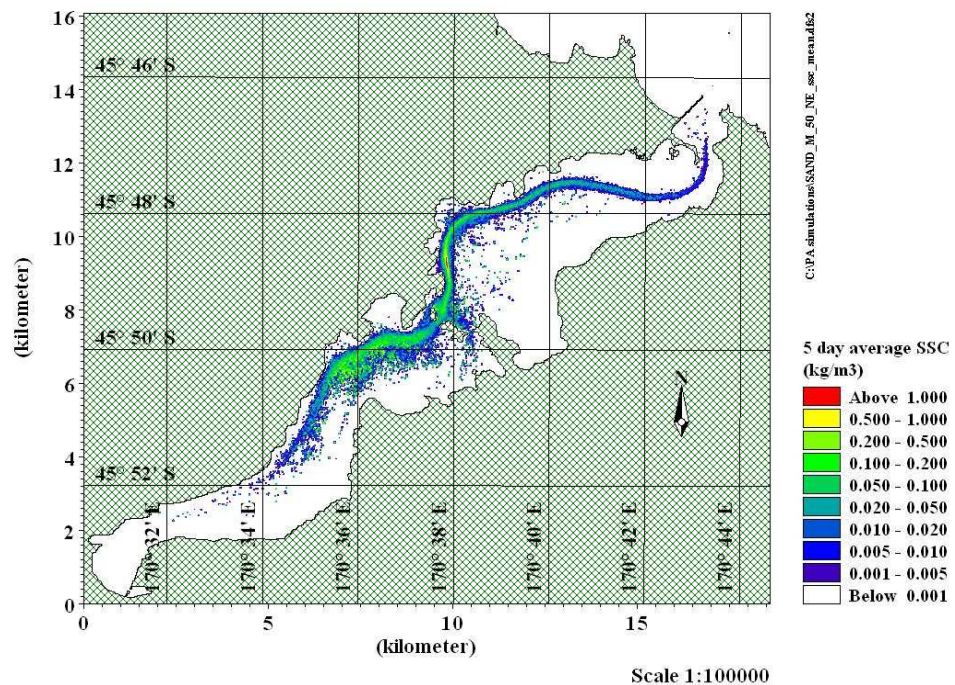


Figure 6.10b: 5-day average suspended sediment concentration (kg/m^3) for mid-range dispersion coefficients, median silt distribution and north-east wind event.

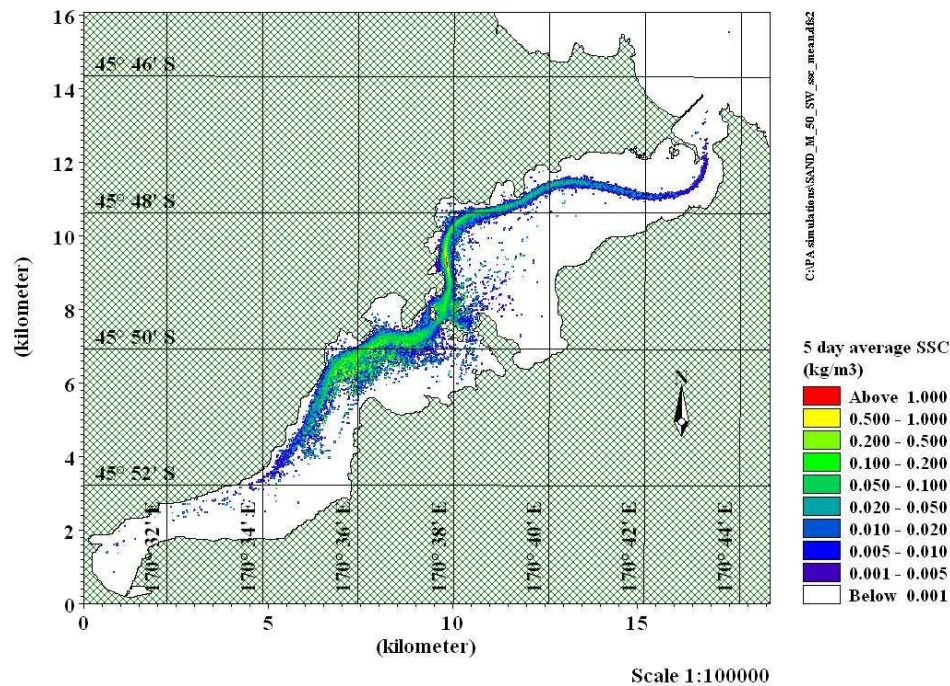


Figure 6.10c: 5-day average suspended sediment concentration (kg/m^3) for mid-range dispersion coefficients, median silt distribution and south-west wind event.

6.9 Overall results from sensitivity testing

In general the application of the MIKE21 PA model for dredging discharges in Otago Harbour shows the results are relatively insensitive to the effect of winds, the choice of dispersion coefficients and the use of different quartile silt distributions examined for a sand dredging claim within the Port Chalmers Turning Basin.

This means that for discharged sediments, dispersion and mixing processes (excluding settling of silts versus sands) and wind-driven effects on currents play a relatively minor role in determining the fate of sediment discharges from the trailing suction dredging operation. The key reason is the dredging operation would occur within the deep main channel of an otherwise shallow intertidal harbour, so advection of sediments and seawater to and fro along the channel would dominate the transport of slowly-settling sediment away from the dredged site. Discharge sources well below the water surface i.e., near the bed (nominally 1 m) and 5 m below the surface for the overflow, also contribute to constraining the settling sediments within the channel systems, rather than leading to substantial spreading out across the adjoining intertidal flats, with the only opportunities for wider spreading occurring around high tide.

The sensitivity test results also indicate that the choice of which quartile silt-grain size distribution to use (upper quartile, median, or lower-quartile) is also somewhat insensitive, again because of the dominance of the channel advection and general containment within the channel system. While there are significant differences in the percentage of each grain size material within the upper, median and lower range sediment distributions (see Fig. 6.3) these different silt-size distributions produce only subtle differences in both the predicted suspended sediment concentrations and bed deposition (as shown above). The effects of winds are also relatively minor as both the sources are well below the surface and not directly influenced by modification of the tidal currents by increased winds (surface wind waves were not included). This emphasizes that the to and fro tidal advection in the channel is a dominant factor in determining the transport of suspended-sediment plumes.

6.10 Decisions on Harbour plume model parameters

For subsequent plume modelling of scenarios from each dredge claim sub-area (Chapter 7), we adopted the mid-range dispersion coefficients and the median silt-grain size distributions. For winds, as used in the Newark (USA) dredging operation situation (USACE, 2005), we used an extract of a real 14-day neap/spring tide cycle along with typical winds (rather than simply assume calm conditions). An extract of a previously recorded 14-day spring/neap period was also found such that the 14-day average wind speed mimics the average wind speed from the long-term wind record at Taiaroa Head. Subtleties in terms of the differences in predicted SSC and bed deposition that may occur under strong winds from the south west and north east can be quantified by referring to the model sensitivity runs (Figs. 6.7 and 6.10).

Based on the long-term record at Taiaroa Head, a portion of the wind record from January 2007 was used for subsequent Harbour plume modelling that is discussed in Chapter 7. This wind record, shown in Figure 6.11 contains the same distribution of wind directions and the same mean wind speed in the north-south and east-west components as the long-term record at Taiaroa Head. The peak wind speed reached just over 11 m/s (22 knots).

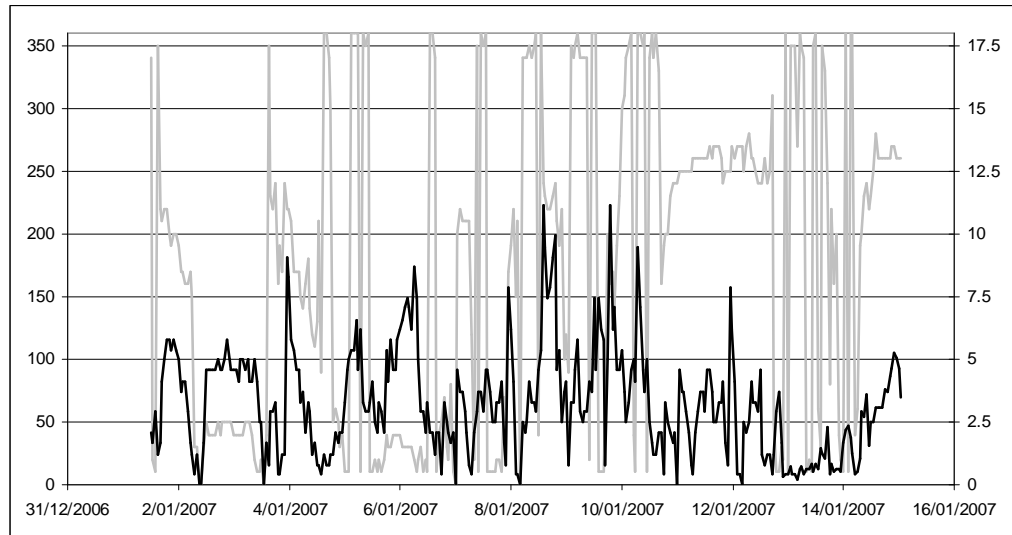


Figure 6.11: The 14-day wind time series from January 2007 adopted for subsequent Harbour plume model simulations discussed in Chapter 7. Wind direction (grey line) is on left axis [$^{\circ}$ True N] and wind speed (dark line) on right axis [(m/s)]. This portion of wind record contains the same relative distribution of wind directions as the long-term wind record and has the same average wind speeds for the north-east and south-west components as does the long-term record.

7. Modelling results for turbidity and deposition of Harbour dredging operations

7.1 Types of dredgers to be used

Model parameters describing discharge sources for the relevant sediment-plume model simulations are specific to the type of dredger that will be contracted.

A mid-size trailing suction hopper dredger (TSHD), with a hopper capacity of between 8,000 m³ to 11,000 m³, is the type of dredger that is proposed for undertake the majority of dredging of the deepened shipping channel. However, where substantial channel widening is required across existing shallow areas, mainly the adjacent intertidal banks to the east of the Port Chalmers Turning Basin, there would be insufficient draught for a mid-size TSHD to operate. So an alternative method will be required to remove seabed material down to the required operational depth for the mid-size TSHD. An allowance for this was built into the sediment plume simulations for the eastern side of the Turning Basin by setting the overflow discharge point much nearer the surface in the plume model for the initial half of the dredging on the eastern side.

A Back Hoe Dredger (BHD) is proposed for the three localised rock outcrops at Rocky Point, Acheron Head and Pulling Point (Fig. 1.1) on the flanks of the widened channel, due to the stronger breakout forces required for the rock substrate. This Report doesn't specifically cover the modelling of sediment plumes from the BHD working on rocky areas, as suspended-sediment concentrations are likely to be substantially less than for the TSHD, and the volumes involved are much smaller (~25,000 m³) than the overall volume of dredging claims (less than 0.5% of total bulk volume).

7.2 Trailing Suction Hopper Dredger operations

A trailing suction hopper dredger (TSHD) is a self-propelled vessel (Fig. 7.1) with a large hopper (CIRIA, 2000) that stores the dredged material for transport to the disposal area before emptying its contents.

The suction pipe, which is lowered to the seabed by derricks, terminates in a draghead (Fig. 7.1). The type of draghead used is specific to the type and stiffness of material being dredged and may be of the plain type or may incorporate a water jet system, blades or teeth, for dislodging compacted materials. The function of the draghead is to allow the seabed material to flow to the suction inlet as efficiently as possible. A TSHD operates very much like a floating vacuum cleaner. It sails slowly over a pre-set track to be dredged, filling its hopper as it proceeds (Fig. 7.1).



Figure 7.1: Artists impression of a trailing suction hopper dredger (TSHD) [Source: TUDelft University: <http://www.dcsc.tudelft.nl/Research/Current/matrix-28.html>]

The hopper acts as a large settling tank where the heavier particles settle to the bottom leaving the finer material suspended in the supernatant water. The amount of material that settles depends on the nature of the material. As a guide, sands of grain size greater than 0.063-0.075 mm, will quickly settle in the hopper, while silt-sized material (<0.063 mm) generally remains suspended, especially fine silts.

On completion of loading, the dredger sails to the disposal site where the cargo can be discharged, either by opening the doors or valves in the hopper bottom. A TSHD hopper can normally be emptied of the majority of water remaining when the bottom doors are closed after each load has been discharged. Hence the first phase of dredging is to fill the hopper with the dredged water-sediment mixture, of which typically less than one-third will be particulates. If dredging ceased at this time, there would be no “overflow” discharge of water and suspended solids into the Harbour. This would be the case when dredging non-cohesive silts which do not readily settle in the hopper. Otherwise from the time the hopper has filled with the water-silt mixture, all the subsequent volume of material being dredged will flow back into the sea through the overflow weir with no further increase in productivity. Therefore there are both environmental and economic reasons to minimise overflows when dredging predominantly-silt claims.

When dredging coarser materials, such as sands, the operator would continue until the hopper is full of seabed material, or almost full, subject to a bulking factor¹⁴ and the dredger density (packing) capacity compared with volume capacity. This greatly increases the efficiency of the dredging operation as fewer trips to the disposal site are required. Up until the hopper is full of the water-sediment mixture, the dredger is in a “no-overflow phase”. Once the hopper is full, the supernatant water (and any material still in suspension near the top of the supernatant) is discharged into the seawater via an overflow. The amount of material in suspension depends on the percentage of fine sediments (silts) in the in-situ sediments.

Smaller TSHDs, such as the Port Otago Ltd maintenance dredger *New Era*, overflow the supernatant water and sediment mix via a weir over the side of the vessel and onto the water surface. However, larger contract TSHD dredgers, of the size that would undertake the channel-dredging project, discharge via a weir down a large pipe that passes out from the bottom of the vessel and therefore any suspended sediment re-enters the sea from under the vessel well below the water surface (typically 5–9 m below the surface). Modern dredges also use a specially-designed valve that minimises the amount of air entrainment into the overflow and therefore minimises the tendency of the discharged water/sediment mix to come to the surface due to enhanced buoyancy.

When the loading of the dredger hopper is complete, the dragheads and suction pipes are lifted on board and the ship sails to the disposal site via the Harbour channel and the shortest line to the designated area. Once the dredger is over the disposal site, the bottom doors or valves are opened to discharge the dredged material, which descends to the seabed. When discharging, the dredger will either stop to discharge or move at a slow speed to help flush the material from the hopper. In each case the position of the dredger when the doors are open is predetermined and the track recorded to ensure an even distribution of sediments across the disposal area.

The sources of turbidity during the dredging operations are therefore:

1. The draghead as it moves over the seabed. This is normally a relatively low-volume source as most material loosened and put into suspension will be sucked through the draghead into the pipe leading to the ship’s pump and hopper. This is a similar action to a household vacuum cleaner over a dusty floor. The ship’s propellers also produce high-energy water movement that

¹⁴ Bulking refers to the increase in volume of the same weight of sediment, from a higher undisturbed in-situ bulk density to a lower density in the hopper caused by the pumping process and mixing of seawater.

can put loosened bed material into suspension and entrain the water from the overflow pipe under the ship. This is also a relatively low-volume source.

2. The overflow from the dredger's hopper. The material that re-enters the water column of the Harbour will be mainly derived from the silt content within the predominately-sand substrates of the Harbour. When dredging predominantly-silt claims, the operations will cease just prior to overflow (although in the plume modelling we have also included a pragmatic 4-minute overflow to allow for the plant and pumps to be turned off). The overflow can be a significant source of suspended material depending on the silt content in the sand and the stage in the dredging cycle. The amount of suspended material in the overflow depends on the settlement rates within the hopper and will vary throughout the dredging cycle as the hopper becomes full with less surface water (supernatant).
3. The discharge at the disposal site. The material retained within the hopper of the dredger will be ejected over the designated disposal site. Sand will act differently during disposal than silt and the hopper volume will be considerably greater. The hopper will be full, or near full, with sand that has had the silt content washed out. When dredging silt or sandy silt, the hopper will only be about a third full of solid material, but the silt content will remain in suspension or quickly become suspended as it drops through the water column. Cohesive clay, silty clay and clayey silts tend to remain grouped in balls and therefore a reasonable proportion is likely to act similarly to sand.

Modelling of the first two discharges in the Otago Harbour environment is discussed in the following sections, while plume modelling for the offshore disposal is described later in Chapter 11.

7.3 Dredging parameters for Harbour plume modelling

The input hopper load is dependent on the material being dredged, the type and size of dredger and its load (pumping) rate. The volume of dredging for Project Next Generation suits a mid-size TSHD, of the range 8,000–11,000 m³ hopper capacity (Lincoln Coe, POL, pers. comm.). Using an upper-range hopper capacity of 10,800 m³, input hopper loads for the plume modelling covering claims from two types of sediment sources were estimated.

Note: Sand-size material was not specifically included in the plume model because they settle quickly in the hopper of a TSHD and little is passed through the overflow.

Likewise, bottom disturbances of sand-sized material quickly settle back on the seabed. Therefore, all the results from the plume modelling below relate to silt-sized material that is found in both predominantly-sand (“sand”) and more so in predominantly-silt (“silt”) dredging claims.

7.3.1 Dredging predominantly sand areas

Based on a mid-sized hopper capacity of 10,800 m³ the in-situ volume dredged per load would be around 8660 m³. This would occur over approximately 80 minutes (1.33 hours) of pumping at a rate of around 108 m³/minute. This hopper loading rate also compares with various overseas projects using mid-size TSHDs that range between 54–115 m³/minute (Stuart Hughes & Assoc., pers. comm.).

Based on results from geotechnical core sampling (Opus International Consultants, 2008), the following sediment discharge rates (Table 7.1) were estimated:

- Draghead and propeller disturbance—a discharge source of 30 kg/s was assigned to cover these near-bed disturbances of the silt-content in the sands. This rate is conservatively higher compared with values for sediment resuspension from two example TSHDs provided by CIRIA (2000) although these were for dredging in predominantly silty sediments. This discharge was nominally located in the plume model at 1 m above the seabed.
- Overflow discharge—a pumping rate of 108 m³/min, with an in-situ wet bulk density of 1800 kg/m³ and an average of 2% silt content by mass in “sand” claims would produce an overflow of around 60 kg/s. No sand-sized material is assumed to be in the overflow discharge as it settles much more quickly in the dredge hopper. The overflow discharge in the plume model was located at 5 m below the surface at the time of dredging (depending on the tide level).

Given that the in-situ and dredging volumes above are in wet bulk densities, the plume modelling will be in terms of saturated-weight of sediment for the above sediment source fluxes. The model results translate easily to sediment deposition thicknesses (when an appropriate recently-settled wet bulk density is used) but means the suspended-sediment concentrations (normally expressed in dry weight per volume for monitoring analyses) will be overestimated although conservative. Using a range of estimated dry bulk densities of 1300 to 1500 kg/m³ obtained for similar consolidated in-situ silty sands in sub-tidal channels of the central Waitemata Harbour in Auckland (Andrew Swales, NIWA pers. comm.), means the suspended-sediment concentrations may realistically be 70–80% of the suspended-sediment concentrations presented in this Chapter.

7.3.2 Dredging predominantly silt areas

Based on results from geotechnical core sampling (Opus International Consultants, 2008), the following likely discharge rates (Table 7.1) were estimated:

- Draghead and propeller disturbance - the same discharge source of 30 kg/s was assigned to cover these near-bed disturbances. The discharge was located nominally at 1 m above the seabed.
- Overflow discharge - normally the pumping would cease immediately prior to overflows occurring, estimated to be 20 minutes (0.33 hours). However, conservatively we have included an additional short 4-minute overflow discharge of 1000 kg/s in the plume modelling to cover a pragmatic shut-down of the dredging operation, especially when dredging claims having isolated layers (lenses) of silt embedded within mainly sands.

7.3.3 Dredging cycles including disposal trips

Once loading ceases, after 1.33 hrs for “sand” claims and 0.4 hrs for ‘silt’ claims (Table 7.2), the TSHD would proceed to the disposal ground to discharge the hopper and return to repeat another cycle of dredging. The turnaround times will be substantially longer for the dredging that takes place around Port Chalmers compared to the dredging off The Mole for example. Turn-around times used in the simulations for an offshore disposal area are listed in Table 7.2 for the five channel source-areas selected as representative discharge points for the suspended-sediment plume simulations (Fig. 7.2). The loading times and the round-trip times were used to construct a sequence of on/off discharges at the rates listed in Table 7.1. Note: Turn-around times for the selected A0 disposal area (which was selected at the end of the modelling process – see Chapter 11) will be longer than that modelled and listed in Table 7.2 (which was set for an initial disposal option at A1). However, the plume modelling presented here will be more conservative in relation to suspended-sediment concentrations with less time between discharges in the model than will be the case in practice if a disposal ground further offshore is used. The discharge itself will be unaffected by turn-around times.

The discharge heights for each source area are also listed in Table 7.1. The exception is the eastern side of the Turning Basin, where the overflow for the first 7 days was set to 1 m below the surface (for a smaller-draught dredger), followed by 7 days at 5 m below the surface, when a mid-range TSHD can commence operations in the deepened section of the widened Turning Basin.

Table 7.1: Source discharge rates to be used for the combination of near-bed disturbances and overflow sources, time windows for these sources ($t = 0$ minutes being the start of pumping) and the total average hopper load (kg) of each sediment-source type. [Source: Stuart Hughes & Associates and POL].

Sediment source	Discharge height	Sediment discharge rate (kg/s)	Timing (min)	Total mass in hopper load [†] (kg)
"Sand" claims	1 m above bed	30	0–80 min	15,600
	5 m below surface [‡]	60	20–80 min	
"Silt" claims	1 m above bed	30	0–24 min	6,067
	5 m below surface [‡]	1000	20–24 min	

[‡] except for the eastern side of the Turning Basin, where initially (1st 7 days of the 14-day simulation) the overflow was set to 1 m below the surface.

[†] assuming a wet bulk density of 1800 kg/m³ for sands and 1600 kg/m³ for silts.

Based on the round-trip times (Table 7.2) and the respective in-situ volumes of "silts" and "sands" in each of the representative channel source-area claims, the total number of dredging days (24-hour units) for each source-area was determined for the 15-m Harbour channel (final design) which sum up to the total dredged volume of 7.06 Mm³. These dredging days were then used to calculate the factors listed in Table 7.3 to pro-rata the accumulated sediment deposition obtained from each 14-day plume model simulation of "sand" and "silt" claims for each of the five source sites.

The total number of dredging days to dredge the entire 15-m channel option out to Landfall Tower (excluding rock volumes) depends on a number of variables including the capacity of the TSHD used, the distance to the offshore disposal site and down-time due to maintenance and weather contingencies. For lower-bound estimates of the total time for accumulated deposition (which will yield an upper-bound on deposition rates), we have used the largest mid-size TSHD likely to be suitable for this project (10,800m³ hopper capacity), and turn-around times to the preferred A0 disposal area (see Chapter 11), with and without down-time. Based on these (conservative) assumptions, the estimated dredging season is estimated at approximately 120 days, extending to around 150 days if a 20% down-time factor is assumed (Stuart Hughes & Associates, pers. comm. and POL).

For assessing the accumulated deposition within Otago Harbour over the dredging season, only one-third of the estimated dredging volume of sands for the outer approach channel was lumped in with the Harington Bend source discharge site (Fig. 7.2). The rationale is that the majority of the "sand" discharges from the outer

approach channel claim, where there is negligible silt content, are unlikely to be deposited inside the Harbour, apart from the seafloor of the main channel in and around the wider Entrance area. This means the lower-bound dredging period relevant to Harbour silt deposition would reduce by around 9 days to be approximately 111 dredging days excluding downtime or around 140 days using a 20% down-time factor. Because the length of the dredging programme is not definite, the resulting dredging effort required for each discharge source location used in the plume/deposition modelling is expressed in Table 7.3 as a % of total dredging days that would affect the Harbour.

Table 7.2: Dredge loading times and round-trip cycles used for modelling discharge plumes from 5 representative channel source-areas (Fig. 7.2). Loading and round-trip times were used to construct sediment discharge on/off cycles for each sub-area. [*Source:* Stuart Hughes & Associates]. *Note:* Values for the time away are relevant to the initial A1 disposal option.

Channel source-area	Loading time (hrs)		Round-trip (loading, disposal, turning and return time) (hrs)		Time away from dredged site (hrs)	
	“Sands”	“Silts”	“Sands”	“Silts”	“Sands”	“Silts”
Harington Bend	1.33	0.4	2.29	1.29	0.96	0.96
Cross-channel	1.33	0.4	2.52	1.52	1.19	1.19
Taylers Bend	1.33	0.4	2.74	1.74	1.41	1.41
Basin–west	1.33	0.4	3.16	2.16	1.82	1.82
Basin–east	1.33	0.4	3.16	2.16	1.82	1.82

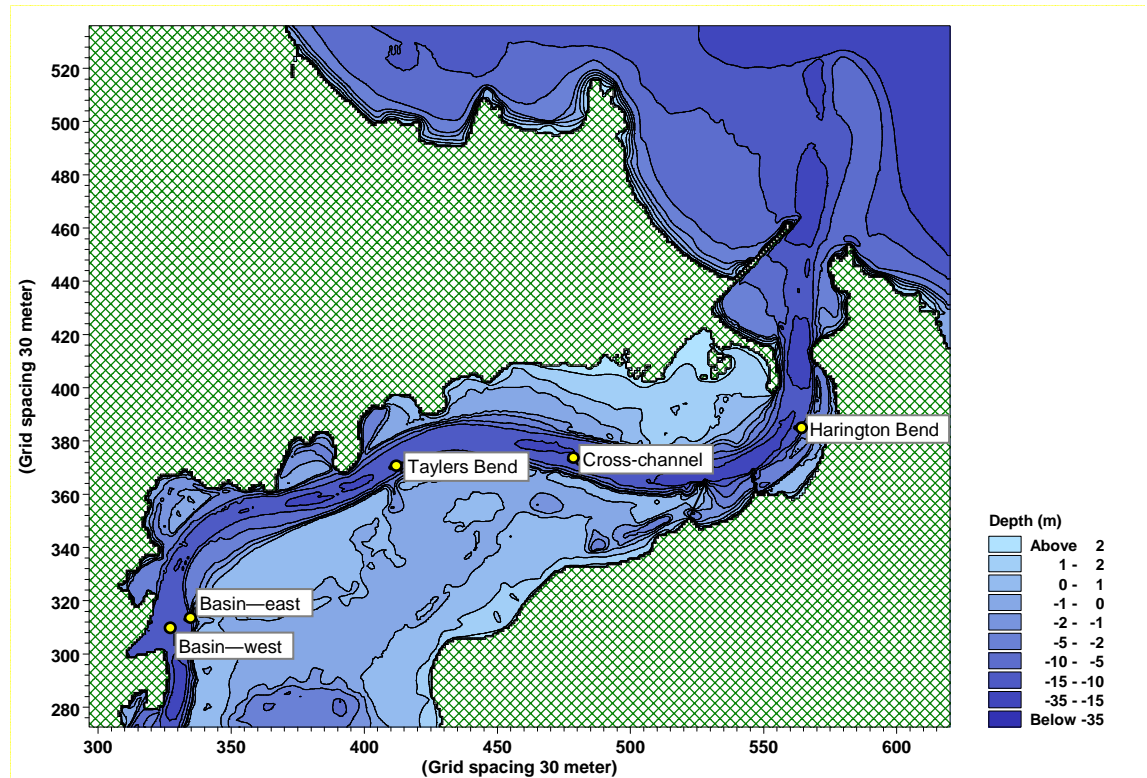


Figure 7.2: The five representative channel source-area sites used as the discharge source locations for dredged-cycle suspended-sediment plume simulations.

Table 7.3: Factors used to pro-rata the accumulated deposition depths from the 14-day plume model simulations for each source-area for a summation of the total deposition over the dredging programme. They were estimated from required dredging volumes clumped together into five channel discharge source locations (Fig. 7.2) and partitioned separately for “sand” and “silt” claims. Values apply to the 15-m dredged harbour-channel (final design). Because the dredging period is not definite, the dredging effort required for each discharge source location is expressed as a % of total dredging days that would affect the Harbour.

Channel discharge source (Fig. 7.2)	Model output factor (“sand” sources)	% of total dredging days (“sands”)	Model output factor (“silt” sources)	% of total dredging days (“silts”)
Harington Bend	1.44	20.4%	0.57	8.1%
Cross-channel	0.44	6.2%	0.32	4.5%
Taylers Bend	0.28	4.0%	1.22	17.3%
Basin—west	0.03	0.4%	0.62	8.8%
Basin—east	1.18	16.7%	0.96	13.6%

Note: dredging days for “sand” and “silt” claims are not proportional to volumes dredged as dredging sands is more efficient than for predominantly-silt sediments.

7.4 Harbour plume modelling approach

Flow fields for the sediment plume modelling were extracted from the MIKE-21 hydrodynamic simulations for the existing channel bathymetry, rather than the simulations for the completed 15-m deep channel option. Simulations for the existing channel hydrodynamics and depths are relevant to conditions at the commencement of the dredging project, while the other set of hydrodynamic simulations only relate to the final design channel depth at the completion of the project. Using the existing hydrodynamics will be more conservative in terms of both seabed deposition and suspended-sediment concentrations (SSC) because the channel will be shallower and the near-bed discharges from draghead and propeller disturbances will be higher relative to Chart Datum than at design channel depths. (Note: overflows will be at a constant depth below the water surface, which won't change much before or after dredging). As the channel dredging approaches its final design depth, the sediment plumes are likely to be more constrained within the main channel, especially as the flanks of the channel adjacent to intertidal banks are cut down to design depth, and channel velocities generally slow down somewhat relative to existing situation.

Suspended-sediment plume simulations were set up for each of the 5 source areas (Fig. 7.2), running for the same 14-day neap/spring tide cycle with typical winds, as discussed in Section 6.10. Two 14-day simulations were undertaken per source area for predominantly “sand” claims and predominantly “silt” claims.

On/off cycles for the two sediment types and the two types of discharge source (near-bed disturbances and overflows in Table 7.1) were constructed for a 14-day sequence as input to the plume model simulations. As discussed in Section 6.10, we adopted mid-range dispersion coefficients and the median silt-grain size distributions.

Subsequent resuspension of settled sediments was not included in the simulations (see also Chapter 6), so the predicted seabed deposition depths will generally be conservative, except those areas of the Harbour unaffected by initial deposition within a 14-day neap/spring tide simulation.

The results from the 14-day sediment-plume simulations were processed as follows:

- SSC in each model grid cell was averaged over the 14-day simulation and plots of the depth-averaged concentration in kg/m^3 produced for dredging from both “sand” and “silt” claims for each of the source-area discharges.
- Seabed deposition accumulated at the end of the 14-day simulation in each model grid cell was plotted in mass per unit area (kg/m^2) for both “sand” and “silt” claims for each of the source-area discharges.

- The Harbour receiving environment was divided into a number of distinct sub-areas as shown in Figure 7.3, and the results for each sub-area tabulated in the form:
 - % of time the SSC was in various concentration ranges within a sub-area.
 - % area across the total sub-area that the accumulated deposition reaches specified bands of deposition depths plus average and maximum deposition depth.
- Finally, the deposition in each sub-area of the Harbour was integrated up to cover 120 continuous dredging days by applying the factors from Table 7.3 to pro-rata the accumulated deposition values from the relevant 14-day plume simulations for each of the discharge sources.

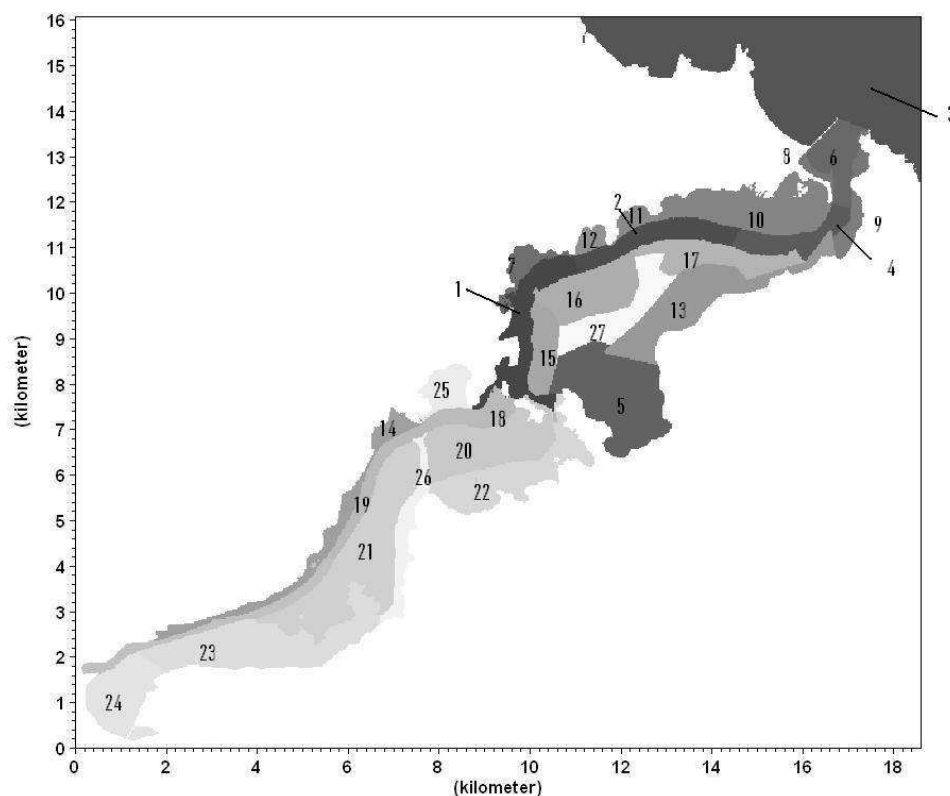


Figure 7.3: The Otago Harbour receiving environment divided into sub-areas for integrating the seabed sediment deposition results from dredging sediment sources at five different channel discharge locations. The numbers for each sub-area are used along with a descriptive location name in the tabulated results below. Areas in hectares of these sub-areas are listed in Table 7.6.

7.5 Predicted results for SSC and deposition from Harbour dredging

This section presents plots and tables of the plume-model results based on five source-area sites in the channel for both predominantly “sand” and “silt” dredging claims. Note: the plume modelling only considered the silt-sized fraction from the “sand” and “silt” dredging claims.

The results for suspended-sediment concentrations (SSC) relate to a shorter turn-around time for the dredger based on a return voyage to an initial offshore disposal area at A1, whereas the final choice of disposal area at A0 is 3.2 km further offshore (which adds about 15 minutes to the turn-around times). This means the modelled SSC variations over time will be slightly more conservative because in the model simulations there is less time to recover between dredging runs. However, maximum SSC values will be the same irrespective of turnaround times, as they are a function of the dredger’s pumping and discharge rates.

7.5.1 Average SSC over a 14-day spring/neap cycle

Suspended-sediment concentration (SSC) averaged over each 14-day plume simulation was calculated for each model grid cell (30 m × 30 m) and plotted in Figures 7.4 to 7.8 for each of the five discharge sources. Concentrations are presented in kg/m³, where 1 kg/m³ is equivalent to 1000 mg/L and 0.1 kg/m³ is equivalent to 100 mg/L.

Concentrations from the MIKE-21 PA plume model are averaged over the entire depth of the water column at the time of calculation, so the 14-day SSC averages shown in the plots are also averages over the water depth (mid-tide to seabed level). However, because the sediments are discharged at depth and they preferentially settle (even though there will be some upwards vertical dispersion), the SSC will be distributed unevenly through the water column, skewed towards much higher-than-average SSC near the seabed compared to a lower-than-average SSC at the water surface. This skewed distribution also occurs naturally with tidal current or wave stirring of bottom sediments, where the SSC is far greater just above the seabed than at the surface - more so the deeper the water column and the larger the grain size.

The plots show the following key results:

- the dredger discharges in the Turning Basin (Figs. 7.4 & 7.5) would have the most influence on elevating average SSC above background levels in the Upper Harbour, in contrast to dredging at Harington Bend and beyond (Fig.

7.8), which would have little influence on SSC in the Upper Harbour beyond Goat and Quarantine Islands;

- the highest depth-average SSC values (e.g., over 100 mg/L with some patches up around 1000 mg/L) would occur in the main shipping channel, subsidiary side channels e.g., channel north of Quarantine Island through to Portobello Peninsula (Figs. 7.5–7.7), and on the intertidal banks adjacent to these channels e.g., the mid-harbour intertidal banks from discharges at Harington Bend (Fig 7.8);
- discharges from predominantly-silt areas (top panels of Figs. 7.4–7.8) show a wider spread of affected areas onto intertidal flats and side channels than discharges of silt-sized material from predominantly-sand areas (bottom panels). This difference relates directly to the magnitude of the discharge or flux of silt-sized material, which was set to 1000 kg/s for “silt” claims compared to 60 kg/s for “sand” claims, even though the latter discharge would run for much longer. However, there wouldn’t be widespread dispersion of these finer silt-sized sediments over large tracts of the Harbour, as the channel tidal streams dominate the transport of suspended sediments rather than dispersion/spreading processes. Also there would be only limited opportunities around the more quiescent period either side of high tide when diluted plumes from the overflow sources - that discharge most of the time at 5 m below the surface (except at Turning Basin–East) - can spread out further over adjacent intertidal or shallow sub-tidal areas;
- while there is only a short distance separating the two Turning Basin source locations (east and west on Fig. 7.2), there would be a substantial divergence in areas affected by suspended-sediment plumes due to the strong flow divergence at Quarantine Island. From the “west” source location, discharge plumes would be transported up the Victoria Channel partway into the Upper Harbour (Fig. 7.4), while plumes from the “east” source location would be preferentially transported and dispersed to areas around the Portobello Peninsula and into the Latham Bay area of the Upper Harbour (Fig. 7.5). The wider spread of average SSC in Figure 7.5 (compared to Fig. 7.4) is also a function of the overflow discharge being set to only 1 m below the surface for the first half of the 14-day simulation for the eastern side of the Turning Basin;
- most of the eastern side of the Lower Harbour from Te Rauone Beach to Harwood would be largely unaffected by discharge sources other than the Harington Bend discharge location, and then only in patches (Fig. 7.8);

- the eastern side of the Upper Harbour from Grassy Point to Dunedin would be also largely unaffected by sediment discharge sources;
- 14-day average SSC will be low in the plume that emanates from the Mole to Taiaroa Head channel section for dredging claims in the Turning Basin, but will gradually increase up to a depth-average SSC of 100–200 mg/L for discharge sources at Harington Bend. These average SSC levels offshore from the Mole would reduce somewhat as the dredger works the Howlett claim (between Harington Point and the Mole) and further reduce in the Outer Channel claim as the silt content of the sandy seabed sediments reduces considerably to virtually nil.

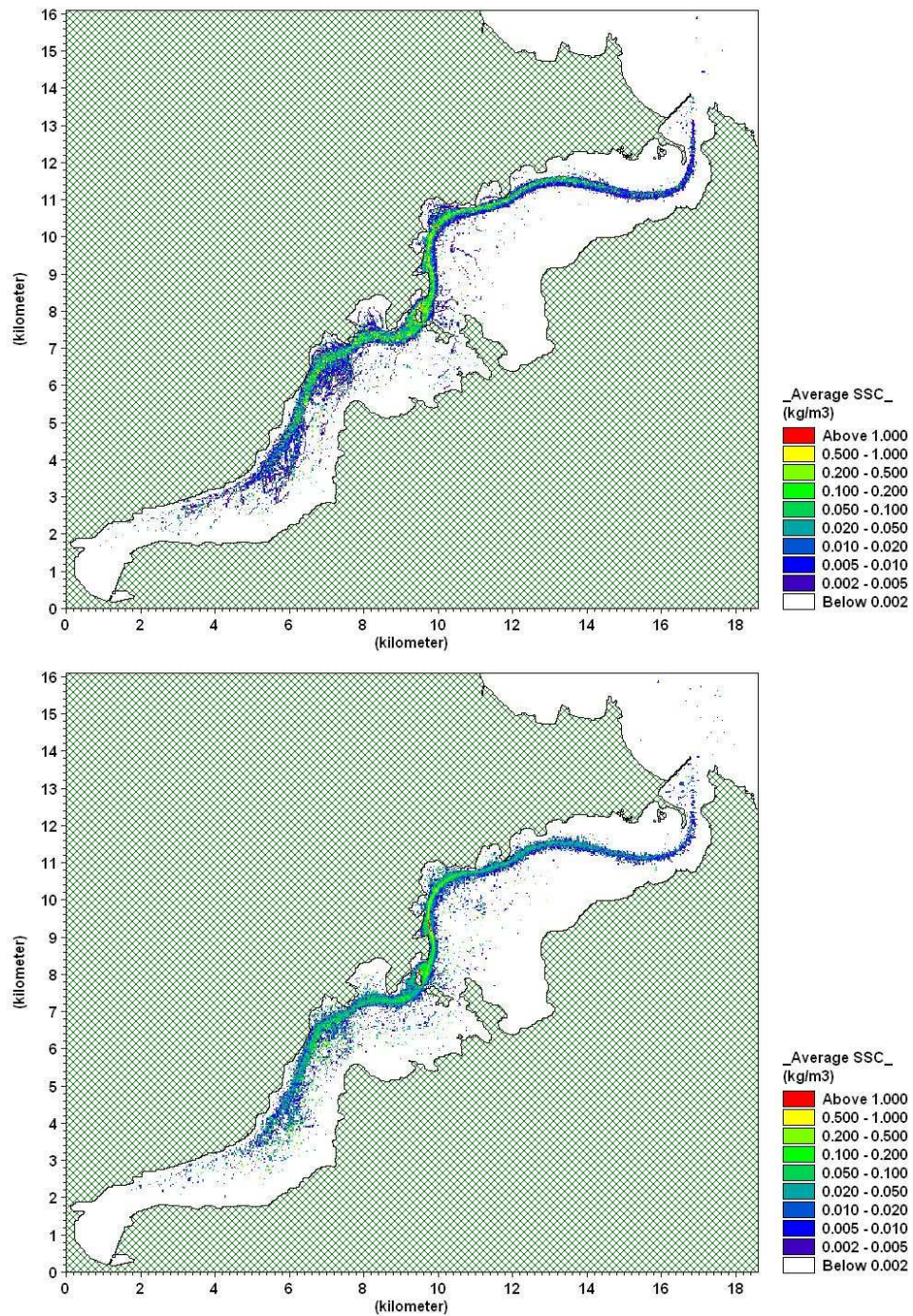


Figure 7.4: 14-day average SSC in kg/m³ for a Basin-west discharge source for predominantly-silt claims (TOP) and predominantly-sand claims (BOTTOM).

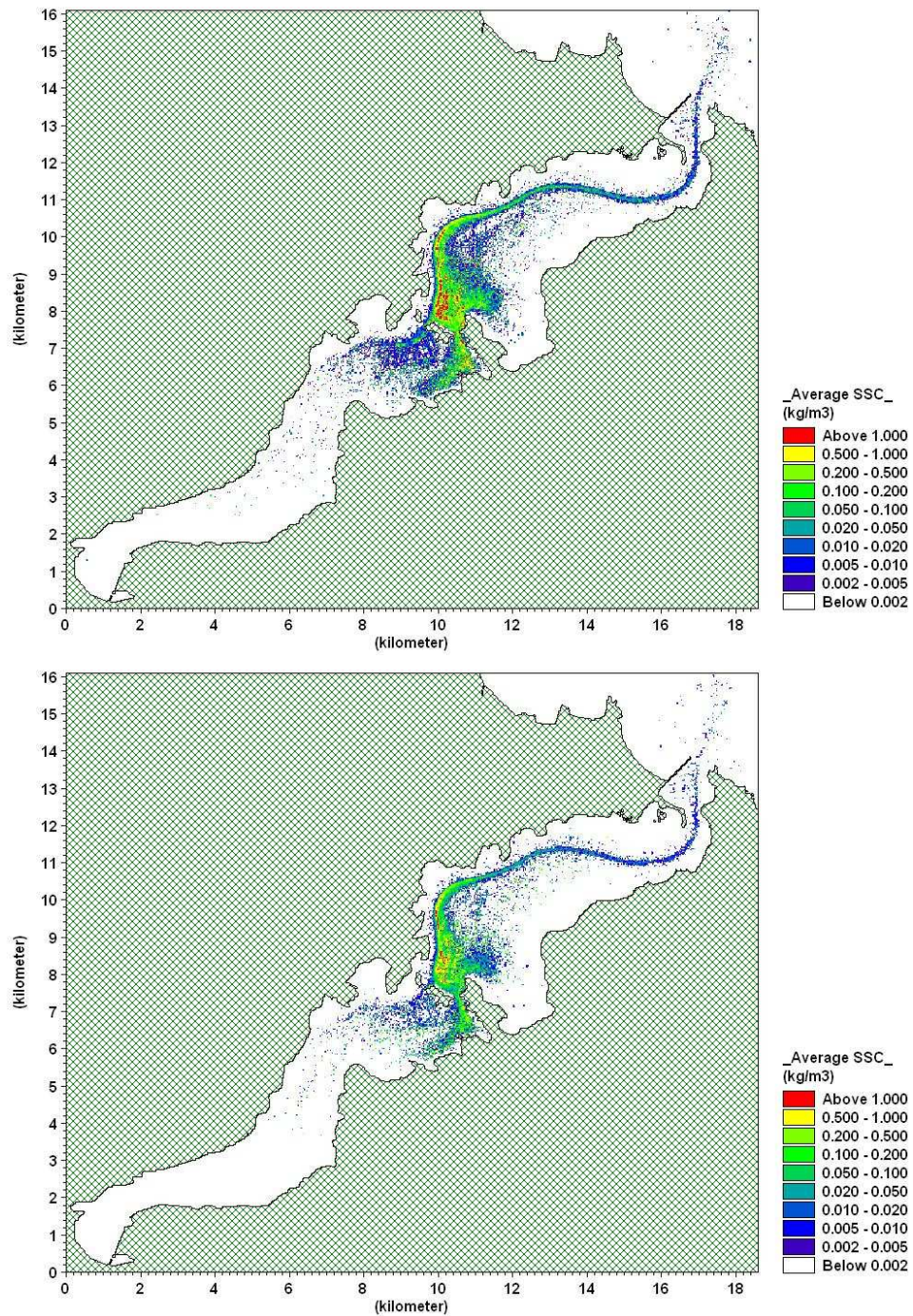


Figure 7.5: 14-day average SSC in kg/m³ for a Basin-east discharge source for predominantly-silt claims (TOP) and predominantly-sand claims (BOTTOM).

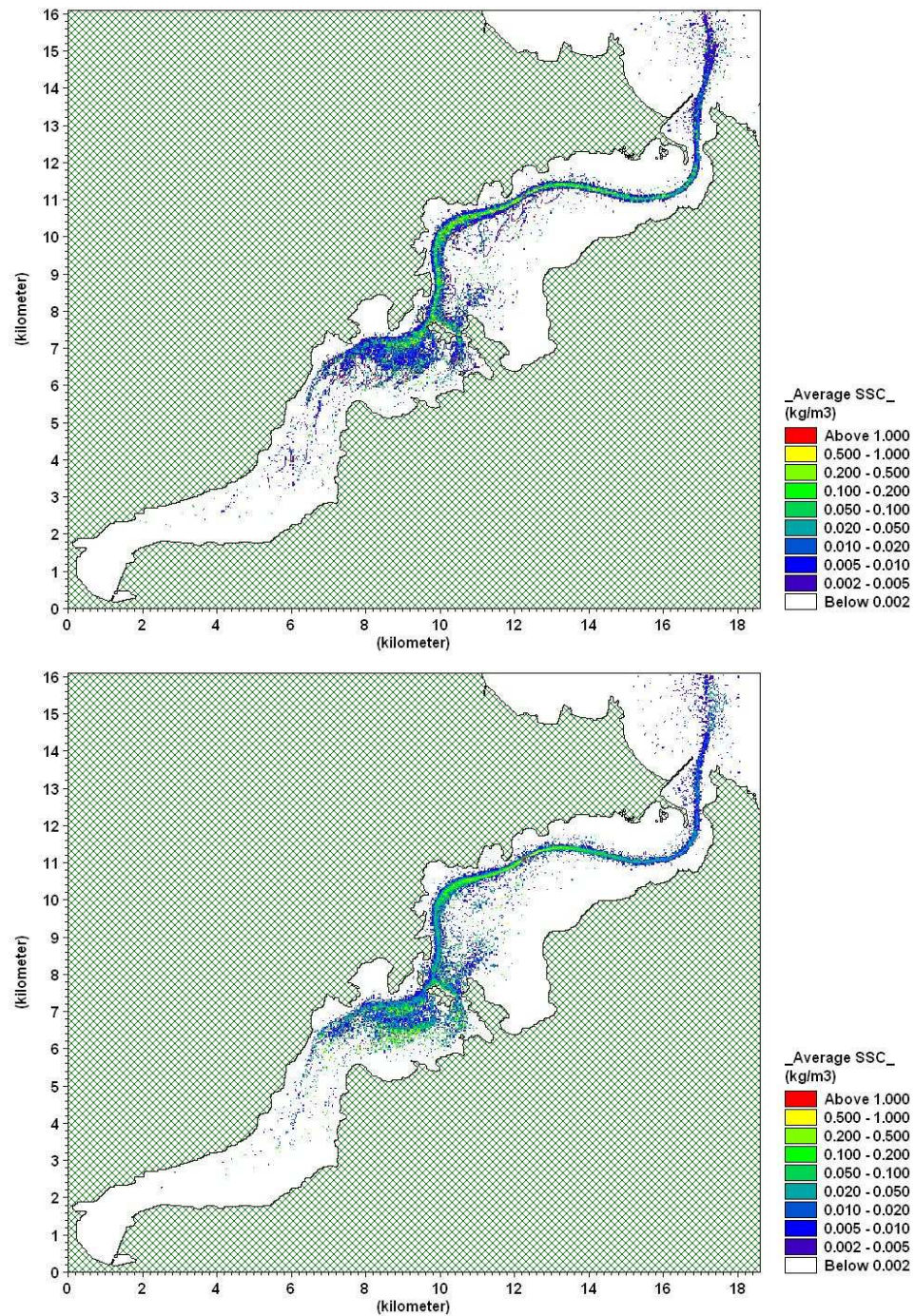


Figure 7.6: 14-day average SSC in kg/m³ for a Taylers Bend discharge source for predominantly-silt claims (TOP) and predominantly-sand claims (BOTTOM).

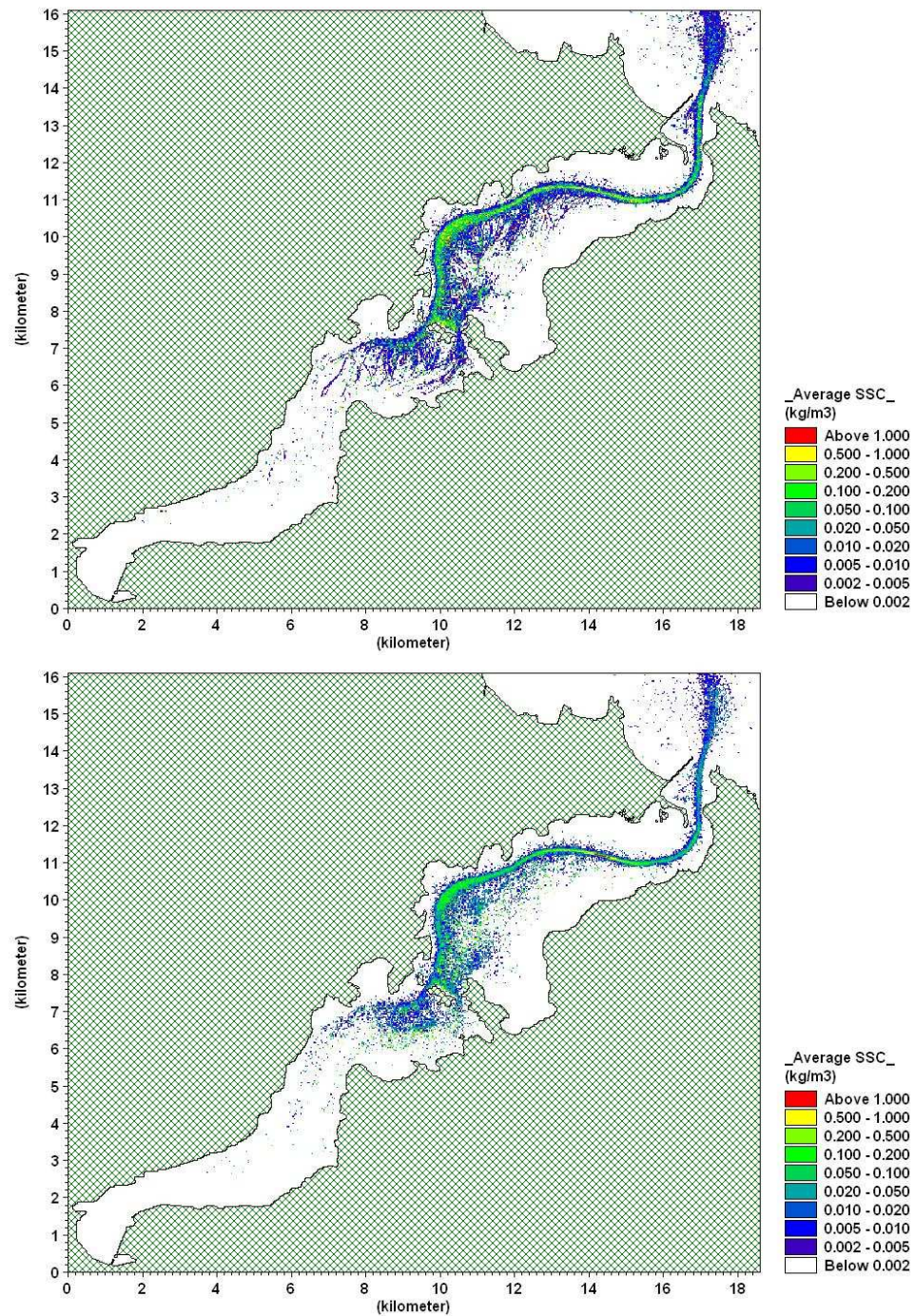


Figure 7.7: 14-day average SSC in kg/m³ for a Cross-channel discharge source for predominantly-silt claims (TOP) and predominantly-sand claims (BOTTOM).

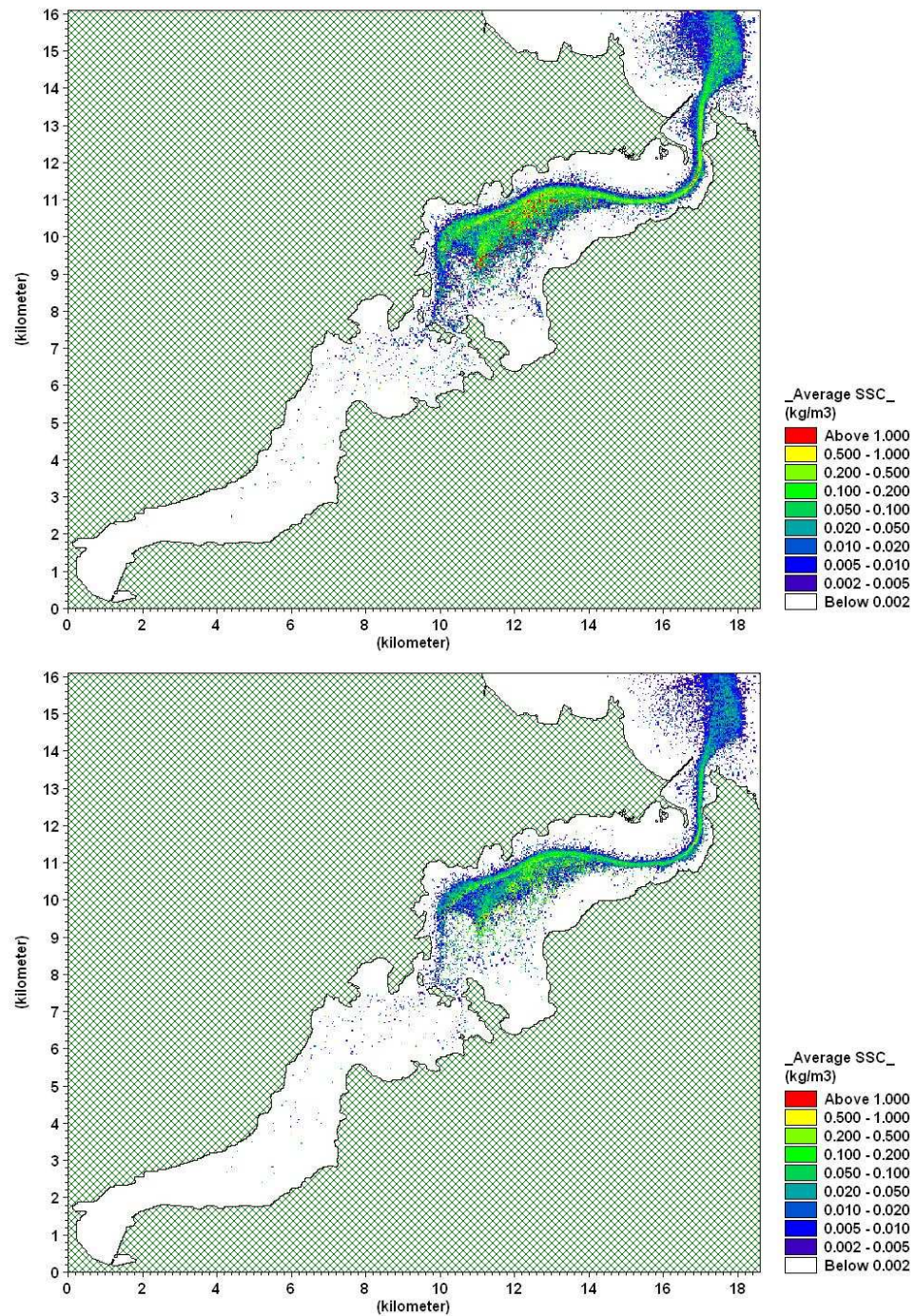


Figure 7.8: 14-day average SSC in kg/m³ for a Harington Bend discharge source for predominantly-silt claims (TOP) and predominantly-sand claims (BOTTOM).

7.5.2 Statistics of 14-day plume model results for SSC

The above results show the spatial distribution of the depth-average SSC, averaged in each model cell over a fortnight. A statistical summary of the SSC plume model simulations for each discharge source area is provided at the end of the Chapter in Table 7.4. The % of time that the depth-averaged SSC is in various brackets of excess concentration (above background) from zero to >400 mg/L is listed for each of the 27 sub-areas of the Otago Harbour environment (Fig. 7.3), for different source discharge areas (5 sites in Fig. 7.2) and for predominantly-sand and predominantly-silt dredging simulations.

The most obvious result from Table 7.4 is that in all sections of the Harbour (leaving aside the main shipping channel), the % of time that the excess SSC is zero is quite high - often 80% of the time or more. This would occur because the dredging discharges are not continuous, but cyclic with gaps of up to 1.8 hours (Table 7.2), and the tidal flows reverse every 6 to 6.5 hours, providing lengthy periods at “upstream” sites for silt-sized material to settle out.

Conversely, Table 7.4 shows there would be few Harbour sub-areas where the depth-averaged SSC exceeds 400 mg/L for 5% of the time or more (over and above the background concentration). This would only occur in sub-areas covering the main shipping channel, close to the relevant discharge source, and three intertidal sub-areas adjacent to the main shipping channel in the middle of the Lower Harbour: a) sub-area 15 (Port Inter-tidal) for a Basin–West and a Taylers Bend discharge; b) sub-area 16 (Pulling Inter-tidal) and sub-area 17 (Tayler Inter-tidal) for a Cross-channel discharge site.

Because of the high % of time at near zero excess SSC, but with short bursts of high concentrations (see > 400 mg/L column in Table 7.4), the variation of SSC with time is quite skewed. This means the 14-day average SSC values presented in the previous section are also skewed to higher magnitudes than if medians (i.e., concentration which was exceeded for 50% of the time) were calculated, so using averages is more conservative.

7.5.3 Accumulated seabed deposition over a 14-day spring/neap cycle

Accumulated seabed deposition over each 14-day plume simulation was calculated for each model grid cell (30 m × 30 m) and plotted in Figures 7.9 to 7.13 for each of the five discharge sources. Deposition is presented in mass of sediment per unit area of seabed (kg/m²). These deposition values are generally conservative as no subsequent

resuspension by competent tidal currents or wind-wave stirring was included in the plume model simulations, which will act to further spread and disperse some of the initially-settled material.

To convert to the predicted thickness of deposition (mm), a settled wet bulk density has to be assumed. For this analysis, and the accumulated deposition heights presented in the next section, a wet bulk density for recently-settled sediments was assumed to be around 1300 kg/m^3 . This value is substantially lower than the range of in-situ bulk densities currently in the channel, and therefore conservative as it will produce higher estimates of deposition thickness than may be the case in practice. Consequently, the highest band of deposition above 5 kg/m^2 (red) in Figures 7.9–7.13 equates to a 3.8 mm thickness (dividing 5 by the density 1300) that would be accumulated over the 14-day simulation period, which converts to a rate of 0.3 mm per day.

The plots (Figs. 7.9–7.13) show the following key results for seabed deposition over a 14-day neap/spring tide cycle with varying winds:

- Deposition at or above 5 kg/m^2 (red) or approximately 3.8 mm over a fortnightly period is largely confined to: a) the main shipping channel (all discharge sources); b) the subsidiary channel to the east from Quarantine Island (Figs. 7.10–7.12); c) around Goat Island and up Victoria Channel to opposite St. Leonards for a discharge source at Turning Basin–west (Fig. 7.9); and d) some of the flanking intertidal flats to these channels.
- Discharges from predominantly-silt claims (top panels in Fig. 7.9–7.13) would cause higher deposition thicknesses (and daily deposition rates) than from predominantly-sand claims (bottom panels), even though the overflows would occur much longer (60 minutes) for the latter. This is because the discharge rate or flux of silt-sized material has been set to a much higher rate of 1000 kg/s for “silt” claims, than when dredging “sand” claims (silt flux of only 60 kg/s). The much smaller but longer overflow discharge of silty material when dredging “sandy” sites, allows the silt-sized material to disperse more widely causing lower local deposition rates. This result shows that any measures targeted at reducing overflows to a minimum, when dredging predominantly-silt areas of the channel, would substantially reduce environmental effects arising from deposition of fine sediments.
- The Upper Harbour would have virtually no discernable seabed deposition arising from discharge sources at Harington Bend and further seaward (Fig. 7.13).

- Most of the eastern parts of the Lower and Upper Harbours would be subject to little or no deposition, apart from the reach from Latham Bay to Yellow Head (west of Portobello Peninsula) for discharges from the eastern side of the Turning Basin, Taylers Bend through to the Cross-channel, and in the subsidiary channel from Te Rauone Beach to Ohinetu Point from Harington Bend discharge sources.
- Deposition rates would gradually increase from 0.5 to 5 kg/m² (or 0.4 to 3.8 mm) per fortnight in the area centred on the outer approach channel and ebb-tide bar, seaward of the Mole, as the dredger works the Harington Bend area and seawards (Fig. 7.13). However, these deposits in the area beyond the Mole are unlikely to remain in place for long due to the active wave climate which will continue to re-mobilise these sediments and in conjunction with currents, further spread the seabed material offshore, alongshore and some back through the Harbour Entrance.

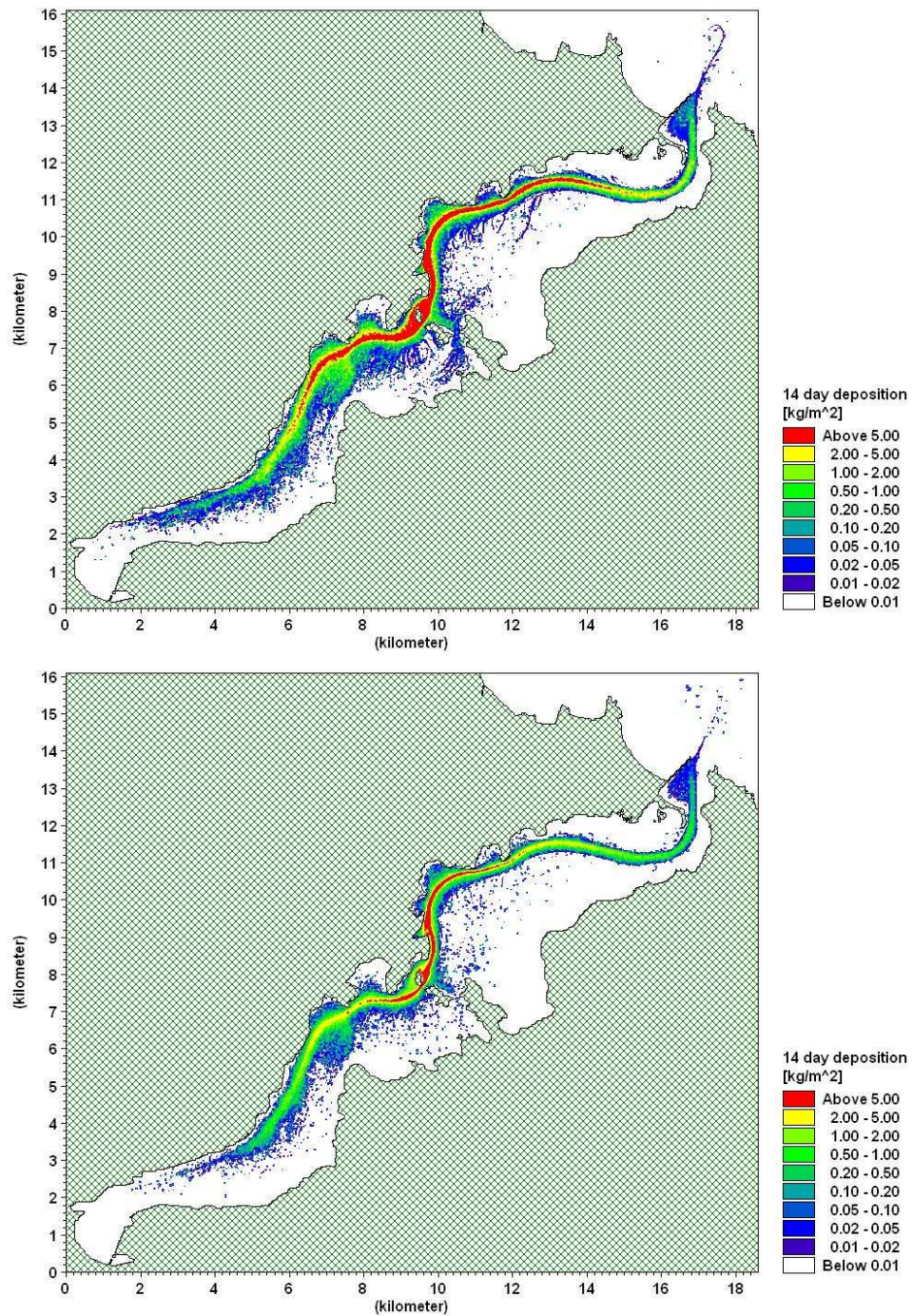


Figure 7.9: 14-day accumulated seabed deposition in kg/m^2 for a Basin-west discharge source for predominantly-silt claims (TOP) and predominantly-sand claims (BOTTOM).

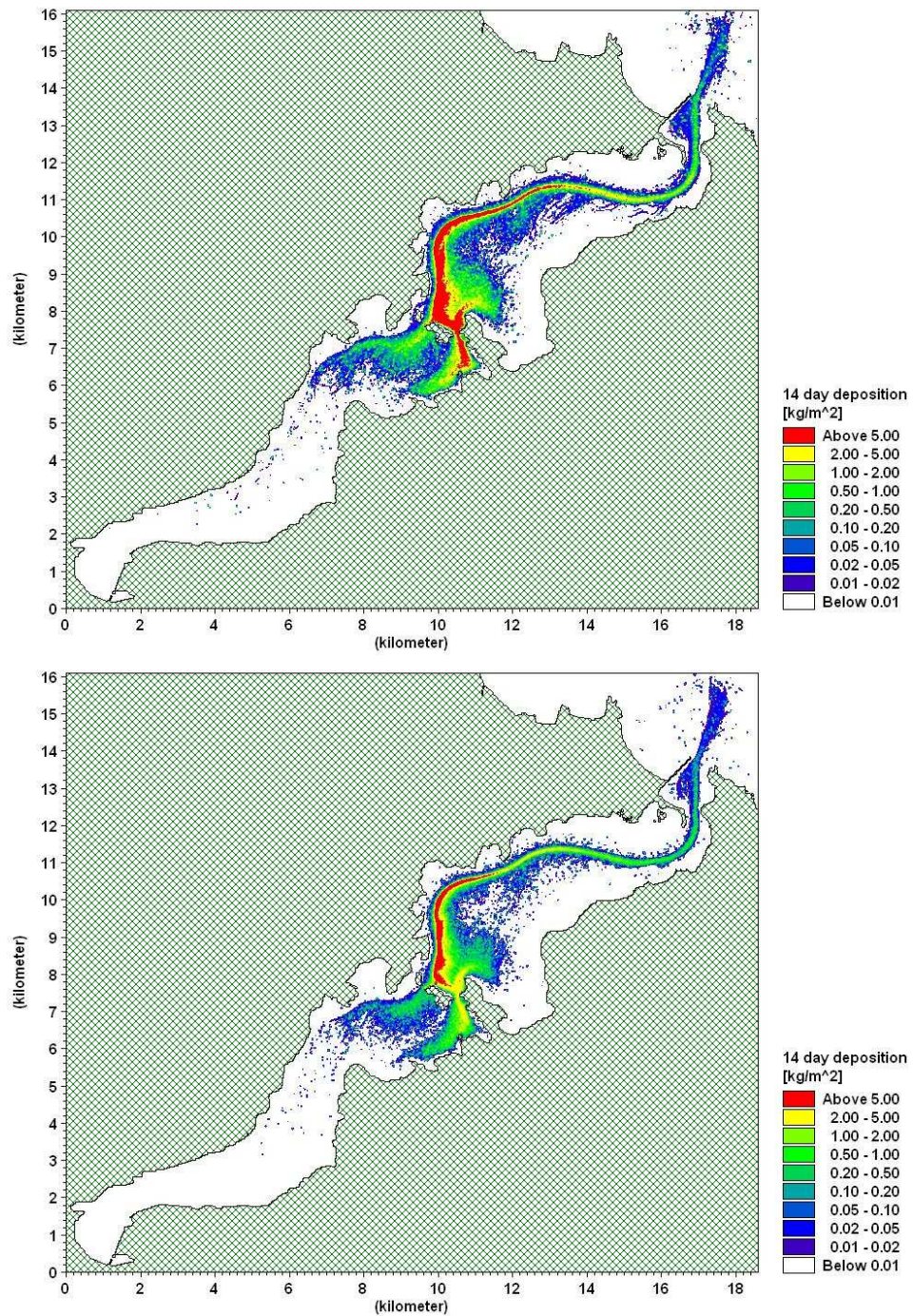


Figure 7.10: 14-day accumulated seabed deposition in kg/m² for a Basin-east discharge source for predominantly-silt claims (TOP) and predominantly-sand claims (BOTTOM).

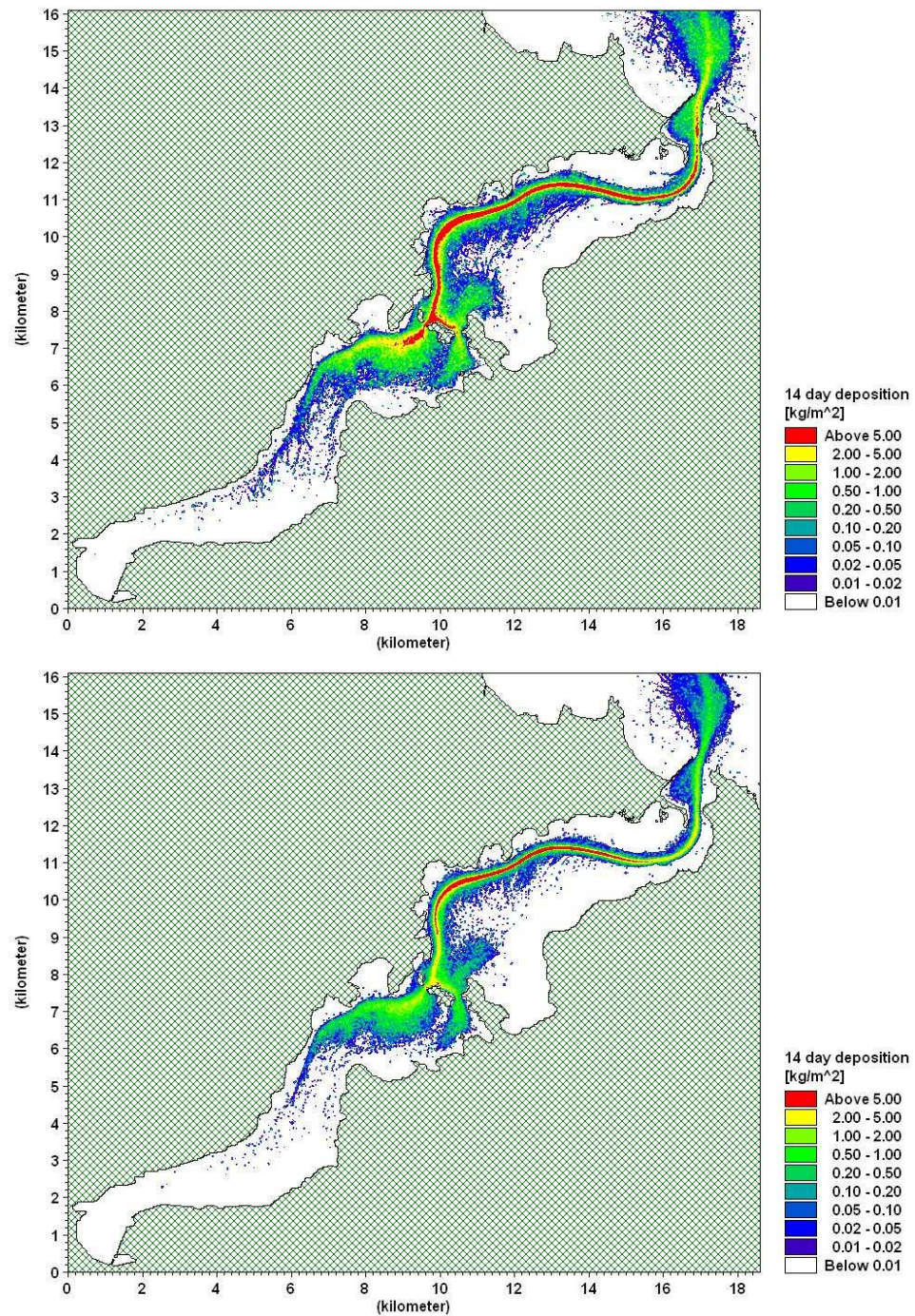


Figure 7.11: 14-day accumulated seabed deposition in kg/m² for a Taylers Bend discharge source for predominantly-silt claims (TOP) and predominantly-sand claims (BOTTOM).

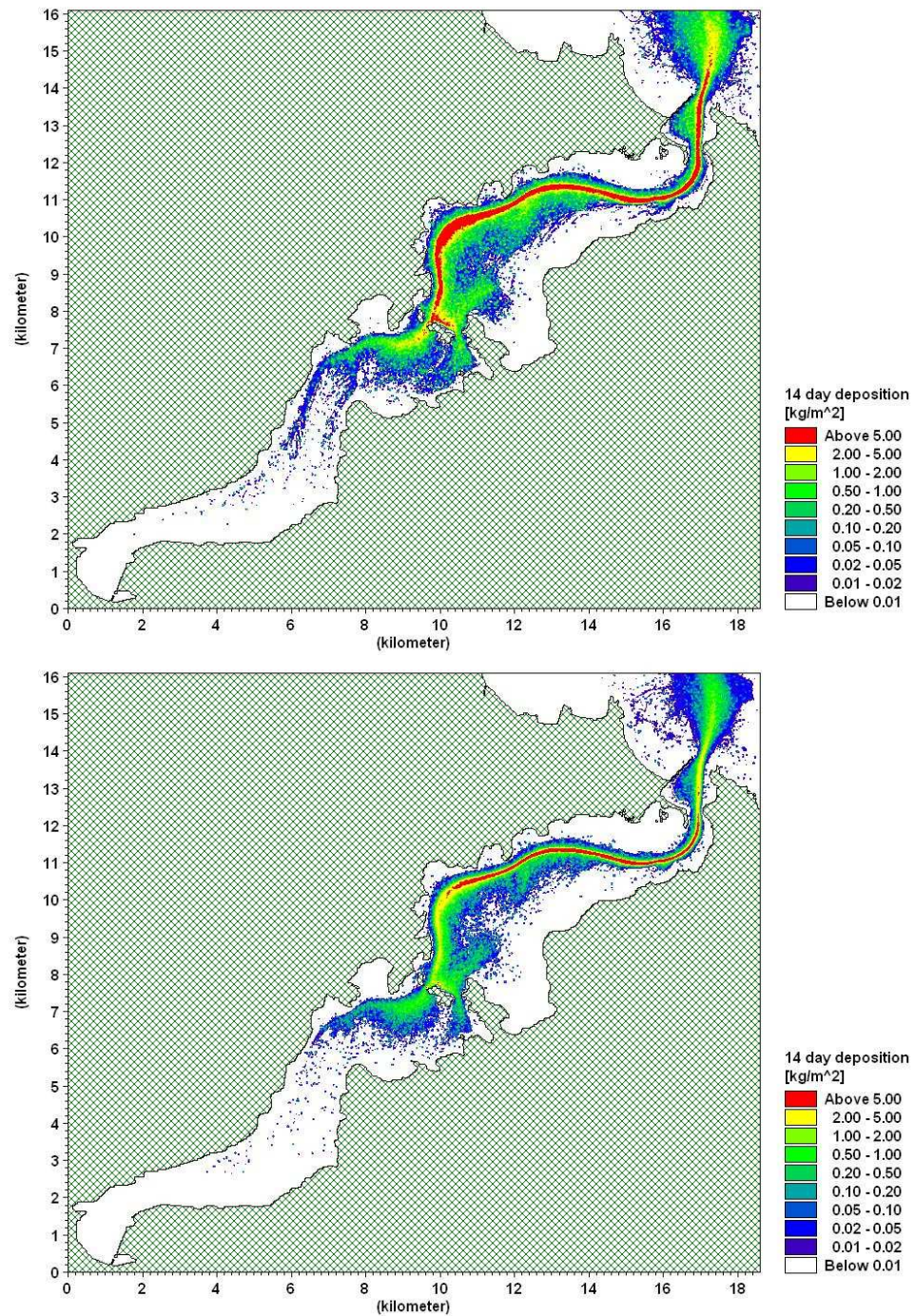


Figure 7.12: 14-day accumulated seabed deposition in kg/m² for a Cross-channel discharge source for predominantly-silt claims (TOP) and predominantly-sand claims (BOTTOM).

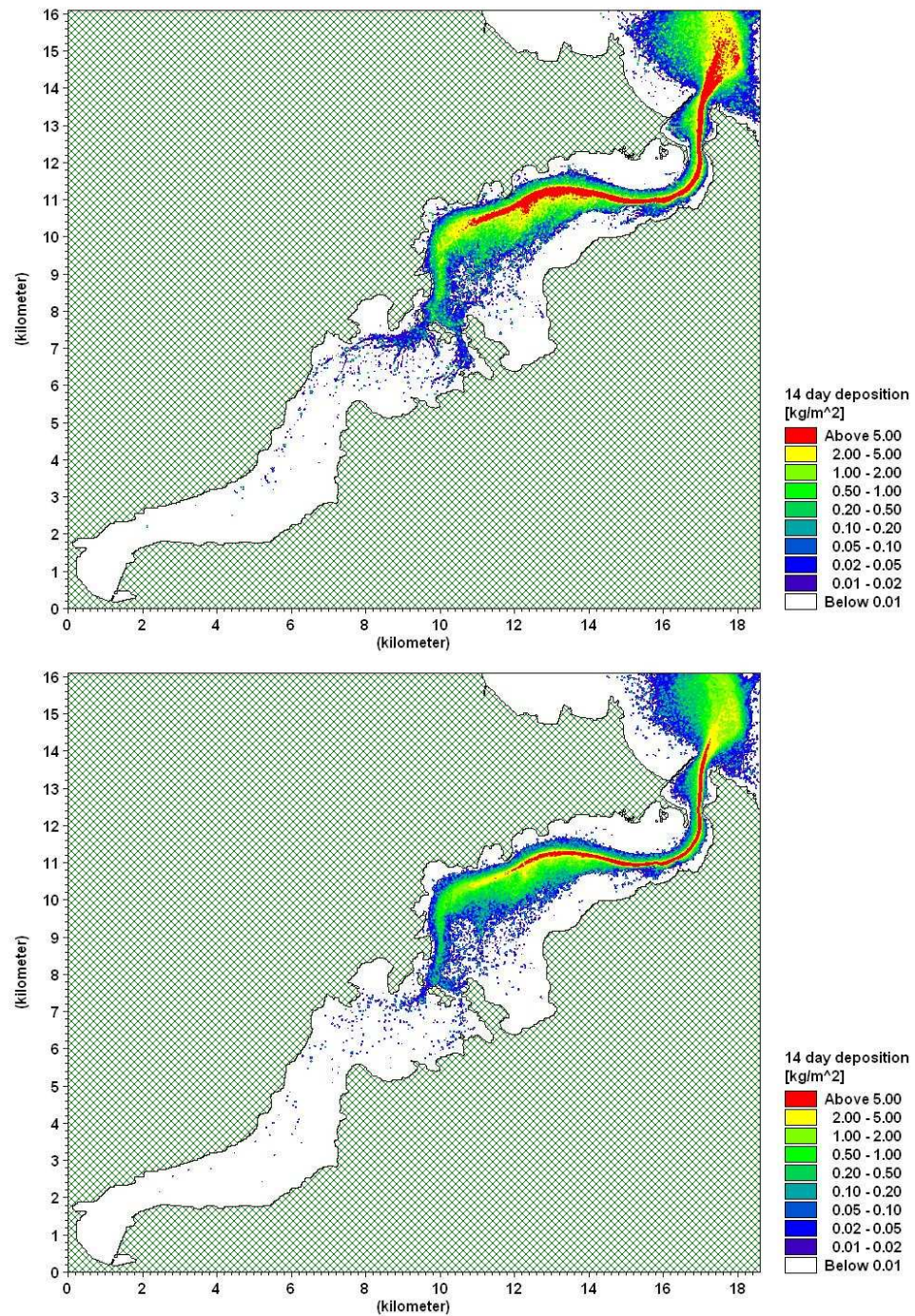


Figure 7.13: 14-day accumulated seabed deposition in kg/m^2 for a Harington Bend discharge source for predominantly-silt claims (TOP) and predominantly-sand claims (BOTTOM).

7.5.4 Statistics of 14-day plume model results for accumulated deposition

The above results show the spatial distribution of the accumulated deposition in each model cell over a fortnight for different source areas. A statistical summary of the accumulated deposition from the plume model simulations for each discharge source area is provided at the end of the Chapter in Table 7.5. The % of each of the Harbour sub-areas that the deposition thickness would be in various brackets from zero to >5 mm in height is listed for each of the 27 sub-areas of the Otago Harbour environment (Fig. 7.3), for different source discharge areas (5 sites in Fig. 7.2) and for both predominantly-sand and predominantly-silt dredging simulations.

The most obvious result from Table 7.5 is that most sub-areas, except the main or subsidiary channels and adjacent intertidal sub-areas, only small thicknesses of settled sediments of <0.1 mm would occur over a fortnight (1st and 2nd result columns in Table 7.5).

Sub-areas that would generally experience higher deposition thicknesses >5 mm in a fortnight are in the main shipping channel from the Mole to Port Chalmers and while other sub-areas for >5 mm deposition over more than 5% of the sub-area would be more specific to the source discharge site:

- Basin–west sources: sub-area 18–Goat Channel (29% of this sub-area for “silt” claims).
- Basin–east sources: sub-area 15–Port Inter-tidal (29% and 12% of this sub-area for “silt” and “sand” claims respectively); sub-area 22–Pudding Inter-tidal (5% of sub-area for “silt” claims).
- Cross-channel sources: sub-area 17–Tayler Inter-tidal (8% of sub-area for “silt” claims).

As mentioned earlier, it would be discharges from the “silt” claims which produce the highest % of sub-area with deposition >5 mm, so any measures to reduce the time of overflows working “silt” claims would bring about reductions in deposition thicknesses and rates.

7.5.5 Deposition accumulated over the entire dredging programme

Silt deposition in each sub-area of Otago Harbour (Fig. 7.3 or 7.14) was finally integrated up by applying the factors from Table 7.3 to the accumulated deposition values from the relevant 14-day plume simulations for each of the discharge sources. No subsequent resuspension of these settled silts was included.

The results of predicted accumulated silt deposition from dredging in the Harbour are summarised in Table 7.6, based on units of 30×30 m model cells. A range of statistics were used to summarise the accumulated deposition, including % of the sub-area where deposition was nil, the average thickness in model cells across the sub-area, and three percentage deposition values (median or 50%, 90% and 99%) that relate to the percentage of cells with less than that deposition thickness within the sub-area. For example, the 90% deposition thickness means that 90% of the cells in the sub-area would be below that accumulated thickness (or another way, the thickness exceeded within 10% of all cells in that sub-area). Each sub-area has a different areal extent, so Table 7.6 also provides the area in hectares that relate to the various statistics on predicted deposition thickness in Table 7.6.

The average sediment deposition across all cells in any sub-area is higher than the median deposition because of the skewed distribution of most model cells showing minimal or low deposition thicknesses but a small number of cells receiving higher deposition. Therefore, the median will be smaller than the average across any sub-area.

Model results for accumulated deposition show a marked difference between predictions of accumulated deposition on the seafloor of the main shipping channel and all other sub-areas. In the shipping channel, deposition values are much higher and few areas are untouched. 90%-deposition values within the main shipping channel in various sections range from 21 mm (sub-area #6–Spit Channel) to 55 mm (sub-areas #1,2–Port Chalmers and Cross Channel). These high predicted deposition values on the channel floor don't include subsequent resuspension by tidal currents and/or wind waves, so are somewhat unrealistic. They occur in the model when sediments settle out in more quiescent periods of the ebb or flood tide slack periods, but in the model they remain fixed to the bed thereafter. In practice, these sediments will be re-mobilised frequently by stronger tidal currents, until eventually a proportion is flushed through the main channel system and some exported, while some material re-settles in areas of the channel and consolidates into the fabric of sands on the channel floor.

As listed in Table 7.6, other Harbour sub-areas (see Fig. 7.3 or 7.14) which would exhibit 99%-deposition levels of up to 10 mm or more during the dredging programme (i.e., level exceeded in only 1% of model cells), would be:

- Sub-area #18–Goat Channel: the reach of Victoria Channel to Kilgours Point (99% of model cells would have accumulated deposition thickness of less than 14 mm).

- Sub-area #5–Portobello: sub-area covers Portobello Bay, but most of the deposition would occur in the side channel off Quarantine Point at the tip of Portobello Peninsula (99% of model cells would have accumulated deposition thickness of less than 10 mm).
- Sub-area #13–Harwood Inter-Tidal: this sub-area covers much of the eastern section of the Lower Harbour from Te Rauone Beach to Harwood, but most of the higher sediment deposition would occur in the central intertidal banks and shallows adjacent to sub-area #17–Tayler Inter-tidal, and arise from a Harington Bend discharge source (99% of model cells would have accumulated deposition thickness of less than 24 mm).
- Sub-area #15–Port Inter-tidal, Sub-area #16–Pulling Inter-tidal and Sub-area #17–Tayler Inter-tidal: these three sub-areas that make up the contiguous central Lower Harbour sandbanks adjacent (port side) to the main shipping channel and would experience in 99% of model cells, accumulated deposition thicknesses of less than 82 mm, 15 mm, and 13 mm respectively. The much higher accumulated deposition for the Port intertidal banks (from Port Chalmers to Quarantine Island) would arise mostly from dredging on the eastern side of the Turning Basin (see Fig. 7.10).
- Sub-area #22–Pudding Inter-tidal: this sub-area extends from Quarantine Island to Grassy Point, but most of the deposition would occur in the subsidiary channel from Quarantine Island to Latham Bay from a Basin-east discharge source (99% of model cells would have an accumulated deposition thickness of less than of 13 mm). See Figure 7.10 for locations of highest deposition.

Outside the main shipping channel, the highest median deposition in any other sub-area would occur for sub-area #15–Port Inter-tidal with half the model cells showing accumulated deposition of 4 mm or more during the dredging programme, followed by 3 mm or more for half the cells in sub-area #18–Goat Channel. Otherwise, the median deposition in all other sub-areas is small at less than 1 mm during the dredging programme.

The *rate* of deposition is also important in assessing the effects of any deposition on benthic ecosystems. This requires an estimate of the time to complete the dredging claims that would affect the Harbour (excluding a portion of the dredging claims in the outer approach channel). To obtain an average daily deposition rate over the dredging season simply requires the values in Table 7.6 to be divided by the relevant number of total dredging days. A lower-bound estimate using a 10,800 m³ capacity TSHD is 111

days for discharges likely to influence the Harbour excluding any downtime or around 140 days assuming a 20% down-time factor (see Section 7.3.3). If a smaller dredger is used for part of the dredging programme, a longer dredging season would be needed. However, in reality, each sub-area of the Harbour will be more affected by a source discharge in a particular section of the channel e.g., Quarantine Island to Latham Bay would be mainly affected by dredging from the eastern Turning Basin source, but not much by the Harington Bend claims. In such cases, the daily deposition rate would be higher than the average when dredging occurs at claim sites that more directly affect a particular sub-area of the Harbour. To derive these higher daily deposition rates, the values in Table 7.6 can be divided by the combined total of “sand” and “silt” dredging days for the relevant discharge sources using the % of dredging days listed in Table 7.3. There are other sub-areas though that would experience deposition from dredging in several sections of the channel, particularly the intertidal banks in the central Lower Harbour adjacent to the shipping channel. These banks would be affected by most of the channel discharge sources modelled except Basin-west. Again, the % dredging days in Table 7.3 can be used to combine a total number of dredging days from the relevant sources, and divided into the values in Table 7.6 to calculate daily rates. Apart from the seabed of the main channels, the daily deposition rate in 99% of cells in any Harbour sub-area would be less than 1 mm/day (highest on the intertidal bank opposite Port Chalmers), but mostly less than 0.1 mm/day. These rates would be lower again for a longer dredging season.

Finally, the question of the long-term fate of silts within the Harbour is a difficult one to address with suspended-sediment modelling, as it would involve lengthy computer simulations with a combination of wave, tide and silt-transport models. However, some general tendencies can be inferred from the plume modelling results and our understanding of silt transport in harbours. Firstly, the plume modelling shows that only the main channel and the side channel between Quarantine Island and Portobello Peninsula would be subject to the highest initial deposition thicknesses of greater than 5 kg/m² in 14-days (Fig. 7.9–7.13). These silts would be reworked regularly by tidal currents, especially on spring tides, and spread throughout the entire shipping channel, preferentially settling in more quiescent sections of the channel system and also with a sizeable proportion being exported out the Entrance (as shown by the 14-day plume model simulations). For the exported silts, based on the similar calculations as shown in Table 7.6, sub-area #3 beyond the Mole (Fig. 7.3 or 7.14) would experience in 99% of model cells, accumulated deposition thicknesses of less than 10 mm over the dredging programme. However, given the wave climate outside the Mole, these silts are likely to be resuspended often and disperse widely, with some preferentially settling in the naturally-occurring silt zone further offshore (shown later in Figure 12.26).

Inside the Harbour, on the shallower sub-tidal areas, and intertidal banks, some of the initially settled silts from the dredging operation will be more likely to be remobilized by wind waves rather than currents, and then transported elsewhere in suspension by the current until settling again. Wave remobilization of silts also depends on the interim bed consolidation, cohesiveness and bioturbation. Assuming no cohesiveness, medium silt-size sediments of 0.01 mm diameter, would require exceedance of a wave orbital velocity threshold of 0.05 m/s (using Komar & Miller, 1974 cited in Raudkivi (1990; p 405). For a typical 3-second wave, and a moderately high significant wave height of 0.6 m (see simulations in Section 9.3), this threshold would be exceeded in depths less than about 7 m, which includes most of the Harbour outside the main shipping channels, except a small part of the basin in Portobello Bay (Fig. 3.7). Consequently, during moderate to high waves, silts available for reworking will be winnowed from the seabed surface, especially off exposed shallow areas and intertidal flats where wave orbital velocities can be high. Silts originating from dredging operations inside the Harbour in the long-term would be dispersed further and more thinly throughout the Harbour, eventually finding their way into the main channel system to be exported to the ocean or preferentially settle “permanently” in quiescent areas where wave activity and currents are low or sporadic e.g., the Dunedin basin, behind the railway embankments, sheltered sub-tidal embayments, the lee of groynes or half-tide training walls and in the upper-tide inter-tidal beaches of sheltered embayments. In the Upper Harbour, a guide to where silts could preferentially settle in the long term are those areas that already show a predominance of silt material in seabed samples, as measured by Grove & Probert (1999).

7.6 Summary of Harbour sediment-plume modelling results

We have put together a complex set of sediment plume simulations that are cognizant of realistic dredging operations such as sources of discharge (bottom disturbances and overflows via a pipe underneath the dredger) and detailed estimates of the volumes for dredging claims of predominantly “sands” and “silts” along the channel and using a mid-size Trailing Suction Hopper Dredger (TSHD) of 10,800 m³ hopper capacity.

Where possible, model parameters or set-ups have erred on the conservative side to provide more confidence in using the results for assessing environmental impacts, given field calibration of the plume model in Otago Harbour is not possible for a particular TSHD. Some examples of decisions made to keep the modelling conservative are:

- a) incorporating a sizeable 4-minute overflow discharge of 1000 kg/s when dredging predominantly-silt claims, whereas in reality, pumping would cease just prior to overflows occurring;

- b) discharge rates of sediment have been set at the higher end of the range of values for which field measurements are available e.g., CRIA (2000) and we have assumed a hopper capacity at the higher end of a mid-sized TSHD that is likely to be appropriate for the Otago Harbour situation;
- c) suspended-sediment concentration results from the plume modelling have been presented in terms of saturated-weight of sediment (rather than the normal dry-weight per volume), which means realistically the actual SSC may only be 70-80% of the SSC values presented in this report;
- d) the overflow depth was set to only 1 m below the surface for half the dredging period to accommodate a smaller dredger working on the claim on the eastern side of the Turning Basin—otherwise the overflow was set to 5 m below the surface. Overflows from different mid-size TSHDs can discharge from between 5 and 9 m below the surface;
- e) the full range of tides (spring/neap) have been simulated in 14-day runs, along with a typical sequence of winds (although sensitivity testing showed winds are only a minor factor);
- f) for expediency, the dredging claims from various sections of the channel were all lumped together into only 5 discharge sites. This concentration of the discharges from one point for a 14-day simulation will produce results that are somewhat larger than in reality, particularly for deposition outside the channel. A constantly-moving discharge will tend to spread out the deposited sediments more than a fixed discharge site;
- g) no resuspension of settled sediments was included in the model simulations, which will be conservative for seabed deposition, but re-mobilised silts, could contribute further to background suspended-sediment concentrations, especially during active wind-wave periods or strong spring tidal flows.

Averages and statistics of suspended-sediment concentrations (SSC) were obtained from 14-day simulations for each of five “lumped” discharge locations with two different sources of both predominantly “silt” material and predominantly “sand” material (with a small 2% silt content). Suspended-sediment concentrations from the MIKE-21 PA plume model are averaged over the entire depth of the water column at the time of calculation. However, because the sediments are discharged at depth and they preferentially settle downwards (even though there will be some upwards vertical dispersion), the SSC will be distributed unevenly through the water column, skewed towards much higher-than-average SSC near the seabed compared to a lower-than-average SSC at the water surface. This skewed distribution also occurs naturally with tidal current or wave stirring of bottom sediments, where the SSC is far greater just above the seabed than at the surface—more so the deeper the water column and the larger the sediment grain size.

Key results from the SSC simulations show:

- The dredger discharges in the Turning Basin would have the most influence on elevating average SSC above background levels in the Upper Harbour, in contrast to dredging at Harington Bend and beyond, which would have little influence on SSC in the Upper Harbour beyond Goat and Quarantine Islands.
- The highest depth-average SSC values (e.g., over 100 mg/L with some patches up around 1000 mg/L) would occur in the main shipping channel, subsidiary side channels e.g., channel north of Quarantine Island through to Portobello Peninsula, and on the intertidal banks adjacent to these channels e.g., the mid-harbour intertidal banks from discharges at Harington Bend.
- Discharges from predominantly-silt claims generally show a wider spread of affected areas onto intertidal flats and side channels than discharges of silt-sized material from predominantly-sand areas. This difference is related directly to the magnitude of the discharge or flux of silt-sized material, which was set to 1000 kg/s for “silt” claims compared to 60 kg/s for “sand” claims, even though the latter discharge would run for much longer. However, there wouldn’t be widespread dispersion of these finer silt-sized sediments over large tracts of the Harbour, as the channel tidal streams dominate the transport of suspended sediments rather than dispersion/spreading processes. Also there would be only limited opportunities around the more quiescent period either side of high tide when diluted plumes from the overflow sources - that discharge most of the time at 5 m below the surface (except at Turning Basin - east) - can spread out further over adjacent intertidal or shallow sub-tidal areas.
- While there is only a short distance separating the two Turning Basin source locations (east and west sides), there would be a substantial divergence in areas affected by suspended-sediment plumes due to the strong flow divergence at Quarantine Island. From the “west” source location, discharge plumes would be transported up the Victoria Channel partway into the Upper Harbour while plumes from the “east” source location would be preferentially transported and dispersed to areas around the Portobello Peninsula and into the Latham Bay area of the Upper Harbour. The wider spread of average SSC from the east-side Basin discharge is also a function of the overflow discharge being set to only 1 m below the surface for the first half of the 14-day simulation.

- Most of the eastern side of the Lower Harbour from Te Rauone Beach to Harwood would be largely unaffected by discharge sources other than the Harington Bend discharge location, and then only in patches.
- The eastern side of the Upper Harbour from Grassy Point to Dunedin would be also largely unaffected by sediment discharge sources.
- 14-day average SSC will be low in the plume that emanates from the Mole to Taiaroa Head channel section for dredging claims in the Turning Basin, but will gradually increase up to a depth-average SSC of 100–200 mg/L for discharge sources at Harington Bend. These average SSC levels offshore from the Mole would reduce somewhat as the dredger works the Howlett claim (between Harington Point and the Mole) and further reduce in the Outer Channel claim as the silt content of the sandy seabed sediments reduces considerably to virtually nil.

Key results for predicted sediment deposition over a 14-day spring/neap tide cycle show:

- deposition at or above 5 kg/m² or approximately 3.8 mm over a fortnightly period is largely confined to the channels: a) the main shipping channel (all dredger discharge sources); b) the subsidiary channel to the east from Quarantine Island; c) around Goat Island and up Victoria Channel to opposite St. Leonards for a discharge source on the west side of the Turning Basin; and d) some of the flanking intertidal flats to these channels;
- discharges from predominantly-silt claims would cause higher deposition thicknesses (and daily deposition rates) than from predominantly-sand claims, even though the overflows would occur much longer (60 minutes) for the latter. The much smaller but longer overflow discharge of silty material when dredging “sandy” sites, allows the silt-sized material to disperse more widely causing lower local deposition rates. This result shows that any measures targeted at reducing overflows to a minimum when dredging predominantly-silt areas of the channel would substantially reduce environmental effects arising from deposition of fine sediments;
- the Upper Harbour would have virtually no discernable seabed deposition arising from dredger discharge sources seaward of Harington Bend;

- most of the eastern parts of the Lower and Upper Harbours would be subject to little or no deposition, apart from the reach from Latham Bay to Yellow Head (west of Portobello Peninsula) for discharges from the eastern side of the Turning Basin, Taylers Bend and through to the Cross-channel reach, and in the subsidiary channel from Te Rauone Beach to Ohinetu Point from Harington Bend discharge sources.

Key results for predicted sediment deposition accumulated over the entire dredging programme (assuming no subsequent resuspension of settled silts):

- silt deposition shows a marked difference between the predicted deposition in the main shipping channel and all other Harbour sub-areas, with deposition values much higher and few areas untouched within the main channel. These high predicted deposition values exclude subsequent resuspension by tidal currents and/or wind waves, so are mostly unrealistic. They occur in the plume dispersion model when sediments settle out eventually in more quiescent periods of the ebb or flood tide slack periods, and remain fixed to the bed in the simulations. In practice, these sediments will be re-mobilised frequently by stronger tidal currents, until eventually a proportion is flushed through the main channel system and some exported, while some material re-settles in areas of the channel and consolidates into the fabric of sands on the channel floor;
- considering all other Harbour sub-areas (outside the main shipping channel), based on accumulated deposition thicknesses which are not exceeded within 99% of model cells in each sub-area, there are only a few sub-areas where this exceeds a threshold of 10 mm deposition over the dredging programme. These sub-areas would be: a) the reach of Victoria Channel to Kilgours Point (99% of cells would be below 14 mm deposition over the dredging programme); b) the side channel off Quarantine Point at the tip of Portobello Peninsula (99% of cells would be below 10 mm); c) the southern side of the central intertidal bank and adjacent shallows that separate the shipping channel from the side channel through Ohinetu Point, which would arise primarily from discharge sources in the Harington Bend and The Spit areas (99% of cells would be below 24 mm); d) the sequence of central intertidal banks adjacent to the shipping channel, which would receive the most silt accumulation outside the shipping channel, with the highest occurring on the sandbank opposite Port Chalmers (99% of cells would be below 82 mm deposition) arising mostly from dredging of the eastern side of the Turning Basin; e) the subsidiary channel from Quarantine Island through to Latham Bay, again from dredging the eastern side of the Turning Basin (99% of cells would be below 13 mm);

- considering medians (i.e., half the cells in a sub-area) for potential deposition outside the main shipping channel, the highest median deposition in any sub-area of the Harbour would occur on the intertidal sandbank opposite Port Chalmers, with half the model cells in this sub-area showing a total deposition of nearly 4 mm or more. In most other sub-areas outside the main channels, the median deposition is small at less than 1 mm over the dredging programme.

Rate of deposition—The *rate* of deposition is also important in assessing the effects of any deposition on benthic ecosystems. This requires an estimate of the time to complete the dredging claims that would affect the Harbour (excluding a portion of the dredging claims in the outer approach channel). To obtain an average daily deposition rate over the dredging season simply requires the values in Table 7.6 to be divided by the relevant number of total dredging days. A lower-bound estimate using a 10,800 m³ capacity TSHD is 111 days for discharges likely to influence the Harbour excluding any downtime or around 140 days assuming a 20% down-time factor (see Section 7.3.3). If a smaller dredger is used for part of the dredging programme, a longer dredging season would be needed. However, in reality, each sub-area of the Harbour will be more affected by a source discharge in a particular section of the channel e.g., Quarantine Island to Latham Bay would be mainly affected by dredging from the eastern Turning Basin source, but not much by the Harington Bend claims. In such cases, the daily deposition rate would be higher than the average when dredging occurs at claim sites that more directly affect a particular sub-area of the Harbour. To derive these higher daily deposition rates, the values in Table 7.6 can be divided by the combined total of “sand” and “silt” dredging days for the relevant discharge sources using the % of dredging days listed in Table 7.3. There are other sub-areas though that would experience deposition from dredging in several sections of the channel, particularly the intertidal banks in the central Lower Harbour adjacent to the shipping channel. These banks would be affected by most of the channel discharge sources modelled except Basin-west. Again, the % dredging days in Table 7.3 can be used to combine a total number of dredging days from the relevant sources, and divided into the values in Table 7.6 to calculate daily rates. Apart from the seabed of the main channels, the daily deposition rate in 99% of cells in any Harbour sub-area would be less than 1 mm/day (highest on the intertidal bank opposite Port Chalmers), but mostly less than 0.1 mm/day.

Deposition relative to the dredging operations—Due to the differing capacities of dredging vessels, the contracted operator would take at least 120 days (excluding downtime) to complete the dredging for the 15-m Harbour channel. However, accumulated deposition is governed predominantly by the volumes of the dredging claims in different sections of the channel, which means the total deposition

thicknesses wouldn't change much for longer dredging programmes. However, daily rates of deposition would change depending on the capacity of the dredger that is contracted, with longer dredging periods simply reducing the rates of deposition proportionately. On the other hand, a longer dredging programme means the environment is disturbed for longer, albeit at a lower level of daily impact. Minimising the time when hopper overflows occur for dredging predominantly-silt claims (4 minutes allowed for in the modelling) would substantially reduce accumulated deposition thicknesses and deposition rates.

Long-term fate of silts in the Harbour—Finally, the question of the long-term fate of silts within the Harbour is a difficult one to address with suspended-sediment modelling, as it would involve lengthy computer simulations with a combination of wave, tide and silt-transport models. However, some general tendencies can be inferred from the plume modelling results and our understanding of silt transport in harbours. Firstly, the plume modelling shows that only the main channel and the side channel between Quarantine Island and Portobello Peninsula would be subject to the highest initial deposition thicknesses of greater than 5 kg/m² in 14-days (Fig. 7.9–7.13). These silts would be reworked regularly by tidal currents, especially on spring tides, and spread throughout the entire shipping channel, preferentially settling in more quiescent sections of the channel system and also with a sizeable proportion being exported out the Entrance (as shown by the 14-day plume model simulations). For the exported silts, based on the similar calculations as shown in Table 7.6, sub-area #3 beyond the Mole (Fig. 7.3 or 7.14) would experience in 99% of model cells, accumulated deposition thicknesses of less than 10 mm over the dredging programme. However, given the wave climate outside the Mole, these silts are likely to be resuspended often and disperse widely, with some preferentially settling in the naturally-occurring silt zone further offshore (shown later in Figure 12.26).

Inside the Harbour, on the shallower sub-tidal areas, and intertidal banks, some of the initially settled silts from the dredging operation will be more likely to be remobilized by wind waves rather than currents, and then transported elsewhere in suspension by the current until settling again. Wave remobilization of silts also depends on the interim bed consolidation, cohesiveness and bioturbation. Assuming no cohesiveness, medium silt-size sediments of 0.01 mm diameter, would require exceedance of a wave orbital velocity threshold of 0.05 m/s (using Komar & Miller, 1974 cited in Raudkivi 1990; p 405). For a typical 3-second wave, and a moderately high significant wave height of 0.6 m (see simulations in Section 9.3), this threshold would be exceeded in depths less than about 7 m, which includes most of the Harbour outside the main shipping channels, except a small part of the basin in Portobello Bay (Fig. 3.7). Consequently, during moderate to high waves, silts available for reworking will be winnowed from the seabed surface, especially off exposed shallow areas and intertidal

flats where wave orbital velocities can be high. Silts originating from dredging operations inside the Harbour in the long-term would be dispersed further and more thinly throughout the Harbour, eventually finding their way into the main channel system to be exported to the ocean or preferentially settle “permanently” in quiescent areas where wave activity and currents are low or sporadic e.g., the Dunedin basin, behind the railway embankments, sheltered sub-tidal embayments, the lee of groynes or half-tide training walls and in the upper-tide inter-tidal beaches of sheltered embayments. In the Upper Harbour, a guide to where silts could preferentially settle in the long term are those areas that already show a predominance of silt material in seabed samples, as measured by Grove & Probert (1999).

Table 7.4: % of the time (14-day period) that the depth-averaged suspended-sediment concentration (SSC) on a saturated sediment weight basis would occur in different brackets from zero to >400 mg/L above background concentrations, for the 5 different source-discharge areas and split into the sub-areas of the Harbour (Fig. 7.3). Note: realistic SSC in terms of dry-weight per volume would be about 70–80% of these predicted values.

Dredged site	Type	Harbour sub-area	% time for each suspended-sediment concentration range (mg/L) over 14-day periods									
			0	<1	1–5	5–10	10–20	20–50	50–100	100–200	200–400	>400
Basin–west	sand	1–Port Channel	39.5	6.3	9.0	3.6	4.3	11.7	9.6	8.7	4.8	2.5
Basin–west	silt	1–Port Channel	27.9	25.4	6.0	5.6	6.4	6.4	4.2	6.4	6.6	5.2
Basin–west	sand	2–Cross Channel	41.6	8.2	11.1	4.7	5.9	15.1	9.5	3.5	0.3	0.0
Basin–west	silt	2–Cross Channel	30.4	26.7	8.0	6.5	6.0	5.7	3.9	6.7	4.9	1.2
Basin–west	sand	3–Exported	99.6	0.2	0.1	0.0	0.0	0.0	0.0	0.0	0.0	0.0
Basin–west	silt	3–Exported	99.7	0.3	0.0	0.0	0.0	0.0	0.0	0.0	0.0	0.0
Basin–west	sand	4–Harington Channel	62.6	5.4	8.1	4.1	5.5	10.1	3.7	0.5	0.0	0.0
Basin–west	silt	4–Harington Channel	49.3	27.9	6.3	4.1	3.4	2.7	2.0	3.2	1.1	0.1
Basin–west	sand	5–Portobello	99.5	0.1	0.1	0.1	0.0	0.1	0.0	0.1	0.1	0.0
Basin–west	silt	5–Portobello	98.4	1.6	0.0	0.0	0.0	0.0	0.0	0.0	0.0	0.0
Basin–west	sand	6–Spit Channel	87.9	2.8	3.2	1.5	1.6	2.3	0.5	0.1	0.0	0.0
Basin–west	silt	6–Spit Channel	79.4	17.1	1.6	0.8	0.3	0.3	0.2	0.3	0.0	0.0
Basin–west	sand	7–Deborah Bay	88.7	0.7	1.4	1.1	1.1	1.2	1.3	2.1	1.5	0.8
Basin–west	silt	7–Deborah Bay	77.1	18.1	0.6	0.4	0.8	1.6	0.6	0.2	0.2	0.6
Basin–west	sand	8–Spit Inter Tidal	99.0	0.1	0.2	0.0	0.0	0.1	0.2	0.2	0.2	0.0
Basin–west	silt	8–Spit Inter Tidal	98.8	1.2	0.0	0.0	0.0	0.0	0.0	0.0	0.0	0.0
Basin–west	sand	9–Te Rauone Beach	100.0	0.0	0.0	0.0	0.0	0.0	0.0	0.0	0.0	0.0
Basin–west	silt	9–Te Rauone Beach	99.6	0.4	0.0	0.0	0.0	0.0	0.0	0.0	0.0	0.0
Basin–west	sand	10–Aramoana	99.1	0.1	0.2	0.1	0.1	0.1	0.1	0.2	0.1	0.0
Basin–west	silt	10–Aramoana	98.6	1.4	0.0	0.0	0.0	0.0	0.0	0.0	0.0	0.0
Basin–west	sand	11–Dowling Bay	95.9	0.4	0.8	0.5	0.4	0.5	0.5	0.5	0.3	0.2
Basin–west	silt	11–Dowling Bay	90.9	8.4	0.1	0.1	0.1	0.3	0.1	0.0	0.0	0.1

Dredged site	Type	Harbour sub-area	% time for each suspended-sediment concentration range (mg/L) over 14-day periods									
			0	<1	1–5	5–10	10–20	20–50	50–100	100–200	200–400	>400
Basin–west	sand	12–Hamilton Bay	93.3	0.3	0.6	0.5	0.5	0.7	0.8	1.7	1.3	0.3
Basin–west	silt	12–Hamilton Bay	92.0	7.5	0.1	0.0	0.1	0.2	0.1	0.0	0.0	0.1
Basin–west	sand	13–Harwood Inter Tidal	99.7	0.1	0.1	0.0	0.0	0.0	0.0	0.0	0.0	0.0
Basin–west	silt	13–Harwood Inter Tidal	99.7	0.3	0.0	0.0	0.0	0.0	0.0	0.0	0.0	0.0
Basin–west	sand	14–Dunedin Bays	91.0	0.8	1.3	0.8	0.7	0.8	1.0	1.6	1.3	0.7
Basin–west	silt	14–Dunedin Bays	81.0	15.7	0.3	0.2	0.4	1.0	0.5	0.2	0.2	0.5
Basin–west	sand	15–Port Inter Tidal	96.8	0.2	0.4	0.2	0.2	0.3	0.3	0.5	0.6	0.5
Basin–west	silt	15–Port Inter Tidal	93.3	6.3	0.1	0.0	0.0	0.1	0.1	0.0	0.0	0.0
Basin–west	sand	16–Pulling Inter Tidal	98.1	0.2	0.3	0.1	0.1	0.2	0.2	0.2	0.2	0.3
Basin–west	silt	16–Pulling Inter Tidal	96.8	3.1	0.0	0.0	0.0	0.0	0.0	0.0	0.0	0.0
Basin–west	sand	17–Tayler Inter Tidal	99.7	0.0	0.1	0.0	0.0	0.0	0.0	0.1	0.0	0.1
Basin–west	silt	17–Tayler Inter Tidal	99.5	0.5	0.0	0.0	0.0	0.0	0.0	0.0	0.0	0.0
Basin–west	sand	18–Goat Channel	28.1	5.4	9.6	5.6	6.7	15.4	15.2	10.8	2.8	0.4
Basin–west	silt	18–Goat Channel	13.3	15.2	4.7	5.7	9.7	13.9	8.5	8.2	12.2	8.6
Basin–west	sand	19–Dunedin Channel	80.7	4.0	4.1	1.5	1.6	4.0	2.7	1.0	0.4	0.0
Basin–west	silt	19–Dunedin Channel	59.4	27.3	2.6	3.0	2.5	1.9	0.8	0.7	1.2	0.6
Basin–west	sand	20–Goat Inter Tidal	97.6	0.2	0.3	0.2	0.2	0.2	0.1	0.3	0.5	0.5
Basin–west	silt	20–Goat Inter Tidal	92.8	6.8	0.1	0.0	0.0	0.1	0.1	0.0	0.0	0.1
Basin–west	sand	21–Dunedin Inter Tidal	93.0	0.2	0.5	0.5	0.6	0.6	0.4	1.0	1.5	1.6
Basin–west	silt	21–Dunedin Inter Tidal	83.2	14.2	0.4	0.1	0.2	0.6	0.5	0.3	0.1	0.4
Basin–west	sand	22–Pudding Inter Tidal	99.3	0.1	0.2	0.1	0.1	0.1	0.0	0.2	0.1	0.0
Basin–west	silt	22–Pudding Inter Tidal	97.2	2.8	0.0	0.0	0.0	0.0	0.0	0.0	0.0	0.0
Basin–west	sand	23–Challis Inter Tidal	99.0	0.0	0.1	0.1	0.1	0.1	0.2	0.3	0.1	0.0
Basin–west	silt	23–Challis Inter Tidal	94.1	5.6	0.0	0.0	0.1	0.1	0.0	0.0	0.0	0.0
Basin–west	sand	24–Dunedin Embayment	100.0	0.0	0.0	0.0	0.0	0.0	0.0	0.0	0.0	0.0
Basin–west	silt	24–Dunedin Embayment	99.8	0.2	0.0	0.0	0.0	0.0	0.0	0.0	0.0	0.0
Basin–west	sand	25–Sawyers Bay	95.6	0.2	0.5	0.3	0.4	0.4	0.4	0.8	0.9	0.5
Basin–west	silt	25–Sawyers Bay	87.0	11.4	0.1	0.1	0.1	0.5	0.3	0.1	0.1	0.3

Dredged site	Type	Harbour sub-area	% time for each suspended-sediment concentration range (mg/L) over 14-day periods									
			0	<1	1–5	5–10	10–20	20–50	50–100	100–200	200–400	>400
Basin–west	sand	26–Eastern Channel	96.0	0.4	0.8	0.4	0.4	0.4	0.6	0.8	0.3	0.0
Basin–west	silt	26–Eastern Channel	89.2	9.8	0.1	0.1	0.2	0.3	0.1	0.0	0.0	0.1
Basin–west	sand	27–Hamilton Inter Tidal	99.5	0.0	0.0	0.0	0.0	0.0	0.0	0.1	0.2	0.1
Basin–west	silt	27–Hamilton Inter Tidal	98.8	1.2	0.0	0.0	0.0	0.0	0.0	0.0	0.0	0.0
Basin–east	sand	1–Port Channel	54.6	8.5	5.2	2.0	2.7	6.5	5.7	5.9	4.8	4.0
Basin–east	silt	1–Port Channel	44.7	30.4	4.5	2.2	2.1	2.6	2.0	2.8	3.2	5.5
Basin–east	sand	2–Cross Channel	53.4	12.5	8.5	3.2	4.0	10.5	5.7	2.0	0.3	0.0
Basin–east	silt	2–Cross Channel	40.1	32.4	7.2	4.5	3.7	3.1	2.5	3.5	2.5	0.7
Basin–east	sand	3–Exported	98.8	0.4	0.4	0.1	0.1	0.2	0.0	0.0	0.0	0.0
Basin–east	silt	3–Exported	98.2	1.8	0.0	0.0	0.0	0.0	0.0	0.0	0.0	0.0
Basin–east	sand	4–Harington Channel	66.6	9.2	8.0	3.5	4.7	6.8	1.2	0.1	0.0	0.0
Basin–east	silt	4–Harington Channel	53.4	29.7	6.6	3.2	1.8	1.8	1.3	1.8	0.3	0.0
Basin–east	sand	5–Portobello	87.0	0.5	1.1	1.0	1.1	1.6	2.6	2.9	1.7	0.5
Basin–east	silt	5–Portobello	78.8	16.9	0.3	0.3	0.7	1.0	0.5	0.3	0.3	0.9
Basin–east	sand	6–Spit Channel	84.7	4.2	3.9	1.5	2.1	3.1	0.4	0.0	0.0	0.0
Basin–east	silt	6–Spit Channel	78.1	18.3	1.9	0.6	0.3	0.3	0.2	0.2	0.0	0.0
Basin–east	sand	7–Deborah Bay	99.9	0.0	0.0	0.0	0.0	0.0	0.0	0.0	0.0	0.0
Basin–east	silt	7–Deborah Bay	99.7	0.3	0.0	0.0	0.0	0.0	0.0	0.0	0.0	0.0
Basin–east	sand	8–Spit Inter Tidal	99.8	0.0	0.1	0.0	0.0	0.0	0.0	0.0	0.0	0.0
Basin–east	silt	8–Spit Inter Tidal	99.5	0.5	0.0	0.0	0.0	0.0	0.0	0.0	0.0	0.0
Basin–east	sand	9–Te Rauone Beach	99.5	0.1	0.1	0.0	0.0	0.0	0.1	0.2	0.0	0.0
Basin–east	silt	9–Te Rauone Beach	99.1	0.9	0.0	0.0	0.0	0.0	0.0	0.0	0.0	0.0
Basin–east	sand	10–Aramoana	99.5	0.0	0.1	0.0	0.0	0.0	0.1	0.1	0.1	0.0
Basin–east	silt	10–Aramoana	99.4	0.6	0.0	0.0	0.0	0.0	0.0	0.0	0.0	0.0
Basin–east	sand	11–Dowling Bay	99.3	0.1	0.1	0.1	0.1	0.0	0.2	0.1	0.1	0.0
Basin–east	silt	11–Dowling Bay	98.6	1.4	0.0	0.0	0.0	0.0	0.0	0.0	0.0	0.0
Basin–east	sand	12–Hamilton Bay	99.8	0.0	0.1	0.0	0.0	0.0	0.0	0.0	0.0	0.0
Basin–east	silt	12–Hamilton Bay	99.1	0.9	0.0	0.0	0.0	0.0	0.0	0.0	0.0	0.0

Dredged site	Type	Harbour sub-area	% time for each suspended-sediment concentration range (mg/L) over 14-day periods									
			0	<1	1–5	5–10	10–20	20–50	50–100	100–200	200–400	>400
Basin–east	sand	13–Harwood Inter Tidal	99.1	0.1	0.2	0.1	0.1	0.2	0.0	0.1	0.1	0.0
Basin–east	silt	13–Harwood Inter Tidal	98.4	1.6	0.0	0.0	0.0	0.0	0.0	0.0	0.0	0.0
Basin–east	sand	14–Dunedin Bays	100.0	0.0	0.0	0.0	0.0	0.0	0.0	0.0	0.0	0.0
Basin–east	silt	14–Dunedin Bays	99.7	0.3	0.0	0.0	0.0	0.0	0.0	0.0	0.0	0.0
Basin–east	sand	15–Port Inter Tidal	50.3	0.6	1.4	1.3	2.1	3.4	2.9	5.0	9.2	23.9
Basin–east	silt	15–Port Inter Tidal	37.3	24.3	2.1	1.2	1.3	4.0	5.4	5.8	4.1	14.4
Basin–east	sand	16–Pulling Inter Tidal	92.1	0.5	1.1	0.7	0.6	0.7	0.8	1.1	1.3	1.0
Basin–east	silt	16–Pulling Inter Tidal	84.0	13.7	0.4	0.2	0.2	0.5	0.4	0.2	0.1	0.3
Basin–east	sand	17–Tayler Inter Tidal	97.0	0.2	0.5	0.3	0.3	0.2	0.2	0.4	0.4	0.4
Basin–east	silt	17–Tayler Inter Tidal	94.6	5.1	0.0	0.0	0.0	0.1	0.0	0.0	0.0	0.0
Basin–east	sand	18–Goat Channel	86.3	4.4	3.4	1.0	1.1	1.8	1.1	0.6	0.3	0.0
Basin–east	silt	18–Goat Channel	71.7	23.2	1.5	1.2	0.8	0.6	0.3	0.3	0.3	0.2
Basin–east	sand	19–Dunedin Channel	99.8	0.1	0.1	0.0	0.0	0.0	0.0	0.0	0.0	0.0
Basin–east	silt	19–Dunedin Channel	98.0	2.0	0.0	0.0	0.0	0.0	0.0	0.0	0.0	0.0
Basin–east	sand	20–Goat Inter Tidal	91.3	0.3	0.8	0.7	0.8	0.8	0.5	1.2	1.8	1.9
Basin–east	silt	20–Goat Inter Tidal	81.9	15.0	0.4	0.2	0.2	0.7	0.6	0.3	0.1	0.5
Basin–east	sand	21–Dunedin Inter Tidal	99.4	0.0	0.1	0.0	0.0	0.1	0.0	0.1	0.1	0.1
Basin–east	silt	21–Dunedin Inter Tidal	98.7	1.3	0.0	0.0	0.0	0.0	0.0	0.0	0.0	0.0
Basin–east	sand	22–Pudding Inter Tidal	81.5	0.5	1.1	1.1	1.3	1.6	1.6	4.8	4.2	2.3
Basin–east	silt	22–Pudding Inter Tidal	70.3	21.2	0.4	0.3	0.6	2.3	1.3	0.8	0.5	2.4
Basin–east	sand	23–Challis Inter Tidal	100.0	0.0	0.0	0.0	0.0	0.0	0.0	0.0	0.0	0.0
Basin–east	silt	23–Challis Inter Tidal	99.9	0.1	0.0	0.0	0.0	0.0	0.0	0.0	0.0	0.0
Basin–east	sand	24–Dunedin Embayment	100.0	0.0	0.0	0.0	0.0	0.0	0.0	0.0	0.0	0.0
Basin–east	silt	24–Dunedin Embayment	100.0	0.0	0.0	0.0	0.0	0.0	0.0	0.0	0.0	0.0
Basin–east	sand	25–Sawyers Bay	99.9	0.0	0.0	0.0	0.0	0.0	0.0	0.0	0.0	0.0
Basin–east	silt	25–Sawyers Bay	99.8	0.2	0.0	0.0	0.0	0.0	0.0	0.0	0.0	0.0
Basin–east	sand	26–Eastern Channel	98.7	0.2	0.4	0.1	0.1	0.1	0.1	0.2	0.1	0.0
Basin–east	silt	26–Eastern Channel	95.9	4.0	0.0	0.0	0.0	0.0	0.0	0.0	0.0	0.0

Dredged site	Type	Harbour sub-area	% time for each suspended-sediment concentration range (mg/L) over 14-day periods									
			0	<1	1–5	5–10	10–20	20–50	50–100	100–200	200–400	>400
Basin–east	sand	27–Hamilton Inter Tidal	92.8	0.2	0.4	0.4	0.5	0.6	0.5	1.5	1.9	1.1
Basin–east	silt	27–Hamilton Inter Tidal	84.4	13.3	0.2	0.1	0.1	0.7	0.5	0.2	0.1	0.4
Taylers Bend	sand	1–Port Channel	50.1	8.9	7.9	3.0	4.4	10.2	7.5	5.4	2.1	0.3
Taylers Bend	silt	1–Port Channel	35.3	28.7	6.3	4.4	3.9	4.5	3.4	4.8	4.5	4.1
Taylers Bend	sand	2–Cross Channel	35.0	13.8	10.4	3.5	4.8	12.4	8.0	6.3	3.5	2.3
Taylers Bend	silt	2–Cross Channel	19.7	25.0	10.4	8.5	6.9	6.2	4.5	6.9	6.5	5.4
Taylers Bend	sand	3–Exported	92.5	1.3	2.0	0.9	1.1	1.6	0.5	0.0	0.0	0.0
Taylers Bend	silt	3–Exported	87.8	11.0	0.4	0.2	0.1	0.1	0.1	0.1	0.0	0.0
Taylers Bend	sand	4–Harington Channel	42.8	10.8	9.0	3.2	5.0	12.7	8.4	4.8	1.9	1.4
Taylers Bend	silt	4–Harington Channel	29.4	28.0	8.6	7.0	5.5	4.7	3.9	6.8	4.0	2.2
Taylers Bend	sand	5–Portobello	94.3	0.3	0.7	0.6	0.6	0.7	1.1	1.1	0.5	0.1
Taylers Bend	silt	5–Portobello	87.2	11.2	0.2	0.1	0.3	0.4	0.1	0.1	0.1	0.2
Taylers Bend	sand	6–Spit Channel	63.6	7.0	6.9	3.0	4.5	9.7	4.3	1.0	0.0	0.0
Taylers Bend	silt	6–Spit Channel	50.0	28.5	4.8	4.0	2.9	2.6	2.2	3.4	1.5	0.2
Taylers Bend	sand	7–Deborah Bay	99.6	0.0	0.1	0.0	0.0	0.0	0.0	0.1	0.1	0.1
Taylers Bend	silt	7–Deborah Bay	97.5	2.4	0.0	0.0	0.0	0.0	0.0	0.0	0.0	0.0
Taylers Bend	sand	8–Spit Inter Tidal	99.1	0.1	0.2	0.1	0.1	0.1	0.2	0.2	0.0	0.0
Taylers Bend	silt	8–Spit Inter Tidal	97.6	2.3	0.0	0.0	0.0	0.0	0.0	0.0	0.0	0.0
Taylers Bend	sand	9–Te Rauone Beach	98.7	0.3	0.4	0.1	0.1	0.1	0.1	0.2	0.1	0.0
Taylers Bend	silt	9–Te Rauone Beach	95.4	4.4	0.0	0.0	0.1	0.1	0.0	0.0	0.0	0.0
Taylers Bend	sand	10–Aramoana	99.8	0.0	0.1	0.0	0.0	0.0	0.0	0.0	0.0	0.0
Taylers Bend	silt	10–Aramoana	98.8	1.2	0.0	0.0	0.0	0.0	0.0	0.0	0.0	0.0
Taylers Bend	sand	11–Dowling Bay	99.4	0.0	0.1	0.1	0.1	0.1	0.1	0.0	0.0	0.0
Taylers Bend	silt	11–Dowling Bay	96.1	3.8	0.0	0.0	0.0	0.0	0.0	0.0	0.0	0.0
Taylers Bend	sand	12–Hamilton Bay	99.4	0.0	0.1	0.0	0.0	0.0	0.0	0.0	0.1	0.2
Taylers Bend	silt	12–Hamilton Bay	97.3	2.6	0.0	0.0	0.0	0.0	0.0	0.0	0.0	0.0
Taylers Bend	sand	13–Harwood Inter Tidal	98.6	0.1	0.2	0.1	0.1	0.3	0.3	0.2	0.1	0.0
Taylers Bend	silt	13–Harwood Inter Tidal	97.6	2.4	0.0	0.0	0.0	0.0	0.0	0.0	0.0	0.0

Dredged site	Type	Harbour sub-area	% time for each suspended-sediment concentration range (mg/L) over 14-day periods									
			0	<1	1–5	5–10	10–20	20–50	50–100	100–200	200–400	>400
Taylers Bend	sand	14–Dunedin Bays	100.0	0.0	0.0	0.0	0.0	0.0	0.0	0.0	0.0	0.0
Taylers Bend	silt	14–Dunedin Bays	99.3	0.7	0.0	0.0	0.0	0.0	0.0	0.0	0.0	0.0
Taylers Bend	sand	15–Port Inter Tidal	74.4	0.6	1.6	1.5	2.0	2.5	1.9	3.5	5.8	6.0
Taylers Bend	silt	15–Port Inter Tidal	57.5	25.2	1.8	0.9	0.9	3.1	3.2	2.3	1.0	4.1
Taylers Bend	sand	16–Pulling Inter Tidal	86.4	0.5	1.3	1.1	1.3	1.4	1.3	2.2	2.6	1.8
Taylers Bend	silt	16–Pulling Inter Tidal	69.6	21.7	1.1	0.5	0.6	1.6	1.7	1.0	0.5	1.9
Taylers Bend	sand	17–Tayler Inter Tidal	93.8	0.4	0.9	0.6	0.6	0.5	0.5	0.9	1.0	0.8
Taylers Bend	silt	17–Tayler Inter Tidal	85.5	12.7	0.4	0.1	0.2	0.5	0.3	0.1	0.0	0.2
Taylers Bend	sand	18–Goat Channel	78.5	5.3	4.8	2.0	2.1	3.6	2.3	1.1	0.3	0.0
Taylers Bend	silt	18–Goat Channel	57.1	29.6	3.3	2.9	2.2	1.9	0.9	0.8	0.8	0.6
Taylers Bend	sand	19–Dunedin Channel	99.1	0.5	0.2	0.0	0.0	0.0	0.1	0.0	0.0	0.0
Taylers Bend	silt	19–Dunedin Channel	96.2	3.8	0.0	0.0	0.0	0.0	0.0	0.0	0.0	0.0
Taylers Bend	sand	20–Goat Inter Tidal	89.7	0.4	0.7	0.6	0.8	0.9	0.6	1.6	2.4	2.3
Taylers Bend	silt	20–Goat Inter Tidal	81.4	15.3	0.4	0.2	0.2	0.8	0.6	0.3	0.1	0.5
Taylers Bend	sand	21–Dunedin Inter Tidal	99.2	0.0	0.1	0.1	0.1	0.1	0.0	0.1	0.2	0.1
Taylers Bend	silt	21–Dunedin Inter Tidal	97.4	2.6	0.0	0.0	0.0	0.0	0.0	0.0	0.0	0.0
Taylers Bend	sand	22–Pudding Inter Tidal	96.1	0.3	0.6	0.4	0.3	0.3	0.4	0.9	0.6	0.1
Taylers Bend	silt	22–Pudding Inter Tidal	87.5	11.1	0.2	0.1	0.2	0.5	0.1	0.0	0.0	0.2
Taylers Bend	sand	23–Challis Inter Tidal	99.9	0.0	0.0	0.0	0.0	0.0	0.0	0.0	0.0	0.0
Taylers Bend	silt	23–Challis Inter Tidal	99.7	0.3	0.0	0.0	0.0	0.0	0.0	0.0	0.0	0.0
Taylers Bend	sand	24–Dunedin Embayment	100.0	0.0	0.0	0.0	0.0	0.0	0.0	0.0	0.0	0.0
Taylers Bend	silt	24–Dunedin Embayment	100.0	0.0	0.0	0.0	0.0	0.0	0.0	0.0	0.0	0.0
Taylers Bend	sand	25–Sawyers Bay	100.0	0.0	0.0	0.0	0.0	0.0	0.0	0.0	0.0	0.0
Taylers Bend	silt	25–Sawyers Bay	99.5	0.5	0.0	0.0	0.0	0.0	0.0	0.0	0.0	0.0
Taylers Bend	sand	26–Eastern Channel	97.4	0.4	0.6	0.2	0.2	0.2	0.5	0.5	0.1	0.0
Taylers Bend	silt	26–Eastern Channel	92.1	7.4	0.1	0.0	0.1	0.1	0.0	0.0	0.0	0.1
Taylers Bend	sand	27–Hamilton Inter Tidal	92.7	0.2	0.5	0.5	0.5	0.6	0.5	1.5	2.0	1.1
Taylers Bend	silt	27–Hamilton Inter Tidal	78.6	17.1	0.5	0.2	0.2	1.4	1.0	0.3	0.1	0.6

Dredged site	Type	Harbour sub-area	% time for each suspended-sediment concentration range (mg/L) over 14-day periods									
			0	<1	1–5	5–10	10–20	20–50	50–100	100–200	200–400	>400
Cross-channel	sand	1–Port Channel	64.1	12.1	7.8	2.7	3.1	5.7	2.9	1.3	0.3	0.0
Cross-channel	silt	1–Port Channel	51.0	31.7	5.6	3.3	2.5	2.0	1.1	1.4	1.0	0.6
Cross-channel	sand	2–Cross Channel	35.9	15.7	11.9	3.7	4.6	11.3	7.8	6.5	2.4	0.2
Cross-channel	silt	2–Cross Channel	24.8	29.5	10.8	6.4	5.0	4.9	3.7	5.8	5.2	3.9
Cross-channel	sand	3–Exported	82.0	2.0	3.5	2.0	3.0	5.0	2.0	0.4	0.0	0.0
Cross-channel	silt	3–Exported	76.0	19.0	1.3	0.9	0.6	0.7	0.5	0.6	0.3	0.1
Cross-channel	sand	4–Harington Channel	35.8	13.6	11.4	3.4	4.6	11.5	9.5	6.5	2.5	1.1
Cross-channel	silt	4–Harington Channel	26.6	28.4	9.3	6.3	5.0	4.6	3.6	6.2	5.7	4.2
Cross-channel	sand	5–Portobello	97.4	0.1	0.3	0.2	0.2	0.3	0.4	0.6	0.3	0.1
Cross-channel	silt	5–Portobello	95.3	4.5	0.0	0.0	0.0	0.1	0.0	0.0	0.0	0.0
Cross-channel	sand	6–Spit Channel	55.2	8.0	8.3	3.5	4.4	9.2	5.7	4.0	1.4	0.1
Cross-channel	silt	6–Spit Channel	44.2	29.0	5.6	4.5	3.5	2.9	2.1	3.5	2.9	1.8
Cross-channel	sand	7–Deborah Bay	99.5	0.0	0.1	0.0	0.1	0.1	0.0	0.1	0.0	0.0
Cross-channel	silt	7–Deborah Bay	98.1	1.9	0.0	0.0	0.0	0.0	0.0	0.0	0.0	0.0
Cross-channel	sand	8–Spit Inter Tidal	97.5	0.3	0.6	0.2	0.1	0.2	0.4	0.5	0.1	0.1
Cross-channel	silt	8–Spit Inter Tidal	96.1	3.7	0.0	0.0	0.0	0.0	0.0	0.0	0.0	0.0
Cross-channel	sand	9–Te Rauone Beach	89.5	1.1	1.8	1.1	1.0	1.4	2.1	1.5	0.5	0.1
Cross-channel	silt	9–Te Rauone Beach	84.6	13.3	0.3	0.2	0.4	0.5	0.2	0.1	0.1	0.2
Cross-channel	sand	10–Aramoana	99.7	0.0	0.1	0.0	0.0	0.0	0.0	0.1	0.0	0.0
Cross-channel	silt	10–Aramoana	99.3	0.7	0.0	0.0	0.0	0.0	0.0	0.0	0.0	0.0
Cross-channel	sand	11–Dowling Bay	99.1	0.1	0.1	0.1	0.1	0.1	0.3	0.1	0.1	0.0
Cross-channel	silt	11–Dowling Bay	97.2	2.7	0.0	0.0	0.0	0.0	0.0	0.0	0.0	0.0
Cross-channel	sand	12–Hamilton Bay	99.5	0.0	0.1	0.0	0.0	0.0	0.1	0.1	0.0	0.0
Cross-channel	silt	12–Hamilton Bay	98.0	1.9	0.0	0.0	0.0	0.0	0.0	0.0	0.0	0.0
Cross-channel	sand	13–Harwood Inter Tidal	96.1	0.2	0.4	0.3	0.3	0.6	0.6	0.5	0.6	0.4
Cross-channel	silt	13–Harwood Inter Tidal	93.5	6.1	0.0	0.0	0.0	0.1	0.1	0.0	0.0	0.1
Cross-channel	sand	14–Dunedin Bays	99.8	0.0	0.0	0.0	0.0	0.0	0.0	0.1	0.0	0.0
Cross-channel	silt	14–Dunedin Bays	99.8	0.2	0.0	0.0	0.0	0.0	0.0	0.0	0.0	0.0

Dredged site	Type	Harbour sub-area	% time for each suspended-sediment concentration range (mg/L) over 14-day periods									
			0	<1	1–5	5–10	10–20	20–50	50–100	100–200	200–400	>400
Cross-channel	sand	15–Port Inter Tidal	88.8	0.5	1.2	0.8	1.0	1.2	0.9	1.9	2.1	1.5
Cross-channel	silt	15–Port Inter Tidal	80.2	16.1	0.5	0.2	0.3	1.0	0.6	0.3	0.1	0.6
Cross-channel	sand	16–Pulling Inter Tidal	69.2	0.8	2.1	1.7	2.5	3.9	2.8	4.0	5.9	7.0
Cross-channel	silt	16–Pulling Inter Tidal	53.8	25.5	1.5	0.9	1.2	3.4	3.9	3.2	1.7	4.9
Cross-channel	sand	17–Tayler Inter Tidal	72.6	0.9	2.0	1.7	2.3	3.0	2.1	3.8	5.6	6.0
Cross-channel	silt	17–Tayler Inter Tidal	60.0	24.8	1.4	0.6	1.0	2.8	2.9	2.1	1.0	3.5
Cross-channel	sand	18–Goat Channel	92.3	4.3	1.4	0.3	0.4	0.8	0.3	0.1	0.0	0.0
Cross-channel	silt	18–Goat Channel	85.7	13.4	0.4	0.2	0.1	0.1	0.0	0.0	0.0	0.0
Cross-channel	sand	19–Dunedin Channel	99.3	0.4	0.1	0.0	0.0	0.1	0.0	0.0	0.0	0.0
Cross-channel	silt	19–Dunedin Channel	99.4	0.6	0.0	0.0	0.0	0.0	0.0	0.0	0.0	0.0
Cross-channel	sand	20–Goat Inter Tidal	99.2	0.1	0.1	0.1	0.1	0.1	0.0	0.1	0.1	0.1
Cross-channel	silt	20–Goat Inter Tidal	97.8	2.1	0.0	0.0	0.0	0.0	0.0	0.0	0.0	0.0
Cross-channel	sand	21–Dunedin Inter Tidal	99.9	0.0	0.0	0.0	0.0	0.0	0.0	0.0	0.0	0.0
Cross-channel	silt	21–Dunedin Inter Tidal	99.6	0.4	0.0	0.0	0.0	0.0	0.0	0.0	0.0	0.0
Cross-channel	sand	22–Pudding Inter Tidal	98.9	0.2	0.2	0.1	0.1	0.1	0.1	0.2	0.1	0.0
Cross-channel	silt	22–Pudding Inter Tidal	97.4	2.6	0.0	0.0	0.0	0.0	0.0	0.0	0.0	0.0
Cross-channel	sand	23–Challis Inter Tidal	99.9	0.0	0.0	0.0	0.0	0.0	0.0	0.0	0.0	0.0
Cross-channel	silt	23–Challis Inter Tidal	100.0	0.0	0.0	0.0	0.0	0.0	0.0	0.0	0.0	0.0
Cross-channel	sand	24–Dunedin Embayment	100.0	0.0	0.0	0.0	0.0	0.0	0.0	0.0	0.0	0.0
Cross-channel	silt	24–Dunedin Embayment	100.0	0.0	0.0	0.0	0.0	0.0	0.0	0.0	0.0	0.0
Cross-channel	sand	25–Sawyers Bay	99.8	0.0	0.0	0.0	0.0	0.0	0.0	0.1	0.0	0.0
Cross-channel	silt	25–Sawyers Bay	99.9	0.1	0.0	0.0	0.0	0.0	0.0	0.0	0.0	0.0
Cross-channel	sand	26–Eastern Channel	99.3	0.1	0.1	0.0	0.0	0.1	0.2	0.1	0.0	0.0
Cross-channel	silt	26–Eastern Channel	98.9	1.1	0.0	0.0	0.0	0.0	0.0	0.0	0.0	0.0
Cross-channel	sand	27–Hamilton Inter Tidal	76.6	0.6	1.2	1.2	1.6	1.9	1.4	4.5	6.2	4.7
Cross-channel	silt	27–Hamilton Inter Tidal	59.7	24.6	1.0	0.4	0.7	4.0	3.6	1.7	0.7	3.5
Harington Bend	sand	1–Port Channel	46.2	8.7	8.8	3.4	4.6	11.5	8.8	5.6	2.0	0.4
Harington Bend	silt	1–Port Channel	35.4	28.7	6.0	4.6	4.9	5.0	3.5	4.8	4.4	2.8

Dredged site	Type	Harbour sub-area	% time for each suspended-sediment concentration range (mg/L) over 14-day periods									
			0	<1	1–5	5–10	10–20	20–50	50–100	100–200	200–400	>400
Harington Bend	sand	2–Cross Channel	38.2	12.8	10.2	3.3	4.5	11.8	7.3	5.8	3.6	2.5
Harington Bend	silt	2–Cross Channel	26.8	28.8	9.6	7.3	5.7	4.8	3.4	6.0	4.6	2.9
Harington Bend	sand	3–Exported	94.7	1.1	1.5	0.7	0.8	1.0	0.2	0.0	0.0	0.0
Harington Bend	silt	3–Exported	91.1	8.3	0.3	0.1	0.1	0.1	0.0	0.0	0.0	0.0
Harington Bend	sand	4–Harington Channel	50.6	11.6	9.2	3.9	6.0	11.9	5.4	1.5	0.1	0.0
Harington Bend	silt	4–Harington Channel	39.1	30.8	8.0	5.2	4.1	3.6	2.8	4.4	1.7	0.2
Harington Bend	sand	5–Portobello	96.2	0.3	0.6	0.4	0.4	0.5	0.7	0.6	0.2	0.0
Harington Bend	silt	5–Portobello	91.1	8.2	0.1	0.1	0.2	0.2	0.0	0.0	0.0	0.1
Harington Bend	sand	6–Spit Channel	68.6	7.2	7.1	3.4	4.3	7.2	2.1	0.1	0.0	0.0
Harington Bend	silt	6–Spit Channel	57.5	27.9	4.6	2.9	2.0	1.7	1.2	1.7	0.5	0.0
Harington Bend	sand	7–Deborah Bay	99.6	0.1	0.1	0.1	0.0	0.0	0.0	0.0	0.0	0.0
Harington Bend	silt	7–Deborah Bay	98.1	1.8	0.0	0.0	0.0	0.0	0.0	0.0	0.0	0.0
Harington Bend	sand	8–Spit Inter Tidal	99.2	0.1	0.2	0.1	0.1	0.1	0.1	0.0	0.0	0.0
Harington Bend	silt	8–Spit Inter Tidal	98.8	1.2	0.0	0.0	0.0	0.0	0.0	0.0	0.0	0.0
Harington Bend	sand	9–Te Rauone Beach	99.6	0.1	0.1	0.0	0.0	0.0	0.0	0.0	0.0	0.0
Harington Bend	silt	9–Te Rauone Beach	99.5	0.5	0.0	0.0	0.0	0.0	0.0	0.0	0.0	0.0
Harington Bend	sand	10–Aramoana	99.4	0.1	0.2	0.1	0.1	0.0	0.1	0.1	0.0	0.0
Harington Bend	silt	10–Aramoana	98.7	1.3	0.0	0.0	0.0	0.0	0.0	0.0	0.0	0.0
Harington Bend	sand	11–Dowling Bay	99.4	0.1	0.1	0.1	0.0	0.0	0.0	0.1	0.1	0.0
Harington Bend	silt	11–Dowling Bay	97.2	2.7	0.0	0.0	0.0	0.0	0.0	0.0	0.0	0.0
Harington Bend	sand	12–Hamilton Bay	98.9	0.1	0.1	0.1	0.1	0.1	0.0	0.4	0.2	0.0
Harington Bend	silt	12–Hamilton Bay	98.5	1.5	0.0	0.0	0.0	0.0	0.0	0.0	0.0	0.0
Harington Bend	sand	13–Harwood Inter Tidal	99.3	0.2	0.1	0.1	0.1	0.2	0.1	0.0	0.0	0.0
Harington Bend	silt	13–Harwood Inter Tidal	98.7	1.3	0.0	0.0	0.0	0.0	0.0	0.0	0.0	0.0
Harington Bend	sand	14–Dunedin Bays	99.8	0.1	0.0	0.0	0.0	0.0	0.0	0.0	0.0	0.0
Harington Bend	silt	14–Dunedin Bays	98.8	1.2	0.0	0.0	0.0	0.0	0.0	0.0	0.0	0.0
Harington Bend	sand	15–Port Inter Tidal	87.1	0.5	1.2	0.9	1.1	1.2	1.1	2.1	2.5	2.2
Harington Bend	silt	15–Port Inter Tidal	78.1	17.4	0.6	0.3	0.4	1.1	0.8	0.4	0.2	0.6

Dredged site	Type	Harbour sub-area	% time for each suspended-sediment concentration range (mg/L) over 14-day periods									
			0	<1	1–5	5–10	10–20	20–50	50–100	100–200	200–400	>400
Harington Bend	sand	16–Pulling Inter Tidal	94.8	0.4	0.9	0.4	0.4	0.4	0.6	0.7	0.7	0.6
Harington Bend	silt	16–Pulling Inter Tidal	88.4	10.4	0.2	0.1	0.1	0.3	0.2	0.1	0.0	0.1
Harington Bend	sand	17–Tayler Inter Tidal	98.5	0.1	0.3	0.1	0.1	0.1	0.2	0.3	0.2	0.1
Harington Bend	silt	17–Tayler Inter Tidal	96.3	3.6	0.0	0.0	0.0	0.0	0.0	0.0	0.0	0.0
Harington Bend	sand	18–Goat Channel	62.8	7.8	6.8	2.9	3.5	6.9	5.0	3.0	1.1	0.2
Harington Bend	silt	18–Goat Channel	43.0	31.6	4.4	4.2	3.8	4.1	2.5	2.3	2.4	1.7
Harington Bend	sand	19–Dunedin Channel	98.5	0.8	0.3	0.1	0.1	0.1	0.0	0.0	0.0	0.0
Harington Bend	silt	19–Dunedin Channel	93.2	6.6	0.1	0.1	0.0	0.0	0.0	0.0	0.0	0.0
Harington Bend	sand	20–Goat Inter Tidal	81.2	0.5	1.2	1.1	1.5	1.8	1.1	2.6	4.3	4.7
Harington Bend	silt	20–Goat Inter Tidal	69.2	21.8	1.0	0.5	0.6	2.1	1.8	1.0	0.4	1.7
Harington Bend	sand	21–Dunedin Inter Tidal	97.6	0.1	0.2	0.1	0.2	0.2	0.1	0.4	0.5	0.5
Harington Bend	silt	21–Dunedin Inter Tidal	94.0	5.7	0.1	0.0	0.0	0.1	0.1	0.0	0.0	0.0
Harington Bend	sand	22–Pudding Inter Tidal	93.0	0.4	0.7	0.6	0.5	0.6	0.8	2.1	1.2	0.2
Harington Bend	silt	22–Pudding Inter Tidal	84.6	13.2	0.2	0.1	0.3	0.8	0.2	0.1	0.1	0.3
Harington Bend	sand	23–Challis Inter Tidal	99.9	0.0	0.0	0.0	0.0	0.0	0.0	0.0	0.0	0.0
Harington Bend	silt	23–Challis Inter Tidal	99.5	0.5	0.0	0.0	0.0	0.0	0.0	0.0	0.0	0.0
Harington Bend	sand	24–Dunedin Embayment	100.0	0.0	0.0	0.0	0.0	0.0	0.0	0.0	0.0	0.0
Harington Bend	silt	24–Dunedin Embayment	100.0	0.0	0.0	0.0	0.0	0.0	0.0	0.0	0.0	0.0
Harington Bend	sand	25–Sawyers Bay	99.8	0.0	0.0	0.0	0.0	0.0	0.0	0.0	0.1	0.0
Harington Bend	silt	25–Sawyers Bay	99.7	0.3	0.0	0.0	0.0	0.0	0.0	0.0	0.0	0.0
Harington Bend	sand	26–Eastern Channel	95.6	0.6	0.8	0.4	0.4	0.4	0.5	0.7	0.6	0.1
Harington Bend	silt	26–Eastern Channel	86.1	12.3	0.2	0.1	0.4	0.5	0.1	0.1	0.1	0.2
Harington Bend	sand	27–Hamilton Inter Tidal	97.9	0.1	0.2	0.2	0.2	0.2	0.1	0.5	0.5	0.2
Harington Bend	silt	27–Hamilton Inter Tidal	93.8	5.9	0.0	0.0	0.0	0.1	0.1	0.0	0.0	0.1

Table 7.5: % of the Harbour environment sub-area that the seabed deposition is predicted to occur in different brackets of thickness from zero to >5 mm in a 14-day period for the 5 different source-discharge areas, with sub-areas shown in Figure 7.3. Assumes wet bulk density is 1300 kg/m³.

Dredged site	Type	Harbour sub-area	% of Harbour sub-area in each deposition range (mm) over a 14-day period						
			0	< 0.1	0.1–0.2	0.2–0.5	0.5–1	1–2	> 5
Basin–west	sand	1–Port Channel	3.9	27.5	7.6	12.1	11.8	11.4	10.1
Basin–west	silt	1–Port Channel	3.6	18.6	8.4	9.8	8.0	11.2	12.9
Basin–west	sand	2–Cross Channel	0.0	34.0	7.8	16.0	14.4	14.1	12.6
Basin–west	silt	2–Cross Channel	0.0	26.3	7.0	11.2	10.1	12.4	16.3
Basin–west	sand	3–Exported	72.6	27.3	0.1	0.1	0.0	0.0	0.0
Basin–west	silt	3–Exported	80.6	19.3	0.0	0.0	0.0	0.0	0.0
Basin–west	sand	4–Harington Channel	5.1	46.5	8.9	18.2	14.8	6.2	0.3
Basin–west	silt	4–Harington Channel	4.4	39.0	6.6	11.6	10.9	15.1	11.7
Basin–west	sand	5–Portobello	83.6	15.8	0.4	0.3	0.0	0.0	0.0
Basin–west	silt	5–Portobello	72.4	27.1	0.1	0.2	0.1	0.1	0.0
Basin–west	sand	6–Spit Channel	12.6	71.5	8.4	6.5	0.9	0.0	0.0
Basin–west	silt	6–Spit Channel	5.0	72.2	7.5	6.7	4.2	4.0	0.4
Basin–west	sand	7–Deborah Bay	26.5	50.1	5.3	13.7	4.2	0.2	0.0
Basin–west	silt	7–Deborah Bay	21.3	48.1	9.5	8.9	5.4	5.4	1.4
Basin–west	sand	8–Spit Inter Tidal	84.2	15.1	0.5	0.2	0.0	0.0	0.0
Basin–west	silt	8–Spit Inter Tidal	78.1	21.7	0.2	0.0	0.0	0.0	0.0
Basin–west	sand	9–Te Rauone Beach	97.2	2.8	0.0	0.0	0.0	0.0	0.0
Basin–west	silt	9–Te Rauone Beach	86.9	13.1	0.0	0.0	0.0	0.0	0.0
Basin–west	sand	10–Aramoana	81.9	17.0	0.5	0.5	0.1	0.0	0.0
Basin–west	silt	10–Aramoana	77.4	21.8	0.3	0.3	0.1	0.1	0.0
Basin–west	sand	11–Dowling Bay	35.6	55.2	2.8	6.4	0.0	0.0	0.0
Basin–west	silt	11–Dowling Bay	28.8	64.6	3.1	1.3	1.0	1.3	0.0
Basin–west	sand	12–Hamilton Bay	37.2	52.6	5.7	4.5	0.0	0.0	0.0

Dredged site	Type	Harbour sub-area	% of Harbour sub-area in each deposition range (mm) over a 14-day period							
			0	< 0.1	0.1–0.2	0.2–0.5	0.5–1	1–2	2–5	> 5
Basin–west	silt	12–Hamilton Bay	16.5	72.7	5.4	2.3	1.1	2.0	0.0	0.0
Basin–west	sand	13–Harwood Inter Tidal	96.4	3.5	0.1	0.1	0.0	0.0	0.0	0.0
Basin–west	silt	13–Harwood Inter Tidal	97.1	2.5	0.1	0.3	0.0	0.0	0.0	0.0
Basin–west	sand	14–Dunedin Bays	35.5	49.0	6.1	7.2	2.2	0.1	0.0	0.0
Basin–west	silt	14–Dunedin Bays	25.9	51.6	6.1	6.4	4.5	4.4	1.2	0.0
Basin–west	sand	15–Port Inter Tidal	28.3	65.8	3.1	2.8	0.0	0.0	0.0	0.0
Basin–west	silt	15–Port Inter Tidal	5.5	87.7	2.8	1.3	1.5	1.2	0.0	0.0
Basin–west	sand	16–Pulling Inter Tidal	32.1	65.6	1.3	0.9	0.1	0.0	0.0	0.0
Basin–west	silt	16–Pulling Inter Tidal	9.4	88.7	0.6	0.6	0.5	0.3	0.0	0.0
Basin–west	sand	17–Tayler Inter Tidal	76.7	23.1	0.1	0.2	0.0	0.0	0.0	0.0
Basin–west	silt	17–Tayler Inter Tidal	69.7	30.1	0.1	0.0	0.1	0.1	0.0	0.0
Basin–west	sand	18–Goat Channel	0.1	8.5	5.1	16.1	23.8	25.1	18.0	3.3
Basin–west	silt	18–Goat Channel	0.1	2.4	3.5	6.3	7.6	16.9	34.4	28.9
Basin–west	sand	19–Dunedin Channel	24.9	51.0	8.1	11.3	4.1	0.6	0.0	0.0
Basin–west	silt	19–Dunedin Channel	14.6	49.9	8.1	9.3	7.4	6.9	3.8	0.1
Basin–west	sand	20–Goat Inter Tidal	22.3	72.2	3.1	2.2	0.2	0.0	0.0	0.0
Basin–west	silt	20–Goat Inter Tidal	4.0	84.7	5.2	2.6	2.0	1.4	0.2	0.0
Basin–west	sand	21–Dunedin Inter Tidal	18.2	65.7	6.0	7.8	2.0	0.3	0.0	0.0
Basin–west	silt	21–Dunedin Inter Tidal	3.3	70.4	7.5	8.1	4.9	4.5	1.2	0.1
Basin–west	sand	22–Pudding Inter Tidal	69.7	29.6	0.3	0.4	0.0	0.0	0.0	0.0
Basin–west	silt	22–Pudding Inter Tidal	50.3	48.2	0.3	0.5	0.5	0.2	0.0	0.0
Basin–west	sand	23–Challis Inter Tidal	75.0	24.3	0.5	0.2	0.0	0.0	0.0	0.0
Basin–west	silt	23–Challis Inter Tidal	47.2	49.5	1.1	0.9	0.9	0.4	0.0	0.0
Basin–west	sand	24–Dunedin Embayment	100.0	0.0	0.0	0.0	0.0	0.0	0.0	0.0
Basin–west	silt	24–Dunedin Embayment	91.2	8.6	0.1	0.0	0.0	0.0	0.0	0.0
Basin–west	sand	25–Sawyers Bay	57.8	32.9	3.5	4.8	0.9	0.1	0.0	0.0
Basin–west	silt	25–Sawyers Bay	45.0	35.5	5.0	5.0	3.5	4.3	1.6	0.1
Basin–west	sand	26–Eastern Channel	63.9	28.7	2.6	2.8	1.4	0.6	0.0	0.0

Dredged site	Type	Harbour sub-area	% of Harbour sub-area in each deposition range (mm) over a 14-day period							
			0	< 0.1	0.1–0.2	0.2–0.5	0.5–1	1–2	2–5	> 5
Basin–west	silt	26–Eastern Channel	40.4	46.1	1.6	5.1	2.3	3.4	1.1	0.1
Basin–west	sand	27–Hamilton Inter Tidal	65.8	33.8	0.3	0.1	0.0	0.0	0.0	0.0
Basin–west	silt	27–Hamilton Inter Tidal	43.2	56.2	0.2	0.2	0.2	0.1	0.0	0.0
Basin–east	sand	1–Port Channel	15.3	40.7	4.5	5.3	4.8	7.3	9.5	12.6
Basin–east	silt	1–Port Channel	12.1	40.8	3.0	4.4	3.7	4.1	8.7	23.3
Basin–east	sand	2–Cross Channel	0.0	54.1	7.9	12.5	8.4	9.4	6.7	0.9
Basin–east	silt	2–Cross Channel	0.0	46.5	6.0	9.2	6.7	9.5	12.8	9.2
Basin–east	sand	3–Exported	53.7	45.6	0.4	0.3	0.0	0.0	0.0	0.0
Basin–east	silt	3–Exported	66.2	32.9	0.3	0.3	0.2	0.2	0.0	0.0
Basin–east	sand	4–Harington Channel	0.5	62.7	8.2	15.3	11.0	2.4	0.0	0.0
Basin–east	silt	4–Harington Channel	0.0	55.3	7.5	9.6	7.8	13.0	6.6	0.2
Basin–east	sand	5–Portobello	50.6	31.5	4.9	7.4	3.0	1.7	0.9	0.0
Basin–east	silt	5–Portobello	47.0	30.0	3.9	5.7	4.7	4.6	3.4	0.8
Basin–east	sand	6–Spit Channel	8.2	75.8	7.2	7.4	1.4	0.1	0.0	0.0
Basin–east	silt	6–Spit Channel	8.2	68.7	6.8	8.8	3.6	3.7	0.2	0.0
Basin–east	sand	7–Deborah Bay	88.2	11.5	0.2	0.2	0.0	0.0	0.0	0.0
Basin–east	silt	7–Deborah Bay	82.7	17.3	0.0	0.0	0.0	0.0	0.0	0.0
Basin–east	sand	8–Spit Inter Tidal	81.1	18.7	0.2	0.0	0.0	0.0	0.0	0.0
Basin–east	silt	8–Spit Inter Tidal	89.7	9.6	0.0	0.0	0.7	0.0	0.0	0.0
Basin–east	sand	9–Te Rauone Beach	75.5	23.9	0.6	0.0	0.0	0.0	0.0	0.0
Basin–east	silt	9–Te Rauone Beach	73.4	26.6	0.0	0.0	0.0	0.0	0.0	0.0
Basin–east	sand	10–Aramoana	85.6	14.1	0.2	0.1	0.0	0.0	0.0	0.0
Basin–east	silt	10–Aramoana	85.1	14.8	0.0	0.0	0.1	0.0	0.0	0.0
Basin–east	sand	11–Dowling Bay	65.9	33.3	0.5	0.3	0.0	0.0	0.0	0.0
Basin–east	silt	11–Dowling Bay	49.6	50.1	0.0	0.3	0.0	0.0	0.0	0.0
Basin–east	sand	12–Hamilton Bay	70.2	29.2	0.3	0.3	0.0	0.0	0.0	0.0
Basin–east	silt	12–Hamilton Bay	61.9	37.8	0.0	0.3	0.0	0.0	0.0	0.0
Basin–east	sand	13–Harwood Inter Tidal	87.9	11.0	0.4	0.6	0.1	0.0	0.0	0.0

Dredged site	Type	Harbour sub-area	% of Harbour sub-area in each deposition range (mm) over a 14-day period							
			0	< 0.1	0.1–0.2	0.2–0.5	0.5–1	1–2	2–5	> 5
Basin–east	silt	13–Harwood Inter Tidal	58.0	40.9	0.2	0.2	0.4	0.4	0.0	0.0
Basin–east	sand	14–Dunedin Bays	97.1	2.8	0.1	0.0	0.0	0.0	0.0	0.0
Basin–east	silt	14–Dunedin Bays	81.4	18.5	0.0	0.0	0.0	0.1	0.0	0.0
Basin–east	sand	15–Port Inter Tidal	0.0	14.1	6.4	14.2	16.6	18.1	18.7	11.9
Basin–east	silt	15–Port Inter Tidal	0.0	8.2	6.0	8.4	7.3	15.1	26.2	28.9
Basin–east	sand	16–Pulling Inter Tidal	2.3	81.8	5.8	7.2	1.3	1.3	0.2	0.1
Basin–east	silt	16–Pulling Inter Tidal	0.0	76.5	8.5	6.1	3.8	3.0	1.7	0.5
Basin–east	sand	17–Tayler Inter Tidal	27.7	66.8	2.5	2.7	0.2	0.0	0.0	0.0
Basin–east	silt	17–Tayler Inter Tidal	11.0	84.6	2.1	1.1	0.6	0.5	0.0	0.0
Basin–east	sand	18–Goat Channel	5.2	80.1	5.9	6.4	1.5	0.4	0.4	0.0
Basin–east	silt	18–Goat Channel	0.3	76.3	6.3	6.6	4.5	4.4	1.0	0.6
Basin–east	sand	19–Dunedin Channel	70.9	29.0	0.1	0.0	0.0	0.0	0.0	0.0
Basin–east	silt	19–Dunedin Channel	35.7	64.1	0.0	0.0	0.1	0.1	0.0	0.0
Basin–east	sand	20–Goat Inter Tidal	3.3	74.9	8.5	8.8	3.3	1.0	0.1	0.1
Basin–east	silt	20–Goat Inter Tidal	1.3	62.1	13.8	9.9	5.2	5.3	2.1	0.2
Basin–east	sand	21–Dunedin Inter Tidal	72.1	27.0	0.6	0.2	0.0	0.0	0.0	0.0
Basin–east	silt	21–Dunedin Inter Tidal	45.6	53.4	0.3	0.3	0.2	0.2	0.0	0.0
Basin–east	sand	22–Pudding Inter Tidal	33.3	37.6	4.8	8.8	7.6	5.1	3.0	0.0
Basin–east	silt	22–Pudding Inter Tidal	25.1	40.8	4.5	5.4	4.7	6.5	8.3	4.7
Basin–east	sand	23–Challis Inter Tidal	100.0	0.0	0.0	0.0	0.0	0.0	0.0	0.0
Basin–east	silt	23–Challis Inter Tidal	96.3	3.6	0.0	0.0	0.0	0.0	0.0	0.0
Basin–east	sand	24–Dunedin Embayment	100.0	0.0	0.0	0.0	0.0	0.0	0.0	0.0
Basin–east	silt	24–Dunedin Embayment	99.4	0.6	0.0	0.0	0.0	0.0	0.0	0.0
Basin–east	sand	25–Sawyers Bay	94.3	5.6	0.0	0.1	0.0	0.0	0.0	0.0
Basin–east	silt	25–Sawyers Bay	93.6	6.4	0.0	0.0	0.0	0.0	0.0	0.0
Basin–east	sand	26–Eastern Channel	67.8	30.3	0.5	1.3	0.2	0.0	0.0	0.0
Basin–east	silt	26–Eastern Channel	42.4	54.5	1.3	0.9	0.3	0.6	0.0	0.0
Basin–east	sand	27–Hamilton Inter Tidal	10.9	78.4	5.6	4.7	0.4	0.0	0.0	0.0

Dredged site	Type	Harbour sub-area	% of Harbour sub-area in each deposition range (mm) over a 14-day period							
			0	< 0.1	0.1–0.2	0.2–0.5	0.5–1	1–2	2–5	> 5
Basin–east	silt	27–Hamilton Inter Tidal	0.4	84.6	5.0	4.2	2.9	2.8	0.1	0.0
Taylers Bend	sand	1–Port Channel	11.4	37.4	5.5	8.6	9.1	13.6	12.7	1.8
Taylers Bend	silt	1–Port Channel	8.5	29.7	6.9	7.0	5.9	6.7	14.6	20.6
Taylers Bend	sand	2–Cross Channel	0.2	33.3	7.8	14.3	12.0	8.2	8.8	15.3
Taylers Bend	silt	2–Cross Channel	0.0	20.2	11.0	9.0	8.1	11.3	15.0	25.5
Taylers Bend	sand	3–Exported	33.5	56.1	2.9	4.0	2.3	1.1	0.1	0.0
Taylers Bend	silt	3–Exported	39.2	43.4	3.9	4.8	3.2	3.0	2.2	0.3
Taylers Bend	sand	4–Harington Channel	0.1	40.2	7.6	13.7	9.4	7.9	8.0	13.0
Taylers Bend	silt	4–Harington Channel	0.0	25.5	11.8	11.0	8.2	10.4	10.1	23.1
Taylers Bend	sand	5–Portobello	63.4	28.0	3.2	4.3	1.0	0.1	0.0	0.0
Taylers Bend	silt	5–Portobello	53.3	31.8	4.0	5.1	3.7	1.9	0.3	0.0
Taylers Bend	sand	6–Spit Channel	1.1	56.2	9.0	11.5	5.6	5.6	10.3	0.6
Taylers Bend	silt	6–Spit Channel	0.1	36.0	12.0	14.3	7.8	8.3	8.4	13.2
Taylers Bend	sand	7–Deborah Bay	83.7	16.0	0.2	0.2	0.0	0.0	0.0	0.0
Taylers Bend	silt	7–Deborah Bay	44.6	52.8	1.2	0.6	0.5	0.3	0.0	0.0
Taylers Bend	sand	8–Spit Inter Tidal	64.4	34.2	0.9	0.5	0.0	0.0	0.0	0.0
Taylers Bend	silt	8–Spit Inter Tidal	53.0	45.9	0.0	0.5	0.2	0.5	0.0	0.0
Taylers Bend	sand	9–Te Rauone Beach	50.7	47.5	1.2	0.6	0.0	0.0	0.0	0.0
Taylers Bend	silt	9–Te Rauone Beach	41.4	54.2	1.6	2.0	0.4	0.4	0.0	0.0
Taylers Bend	sand	10–Aramoana	88.8	10.8	0.2	0.2	0.0	0.0	0.0	0.0
Taylers Bend	silt	10–Aramoana	79.0	20.2	0.2	0.2	0.2	0.2	0.0	0.0
Taylers Bend	sand	11–Dowling Bay	68.7	29.8	0.8	0.8	0.0	0.0	0.0	0.0
Taylers Bend	silt	11–Dowling Bay	45.0	53.0	0.8	0.5	0.3	0.5	0.0	0.0
Taylers Bend	sand	12–Hamilton Bay	76.4	22.7	0.6	0.3	0.0	0.0	0.0	0.0
Taylers Bend	silt	12–Hamilton Bay	35.8	62.8	0.6	0.3	0.3	0.3	0.0	0.0
Taylers Bend	sand	13–Harwood Inter Tidal	82.7	15.7	0.4	0.4	0.1	0.1	0.4	0.3
Taylers Bend	silt	13–Harwood Inter Tidal	59.6	38.6	0.3	0.3	0.3	0.1	0.1	0.7
Taylers Bend	sand	14–Dunedin Bays	94.0	6.0	0.0	0.0	0.0	0.0	0.0	0.0

Dredged site	Type	Harbour sub-area	% of Harbour sub-area in each deposition range (mm) over a 14-day period							
			0	< 0.1	0.1–0.2	0.2–0.5	0.5–1	1–2	2–5	> 5
Taylers Bend	silt	14–Dunedin Bays	68.2	31.5	0.2	0.1	0.1	0.1	0.0	0.0
Taylers Bend	sand	15–Port Inter Tidal	0.0	36.1	13.9	26.4	16.8	6.2	0.6	0.0
Taylers Bend	silt	15–Port Inter Tidal	0.0	21.3	14.2	19.8	14.7	16.0	11.9	2.0
Taylers Bend	sand	16–Pulling Inter Tidal	0.5	63.5	11.2	13.7	6.8	3.2	1.1	0.0
Taylers Bend	silt	16–Pulling Inter Tidal	0.0	35.9	18.8	17.5	10.3	8.3	6.7	2.4
Taylers Bend	sand	17–Tayler Inter Tidal	12.9	69.8	5.8	9.4	2.0	0.1	0.0	0.0
Taylers Bend	silt	17–Tayler Inter Tidal	7.6	59.9	11.3	10.8	5.1	4.5	0.9	0.0
Taylers Bend	sand	18–Goat Channel	3.4	71.6	6.5	11.8	5.8	0.9	0.0	0.0
Taylers Bend	silt	18–Goat Channel	0.0	64.1	6.1	9.2	7.4	8.2	4.7	0.2
Taylers Bend	sand	19–Dunedin Channel	58.9	40.9	0.2	0.0	0.0	0.0	0.0	0.0
Taylers Bend	silt	19–Dunedin Channel	30.8	68.3	0.5	0.2	0.1	0.1	0.0	0.0
Taylers Bend	sand	20–Goat Inter Tidal	3.3	73.8	9.5	10.9	2.0	0.3	0.2	0.1
Taylers Bend	silt	20–Goat Inter Tidal	1.6	66.6	9.7	10.8	5.0	5.2	1.0	0.2
Taylers Bend	sand	21–Dunedin Inter Tidal	64.9	33.9	0.7	0.4	0.1	0.0	0.0	0.0
Taylers Bend	silt	21–Dunedin Inter Tidal	25.6	72.4	0.5	1.0	0.3	0.2	0.0	0.0
Taylers Bend	sand	22–Pudding Inter Tidal	46.3	48.4	2.3	2.4	0.5	0.1	0.0	0.0
Taylers Bend	silt	22–Pudding Inter Tidal	33.8	55.6	4.0	2.9	1.8	1.7	0.3	0.0
Taylers Bend	sand	23–Challis Inter Tidal	97.4	2.5	0.1	0.0	0.0	0.0	0.0	0.0
Taylers Bend	silt	23–Challis Inter Tidal	87.8	12.2	0.0	0.0	0.0	0.0	0.0	0.0
Taylers Bend	sand	24–Dunedin Embayment	100.0	0.0	0.0	0.0	0.0	0.0	0.0	0.0
Taylers Bend	silt	24–Dunedin Embayment	99.3	0.7	0.0	0.0	0.0	0.0	0.0	0.0
Taylers Bend	sand	25–Sawyers Bay	98.1	1.9	0.0	0.0	0.0	0.0	0.0	0.0
Taylers Bend	silt	25–Sawyers Bay	88.9	11.1	0.0	0.0	0.0	0.0	0.0	0.0
Taylers Bend	sand	26–Eastern Channel	47.1	49.8	1.7	1.4	0.0	0.0	0.0	0.0
Taylers Bend	silt	26–Eastern Channel	41.1	53.9	2.3	1.1	1.0	0.6	0.1	0.0
Taylers Bend	sand	27–Hamilton Inter Tidal	11.2	77.9	4.9	5.4	0.5	0.1	0.0	0.0
Taylers Bend	silt	27–Hamilton Inter Tidal	0.1	82.3	6.3	5.7	2.8	2.9	0.1	0.0
Cross-channel	sand	1–Port Channel	12.3	55.7	8.5	12.7	7.1	3.3	0.5	0.0

Dredged site	Type	Harbour sub-area	% of Harbour sub-area in each deposition range (mm) over a 14-day period							
			0	< 0.1	0.1–0.2	0.2–0.5	0.5–1	1–2	2–5	> 5
Cross-channel	silt	1–Port Channel	10.6	43.8	12.5	10.7	7.5	8.3	6.1	0.6
Cross-channel	sand	2–Cross Channel	0.0	37.8	12.2	12.7	5.4	7.2	16.7	7.9
Cross-channel	silt	2–Cross Channel	0.0	22.2	13.6	13.1	9.0	7.9	8.6	25.6
Cross-channel	sand	3–Exported	36.6	37.7	4.8	6.8	5.4	6.7	1.8	0.1
Cross-channel	silt	3–Exported	33.5	36.1	4.3	4.9	4.6	5.4	8.7	2.6
Cross-channel	sand	4–Harington Channel	0.0	35.7	10.2	14.0	8.5	6.9	7.8	16.8
Cross-channel	silt	4–Harington Channel	0.0	22.9	11.8	11.1	8.8	9.1	10.7	25.6
Cross-channel	sand	5–Portobello	62.5	36.4	0.8	0.3	0.0	0.0	0.0	0.0
Cross-channel	silt	5–Portobello	54.5	44.1	0.5	0.5	0.4	0.1	0.0	0.0
Cross-channel	sand	6–Spit Channel	1.9	43.9	10.1	15.7	8.1	4.8	5.2	10.4
Cross-channel	silt	6–Spit Channel	0.4	33.2	8.3	13.0	9.7	10.7	8.8	15.9
Cross-channel	sand	7–Deborah Bay	80.4	19.1	0.3	0.2	0.0	0.0	0.0	0.0
Cross-channel	silt	7–Deborah Bay	44.8	53.8	0.0	0.5	0.3	0.6	0.0	0.0
Cross-channel	sand	8–Spit Inter Tidal	56.2	40.4	2.1	1.1	0.2	0.0	0.0	0.0
Cross-channel	silt	8–Spit Inter Tidal	48.2	45.9	2.5	1.6	0.7	1.1	0.0	0.0
Cross-channel	sand	9–Te Rauone Beach	47.7	34.0	4.6	7.6	3.6	2.2	0.2	0.0
Cross-channel	silt	9–Te Rauone Beach	40.0	36.6	4.4	6.4	4.6	4.8	2.8	0.2
Cross-channel	sand	10–Aramoana	82.0	17.6	0.3	0.1	0.0	0.0	0.0	0.0
Cross-channel	silt	10–Aramoana	82.3	17.2	0.1	0.2	0.2	0.0	0.0	0.0
Cross-channel	sand	11–Dowling Bay	64.6	34.4	0.8	0.3	0.0	0.0	0.0	0.0
Cross-channel	silt	11–Dowling Bay	49.9	49.3	0.3	0.3	0.3	0.0	0.0	0.0
Cross-channel	sand	12–Hamilton Bay	80.4	18.2	1.1	0.3	0.0	0.0	0.0	0.0
Cross-channel	silt	12–Hamilton Bay	49.7	49.2	0.3	0.0	0.6	0.3	0.0	0.0
Cross-channel	sand	13–Harwood Inter Tidal	54.1	42.3	1.0	0.8	0.3	0.5	0.3	0.7
Cross-channel	silt	13–Harwood Inter Tidal	34.7	60.7	1.2	1.0	0.5	0.4	0.5	1.0
Cross-channel	sand	14–Dunedin Bays	86.9	13.0	0.1	0.1	0.0	0.0	0.0	0.0
Cross-channel	silt	14–Dunedin Bays	82.1	17.9	0.0	0.0	0.0	0.0	0.0	0.0
Cross-channel	sand	15–Port Inter Tidal	0.0	80.3	8.4	8.4	2.6	0.3	0.0	0.0

Dredged site	Type	Harbour sub-area	% of Harbour sub-area in each deposition range (mm) over a 14-day period							
			0	< 0.1	0.1–0.2	0.2–0.5	0.5–1	1–2	2–5	> 5
Cross-channel	silt	15–Port Inter Tidal	0.0	70.8	9.6	8.8	5.2	4.5	1.1	0.0
Cross-channel	sand	16–Pulling Inter Tidal	0.0	31.0	13.7	25.3	17.6	8.2	4.0	0.2
Cross-channel	silt	16–Pulling Inter Tidal	0.0	17.2	11.2	17.7	16.3	18.2	15.1	4.4
Cross-channel	sand	17–Tayler Inter Tidal	3.7	41.1	8.4	15.3	13.5	11.6	6.1	0.3
Cross-channel	silt	17–Tayler Inter Tidal	0.9	35.3	8.3	11.3	8.7	12.0	15.8	7.7
Cross-channel	sand	18–Goat Channel	2.3	95.3	1.8	0.5	0.0	0.0	0.0	0.0
Cross-channel	silt	18–Goat Channel	0.6	95.0	1.6	1.2	1.4	0.2	0.0	0.0
Cross-channel	sand	19–Dunedin Channel	53.9	46.0	0.1	0.0	0.0	0.0	0.0	0.0
Cross-channel	silt	19–Dunedin Channel	49.9	49.9	0.1	0.1	0.1	0.0	0.0	0.0
Cross-channel	sand	20–Goat Inter Tidal	51.3	47.4	0.8	0.5	0.0	0.0	0.0	0.0
Cross-channel	silt	20–Goat Inter Tidal	17.7	80.2	0.7	0.7	0.5	0.2	0.0	0.0
Cross-channel	sand	21–Dunedin Inter Tidal	81.8	18.1	0.1	0.0	0.0	0.0	0.0	0.0
Cross-channel	silt	21–Dunedin Inter Tidal	73.5	26.3	0.1	0.1	0.0	0.1	0.0	0.0
Cross-channel	sand	22–Pudding Inter Tidal	68.9	30.3	0.5	0.3	0.0	0.0	0.0	0.0
Cross-channel	silt	22–Pudding Inter Tidal	56.2	42.4	0.3	0.5	0.4	0.2	0.0	0.0
Cross-channel	sand	23–Challis Inter Tidal	97.0	3.0	0.0	0.0	0.0	0.0	0.0	0.0
Cross-channel	silt	23–Challis Inter Tidal	98.8	1.2	0.0	0.0	0.0	0.0	0.0	0.0
Cross-channel	sand	24–Dunedin Embayment	100.0	0.0	0.0	0.0	0.0	0.0	0.0	0.0
Cross-channel	silt	24–Dunedin Embayment	100.0	0.0	0.0	0.0	0.0	0.0	0.0	0.0
Cross-channel	sand	25–Sawyers Bay	90.3	9.7	0.0	0.0	0.0	0.0	0.0	0.0
Cross-channel	silt	25–Sawyers Bay	92.9	7.1	0.0	0.0	0.0	0.0	0.0	0.0
Cross-channel	sand	26–Eastern Channel	68.8	30.9	0.2	0.2	0.0	0.0	0.0	0.0
Cross-channel	silt	26–Eastern Channel	67.9	31.8	0.1	0.1	0.1	0.0	0.0	0.0
Cross-channel	sand	27–Hamilton Inter Tidal	0.1	74.9	8.5	9.2	4.7	2.4	0.2	0.0
Cross-channel	silt	27–Hamilton Inter Tidal	0.0	69.2	7.5	7.2	5.1	6.2	4.5	0.5
Harington Bend	sand	1–Port Channel	11.4	29.1	7.5	11.8	10.4	10.7	13.1	5.9
Harington Bend	silt	1–Port Channel	9.1	26.1	5.3	6.6	6.9	10.6	14.6	20.8
Harington Bend	sand	2–Cross Channel	0.0	36.5	10.9	16.6	8.9	5.1	6.4	15.6

Dredged site	Type	Harbour sub-area	% of Harbour sub-area in each deposition range (mm) over a 14-day period							
			0	< 0.1	0.1–0.2	0.2–0.5	0.5–1	1–2	2–5	> 5
Harington Bend	silt	2–Cross Channel	0.0	21.5	12.0	14.1	11.2	10.9	9.2	21.0
Harington Bend	sand	3–Exported	41.3	51.9	2.6	3.1	1.0	0.1	0.0	0.0
Harington Bend	silt	3–Exported	38.2	48.7	4.5	4.1	2.2	1.9	0.5	0.0
Harington Bend	sand	4–Harington Channel	1.4	46.5	9.0	12.0	7.5	8.8	12.7	2.2
Harington Bend	silt	4–Harington Channel	0.2	36.7	10.3	10.4	6.9	8.2	11.7	15.6
Harington Bend	sand	5–Portobello	68.5	24.9	2.9	3.3	0.3	0.0	0.0	0.0
Harington Bend	silt	5–Portobello	59.3	28.1	4.3	4.4	2.2	1.5	0.2	0.0
Harington Bend	sand	6–Spit Channel	1.1	59.8	7.7	12.6	8.5	8.8	1.5	0.0
Harington Bend	silt	6–Spit Channel	0.6	37.2	17.8	13.3	8.0	8.8	12.2	2.0
Harington Bend	sand	7–Deborah Bay	68.8	30.0	0.8	0.5	0.0	0.0	0.0	0.0
Harington Bend	silt	7–Deborah Bay	44.3	54.2	0.2	0.9	0.3	0.2	0.0	0.0
Harington Bend	sand	8–Spit Inter Tidal	68.3	29.6	0.9	0.9	0.2	0.0	0.0	0.0
Harington Bend	silt	8–Spit Inter Tidal	65.1	32.6	0.9	1.1	0.0	0.2	0.0	0.0
Harington Bend	sand	9–Te Rauone Beach	74.8	24.6	0.6	0.0	0.0	0.0	0.0	0.0
Harington Bend	silt	9–Te Rauone Beach	70.8	28.8	0.4	0.0	0.0	0.0	0.0	0.0
Harington Bend	sand	10–Aramoana	86.1	12.9	0.5	0.5	0.0	0.0	0.0	0.0
Harington Bend	silt	10–Aramoana	75.5	23.2	0.4	0.2	0.4	0.3	0.0	0.0
Harington Bend	sand	11–Dowling Bay	59.8	39.4	0.3	0.5	0.0	0.0	0.0	0.0
Harington Bend	silt	11–Dowling Bay	49.6	47.1	1.3	1.0	0.5	0.5	0.0	0.0
Harington Bend	sand	12–Hamilton Bay	74.1	24.5	0.6	0.9	0.0	0.0	0.0	0.0
Harington Bend	silt	12–Hamilton Bay	50.0	48.3	0.3	0.3	0.6	0.6	0.0	0.0
Harington Bend	sand	13–Harwood Inter Tidal	93.9	5.3	0.1	0.2	0.1	0.2	0.1	0.0
Harington Bend	silt	13–Harwood Inter Tidal	78.2	20.7	0.2	0.1	0.1	0.2	0.3	0.2
Harington Bend	sand	14–Dunedin Bays	83.1	16.7	0.1	0.1	0.0	0.0	0.0	0.0
Harington Bend	silt	14–Dunedin Bays	67.0	32.5	0.1	0.2	0.1	0.1	0.0	0.0
Harington Bend	sand	15–Port Inter Tidal	0.6	61.9	11.1	16.9	8.1	1.2	0.3	0.0
Harington Bend	silt	15–Port Inter Tidal	0.0	57.5	12.1	12.1	8.1	6.4	3.2	0.6
Harington Bend	sand	16–Pulling Inter Tidal	12.6	76.0	5.1	4.7	1.1	0.4	0.0	0.0

Dredged site	Type	Harbour sub-area	% of Harbour sub-area in each deposition range (mm) over a 14-day period							
			0	< 0.1	0.1–0.2	0.2–0.5	0.5–1	1–2	2–5	> 5
Harington Bend	silt	16–Pulling Inter Tidal	0.2	77.9	9.0	6.2	3.4	2.5	0.7	0.1
Harington Bend	sand	17–Tayler Inter Tidal	49.5	47.5	1.6	1.4	0.1	0.0	0.0	0.0
Harington Bend	silt	17–Tayler Inter Tidal	27.4	67.5	3.0	0.8	0.4	0.7	0.2	0.0
Harington Bend	sand	18–Goat Channel	0.1	55.2	8.2	13.3	13.9	8.8	0.6	0.0
Harington Bend	silt	18–Goat Channel	0.0	45.2	8.2	9.4	7.8	11.8	14.0	3.6
Harington Bend	sand	19–Dunedin Channel	48.6	50.6	0.7	0.1	0.0	0.0	0.0	0.0
Harington Bend	silt	19–Dunedin Channel	22.0	76.5	0.5	0.6	0.2	0.2	0.0	0.0
Harington Bend	sand	20–Goat Inter Tidal	2.3	52.0	14.0	19.0	10.4	1.9	0.2	0.1
Harington Bend	silt	20–Goat Inter Tidal	1.4	39.2	12.9	19.1	11.8	11.3	3.9	0.4
Harington Bend	sand	21–Dunedin Inter Tidal	51.7	43.4	2.1	2.4	0.4	0.0	0.0	0.0
Harington Bend	silt	21–Dunedin Inter Tidal	21.5	71.2	2.0	2.7	1.5	1.0	0.1	0.0
Harington Bend	sand	22–Pudding Inter Tidal	49.2	41.6	2.9	4.4	1.7	0.2	0.0	0.0
Harington Bend	silt	22–Pudding Inter Tidal	33.0	51.9	4.3	4.4	2.6	2.6	1.1	0.1
Harington Bend	sand	23–Challis Inter Tidal	96.6	3.4	0.0	0.0	0.0	0.0	0.0	0.0
Harington Bend	silt	23–Challis Inter Tidal	82.2	17.6	0.0	0.1	0.1	0.0	0.0	0.0
Harington Bend	sand	24–Dunedin Embayment	100.0	0.0	0.0	0.0	0.0	0.0	0.0	0.0
Harington Bend	silt	24–Dunedin Embayment	97.4	2.6	0.0	0.0	0.0	0.0	0.0	0.0
Harington Bend	sand	25–Sawyers Bay	93.3	6.6	0.1	0.0	0.0	0.0	0.0	0.0
Harington Bend	silt	25–Sawyers Bay	86.8	12.8	0.1	0.1	0.1	0.1	0.0	0.0
Harington Bend	sand	26–Eastern Channel	46.9	46.7	2.6	2.5	1.2	0.1	0.0	0.0
Harington Bend	silt	26–Eastern Channel	32.3	56.8	2.2	3.0	2.9	2.0	0.8	0.0
Harington Bend	sand	27–Hamilton Inter Tidal	42.6	52.8	2.6	2.0	0.0	0.0	0.0	0.0
Harington Bend	silt	27–Hamilton Inter Tidal	7.5	88.1	1.6	0.9	1.3	0.7	0.0	0.0

Table 7.6: Statistics and associated areas (hectares) for accumulated deposition predicted in various sub-areas of Otago Harbour (Fig. 7.14 below this Table) from combined “silt” and “sand” claims over the entire dredging programme for the final channel design. The factors applied to each 14-day “silt” and “sand” simulations for each of the 5 discharge source locations are listed in Table 7.3. Note: areas based on units of 30×30 m model cells assigned to each sub-area. [1 ha = 10,000 m²].

Sub-area ID	Harbour sub-area	Total area (ha)	% sub-area where deposition is NIL	Average deposition (mm)	Median deposition (mm)	Deposition in 90% cells (mm)	Area for 90% cells (ha)	Deposition in 99% cells (mm)	Area for 99% cells (ha)
18	GOAT Channel	181.0	0.0	4.2	3.4	≤9.1	18.1	≤14.0	1.8
26	EASTERN Channel	107.2	27.9	0.3	0.01	≤1.0	10.7	≤5.1	1.1
19	DUNEDIN Channel	112.3	11.5	0.2	0.04	≤0.8	11.2	≤2.0	1.1
5	PORTOBELLO	412.8	34.4	0.8	0.1	≤2.4	41.3	≤9.6	4.1
7	DEBORAH BAY	59.7	17.6	0.2	0.04	≤0.6	6.0	≤1.5	0.6
8	SPIT Inter Tidal	39.4	34.9	0.1	0.02	≤0.3	3.9	≤0.9	0.4
9	TE RAUONE Beach	54.2	36.2	0.5	0.1	≤1.4	5.4	≤4.0	0.5
10	ARAMOANA	307.9	63.3	0.1	0.00	≤0.2	30.8	≤1.2	3.1
11	DOWLING Bay	35.4	18.8	0.1	0.02	≤0.2	3.5	≤1.2	0.4
12	HAMILTON Bay	31.7	15.6	0.1	0.02	≤0.2	3.2	≤1.1	0.3
13	HARWOOD Inter Tidal	311.3	26.3	1.0	0.001	≤0.1	31.1	≤24.4	3.1
14	DUNEDIN BAYS	165.5	21.9	0.1	0.01	≤0.5	16.6	≤1.7	1.7
15	PORT Inter Tidal	105.5	0.0	9.2	4.2	≤23.1	10.5	≤81.7	1.1
16	PULLING Inter Tidal	209.2	0.0	2.2	1.1	≤5.6	20.9	≤15.0	2.1
17	TAYLER Inter Tidal	166.2	0.1	1.8	0.6	≤5.1	16.6	≤13.2	1.7
20	GOAT Inter Tidal	288.6	1.1	1.2	0.6	≤2.9	28.9	≤7.5	2.9
21	DUNEDIN Inter Tidal	476.2	1.8	0.2	0.02	≤0.6	47.6	≤2.3	4.8
22	PUDDING Inter Tidal	261.1	19.4	1.5	0.1	≤5.6	26.1	13.2	2.6
23	CHALLIS Inter Tidal	405.5	44.3	0.0	0.001	≤0.04	40.6	≤0.7	4.1
24	DUNEDIN Embayment	203.4	88.5	0.0	0.000	≤0.002	20.3	≤0.2	2.0
25	SAWYERS Bay	85.9	42.0	0.2	0.02	≤0.7	8.6	≤1.8	0.9
27	HAMILTON Inter Tidal	178.1	0.0	0.6	0.2	≤1.6	17.8	≤4.8	1.8

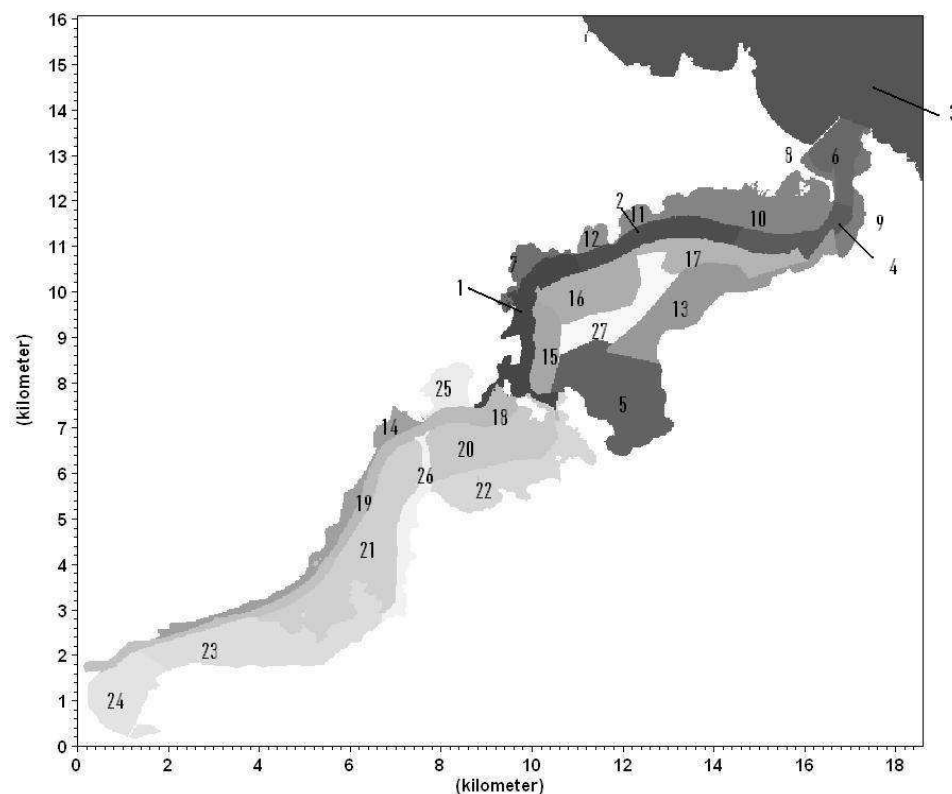


Figure 7.14: (same as Fig. 7.3) Otago Harbour receiving environment divided into sub-areas for integrating the seabed sediment deposition results from dredging sediment sources at five different channel discharge locations. The numbers for each sub-area are used along with a descriptive location name in the tabulated results below. Areas in hectares of these sub-areas are listed above in Table 7.6.

8. Offshore wave modelling

8.1 Wave model

SWAN (Simulating Waves Nearshore) was used for all the wave modelling including the wind-wave simulations for the Lower Harbour (discussed in Chapter 9).

SWAN is a third generation ocean wave propagation model, which solves the spectral action density balance equation for wavenumber-direction spectra. This means that the growth, refraction, and decay of each component of the complete sea state, each with a specific frequency and direction, is solved, giving a complete and realistic description of the wave field as it changes in time and space. Physical processes that are simulated include the generation of waves by surface wind, dissipation by white-capping, resonant nonlinear interaction between the wave components, bottom friction and depth limited breaking. A detailed description of the model equations, parameterizations, and numerical schemes can be found in Holthuijsen et al. (2007). All 3rd generation physics are included. The Collins friction scheme is used for wave dissipation by bottom friction.

The solution of the wavefield is found for the non-stationary (time-stepping) mode. Boundary conditions, wind forcing and resulting solutions are all time dependent, allowing the model to capture the growth, development and decay of the wavefield.

8.2 Model grid domains

Hindcast wave modelling of the existing and proposed dredging development applied a three-level nested scheme:

1. a coarse grid with resolution of 0.045° longitude by 0.044° latitude (~5.0 km by 3.4 km) covering the eastern side of southern New Zealand;
2. a regional grid with resolution of 0.0055° longitude by 0.0065° latitude (~0.6 km by 0.4 km) covering the area offshore the Otago Peninsula; and
3. a local grid of the Harbour Entrance with resolution of 0.0008° longitude by 0.0008° latitude (~90 m by 60 m) for the existing and proposed dredged bathymetry.

The three model domains are shown in Figure 8.1. The two larger domains were used to generate boundary conditions for the high-resolution Harbour Entrance domains (existing and the 15-m dredged initial channel design). Bathymetry data for the

regional and local resolution domains were derived from bathymetric charts and various survey data collected by Port Otago Ltd, as described in Chapter 3.

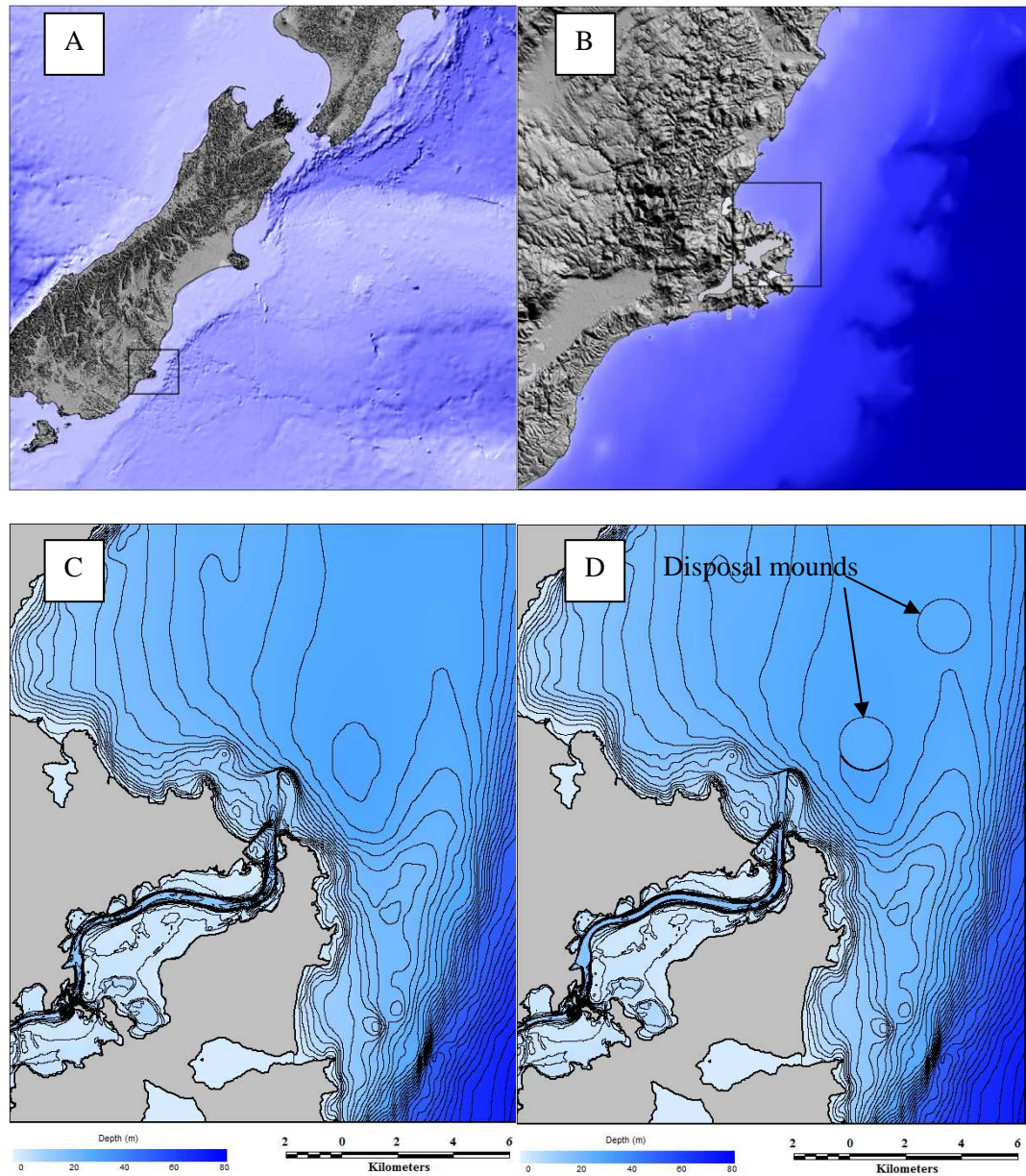


Figure 8.1: Wave model domains showing the regional grids (A and B) and the existing (C) and proposed dredged bathymetry (D) at the entrance region and Lower Harbour. The proposed bathymetry (for the initial channel design) includes two options for disposal mounds.

8.3 Model set-up

8.3.1 Boundary conditions

The wave spectra on the open-ocean boundaries of the coarse domain (eastern side of New Zealand) were obtained from the NOAA WAVEWATCH III (NWW3) solution. NWW3 is a state-of-the-art wave generation, propagation and transformation model for forecasting the evolution of directional wave energy spectra across the global oceans.

Along the open boundaries of the model domain, the primary statistical parameters of the incoming wavefield are interpolated from the NWW3 hindcast solution. Boundary spectra are then reconstructed by assuming a bi-modal Ochi-Hubble shape.

Boundary conditions for the high-resolution nested grids (Fig. 8.1) come directly from the coarse model domain.

8.3.2 Winds

The regional wind field is very important for wave generation. A spatially-varying wind field was specified from a blended global wind product developed by MetOcean Solutions. These data are 10 m elevation wind velocity vectors in a 3-hourly gridded format at a resolution of 0.25° of longitude and latitude. The wind field is a combination of the 6-hourly Blended Sea Winds data¹⁵ and the winds from the NWW3 hindcast. The blended data product combines the benefits of measured satellite data with the temporal resolution and continuous coverage of the modelled re-analysis.

8.3.3 Currents

Tidal current constituents (provided from the NIWA hydrodynamic Harbour model described in Chapter 4) were used to include the effects of the ebb and flood tidal jet on the wave transformation in the vicinity of the Harbour Entrance.

8.3.4 Model output

Directional wave spectra were hindcast at hourly intervals for a 10-year period (1998-2007), and the standard spectral wave parameters (e.g., significant wave height, peak spectral period) were output over the entire domain at 3-hourly intervals. The full directional spectra were also archived for discrete locations within the local domain, as shown on Figure 8.2 and detailed in Table 8.1. Derivation of wave statistics from the full (two-dimensional) directional spectra are described in Appendix I.

¹⁵ From NCDC, NOAA, Zhang et al. (2006).

Table 8.1: Output locations for directional wave spectra from the hindcast wave modelling for sites marked in Figure 8.2.

Location	Longitude (E)	Latitude (N)
Fairway Beacon	170.726933	-45.751173
CL1	170.726441	-45.747211
CL2	170.72554	-45.752749
CL3	170.72502	-45.756042
CL4	170.724278	-45.760833
CL5	170.723689	-45.764553
CL6	170.723226	-45.767543
CL7	170.722807	-45.77025
ADCP_DM	170.761933	-45.744917
ADCP_War	170.6381	-45.707717
A1	170.7119123	-45.77256352
A10	170.6240056	-45.73737116
A11	170.6127281	-45.72983225
A12	170.6080369	-45.72287302
A13	170.6071653	-45.71247963
A2	170.7060997	-45.76994478
A3	170.7024137	-45.7666724
A4	170.7001665	-45.76261542
A5	170.6834391	-45.758499
A6	170.6713394	-45.76005591
A7	170.6617056	-45.7572235
A8	170.6533445	-45.75208667
A9	170.6492974	-45.74554
I1	170.7139982	-45.7793576
Ref1	170.733442	-45.751175
S1	170.724267	-45.75412
S2	170.7232	-45.7627
S3	170.72213	-45.77485
S4	170.71999	-45.7884
B1	170.71617	-45.7785
B2	170.72371	-45.77784
B3	170.7232	-45.78881
B4	170.7121	-45.79675

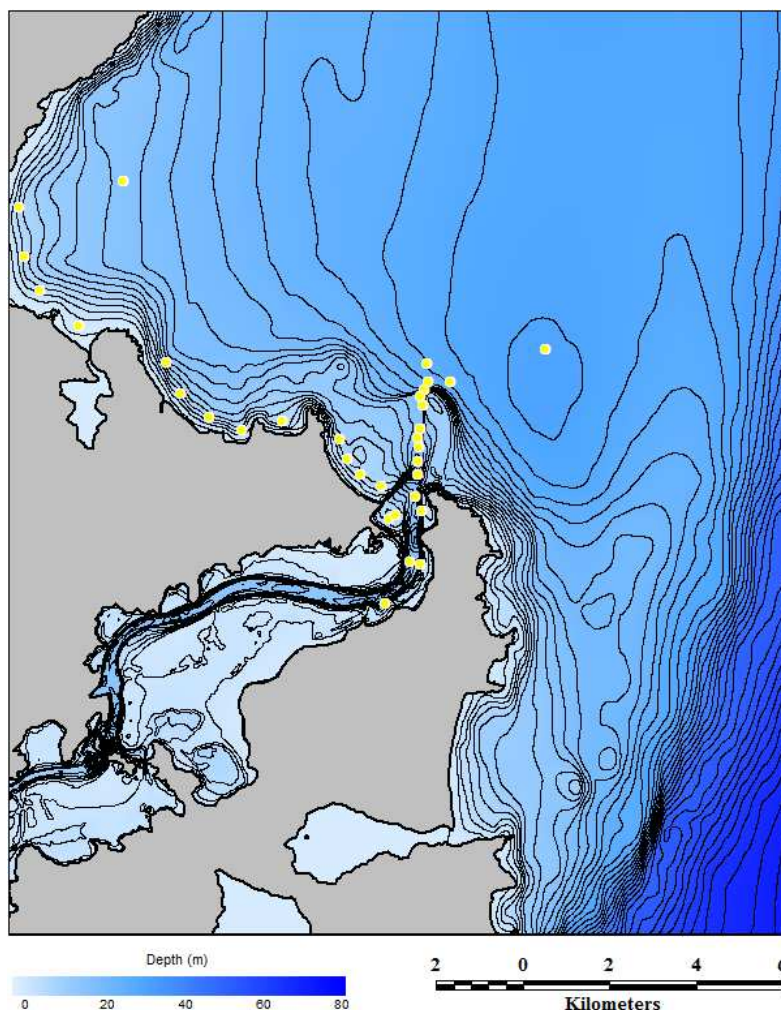


Figure 8.2: Output locations for directional spectra from the wave hindcast modelling that are listed in Table 8.1.

8.4 Wave hindcast validation

The hindcast wave model outputs have been validated with wave buoy data from numerous locations around New Zealand, in water depths ranging from 10–110 m (Figure 8.3). For the present study, a site-specific validation was undertaken using measured waverider data from the Tahuna outfall on the southern side of Otago Heads (Lawyers Head), which were observed from January to May 2007.

A time-series validation plot of the measured and hindcast significant wave heights is presented in Figure 8.4, indicating the numerical wave model for the Otago shelf is faithfully representing the periods of high and low energy. The measured and hindcast data have similar statistical means (1.40 m and 1.59 m, respectively) and medians (1.21 m and 1.36 m, respectively). Linear regression of the measured and hindcast wave heights show an R^2 correlation coefficient of 0.80, with slope of 1.08.

Further quantitative measures of the accuracy of the hindcast are calculated from the measured, x_m and hindcast, x_h , data. These are defined as:

$$\text{Mean absolute error: } \overline{|x_h - x_m|} \quad (8.1)$$

$$\text{RMS error: } \sqrt{\overline{(x_h - x_m)^2}} \quad (8.2)$$

$$\text{Mean relative absolute error: } \overline{\left| \frac{x_h - x_m}{x_m} \right|} \quad (8.3)$$

$$\text{Bias: } \overline{x_h - x_m} \quad (8.4)$$

where the line indicates an average over all pairs of measured/hindcast data. These four measures of accuracy are listed in Table 8.2.

The mean absolute error (MAE) is the most direct representation of what the typical deviation of the hindcast from the measured value. The RMS error exaggerates large differences in measured and hindcast wave heights and is therefore larger than the MAE. The mean relative absolute errors are an expression in percentage terms of the error compared to actual, and shown that the hindcast wave heights are on, average, within $\pm 15\%$ of the measured values (Table 8.2). The bias, which represents a constant ‘offset’ in the hindcast significant wave heights, indicates that overall the model slightly over predicts the wave heights by ~ 0.19 m. Notably, some of the error in the hindcast wave heights is due to timing of the wave events, as the hindcasting technique has an inherent phase resolution of ~ 3 hours. Also, the waverider buoy at Tahuna outfall was located close to the shore, and the regional wave model used in this validation has a resolution of approximately 0.5 km.

Table 8.2: Accuracy measures for hindcast significant wave heights based on Tahuna outfall wave buoy measurements. MAE: mean absolute error, RMSE: RMS error, MRAE: mean relative absolute error, BIAS: bias

MAE (m)	RMSE (m)	MRAE (%)	Bias (m)
0.33	0.42	0.15	0.19

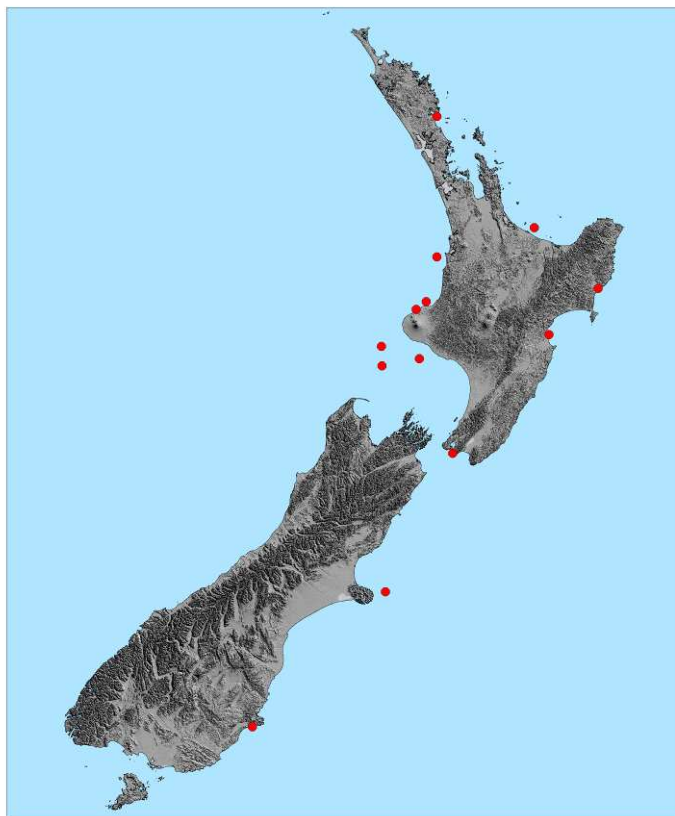


Figure 8.3: Wave hindcast validation sites around New Zealand.

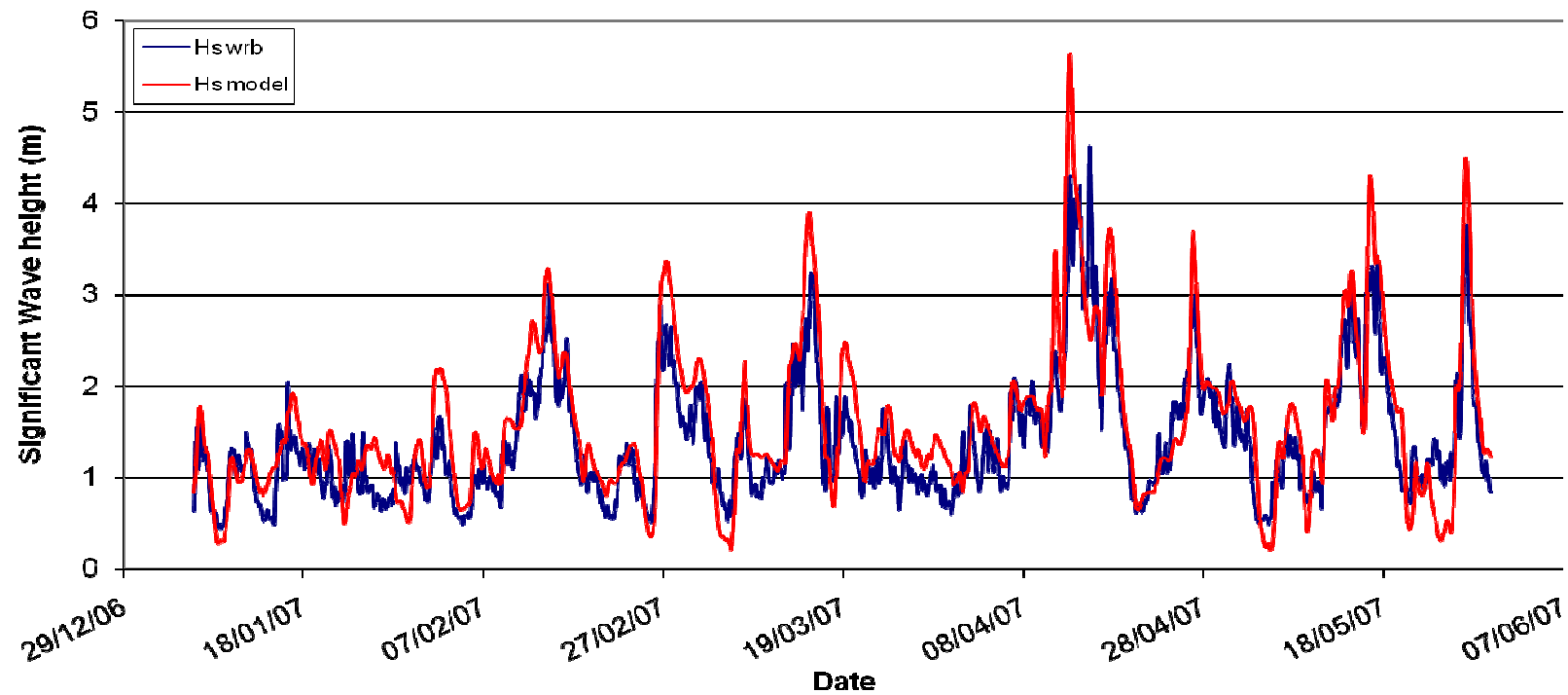


Figure 8.4: Time-series validation plot of the measured (waverider buoy—wrb) and hindcast (model) significant wave heights at Tahuna, Dunedin (Jan–May 2007).

8.5 Offshore and coastal wave climate

The Otago Peninsula provides a considerable wave shelter effect to the Harbour Entrance for the dominant incident wave conditions. Typically, sea and swell approach from the SE sector, and wave refraction is an important process in transferring wave energy from deepwater offshore to the entrance zone. This effect is clearly shown in the summary wave height maps on Figure 8.5. Here, the mean and the maximum significant wave heights from a 5-year period (2003–2007) are presented. Focussing of the wave energy by the ebb tidal bar is also evident on these maps.

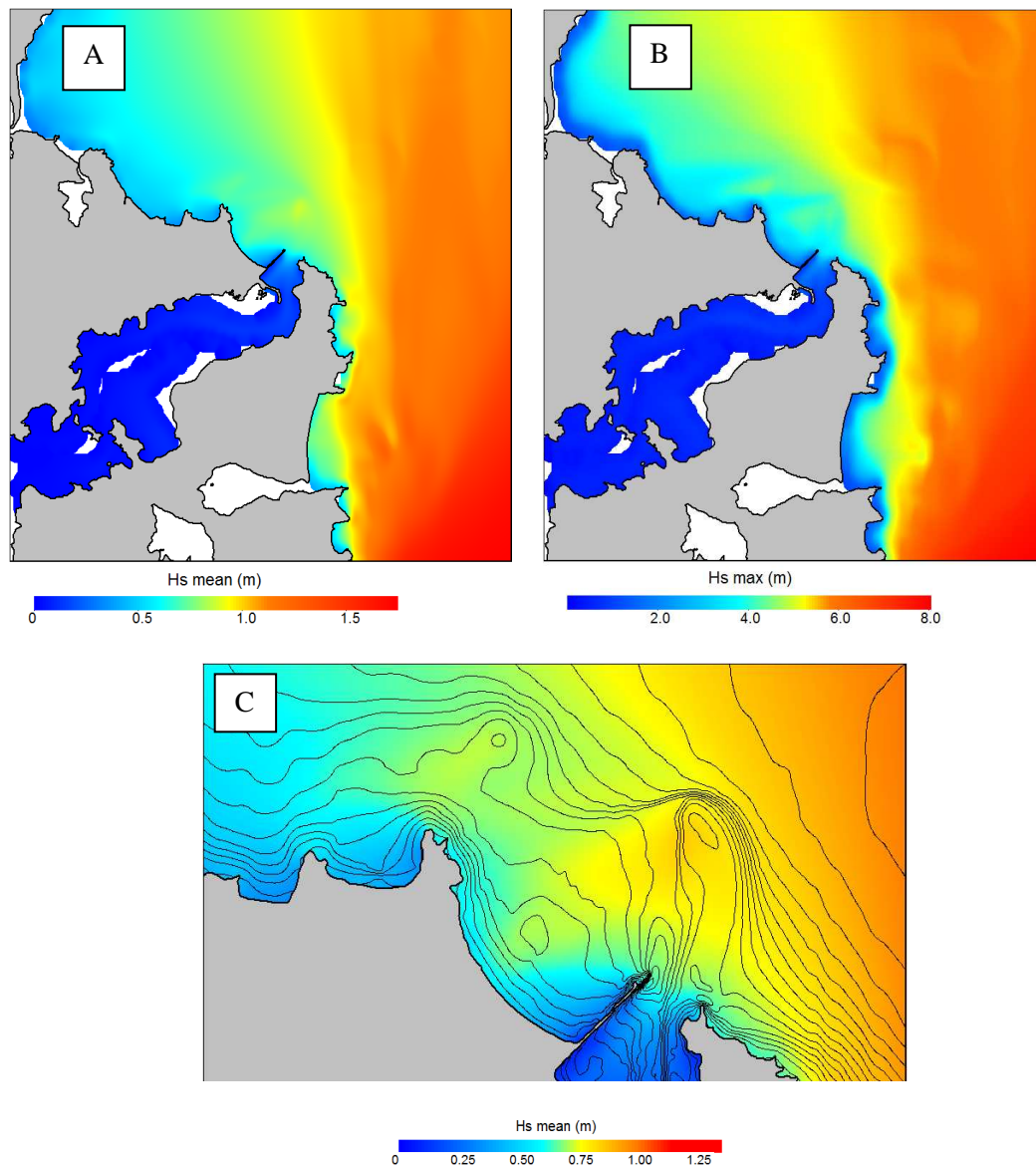


Figure 8.5: Mean (A) and maximum (B) significant wave heights over a 5-year period (2003–2007). A close-up of the mean wave heights near the entrance is provided on panel C.

Waves also approach the Harbour Entrance from the northeast, where there is no shelter afforded by the adjacent coast. Examples of the contrasting wave height patterns for SE and NE waves are provided in Figure 8.6.

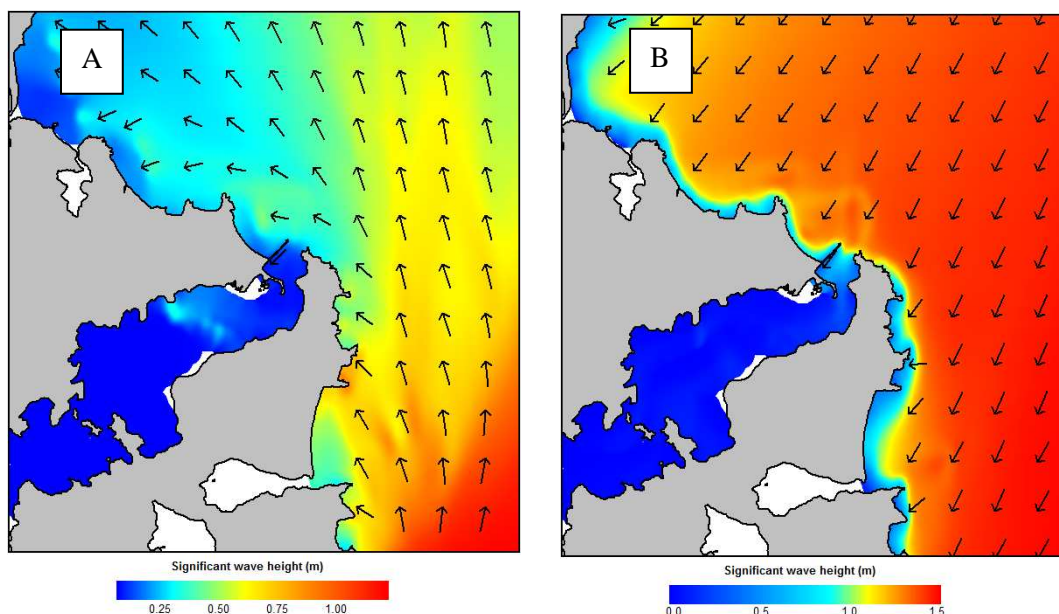


Figure 8.6: Typical wave height patterns for waves from the southeast (A) and the northeast (B).

A detailed analysis of the wave climate has been undertaken for two representative locations; an offshore site (labelled ADCP-DM, which is also known as disposal option A1) and a location near the fairway beacon on Landfall Tower (labelled Ref-1). These sites are shown on Figure 8.7.

Annual, seasonal and monthly significant wave height statistics for each site are presented in Table 8.3. Site Ref-1 clearly receives more wave sheltering than the offshore ADCP-DM location; the mean annual significant wave height (H_s) at ADCP-DM is 1.06 m while at Ref-1 it is 0.85 m. As expected, the winter and autumn months are more energetic, while November is the least energetic month.

The annual joint probability distributions of significant wave height and peak wave period are presented in Tables 8.4 and 8.5 for ADCP-DM and Ref-1, respectively. The largest waves tend to have peak periods in the range 10–13 seconds, and the height–period distribution is similar for both locations. The annual joint probability distributions of significant wave height and wave direction are presented in Tables 8.6 and 8.7 for ADCP-DM and Ref-1, respectively. At the offshore location (ADCP-DM), two directional modes are evident from the NE and the SE. Wave directions are constrained near the entrance region (Table 8.7).

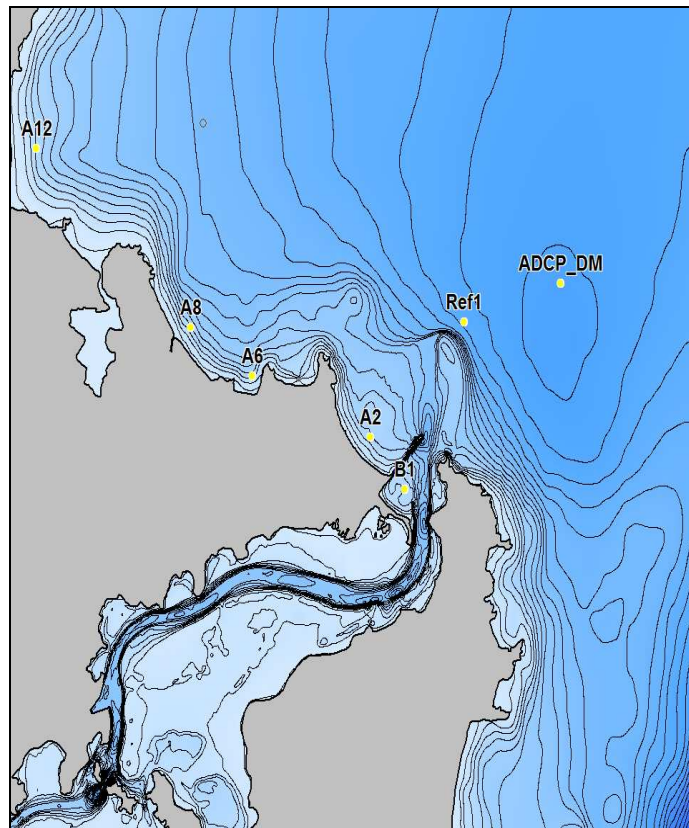


Figure 8.7: Wave model hindcast output locations. Note: ADCP-DM is also otherwise known as disposal site option A1 in other sections of this report and in Bell & Hart (2008).

Table 8.3: Annual, seasonal and monthly significant wave height statistics for sites ADCP-DM and Ref-1 (shown in Fig. 8.7).

Site	Mean (m)		Median (m)		90th percentile (m)		95th percentile (m)		99th percentile (m)	
	ADCP-DM	Ref-1	ADCP-DM	Ref-1	ADCP-DM	Ref-1	ADCP-DM	Ref-1	ADCP-DM	Ref-1
Annual	1.06	0.85	0.93	0.74	1.78	1.49	2.13	1.81	2.93	2.53
Winter	1.22	0.98	1.06	0.84	2.13	1.83	2.59	2.22	3.39	2.84
Autumn	1.09	0.86	0.96	0.74	1.85	1.49	2.19	1.78	2.93	2.60
Spring	0.95	0.75	0.87	0.68	1.53	1.22	1.78	1.42	2.37	1.98
Summer	0.97	0.82	0.86	0.70	1.60	1.45	1.88	1.68	2.69	2.30
January	0.91	0.80	0.79	0.67	1.48	1.38	1.81	1.64	2.90	2.74
February	1.04	0.87	0.94	0.77	1.71	1.53	1.91	1.75	2.67	2.10
March	1.00	0.81	0.88	0.69	1.62	1.31	2.02	1.59	2.90	2.79
April	1.12	0.86	0.95	0.72	2.02	1.61	2.41	2.03	3.14	2.65
May	1.14	0.91	1.05	0.81	1.84	1.53	2.05	1.72	2.61	2.02
June	1.18	0.89	1.07	0.81	1.89	1.51	2.44	1.88	3.40	2.36
July	1.16	0.95	0.99	0.82	2.04	1.79	2.29	2.09	3.19	3.10
August	1.32	1.11	1.16	0.93	2.46	2.18	2.82	2.42	3.44	2.98
September	0.99	0.80	0.87	0.72	1.64	1.30	2.03	1.53	2.68	2.13
October	0.95	0.75	0.88	0.68	1.53	1.21	1.73	1.41	2.10	1.97
November	0.91	0.69	0.85	0.64	1.46	1.11	1.65	1.34	2.05	1.73
December	0.97	0.80	0.85	0.68	1.65	1.42	1.90	1.63	2.27	1.93

Table 8.4: Annual significant wave height and peak period joint-probability at site ADCP-DM in parts-per-thousand (ppt). For example, 15.2 ppt is equivalent to 1.52%.

	Annual	Peak wave period (s)																				
		0 to 1	1 to 2	2 to 3	3 to 4	4 to 5	5 to 6	6 to 7	7 to 8	8 to 9	9 to 10	10 to 11	11 to 12	12 to 13	13 to 14	14 to 15	15 to 16	16 to 17	17 to 18	18 to 19	19 to 20	SUM
Significant wave height (m)	> 0 ≤ 0.5	0	0.1	15.2	2.2	6.8	4.8	3.7	3.3	3.2	3.3	8.7	19.5	19.3	15.4	3.7	1	0.3	0	0.1	0	110.6
	> 0.5 ≤ 1	0	0	10.1	38.1	15.9	17.4	19.6	22.9	23.6	25.4	36	59.1	71.3	75.7	21.3	9.3	1.9	0.8	0.2	0	448.6
	> 1 ≤ 1.5	0	0	0	6.2	14.3	13.6	9.9	17.8	31.4	33.7	31.2	35	30.8	33	9.8	2.8	0.3	0.1	0	0	269.9
	> 1.5 ≤ 2	0	0	0	0	0.5	5.7	5.4	4.1	7.1	16.2	20.7	18.1	12.1	12	3.8	0.8	0.1	0	0	0	106.6
	> 2 ≤ 2.5	0	0	0	0	0	0.3	3.4	1.7	1	2.9	7.4	8.5	5.8	4.7	1.7	0.7	0	0	0	0	38.1
	> 2.5 ≤ 3	0	0	0	0	0	0	0.3	0.6	0.9	1.2	1.9	5.7	3.9	2.5	0.3	0	0	0	0	0	17.3
	> 3 ≤ 3.5	0	0	0	0	0	0	0	0.4	0.6	0.3	0.2	1.3	1.4	1.4	0.6	0	0	0	0	0	6.2
	> 3.5 ≤ 4	0	0	0	0	0	0	0	0	0.1	0	0	0.1	0.3	0.7	0.1	0	0	0	0	0	1.3
	> 4 ≤ 4.5	0	0	0	0	0	0	0	0	0.1	0	0	0.1	0.1	0	0	0	0	0	0	0	0.3
	> 4.5 ≤ 5	0	0	0	0	0	0	0	0	0	0.2	0.1	0	0.1	0	0	0	0	0	0	0	0.4
	> 5 ≤ 5.5	0	0	0	0	0	0	0	0	0	0	0.1	0.1	0.1	0	0	0	0	0	0	0	0.3
	> 5.5 ≤ 6	0	0	0	0	0	0	0	0	0	0	0	0.1	0	0	0	0	0	0	0	0	0.1
	SUM	0	0.1	25.3	46.5	37.5	41.8	42.3	50.8	68	83.2	106.3	147.6	145.2	145.4	41.3	14.6	2.6	0.9	0.3	0	1000

Table 8.5: Annual significant wave height and peak period joint-probability at site Ref-1 in parts-per-thousand (ppt). For example, 34.5 ppt is equivalent to 3.45%.

		Peak wave period (s)																				
		0 to 1	1 to 2	2 to 3	3 to 4	4 to 5	5 to 6	6 to 7	7 to 8	8 to 9	9 to 10	10 to 11	11 to 12	12 to 13	13 to 14	14 to 15	15 to 16	16 to 17	17 to 18	18 to 19	19 to 20	SUM
Significant wave height (m)	> 0 ≤ 0.5	0	0.5	34.5	5.9	11.1	11.3	10.2	8.2	4.4	4.7	15.2	30.1	35.3	46.8	14.2	4.6	1.3	0.4	0.1	0	238.8
	> 0.5 ≤ 1	0	0	24.6	65.8	27.7	25.3	28.2	31.6	40.1	31.5	25.1	36.3	44.3	61.8	28.9	10.2	3.7	0.6	0.3	0	486
	> 1 ≤ 1.5	0	0	0	5.7	13.4	12.7	9.4	14.6	23	29.3	23.2	15.1	8.9	13.4	7.8	2.3	0.1	0.1	0	0	179
	> 1.5 ≤ 2	0	0	0	0	0.2	5.5	4.6	2.9	3.9	10.2	15.4	10.3	4.9	4	0.5	0.5	0	0	0	0	62.9
	> 2 ≤ 2.5	0	0	0	0	0	0.2	2.4	1	0.6	0.9	2.6	8.3	3.8	2.4	0.6	0.3	0	0	0	0	23.1
	> 2.5 ≤ 3	0	0	0	0	0	0	0.2	0.6	0.8	0.8	0.9	1.3	1.6	1.6	0	0	0	0	0	0	7.8
	> 3 ≤ 3.5	0	0	0	0	0	0	0	0.3	0.6	0	0	0.2	0.1	0.5	0	0	0	0	0	0	1.7
	> 3.5 ≤ 4	0	0	0	0	0	0	0	0	0.1	0.1	0	0.1	0.1	0	0	0	0	0	0	0	0.4
	> 4 ≤ 4.5	0	0	0	0	0	0	0	0	0	0.1	0.1	0.1	0.1	0	0	0	0	0	0	0	0.4
	> 4.5 ≤ 5	0	0	0	0	0	0	0	0	0	0	0.2	0.1	0.1	0	0	0	0	0	0	0	0.4
	> 5 ≤ 5.5	0	0	0	0	0	0	0	0	0	0	0	0	0	0	0	0	0	0	0	0	0
	> 5.5 ≤ 6	0	0	0	0	0	0	0	0	0	0	0	0	0	0	0	0	0	0	0	0	0
	SUM	0	0.5	59.1	77.4	52.4	55	55	59.2	73.5	77.6	82.7	101.9	99.2	130.5	52	17.9	5.1	1.1	0.4	0	1000

Table 8.6: Annual significant wave height and direction joint-probability at site ADCP-DM in parts-per-thousand (ppt). For example, 14.3 ppt is equivalent to 1.43%.

		Wave direction (°T)																
		348.75 to 11.25	11.25 to 33.75	33.75 to 56.25	56.25 to 78.75	78.75 to 101.25	101.25 to 123.75	123.75 to 146.25	146.25 to 168.75	168.75 to 191.25	191.25 to 213.75	213.75 to 236.25	236.25 to 258.75	258.75 to 281.25	281.25 to 303.75	303.75 to 326.25	326.25 to 348.75	SUM
Significant wave height (m)	> 0 ≤ 0.5	6.5	5.6	7.9	8.2	7.6	8	8.1	20.5	11.9	3.5	2.9	2.4	2.6	3.3	5.4	6.3	110.7
	> 0.5 ≤ 1	14.3	23.1	36.8	47.7	37	29.1	34.4	88.3	39.2	20.2	14.5	13.3	14.6	13.5	10.6	11.9	448.5
	> 1 ≤ 1.5	2.7	7.8	24.1	43.6	29.2	17.9	19	59.2	34.8	13.6	7.1	4.5	3.1	1	1.2	1.2	270
	> 1.5 ≤ 2	0.1	0.6	6.6	18.4	15.5	11.1	11.4	21.6	15.7	3.8	0.9	0.7	0.1	0	0	0	106.5
	> 2 ≤ 2.5	0	0.2	2	4.2	6	5.8	6.3	7.3	6	0.4	0	0	0	0	0	0	38.2
	> 2.5 ≤ 3	0	0	0.3	1.2	2.7	4.7	4.3	2.1	2.1	0	0	0	0	0	0	0	17.4
	> 3 ≤ 3.5	0	0	0.1	0.9	0.3	1.5	1.3	1.3	0.8	0	0	0	0	0	0	0	6.2
	> 3.5 ≤ 4	0	0	0	0.1	0	0.2	0.6	0.2	0.2	0	0	0	0	0	0	0	1.3
	> 4 ≤ 4.5	0	0	0	0.1	0	0.1	0.1	0	0	0	0	0	0	0	0	0	0.3
	> 4.5 ≤ 5	0	0	0	0.1	0	0.1	0.1	0	0	0	0	0	0	0	0	0	0.3
	> 5 ≤ 5.5	0	0	0	0	0	0.2	0.1	0	0	0	0	0	0	0	0	0	0.3
	> 5.5 ≤ 6	0	0	0	0	0	0	0.1	0	0	0	0	0	0	0	0	0	0.1
		SUM	23.6	37.3	77.8	124.5	98.3	78.7	85.8	200.5	110.7	41.5	25.4	20.9	20.4	17.8	17.2	19.4

Table 8.7: Annual significant wave height and direction joint-probability at site Ref-1 in parts-per-thousand (ppt). For example, 14.3 ppt is equivalent to 1.43%.

		Wave direction (°T)																SUM
		348.75 to 11.25	11.25 to 33.75	33.75 to 56.25	56.25 to 78.75	78.75 to 101.25	101.25 to 123.75	123.75 to 146.25	146.25 to 168.75	168.75 to 191.25	191.25 to 213.75	213.75 to 236.25	236.25 to 258.75	258.75 to 281.25	281.25 to 303.75	303.75 to 326.25	326.25 to 348.75	
Significant wave height (m)	> 0 ≤ 0.5	14.3	15.9	22.1	26.2	16.3	19.3	36.9	17.5	6.4	4.3	3.8	4.6	8.7	13.1	14.9	14.3	238.6
	> 0.5 ≤ 1	22.4	36.5	60.2	70	34.8	29.4	61.9	29.8	14.2	10.2	10.6	12.3	24.1	30.7	20.4	18.3	485.8
	> 1 ≤ 1.5	1.8	6.8	25.8	47.1	28.5	16.4	17.1	11	6.7	4.9	3.3	3	2.8	2.7	0.8	0.4	179.1
	> 1.5 ≤ 2	0	0.4	6.9	19.9	14.4	10.4	5.5	1.4	1.8	1.3	0.6	0.2	0	0	0	0	62.8
	> 2 ≤ 2.5	0	0	1.8	4.1	7.1	6.8	1.3	1	0.7	0.1	0	0	0	0	0	0	22.9
	> 2.5 ≤ 3	0	0	0.2	1.5	2.6	3.1	0.2	0	0	0	0	0	0	0	0	0	7.6
	> 3 ≤ 3.5	0	0	0	1	0.1	0.7	0	0	0	0	0	0	0	0	0	0	1.8
	> 3.5 ≤ 4	0	0	0	0.1	0.1	0.1	0	0	0	0	0	0	0	0	0	0	0.3
	> 4 ≤ 4.5	0	0	0	0.1	0.1	0.2	0	0	0	0	0	0	0	0	0	0	0.4
	> 4.5 ≤ 5	0	0	0	0.1	0.1	0.2	0	0	0	0	0	0	0	0	0	0	0.4
	> 5 ≤ 5.5	0	0	0	0	0	0	0	0	0	0	0	0	0	0	0	0	0
	> 5.5 ≤ 6	0	0	0	0	0	0	0	0	0	0	0	0	0	0	0	0	0
	SUM	38.5	59.6	117	170.1	104.1	86.6	122.9	60.7	29.8	20.8	18.3	20.1	35.6	46.5	36.1	33	1000

8.6 Effects of dredging on the offshore wave climate

Waves refract, shoal and dissipate as they approach the shore, and the nearshore wave climate will respond to changes to the offshore bathymetry. The proposed Harbour developments include the creation of an offshore disposal site (see Section 11.2 for more details) and a deeper entrance channel—these changes have the potential to influence the adjacent wave climate. To examine and quantify these changes, the numerical wave hindcast model was used to simulate waves over a 5-year period (2003–2007) using the modified bathymetry (initial channel design), and then the model outputs were compared directly with the existing bathymetry simulation. The existing and proposed bathymetries are illustrated in Figure 8.1 (panel C and D), while Figure 8.8 illustrates the difference in the bathymetries used (positive depth change for two options for a dredged-material disposal site and negative depth change for dredged areas associated with the 15-m deep Harbour channel (initial design). Note: the two disposal area options were modelled simultaneously in the wave hindcast model, assuming the distance between the offshore mounds in the model would be sufficient for the effects to be independent.

The comparisons between the mean and maximum significant wave heights over the 5-year hindcast are shown on Figures 8.9 and 8.10, respectively. The furthest offshore disposal mound option [A2] on the offshore submergent Peninsula Spit would have little discernable impact on the wave patterns, especially mean wave height (Fig. 8.9), while the mound option closer to Taiaroa Head [A1] has a minor focussing effect in the lee of the mound (i.e., to the NW). The biggest changes associated with dredging for maximum significant wave heights would be only 3–5% of the wave heights for the existing situation, and the maps (Figs. 8.9–8.10) show no evidence of persistent shoreline effects that would: i) be detrimental to surfing conditions; or ii) give rise to adverse coastal erosion impacts.

The impacts are further quantified by a detailed analysis of the time-series of wave hindcast data (existing versus modified) at discrete locations along the coast (as shown on Figure 8.7). Annual, seasonal and monthly significant wave height statistics have been used to quantify the expected changes in the wave height at various locations along the coast, and the results are presented in Tables 8.8–8.14.

With regard to coastal effects, there would be a very slight reduction in wave heights at some locations near the entrance. For example, in the middle of Aramoana Beach (coastal site A2 on Fig. 8.7 and Table 8.10) the reduction in height would be around 0.01 m for a dredged channel associated with the 15-m deep Harbour channel option. At Shelly Beach near The Mole (coastal site B1 on Fig. 8.7 and Table 8.14) the wave height reduction would be around 0.02–0.04 m. These effects would be due to the dredged approach channel and wave refraction over the nearshore disposal mound option (Fig. 8.10).

Following subsequent fine-tuning of the initial channel design, minor changes were made to the channel dimensions resulting in a slight reduction of 6% in the overall volume to be dredged for the final channel design. In the offshore half of the approach channel where the wave exposure is greatest, the channel design depths remain the same as that modelled (17.5 m relative to Chart Datum), but the width at the offshore end has been reduced.

Notably, the disposal mounds that have been modelled and discussed above represent the original base-case assessment, which is some 6% larger by volume. Accordingly, these wave model results provide a more conservative estimate of the effects for the modifications to the channel design. Because the mound will be around 6% lower (but same area), the effects on the wave climate will be lessened somewhat.

The wave modelling also included the effect of wave refraction due to the ebb and flood tidal currents. These flow patterns for the final dredged channel design will vary only slightly from the modelled configurations (e.g., channel depths are the same in the approach channel), and are not expected to have shown any significant change in the results of effects on inshore wave patterns.

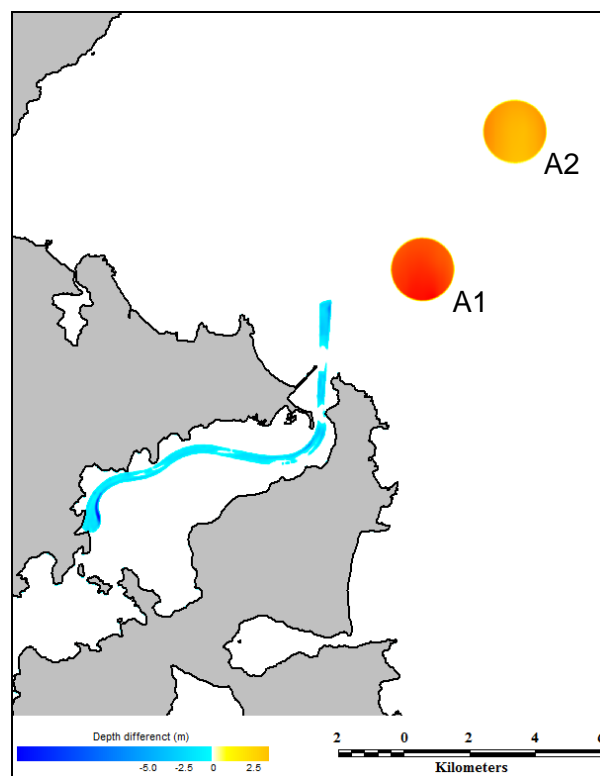


Figure 8.8: Bathymetry difference between the existing bathymetry and proposed modifications for the dredged 15-m option (initial design) and two disposal area options, A1 and A2.

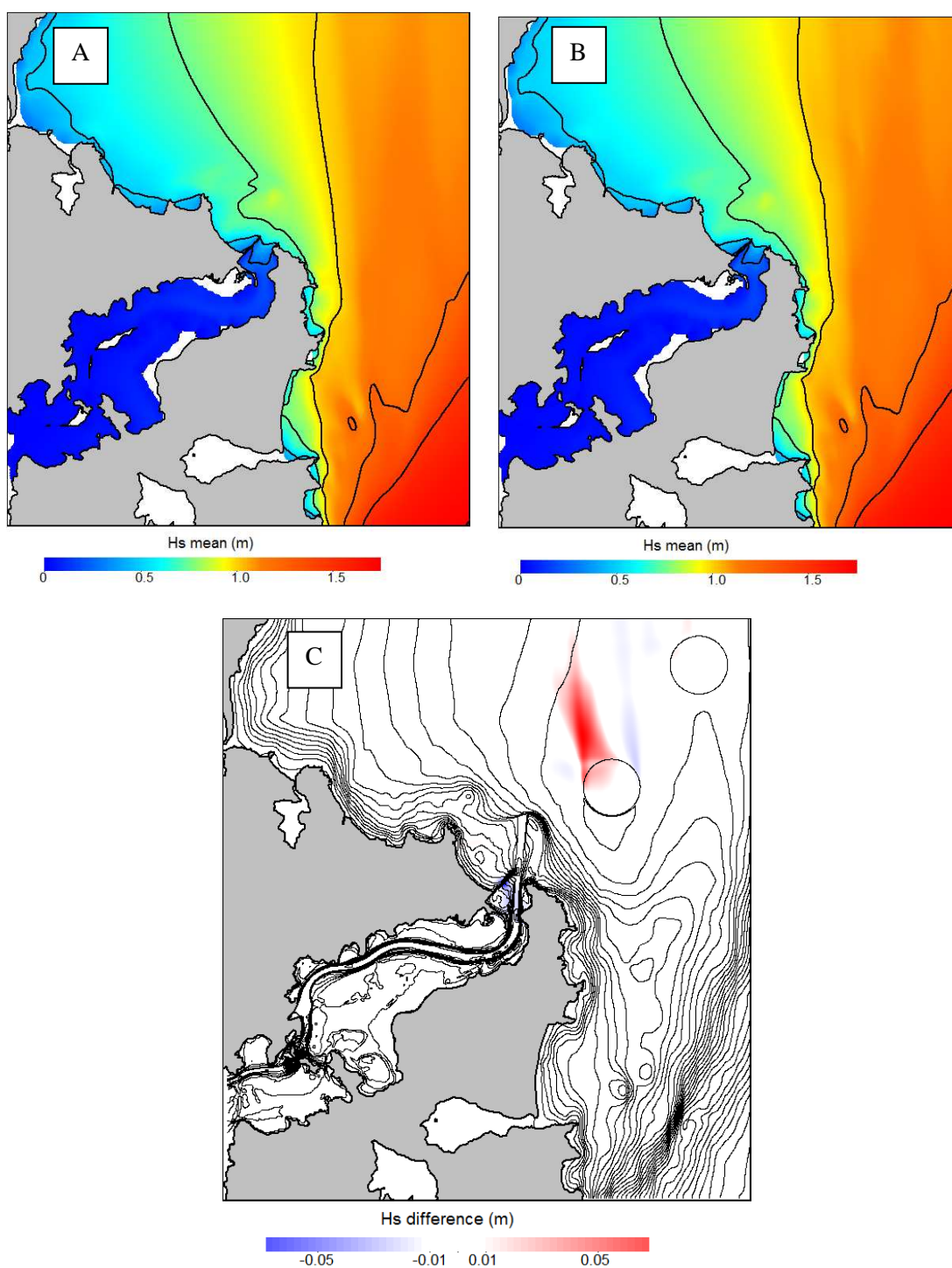


Figure 8.9: Mean significant wave height (m) over 2003–2007 for the existing (A) and modified (B) bathymetries, plus the predicted differences in mean wave height (C).

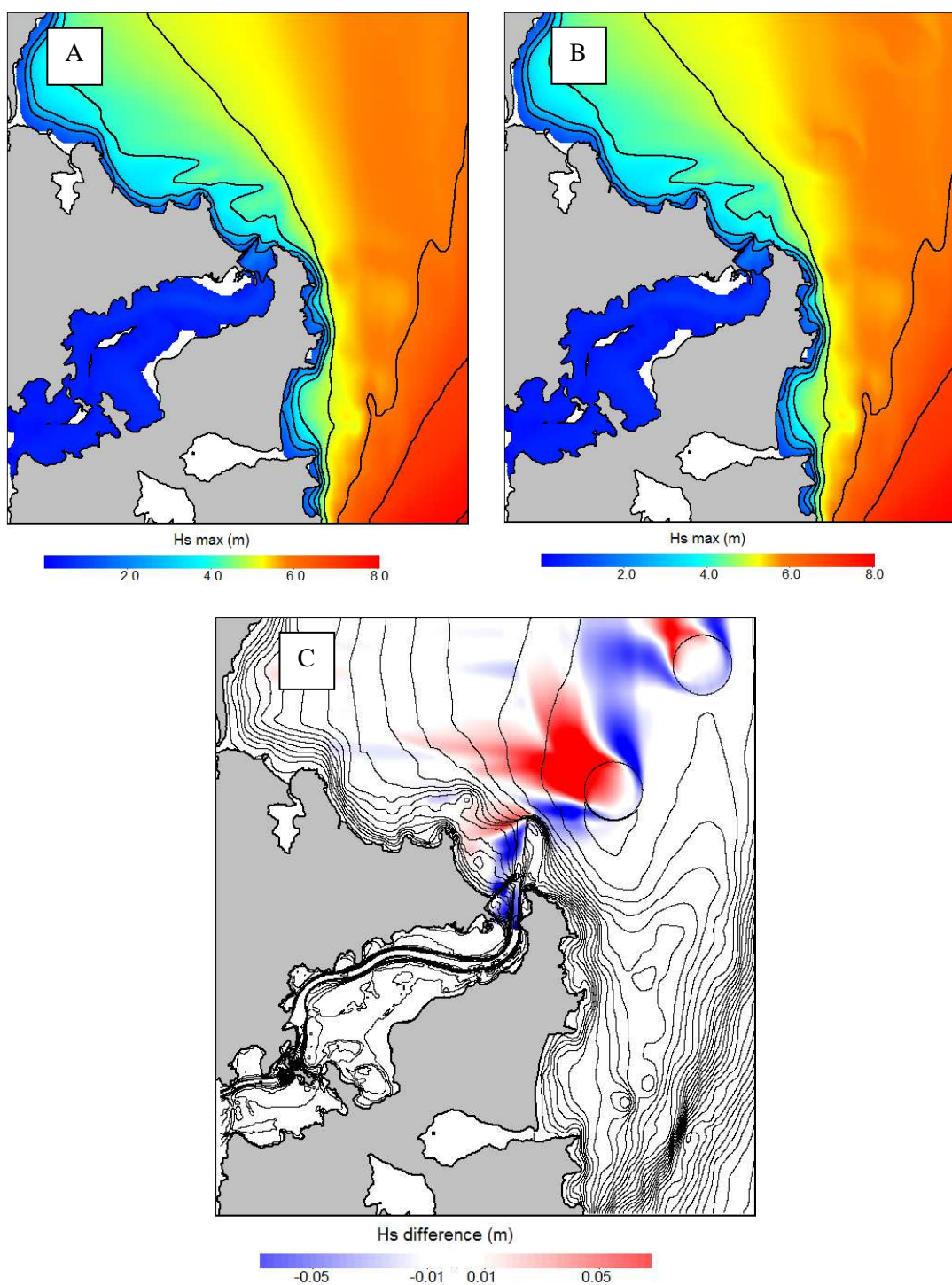


Figure 8.10: Maximum significant wave height (m) for 2003–2007 for the existing (A) and modified (B) bathymetries, plus the differences in maximum wave height (C).

Table 8.8: Annual, seasonally and monthly wave statistics for the existing and proposed bathymetry at site ADCP-DM (also known as disposal site A1).

ADCP-DM	Mean (m)			Median (m)			90th percentile (m)			95th percentile (m)			99th percentile (m)			Mean
	Existing	Proposed	Difference	Existing	Proposed	Difference	Existing	Proposed	Difference	Existing	Proposed	Difference	Existing	Proposed	Difference	
Annual	1.06	1.07	0.01	0.93	0.94	0.01	1.78	1.80	0.02	2.13	2.15	0.02	2.93	2.97	0.04	0.02
Winter	1.22	1.24	0.02	1.06	1.07	0.01	2.13	2.16	0.03	2.59	2.62	0.03	3.39	3.46	0.07	0.03
Autumn	1.09	1.10	0.01	0.96	0.97	0.01	1.85	1.87	0.02	2.19	2.22	0.03	2.93	2.98	0.05	0.02
Spring	0.95	0.96	0.01	0.87	0.88	0.01	1.53	1.54	0.01	1.78	1.80	0.02	2.37	2.40	0.03	0.02
Summer	0.97	0.97	0.00	0.86	0.87	0.01	1.60	1.61	0.01	1.88	1.89	0.01	2.69	2.71	0.02	0.01
January	0.91	0.92	0.01	0.79	0.79	0.00	1.48	1.48	0.00	1.81	1.81	0.00	2.90	2.91	0.01	0.00
February	1.04	1.05	0.01	0.94	0.95	0.01	1.71	1.72	0.01	1.91	1.91	0.00	2.67	2.68	0.01	0.01
March	1.00	1.01	0.01	0.88	0.88	0.00	1.62	1.63	0.01	2.02	2.03	0.01	2.90	2.95	0.05	0.02
April	1.12	1.14	0.02	0.95	0.96	0.01	2.02	2.05	0.03	2.41	2.44	0.03	3.14	3.20	0.06	0.03
May	1.14	1.15	0.01	1.05	1.07	0.02	1.84	1.85	0.01	2.05	2.08	0.03	2.61	2.65	0.04	0.02
June	1.18	1.19	0.01	1.07	1.08	0.01	1.89	1.90	0.01	2.44	2.48	0.04	3.40	3.47	0.07	0.03
July	1.16	1.17	0.01	0.99	1.00	0.01	2.04	2.07	0.03	2.29	2.31	0.02	3.19	3.19	0.01	0.01
August	1.32	1.34	0.02	1.16	1.17	0.01	2.46	2.48	0.02	2.82	2.86	0.04	3.44	3.51	0.06	0.03
September	0.99	1.00	0.01	0.87	0.88	0.01	1.64	1.66	0.02	2.03	2.06	0.03	2.68	2.73	0.05	0.02
October	0.95	0.96	0.01	0.88	0.89	0.01	1.53	1.54	0.01	1.73	1.74	0.01	2.10	2.10	0.00	0.01
November	0.91	0.91	0.00	0.85	0.86	0.01	1.46	1.48	0.02	1.65	1.66	0.01	2.05	2.07	0.02	0.01
December	0.97	0.97	0.00	0.85	0.85	0.00	1.65	1.66	0.01	1.90	1.92	0.02	2.27	2.30	0.03	0.01
Mean			0.01			0.01			0.02			0.02			0.04	

Table 8.9: Annual, seasonally and monthly wave statistics for the existing and proposed bathymetry at site Ref-1 (Landfall Tower).

	Mean (m)			Median (m)			90th percentile (m)			95th percentile (m)			99th percentile (m)			
Ref-1	Existing	Proposed	Difference	Existing	Proposed	Difference	Existing	Proposed	Difference	Existing	Proposed	Difference	Existing	Proposed	Difference	Mean
Annual	0.85	0.86	0.01	0.74	0.74	0.00	1.49	1.50	0.01	1.81	1.83	0.02	2.53	2.53	0.00	0.01
Winter	0.98	0.99	0.01	0.84	0.85	0.01	1.83	1.84	0.01	2.22	2.24	0.02	2.84	2.79	-0.05	0.00
Autumn	0.86	0.86	0.00	0.74	0.74	0.00	1.49	1.49	0.00	1.78	1.79	0.01	2.60	2.61	0.01	0.00
Spring	0.75	0.75	0.00	0.68	0.68	0.00	1.22	1.22	0.00	1.42	1.43	0.01	1.98	1.99	0.01	0.00
Summer	0.82	0.83	0.01	0.70	0.70	0.00	1.45	1.47	0.02	1.68	1.69	0.01	2.30	2.27	-0.03	0.00
January	0.80	0.80	0.00	0.67	0.67	0.00	1.38	1.39	0.01	1.64	1.63	-0.01	2.74	2.73	-0.01	0.00
February	0.87	0.88	0.01	0.77	0.77	0.00	1.53	1.55	0.02	1.75	1.79	0.04	2.10	2.10	0.00	0.01
March	0.81	0.81	0.00	0.69	0.69	0.00	1.31	1.33	0.02	1.59	1.60	0.01	2.79	2.91	0.12	0.03
April	0.86	0.86	0.00	0.72	0.72	0.00	1.61	1.62	0.01	2.03	2.04	0.01	2.65	2.67	0.02	0.01
May	0.91	0.91	0.00	0.81	0.82	0.01	1.53	1.55	0.02	1.72	1.72	0.00	2.02	2.03	0.01	0.01
June	0.89	0.89	0.00	0.81	0.81	0.00	1.51	1.51	0.00	1.88	1.88	0.00	2.36	2.36	0.00	0.00
July	0.95	0.96	0.01	0.82	0.82	0.00	1.79	1.80	0.01	2.09	2.17	0.08	3.10	3.09	-0.01	0.02
August	1.11	1.11	0.00	0.93	0.93	0.00	2.18	2.19	0.01	2.42	2.37	-0.05	2.98	2.92	-0.07	-0.02
September	0.80	0.80	0.00	0.72	0.72	0.00	1.30	1.31	0.01	1.53	1.53	0.00	2.13	2.10	-0.03	0.00
October	0.75	0.75	0.00	0.68	0.68	0.00	1.21	1.21	0.00	1.41	1.42	0.01	1.97	1.97	0.00	0.00
November	0.69	0.69	0.00	0.64	0.64	0.00	1.11	1.11	0.00	1.34	1.34	0.00	1.73	1.75	0.02	0.00
December	0.80	0.80	0.00	0.68	0.68	0.00	1.42	1.43	0.01	1.63	1.64	0.01	1.93	2.02	0.09	0.02
Mean			0.00			0.00			0.01			0.01			0.00	

Table 8.10: Annual, seasonally and monthly wave statistics for the existing and proposed bathymetry at coastal site A2.

A2	Mean (m)			Median (m)			90th percentile (m)			95th percentile (m)			99th percentile (m)			Mean
	Existing	Proposed	Difference	Existing	Proposed	Difference	Existing	Proposed	Difference	Existing	Proposed	Difference	Existing	Proposed	Difference	
Annual	0.60	0.59	-0.01	0.46	0.46	0.00	1.20	1.20	0.00	1.49	1.48	-0.01	2.04	2.04	0.00	0.00
Winter	0.68	0.68	0.00	0.52	0.51	-0.01	1.42	1.41	-0.01	1.77	1.76	-0.01	2.17	2.16	-0.01	-0.01
Autumn	0.60	0.59	-0.01	0.47	0.46	-0.01	1.18	1.17	-0.01	1.43	1.43	0.00	2.18	2.16	-0.02	-0.01
Spring	0.50	0.49	-0.01	0.40	0.40	0.00	0.96	0.95	-0.01	1.17	1.17	0.00	1.61	1.60	-0.01	-0.01
Summer	0.61	0.60	-0.01	0.48	0.47	-0.01	1.24	1.24	0.00	1.48	1.48	0.00	1.86	1.86	0.00	0.00
January	0.60	0.60	0.00	0.48	0.48	0.00	1.24	1.23	-0.01	1.50	1.50	0.00	1.98	1.98	0.00	0.00
February	0.66	0.66	0.00	0.54	0.54	0.00	1.38	1.38	0.00	1.56	1.55	-0.01	1.84	1.84	0.00	0.00
March	0.59	0.59	0.00	0.46	0.45	-0.01	1.13	1.13	0.00	1.37	1.36	-0.01	2.44	2.44	0.00	-0.01
April	0.55	0.55	0.00	0.41	0.40	-0.01	1.09	1.08	-0.01	1.51	1.51	0.00	2.09	2.10	0.01	0.00
May	0.65	0.64	-0.01	0.56	0.55	-0.01	1.23	1.23	0.00	1.42	1.41	-0.01	1.76	1.75	-0.01	-0.01
June	0.57	0.57	0.00	0.46	0.45	-0.01	1.03	1.03	0.00	1.38	1.38	0.00	2.02	2.02	0.00	0.00
July	0.69	0.68	-0.01	0.51	0.50	-0.01	1.42	1.41	-0.01	1.91	1.91	0.00	2.45	2.44	-0.01	-0.01
August	0.79	0.78	-0.01	0.63	0.62	-0.01	1.61	1.60	-0.01	1.82	1.81	-0.01	2.18	2.17	-0.01	-0.01
September	0.57	0.56	-0.01	0.49	0.49	0.00	1.09	1.08	-0.01	1.23	1.22	-0.01	1.60	1.59	-0.01	-0.01
October	0.50	0.50	0.00	0.41	0.41	0.00	0.94	0.94	0.00	1.21	1.20	-0.01	1.63	1.62	-0.01	0.00
November	0.43	0.42	-0.01	0.34	0.34	0.00	0.80	0.80	0.00	1.05	1.04	-0.01	1.61	1.60	-0.01	-0.01
December	0.56	0.55	-0.01	0.43	0.43	0.00	1.16	1.15	-0.01	1.35	1.35	0.00	1.86	1.87	0.01	0.00
Mean			-0.01			-0.01			-0.01			-0.01			-0.01	

Table 8.11: Annual, seasonally and monthly wave statistics for the existing and proposed bathymetry at coastal site A6.

A6	Mean (m)			Median (m)			90th percentile (m)			95th percentile (m)			99th percentile (m)			Mean
	Existing	Proposed	Difference	Existing	Proposed	Difference	Existing	Proposed	Difference	Existing	Proposed	Difference	Existing	Proposed	Difference	
Annual	0.43	0.42	-0.01	0.36	0.36	0.00	0.78	0.78	0.00	0.96	0.95	-0.01	1.32	1.31	-0.01	-0.01
Winter	0.48	0.48	0.00	0.40	0.40	0.00	0.93	0.92	-0.01	1.16	1.15	-0.01	1.41	1.41	0.00	0.00
Autumn	0.43	0.43	0.00	0.36	0.36	0.00	0.76	0.76	0.00	0.92	0.91	-0.01	1.40	1.39	-0.01	0.00
Spring	0.37	0.37	0.00	0.33	0.33	0.00	0.64	0.64	0.00	0.77	0.77	0.00	1.03	1.03	0.00	0.00
Summer	0.42	0.42	0.00	0.36	0.36	0.00	0.81	0.80	-0.01	0.95	0.95	0.00	1.20	1.20	0.00	0.00
January	0.42	0.42	0.00	0.36	0.36	0.00	0.80	0.80	0.00	0.95	0.95	0.00	1.28	1.28	0.00	0.00
February	0.46	0.46	0.00	0.39	0.39	0.00	0.89	0.89	0.00	0.99	0.99	0.00	1.17	1.16	-0.01	0.00
March	0.42	0.42	0.00	0.35	0.35	0.00	0.73	0.73	0.00	0.88	0.88	0.00	1.65	1.64	-0.01	0.00
April	0.40	0.39	-0.01	0.32	0.32	0.00	0.73	0.73	0.00	0.96	0.95	-0.01	1.34	1.32	-0.02	-0.01
May	0.46	0.46	0.00	0.42	0.42	0.00	0.80	0.79	-0.01	0.91	0.91	0.00	1.09	1.09	0.00	0.00
June	0.43	0.42	-0.01	0.39	0.39	0.00	0.70	0.70	0.00	0.90	0.90	0.00	1.33	1.33	0.00	0.00
July	0.48	0.48	0.00	0.40	0.40	0.00	0.92	0.92	0.00	1.24	1.24	0.00	1.60	1.60	0.00	0.00
August	0.54	0.53	-0.01	0.44	0.43	-0.01	1.05	1.04	-0.01	1.18	1.18	0.00	1.43	1.43	0.00	-0.01
September	0.42	0.42	0.00	0.39	0.39	0.00	0.70	0.70	0.00	0.81	0.80	-0.01	1.02	1.02	0.00	0.00
October	0.37	0.36	-0.01	0.32	0.32	0.00	0.61	0.61	0.00	0.76	0.76	0.00	1.06	1.05	-0.01	0.00
November	0.33	0.33	0.00	0.29	0.29	0.00	0.55	0.55	0.00	0.70	0.70	0.00	1.01	1.01	0.00	0.00
December	0.40	0.40	0.00	0.34	0.34	0.00	0.73	0.73	0.00	0.86	0.86	0.00	1.20	1.19	-0.01	0.00
Mean			0.00			0.00			0.00			0.00			0.00	

Table 8.12: Annual, seasonally and monthly wave statistics for the existing and proposed bathymetry at coastal site A8.

	Mean (m)			Median (m)			90th percentile (m)			95th percentile (m)			99th percentile (m)			
A8	Existing	Proposed	Difference	Existing	Proposed	Difference	Existing	Proposed	Difference	Existing	Proposed	Difference	Existing	Proposed	Difference	Mean
Annual	0.52	0.51	-0.01	0.40	0.40	0.00	1.03	1.02	-0.01	1.26	1.26	0.00	1.68	1.68	0.00	0.00
Winter	0.59	0.59	0.00	0.45	0.45	0.00	1.19	1.18	-0.01	1.44	1.44	0.00	1.91	1.90	-0.01	0.00
Autumn	0.52	0.52	0.00	0.41	0.41	0.00	1.01	1.00	-0.01	1.23	1.23	0.00	1.82	1.82	0.00	0.00
Spring	0.43	0.43	0.00	0.35	0.35	0.00	0.82	0.82	0.00	1.00	1.00	0.00	1.36	1.36	0.00	0.00
Summer	0.52	0.52	0.00	0.41	0.41	0.00	1.06	1.06	0.00	1.26	1.26	0.00	1.61	1.61	0.00	0.00
January	0.52	0.52	0.00	0.42	0.42	0.00	1.05	1.05	0.00	1.29	1.28	-0.01	1.76	1.76	0.00	0.00
February	0.56	0.56	0.00	0.47	0.47	0.00	1.11	1.11	0.00	1.31	1.31	0.00	1.61	1.61	0.00	0.00
March	0.51	0.51	0.00	0.39	0.39	0.00	0.96	0.95	-0.01	1.14	1.14	0.00	2.02	2.03	0.01	0.00
April	0.48	0.48	0.00	0.35	0.35	0.00	0.95	0.95	0.00	1.29	1.28	-0.01	1.70	1.70	0.00	0.00
May	0.56	0.56	0.00	0.48	0.48	0.00	1.08	1.08	0.00	1.22	1.22	0.00	1.52	1.52	0.00	0.00
June	0.50	0.49	-0.01	0.40	0.40	0.00	0.90	0.90	0.00	1.16	1.16	0.00	1.66	1.66	0.00	0.00
July	0.59	0.59	0.00	0.44	0.44	0.00	1.16	1.15	-0.01	1.51	1.51	0.00	2.28	2.28	0.00	0.00
August	0.67	0.67	0.00	0.55	0.55	0.00	1.33	1.32	-0.01	1.50	1.49	-0.01	1.95	1.94	-0.01	-0.01
September	0.49	0.48	-0.01	0.42	0.42	0.00	0.91	0.91	0.00	1.05	1.05	0.00	1.32	1.32	0.00	0.00
October	0.44	0.44	0.00	0.35	0.35	0.00	0.82	0.82	0.00	1.00	0.99	-0.01	1.45	1.44	-0.01	0.00
November	0.37	0.37	0.00	0.30	0.30	0.00	0.67	0.67	0.00	0.88	0.88	0.00	1.35	1.35	0.00	0.00
December	0.49	0.48	-0.01	0.38	0.38	0.00	1.01	1.01	0.00	1.18	1.18	0.00	1.50	1.50	0.00	0.00
Mean			0.00			0.00			0.00			0.00			0.00	

Table 8.13: Annual, seasonally and monthly wave statistics for the existing and proposed bathymetry at coastal site A12.

A12	Mean (m)			Median (m)			90th percentile (m)			95th percentile (m)			99th percentile (m)			Mean
	Existing	Proposed	Difference	Existing	Proposed	Difference	Existing	Proposed	Difference	Existing	Proposed	Difference	Existing	Proposed	Difference	
Annual	0.46	0.46	0.00	0.31	0.31	0.00	1.10	1.10	0.00	1.38	1.38	0.00	1.94	1.94	0.00	0.00
Winter	0.54	0.54	0.00	0.37	0.37	0.00	1.30	1.30	0.00	1.65	1.65	0.00	2.05	2.04	-0.01	0.00
Autumn	0.45	0.45	0.00	0.30	0.30	0.00	1.06	1.06	0.00	1.33	1.33	0.00	2.09	2.09	0.00	0.00
Spring	0.35	0.35	0.00	0.23	0.23	0.00	0.84	0.84	0.00	1.07	1.07	0.00	1.49	1.49	0.00	0.00
Summer	0.49	0.49	0.00	0.35	0.35	0.00	1.15	1.15	0.00	1.39	1.40	0.01	1.80	1.80	0.00	0.00
January	0.50	0.50	0.00	0.36	0.36	0.00	1.13	1.13	0.00	1.35	1.35	0.00	1.86	1.85	-0.02	0.00
February	0.55	0.55	0.00	0.42	0.42	0.00	1.29	1.29	0.00	1.46	1.46	0.00	1.74	1.74	0.00	0.00
March	0.45	0.45	0.00	0.30	0.30	0.00	1.03	1.03	0.00	1.28	1.28	0.00	2.38	2.37	-0.01	0.00
April	0.42	0.42	0.00	0.24	0.24	0.00	0.93	0.93	0.00	1.45	1.45	0.00	2.07	2.07	0.00	0.00
May	0.49	0.49	0.00	0.39	0.39	0.00	1.10	1.09	-0.01	1.28	1.28	0.00	1.59	1.59	0.00	0.00
June	0.40	0.40	0.00	0.27	0.28	0.01	0.92	0.93	0.01	1.19	1.19	0.00	1.80	1.80	0.00	0.00
July	0.56	0.56	0.00	0.36	0.36	0.00	1.40	1.40	0.00	1.86	1.86	0.00	2.29	2.28	-0.01	0.00
August	0.66	0.66	0.00	0.52	0.52	0.00	1.47	1.47	0.00	1.71	1.70	-0.01	2.00	1.99	-0.01	0.00
September	0.40	0.40	0.00	0.28	0.28	0.00	0.95	0.95	0.00	1.11	1.11	0.00	1.52	1.52	0.00	0.00
October	0.37	0.37	0.00	0.25	0.25	0.00	0.84	0.84	0.00	1.08	1.08	0.00	1.48	1.48	0.00	0.00
November	0.29	0.29	0.00	0.18	0.18	0.00	0.66	0.65	-0.01	0.95	0.94	-0.01	1.48	1.49	0.01	0.00
December	0.44	0.44	0.00	0.28	0.28	0.00	1.05	1.05	0.00	1.28	1.28	0.00	1.86	1.86	0.00	0.00
Mean			0.00			0.00			0.00			0.00			0.00	

Table 8.14: Annual, seasonally and monthly wave statistics for the existing and proposed bathymetry at coastal site B1.

	Mean (m)			Median (m)			90th percentile (m)			95th percentile (m)			99th percentile (m)			
B1	Existing	Proposed	Difference	Existing	Proposed	Difference	Existing	Proposed	Difference	Existing	Proposed	Difference	Existing	Proposed	Difference	Mean
Annual	0.28	0.26	-0.02	0.21	0.20	-0.01	0.57	0.54	-0.03	0.71	0.67	-0.04	0.99	0.94	-0.05	-0.03
Winter	0.32	0.30	-0.02	0.24	0.23	-0.01	0.66	0.62	-0.04	0.82	0.78	-0.04	1.08	1.05	-0.03	-0.03
Autumn	0.28	0.26	-0.02	0.21	0.20	-0.01	0.56	0.54	-0.02	0.69	0.66	-0.03	1.06	1.00	-0.06	-0.03
Spring	0.23	0.21	-0.02	0.18	0.16	-0.02	0.47	0.45	-0.02	0.56	0.54	-0.02	0.80	0.77	-0.03	-0.02
Summer	0.29	0.27	-0.02	0.22	0.21	-0.01	0.60	0.57	-0.03	0.72	0.68	-0.04	0.93	0.90	-0.03	-0.03
January	0.28	0.26	-0.02	0.23	0.21	-0.02	0.59	0.55	-0.04	0.72	0.69	-0.03	1.06	1.03	-0.03	-0.03
February	0.32	0.30	-0.02	0.25	0.24	-0.01	0.66	0.62	-0.04	0.77	0.73	-0.04	0.91	0.89	-0.02	-0.03
March	0.28	0.26	-0.02	0.21	0.20	-0.01	0.55	0.52	-0.03	0.67	0.64	-0.03	1.24	1.16	-0.08	-0.03
April	0.25	0.24	-0.01	0.18	0.16	-0.02	0.53	0.50	-0.03	0.69	0.65	-0.04	0.99	0.94	-0.05	-0.03
May	0.30	0.28	-0.02	0.25	0.24	-0.01	0.60	0.57	-0.03	0.70	0.67	-0.03	0.89	0.86	-0.03	-0.02
June	0.26	0.25	-0.01	0.21	0.19	-0.02	0.52	0.50	-0.02	0.66	0.62	-0.04	0.96	0.91	-0.05	-0.03
July	0.32	0.30	-0.02	0.25	0.23	-0.02	0.65	0.62	-0.03	0.89	0.83	-0.06	1.23	1.18	-0.05	-0.04
August	0.36	0.34	-0.02	0.30	0.28	-0.02	0.74	0.69	-0.05	0.83	0.79	-0.04	1.11	1.08	-0.03	-0.03
September	0.26	0.25	-0.01	0.23	0.21	-0.02	0.51	0.50	-0.01	0.58	0.57	-0.01	0.75	0.72	-0.03	-0.02
October	0.23	0.22	-0.01	0.18	0.16	-0.02	0.46	0.44	-0.02	0.57	0.54	-0.03	0.86	0.84	-0.02	-0.02
November	0.19	0.18	-0.01	0.15	0.13	-0.02	0.39	0.37	-0.02	0.50	0.47	-0.03	0.79	0.75	-0.04	-0.02
December	0.26	0.24	-0.02	0.20	0.19	-0.01	0.55	0.53	-0.02	0.68	0.65	-0.03	0.89	0.83	-0.06	-0.03
Mean			-0.02			-0.02			-0.03			-0.03			-0.04	

9. Harbour wind-wave modelling

9.1 Introduction

Harbour wind-wave modelling was undertaken for the purposes of characterising the wave climate within the Lower Harbour, and identifying the influence of various wind directions and speeds on wave generation. The modelling was only undertaken on the existing channel bathymetry grid as changes in significant wave heights would be small (less than a few cm) for a deeper channel. The reasoning is that short-period wind waves are not limited or influenced much by the larger depths (e.g., >12 m as in the existing channel or dredged channel option) for the relatively short wind fetches that occur in the Lower Harbour.

The wave information for different wind velocities was used by Port Otago Ltd. for ship-handling assessments. However it also provides insights into the influence the Harbour orientation, channel alignment and varying depths have on the spatial distribution of waves within the Lower Harbour.

9.2 Lower Harbour wave model set-up

Wind wave generation within the Lower Harbour region (Figure 9.1) was simulated with the SWAN model (see Section 8.1) for the existing channel regime. Hourly data from the wind station at Taiaroa Head (May 2003 to May 2008) were used to characterise the wind regime. Extreme events for wave modelling were defined as the 99th percentile wind-speed exceedance velocity for each of the directional octants. These wave scenarios were modelled at Mean High Water Spring (MHWS) to allow maximum wind fetch.

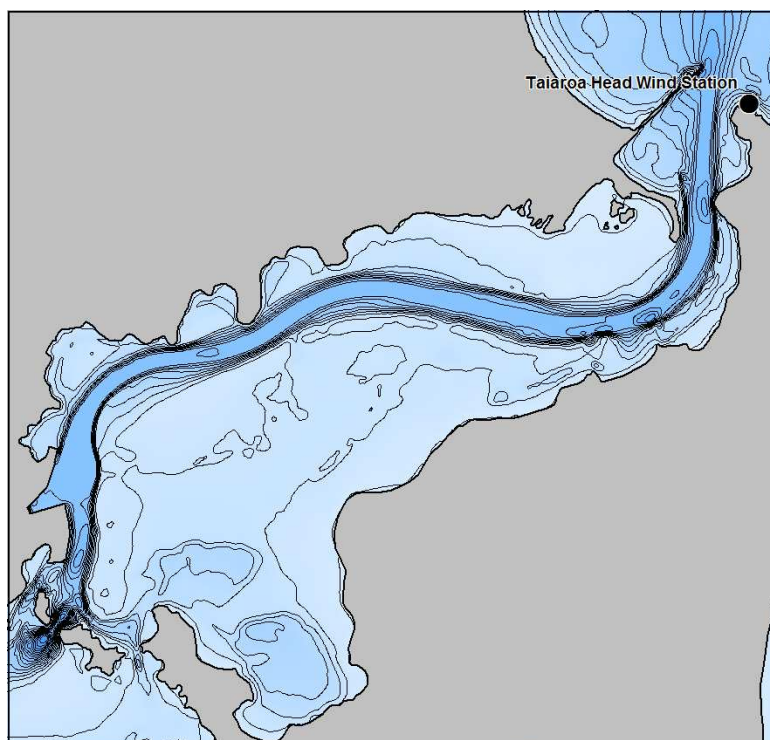


Figure 9.1: Area used to model wind-generated waves in the Lower Harbour including relative shading to represent the bathymetry (for the existing channel) and the location of the Taiaroa Head wind station.

9.3 Lower Harbour wind-generated waves

The area encompassed by the lower section of Otago Harbour is sufficiently large enough to allow wind-generated waves to develop to a considerable size. It is of interest to the project to quantify the likely magnitude of these waves under highly-energetic wind conditions.

Wind data from the Taiaroa Head station for May 2003 to May 2008 are presented as a wind rose in Figure 9.2, and the annual 10-minute wind speed statistics for each directional octant are presented Table 9.1.

The wind speed and wind direction joint-probability distribution is given in Table 9.2. The 99th percentile level was used to characterise the energetic conditions for wave modelling. While the Taiaroa Heads winds data does not represent the true spatial wind conditions at the 10 m reference elevation over the Harbour, it does provide a realistic level for a saturated wind-wave generation simulation. The Taiaroa Head wind data indicate that the 99th percentile wind speeds from the west are the strongest

(25.2 m/s), while winds from the north have the highest probability of occurrence (~28 %).

Example wave model results for significant wave height for the 99th percentile northerly wind condition are presented in Figure 9.3, and the westerly condition in Figure 9.4. These results clearly show the fetch-limitations to wave growth and the attenuation that occurs over the shallow intertidal areas. The wind-generated significant wave heights along the centre-line of the shipping channel (e.g., Fig. 9.5) are presented in Figure 9.6 for each of the directional octants at their respective 99th percentile wind speeds. This transect begins at the Port Chalmers Turning Basin and extends to the offshore breakwater (The Mole) at the entrance to Otago Harbour. The largest significant wave height along this transect reaches ~1.2 m for a 99-percentile wind speed from due west, and occurs in the area of Harington Bend (see Figure 9.4).

Table 9.1: Annual wind statistics from Taiaroa Head (May 2003 to May 2008) by directional octant.

Wind speed Wind direction	Mean (m/s)	Median (m/s)	90th percentile (m/s)	95th percentile (m/s)	99th percentile (m/s)
North (337.5°–22.5°)	5.1	4.1	10.3	11.8	14.9
North-East (22.5°–67.5°)	6.2	5.7	10.8	12.4	14.9
East (67.5°–112.5°)	4.4	3.6	8.2	9.8	15.4
South-East (112.5°–157.5°)	5.6	5.7	9.3	10.8	16.5
South (157.5°–202.5°)	5.8	5.7	9.3	10.8	14.9
South-West (202.5°–247.5°)	7.7	7.2	13.9	15.4	19.6
West (247.5°–292.5°)	11.0	10.8	19.0	21.6	25.2
North-West (292.5°–337.5°)	4.9	3.6	9.8	12.4	18.5

Table 9.2: Wind speed and direction joint-probability distribution in parts-per-thousand (ppt). For example, 3.8 ppt is equivalent to 0.38%.

Speed (m/s)	Wind direction (degrees)								SUM
	337.5 to 22.5	22.5 to 67.5	67.5 to 112.5	112.5 to 157.5	157.5 to 202.5	202.5 to 247.5	247.5 to 292.5	292.5 to 337.5	
> 0 <= 1	46.6	3.8	2.8	1.1	1.5	3.8	4.1	3.2	67
> 1 <= 2	13.6	6.3	3.6	1.1	2.1	7.5	4.3	4.3	43
> 2 <= 3	33.1	18.9	10.7	1.9	4.3	15.9	7.9	9.5	102
> 3 <= 4	35.9	20	12.1	2.6	5.2	15.4	7.3	6.9	105
> 4 <= 5	30.2	17	9.4	3	5.6	16.4	7.3	5.7	95
> 5 <= 6	25.1	16	6.8	3.4	7.1	15.8	7.5	5	87
> 6 <= 7	19.3	15.1	4	3.1	6.6	16.2	8.5	3.9	77
> 7 <= 8	16.1	15.1	2.1	2.4	5.5	17.2	8.5	3.1	70
> 8 <= 9	13	14	2.1	1.8	4.2	14.9	8.4	1.4	60
> 9 <= 10	10.3	12.9	1.6	1.1	3.2	13.6	8.4	1.6	53
> 10 <= 11	9.1	11.2	1.2	0.5	2.1	14.2	8.8	1.3	48
> 11 <= 12	7.9	6.3	0.6	0.5	1.3	10.9	9.6	0.8	38
> 12 <= 13	5.2	5.1	0.4	0.3	0.8	10.3	9.2	0.8	32
> 13 <= 14	3.7	3	0.4	0.1	0.5	8	10	0.5	26
> 14 <= 15	2.4	2.3	0.3	0.2	0.3	6.8	8.9	0.4	22
> 15 <= 16	2	1.6	0.3	0.1	0.3	5.5	8.4	0.3	19
> 16 <= 17	0.8	0.9	0.3	0.1	0.2	4.1	7.3	0.3	14
> 17 <= 18	0.6	0.2	0.2	0.1	0.1	2.5	6	0.1	10
> 18 <= 19	0.3	0.2	0.1	0	0	2.2	5.3	0.2	8
> 19 <= 20	0.2	0.3	0.1	0	0.1	1.4	2.8	0	5
> 20 <= 21	0.1	0.1	0.1	0	0	1.4	4.1	0.1	6
> 21 <= 22	0	0.1	0	0	0	1	2.9	0.1	4
> 22 <= 23	0	0	0	0	0	0.6	1.9	0	3
> 23 <= 24	0	0	0	0	0	0.5	1.7	0.1	2
> 24 <= 25	0	0	0	0	0	0.3	1.2	0	2
> 25 <= 26	0	0	0	0	0	0.3	1.2	0	2
> 26 <= 27	0	0	0	0	0	0.1	0.4	0	1
> 27 <= 28	0	0	0	0	0	0	0.4	0	0
> 28 <= 29	0	0	0	0	0	0.1	0.3	0	0
> 29 <= 30	0	0	0	0	0	0	0.2	0	0
> 30 <= 31	0	0	0	0	0	0	0.1	0	0
SUM	276	170	59	23	51	207	163	50	1000

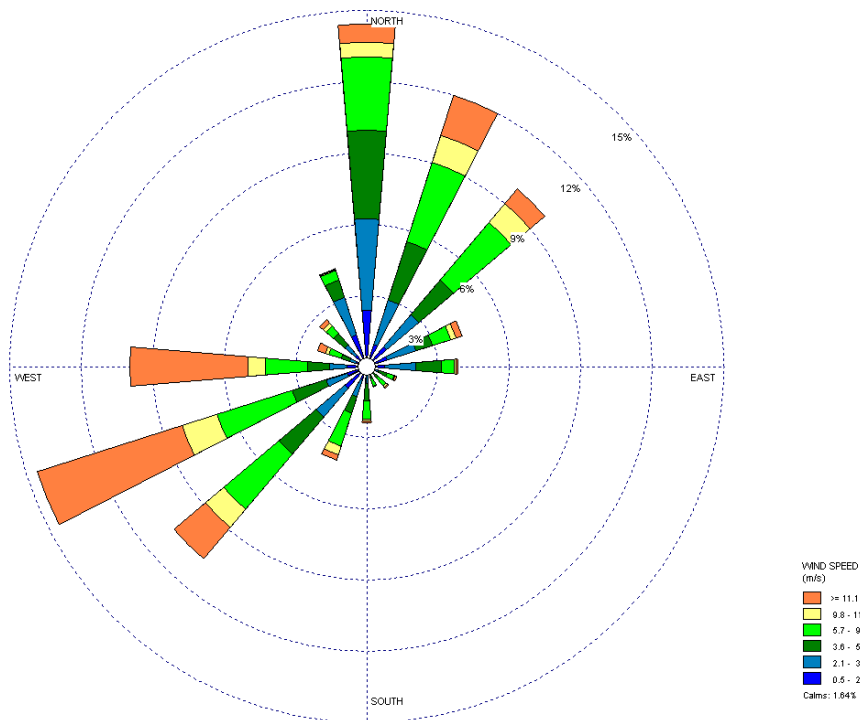


Figure 9.2: Taiaroa Head wind-rose for the period May 2003–May 2008. The top wind-speed category at the end of each sector bar is for wind speeds ≥ 11.1 m/s.

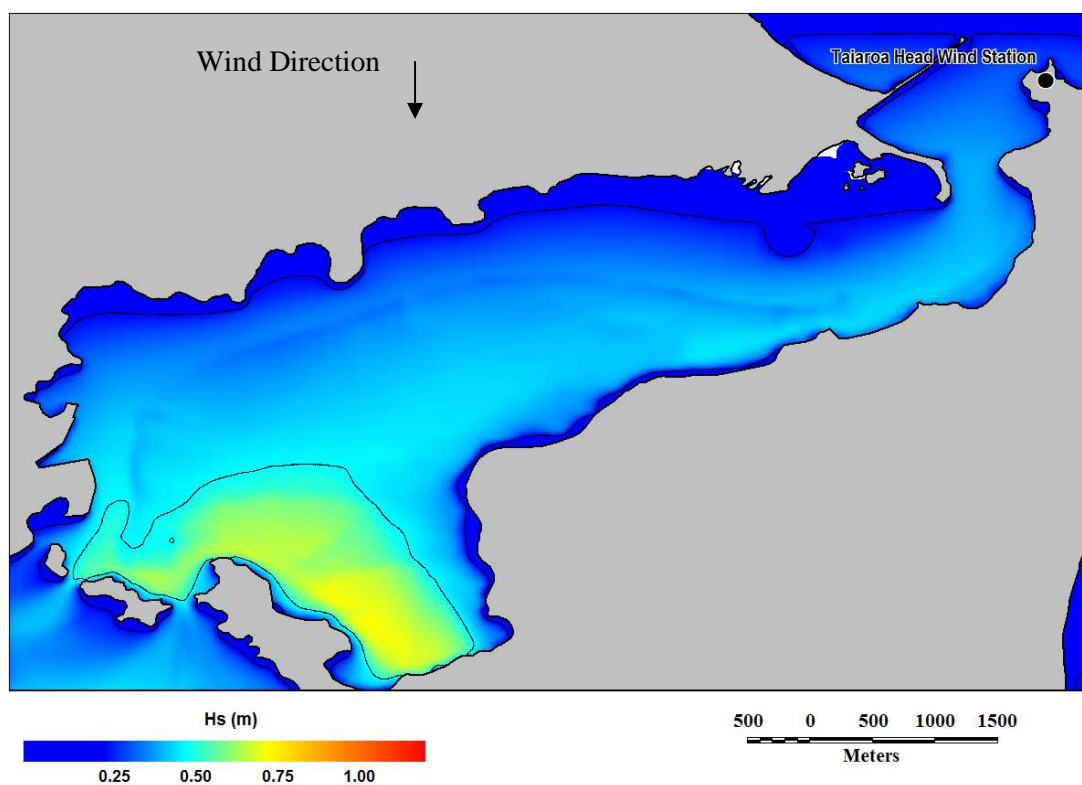


Figure 9.3: Wind-generated significant wave heights from the 99th percentile northerly winds.

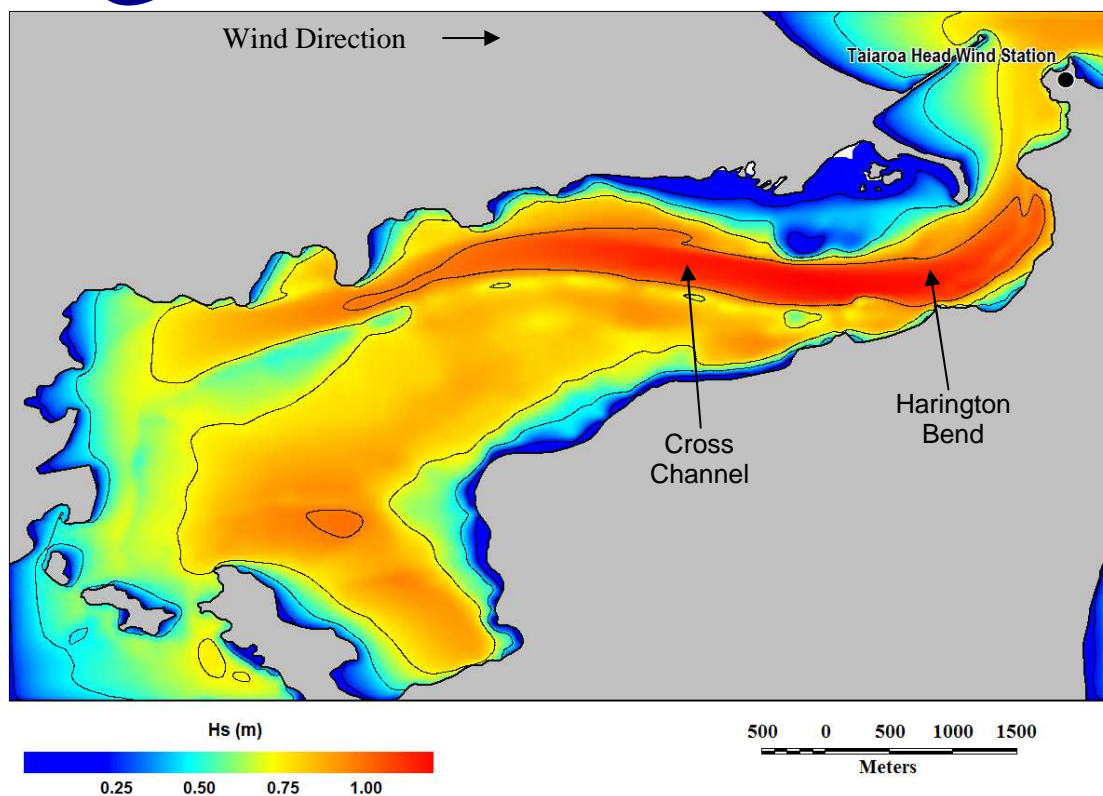


Figure 9.4: Wind-generated significant wave heights from the 99th percentile westerly winds.

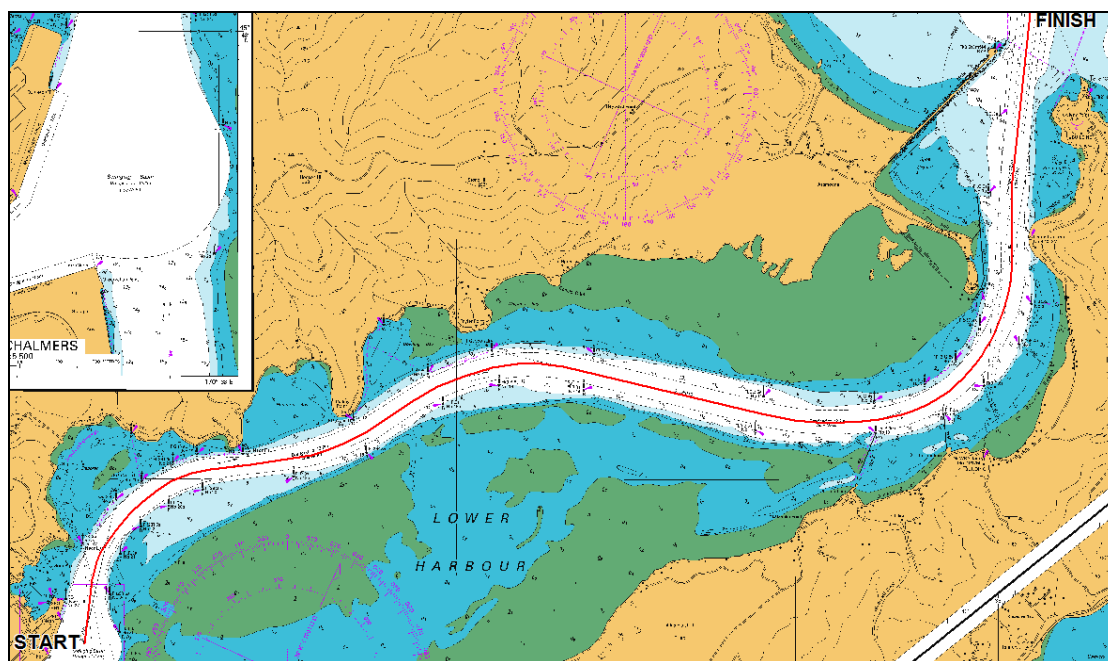


Figure 9.5: Significant wave heights were extracted along this transect.

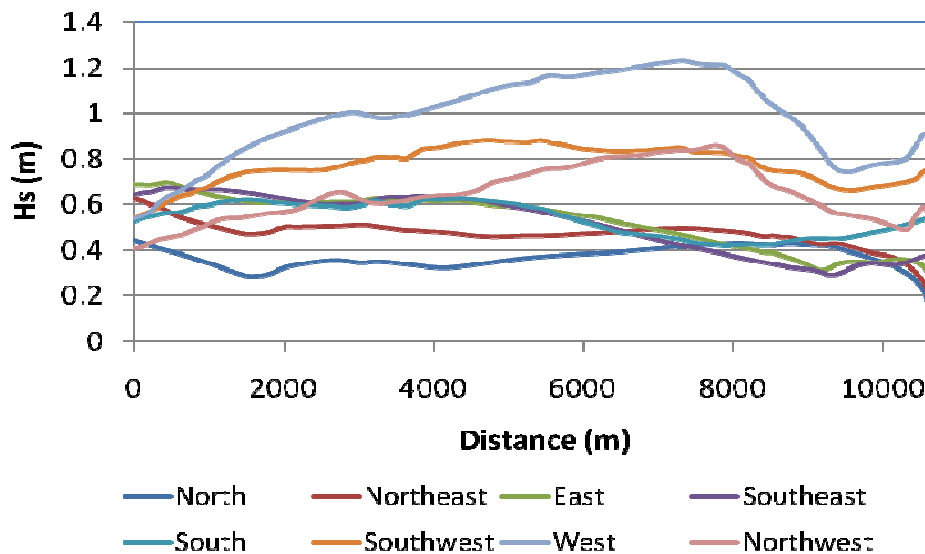


Figure 9.6: Wind-generated significant wave heights along the shipping channel (starting at the Port Chalmers Turning Basin) under the 99th percentile wind speed for each of the directional octants.

9.4 Summary

Wave modelling results show the highest waves in the Lower Harbour originate from westerly winds (highest waves) and south-westerlies (next highest) and also the strongest winds blow from these directions. These predominant winds, combined with the geographical alignment of the Lower Harbour and shipping channel and the associated wind fetches over open-water pathways, result in the largest wind-generated waves occurring in the channel reach from Cross Channel through to and around Harington Bend. The largest significant wave height reaches approximately 1.2 m in the Harington Bend area for a 99-percentile wind (25 m/s or 49 knots) from due west.

Increases in significant wave height for a 15-m channel option would be quite small (less than a few cm) in the main channel with negligible changes outside the footprint of the proposed widened channel. Wave heights (relative to existing conditions) would change most in two specific areas where the channel bends (east side of Turning Basin and north side of Harington Bend) would be substantially dredged from approximately intertidal depths presently to the new channel base depth or lesser depth if on the batter side-slope. In this case, these localised areas would begin to experience similar wave characteristics to the existing channel (because they would be deeper and amalgamated with the main channel), rather than the intertidal depth-limited waves experienced presently.

10. Offshore hydrodynamic model

10.1 Offshore hydrodynamic model set-up

The 3-dimensional DHI MIKE-3 Flexible Mesh (FM)¹⁶ model was used to simulate current flows on the Otago shelf. A flexible mesh comprising triangular elements was constructed from the bathymetry datasets described in Section 3, with the depth contours within the model domain shown in Figure 10.1. A closer view of the final mesh layout in the region of Otago Heads is shown in Figure 10.2. The southern coastal boundary point in the model grid was at Taieri River mouth (-46.053°N) and the northernmost was at Shag Point (-45.473°N).

A flexible mesh is conducive to efficient model run times, by having larger elements in the offshore area where calculations can be done at broader spatial scales, but more highly resolved in the area of interest using smaller elements. To further speed up run times and ease the computational demands for the subsequent plume modelling for the offshore disposal grounds, the mesh inside Otago Harbour was made very coarse and a volume point source was introduced at the Entrance that matches the ebb and flood tidal flux in and out of the Harbour. This approach is warranted as the Harbour investigations were carried out using a separate high-resolution model (presented in earlier sections) and the selection of an appropriate disposal ground would be on the basis of no discernable direct re-entry to the Harbour of suspended-sediment plumes. Therefore in all subsequent plots using the offshore model, the velocities inside Otago Harbour should be ignored.

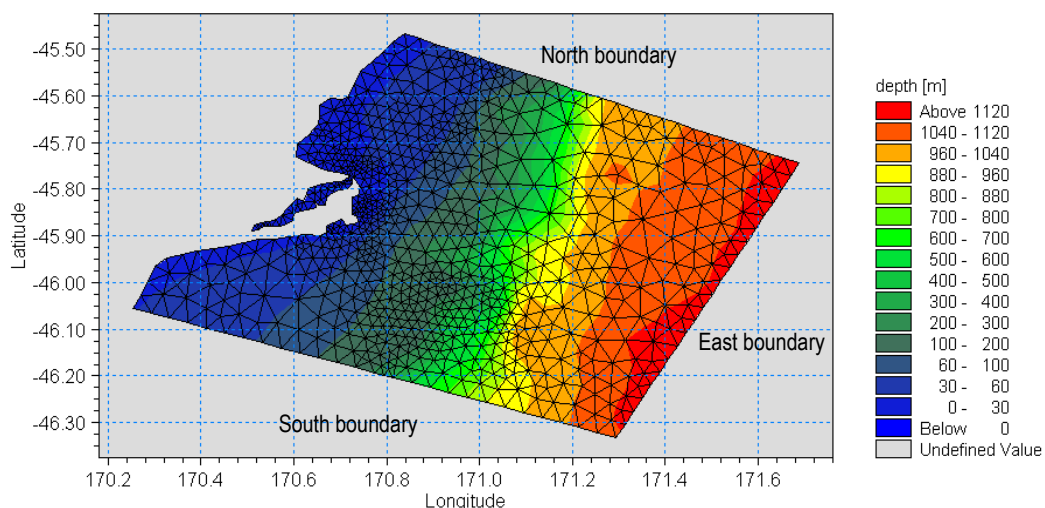


Figure 10.1: Extent and location of the offshore hydrodynamic grid and the underlying bathymetry plotted in WGS-84 coordinates.

¹⁶ <http://www.dhigroup.com/Software/Marine.aspx>

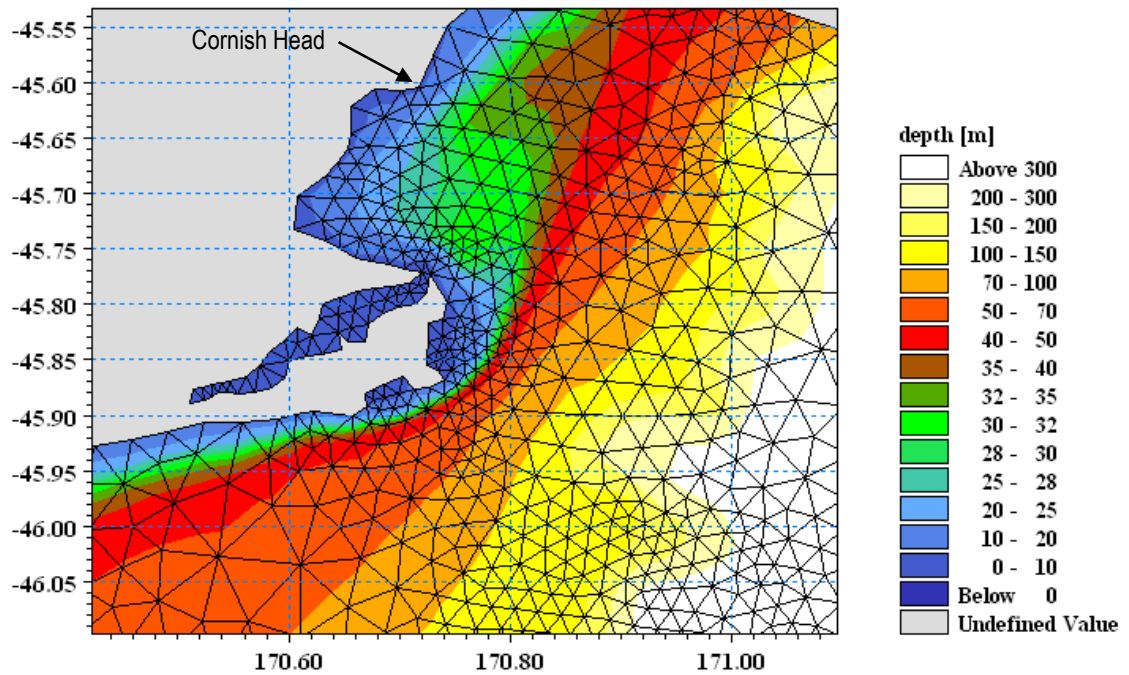


Figure 10.2: Close-up of the triangular grid of the offshore hydrodynamic model in the area of interest and the underlying bathymetry plotted in WGS-84 coordinates (latitude/longitude).

The 3-dimensional MIKE-3 (FM) offshore model simulates the water column depth in a sigma-coordinate system, which is simply determined as the ratio of the total depth at a grid node. Three depth layers were incorporated in the model to simulate the hydrodynamics from wind-generated shear, but water density stratification was not included in the simulation on the basis of the field results which showed generally well-mixed conditions below the top few metres in the inner shelf area where disposal would occur (Bell & Hart, 2008).¹⁷ These three vertical layers (L1 to L3) change in height with total depth, but is always in the following ratios: a) Layer 1 (L1) is the bottom layer (the bottom 20% of the water depth); b) Layer 2 (L2) is the mid-layer (the next 50% of the water depth); and; c) Layer 3 (L3) is the surface layer (top 30% of the water depth).

The offshore hydrodynamic model has 3 open-sea boundaries in the model (Fig. 10.1) that required boundary conditions to be set. The South boundary was forced by a spatially varying Southland Current flux (or velocity) with distance offshore that was constant in time. This prescription for the Southland Current velocity was derived from analysing the output from a larger scale oceanic ROMS model of the Southland

¹⁷ Further offshore in the core of the Southland Current, water-column density gradients will have an influence on currents.

Current (Dr M. Hadfield, NIWA, pers comm.). The East boundary was set as a slip boundary that allows only flows parallel to the boundary (i.e., no inflow or outflow). The North boundary forcing comprised the tide height time series for the deployment periods being applied at the NE corner of the model open-sea boundaries in tandem with automatic tilting of the north boundary that balances the applied wind stress, Coriolis effect and tides.

Horizontal eddy diffusivity was implemented based on the Smagorinsky formulation and vertical eddy diffusivity based on a k-epsilon scheme.

Wind velocity time series for the offshore deployment periods were applied over the entire water surface of the model at each time step, using measurements from the Taiaroa Head automatic weather station. A volume source was introduced at the Entrance to Otago Harbour to simulate the flood and ebb-tide flows in and out of the Harbour to obviate the need to model currents throughout Otago Harbour in what is essentially an offshore model.

10.2 Offshore model calibration and verification

Several flexible mesh variants and different distributions of Southland Current flux through the southern boundary of the model were simulated before settling on the optimal match with the field data observations at site A1 (see Bell & Hart, 2008). Comparisons of the net residual drift during each of the first two deployments at A1 with the residual drifts from Run 10 of the offshore hydrodynamic model are shown in Figure 10.3. The results from this comparison are listed in Table 10.1. The model under predicts the residual drift for deployment 1 and slightly over predicts for the subsequent deployment at A1, but overall combining the two deployments for the calibration phase shows good agreement in the residual drift (last row for Table 10.1). There is a slight offset in the model on the direction of the drift by 12°. However, considering the comparison is between point measurements by an ADCP at A1 versus a computed velocity over a triangular grid element that is about 900 m wide, this is a reasonable result in an area where the residual velocity within an eddy off Taiaroa Head (Fig. 10.3) is changing significantly over such spatial scales in the vicinity of A1.

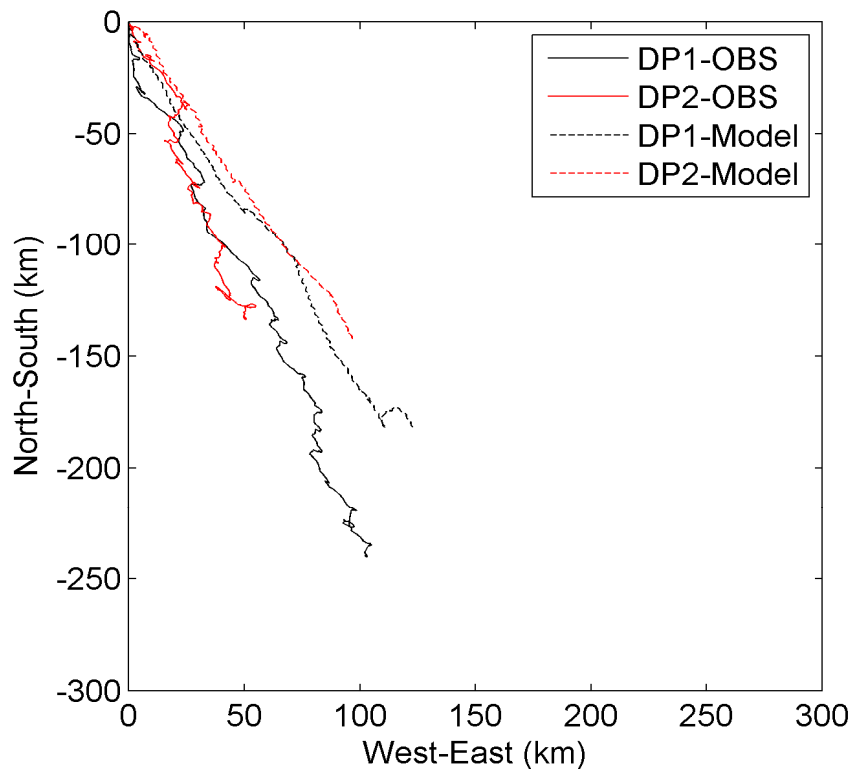


Figure 10.3: Progressive vector traces covering the observations (OBS) from the first two field deployments (DP1 and DP2) at site A1 from mid-March to May 2008 (Bell & Hart, 2008) versus the traces (dashed) from the offshore hydrodynamic model (Run10) for DP1 and DP2.

Table 10.1: Comparison of the depth-averaged velocity residual for deployments 1 & 2 (DP1 & DP2) at site A1 and the calibration run for the offshore hydrodynamic model.

Deployment No.	Measured residual at A1 (km/day)	Modelled residual at A1 (km/day)	Measured residual direction (°)	Modelled residual direction (°)
1	7.7	6.5	157	146
2	5.2	6.3	159	146
Combined	6.6	6.4	158	146

Figure 10.4a shows the depth-averaged residual current vectors computed from the offshore hydrodynamic model run that covered the first two deployments of the field programme at A1 from 18 March to 26 May 2008 (Bell & Hart, 2008). Fig 10.4b also shows the locations of current-meter moorings from the 2008 field programme (Bell & Hart, 2008) and previous moorings in 1988, at Landfall Tower (LF88) and to the SE of Taiaroa Head in 1983 (CM83), discussed in Section 2.

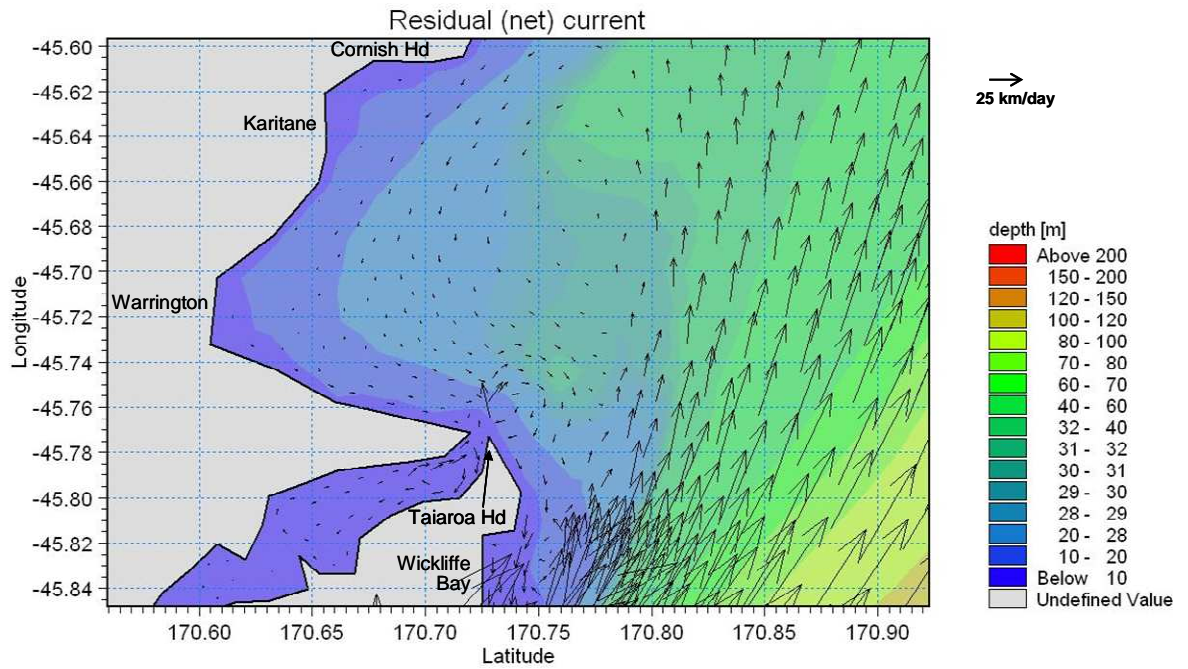


Figure 10.4a: Residual depth-averaged current pattern over the initial two field deployments at A1 from the calibrated Run10 of the offshore hydrodynamic model. [Note: residual currents inside Otago Harbour should be ignored].

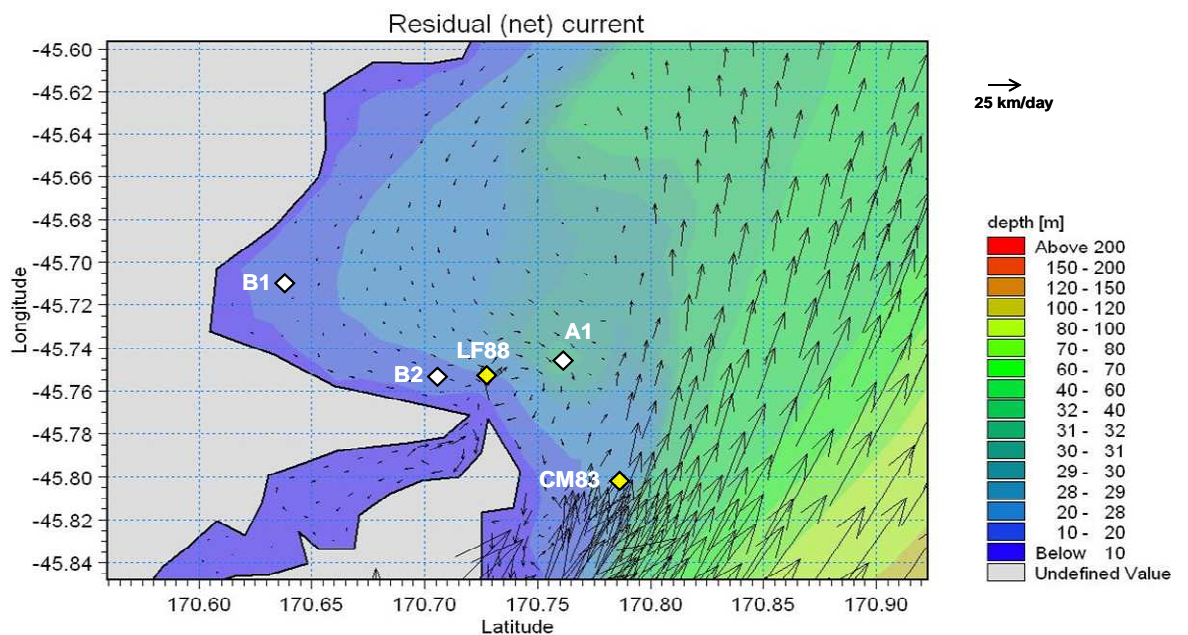


Figure 10.4b: Current-meter mooring sites plotted on the backdrop of the residual depth-averaged current pattern over the initial two field deployments at A1 from the calibrated Run10 of the offshore hydrodynamic model. White diamonds are from the 2008 field programme, and yellow diamonds from previous moorings in the 1980s.

Figure 10.4b is also a useful summary plot to illustrate the validation of the offshore hydrodynamic model, as it is the net or residual velocity that ultimately determines the transport of sediment on the seabed and suspended-sediment plumes generated during the disposal operation. The SSE net current at A1 in comparison with the measured dataset has been discussed previously (see Fig. 10.3). A deployment at B1 in Blueskin Bay coinciding with the first deployment at A1 showed a very small net residual current of about 0.5 km/day that varied by nearly 180° in direction going down the water column, which is indicative of currents being largely influenced by wind shear within the Bay. This matches the small residual at B1 computed by the offshore hydrodynamic model (Fig. 10.4b). A later deployment at B2 (off Heyward Point) at the end of the 2008 field programme (July), showed a more consistent residual current than B1, at an average of 1.7 km/day to the ENE. This matches reasonably well with the modelled residual current to the east at B2 for the March-May period (Fig 10.4b), given the wind is still a major influence on the currents at B2. The net northerly residual current at Landfall Tower (LF88) of 4.5 km/day (Barnett, 1988) fits in with the overall residual flow pattern in Figure 4.10b, as does the short 4-day deployment at CM83 off Otago Heads, where the current was consistently flowing in a NE direction (mean of 40° True North) at a mean speed of 0.2 m/s (equivalent to 17 km/day). In summary, all the current-meter records fit reasonably well with the residual current pattern from the calibration period, thus verifying the pattern relative to measurements from other time periods.

10.3 Residual (net) circulation on the Otago shelf

For sediment plume and seabed sand transport, it is more important to focus on the residual or net-averaged current rather than focus on the distribution of current magnitudes and directions at any given time. A residual current is computed by averaging the current vectors (speed & direction) from the time series of all modelled or measured currents at a location by numerically placing all the vectors progressively nose-to-tail, thus taking into account the backwards and forwards currents, and arriving at a net residual current vector (speed and magnitude). Figure 10.4a is the residual current pattern in km/day averaged over the first two field deployments spanning a total of 61 days (nominally 2 months) from mid-March to mid-May 2008.

Figure 10.4a reveals several features of the averaged residual flow patterns on the Otago inner shelf that improve our understanding from the previous studies summarised in Section 2.3. The inshore component (Subtropical Waters) of the Southland Current is strong and persistent, peeling off from Cape Saunders to the NE, with the net residual current gradually reducing in velocity as it moves more northwards over the submergent Peninsula Spit in outer Blueskin Bay. This outer shelf

flow pattern is very persistent, although actual currents do vary in speed depending on winds through Foveaux Strait (Chiswell, 1996), but seldom flow in the reverse direction (i.e., to the SE).

On the inner shelf, there is an anticlockwise eddy in Blueskin Bay (Fig. 10.4a) as deduced by Murdoch et al. (1990), but it is relatively weak and it sweeps down through the outer part of Blueskin Bay in depths of greater than 20 m, rather than sweep along the coastline.

The main feature on the inner shelf, hitherto not documented, is a relatively small clockwise eddy of about 5 km in diameter off Taiaroa Head, juxtaposed between the ebb-tide jet from the Harbour entrance and the Southland Current flow to the NE offshore. The current-meter mooring site at A1 was located towards the outer edge of the Taiaroa Head eddy, giving rise to a persistent residual current to the SE (Bell & Hart, 2008).

In the nearshore zone along Otago Heads, including Wickcliffe Bay, the depth-averaged current residual is to the south (Fig. 10.4a), which is driven by the return flow of the separation eddy off Cape Saunders. This residual current only includes the influences of winds, tides and the Southland Current. Waves and swell also generate current drift in the nearshore region, with stronger swells arriving from the SE (compared with local seas from the NE) likely to generate a nearshore wave drift to the north in the opposite direction to the current residual (Martin Single, pers. comm.).

10.4 Appraisal of the offshore hydrodynamic model performance

A reasonable calibration of the 3-layer offshore hydrodynamic model was achieved focusing on obtaining a good match with net or residual currents. Residual current patterns and behaviour are more important for longer- and larger-scale plume and sediment transport processes offshore, than tides and responses to winds over short time scales. Further, the availability of current-meter field data was limited to measurements at two concurrent sites during the 2008 field period, with little historic data (Bell & Hart, 2008) and the Southland Current imposes a persistent flow stream to the north-east a few kilometres offshore. Consequently, the approach of matching residual currents to calibrate the offshore hydrodynamic model differs from that used for the Harbour model (Chapter 4), where the focus was on matching intensely-sampled tidal data with model results.

Critical to the success in achieving a realistic match of the modelled residual current to that measured at the offshore site A1 (30 m depth) was the ability to derive a realistic

southern boundary condition to drive the model by quantifying the spatial variation along a shore-normal transect of the mean flow of the Southland Current from NIWA's ocean circulation models (M. Hadfield; pers. comm.).

While the chosen field mooring location (A1) proved eventually to be unsuitable as a disposal site option (Chapter 11), it proved to be an excellent location to test and verify the offshore model because of the complexities that exist there in the circulation pattern. In this locality, a small-scale clockwise eddy off Taiaroa Heads interacts with the ebb-tide jet from the Harbour Entrance, local offshore winds and the Southland Current further offshore. At A1, the SSE residual or drift current was reasonably well predicted after tuning the hydrodynamic model, the boundary conditions and its associated irregular bathymetry grid. If the mooring site had been located further offshore within the Southland Current, the subtleties within the inshore flows may not have been well resolved, particularly the Taiaroa Head eddy, which preferentially transports material towards the coastline of Otago Heads. On the other hand, not having a mooring further offshore within the main Southland Current flow was not critical in this project. Sensitivity tests of the offshore model using realistic variations in the spatial distribution and strength of the Southland Current boundary condition showed the results on the shelf were relatively insensitive compared to the situation of using the mean or average flow of the Southland Current. Local winds play a role in modifying the underlying residual currents offshore that are generated or influenced by the Southland Current, which the model was also able to mimic.

Overall, the MIKE-3 FM offshore hydrodynamic model is performing well in predicting residual or net currents that specifically include the Southland Current, tides and local offshore winds. Therefore simulating transport of suspended sediment and long-term sand transport from the preferred dredge disposal site can be achieved with reasonable confidence.

11. Offshore plume dispersal and deposition

11.1 Plume model set-up

During the disposal operation, when the dredge hopper is emptied at the offshore disposal site, the following processes would occur:

- a major portion of the released sediment load descends rapidly en masse to the seabed and deposits itself there;
- a minor portion of the sediment load goes directly into suspension (especially finer size fractions), increasing the concentration of suspended material in the water column and drifts off with the current, dispersing and gradually settling with time;
- finer material (e.g., silts) within the mass that falls directly to the seabed will spread out radially along the seabed away from the impact zone;
- deposited material can be subsequently resuspended when wave conditions are sufficient strength to mobilise the seabed surface sediments and transported by currents before settling again when conditions allow.

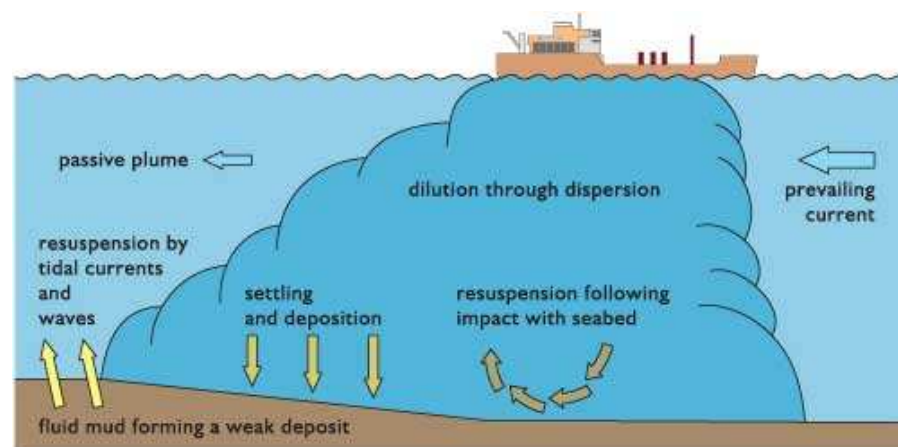


Figure 11.1: Schematic of a dynamic sediment plume discharged from a dredge hopper. [Source: CIRIA (2000)].

The DHI Particle Tracking (PT) module for the Flexible Mesh (FM) version of MIKE-3 was used to simulate the transport and fate of suspended material, and is commonly used worldwide for modelling or monitoring of dredging works. The time history of flow field is supplied from prior runs of MIKE-3 FM in a de-coupled mode.

The sediment discharge is represented by a finite number of particles, which are then transported with the surrounding water body and dispersed as a result of turbulence and shearing processes. Several sediment class sizes can be simulated. To each particle a corresponding sediment class and mass are assigned such that the total number of particles of that sediment class sums up to the total mass discharged for that sediment class. This mass can change during the simulation as a result of deposition on the seabed. For the plume modelling, due to the difficulty of predicting what wave conditions (especially swell) might be present on any future dredging day of a particular wind strength and direction, no subsequent wave resuspension was included (but is considered by way of expert comments later in this Section).

The basic Lagrangian (flow-path tracking) approach used in the PT module involves no other discretizations other than those associated with the description of the bathymetry of the model area and wind, current and water level fields from the MIKE-3 model simulations. This concept of particle-tracking has several advantages including the elimination of numerical dispersion associated with finite-difference model solutions of the dispersion equations and the number of tracked particles can be matched with available computer resources.

The outputs from the PT module are suspended-sediment concentrations for each size class over the model domain (Fig. 10.1) at each time step in the model simulation, with a facility to calculate composite envelopes of minimum and maximum concentrations that occur in each model cell at anytime during the simulation as well as the mean concentration in each cell. Unfortunately, the new PT flexible-mesh module does not output deposition on the seabed (unlike the MIKE-21 regular-grid PA module that was used for the Harbour plume modelling in Chapters 6 & 7). Consequently, Matlab© software was written to analyse the XML file generated at the end of each PT simulation, to calculate the deposition thickness by including those particles deposited on the bed and also assuming all particles remaining in suspension (mostly near the bed) in any cell would also contribute to the total deposition in that cell. This latter assumption is conservative for areas within a few kilometres of the disposal site (as the deposition will be somewhat higher than that modelled), but less so for the far-field deposition impacts, although in reality these thin deposits, comprising mainly fine or medium silts, will be temporary and continue to be mobilised by wave activity.

11.1.1 PT plume model parameters

The following plume model parameters were implemented for the offshore disposal ground:

- Sediment classes - 4 sediment size fractions were simulated by “particles” in the discharge with their respective average settling velocity:
 - *Class 1* - fine silt with grain sizes of <0.00625 mm with a settling velocity of 5.8×10^{-3} mm/s.
 - *Class 2* - medium silt with grain sizes between 0.00625 and 0.02 mm with a settling velocity of 0.415 mm/s.
 - *Class 3* - coarse silt with grain sizes between 0.02 and 0.0625 mm with a settling velocity of 0.584 mm/s.
 - *Class 4* - fine sand with grain sizes of >0.0625 mm with a settling velocity of 4.11 mm/s.
- Discharge height - set to 5 m below the water surface at the time, which is applicable to a mid-size trailer suction hopper dredger (TSHD).
- Discharge sequence - based on an analysis of dredging operations by POL, the discharge at the disposal site was simulated as a 10-minute slug with a 2-hour turn-around window before the next disposal commenced and so on. Note: this average turnaround time was based on a vessel’s passage to the initial disposal area at A1. The later adoption of a disposal site further offshore (see next Section) could increase the turn-around time by up to 10–15 minutes. This slight time difference between discharges won’t affect the model predictions of peak suspended-sediment concentrations or the deposition patterns.
- Discharge location - specified as a latitude and longitude in WGS-84 coordinate system, which is a “point”. Five “points” were selected to cover the finite size of the disposal ground, which for the 15-m dredged channel option would require an area of approximately 2 km in diameter.
- Dredge hopper composition and discharge rates - two variants on the likely sediment composition of a hopper were simulated with their associated discharge rates in kg/s for each sediment class listed in Table 11.1. The wet bulk density of sand in the hopper was assumed to be packed at 1800 kg/m^3 and for silts 1600 kg/m^3 . The majority of the plume model runs used an overall average hopper composition, based on a dredging analysis by Port Otago Ltd. that incorporated the geotechnical findings and sediment size grading curves (Opus International Consultants, 2008). These averaged hopper simulations were part of an approach (see Section 11.3) to integrate the overall seabed deposition pattern likely from the overall dredging programme for the 15-m Harbour channel. In terms of ascertaining peak suspended-sediment concentrations at the disposal site, some

simulations were also performed for a hopper of predominantly silt (e.g., sourced from the Hamilton Bay reach between Beacons 18 and 20). No allowance was made in the hopper volumes for the slight reduction in sediment lost through overflows during dredging of the channel, particularly dredging claims that would be predominantly in sands but with a small fraction of silts. However this makes the results more conservative.

- Dispersion coefficients - these were set automatically with a scaling of 1 to the Smagorinsky eddy diffusivity formulation for the horizontal dispersion coefficient and the k -epsilon formulation for the vertical dispersion coefficient that match with the de-coupled flow-field runs undertaken using MIKE-3 FM.

Table 11.1: Sediment discharge rates (kg/s) on a saturated-weight basis used for the dredge hopper scenarios for each sediment size class covering two variants on hopper sediment composition from dredging the 15-m Harbour channel option.

Hopper load scenarios	Overall silt/sand load averaged over all dredging sites [†]	Predominantly silt load (e.g., from Hamilton reach) [‡]
Sediment class discharge (kg/s)		
C1 (fine silt)	1,530	2,326
C2 (medium silt)	1,995	3,034
C3 (coarse silt)	2,128	3,236
C4 (fine sand)	11,067	1,517

[†] Average hopper load for a mid-size TSHD would be ~5,800 m³ (rounded up) computed by dividing the total estimated dredge volume of 7.06 Mm³ for the 15-m Harbour channel (final design) by 1224 round trips. From the geotechnical findings and POL dredging analysis, overall the sand component (class 4) would be 63.5% of an average hopper load and the remaining 36.5% silt. The silt component was further divided in size classes 1–3 in the ratios 0.271, 0.353, 0.376 based on the average silt-size grading curve from the geo-technical investigations (Opus International Consultants, 2008).

[‡] Predominantly-silt hopper load for the same dredge capacity would be 3,790 m³ assuming a lower hopper loading factor of 0.35. The lower loading factor arises from early cessation of dredging when the hopper starts to overflow and silts don't readily settle in the hopper like sands. From an average of the sediment grading curves from the predominantly silt areas, the ratio of this hopper volume across sediment size classes 1–4 would be 0.23, 0.30, 0.32, 0.15. A hopper load density of 1600 kg/m³ is assumed.

11.2 Offshore disposal ground options

Early in Project Next Generation, an optimisation process was undertaken to identify potential disposal sites based on a variety of constraints such as fishing zones, seabed

sediment characteristics, distance from the Entrance (dredging cost), known ecological zonation etc. Two disposal sites A1 (closer at 4 km NE of Taiaroa Head) and A2 (on the northern end of the submergent Peninsula Spit) were identified from this initial process as being potential sites to investigate further (Fig. 11.2).

To accommodate the estimated dredging volume of 7.06 Mm^3 from the 15-m Harbour channel design, the disposal ground would need to be around 2 km in diameter (see circular zones Fig 11.2) with an average mound height of up to 1.4–1.8 m above the seabed, depending on the proportion of the volume that disperses from the site during disposal, the wet bulk density of the deposited sediments (see Section 12.1 for more analysis), and the losses from in-harbour discharges during channel dredging.

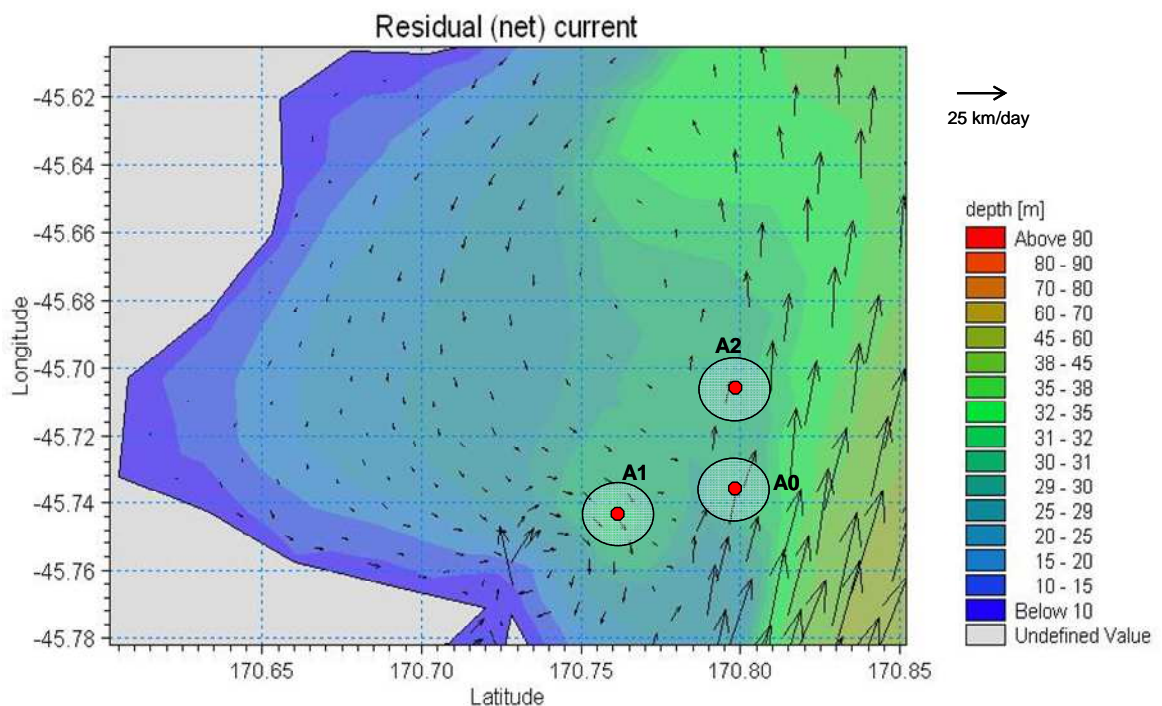


Figure 11.2: Location and extent of disposal site options investigated during the offshore plume modelling process, with a backdrop of the residual current pattern from Figure 10.4a.

As a result of initial plume-model simulations, site A1 was ruled out as a disposal site option. This was due to the tendency for onshore movement of suspended-sediment plumes directly towards Otago Heads coastline with parts of the plume with low concentrations entering the Harbour Entrance. The cause of this preferential onshore transport of the plume arises from the clockwise rotation of the Taiaroa Head eddy within which A1 is located (see Fig. 11.2).

Further plume modelling was undertaken at various sites in the vicinity of A1 and A2, including a site at A0 and one at 2 km further offshore to the east of A2 (which provided only marginal improvement on the A2 results in terms of fine silt dispersal). This process led to a potentially optimal site at A0 on the submergent Peninsula Spit, in terms of suspended-sediment plumes seldom reaching coastal areas or entering the Harbour, and then only occasionally at low excess concentrations above background. Further, current velocities and the residual current are parallel with the Peninsula Spit (Fig. 11.2), so disposal of material at A0 will result in initial settling out of silts downstream at A2 in any case, while sea-bed sediment transport to the north along the Peninsula Spit (see Section 12) will eventually move some of the sand from a disposal mound towards A2. Disposal at the more northern A2 site resulted in almost no direct contact of the plume edge on Otago Heads and The Mole, but increased silt concentrations somewhat for coastal zones north of Cornish Head (see Figs. 10.2 & 10.4a for location), relative to the concentrations using site A0. Site A0 is also a shorter steaming distance to and from the Harbour Entrance for the dredge, rather than A2.

11.3 Plume modelling approach

A plume modelling strategy was developed for the offshore disposal operation to include the uncertainty of when the future dredging would take place and under what wind conditions.

11.3.1 Hydrodynamic model scenarios

The calibration of the offshore hydrodynamic model (Section 10) revealed that tidal effects were minor, once outside the influence of the tidal stream in and out of Otago Harbour, while the Southland Current persistently flows to the NE, although it can vary somewhat in magnitude. This leaves local winds as the main contributor to variations in current flows, especially in creating marked differences between surface and bottom layers in the water column. Consequently, hydrodynamic model runs were set up for different wind scenarios, but the Southland Current flux and an average tidal range were kept constant. Each wind scenario was modelled using a 4-day spin-up period with no wind to allow the tide and Southland Current forcing to reach equilibrium. This was followed by a 48-hour period with the selected wind velocity applied progressively as a half-sine function, reaching the peak wind speed in the mid-point (24 hours) then decreasing again to zero by 48 hours. A couple of hours was added at the end with the wind at zero as run-out phase to allow for tracking the plume after the last dredge-hopper discharge. A 48-hour period was selected as the basis for a wind scenario run as it: a) is around the average time period for a wind event to occur;

b) divides evenly into 24 dredge-hopper discharges at an average turn-around time of 2 hours¹⁸; c) provides for quite a number of wind sequences over the dredging programme.

The aim was to select several wind scenarios to model and assign probabilities of occurrence to these “events” so a Monte Carlo process could be used to “spin the dice” to select the wind scenario for each set of 48-hour time window in the dredging season. The total dredged sediment volume of 7.06 Mm³ was divided by the sub-total of sediment volume released in each simulated 48-hour dredge-disposal sequence to arrive at the requirement of 51 such sequences. Note: this is conservative as we haven’t deducted the loss of sediment via discharges (overflows, bottom disturbance) while dredging in the Harbour, which would only be about 3% of the overall dredging volume (excluding rock).

Long-term wind measurements at Taiaroa Head since 1988 were analysed, assigning wind speeds to either of the two dominant wind sectors NNE or WSW. Then a cumulative frequency distribution of wind speeds was generated for each of these two sectors - summing to 56% of the time for winds from the NNE sector and 44% of the time for the WSW sector (Fig. 11.3). This included calm wind occurrences (2%) of which half were assigned to each sector. Three wind speeds were selected from the cumulative frequency distributions for each sector, that are representative of the first 25% of all winds split between wind sectors (=50% in total), the next highest 20% of all winds (=40% in total) and the upper range of the last 5% of all winds (10% in total). Within each of these sub-ranges, the 66-percentile wind speed was selected to represent that range of speeds and assigned the probability of occurrence for that range. The six representative wind speeds relative to the cumulative wind frequency distributions are shown in Figure 11.3 and the details of the winds speeds and assigned probabilities of occurrence are listed in Table 11.2. The skewness in the representative wind velocities between the two wind sectors arise because winds from the NNE sector occur more often, but at lower wind speeds than from the WSW sector, as shown in Figure 11.3.

¹⁸ Note: this average turn-around time was applicable to the initial A1 option for a disposal site. The subsequent selection of the A0 disposal site would add around 10-15 minutes. However, this won’t affect maximum SSC or accumulated deposition thicknesses.

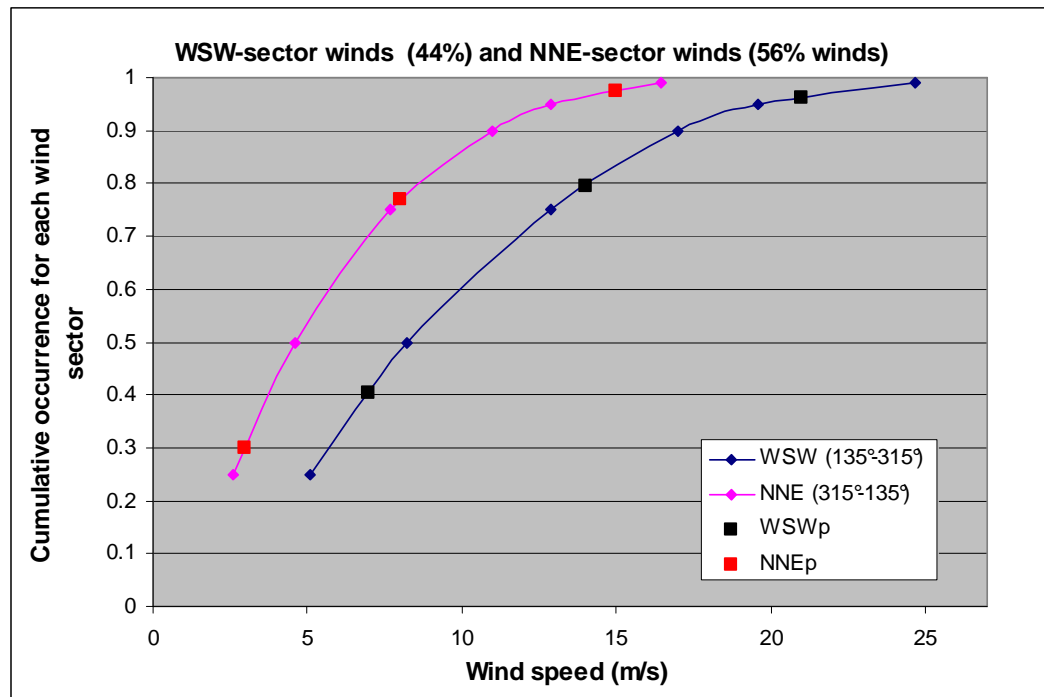


Figure 11.3: Cumulative frequency of occurrence for each of the two wind sectors centred on blowing from WSW and NNE, normalised to a probability of 1.0 for each sector, which is 44% of all winds for the WSW sector and 56% of winds for the NNE sector. The six selected wind scenarios that representative of each wind-sector distribution (see Table 11.2) are shown as WSWp and NNEp respectively.

Table 11.2: Parameters associated with the six wind scenarios used for the offshore plume modelling.

	Wind scenario No.					
	1	2	3	4	5	6
Wind speed range (m/s)	0–9.3	9.3–16.6	16.6–max	0–4	4–11.3	11.3–max
Representative wind speed – 66%ile (m/s)	7	14	21	3	8	15
Wind direction (°)	245	245	245	22.5	22.5	22.5
	WSW	WSW	WSW	NNE	NNE	NNE
Probability of occurrence (0–1)	0.25	0.20	0.05	0.25	0.20	0.05

The six hydrodynamic model runs for these representative winds were undertaken as described above, ramping up to the peak wind speed and back to calm winds again for each 48-hour scenario. The results from these six wind simulations then provided a look-up set of time-varying flow fields in three depth layers that were used as input to the plume model simulations.

11.3.2 Plume model scenarios

The two key aspects for assessing environmental effects that are required from the offshore sediment plume modelling are the: a) magnitude (mean and maximum) of suspended-sediment concentrations and the spatial extent of the plume; and, b) total seabed deposition (mm) and extent of deposition over the dredging season. Both these requirements needed a different approach to the set-up of the plume simulations.

Plume concentrations and spatial extent - these results can be obtained by a single simulation of each of the six 48-hour wind scenarios, applied for each of the five selected discharge sub-sites within the 2 km disposal area. For the preferred disposal site (A0), the locations and spread of the 5 disposal sub-sites are shown in Figure 11.4.

Following each of these individual scenarios (for winds and sub-sites), composite envelopes of the mean and maximum SSC over the 48-hour wind sequence (plus a 2-hour wind-down following the last hopper discharge) were generated for each sediment-size component. To get total suspended concentrations in the plume, the excess SSC values predicted by the model for each sediment-size class (1–4) need to be added together.

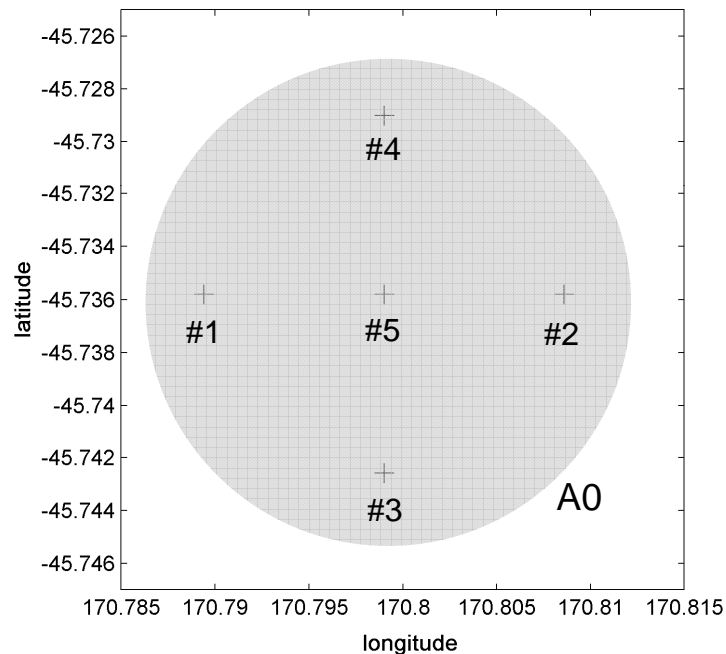


Figure 11.4: Relative location of the 5 sub-sites used as discharge locations within a 2-km diameter disposal site at A0 (central sub-site #5 is at -45.7358°N and 170.799°E).

Note: the plume modelling results for SSC are in terms of saturated-weight (because wet-bulk densities have been used for the source input), whereas normally SSC is expressed in dry-weight per volume. Therefore, the SSC results will be overestimates (conservative) compared with dry-weight SSC values. Realistically, SSC may be 50–90% of the conservative SSC values presented in this Chapter, depending on the equivalent dry bulk density of the sediments in the hopper, with the lower-range percentages applying to silt sizes and the upper-range percentages to fine sands.

Sea-bed deposition—Given the distribution of winds during the actual dredging programme are not known ahead of time, a Monte Carlo approach was used to randomly select one of the 6 wind scenarios for any 48-hour period, where the chance of selection for a wind scenario is governed by the probabilities in Table 11.2. A sequence of 51 sets of 48-hour plume simulations were required to cover the total discharge of 7.06 Mm³, and the deposition pattern and magnitude from each set is accumulated to arrive at an estimate of the total offshore deposition.

This approach was achieved with the following steps:

- (i) cycle consecutively around the sub-sites within the disposal area, starting with #1, then #2 etc;
- (ii) throw the weighted “dice” using a Monte Carlo algorithm to select a wind scenario from 1–6 for that sub-site;
- (iii) run the plume model simulation for that sub-site and the chosen wind scenario using the parameters from Section 11.1;
- (iv) extract the results in the form of the spatial distribution on a 0.005°×0.005° grid (390 m easting × 555 m northing) and magnitudes (kg/m²) of sea-bed sediment deposition for the four sediment size classes;
- (v) go back to step (i) and repeat sequence for the next sub-site;
- (vi) at the end, sum up the 51 sets of spatial deposition patterns, apply a wet bulk density (assumed a conservative value of 1300 kg/m³) and produce plots of deposition in mm for each size class and the grand total for all sediment sizes.

The number of times each wind scenario was selected by step (ii) is listed in Table 11.3 and compared to the assigned probability distribution that the Monte Carlo procedure randomly sampled from. The differences arise because of the relatively small sample size (51). Note: the Monte Carlo algorithm was tested for 10,000 samples, which produced a distribution very close to the final row of Table 11.3.

Table 11.3: No. of times each wind scenario was selected at random by the Monte Carlo procedure for the 51 sets of “48-hour events” compared to the assigned probability distribution.

	Wind scenario No.					
	1	2	3	4	5	6
Wind direction (°)	245 WSW	245 WSW	245 WSW	22.5 NNE	22.5 NNE	22.5 NNE
No. of times selected (total 51)	14	8	1	13	12	3
No. of times selected (ratio) [†]	0.27	0.15	0.02	0.25	0.24	0.06
Probability of occurrence (0–1)	0.25	0.20	0.05	0.25	0.20	0.05

[†] rounding to 2 decimal places means total is not exactly 1.0.

Assumptions - The assumptions implicit in the above approaches are that: a) flow fields for a given band of wind speeds can be represented by a single value, and the entire wind probability distribution can be represented by 6 wind speeds; b) no seasonality for winds is included, as the period for the dredging is not yet determined; c) the local area around each sub-site in the disposal area is worked “continuously” (actually 10 minute slugs every 2 hours) over a period of 48-hours before moving to the next sub-site; d) material remains in place where it is first deposited (i.e., no resuspension by waves is included for this analysis).

With respect to the first two assumptions, the results presented in the following sections were not overly sensitive to changes in wind speed, given the Southland Current dominates the flow regime in the offshore area and at the A0 disposal site. The third assumption is a pragmatic one, and will be similar to the procedure undertaken by the dredger to build up the mound evenly - but however it is sequenced doesn’t affect the overall deposition which depends on the total volume discharged and the relative proportion of each sediment size class (see Table 11.1). The final assumption is the more critical one that will be considered further in this Chapter, as silts in particular will be resuspended by wave action and moved. In terms of total deposition, the assumption of no resuspension will generally be conservative (i.e., lead to higher estimated depths of sediment than would be the case in reality) and therefore provides an upper bound on the likely sediment deposition when considering environmental effects.

11.4 Suspended-sediment concentrations predicted using disposal site A0

Results from the individual 48-hour disposal plume simulations are presented in the form of composite envelopes of both the mean and maximum suspended-sediment concentration (SSC). These composites are not a time snapshot of the plume or its extent - rather they show for each location the maximum SSC that occurred there at any time during the simulation and the average SSC through the 48-hour period for that location.

As expected, SSC was highest in the bottom near-bed layer (L1 as described in Section 10.1) due to the settling of sediment towards the bed and having commenced discharge at 5 m below the water surface. Consequently, most of the results are presented from L1. Results also focus on the finer silt sizes (Size classes 1 and 2) as they settle the slowest contributing to higher SSC for longer periods after the 10-minute disposal window.

11.4.1 Results for different wind scenarios

Figures 11.5 to 11.10 show the mean (a) and the maximum (b) excess SSC composites during 48-hour periods for wind scenarios 1 to 6 described in Section 11.3. All results are for the most landward sub-site #1 within the A0 disposal area (Fig. 11.4), potentially being the most critical in terms of the plume more likely to intersect with the coastal zone and subject to a slower residual current. However, the Monte Carlo approach didn't select wind scenario 6 (strong NNE wind) for sub-site #1, so the SSC composites for this wind scenario were taken from the central sub-site (#5) which is only 0.75 km further east. Only results for size classes 1 and 2 (fine and medium silts) and the bottom layer (L1) only are shown.

Note: the SSC scale was set the same for all plots ranging from 0 to 0.15 kg/m^3 (which is equivalent to 0 to 150 mg/L of saturated-weight per volume), although the predicted SSC reaches higher values of up to 220 mg/L for medium silts in some wind scenarios in the vicinity of the disposal ground. The SSC is the additional concentration arising from the disposal sequence over and above the background concentration at the time (which can vary considerably depending on wave conditions and river run-off).

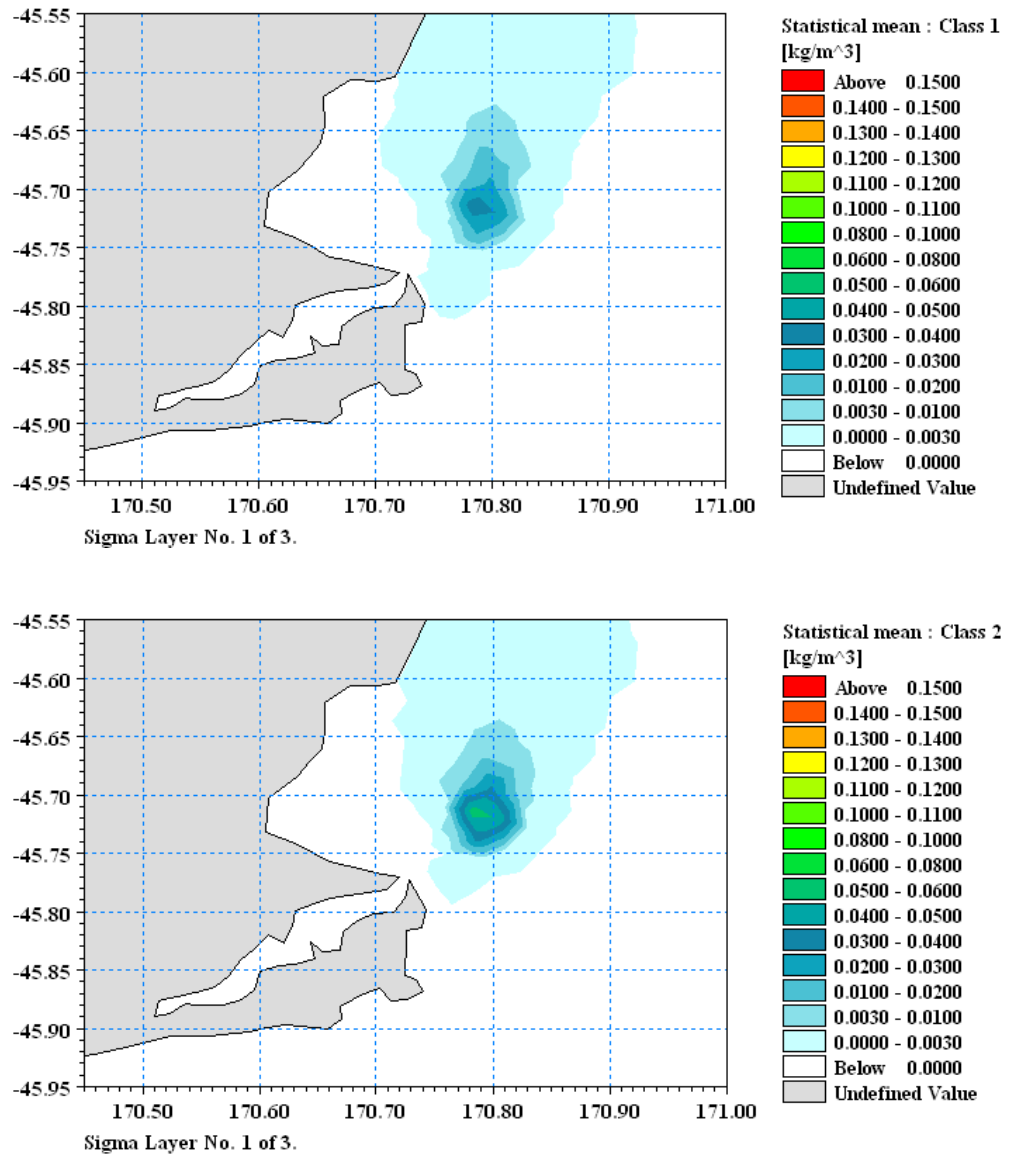


Figure 11.5a: Mean SSC composite envelopes for size class 1 (top) and size class 2 (bottom) over 24 disposal cycles for wind scenario 1 (light WSW wind) at disposal sub-site #1.

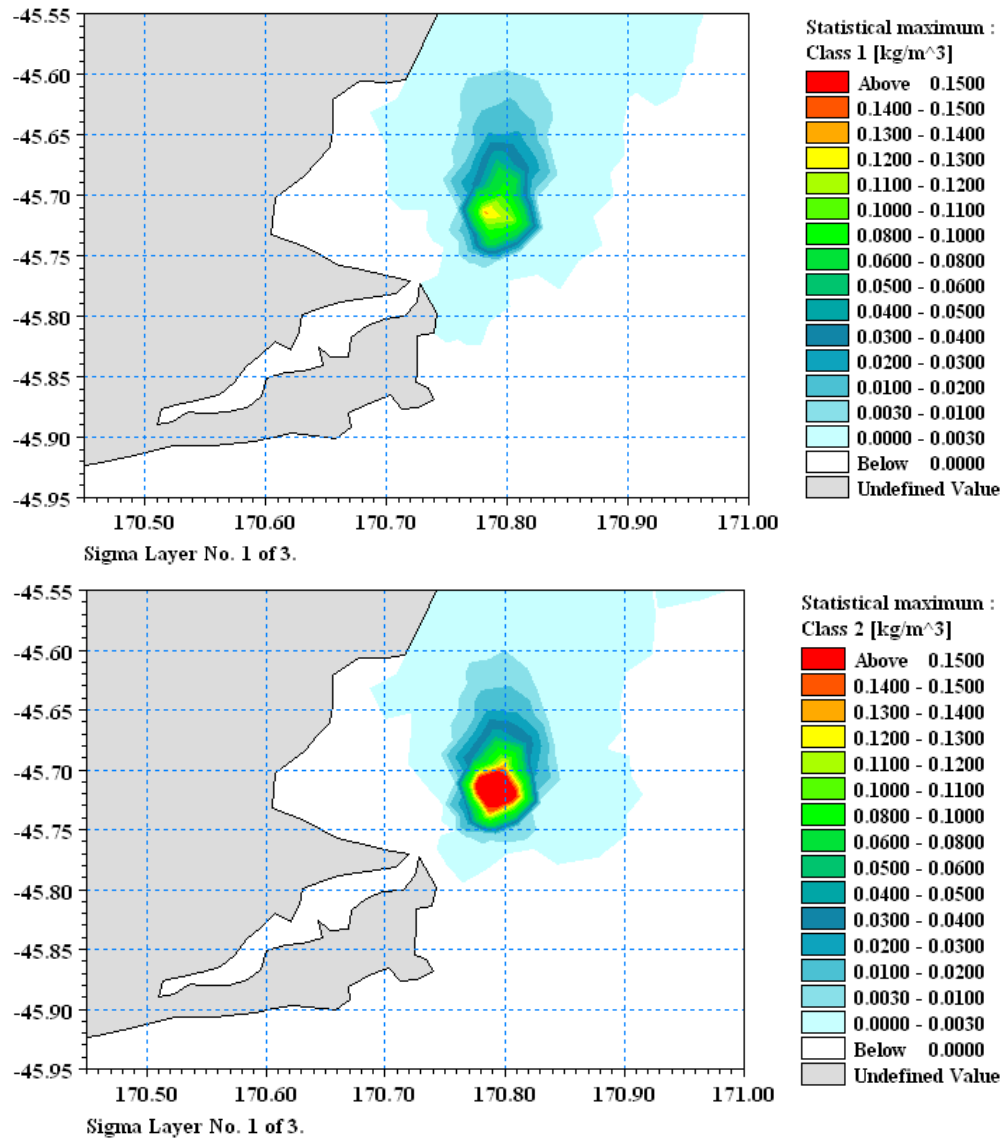


Figure 11.5b: Max. SSC composite envelopes for size class 1 (top) and size class 2 (bottom) over 24 disposal cycles for wind scenario 1 (light WSW wind) at disposal sub-site #1. Note: maximum SSC for size class 2 in this simulation was 0.20 kg/m³ or 200 mg/L.

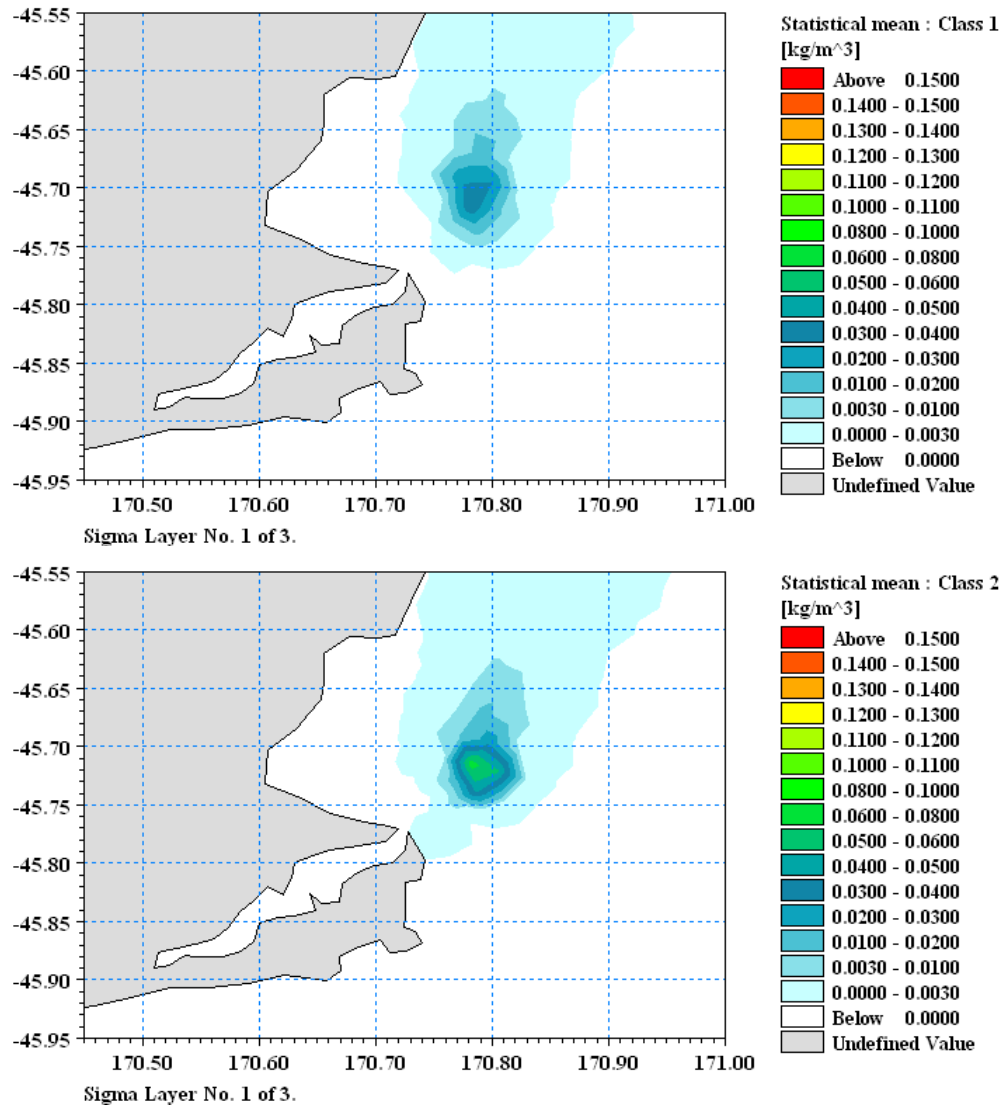


Figure 11.6a: Mean SSC composite envelopes for size class 1 (top) and size class 2 (bottom) over 24 disposal cycles for wind scenario 2 (moderate WSW wind) at disposal sub-site #1.

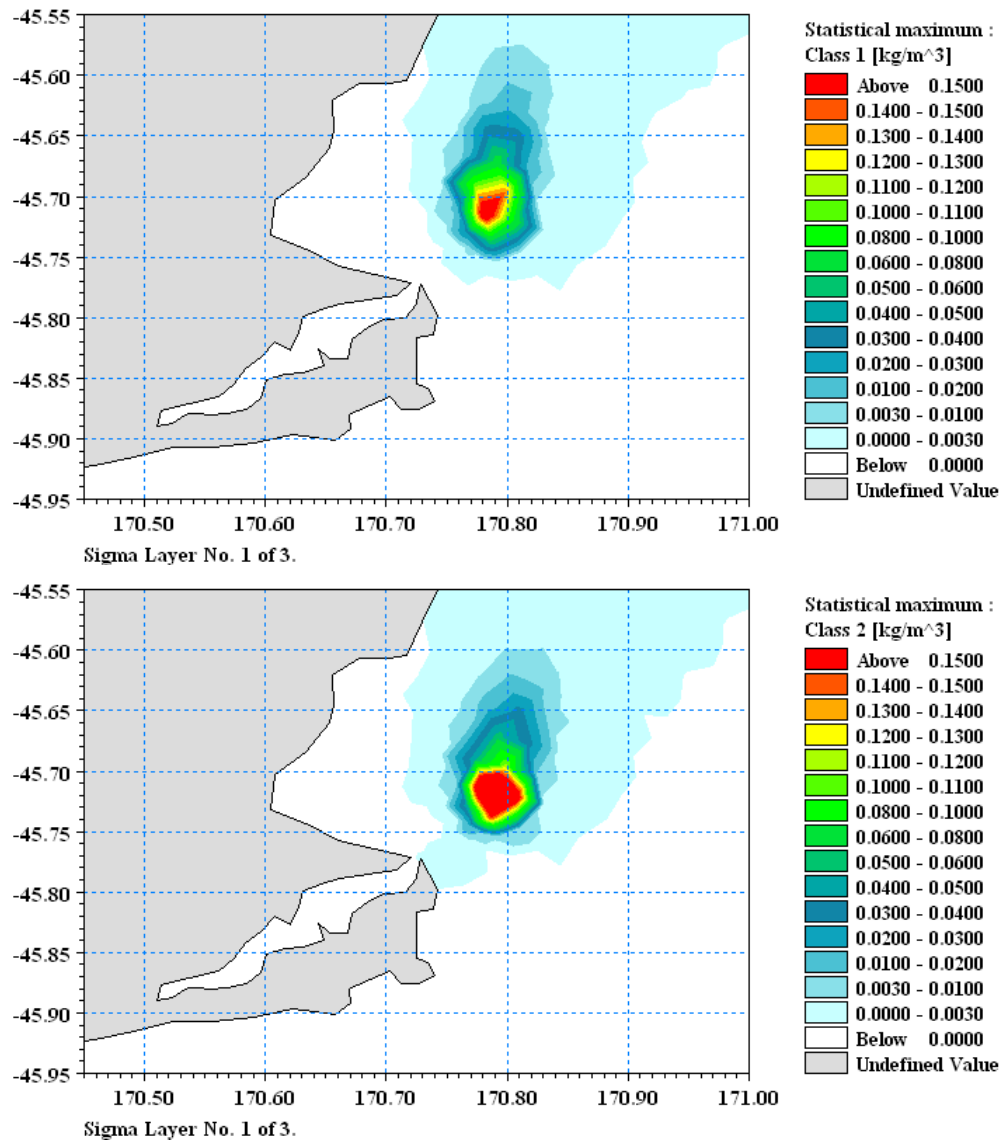


Figure 11.6b: Max. SSC composite envelopes for size class 1 (top) and size class 2 (bottom) over 24 disposal cycles for wind scenario 2 (moderate WSW wind) at disposal sub-site #1. Note: maximum SSC for size class 1 in this simulation was 0.17 kg/m³ or 170 mg/L and for size class 2 was 0.22 kg/m³ or 220 mg/L.

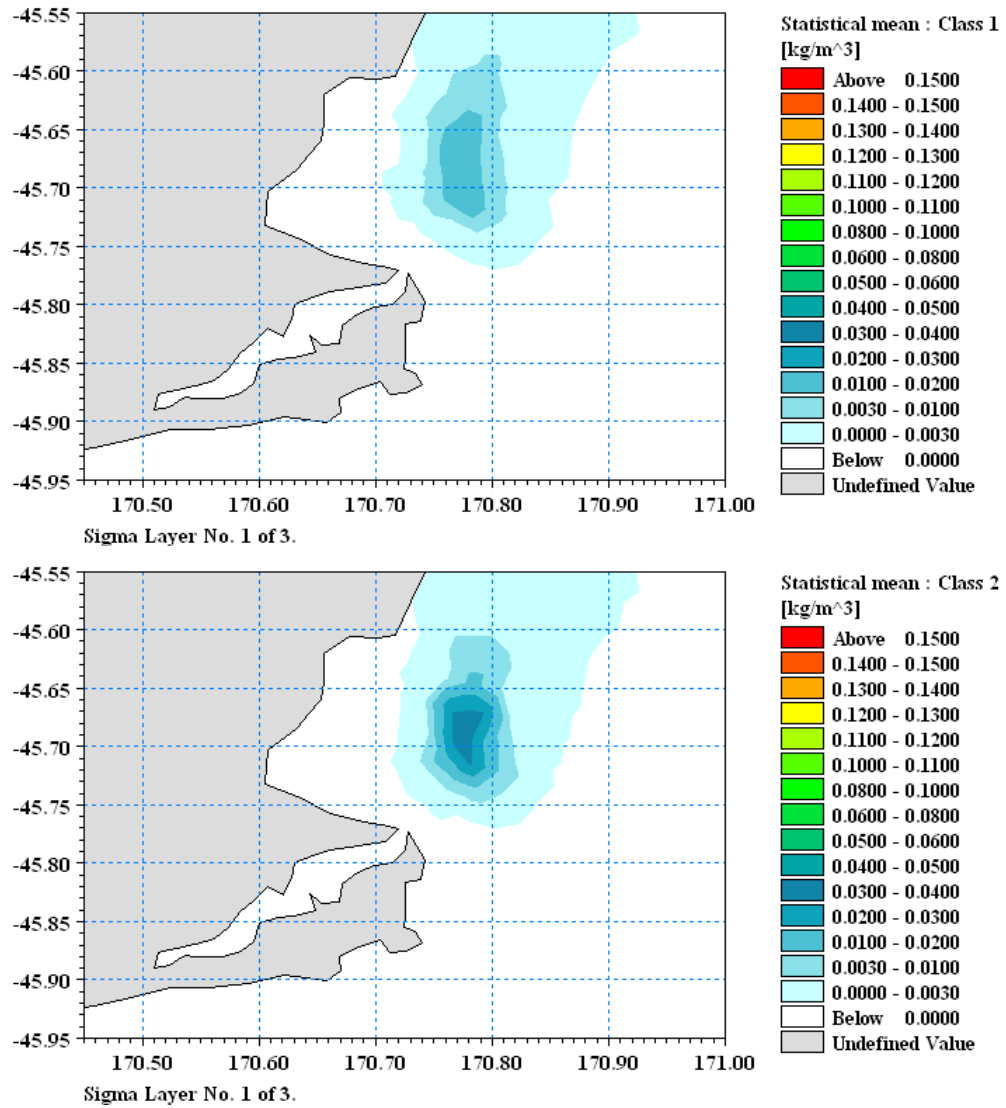


Figure 11.7a: Mean SSC composite envelopes for size class 1 (top) and size class 2 (bottom) over 24 disposal cycles for wind scenario 3 (strong WSW wind) at disposal sub-site #1.

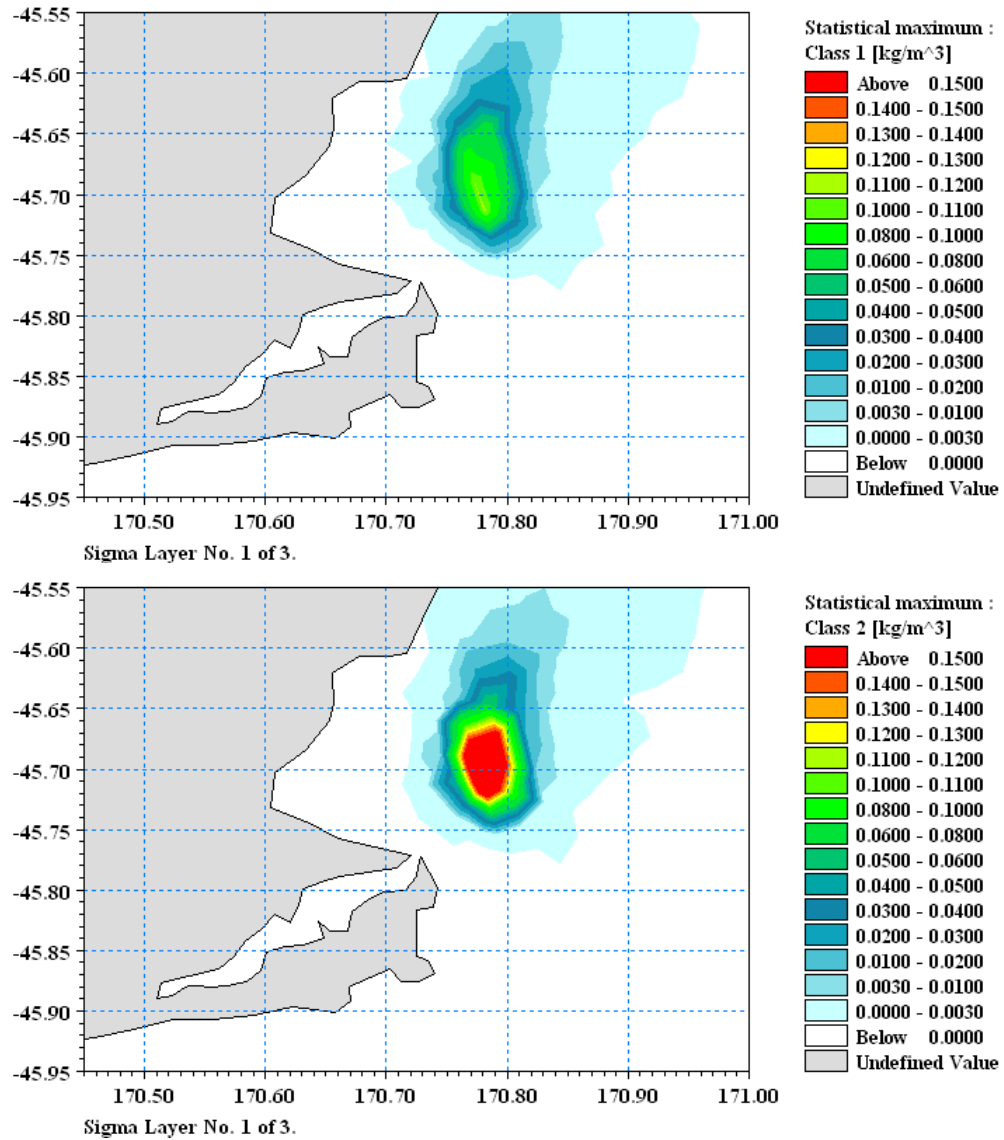


Figure 11.7b: Max. SSC composite envelopes for size class 1 (top) and size class 2 (bottom) over 24 disposal cycles for wind scenario 3 (strong WSW wind) at disposal sub-site #1. Note: maximum SSC for size class 2 in this simulation was 0.21 kg/m³ or 210 mg/L.

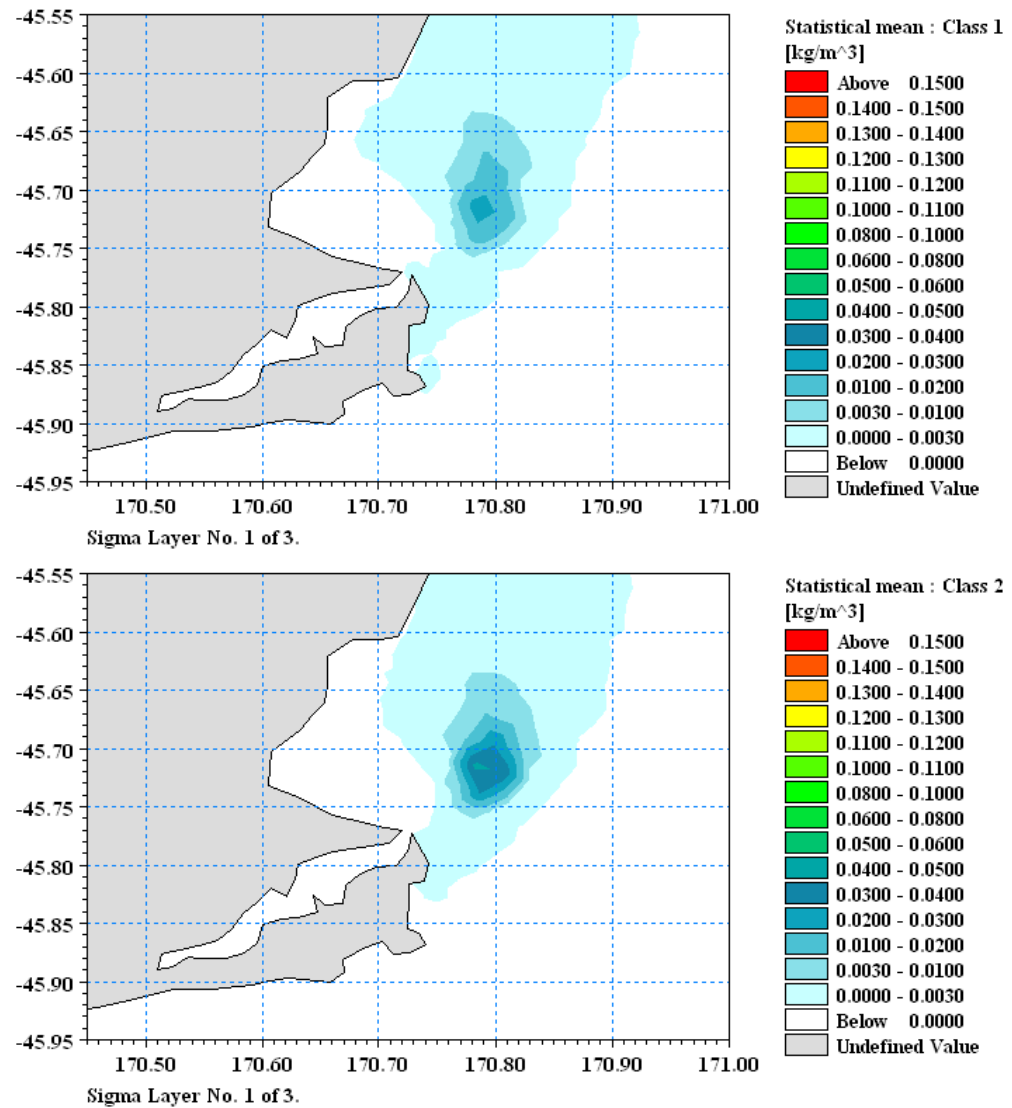


Figure 11.8a: Mean SSC composite envelopes for size class 1 (top) and size class 2 (bottom) over 24 disposal cycles for wind scenario 4 (light NNE wind) at disposal sub-site #1.

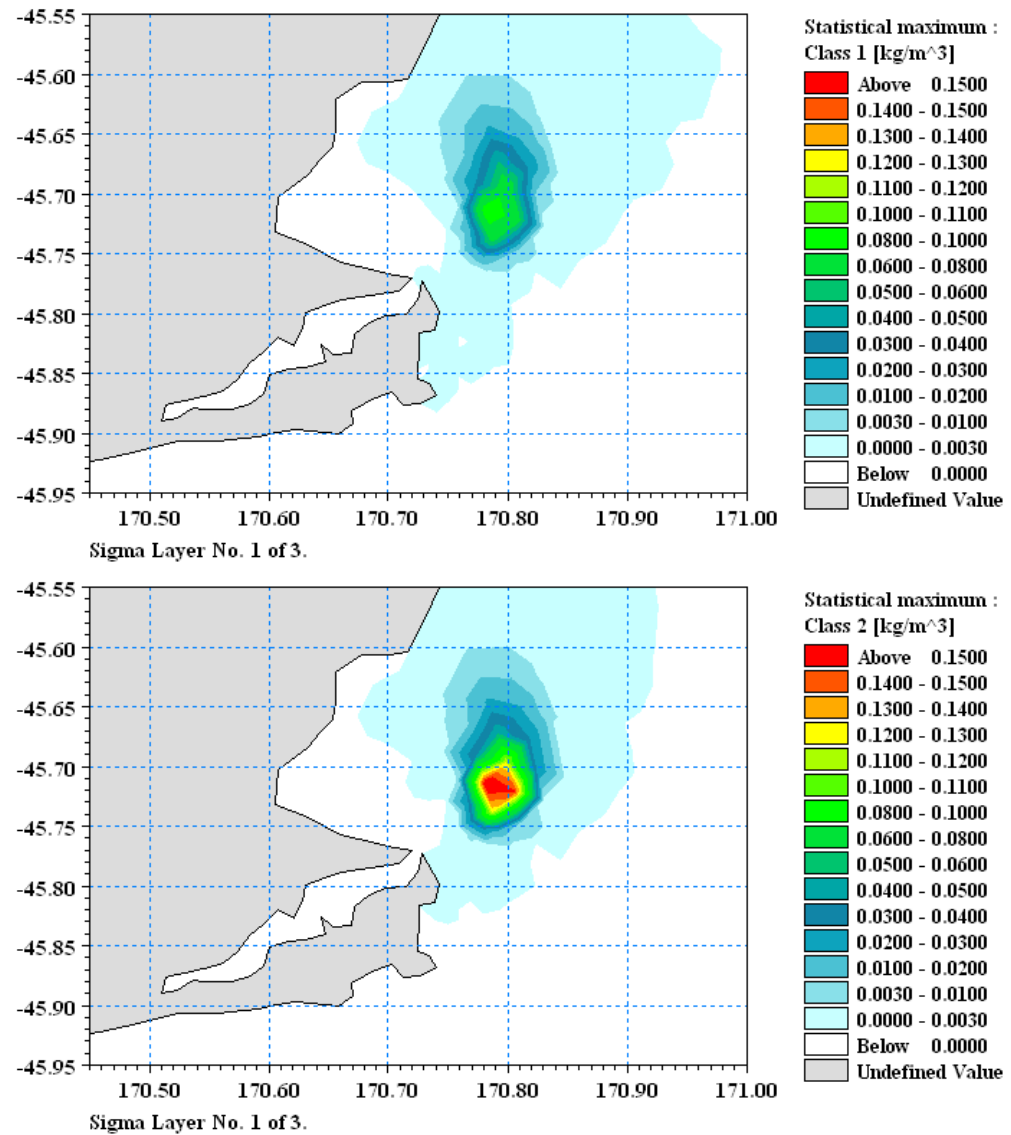


Figure 11.8b: Max. SSC composite envelopes for size class 1 (top) and size class 2 (bottom) over 24 disposal cycles for wind scenario 4 (light NNE wind) at disposal sub-site #1. Note: maximum SSC for size class 2 in this simulation was 0.16 kg/m³ or 160 mg/L.

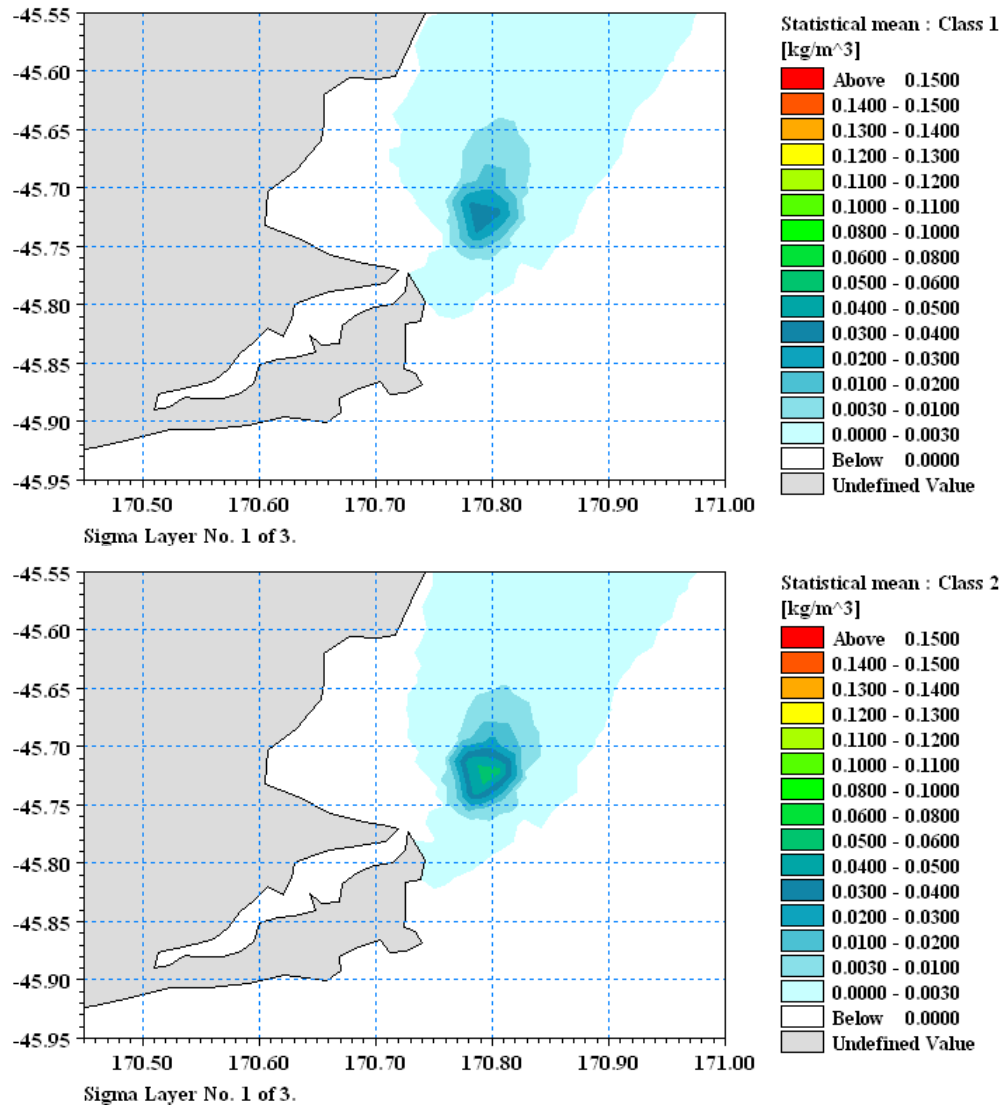


Figure 11.9a: Mean SSC composite envelopes for size class 1 (top) and size class 2 (bottom) over 24 disposal cycles for wind scenario 5 (moderate NNE wind) at disposal sub-site #1.

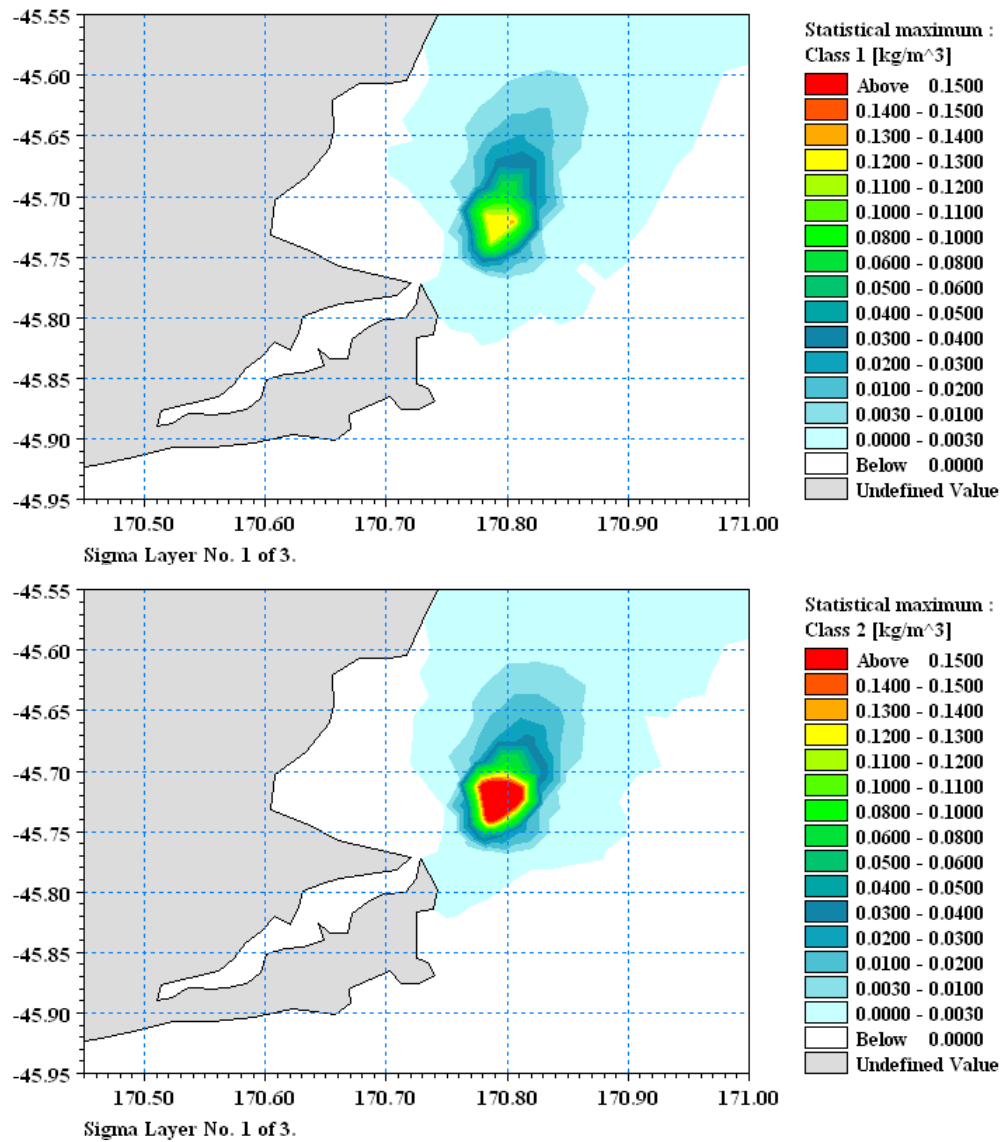


Figure 11.9b: Max. SSC composite envelopes for size class 1 (top) and size class 2 (bottom) over 24 disposal cycles for wind scenario 5 (moderate NNE wind) at disposal sub-site #1. Note: maximum SSC for size class 2 in this simulation was 0.20 kg/m^3 or 200 mg/L .

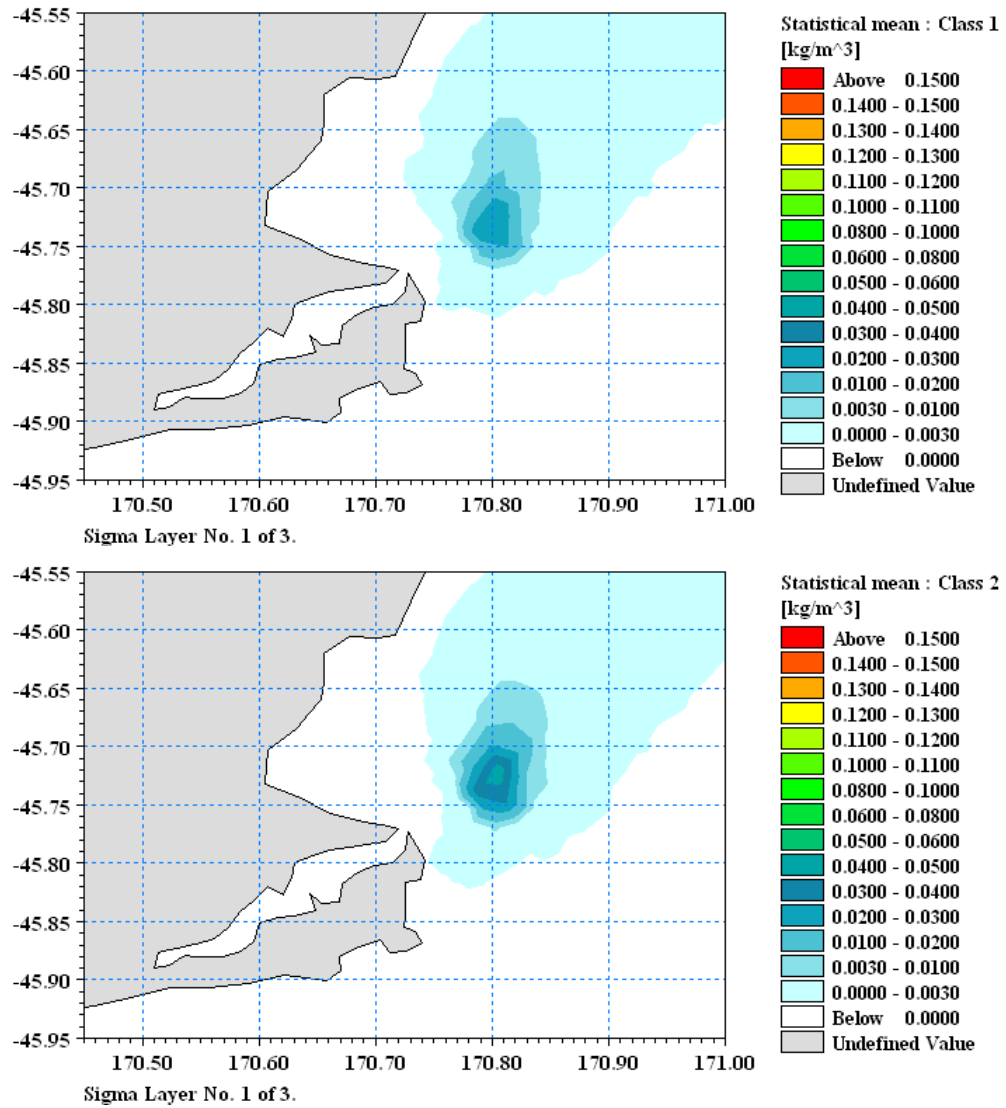


Figure 11.10a: Mean SSC composite envelopes for size class 1 (top) and size class 2 (bottom) over 24 disposal cycles for wind scenario 6 (strong NNE wind) at disposal sub-site #5.

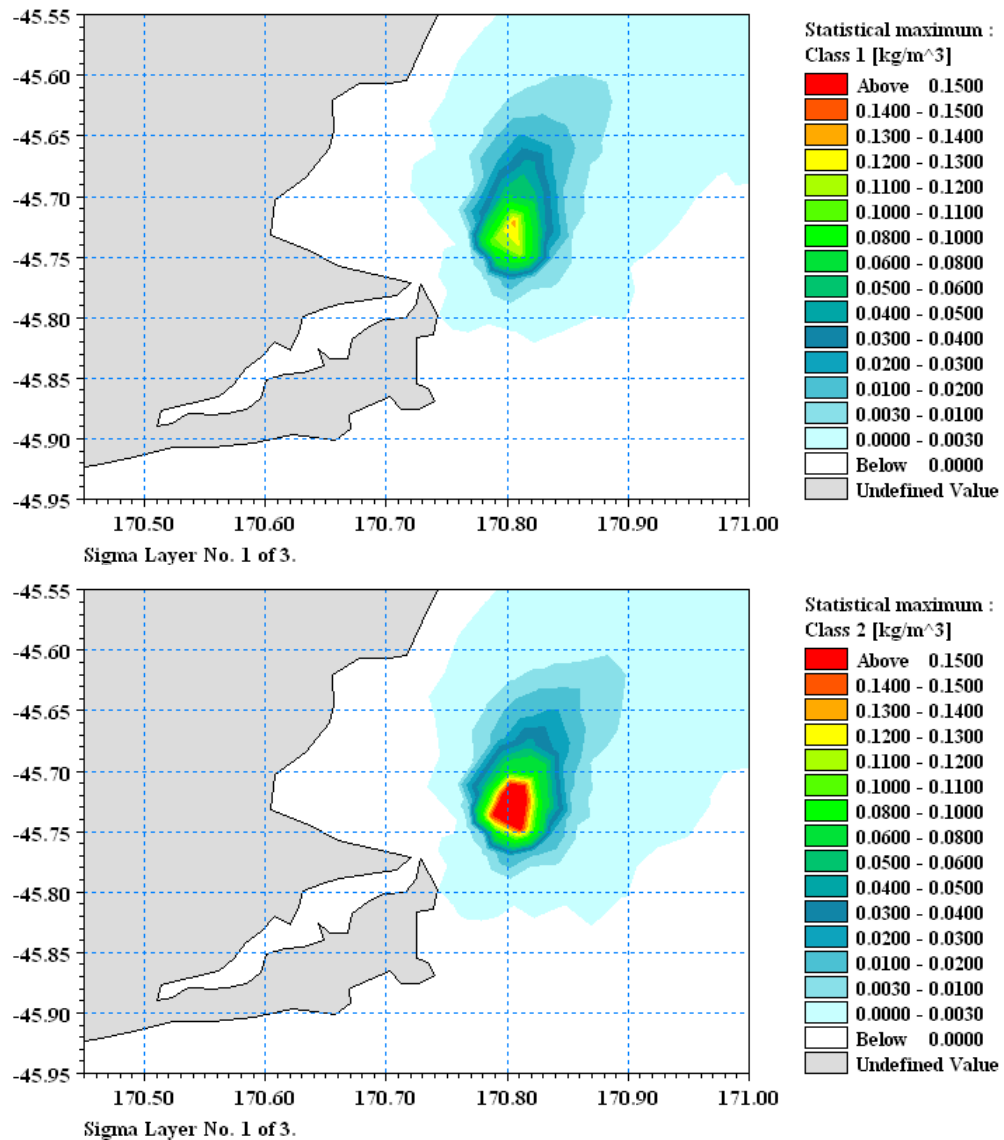


Figure 11.10b: Max. SSC composite envelopes for size class 1 (top) and size class 2 (bottom) over 24 disposal cycles for wind scenario 6 (strong NNE wind) at disposal sub-site #5. Note: maximum SSC for size class 2 in this simulation was 0.19 kg/m³ or 190 mg/L.

Summary of results - the above sequence of SSC composites for the near-bed layer and fine and medium silts only, under the six different wind conditions show that:

- medium silts cause the higher local elevations in SSC in the bottom layer within a few kilometres of the disposal ground, but the fine silts are more dispersive spreading over a wider area (due to their lower settling rate);
- out of the two finer size classes, the highest excess SSC values reached in the vicinity of the disposal site are in the range 160 to 220 mg/L in the bottom

layer for medium silts, with this higher maximum value likely to occur during moderate WSW winds;

- for both fine and medium silts, the most adverse wind conditions for the maximum excess SSC are moderate WSW winds;
- the mean SSC composites show that the average concentrations are substantially lower than the maximum values. Considering only the medium silts (class 2), the highest average SSC in the vicinity of the disposal ground, would reach 70 mg/L in moderate winds (NNE and WSW) and 60 mg/L for all other wind conditions. The much lower average SSC is influenced by the 2-hour gap between disposal from the dredging vessel, allowing the concentrations to reduce from settling and dispersion;
- the dilute edge of the suspended-sediment plume could occasionally reach coastal areas between Taiaroa Head and northern Wickcliffe Bay but not under stronger winds from both the WSW or NNE. When nearshore contact does occur, the maximum concentration contributed to by both fine and medium silts in the plume would be small—no more than 0.07 mg/L on top of the background concentration except in light north-east winds when the maximum excess concentration could reach 2–2.5 mg/L for short periods. No contact of the near-bed plume edge with Otago Heads would occur with strong winds from either WSW or NNE;
- the dilute edge of the suspended-sediment plume could also reach coastal areas north of Cornish Head, except during strong NNE winds when the near-bed flow would be nudged further offshore opposite to the surface wind. In these coastal zones, the maximum concentration contributed to by the plume would be small—no more than 0.3 mg/L (for fine silts) and no more than 0.1 mg/L for medium silts (combined total of 0.41 mg/L for all size classes) in the near-bed layer which would occur under strong WSW winds;
- overall, winds don't appear to substantially affect the plume characteristics and movement as much as plume simulations for disposal site option A1 closer inshore. This is because disposal site A0 is located in the periphery of the Southland Current that drives a persistent residual current to the north and tends to dominate the flow regime.

11.4.2 Differences between size classes and surface vs. bottom layer

Figures 11.11 to 11.12 show the mean (a) and the maximum (b) excess SSC composites during 48-hour periods for all four size classes, starting in the surface layer, then considering the bottom layer, for the light-wind scenario 1 (WSW) described in Section 11.3. A similar sequence is shown in Figure 11.13 to 11.14 for light-wind scenario 4 (NNE). All results are for the most landward sub-site #1 within the A0 disposal area, potentially being the most critical in terms of likelihood of the plume passing near the coast and subject to the slowest residual current.

To obtain the total suspended sediment concentration predicted for the plume, the excess SSC for each sediment-size class needs to be added together.

Note: the SSC scale on each plot was set the same as before, ranging from 0 to 0.15 kg/m³ (which is equivalent to 0 to 150 mg/L), except for class 4 (fine sand) composites in the lower layer (L1) where the scale was expanded up to 1.5 kg/m³ (1500 mg/L). The SSC is the additional concentration arising from the disposal sequence over and above the background concentration at the time.

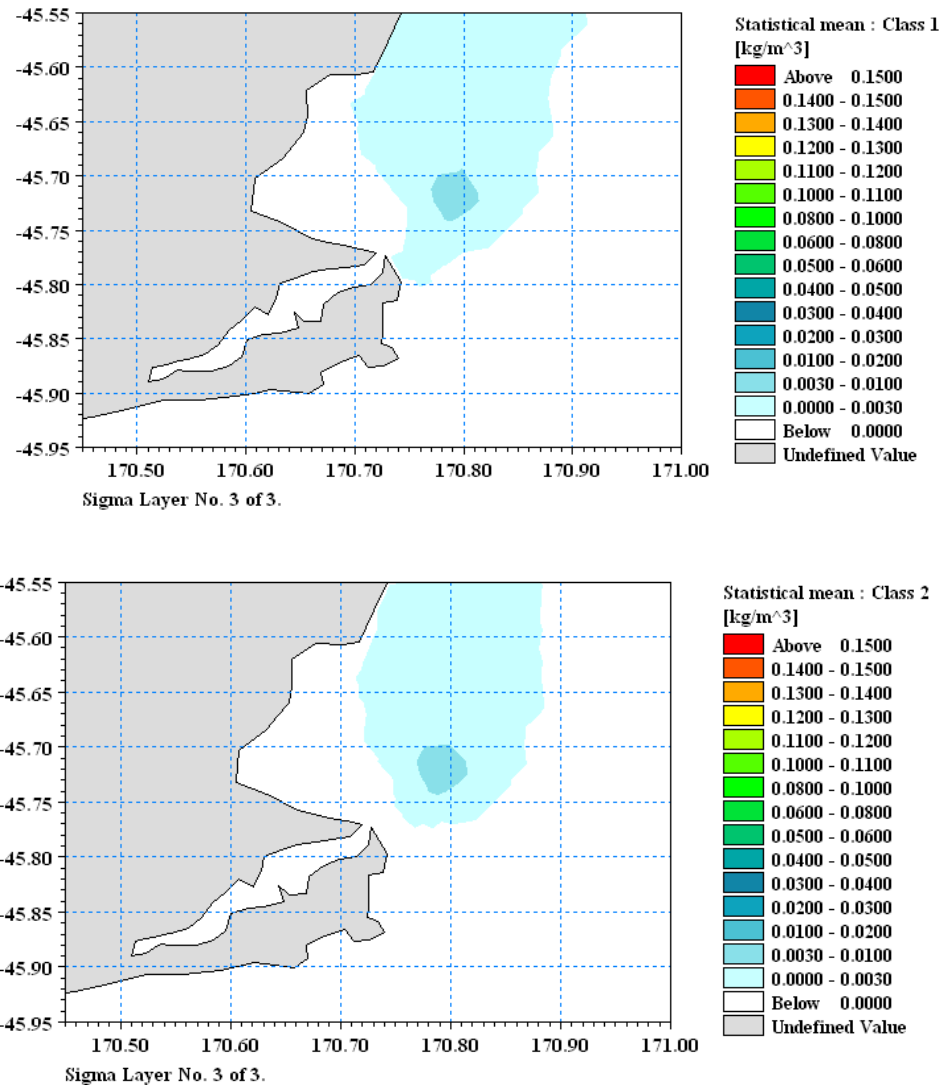


Figure 11.11a: Mean SSC composite envelopes for size class 1 (top) and size class 2 (bottom) in the surface layer (L3) over 24 disposal cycles for wind scenario 1 (light WSW wind) at disposal sub-site #1.

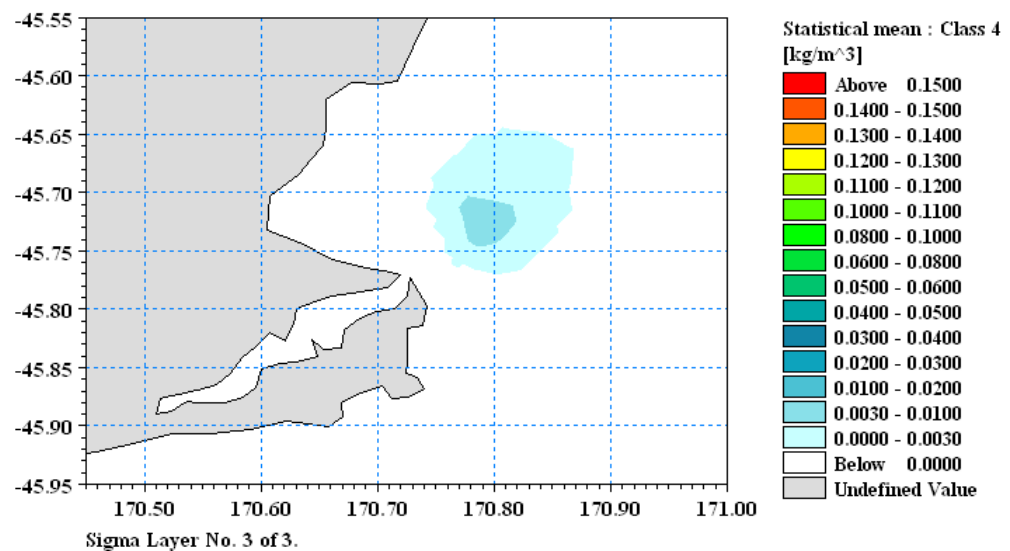
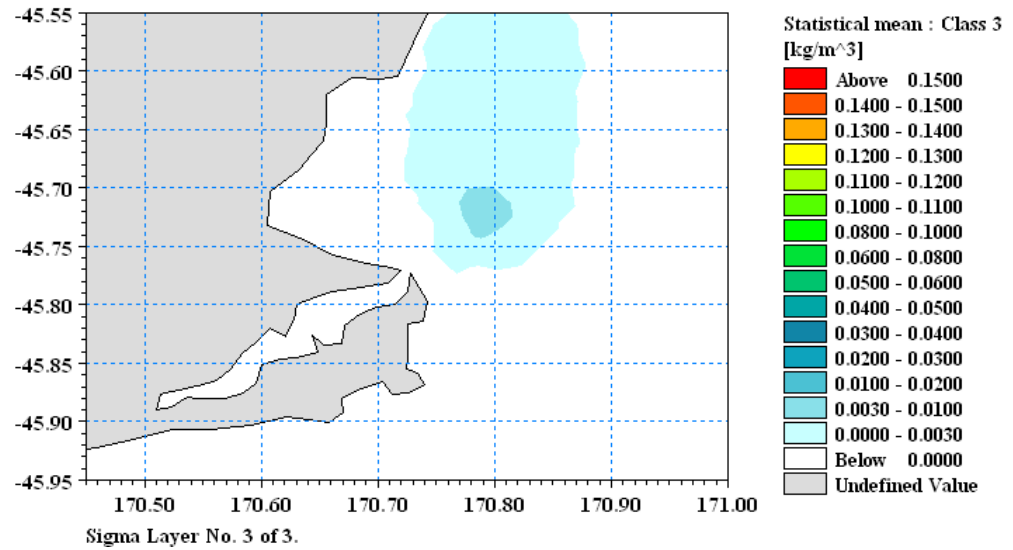


Figure 11.11b: Mean SSC composite envelopes for size class 3 (top) and size class 4 (bottom) in the surface layer (L3) over 24 disposal cycles for wind scenario 1 (light WSW wind) at disposal sub-site #1.

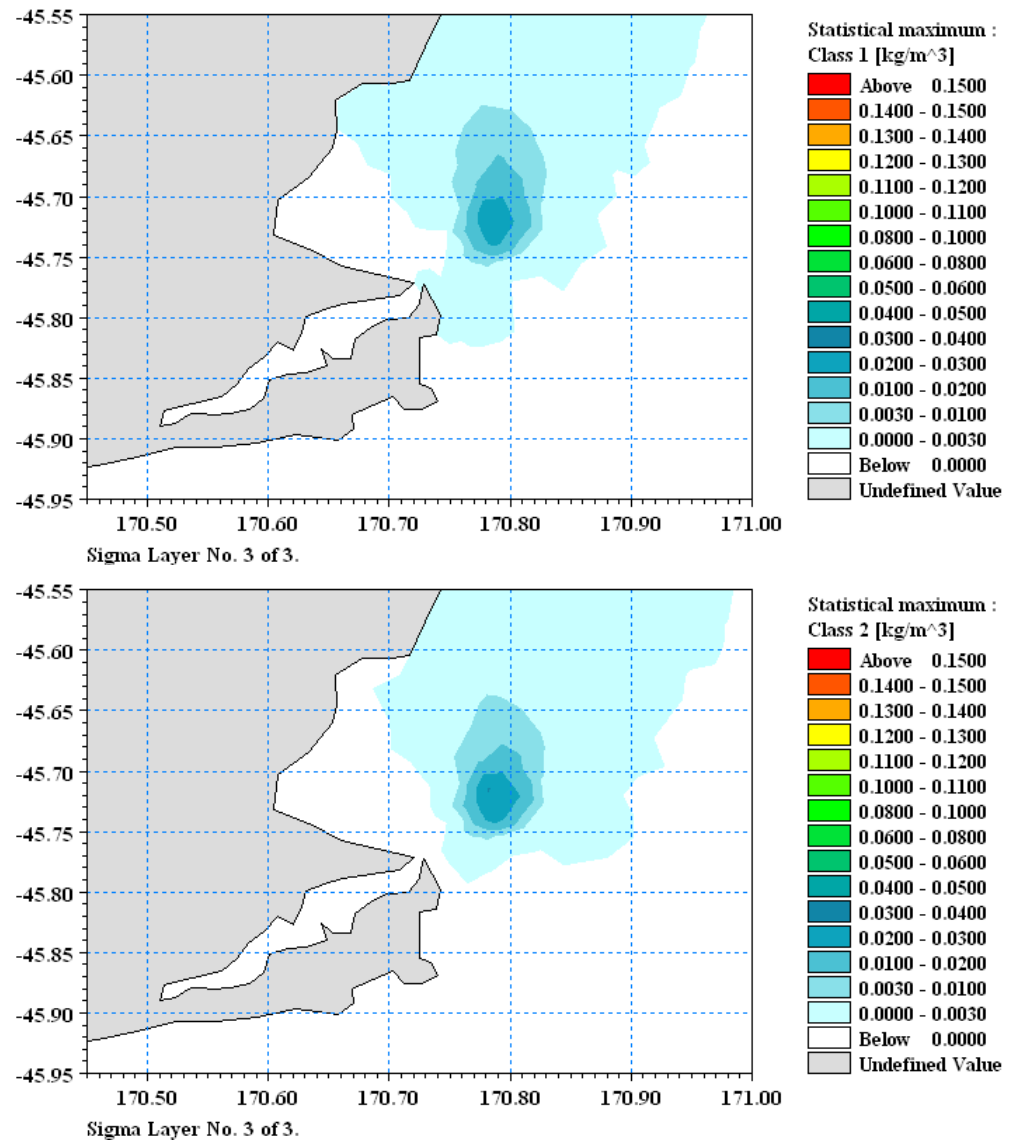


Figure 11.11c: Max. SSC composite envelopes for size class 1 (top) and size class 2 (bottom) in the surface layer (L3) over 24 disposal cycles for wind scenario 1 (light WSW wind) at disposal sub-site #1.

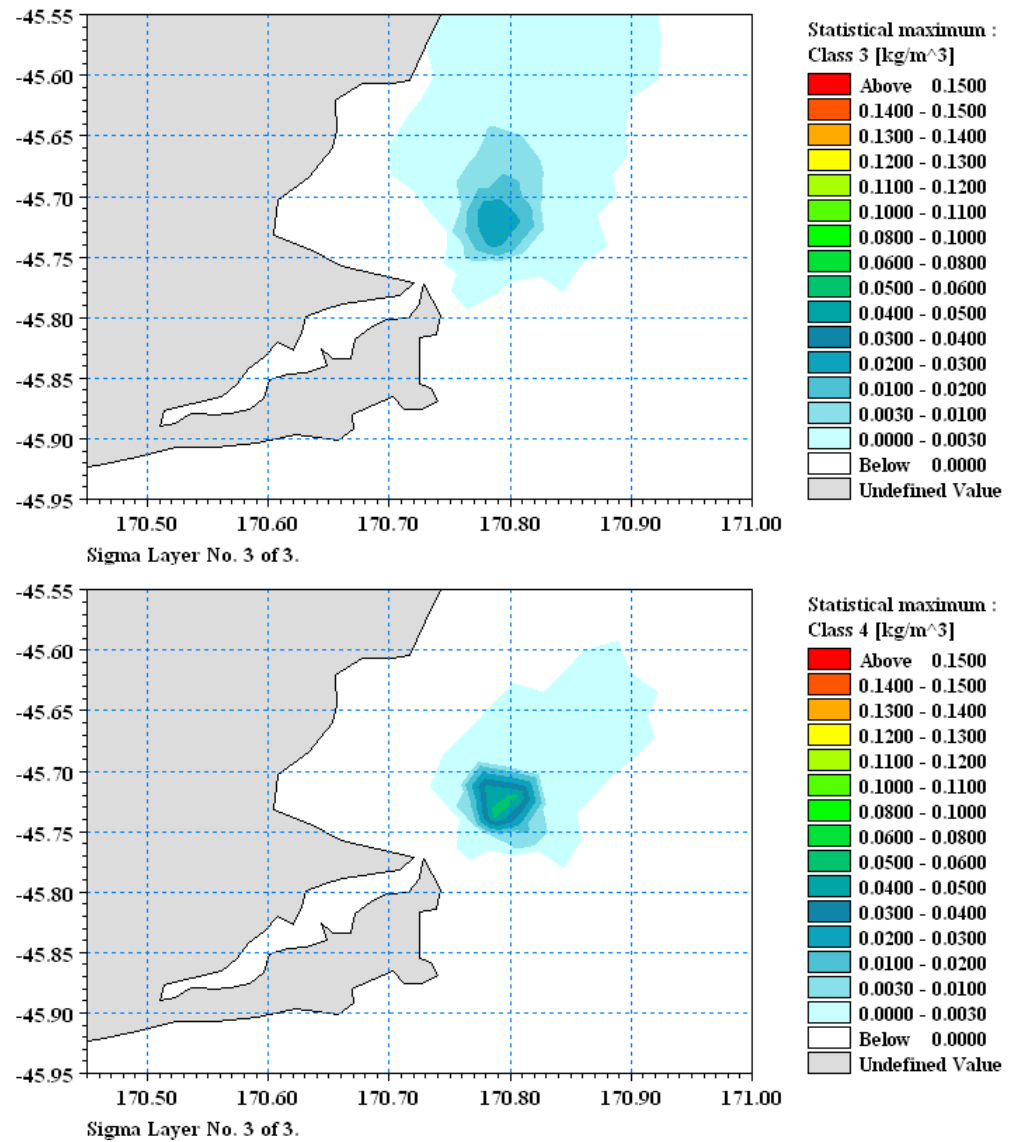


Figure 11.11d: Max. SSC composite envelopes for size class 3 (top) and size class 4 (bottom) in the surface layer (L3) over 24 disposal cycles for wind scenario 1 (light WSW wind) at disposal sub-site #1.

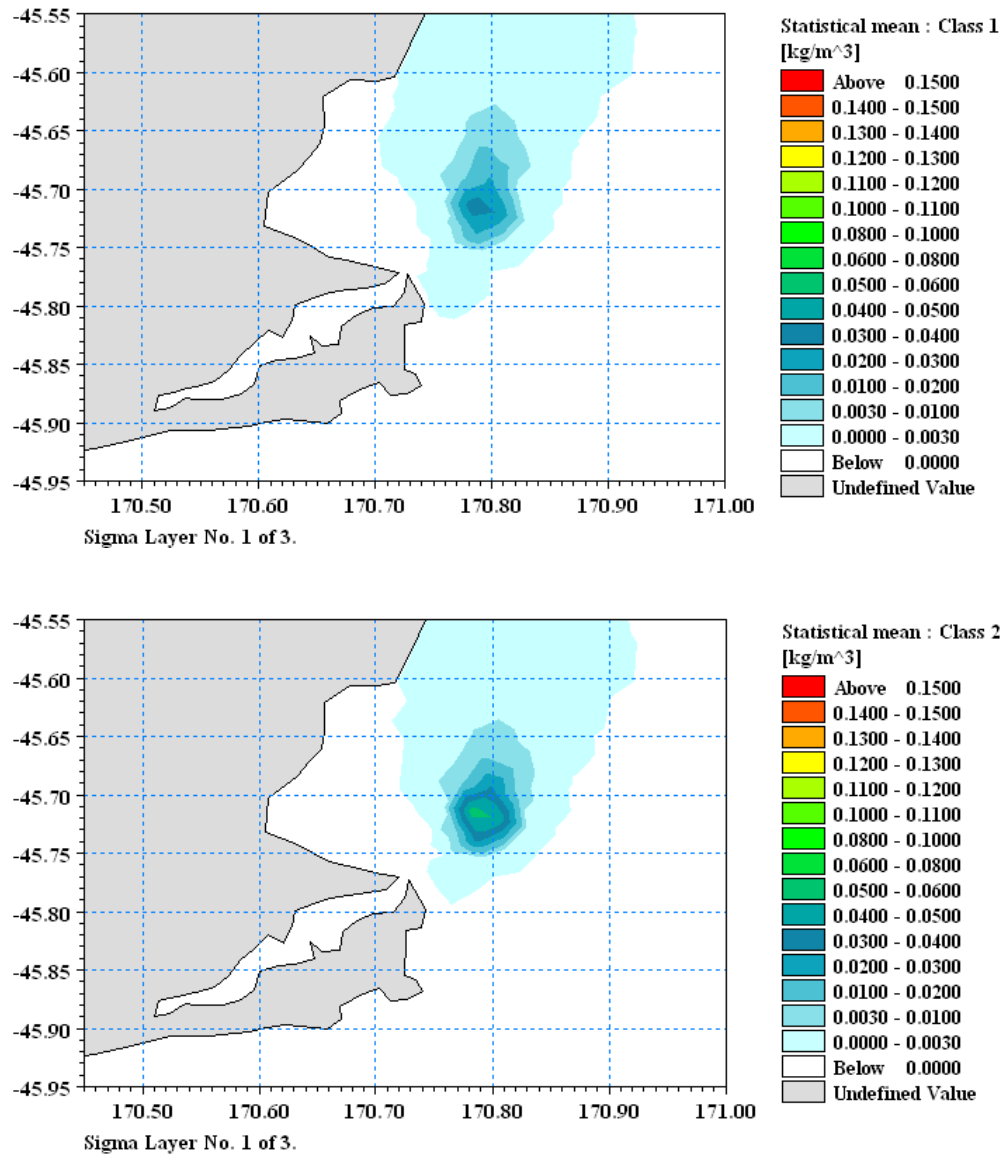


Figure 11.12a: Mean SSC composite envelopes for size class 1 (top) and size class 2 (bottom) in the bottom layer (L1) over 24 disposal cycles for wind scenario 1 (light WSW wind) at disposal sub-site #1.

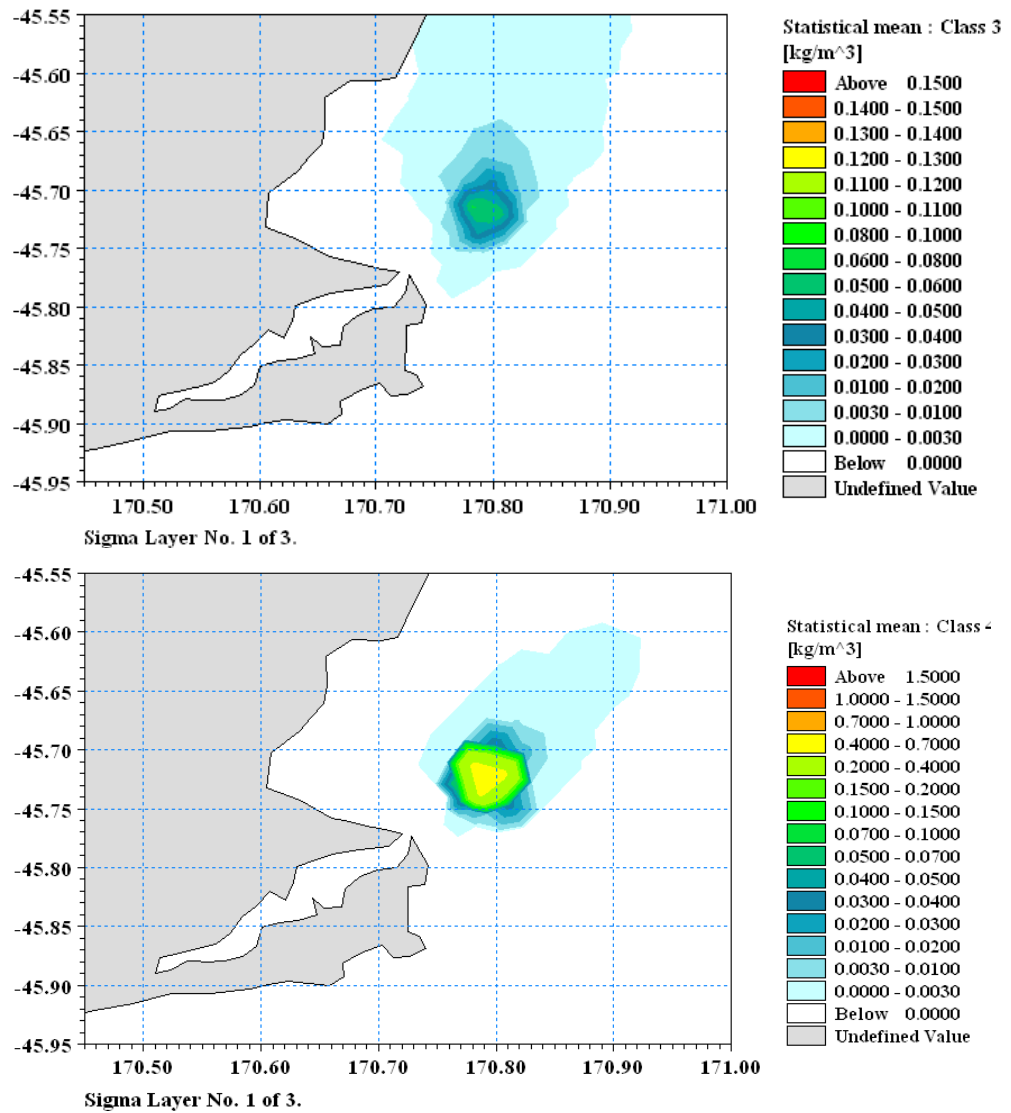


Figure 11.12b: Mean SSC composite envelopes for size class 3 (top) and size class 4 (bottom) in the bottom layer (L1) over 24 disposal cycles for wind scenario 1 (light WSW wind) at disposal sub-site #1. *Note: scale change for class 4.*

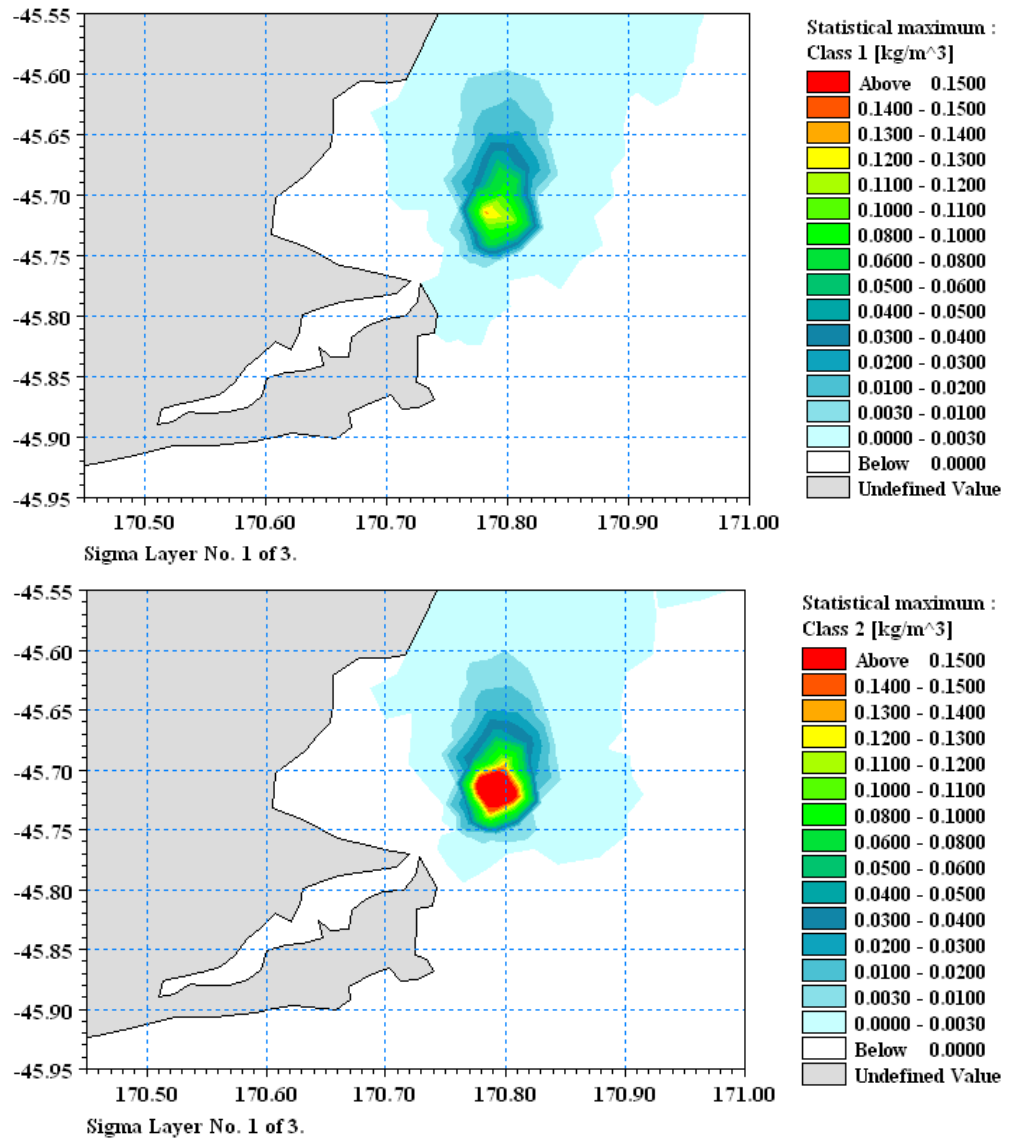


Figure 11.12c: Max. SSC composite envelopes for size class 1 (top) and size class 2 (bottom) in the bottom layer (L1) over 24 disposal cycles for wind scenario 1 (light WSW wind) at disposal sub-site #1. Note: maximum SSC for size class 2 in this simulation was 0.20 kg/m³ or 200 mg/L.

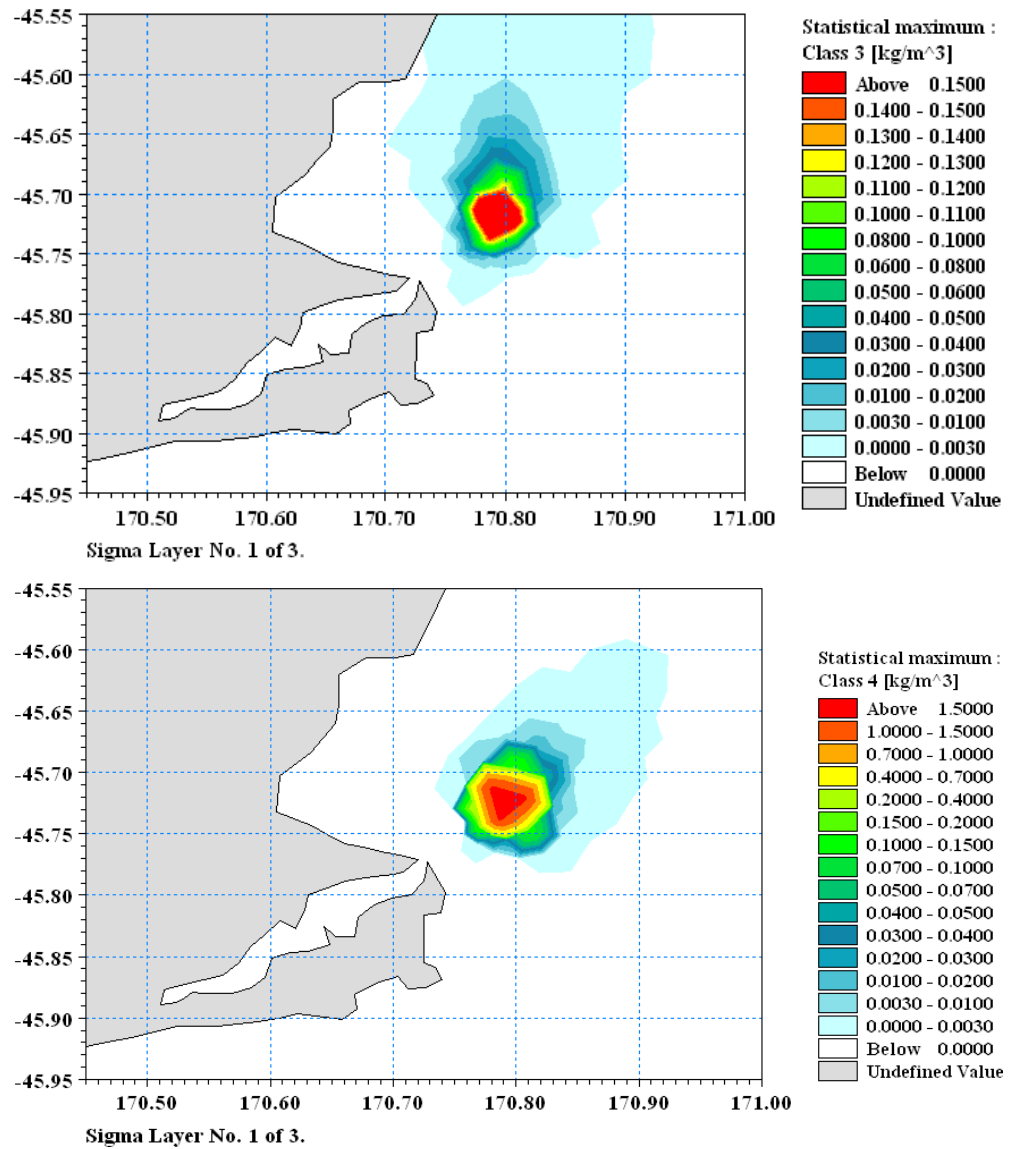


Figure 11.12d: Max. SSC composite envelopes for size class 3 (top) and size class 4 (bottom) in the bottom layer (L1) over 24 disposal cycles for wind scenario 1 (light WSW wind) at disposal sub-site #1. Note: maximum SSC for size class 3 in this simulation was 0.21 kg/m³ or 210 mg/L and for size class 4 peaks at 1.60 kg/m³ or 1600 mg/L. *Note: scale change for class 4.*

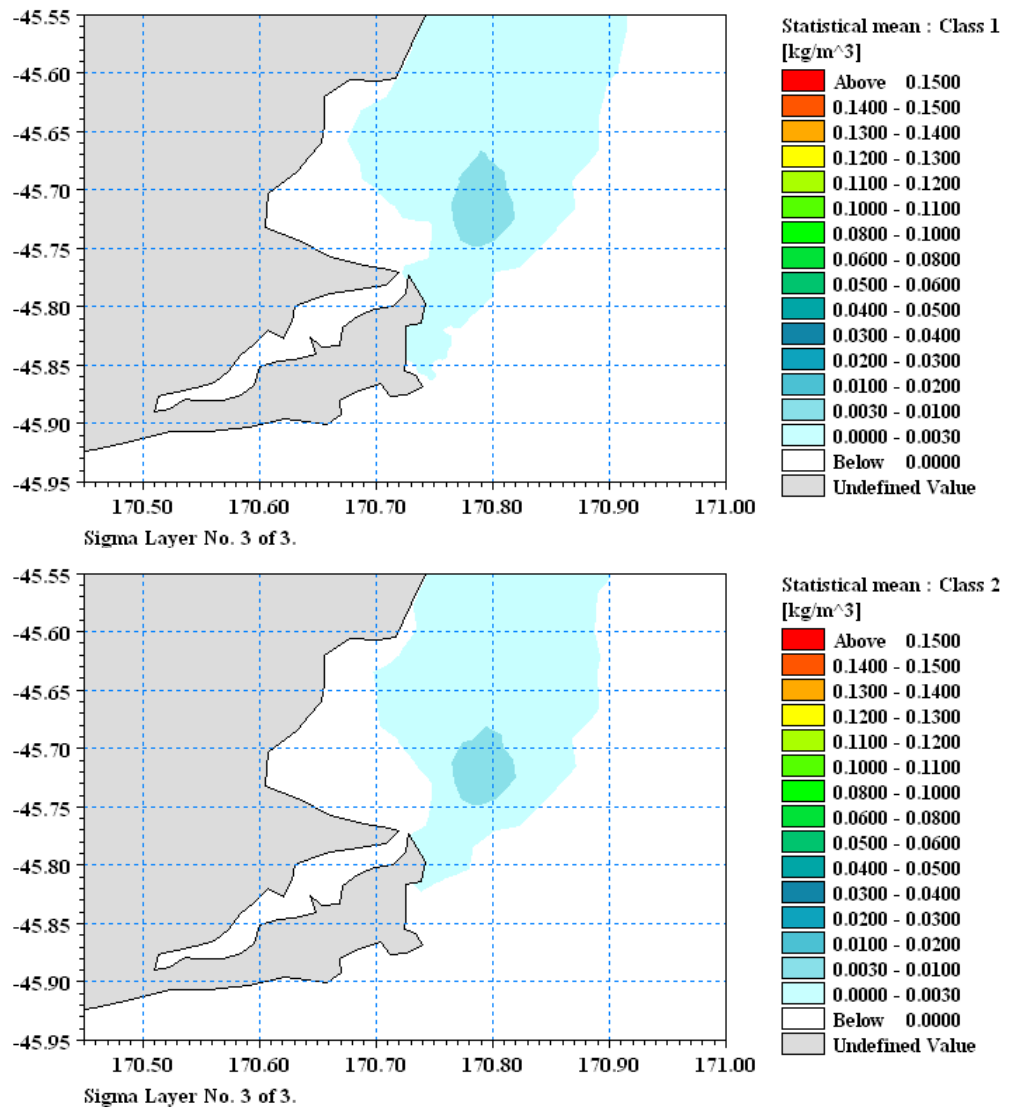


Figure 11.13a: Mean SSC composite envelopes for size class 1 (top) and size class 2 (bottom) in the surface layer (L3) over 24 disposal cycles for wind scenario 4 (light NNE wind) at disposal sub-site #1.

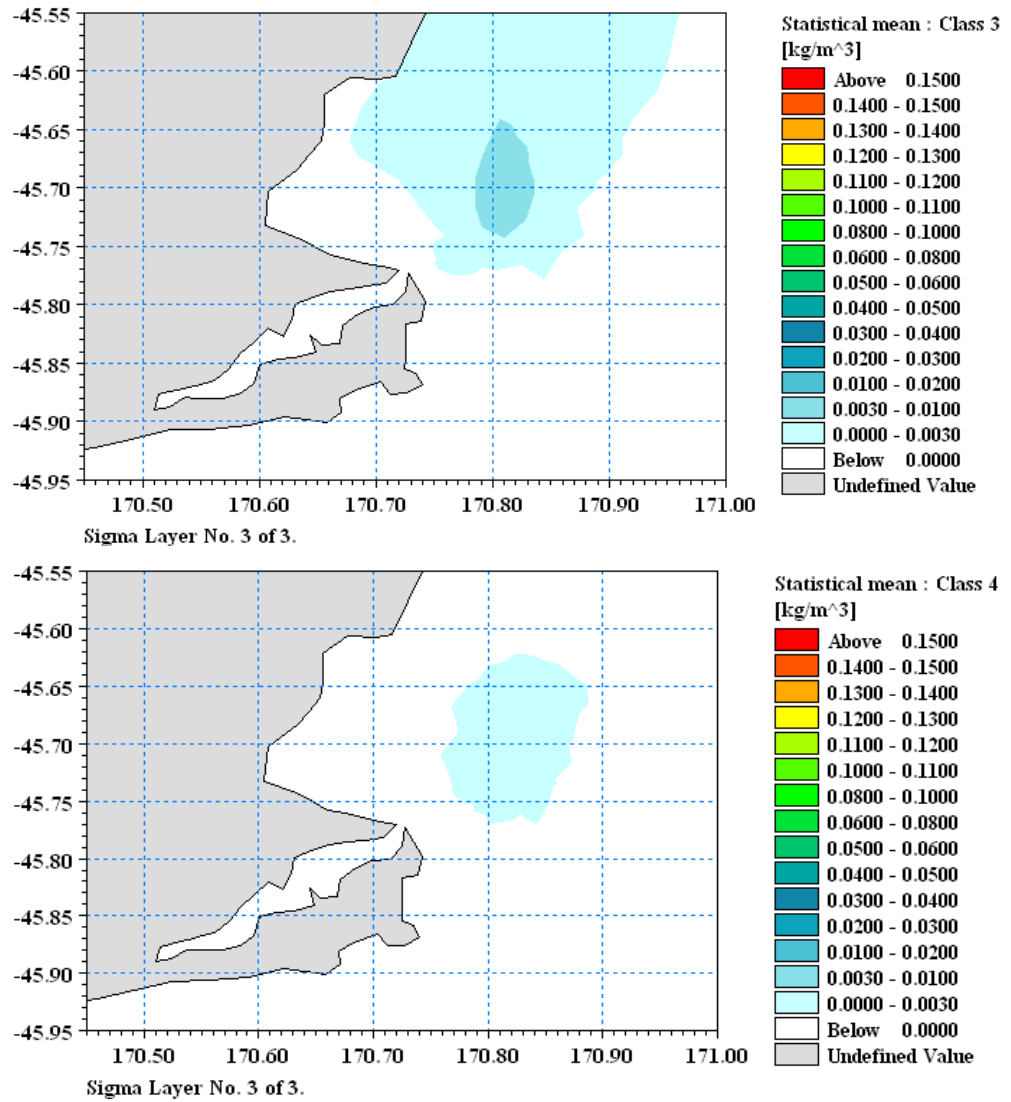


Figure 11.13b: Mean SSC composite envelopes for size class 3 (top) and size class 4 (bottom) in the surface layer (L3) over 24 disposal cycles for wind scenario 4 (light NNE wind) at disposal sub-site #1.

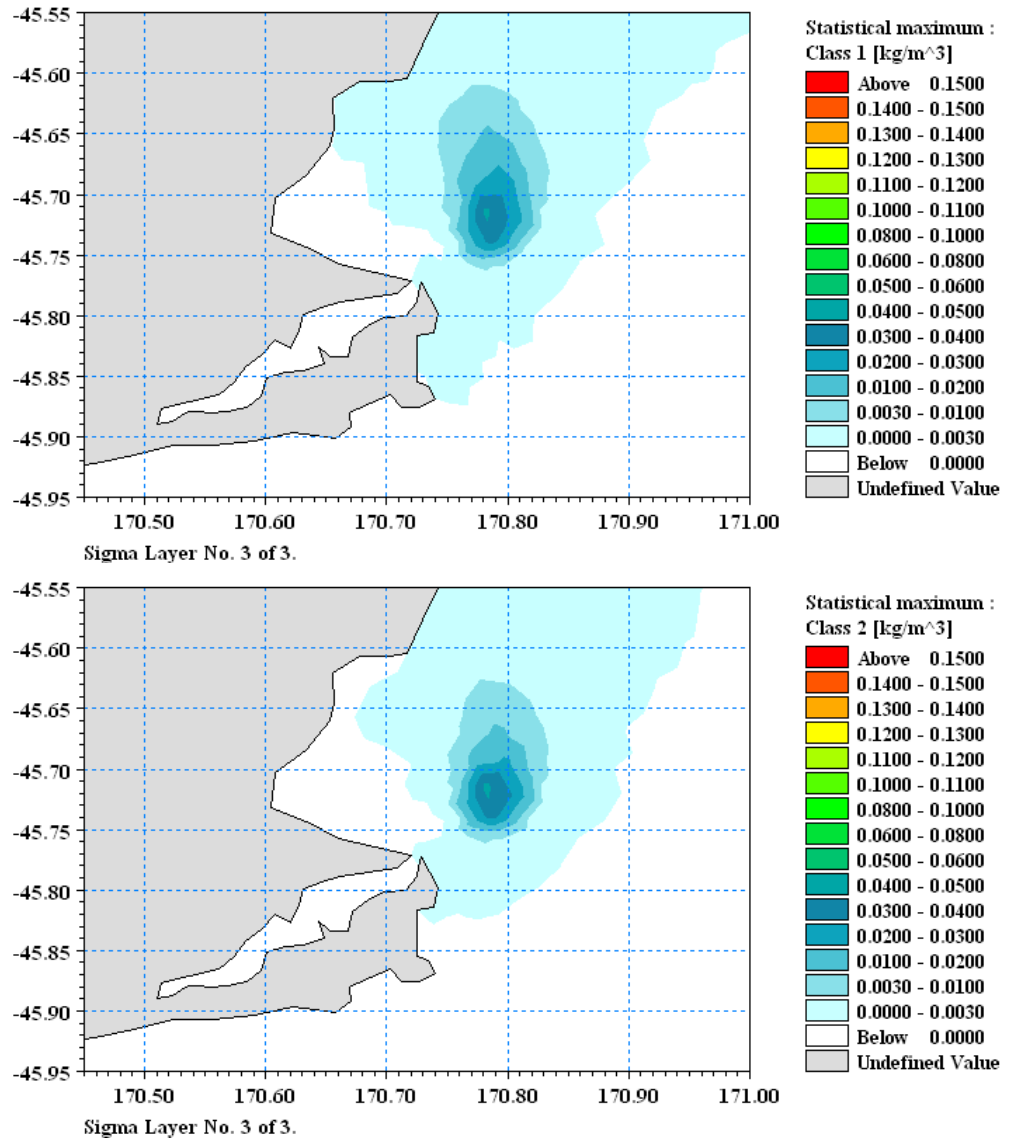


Figure 11.13c: Max. SSC composite envelopes for size class 1 (top) and size class 2 (bottom) in the surface layer (L3) over 24 disposal cycles for wind scenario 4 (light NNE wind) at disposal sub-site #1.

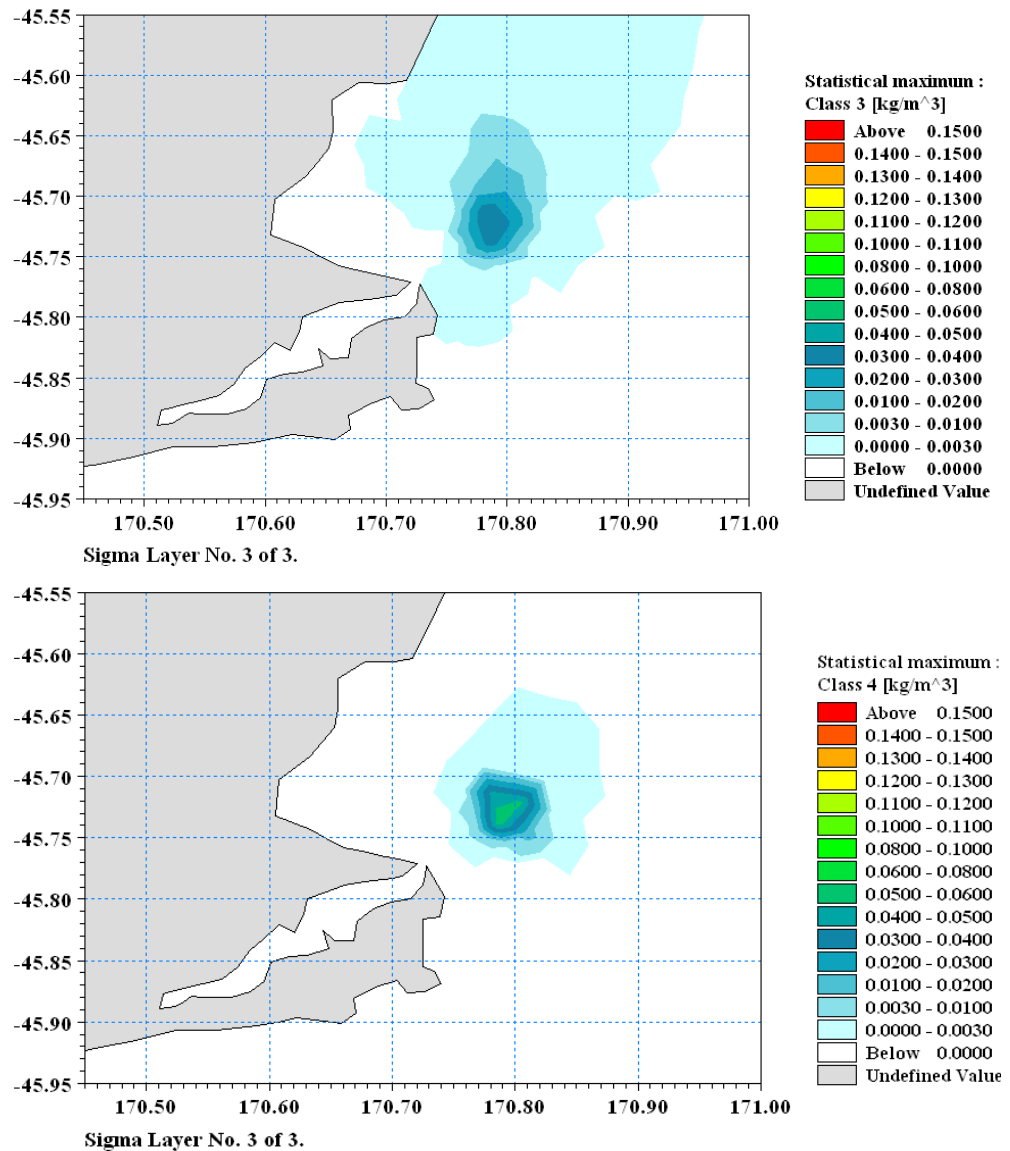


Figure 11.13d: Max. SSC composite envelopes for size class 3 (top) and size class 4 (bottom) in the surface layer (L3) over 24 disposal cycles for wind scenario 4 (light NNE wind) at disposal sub-site #1.

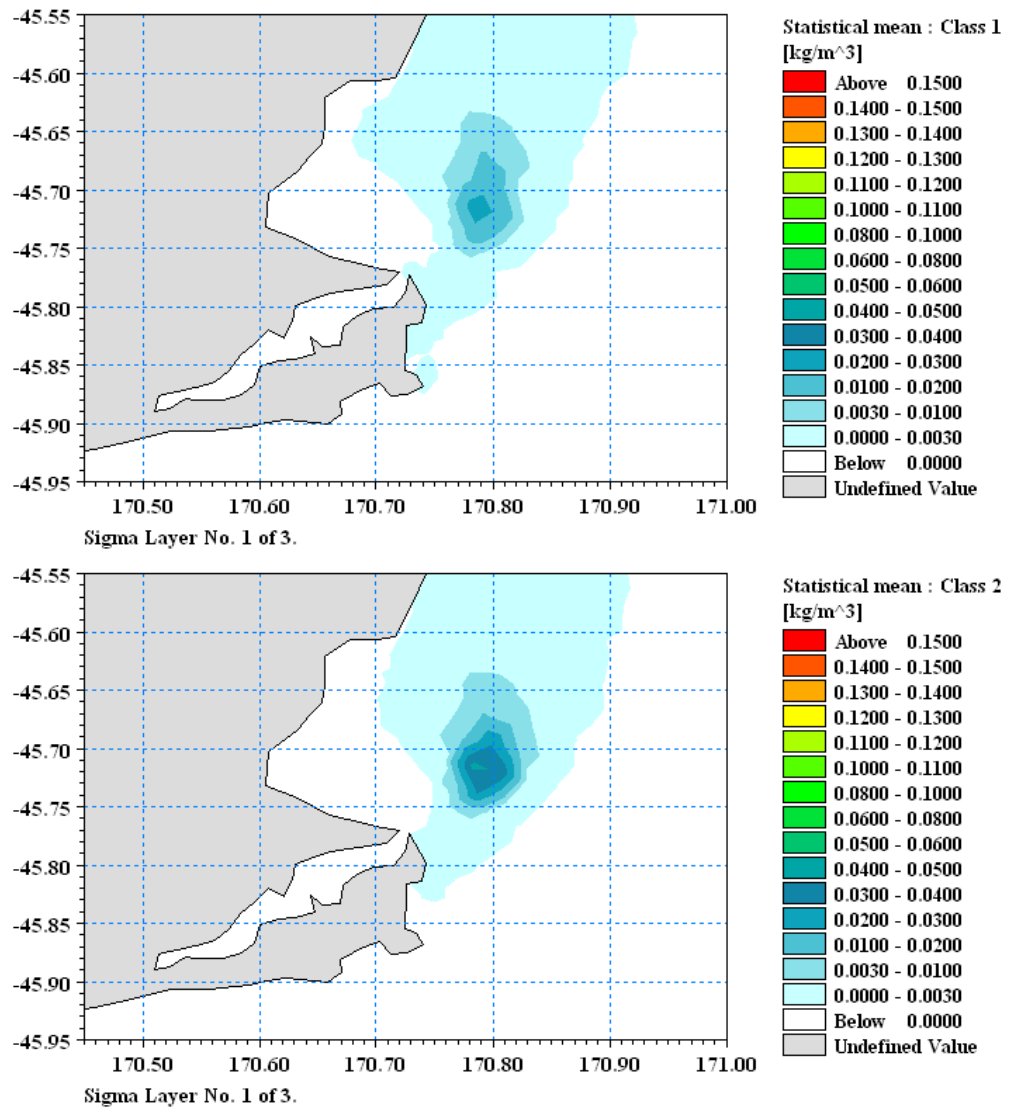


Figure 11.14a: Mean SSC composite envelopes for size class 1 (top) and size class 2 (bottom) in the bottom layer (L1) over 24 disposal cycles for wind scenario 4 (light NNE wind) at disposal sub-site #1.

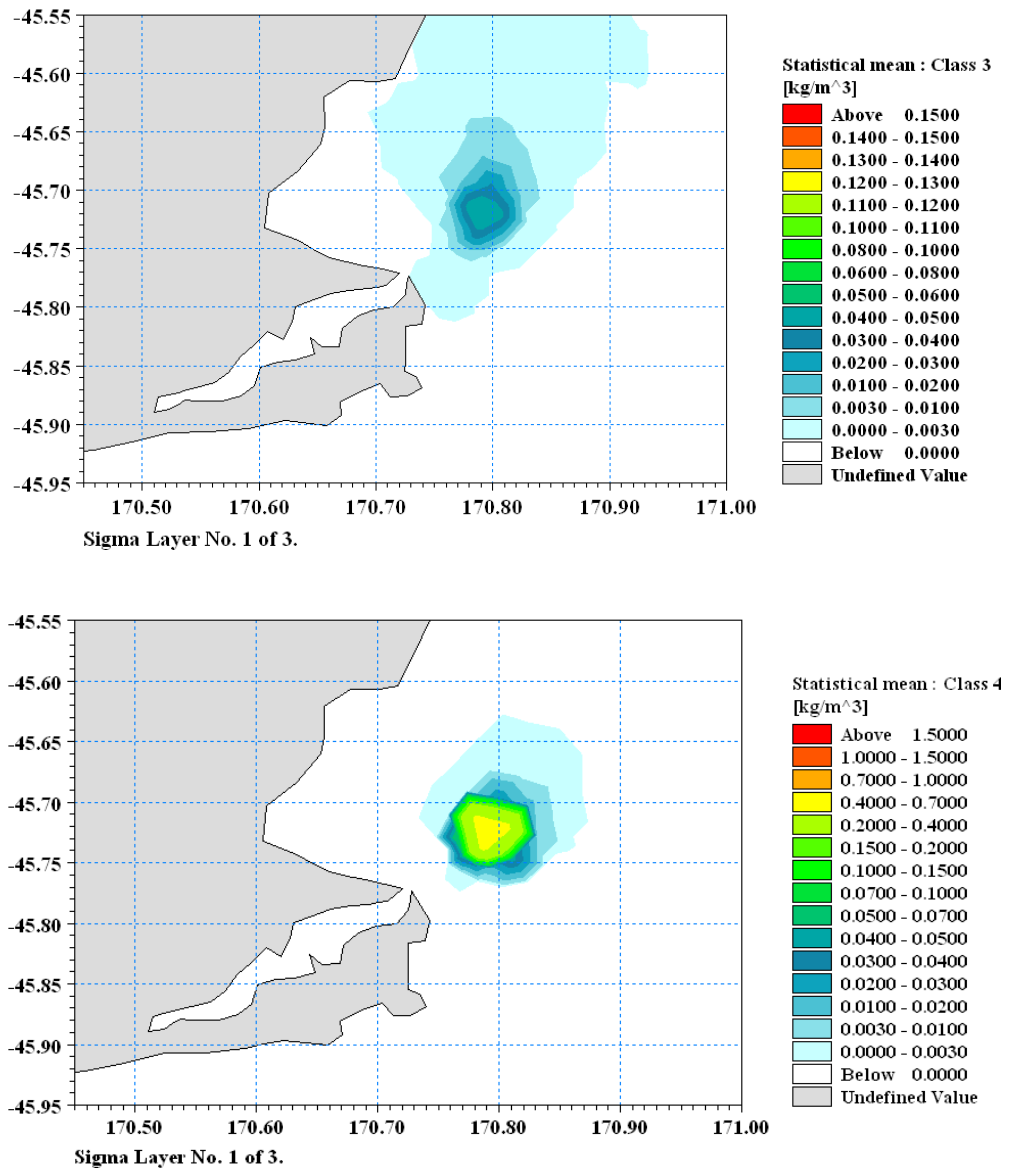


Figure 11.14b: Mean SSC composite envelopes for size class 3 (top) and size class 4 (bottom) in the bottom layer (L1) over 24 disposal cycles for wind scenario 4 (light NNE wind) at disposal sub-site #1. *Note: scale change for class 4.*

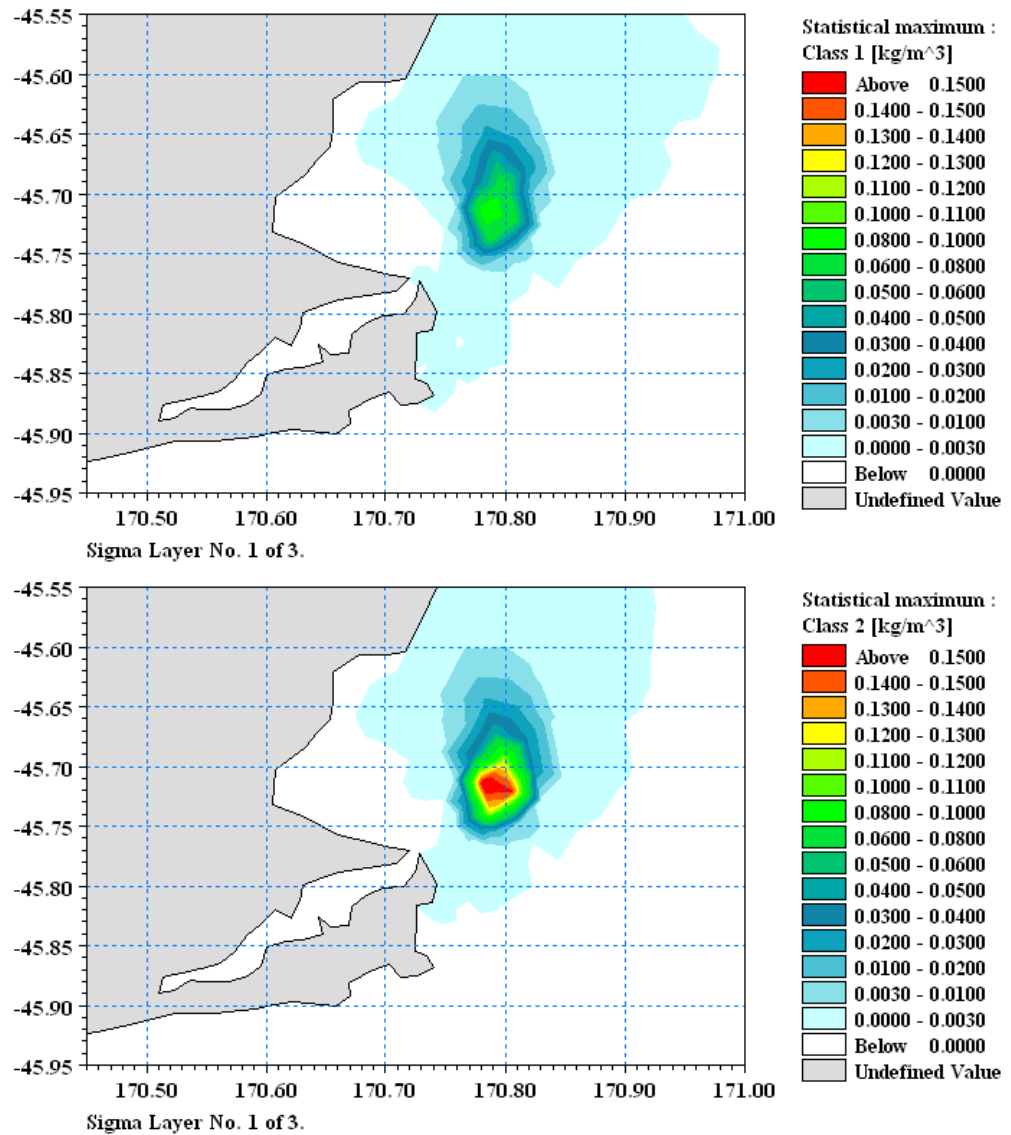


Figure 11.14c: Max. SSC composite envelopes for size class 1 (top) and size class 2 (bottom) in the bottom layer (L1) over 24 disposal cycles for wind scenario 4 (light NNE wind) at disposal sub-site #1. Note: maximum SSC for size class 2 in this simulation was 0.16 kg/m³ or 160 mg/L.

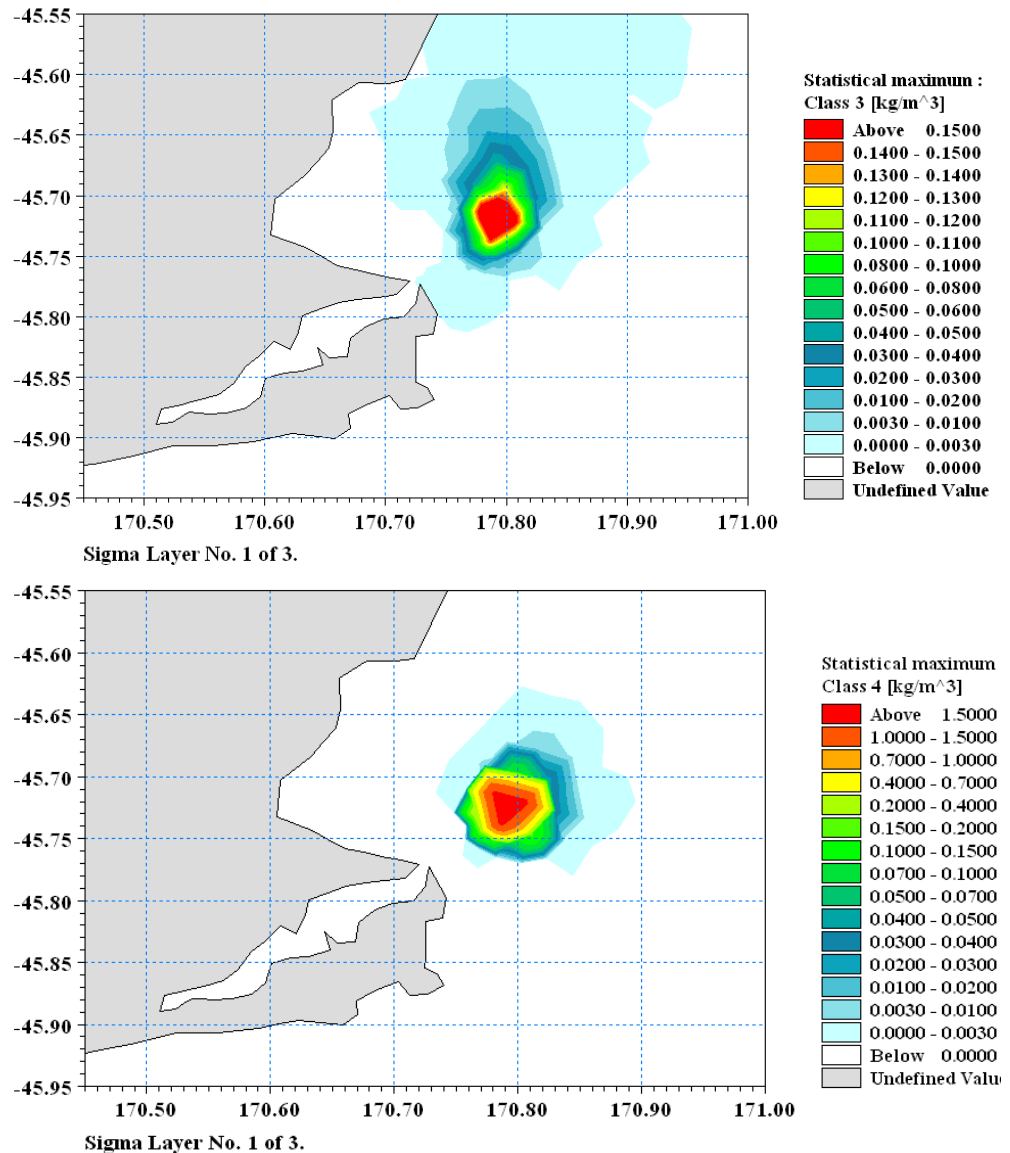


Figure 11.14d: Max. SSC composite envelopes for size class 3 (top) and size class 4 (bottom) in the bottom layer (L1) over 24 disposal cycles for wind scenario 4 (light NNE wind) at disposal sub-site #1. Note: maximum SSC for size class 3 in this simulation was 0.18 kg/m³ or 180 mg/L and for size class 4 peaks at 1.60 kg/m³ or 1600 mg/L. *Note: scale change for class 4.*

Summary of results: the above sequence of SSC composites for the full range of sediment size classes in the surface and bottom layers shows that:

- maximum surface-layer concentrations in the top 30% of the water column would be considerably smaller than for the bottom layer, due to the hopper discharge being several metre's below the surface (5 m in this case), and the physical settling of sediments towards the seabed. The highest maximum

surface-layer concentrations reached in the vicinity of the disposal site during 48-hour simulations were in the range 30–60 mg/L for each of the size classes and across all six wind scenarios, with the higher values occurring during light NNE winds (Fig. 11.13c, d) and combining all size classes, the maximum total surface-layer SSC would be around 185 mg/L;

- occasionally the diluted edge of the plume could reach the coastal zone along the Otago Heads, which would elevate background surface SSC by up to only 0.7–1.5 mg/L, for fine and medium silts (for a total SSC of 2.2 mg/L) under light NNE winds. This situation could also be accompanied by the plume edge reaching the area off The Mole in the Harbour Entrance, but would only generate a maximum total surface SSC of around 0.08 mg/L (Fig. 11.13c). In the bottom layer, maximum total SSC would be somewhat higher at around 0.1 mg/L (off The Mole) and 2.8 mg/L (off Otago Heads and northern Wickliffe Bay) for the light NNE wind conditions (Fig. 11.14c, d);
- the diluted edge of the plume could reach areas of the coast north of Karitane but would elevate the total surface SSC by only about 0.02 mg/L in the Karitane area, and up to 0.9 mg/L further north towards Stony Creek and Shag Rock under light NNE winds (Fig. 11.13c, d). In the bottom layer, maximum total SSC would be marginally higher at around 1 mg/L further north towards Stony Creek and Shag Rock under light NNE winds (Fig. 11.14c, d). Note: strong WSW winds would cause the highest total SSC in the near-bed layer north of Cornish Head as discussed in the previous section);
- in the bottom layer, the highest excess concentrations occur at the disposal ground where the fine sand (class 4) concentrations would reach around 1600–1700 mg/L for light wind conditions (Fig. 11.12d, 11.14d), and less for stronger wind events. Of the silt size classes, medium and coarse silts would contribute similar maximum excess concentrations in the bottom layer of up to 200–230 mg/L “downstream” in the vicinity of the disposal area (Fig. 11.6b-bottom plot and Fig. 11.12c, d), with the higher values occurring during a moderate WSW wind. For this moderate WSW wind scenario, the total maximum SSC in the bottom layer combining all size classes would be around 2100 mg/L in the vicinity of the disposal ground;
- for coastal areas likely to be reached occasionally by the dilute plume, excess surface SSC would be highest for light NNE winds, which are conducive to wider spreading (dispersion) of the plume and less vertical shear in the water column (which occurs in stronger winds). In terms of the bottom layer, light

NNE winds would cause the highest SSC off Otago Heads, but strong WSW winds would cause the highest SSC off the northern coast. In all coastal cases, the maximum SSC would remain quite small and occur periodically depending on the winds;

- in the vicinity of the disposal ground, the highest excess concentrations in the surface water would most likely occur on light NNE winds, with the highest concentrations in the bottom layer for sands also likely to occur during light winds (any direction), while for silts, it would be reached during moderate WSW winds.

11.4.3 Predicted plume concentrations for predominantly-silt hopper loads

Some of the plume simulations for light-wind conditions were also performed for a hopper of predominantly silt (e.g., sourced from the Hamilton Bay reach between Lower Harbour Beacons 18 and 20), in order to provide the ratio of the highest maximum SSC and extent of the plume compared with the average sand/silt hopper discharge. The sediment discharge rates for this hopper discharge scenario are listed in Table 11.1 and should be noted that the total volume of sediment per hopper would be substantially lower at 65% of the volume for the average sand/silt hopper load used in the simulations reported above. This is because of the need to restrict overflows when dredging predominantly silt material and the silt doesn't readily settle in the hopper during the dredging.

Figures 11.15a–d show the maximum excess SSC composites during 48-hour periods for the four size classes in the bottom surface layer for wind scenario 1 (light WSW). The top plots show the result from the predominantly-silt hopper load, and the bottom plot is the equivalent result for the average sand/silt hopper load. Results are only for the most landward sub-site #1 within the A0 disposal area. A similar series for the same sub-site is shown in Figures 11.16a–c for wind scenario 4 (light NNE), excluding the sand-size class which is inconsequential.

Plume simulations were also performed for a moderate WSW wind (scenario 2) to ascertain the likely increase in maximum concentrations in the vicinity of the disposal area for predominantly-silt hopper loads. Moderate WSW winds lead to the highest suspended-sediment concentrations in and around the disposal site (see previous Section).

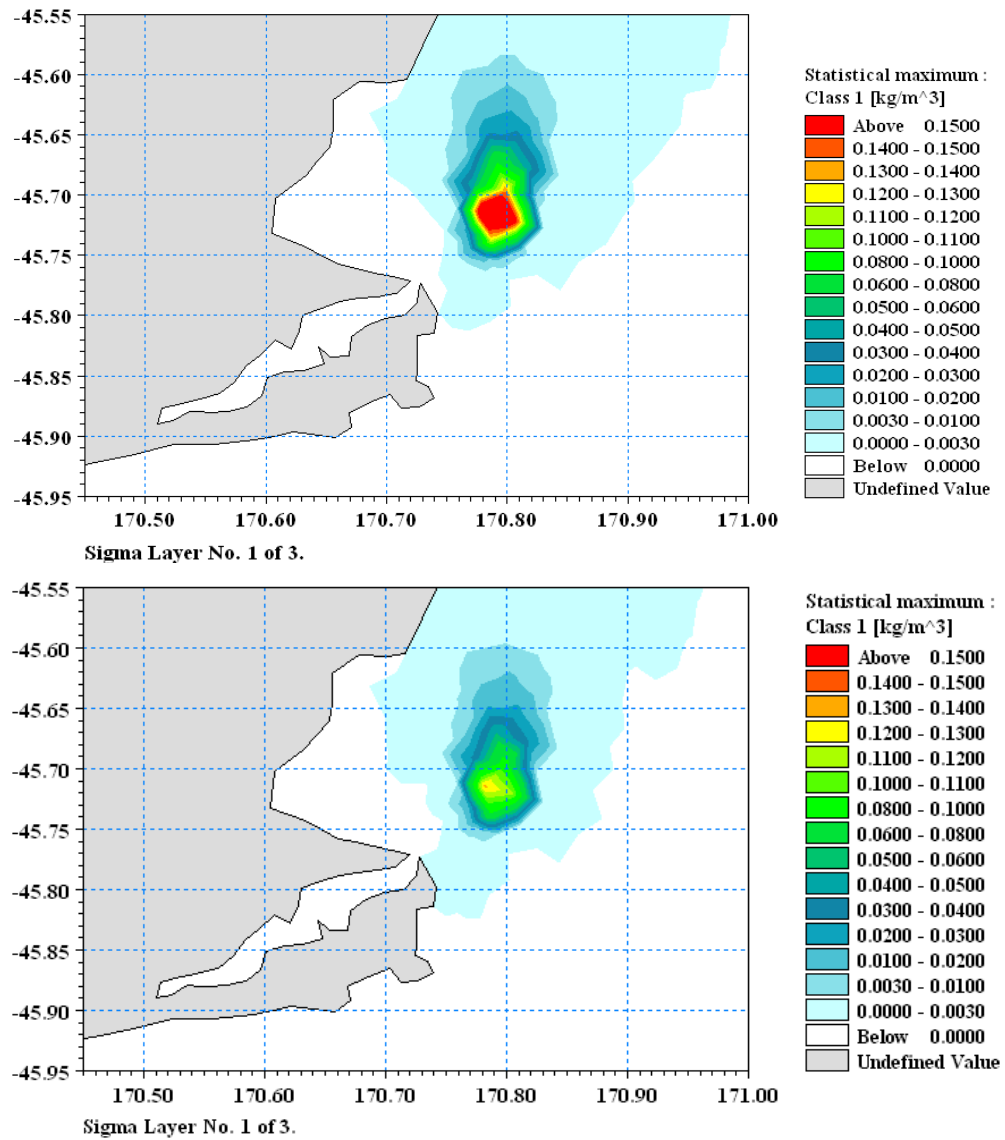


Figure 11.15a: Max. SSC composite envelopes for predominantly-silt hopper load (top) and the average sand/silt hopper load (bottom) for size class 1 in the bottom layer (L1) over 24 disposal cycles for wind scenario 1 (light WSW wind) at disposal sub-site #1. Note: maximum SSC for the top and bottom plots respectively was 160 mg/L and 122 mg/L.

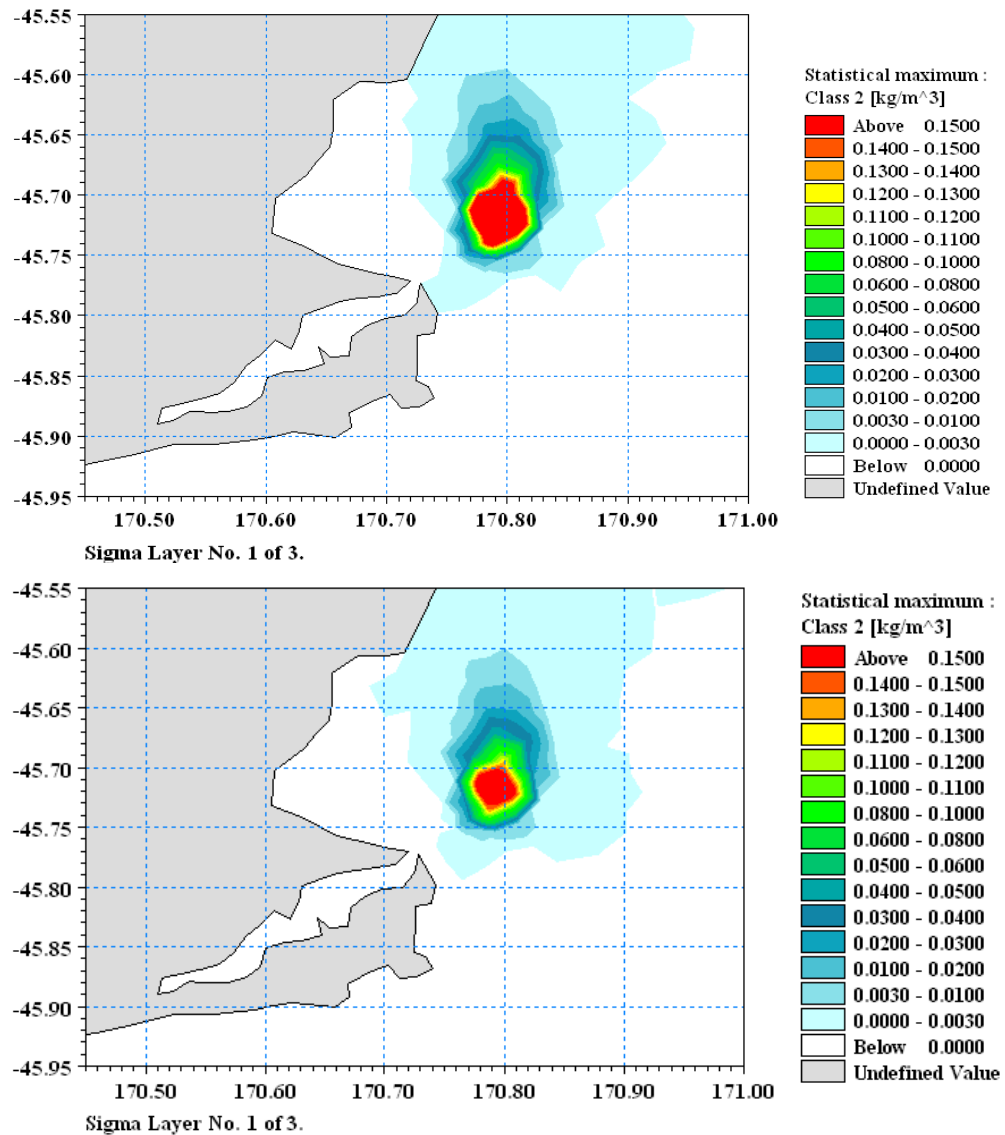


Figure 11.15b: Max. SSC composite envelopes for predominantly-silt hopper load (top) and the average sand/silt hopper load (bottom) for size class 2 in the bottom layer (L1) over 24 disposal cycles for wind scenario 1 (light WSW wind) at disposal sub-site #1. Note: maximum SSC for the top and bottom plots respectively was 280 mg/L and 200 mg/L.

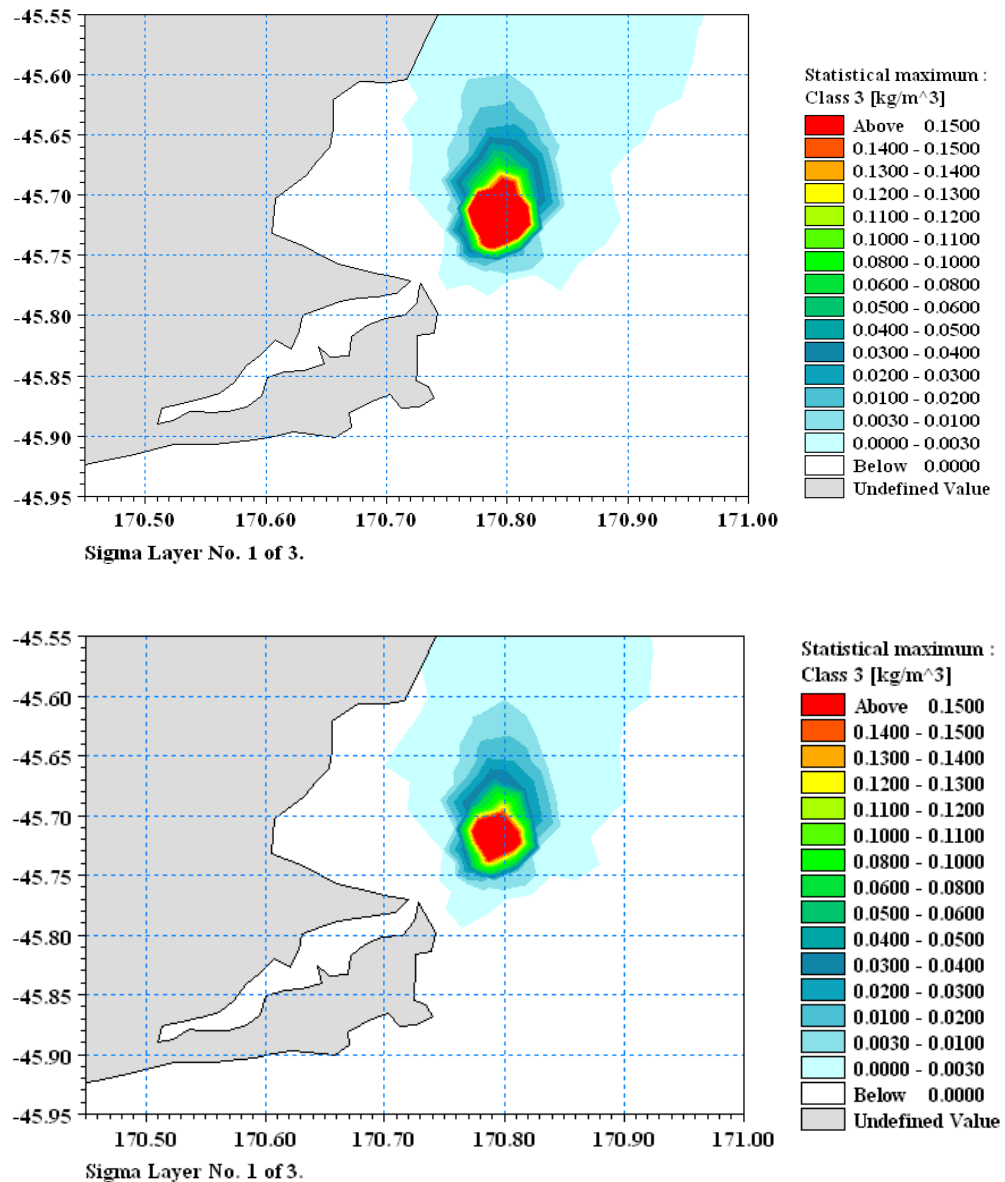


Figure 11.15c: Max. SSC composite envelopes for predominantly-silt hopper load (top) and the average sand/silt hopper load (bottom) for size class 3 in the bottom layer (L1) over 24 disposal cycles for wind scenario 1 (light WSW wind) at disposal sub-site #1. Note: maximum SSC for the top and bottom plots respectively was 320 mg/L and 210 mg/L.

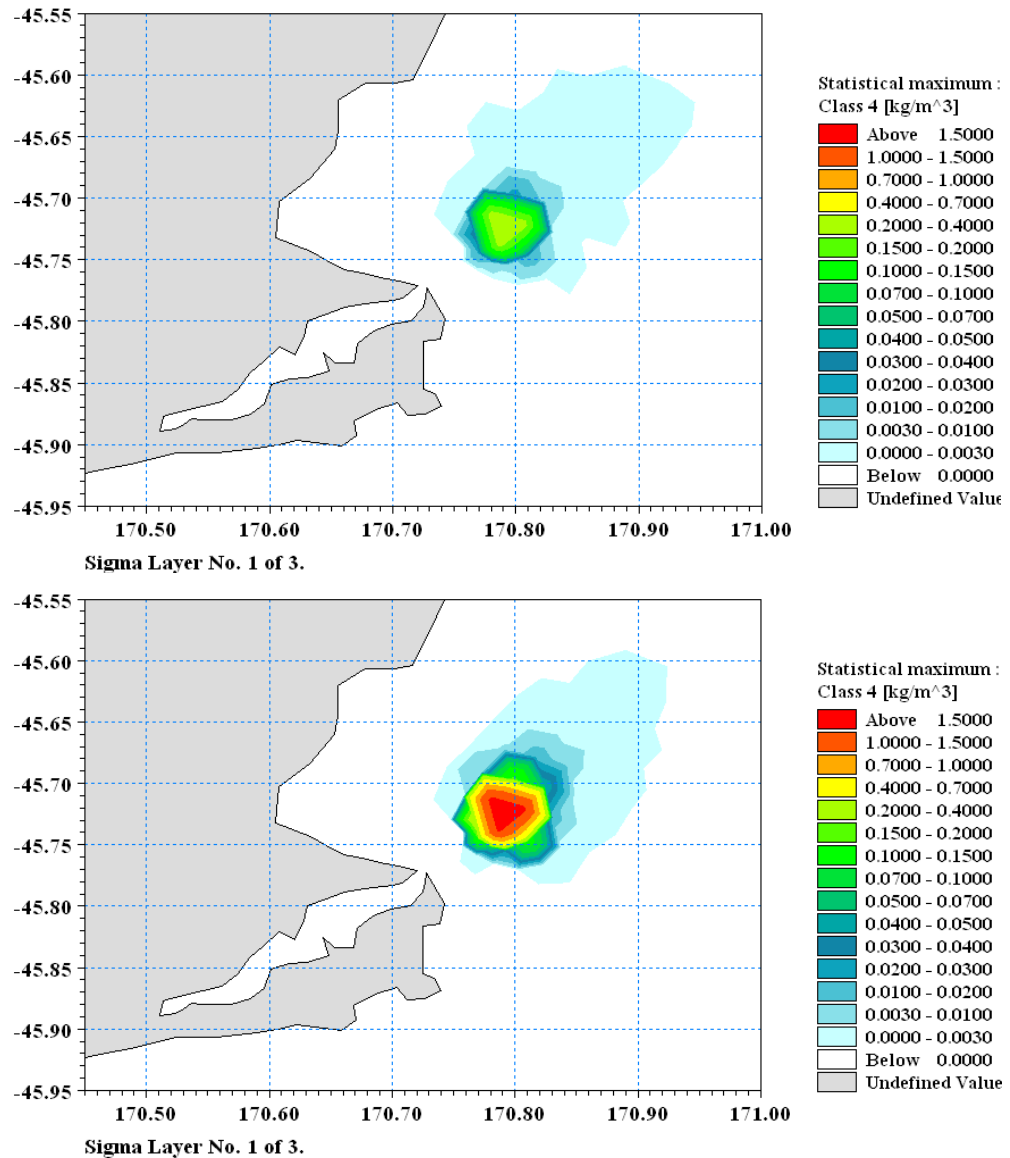


Figure 11.15d: Max. SSC composite envelopes for predominantly-silt hopper load (top) and the average sand/silt hopper load (bottom) for size class 4 in the bottom layer (L1) over 24 disposal cycles for wind scenario 1 (light WSW wind) at disposal sub-site #1. Note: maximum SSC for the top and bottom plots respectively was 235 mg/L and 1600 mg/L.

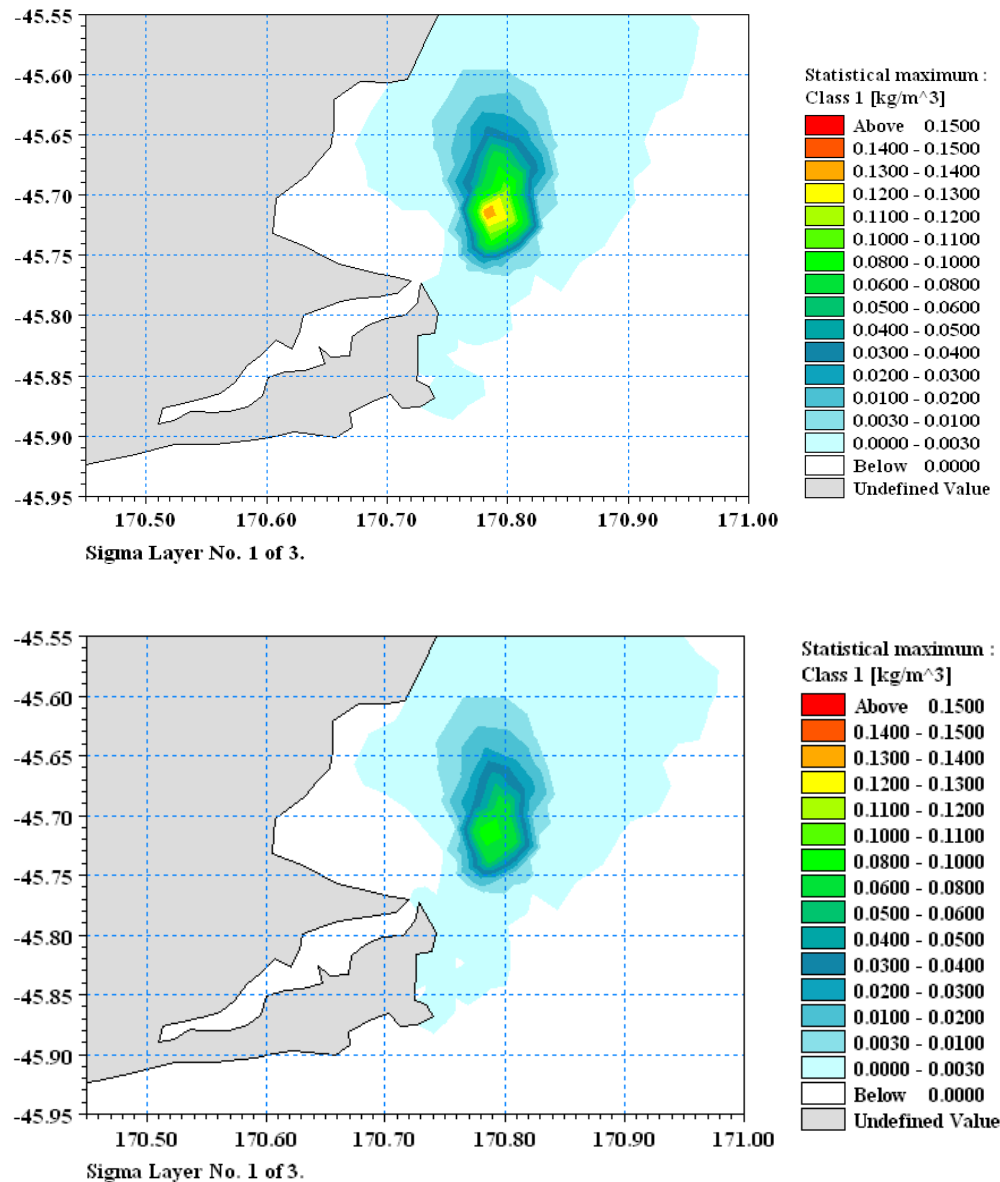


Figure 11.16a: Max. SSC composite envelopes for predominantly-silt hopper load (top) and the average sand/silt hopper load (bottom) for size class 1 in the bottom layer (L1) over 24 disposal cycles for wind scenario 4 (light NNE wind) at disposal sub-site #1. Note: maximum SSC for the top and bottom plots respectively was 135 mg/L and 92 mg/L.

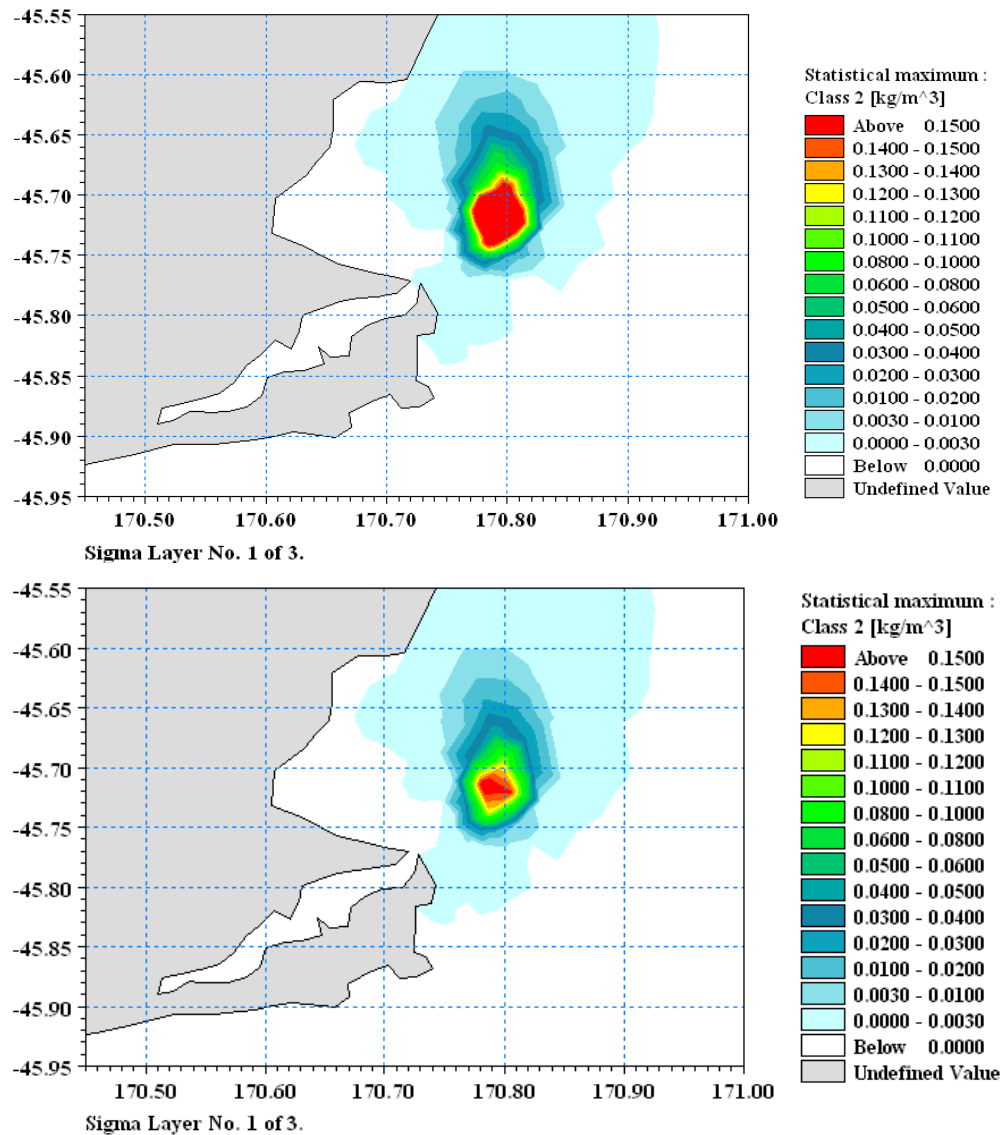


Figure 11.16b: Max. SSC composite envelopes for predominantly-silt hopper load (top) and the average sand/silt hopper load (bottom) for size class 2 in the bottom layer (L1) over 24 disposal cycles for wind scenario 4 (light NNE wind) at disposal sub-site #1. Note: maximum SSC for the top and bottom plots respectively was 230 mg/L and 160 mg/L.

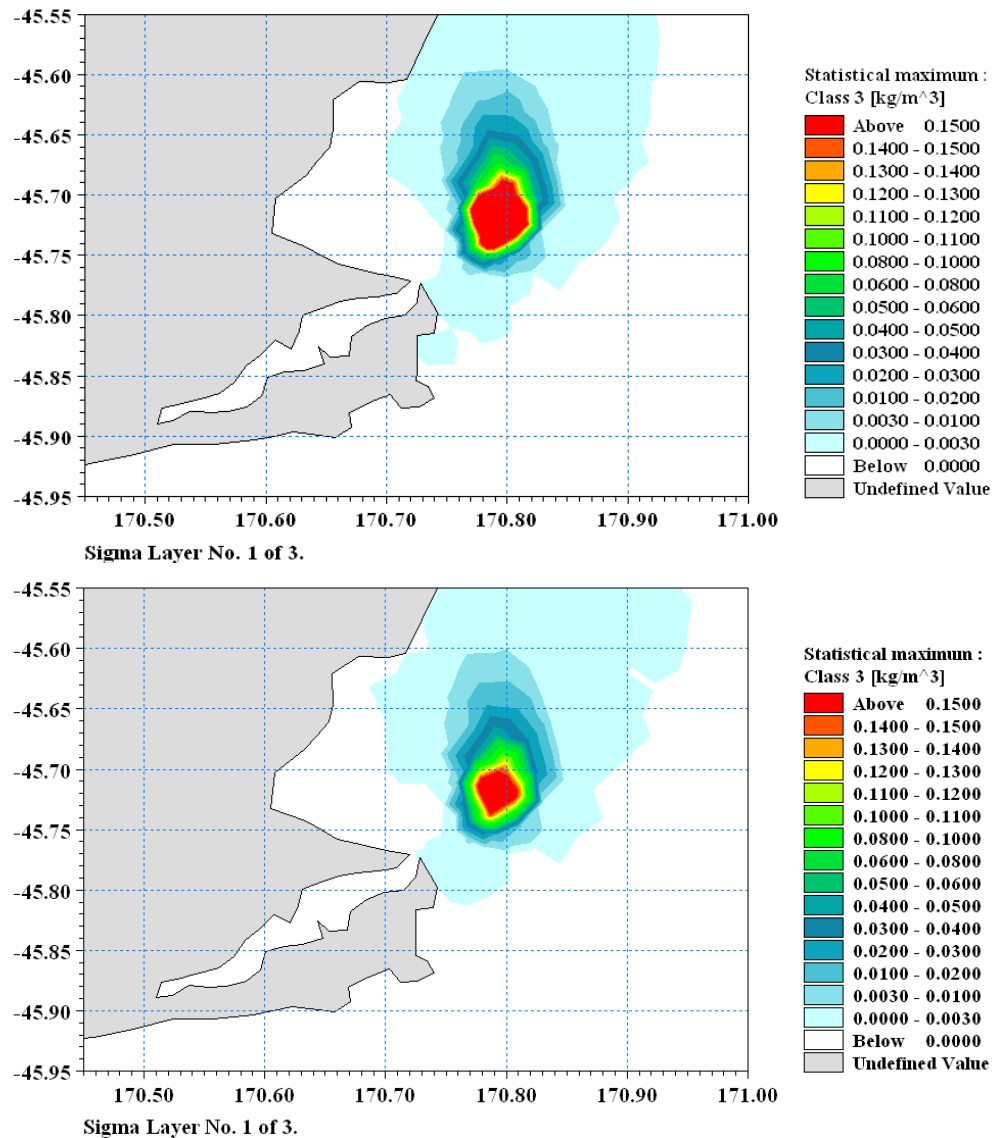


Figure 11.16c: Max. SSC composite envelopes for predominantly-silt hopper load (top) and the average sand/silt hopper load (bottom) for size class 3 in the bottom layer (L1) over 24 disposal cycles for wind scenario 4 (light NNE wind) at disposal sub-site #1. Note: maximum SSC for the top and bottom plots respectively was 270 mg/L and 180 mg/L.

Summary of results: the above comparison of maximum SSC composites between a predominantly-silt hopper load and the overall average sand/silt hopper load for the silt-size classes in the bottom layer shows that:

- maximum bottom-layer concentrations in the vicinity of the disposal ground are considerably higher for the predominantly-silt hopper discharge compared with the average sand/silt hopper loads reported on in the previous sections. For class 1 (fine silts), the increase would be 130% and 145% for light WSW

and light NNE winds respectively, with equivalent increases of 140% and 150% for class 2 sediment size (medium silts) and 150% higher in both cases for class 3 sediment size (coarse silts). However, with respect to light winds, the highest excess concentrations in and around the disposal area would still occur under WSW winds (Fig. 11.15) even though the percentage increase is higher for finer silts under NNE light winds when comparing a predominantly-silt hopper load versus an average silt/sand load;

- overall in the vicinity of the disposal area, the highest maximum excess concentration of any of the silt classes would be reached in moderate WSW winds by the coarse-silt fraction, reaching 350 mg/L compared to 230 mg/L based on an average sand/silt hopper load (an increase of 150%);
- combining all the “silt” size classes, the maximum silt-derived SSC in the bottom layer in the vicinity of the disposal ground, for the worst wind scenario (a moderate WSW wind), would increase from around 620 mg/L for an average sand/silt hopper load to around 910 mg/L for a smaller, but predominantly-silt hopper load—an increase of around 145%;
- combining all size classes, the total maximum SSC in the bottom layer in the vicinity of the disposal ground, for a moderate WSW wind, would actually decrease from around 2100 mg/L for an average sand/silt hopper load to around 1150 mg/L for a smaller, but predominantly silt hopper load—because of the much smaller sand volume in the latter;
- for shoreline areas (e.g., Otago Heads and north of Cornish Head) when the edge of the plume makes contact, the maximum SSC for each silt size class in the bottom layer is not likely to be noticeably higher for the predominantly-silt hopper discharge for light WSW or NNE wind conditions, but the area over which the silts disperse at very low concentrations is slightly more widespread. Both these findings are indicative of the highly dispersive processes for suspended silt that operate on the Otago shelf, once they leave the disposal area.

11.4.4 Predicted upper-bound deposition patterns

As described in Section 11.3.2, the various spatial distributions of seabed deposition accumulated from each of the sets of 48-hour disposal windows were plotted for each size class as shown in Figures 11.17–11.20. Two plots are provided - one to cover the full range of accumulated deposition and the second to cover the lower-end of the

deposition range to focus more on far-field effects. These results were then combined across all four sediment sizes to derive the accumulated deposition (mm) on the seabed at the end of the dredging programme, as shown in Figure 11.21a, b. Finally, the accumulated deposition values were converted into a deposition rate (mm per day) in over the course of the dredging programme, as shown in Figure 11.22 (assuming 120 days continuous dredging (Section 7.3.3) for conservative estimates of deposition rates). These zones for various deposition rates are used by James et al. (2009) to assess the ecological effects. Note: the deposition rate would be lower for a longer dredging programme.

The key assumption on which these distributions were calculated is that sediment that has been deposited on the bed remains there for the duration of the dredging programme. Clearly this is a rather conservative assumption, especially for the finer sizes, which will be regularly mobilised by wave action and moved on in an ever increasing dispersive manner. Also a conservative assumption was made that the wet bulk density of settled sediments would be only 1300 kg/m³, thus erring on the higher side of deposition depths. Finally, losses of silts and sands that may overflow from the hopper into the Harbour waters during dredging were not deducted from the volumes discharged over the disposal ground. Consequently on all counts, the offshore deposition plots provide a conservative upper bound on deposition depths on which to assess environmental effects, bearing in mind the dispersive behaviour of fine sediments on an active, exposed shelf system.

The key results from the deposition distributions are:

- for the A0 disposal site option, the deposition is predominantly on the disposal ground and to the north of it (Fig. 11.21), arising from the persistent northerly residual current. Within the 2-km diameter disposal area, the maximum predicted deposition in any 555×390 m cell from the accumulated plume simulations was 1.75 m near the centre of A0, and averaged 1.1 m depth across the 2-km diameter disposal area. In practice the average mound height would be somewhat higher in the range 1.4–1.8 m as more of the material will fall en-masse from the hopper as a dynamic compared to the passive-plume model which treats each discharged sediment particle as a separate unit;
- the small degree of deposition to the south-east mainly occurs at times during light NNE breezes;
- fine silt deposition (Fig. 11.17) occurs over the widest area as expected in a highly dispersive environment with slowly-settling sediments, which contrasts

with sand (Fig. 11.20), where deposition is much more confined, occurring well offshore and to the north and north-east of the disposal ground;

- deposition would be low along coastal areas, and only where the suspended-sediment plume edge comes in occasional contact, such as Otago Heads (north of Wickliffe Bay) and the northern coast from Cornish Head northwards (Figs. 11.17–11.18). Where deposition is predicted to occur, the accumulation would be less than 0.5 mm thick over the dredging programme. This is an upper-bound estimate, but in reality these “deposited” sediments, being fine and medium silts, will often be mobilised by wave activity in shallow coastal waters and continue to be dispersed over a wide area. The modelling shows no deposition of silts or sands would occur in Blueskin Bay and Karitane within 48 hours of disposal occurring (Fig. 11.17–11.21);
- all silt sizes would be dispersed further north than the northern boundary in the hydrodynamic model at Shag Rock, but deposition would be very small at <0.1 mm;
- based on the use of a 10,800 m³ capacity TSHD and a continuous 120-day dredging programme, the area influenced by various deposition rates are shown in Figure 11.22. The area where a deposition rate of more than 0.08 mm per day would occur (as an upper-bound) extends approximately 18 km in N-S direction (mainly to the north) and 5 km in width (Fig. 11.22) covering 77 km². The area in which the deposition rate would be ≥0.4 mm per day would extend only to the northern terminus of the Peninsula Spit (–45.655°N) covering up to 29 km² while smaller areas where accumulated deposition rates would exceed 0.8 and 1.7 mm/day (Fig. 11.22) could cover 18 km² and 11 km² respectively (including the disposal mound);
- the accumulated deposition pattern for fine sand (Fig. 11.20b) is closely aligned with the results from the sand transport modelling described in Section 12, which indicate persistent net sand transport to the north, with minimal transport in all other directions. Further, the spatial extent of sand deposition over 50 mm in Figure 11.20a shows the likely spatial pattern of where long-term sand transport will head from the A0 disposal area, given the sand fraction in the suspended-sediment plume after disposal would quickly settle and mostly would travel in the bottom layer (comparing Fig. 11.11d with Fig. 11.12d). This is also the layer where long-term sand transport would take place after previously settled dredged material is mobilized by waves and transported by the same northerly-directed residual current, although in

subsequent months and years the transport would predominantly occur much closer to the seabed than when sand is released in the upper water column from a hopper (which is the case for Figure 11.20a, b).

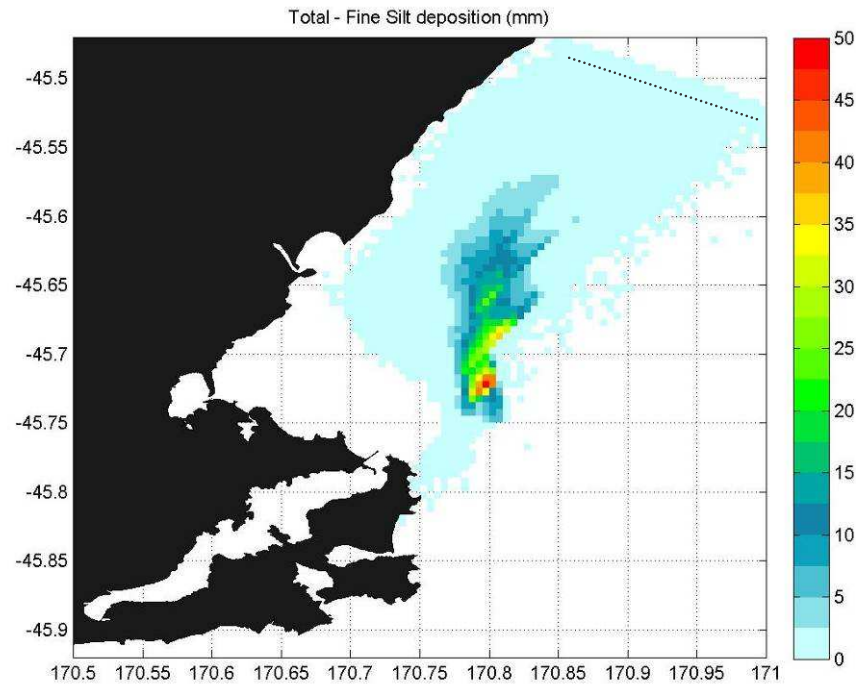


Figure 11.17a: Spatial distribution of deposition (mm) estimated for class size 1 (fine silt) over the dredging programme for the 15-m Harbour channel. Note: the dotted line near the top marks the northern boundary of the model.

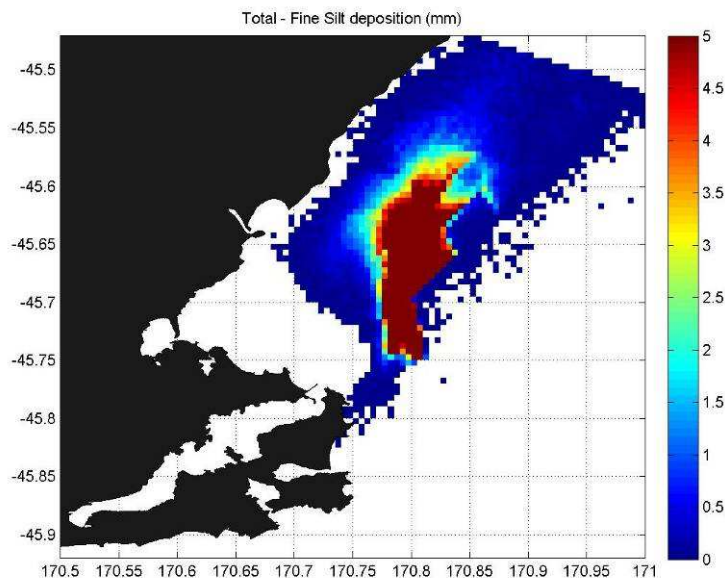


Figure 11.17b: Spatial distribution of deposition (mm) estimated for class size 1 (fine silt) with scale covering the 0–5 mm range.

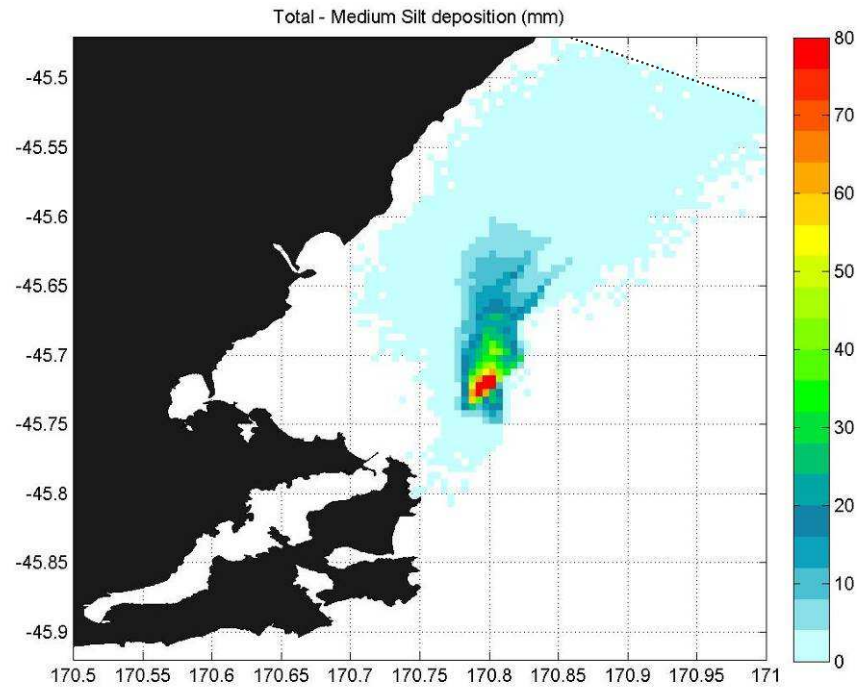


Figure 11.18a: Spatial distribution of deposition (mm) estimated for class size 2 (medium silt) over the dredging programme for the 15-m Harbour channel. Note: the dotted line near the top marks the northern boundary of the model.

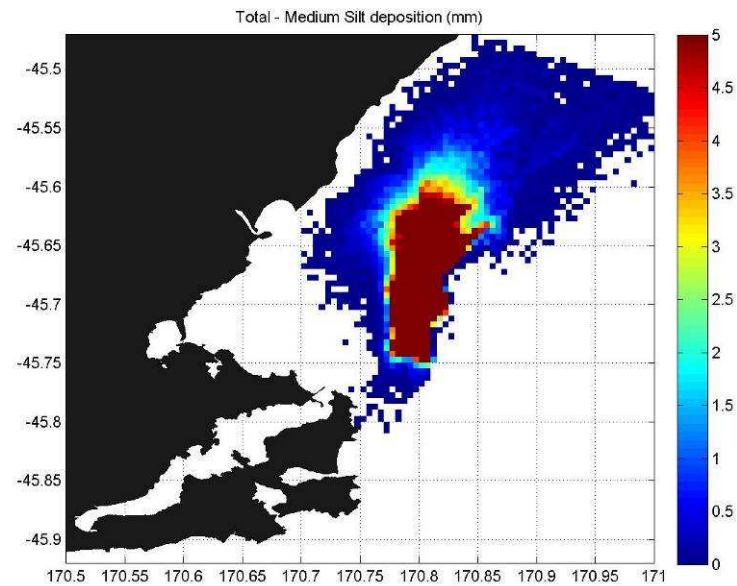


Figure 11.18b: Spatial distribution of deposition (mm) estimated for class size 2 (medium silt) with scale covering the 0–5 mm range.

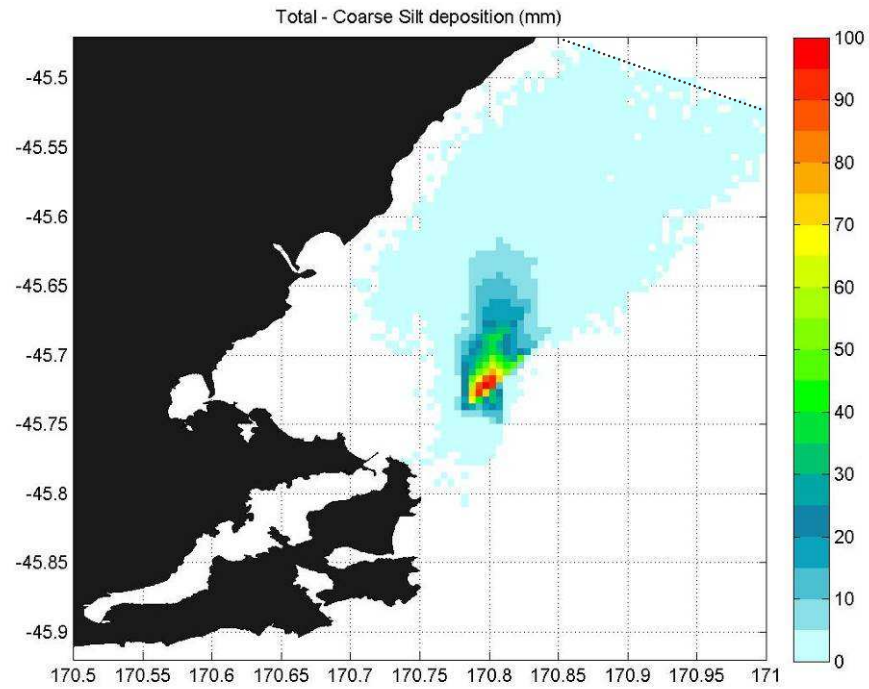


Figure 11.19a: Spatial distribution of deposition (mm) estimated for class size 3 (coarse silt) over the dredging programme for the 15-m Harbour channel. Note: the dotted line near the top marks the northern boundary of the model.

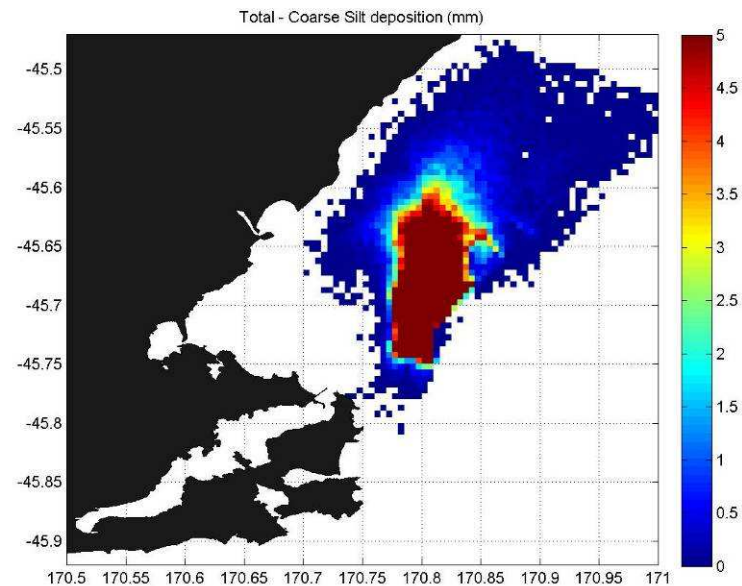


Figure 11.19b: Spatial distribution of deposition (mm) estimated for class size 3 (coarse silt) with scale covering the 0–5 mm range.

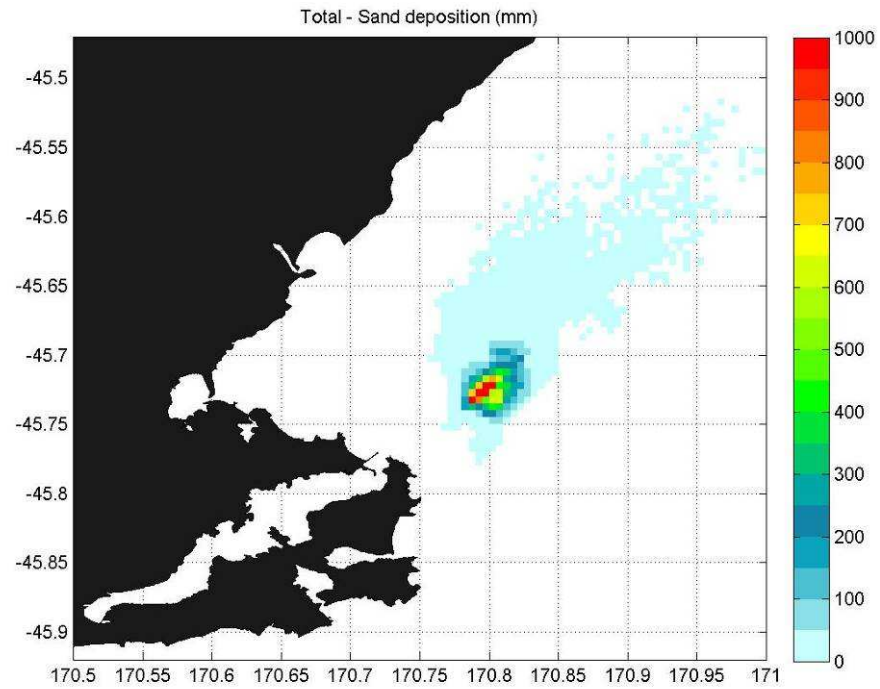


Figure 11.20a: Spatial distribution of deposition (mm) estimated for class size 4 (fine sand) over the dredging programme for the 15-m Harbour channel.

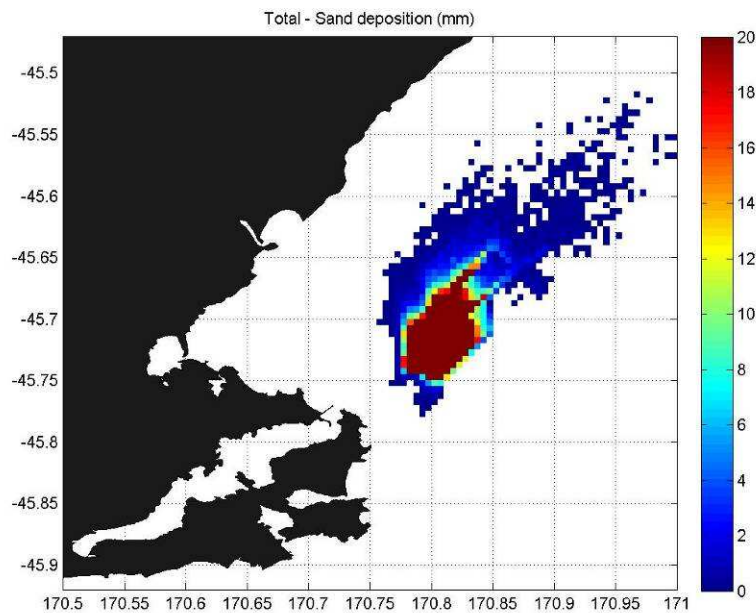


Figure 11.20b: Spatial distribution of deposition (mm) estimated for class size 4 (fine sand) with scale covering the 0–20 mm range.

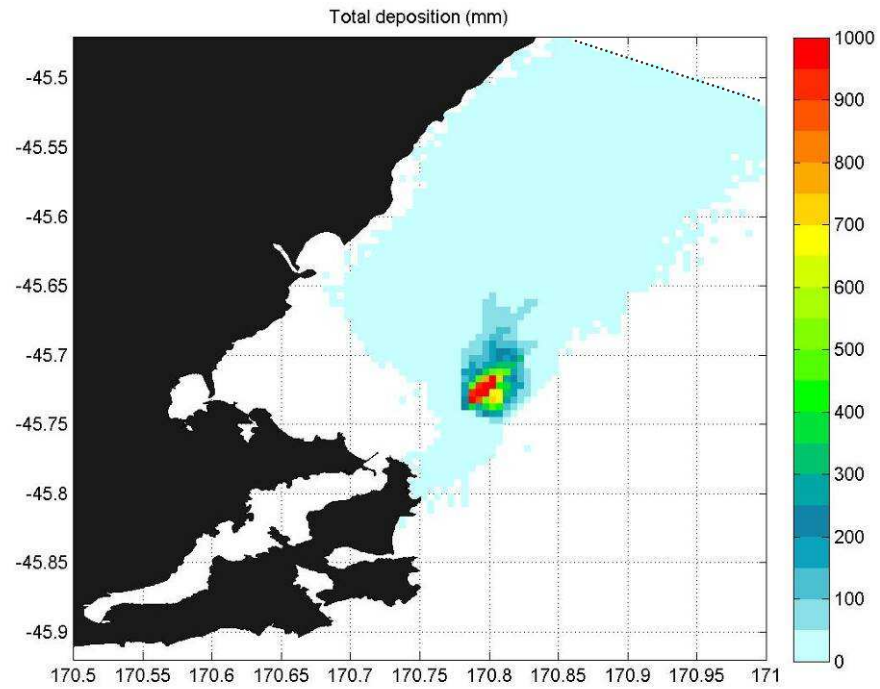


Figure 11.21a: Spatial distribution of total deposition (mm) estimated for all class sizes over the dredging programme for the 15-m Harbour channel. Note: the dotted line near the top marks the northern boundary of the model.

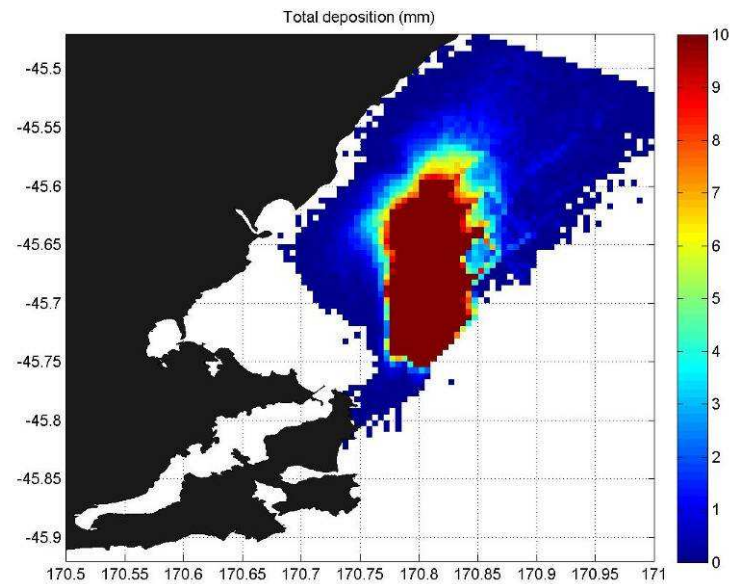


Figure 11.21b: Spatial distribution of deposition (mm) estimated for all class sizes with scale covering the 0–10 mm range.

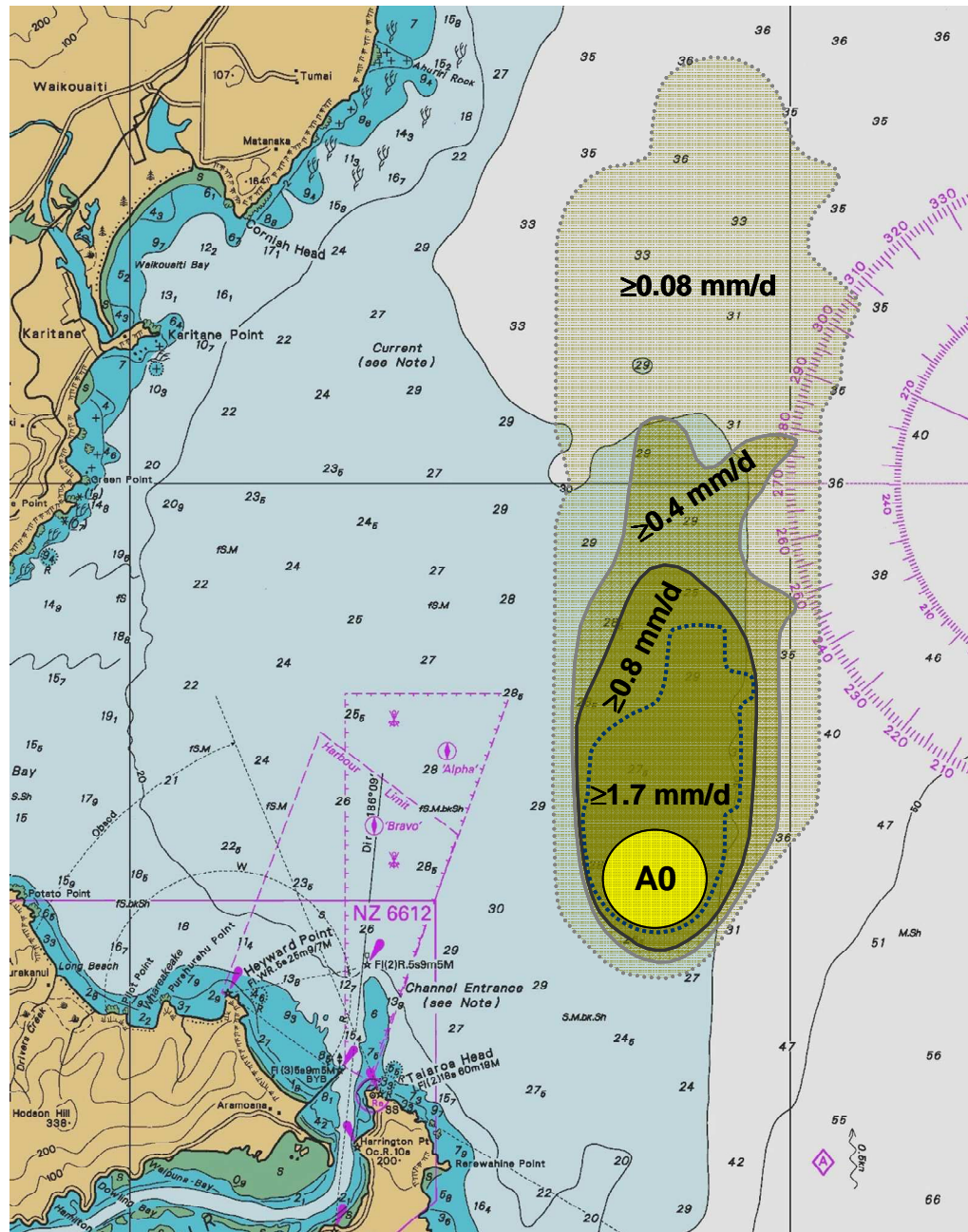


Figure 11.22: Zones within which various average deposition rates (mm per day) are exceeded for all sand/silt fractions from the disposal plume modelling over the entire dredging programme (final channel design). The deposition rates are conservative, being applicable to a mid-size TSHD of 10,800 m³ capacity where the dredging extends for 120 days continuously. [Source of background map: Chart NZ661, LINZ].

12. Long-term sediment transport from the disposal site

12.1 Disposal mound

The Project Next Generation proposal is to dredge and dispose of up to 7.06 Mm³ of sea-bed material dredged from the existing channel for the 15-m Harbour channel design. The process of investigating various options for an appropriate disposal area is discussed in Section 11.2, with the selected site A0 located in Figure 11.2.

A disposal ground would need to be around 2 km in diameter (Fig 11.2) to limit the mound height to under 2 m. In the previous section 11.4.4, the accumulation of the deposition from the plume model runs, assuming a wet bulk density of 1300 kg/m³, resulted in a maximum height of 1.75 m in the centre of A0, but averaging 1.1 m across the A0 circular area, with around 40% export due to dispersion of suspended sediment from the disposal area and its periphery. This export factor may be at the higher end of what is achieved in reality, as trapping of fine sediments would occur in the context of an en masse descent of a large volume of material, which is not specifically included in the passive-plume modelling. The average mound height is expected to be between 1.4 and 1.8 m above the background seabed bathymetry.

12.2 Approach to long-term sand transport from a disposal mound

Two disposal area options were assessed for long-term sediment transport, where “long-term” is defined as spanning months and years after the disposal of sediments has occurred.

The closer A1 site (Fig. 11.2) is where an ADCP measuring both currents and waves was deployed for over 4 months, enabling a comprehensive analysis to be undertaken on sediment transport at the ADCP site. It provided an opportunity to unpack the physical processes that generate sediment transport on the shelf off the Otago Heads, such as the interplay between currents, net residual current and coincidence of currents with wave events from different directions. Armed with this specific knowledge, a subsequent analysis of long-term sediment transport from a second (preferred) disposal site at A0 (Fig. 11.2) was undertaken, using simulated data on waves and currents from the offshore models described respectively in Chapters 8 and 10.

For long-term sediment transport, the assumption is made that the small grain size fractions of < 0.1 mm (particularly silts) in the surface layer of the mound have been winnowed out either during the descent phase of the hopper disposal or resuspended

from the surface layers of the mound by wave activity and widely dispersed in suspension. Consequently, the long-term sediment transport within the surface layer of the mound will be predominantly sand transport. The following sections describe the estimates of long-term transport of a range of grain sizes (0.1 mm to 0.5 mm, which covers fine and medium sands) through the A1 and A0 disposal area, based on the methodology described in detail in Appendix II.

12.3 Sand transport through disposal site A1

The methodology used to estimate sand transport through the A1 disposal area option is described in more technical detail in Appendix II. Note that we have no actual field measurements of sand transport which would be used to validate these estimates.

Initially, a full analysis was undertaken for the nominally 4-month field period from 18 March to 4 August 2008 (with gaps between ADCP deployments) to estimate transport using actual measurements of waves and currents. The waves measured during the 2008 field period were somewhat higher than the long-term hindcast wave climate (described in Chapter 8) as shown in Table 12.1, with all four months producing a mean significant wave height greater than the 5-year average for the particular month. This means the sediment-transport estimates based on the 2008 field period will be higher than the long-term average rate, based on the ability of waves to mobilise fine sands on the seabed.

Table 12.1: Monthly-mean significant wave height at A1 during the 2008 field programme compared to the monthly-mean hindcast wave height for the 5-year period 2003–2007 listed in Table 8.8.

Month	Monthly-mean significant wave height (m)	
	2008 ADCP measurements [†]	5-year hindcast (2003–07)
April	1.30	1.12
May	1.66	1.14
June	1.43	1.18
July	1.88	1.16

[†] contains some absent data, especially during calmer periods when the ADCP is less accurate in deeper water, but also from ADCP deployment turnaround periods when it was calmer to operate with vessels and divers. This introduces a small bias towards slightly higher monthly-mean wave heights.

Finally, in order to estimate long-term effects of wave activity on sediment transport at site A1 (where the ADCP was located), a 10-year hindcast of the wave climate from MetOcean Solutions (described in Chapter 8) was used to determine the percentage of time that waves would be capable of entraining sand at A1.

The sediment grading curves from coring in the Harbour channel show that the predominant sand sizes in the bulk of “sandy” material to be dredged are in the range 0.1–0.3 mm (fine sands), but there is a smaller fraction (<10%) of medium sands from 0.3–0.6 mm and an even smaller fraction of coarse sands and gravels above 0.6 mm (Opus International Consultants, 2008). Note the range of grain sizes that were used in this Chapter to estimate sediment transport were 0.1–0.5 mm, which will form the dominant contribution to sand transport rates.

12.3.1 2008 field period assessment

Figures 12.1 to 12.5 show measured waves and currents at Site A1 with critical wave-orbital speed and critical current speed for initiation of sediment motion both superimposed. Critical speeds are shown for a range of sand grain sizes ($D_s = 0.1, 0.2, 0.3, 0.4$ and 0.5 mm).

Figures 12.6 and 12.7 shows a comparison of the critical speeds (wave-orbital and current, respectively) for all grain sizes on the one graph.

These figures illustrate how larger grain sizes require higher wave-orbital speeds and current speeds to initiate sediment motion on the seabed. Currents rarely exceeded the critical speed required to entrain sediment, even in the case of the smallest grain size ($D_s = 0.1$ mm). Currents were not capable of entraining the largest sand size ($D_s = 0.5$ mm) at all. In comparison to currents, wave-orbital speeds were larger and were frequently capable of entraining all grain sizes. The conclusion is that waves are primarily responsible for entraining seabed sediments at depths of around 30 m, and we focus the rest of this analysis accordingly.

Figure 12.8 shows a vector plot of waves, where the vector magnitude is the significant wave height H_s and the vector direction is the peak spectral wave direction D_p , which is the direction that waves propagate from. Wave direction is divided into five sectors, which will feature in the following analysis (sector 1 denotes $H_s = 0$; sector 2 is $D_p = 0–97^\circ$; sector 3 is $D_p = 97–142^\circ$; sector 4 is $D_p = 142–180^\circ$; sector 5 is $D_p = 180–360^\circ$). Table 12.2 shows the percentage of time that waves came from each sector. Approximately 15% of the time there were no waves (or, to be more precise, waves were not detectable by the ADCP, because of small height and/or short period).

Waves were present for 85% of the time, where “present” in this context means detectable by the ADCP on the seabed. Waves came most frequently from sector 4 (southeast), followed by sectors 2 and 3. Waves from sector 5 (west of south between the site and the shoreline) were rarely detectable.

Table 12.3 shows time that waves were capable of entraining each sediment grain size ($D_s = 0.1, 0.2, 0.3, 0.4$ and 0.5 mm), expressed as a percentage of the total time and as a percentage of the time that waves were present. When waves were present they were often capable of entraining sediment (81% of the time for $D_s = 0.1$ mm, reducing to 36% of the time for $D_s = 0.5$ mm). Since waves were present for 85% of the time, sediment was therefore often in motion.

Table 12.4 shows the same information as Table 12.3 broken down by wave sector.

Figure 12.9 shows a vector plot of currents, where the vector magnitude is the current speed U_c and the vector direction is the direction that currents propagate to. The principal axis of the current ellipse is oriented roughly northwest–southeast and is approximately symmetrical (visual estimation only).

Figure 12.10 shows a progressive vector plot formed from the current speed and direction measured at a height of 2.26 m above the seabed over the whole duration of the ADCP deployment. The net (or “residual”) current was directed approximately to the southeast.

Figure 12.11 shows progressive vector plots for the current formed from the measured current speed and direction over each of 10 individual “events”, defined as periods when waves were more-or-less continuously capable of entraining 0.1 mm grain size bed sediment. The events so defined are shown in Figure 12.12. The net (residual) current over the duration of each event was practically the same (i.e., to the southeast) as the net current over the whole duration of the ADCP deployment (i.e., regardless of whether waves were capable of entraining the 0.1 mm bed sediment). This demonstrates that wave events were typically not associated with any unusual current pattern.

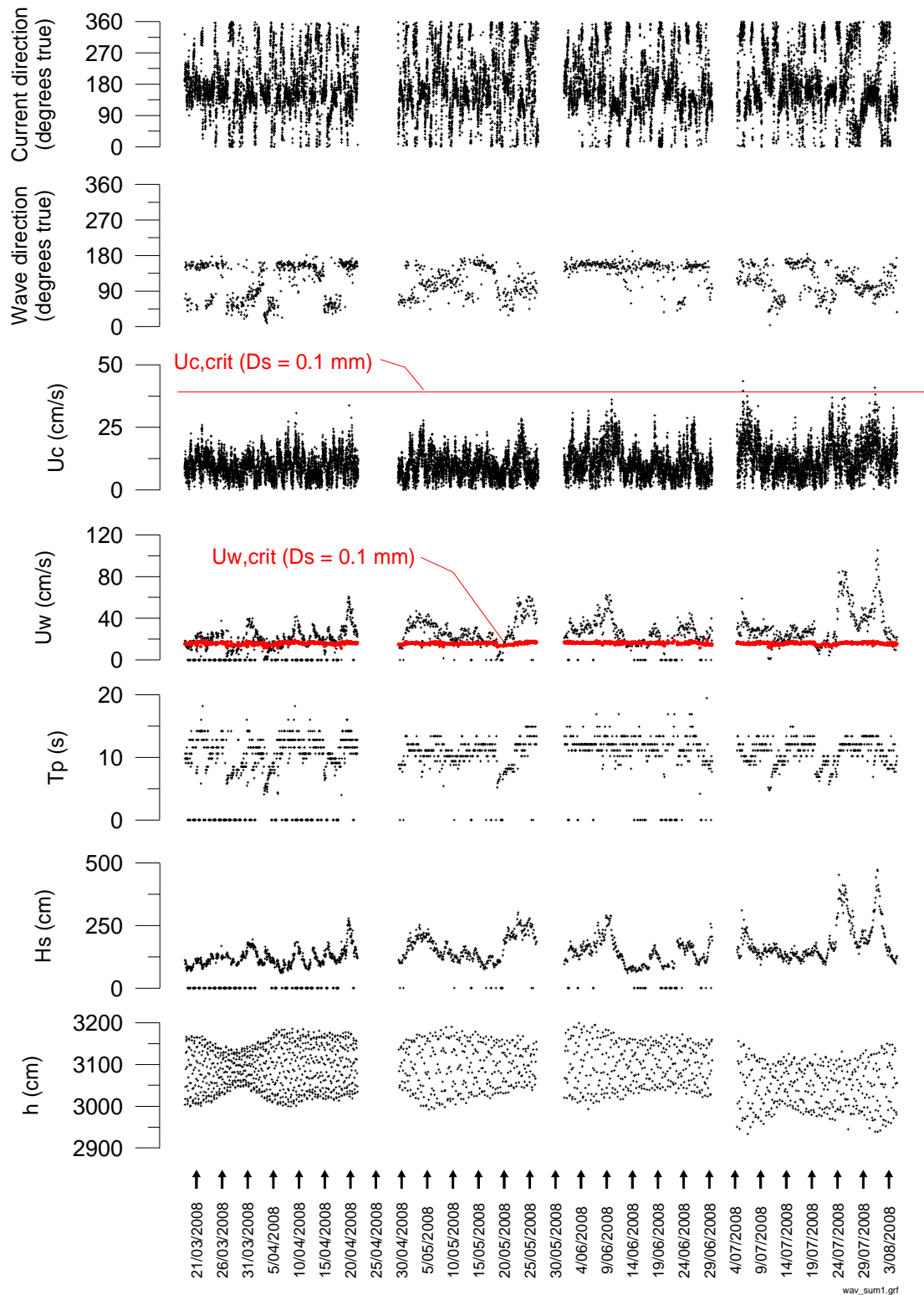


Figure 12.1: Measured waves, currents and depth (h) at site A1 with critical current (U_c) and wave-orbital (U_w) speeds for initiation of sediment motion for $D_s = 0.1$ mm superimposed.

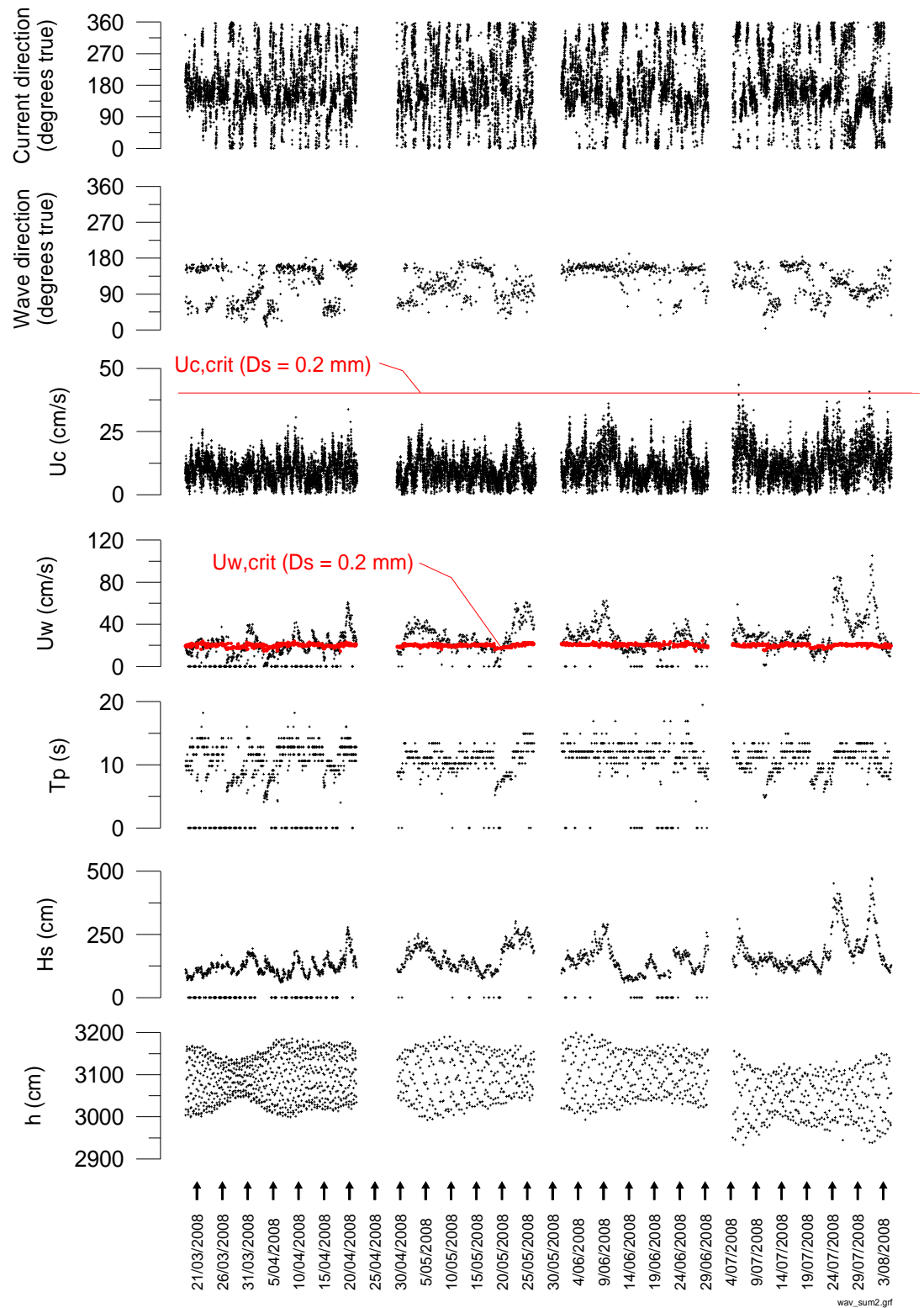


Figure 12.2: Measured waves, currents and depth (h) at site A1 with critical current (U_c) and wave-orbital (U_w) speeds for initiation of sediment motion for $D_s = 0.2$ mm superimposed.

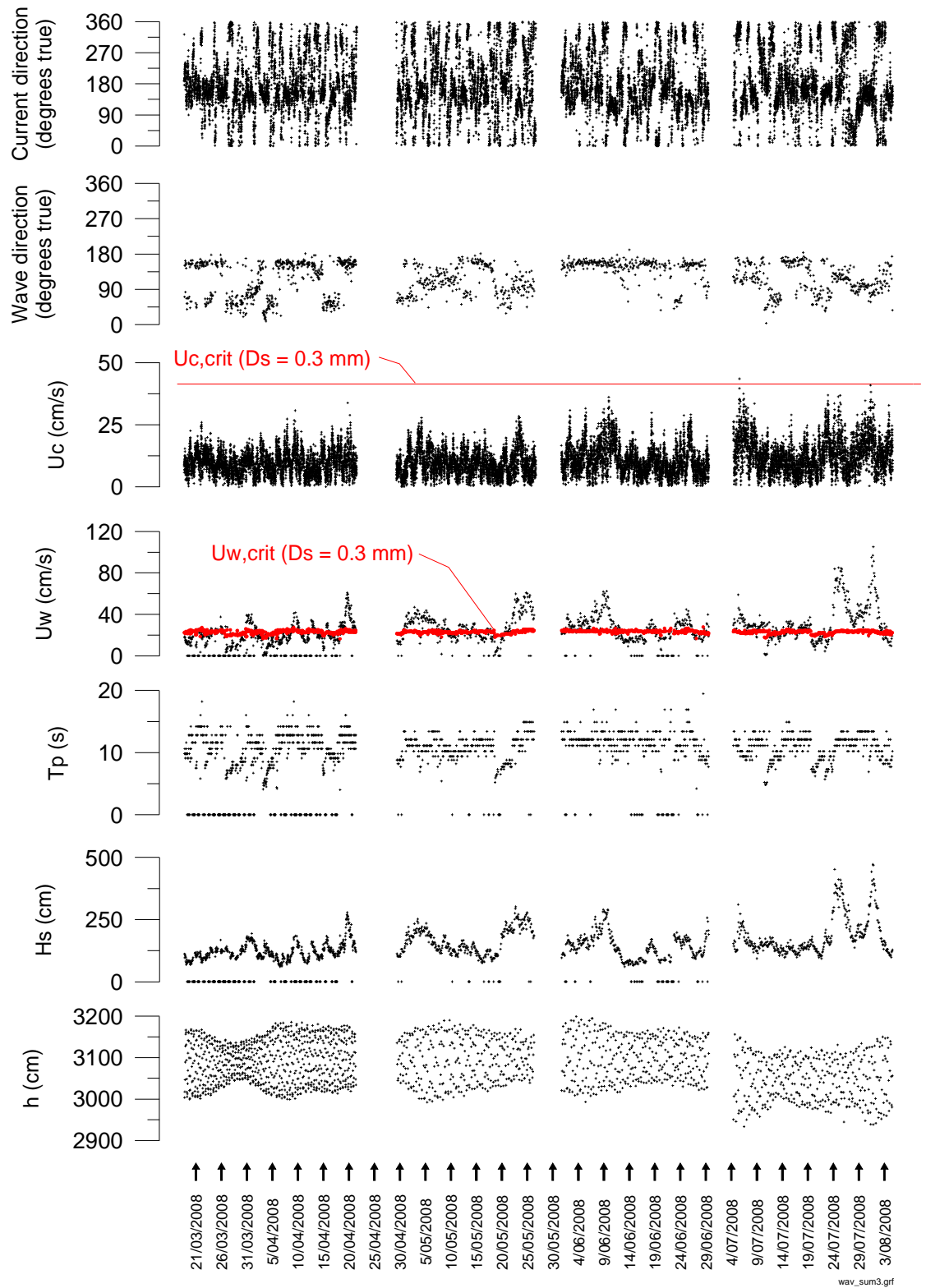


Figure 12.3: Measured waves, currents and depth (h) at site A1 with critical current (U_c) and wave-orbital (U_w) speeds for initiation of sediment motion for $D_s = 0.3$ mm superimposed.

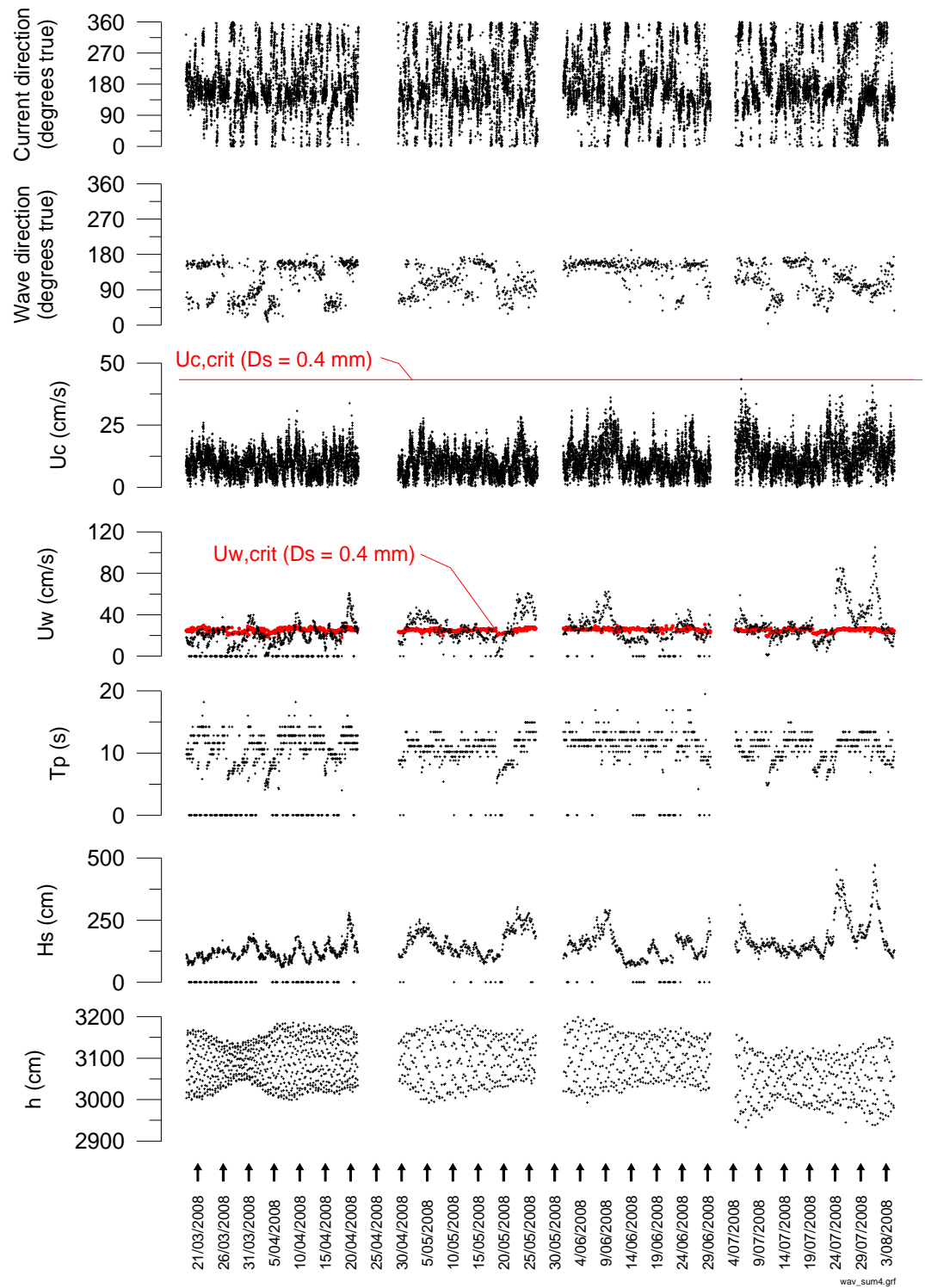


Figure 12.4: Measured waves, currents and depth (h) at site A1 with critical current (U_c) and wave-orbital (U_w) speeds for initiation of sediment motion for $D_s = 0.4$ mm superimposed.

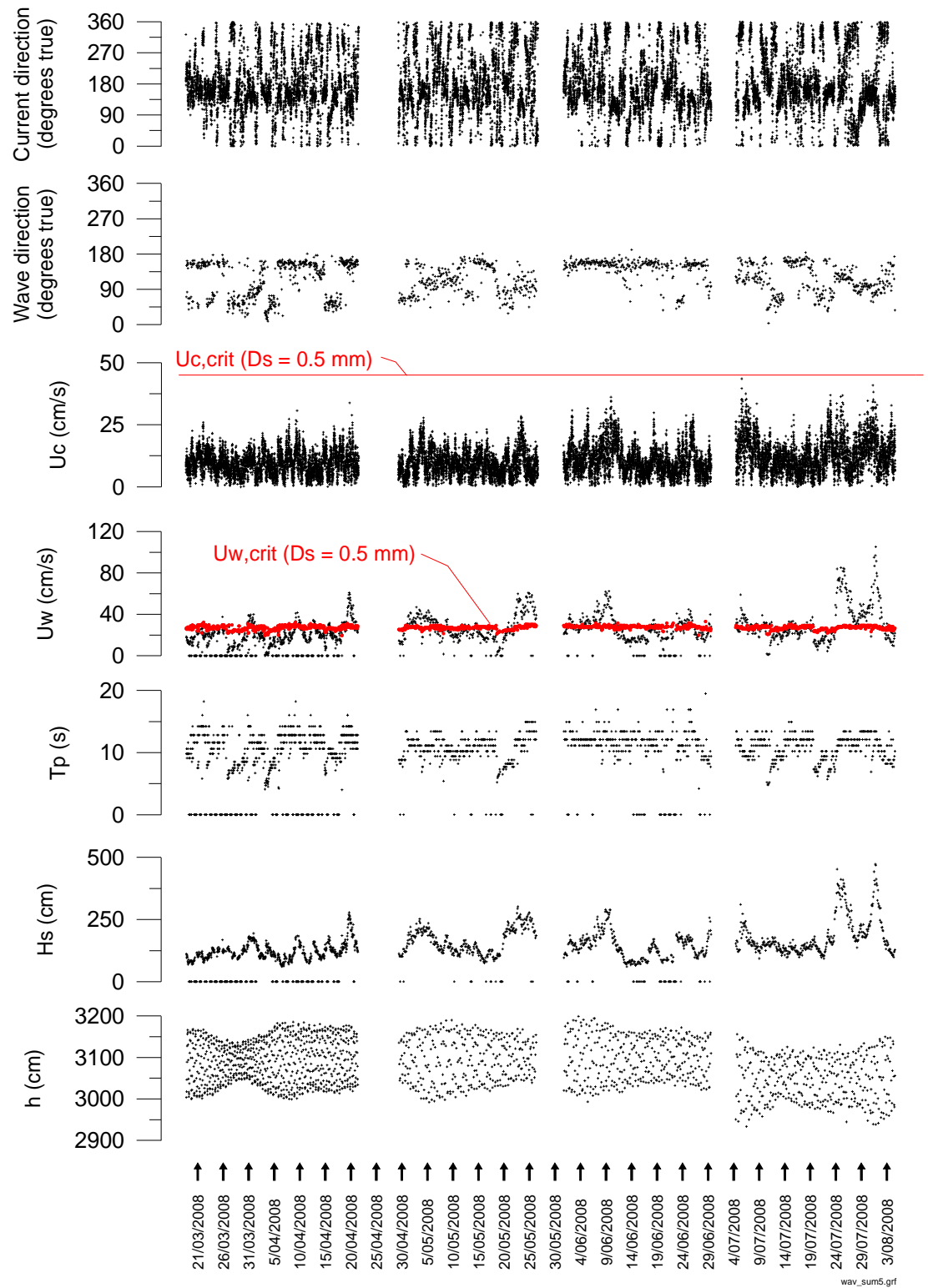


Figure 12.5: Measured waves, currents and depth (h) at site A1 with critical current (U_c) and wave-orbital (U_w) speeds for initiation of sediment motion for $D_s = 0.5$ mm superimposed.

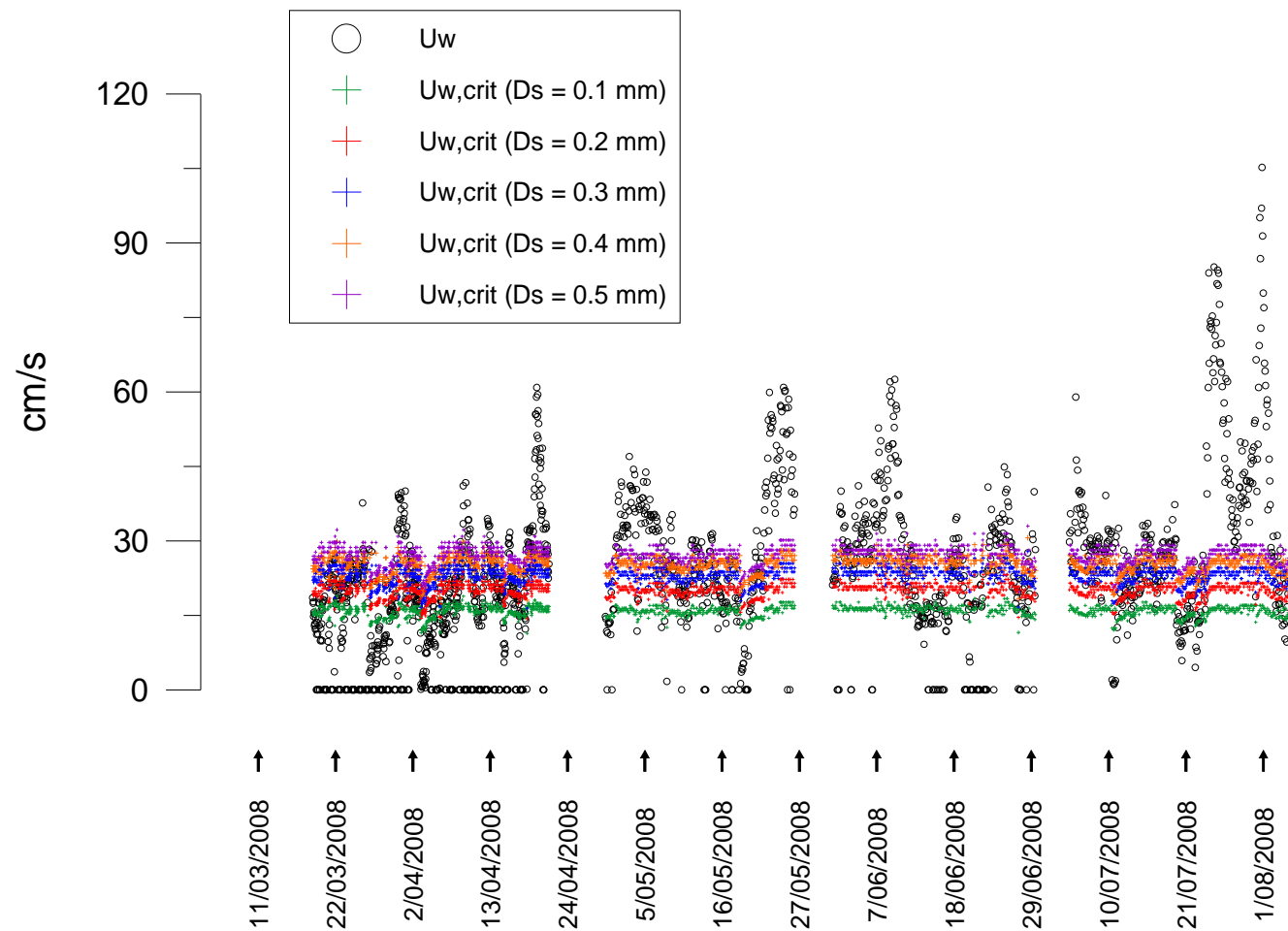


Figure 12.6: A comparison of the critical wave-orbital speed ($U_{w,crit}$) for all grain sizes compared with the measured wave orbital speed (U_w).

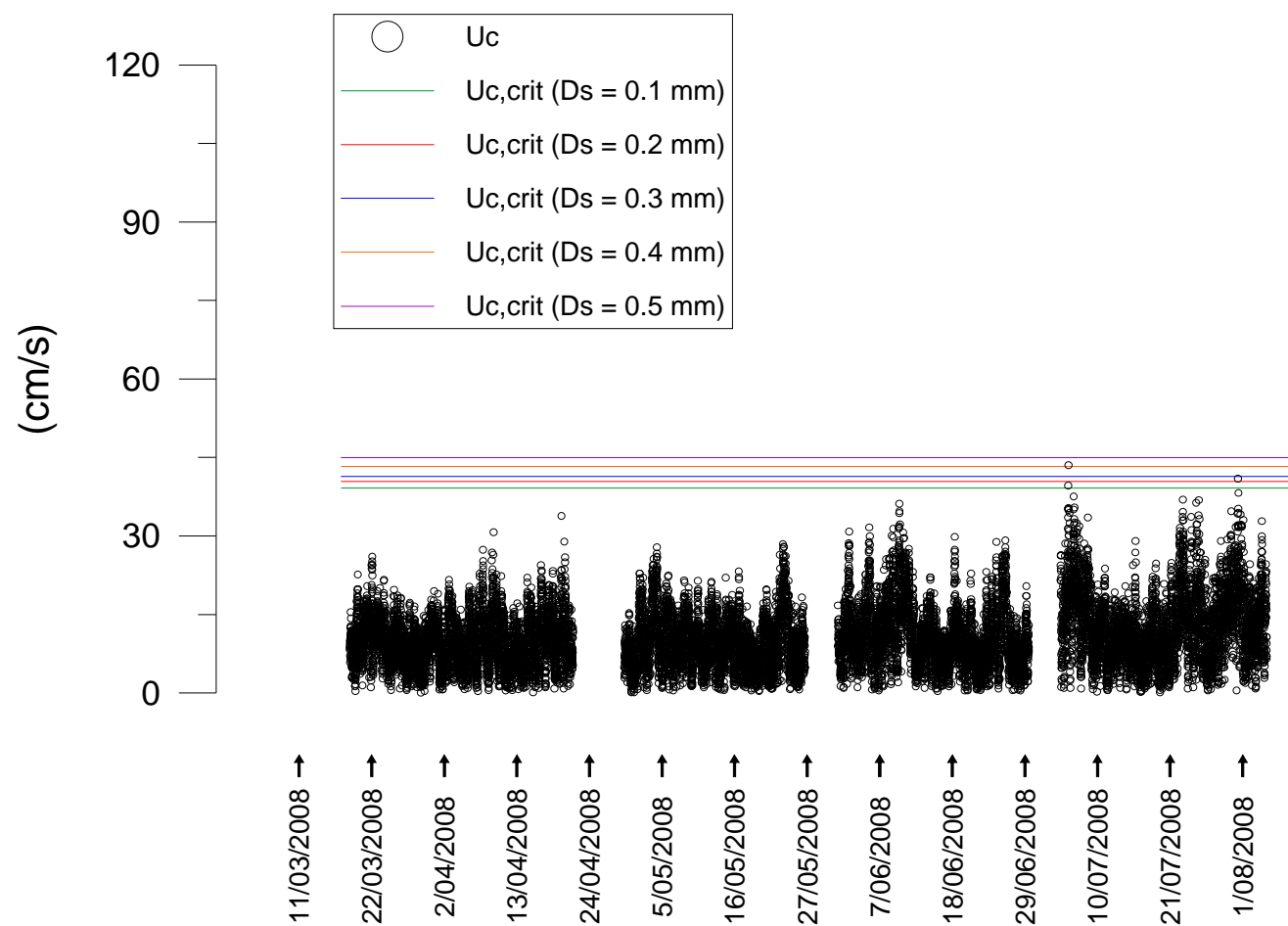


Figure 12.7: A comparison of the critical current-flow speeds ($U_{c,crit}$) for all grain sizes compared with the measured current speed (U_c).

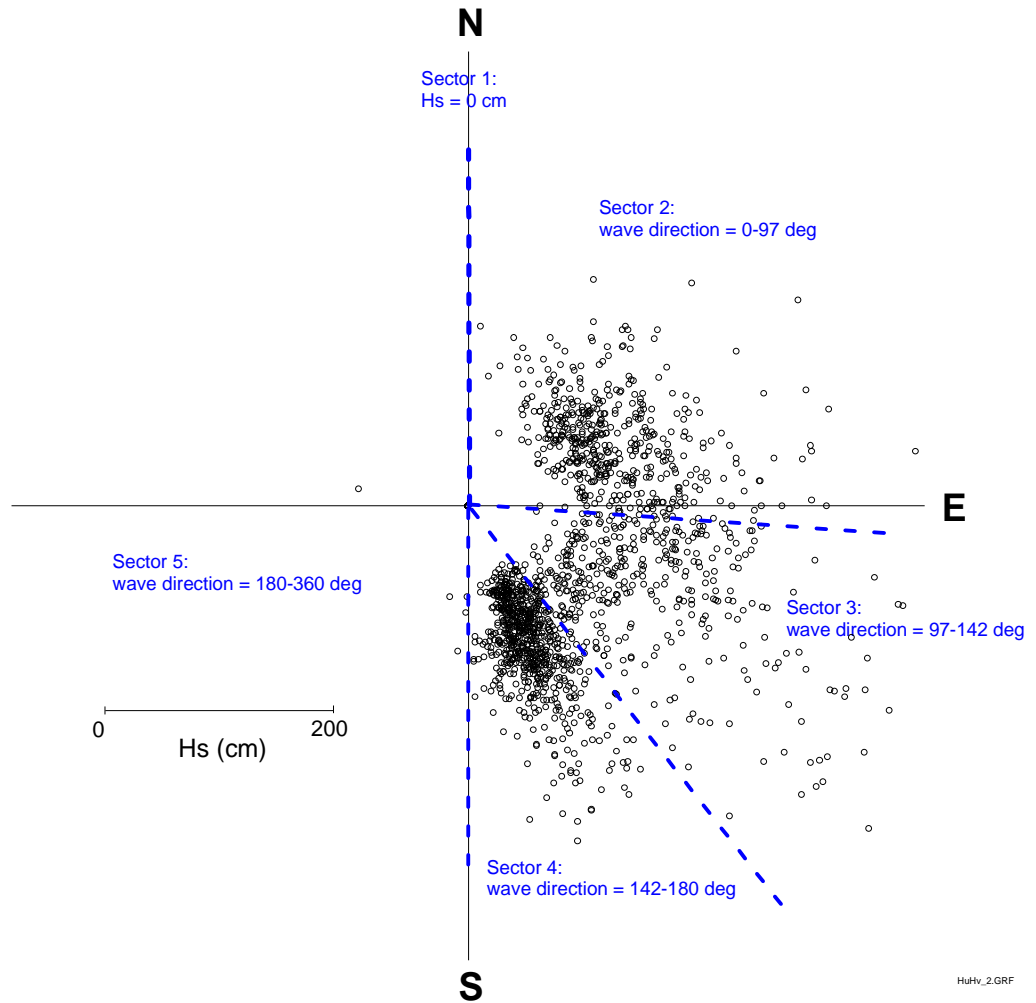


Figure 12.8: Vector plot of waves, where the vector magnitude is significant wave height H_s and the vector direction is D_p (direction that waves propagate from). Wave direction is divided into 5 sectors (sector 1 denotes $H_s = 0$; sector 2 is $D_p = 0-97^\circ$; sector 3 is $D_p = 97-142^\circ$; sector 4 is $D_p = 142-180^\circ$; sector 5 is $D_p = 180-360^\circ$).

Table 12.2: Percentage of time waves came from each sector. (Sector 1 denotes $H_s = 0$.)

Sector				
1	2	3	4	5
14.5	27.3	19.2	38.7	0.2

Table 12.3: Percent of time sediment was mobilized and entrained by waves into the water column (expressed as percentage of total time and as percentage of time that waves were present and detectable by the ADCP at the seabed).

D_s (mm)	Percentage of total time	Percentage of time that waves are present
0.1	70	81
0.2	56	65
0.3	45	53
0.4	37	44
0.5	31	36

Table 12.4: Percent of time sediment was mobilized and entrained into the water column by waves, broken down by wave direction sector, and expressed as (left) percentage of total time and (right) percentage of time that waves were present and detectable by the ADCP at the seabed.

Sector					Sector				
D_s (mm)	2	3	4	5	D_s (mm)	2	3	4	5
0.1	18	18	34	0	0.1	65	94	87	50
0.2	13	15	28	0	0.2	49	77	71	25
0.3	11	13	21	0	0.3	39	67	55	25
0.4	9	11	17	0	0.4	33	59	44	25
0.5	8	10	13	0	0.5	29	52	34	0

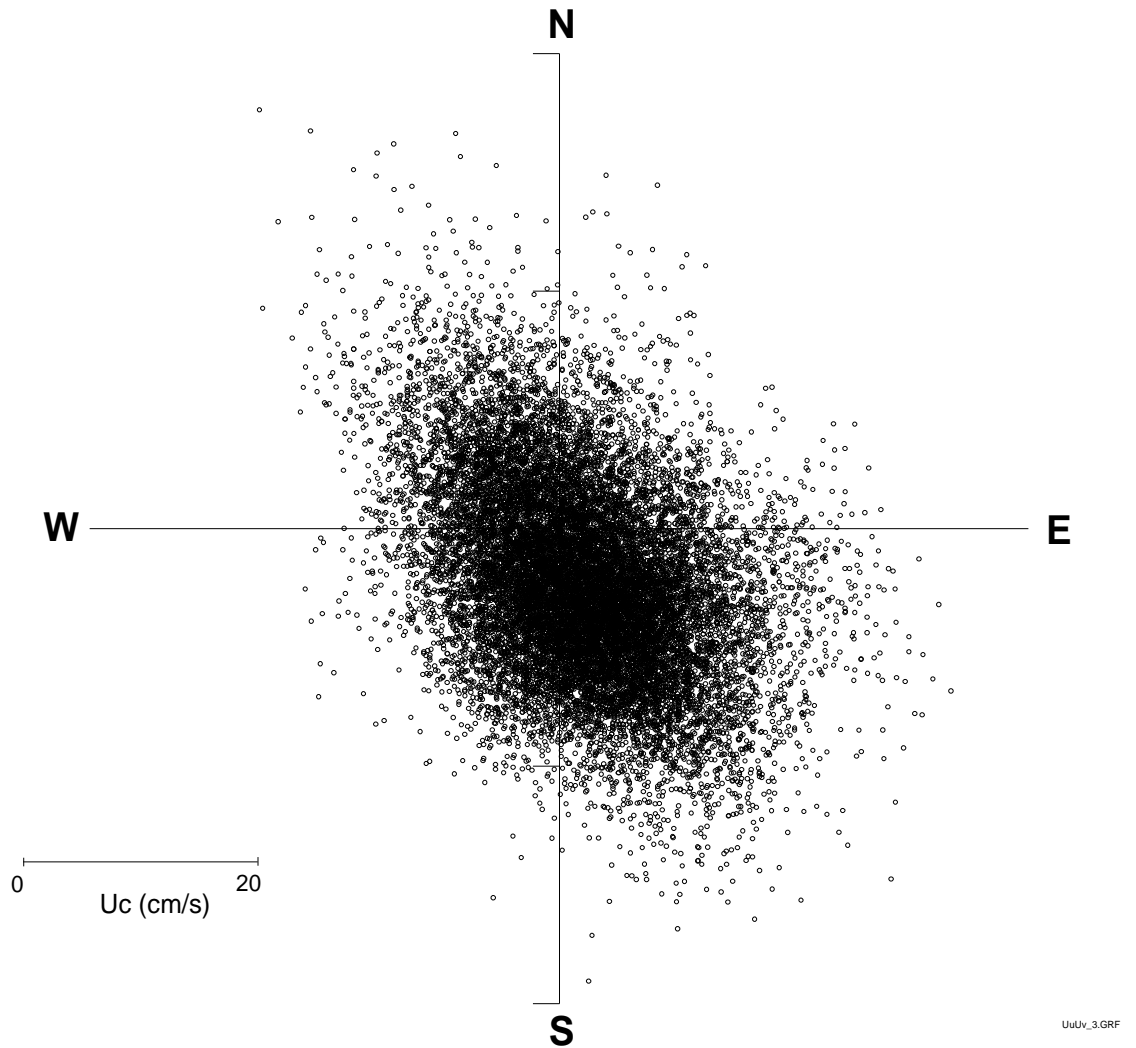


Figure 12.9: Vector plot of currents measured at A1 during the entire field programme (Bell & Hart, 2008), where the vector magnitude is the current speed U_c and the vector direction is the direction that currents propagate towards.

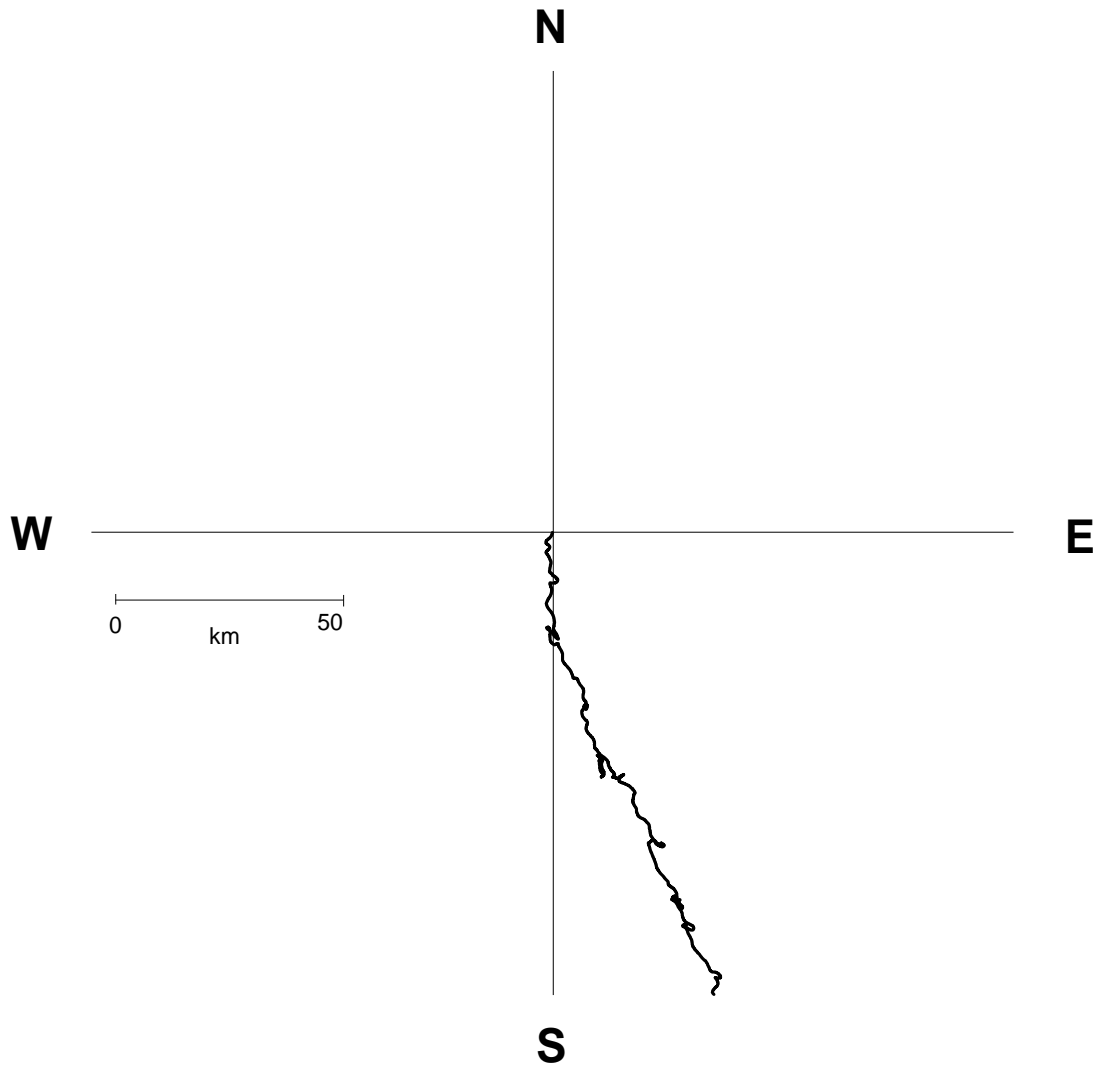


Figure 12.10: Residual (net) current trace formed from the current speed and direction measured at a height of 2.26 m above the seabed over the whole duration of the 2008 ADCP deployments at site A1.

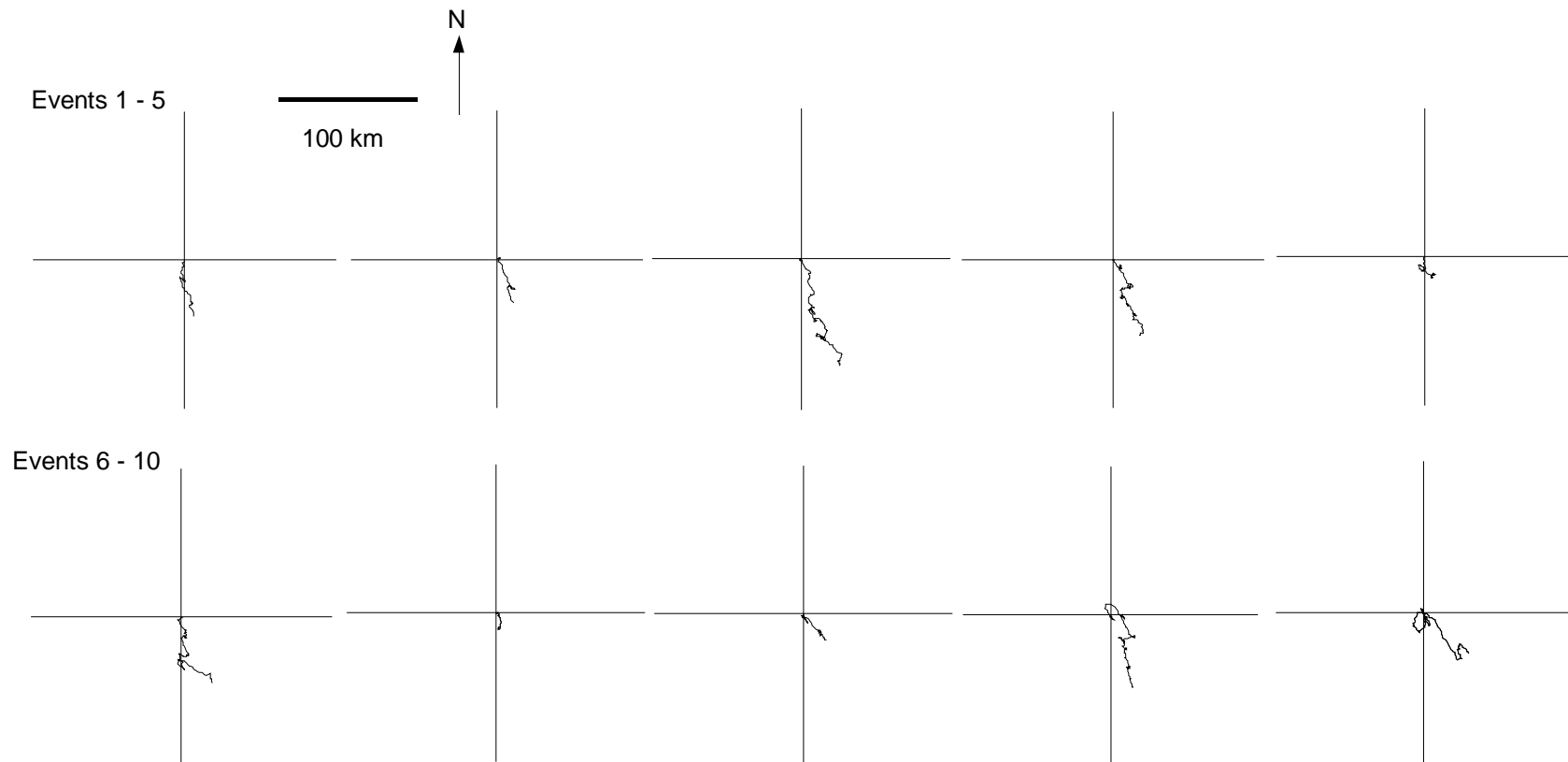


Figure 12.11: Progressive vector plot formed from the measured current speed and direction over each of 10 individual “events” defined as periods when waves were more-or-less continuously capable of entraining 0.1 mm grain size bed sediment. The wave events are defined in Figure 12.12.

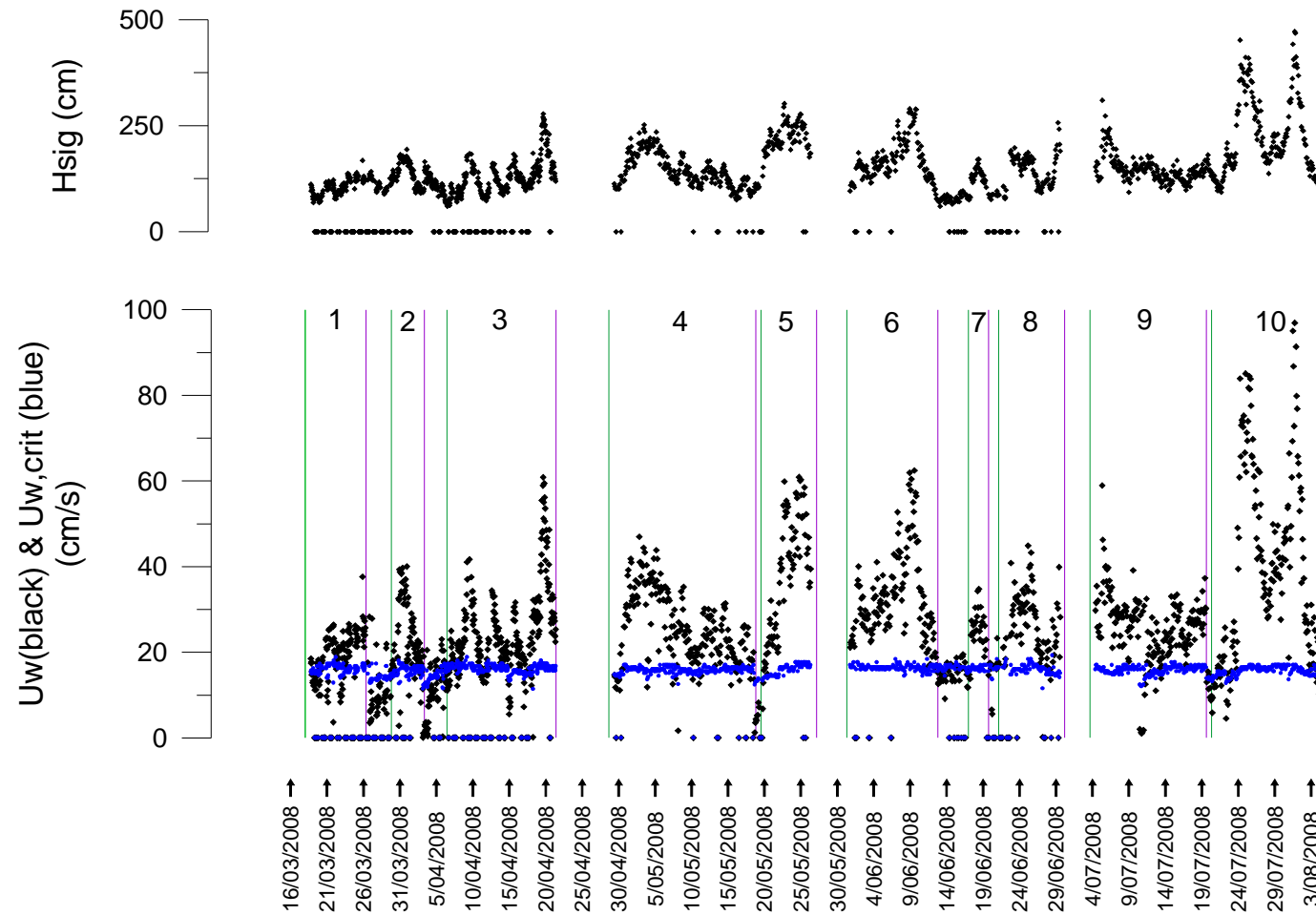


Figure 12.12: Events (periods when waves were more-or-less continuously capable of entraining 0.1 mm grain size bed sediment) used in the analysis of progressive vectors (Figure 12.11). Hsig is the significant wave height and Uw is the wave-orbital speed.

The depth-integrated suspended-sediment transport integrated over the duration of the deployments is denoted as Φ (see Appendix II for how it is calculated). Values for Φ are shown in Table 12.5 for each sediment grain size calculated by each of the two sediment transport models—Rouse, cited in Raudkivi (1990: p. 166–168) and Nielsen (1992). For these calculations, the nearbed current is a scalar only (i.e., speed without direction). This means that Φ is the integral of the scalar instantaneous transport, Q , which can be thought of (loosely) as the “gross” sediment transport. Φ is multiplied by a nominal disposal mound width of 2 km in Table 12.5.

The depth-integrated sediment transport Φ was calculated again, this time treating the transport of sediment Q as a vector with direction corresponding to the measured current speed at 2.26 m above the bed. Sediment transport (Φ) calculated in this way is now a vector itself, with magnitude $MAG[\vec{\Phi}]$ and direction $DIR[\vec{\Phi}]$. This can be thought of (loosely) as the “net” sediment transport. Table 12.6 shows the results, including the magnitude of sediment transport multiplied by a nominal disposal mound width of 2 km (as in Table 12.5).

Figures 12.13a and 12.13b show progressive vector plots of sediment transport formed from the Nielsen and Rouse model predictions (respectively) of $MAG[\vec{\Phi}]$ and $DIR[\vec{\Phi}]$ for 0.1 mm grain size bed sediment for each of the 10 individual events defined in Figure 12. The two models show similar net transport directions, however the transport magnitudes are different, as already illustrated in Table 12.6. For most events the net transport was to the southeast, which is the same direction as the overall residual current (Figure 12.10), but events 6 and 9, in which net sediment transport was directed towards the northwest and north, are exceptions. Furthermore, sediment transport was turned towards the north for short periods within other events (e.g., event 5). Turning of transport to the north is caused by periods of high waves (within events) occurring when the current was setting towards the north.

Table 12.5: Φ , the “gross” sediment transport in grams per unit cm width (see text for explanation), and Φ multiplied by a nominal dredge disposal mound width of 2 km using two sediment transport formulae for various sand grain sizes (D_s) and associated settling velocities (W_s). Note: 1 g/cm width sediment transport is equivalent to 0.1 kg/m width.

		Rouse model		Nielsen model	
D_s (mm)	W_s (cm/s)	Φ (g/cm)	$\Phi \times \text{mound width}$ (tonnes)	Φ (g/cm)	$\Phi \times \text{mound width}$ (tonnes)
0.1	0.64	170,500	34,100	4,601,123	920,224
0.2	1.88	12,145	2,429	278,423	55,684
0.3	3.25	4,653	930	58,708	11,741
0.4	4.75	2,488	489	19,736	3,947
0.5	6.38	1,497	299	8,504	1,700

Table 12.6: Magnitude and direction ($\text{MAG}[\vec{\Phi}]$ and $\text{DIR}[\vec{\Phi}]$) of the “net” sediment transport in grams per cm width (see text for explanation), and $\text{MAG}[\vec{\Phi}]$ multiplied by a nominal dredge disposal mound width of 2 km using two sediment transport models for various sand grain sizes (D_s) and associated settling velocities (W_s). Note: 1 g/cm width sediment transport is equivalent to 0.1 kg/m width.

		Rouse model			Nielsen model		
D_s (mm)	W_s (cm/s)	$\text{MAG}[\vec{\Phi}]$ (g/cm)	$\text{DIR}[\vec{\Phi}]$ (° N)	$\text{MAG}[\vec{\Phi}] \times \text{mound width}$ (tonnes)	$\text{MAG}[\vec{\Phi}]$ (g/cm)	$\text{DIR}[\vec{\Phi}]$ (° N)	$\text{MAG}[\vec{\Phi}] \times \text{mound width}$ (tonnes)
0.1	0.64	116,383	157	23,276	2,850,365	166	570,073
0.2	1.88	6,639	164	1,327	173,311	166	34,662
0.3	3.25	2,447	165	495	36,442	166	7,288
0.4	4.75	1,294	165	258	12,214	166	2,442
0.5	6.38	788	165	157	5,244	166	1,048

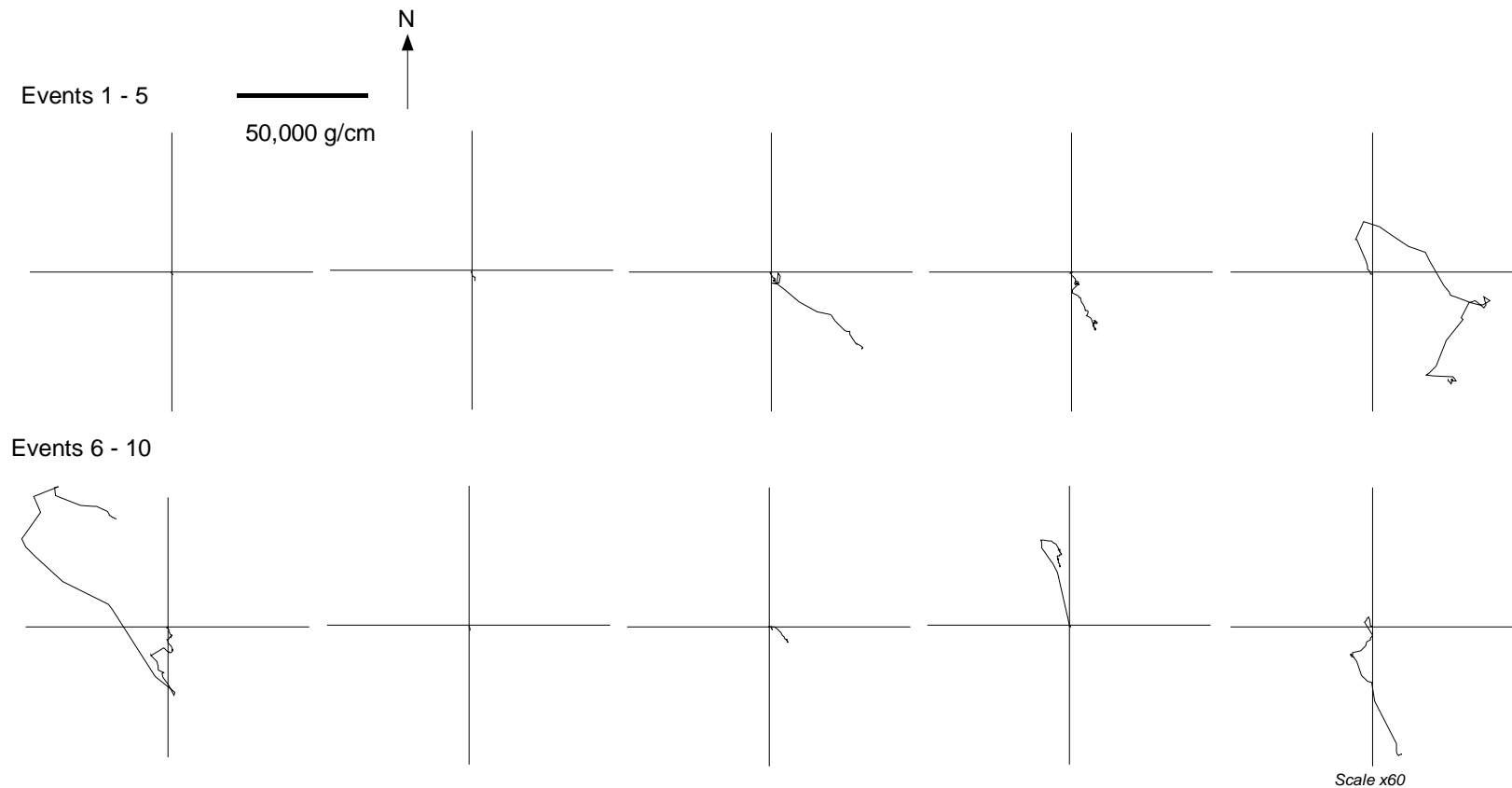


Figure 12.13a: Progressive vector plot formed from Nielsen prediction of sediment transport $MAG[\vec{\Phi}]$ and $DIR[\vec{\Phi}]$ for 0.1 mm grain size bed sediment for each of the 10 individual events (defined in Figure 12.12). Note: the large scale change of 60 \times required for the high wave event #10.

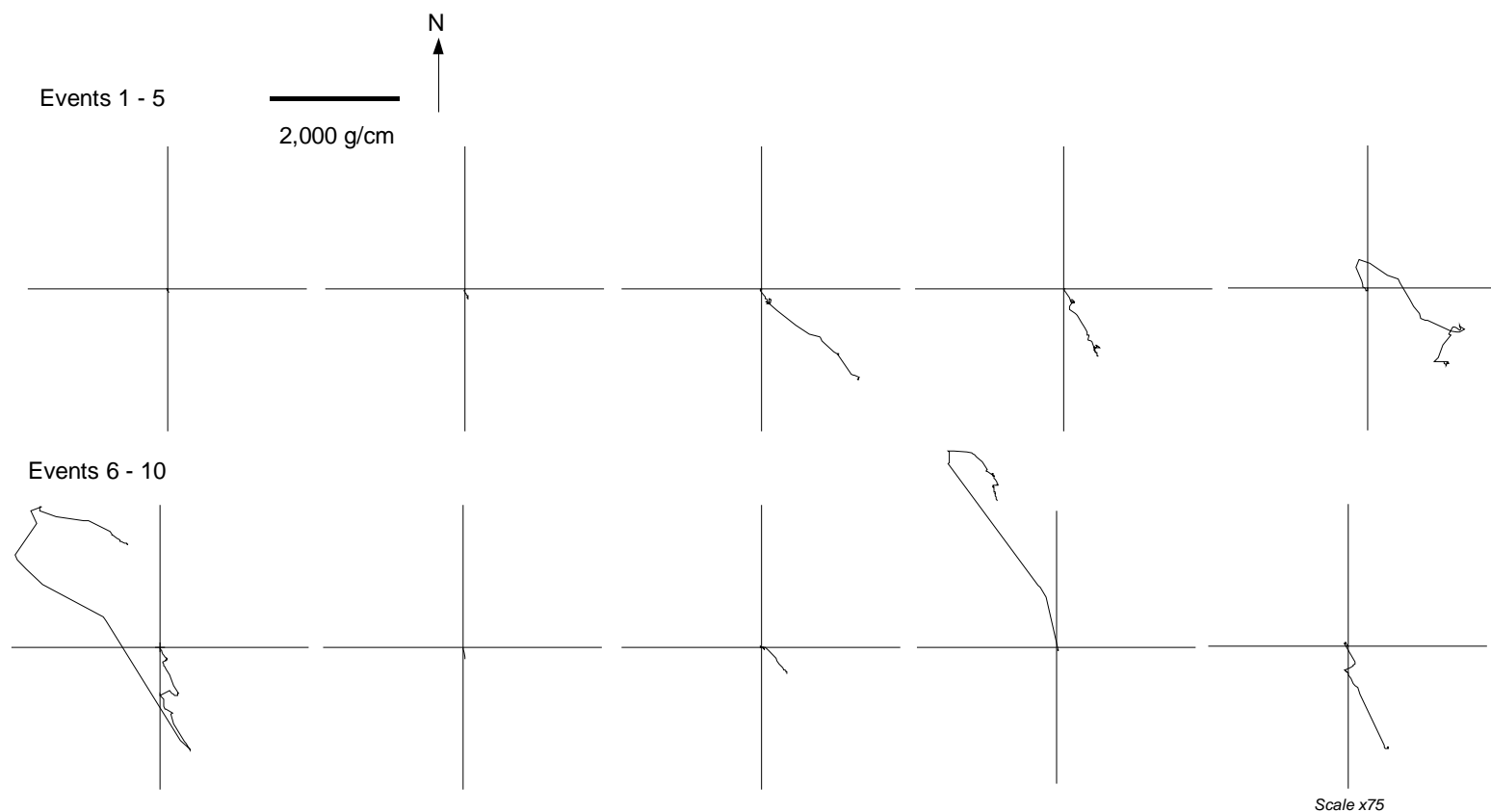


Figure 12.13b: Progressive vector plot formed from Rouse prediction of sediment transport $MAG[\vec{\Phi}]$ and $DIR[\vec{\Phi}]$ for 0.1 mm grain size bed sediment for each of the 10 individual events (defined in Figure 12.12). Note: the large scale change of 75 \times required for the high wave event #10.

12.3.2 10-year wave hindcast estimates of active sand transport occurrences at A1

In order to estimate long-term occurrences of wave activity on sediment transport at site A1 (which is where the ADCP was located), wave statistics from a 10-year hindcast of the wave climate using the SWAN (Simulating Waves Nearshore) model (Chapter 8) were utilised as follows:

- the SWAN model produced directional wave spectra at hourly intervals over the wave model domain for a 10-year period 1998–2007 (Chapter 8), and the standard spectral wave parameters were output at 3-hourly intervals. Wave statistics (H_s , T_p and D_p) from the 10-year hindcast period were extracted from the model for site A1;
- wave orbital speeds U_w and the critical wave orbital speeds $U_{w,crit}$ were calculated from the hindcast data in the same way as described for the ADCP field data (Appendix II);
- the water depth was fixed at 29.5 m.

Figure 12.14 shows the hindcast wave data and calculated wave-orbital speed at the bed over the 10-year period at site A1.

Figure 12.15 shows a comparison of the critical wave-orbital speeds, calculated from the wave hindcast dataset, for all grain sizes on the one graph. Wave-orbital speeds were frequently capable of entraining all grain sizes that were tested, which was also the case with the 4-month ADCP field dataset (Figure 12.6).

Figure 12.16 shows a vector plot of hindcast waves, where the vector magnitude is the significant wave height H_s and the vector direction is D_p , which is the direction that waves propagate from (Figure 12.8 shows a similar plot for the 4-month ADCP field dataset). Waves from the 10-year hindcast dataset approached the site from a similar set of directions and with a similar range of magnitudes as waves measured by the ADCP during the 4-month field period.

Table 12.7 shows time that hindcast waves were capable of entraining each sediment grain size ($D_s = 0.1, 0.2, 0.3, 0.4$ and 0.5 mm), expressed as a percentage of the total hindcast period. Table 12.8 shows the same information as Table 12.7 broken down by wave sector, and can be compared with the field period results in the left-hand side of Table 12.4. Waves were capable of suspending 0.1 mm fine sands for 49% of the time, reducing to 17% of the time for coarser 0.5 mm sands (all wave sectors). This is less often than calculated from the ADCP field data period (81% of the time for $D_s = 0.1$ mm, reducing to 36% of the time for $D_s = 0.5$ mm). An explanation is that there is

seasonal variability in the hindcast wave data and the ADCP data were acquired in a season when wave activity was higher. This suggestion is supported by the analysis of the 10-year wave hindcast at site A1, presented in Table 8.8, which showed that the largest mean significant wave height H_s was in winter (1.22 m), followed by autumn (1.09 m), summer (0.97 m) and spring (0.95 m). The ADCP field data were collected during autumn and winter (18 March – 4 August 2008). There were also gaps in the field data when wave heights were low and unable to be detected by the ADCP to sufficient accuracy at the 30 m depth, which will somewhat bias the monthly-average wave height measurements to be slightly higher.

Table 12.9 presents another seasonal analysis of the hindcast wave data, which shows the time that waves were capable of entraining 0.1 mm fine sands, split into seasons and expressed as a percentage of the season duration. The most energetic season was winter (waves were capable of entraining sediment for 62% of the time) followed by autumn (53%), spring (45%) and summer (33%).

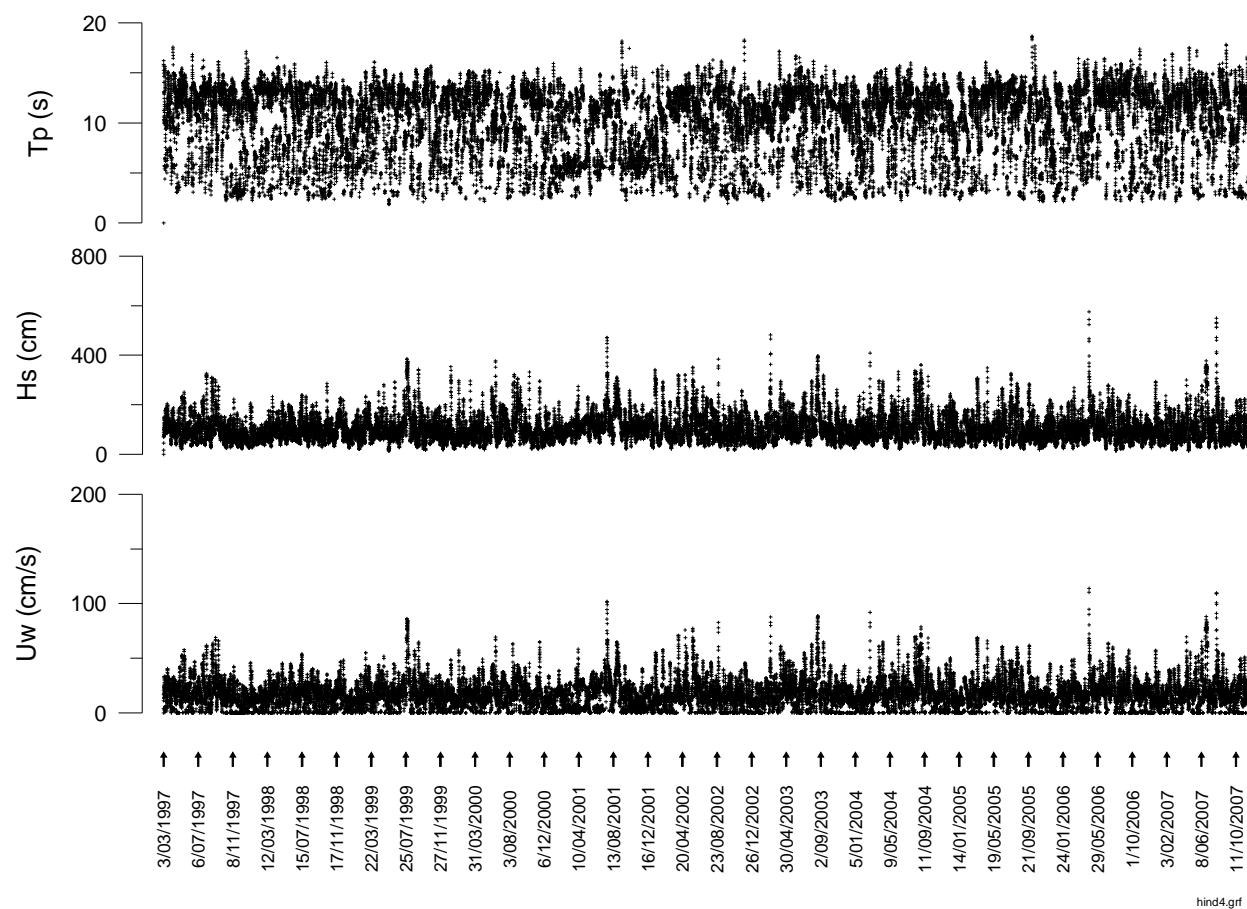


Figure 12.14: Hindcast wave data (peak period T_p and significant wave height H_s) and calculated wave-orbital speed (U_w) at the bed over a 10-year period at site A1.

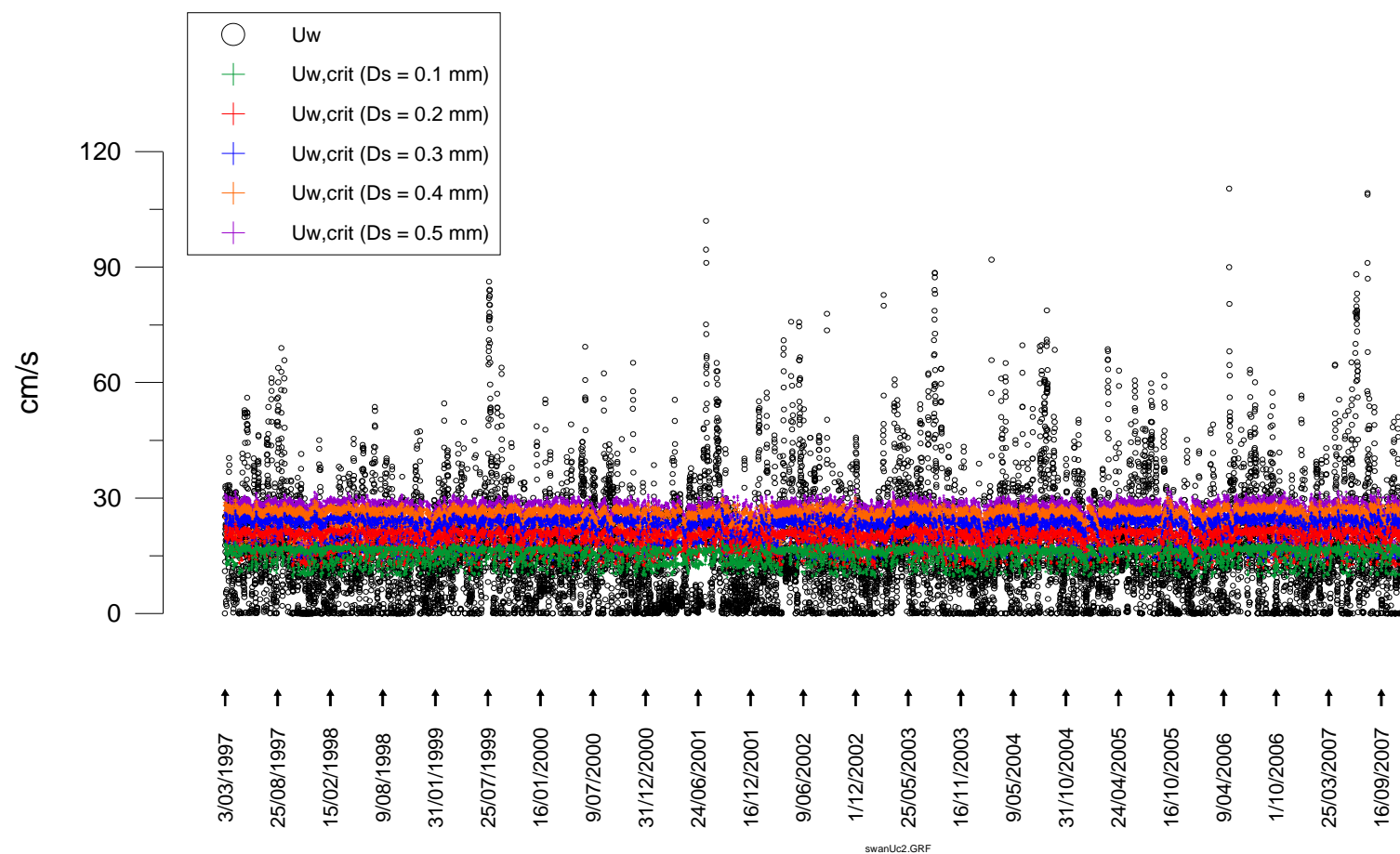


Figure 12.15: A comparison of the critical wave-orbital speed for all grain sizes with the wave-orbital speed at the bed U_w calculated from the 10-year wave hindcast at site A1.

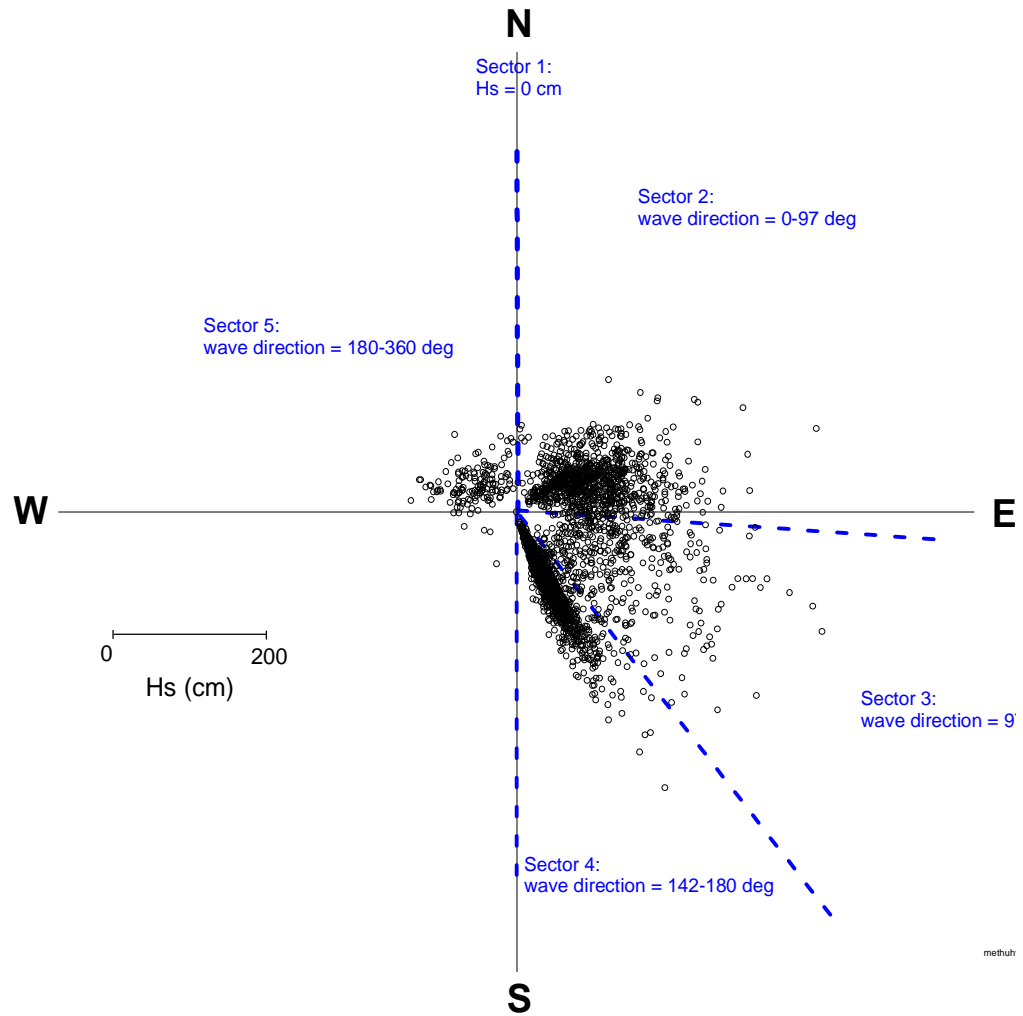


Figure 12.16: Vector plot of hindcast waves, where the vector magnitude is H_s and the vector direction is D_p , which is the direction that waves propagate from.

Table 12.7: Percentage of total time sediment is entrained at A1 by 10 years of hindcast waves.

D_s (mm)	Percentage of total time
0.1	49
0.2	33
0.3	24
0.4	19
0.5	17

Table 12.8: Percentage of total time sediment is entrained at A1 by 10 years of hindcast waves, broken down by wave direction sector (Fig. 12.16).

D_s (mm)	Sector			
	2	3	4	5
0.1	10	7	32	0
0.2	7	6	20	0
0.3	5	5	14	0
0.4	4	4	11	0
0.5	4	4	9	0

Table 12.9: Percent of total time waves are capable of entraining 0.1-mm fine sands at A1, broken down by season and expressed as percentage of the season duration.

Season			
Summer	Autumn	Winter	Spring
33%	53%	62%	45%

12.4 Sand transport through the preferred disposal site A0

12.4.1 Four-month 2008 field period

Sediment transport at site A0 (the preferred disposal site) for the period spanned by the ADCP deployment at site A1 was estimated by the method described in Appendix II (Section 16.2). Wave height, period and direction measured at site A1 by the ADCP during the 2008 field period were assumed to apply without modification to the site A0, which is in the general vicinity of A1, 3 km away. However, the conversion of wave heights and periods to wave orbital speeds at the bed was computed with a water depth that was 2.5 m less than the water depth measured by the ADCP at site A1, to account for the shallower depth on top of the submergent Peninsula Spit. This means for any combination of significant wave height and wave period, that the near-bed wave orbital speeds will be somewhat higher at site A0 compared to A1 (Figure 12.17).

Current speed and direction at site A0 were predicted by the DHI MIKE-3 (FM) hydrodynamic model (described in Chapter 10) that covered the entire 2008 field deployments at A1.

Figure 12.18 shows a vector plot of currents at site A0 predicted by the offshore hydrodynamic model (compare with Figure 12.9, which shows a similar plot for currents measured at site A1). The principal directions of the current vectors were oriented approximately to the north and southeast, but overall elongated towards the north. In contrast, the current ellipse at site A1 was oriented roughly northwest–southeast, and was more symmetrical in either direction, but with a net current bias to the southeast as shown by Bell and Hart (2008).

Figure 12.19 shows a progressive vector plot formed from the current speed and direction at site A0, predicted by the offshore hydrodynamic model (compare Figure 12.10, which shows the same plot for currents measured at site A1, but note that the scales are different in the two figures). The net (residual) current was directed firmly to the north. This contrasts sharply with the net current at site A1, which was directed to the southeast. The magnitude of the net current at site A0 was also much greater than the magnitude of the net current at site A1.

Figure 12.20 shows progressive vector plots for the current formed from the current speed and direction at site A0 (predicted by the DHI model) over each of 10 individual “events”, defined as periods when waves were more-or-less continuously capable of entraining 0.1 mm grain size bed sediment. The equivalent progressive current vector plots for A1 from Figure 12.11 are also shown in Figure 12.20 to contrast the differences between the two disposal site options. The ten wave events are defined in Figure 12.12 above. The net (residual) current at A0 over the duration of each wave event was typically towards the north, which contrasts sharply with the result for site A1 (net residual current over the duration of each event typically to the southeast).

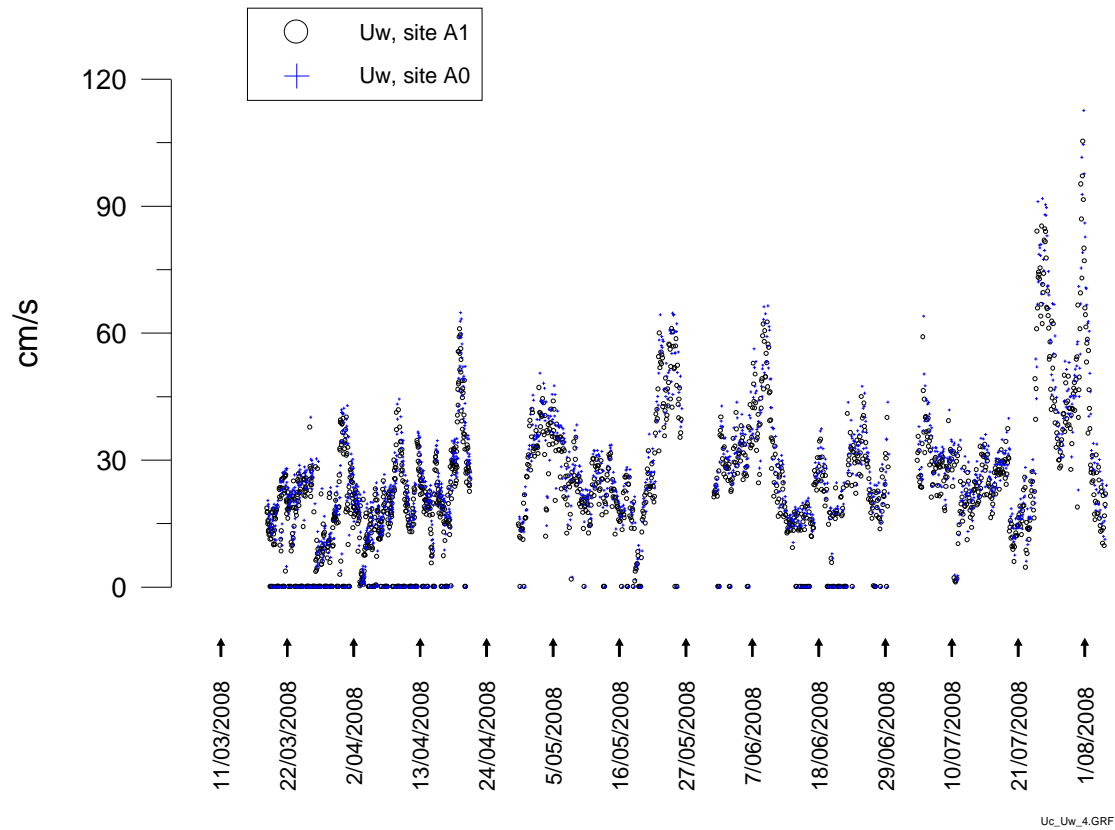


Figure 12.17: Comparison of wave orbital speeds U_w at site A1 (estimated from measured ADCP data) and U_w at site A0 (wave height and period measured at site A1 by the ADCP assumed to apply without modification except for conversion to wave orbital speeds using a water depth that was 2.5 m less than the water depth at site A1).

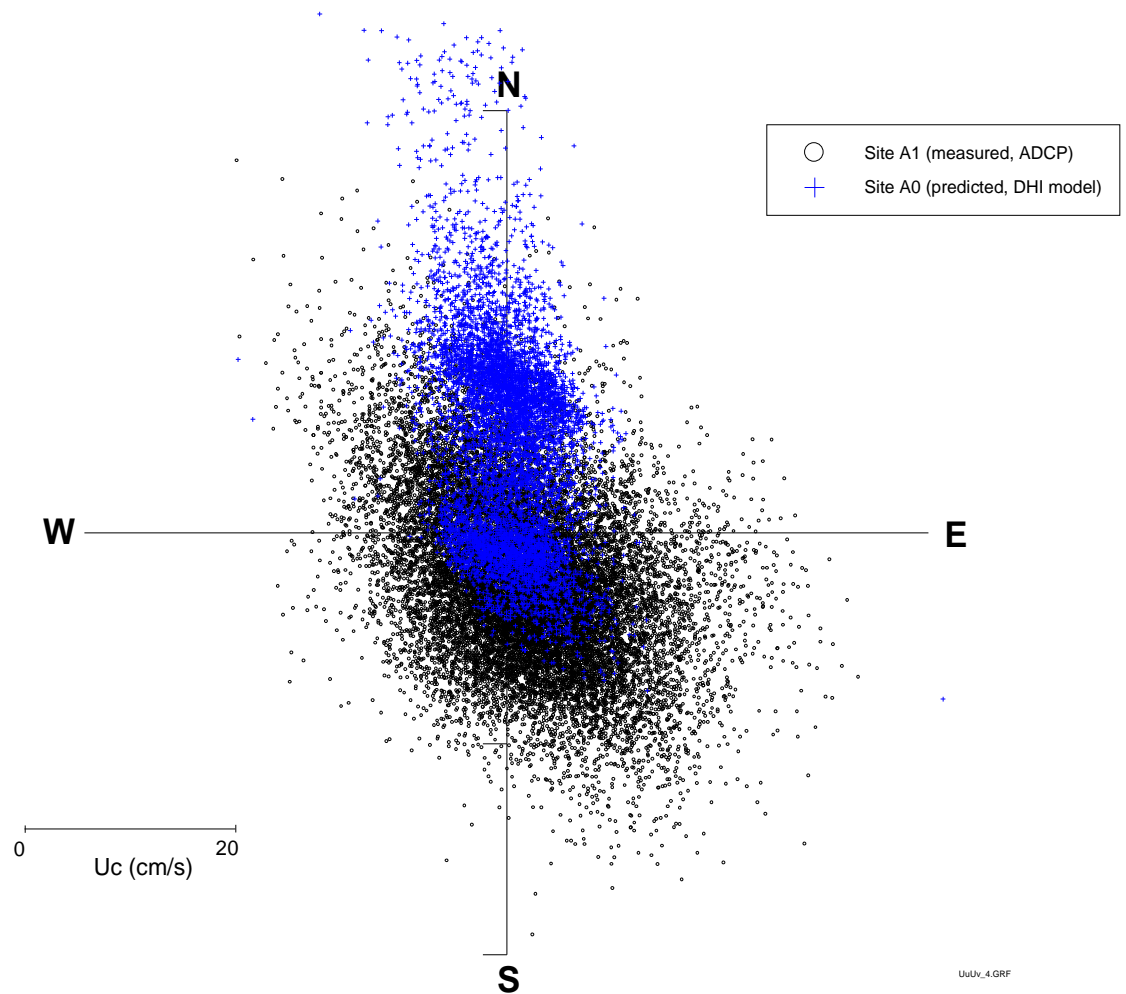


Figure 12.18: Vector plot of currents at site A0, predicted by the offshore hydrodynamic model (small coloured crosses), compared to the current vectors from Figure 12.9 that were measured at site A1 (black dots).

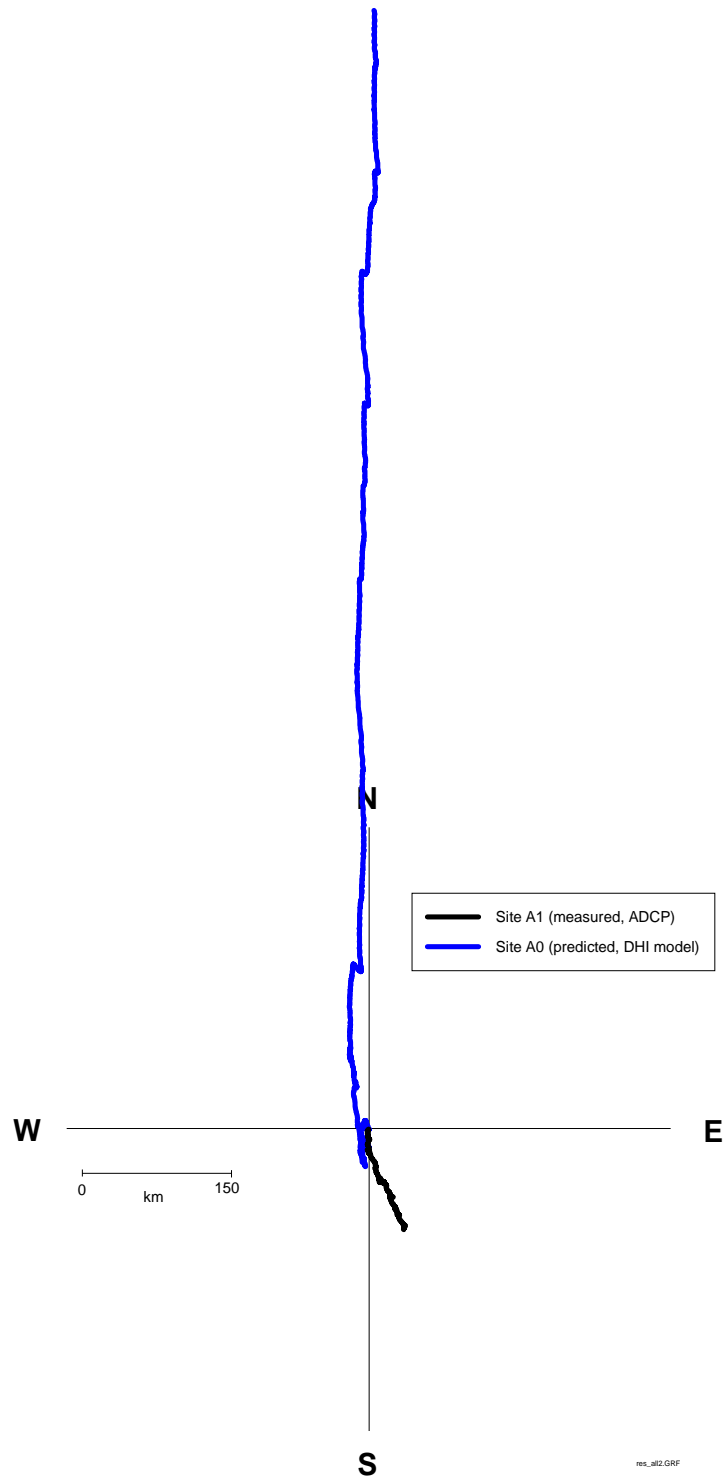


Figure 12.19: Residual (net) current trace formed from the current speed and direction at site A0 (coloured line) predicted by the hydrodynamic model, which is plotted with the measured residual current trace from A1 (black line) shown in Figure 12.10, both covering the 2008 field period. (Note: the length scale is different than Figure 12.10).

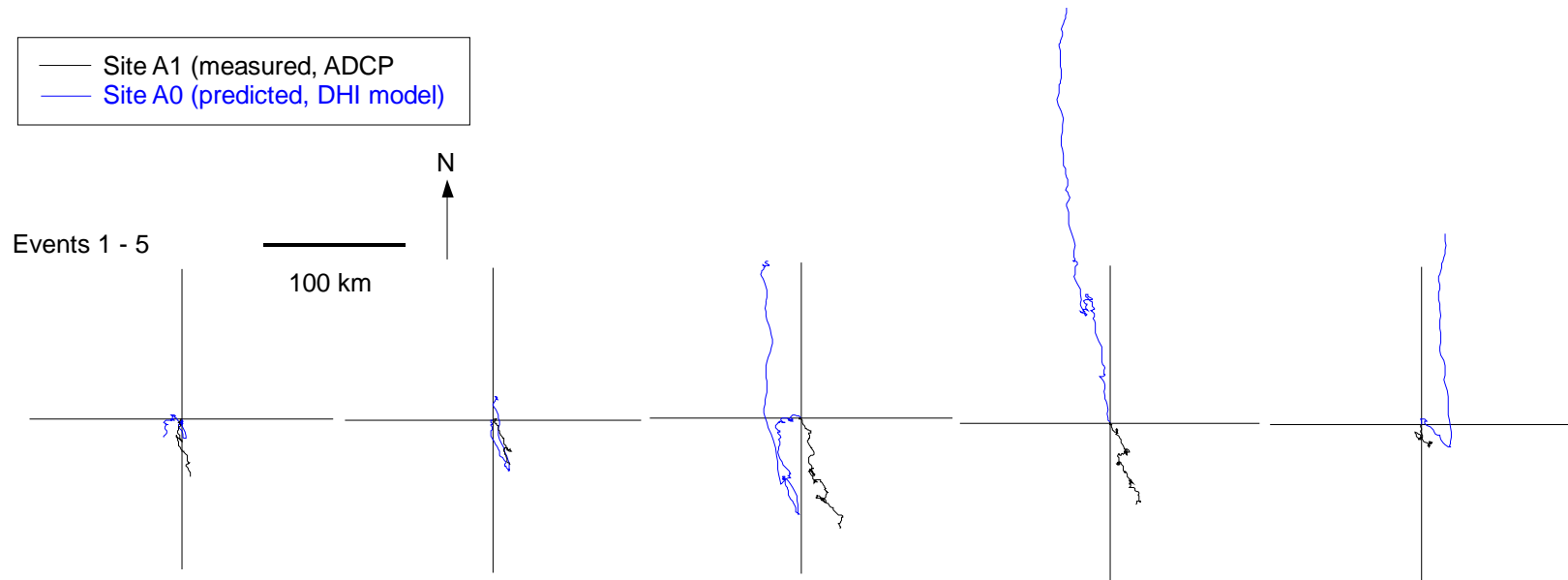


Figure 12.20: (Continued on next page). Residual current plot formed from the current speed and direction at site A0 (predicted by the DHI model), over each of 10 individual “events” defined as periods when waves were more-or-less continuously capable of entraining 0.1 mm grain size bed sediment, plotted with the residual current traces for the same events at site A1 from Figure 12.11. The events are defined in Figure 12.12.

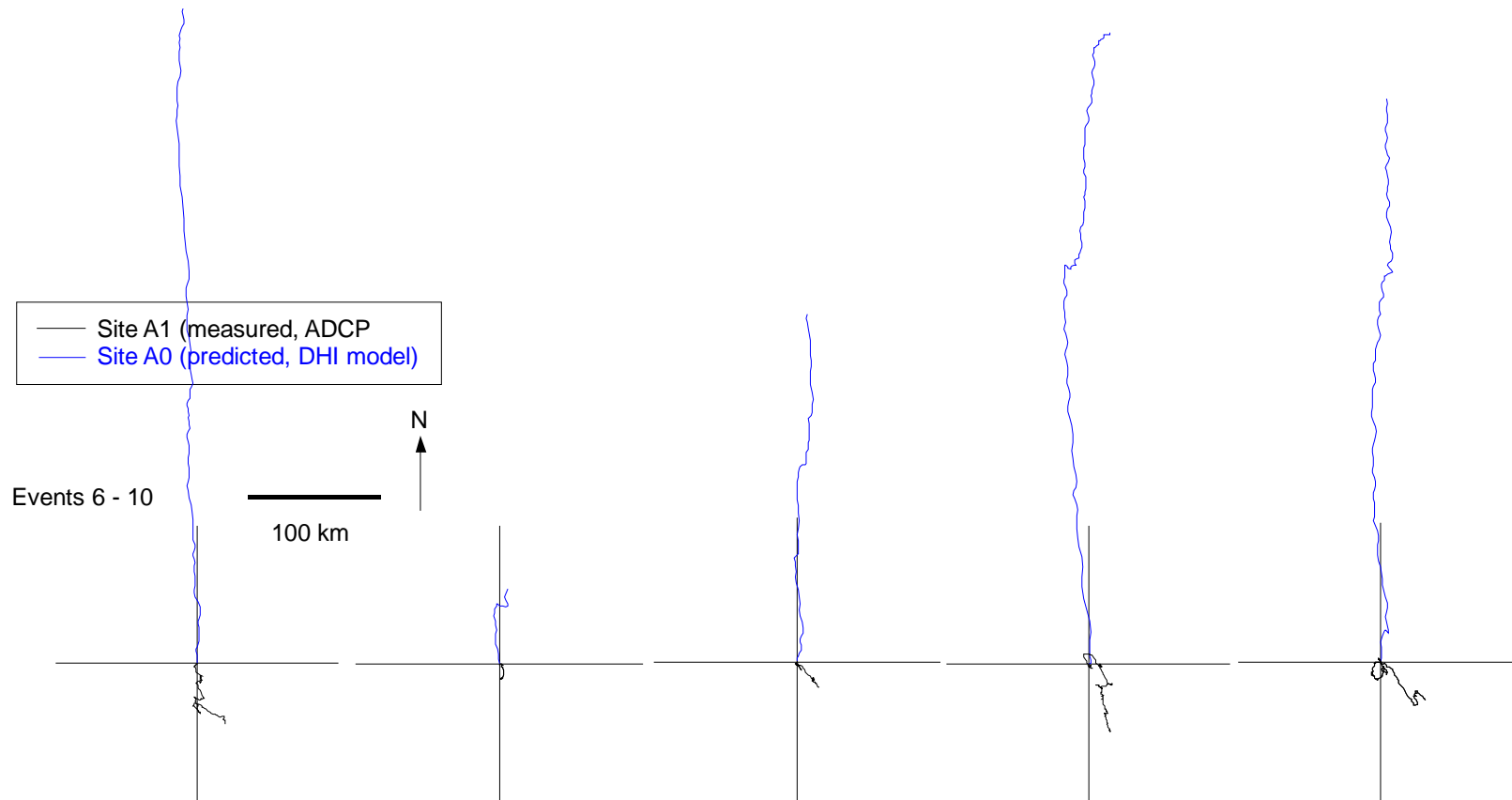


Figure 12.20: (Continued from previous page). Residual current plot formed from the current speed and direction at site A0 (predicted by the DHI model), over each of 10 individual “events” defined as periods when waves were more-or-less continuously capable of entraining 0.1 mm grain size bed sediment, plotted with the residual current traces for the same events at site A1 from Figure 12.11. The events are defined in Figure 12.12.

The “gross” sediment transport at site A0 over the entire 4-month 2008 field period is shown in Table 12.10 for each sand size calculated by each sediment-transport model (Rouse and Nielsen). (Similar information for site A1 is shown in Table 12.5).

The corresponding “net” transport at site A0, taking into account the direction of sediment transport in the summation, is shown in Table 12.11 for each sediment grain size calculated by each model (Rouse and Nielsen). (Similar information for site A1 is shown earlier in Table 12.6).

Sediment transport rates are larger at site A0 compared to site A1, for two reasons: the larger bottom-orbital speeds at the shallower site A0 mobilize more bed sediment; and the stronger currents offshore transport more resuspended sediment.

The other key finding (comparing Tables 12.10 and 12.11) is that the “net” sediment transport at A0 is very close to the “gross” transport (97+%), implying there is very little sediment transport in any other direction apart from towards True North. This compares with site A1 (Tables 12.5 and 12.6), where the “net” is 62–68% of the “gross” transport (depending on the sediment model used), implying there are more occurrences of sediment transport in different directions than the prevailing SSE transport direction. The strong net tendency for northwards transport from A0 is confirmed by Figures 12.21a and 12.21b, which show progressive vector plots of sediment transport formed from the Nielsen and Rouse predictions (respectively) of $MAG[\vec{\Phi}]$ and $DIR[\vec{\Phi}]$ for 0.1 mm fine sands for each of the 10 individual events in the 2008 field period (defined in Figure 12.12 above). Similar information for site A1 is shown in Figures 12.13a and 12.13b (note the various different scales). As was the case for site A1, the two models show similar net transport directions, however the transport magnitudes are different. In contrast to site A1, where for most events the net transport was to the southeast, for most events at site A0 the net transport was to the north.

Consequently, there is more surety of the direction of long-term sediment transport for a disposal site at A0, compared to site A1 closer inshore, with transport predominantly to the north along the submergent Peninsula Spit.

However, the rate of sediment transport is much more difficult to quantify. Estimates are very sensitive to current speed and wave-orbital speed, as exemplified by the large differences of one to two orders of magnitude between the Rouse and Nielsen sediment-transport models in Tables 12.10 and 12.11 (similarly for site A1 in Tables 12.5 and 12.6). The predicted “net” sediment transport rate for the finer 0.1 mm sands is likely to lie somewhere between these two estimates of 0.06 Mt and 1.5 Mt through a 2-km wide E-W section of the disposal area at A0 over the 4-month field period

(Table 12.11). For a 0.3 mm grain size, the two different “net” estimates would be closer together, but much smaller at 0.002 Mt and 0.02 Mt for Rouse and Nielsen models, respectively.

This compares with the total disposal of 7.06 Mm³ of sediment for the 15-m Harbour channel option, which, allowing for an initial loss during disposal due to water-column dispersion, and assuming a wet bulk density of 1300 kg/m³ for newly-settled sediments on the seabed, and taking into account the wider dispersal of finer sediments, leads to an estimated total weight of approximately 8 Mt. In comparing the estimated “net” sediment transport rates above with this total mass of disposed dredged material, one cannot simply divide the 8 Mt by the net rate to obtain the time for the mound to deflate. It needs to be recognized that sediment transport through the 2-km wide cross section of the disposal area also includes transport of “natural” seabed sediments derived from upstream (i.e., south) of the disposal area, so the transport rate wouldn’t solely be derived from the dredged material. This is covered in Section 12.5.2.

Any further refinement in quantifying sediment transport rates would require field experiments on the seabed using instrumented tripods to measure bedload and suspended-sediment load directly under a variety of wave and current conditions to “locally” calibrate a sediment transport model for the area.

Table 12.10: Φ , the “gross” sediment transport (over the 4-month 2008 field period) in grams per unit cm width, and Φ multiplied by the dredge disposal mound width of 2 km using two sediment transport models for various sand grain sizes (D_s) and associated settling velocities (W_s). These are results for site A0; see Table 12.5 for results for site A1. Note: 1 g/cm width sediment transport is equivalent to 0.1 kg/m width.

		Rouse model		Nielsen model	
D_s (mm)	W_s (cm/s)	Φ (g/cm)	$\Phi \times \text{mound width}$ (tonnes)	Φ (g/cm)	$\Phi \times \text{mound width}$ (tonnes)
0.1	0.64	302,089	60,417	7,844,195	1,568,839
0.2	1.88	20,537	4,107	475,485	95,097
0.3	3.25	7,856	1,571	100,306	20,061
0.4	4.75	4,135	827	33,732	6,746
0.5	6.38	2,531	506	14,540	2,908

Table 12.11: Magnitude and direction ($MAG[\vec{\Phi}]$ and $DIR[\vec{\Phi}]$) of the “net” sediment transport in grams per unit cm width over the 4-month 2008 field period, and $MAG[\vec{\Phi}]$ multiplied by a nominal disposal mound width of 2 km to provide estimates of sediment transport in tonnes through the entire disposal mound. These are results for disposal site option A0; see Table 12.5 for corresponding results for disposal site option A1. Note: 1 g/cm width sediment transport is equivalent to 0.1 kg/m width.

		Rouse model			Nielsen model		
D_s (mm)	W_s (cm/s)	$MAG[\vec{\Phi}]$ (g/cm)	$DIR[\vec{\Phi}]$ (° N)	$MAG[\vec{\Phi}] \times$ mound width (tonnes)	$MAG[\vec{\Phi}]$ (g/cm)	$DIR[\vec{\Phi}]$ (° N)	$MAG[\vec{\Phi}] \times$ mound width (tonnes)
0.1	0.64	296,655	356	59,331	7,621,729	358	1,524,345
0.2	1.88	19,852	357	3,970	462,029	358	92,405
0.3	3.25	7,584	358	1,516	97,467	358	19,493
0.4	4.75	3,991	358	798	32,776	358	6,555
0.5	6.38	2,444	358	488	14,128	358	2,825

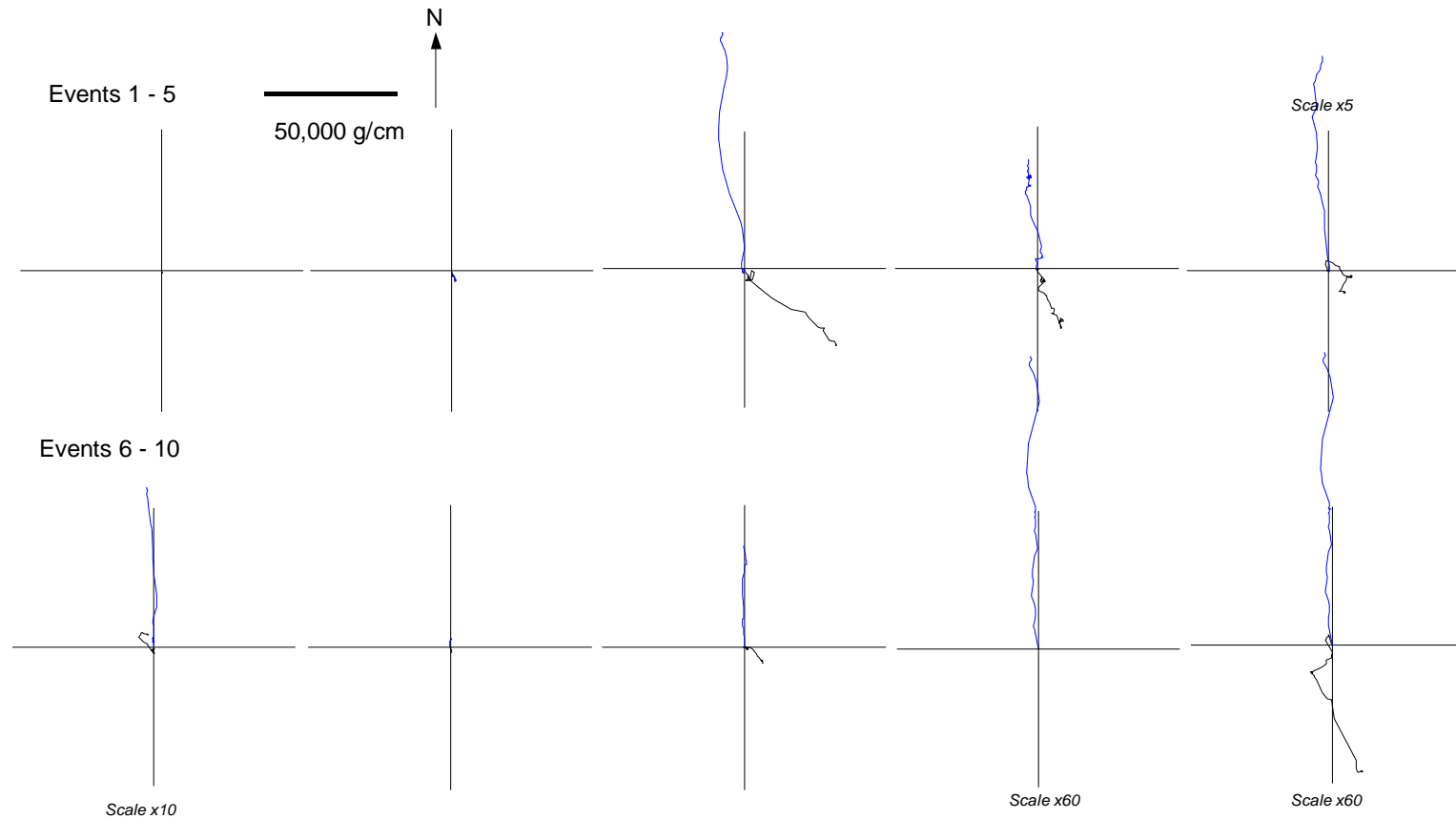


Figure 12.21a: Progressive vector plot formed from Nielsen prediction of sediment transport $MAG[\vec{\Phi}]$ and $DIR[\vec{\Phi}]$ for 0.1 mm grain size bed sediment for each of the 10 individual events defined in Figure 12.12. The results for site A0 (blue traces) are generally heading north and are compared with the equivalent black traces from site A1 (Figure 12.13a). Note: the various different scales for event Nos. 5, 6, 9, 10.

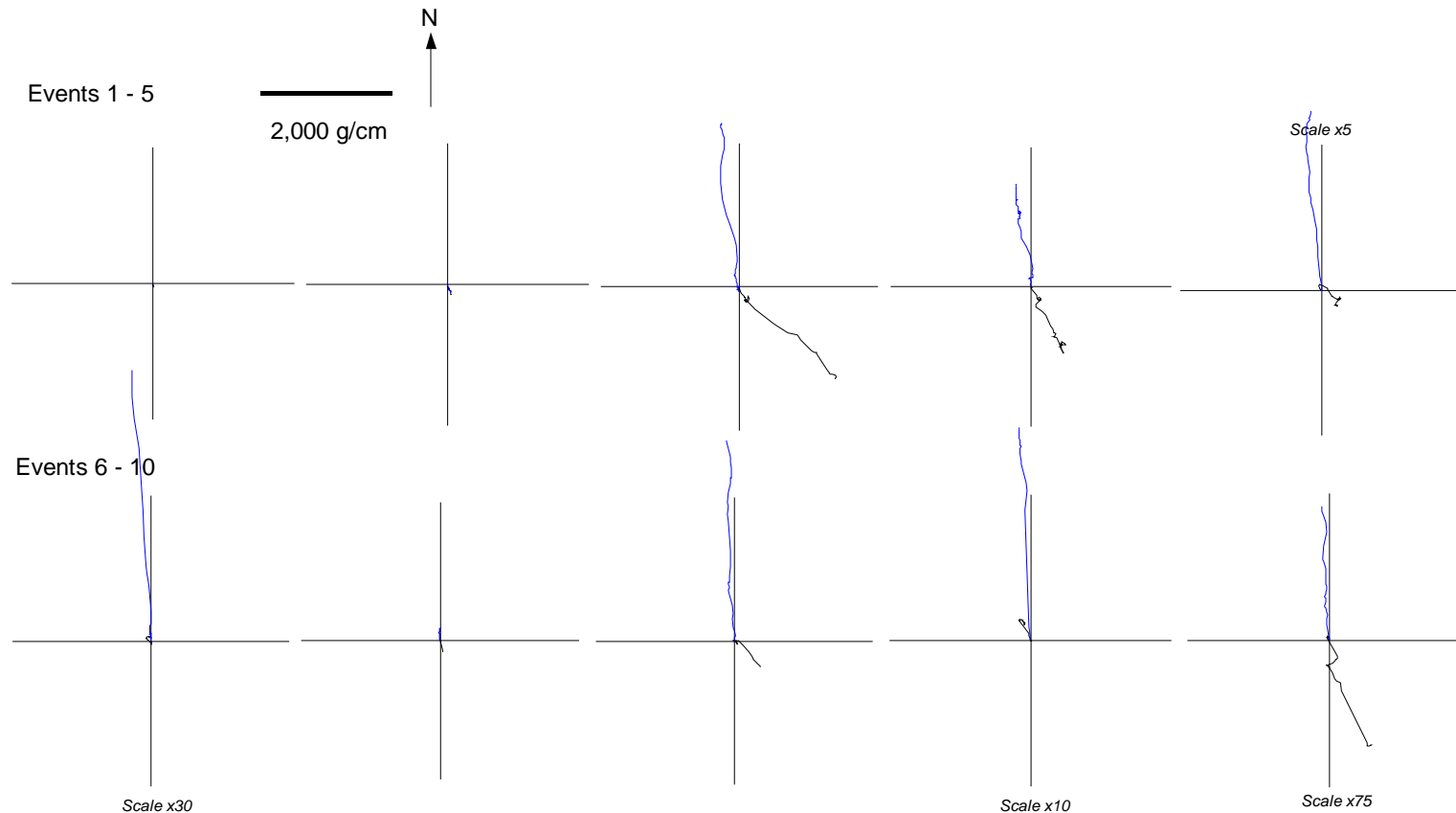


Figure 12.21b: Progressive vector plot formed from Rouse prediction of sediment transport $MAG[\vec{\Phi}]$ and $DIR[\vec{\Phi}]$ for 0.1 mm grain size bed sediment for each of the 10 individual events defined in Figure 12.12. The results for site A0 (blue traces) are generally heading northland are compared with the equivalent black traces from site A1 (Figure 12.13b). Note: the various different scales for event Nos. 5, 6, 9, 10.

12.4.2 10-year wave hindcast estimates of active sand transport occurrences at A0

In order to estimate long-term occurrences of wave activity on sediment transport at the preferred disposal site A0, wave statistics were extracted from the 10-year hindcast of the wave climate using the SWAN model and processed in a similar manner to that outlined in Section 12.3.2 for the ADCP site A1, except the depth of water was set to 27 m (2.5 m shallower than the wave hindcast analysis for A1).

Figure 12.22 shows a comparison of the critical wave-orbital speeds, calculated from the hindcast dataset at site A0, for all grain sizes on the one graph. Wave-orbital speeds at site A0 were frequently capable of mobilizing and resuspending all grain sizes, which was also the case with the hindcast data for site A1 (Figure 12.15). The A0 site was in slightly shallower water, thus the wave-orbital speeds were slightly stronger at the bed due to slightly less attenuation of the wave energy.

Figure 12.23 shows a vector plot of hindcast waves at site A0, where the vector magnitude is the significant wave height H_s and the vector direction is the peak-energy wave direction D_p , which is the direction that waves propagate from (Figure 12.16 shows a similar plot for the hindcast data from site A1). Waves from the 10-year hindcast period approached site A0 from a similar grouping of directions and with a similar range of magnitudes as hindcast waves at site A1 closer to Otago Heads. The only real differences were waves during the hindcast period approached site A0 from a slightly more southerly direction and were slightly larger.

Table 12.12 shows the occurrence of waves at site A0 during the 10-year hindcast that were capable of mobilizing each of the five sand sizes (0.1, 0.2, 0.3, 0.4 and 0.5 mm), expressed as a percentage of the total hindcast period. Table 12.13 shows the same information as Table 12.12 broken down by wave sector. Waves were capable of suspending 0.1 mm sediment for 55% of the time, reducing to 23% of the time for 0.5 mm sands (considering all wave sectors). This is a larger percentage of time than calculated from the hindcast period at the closer inshore site A1 by between 6–9% higher. This is because site A0 is in slightly shallower water, meaning wave-orbital speeds at the bed are slightly stronger (due to less attenuation of wave energy) and waves are therefore capable of entraining sands for more of the time plus slightly higher waves approach from the south (Sector 4 in Table 12.13).

Table 12.14 presents a seasonal analysis of competent waves at A0 from the hindcast period, which shows the time that waves were capable of mobilizing 0.1 mm sand and expressed as a percentage of the season duration. The most energetic season at site A0 was winter (waves were capable of mobilizing and resuspending sediment for 68% of the time) followed by autumn (61%), spring (53%) and summer (42%), which is the

same pattern as at site A1. However waves at A0 are more competent at entraining sand sizes as shown by a higher percentage of occurrences for all seasons at the preferred disposal site A0 in comparison to site A1 (Table 12.9). This is mainly due to site A0 being shallower by 2.5 m than A1 and the slightly higher southerly waves.

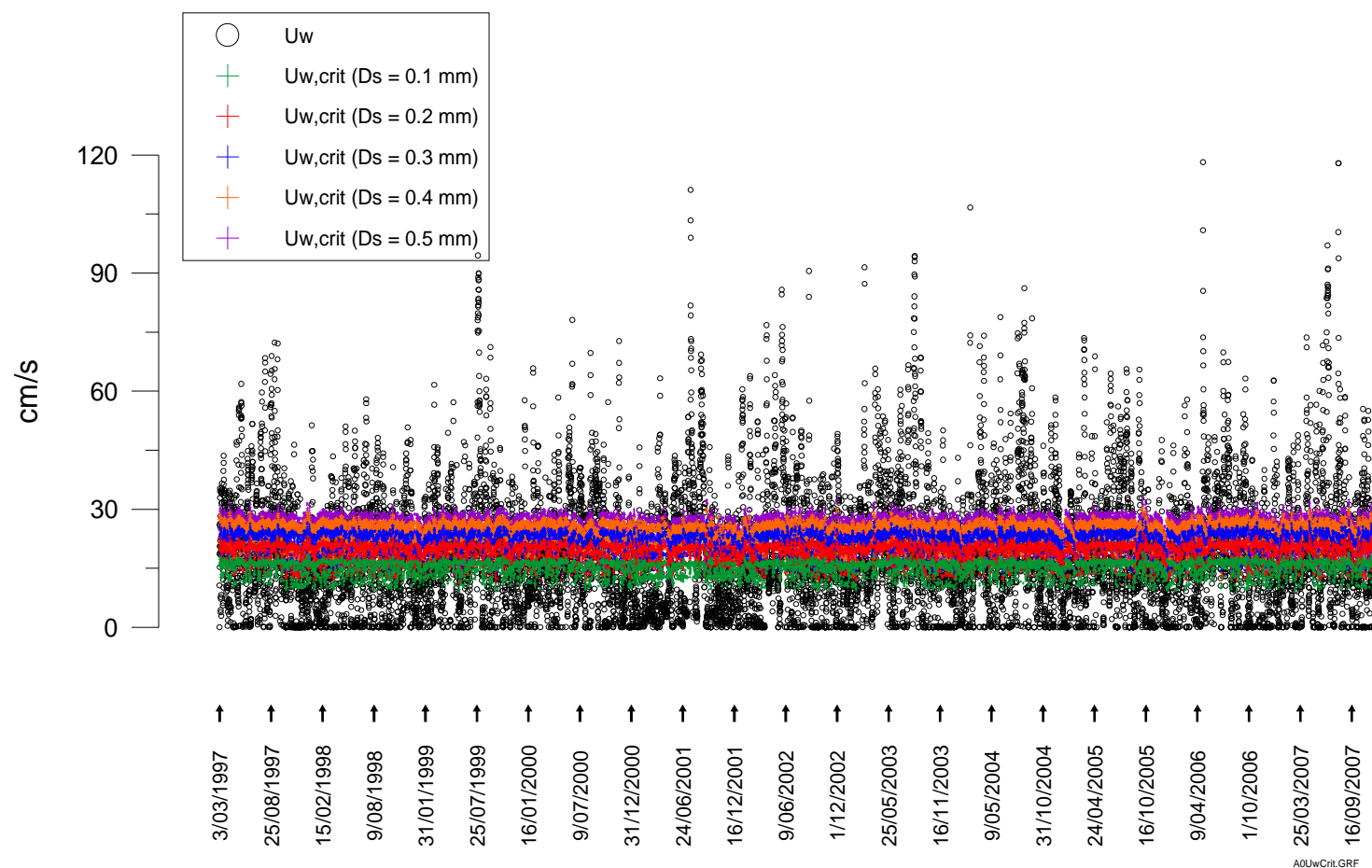


Figure 12.22: A comparison of the critical wave-orbital speed for all five grain sizes with the wave-orbital speed at the bed U_w calculated from the 10-year wave hindcast at site A0. Note: wave orbital speeds above the relevant coloured band will resuspend that grain size.

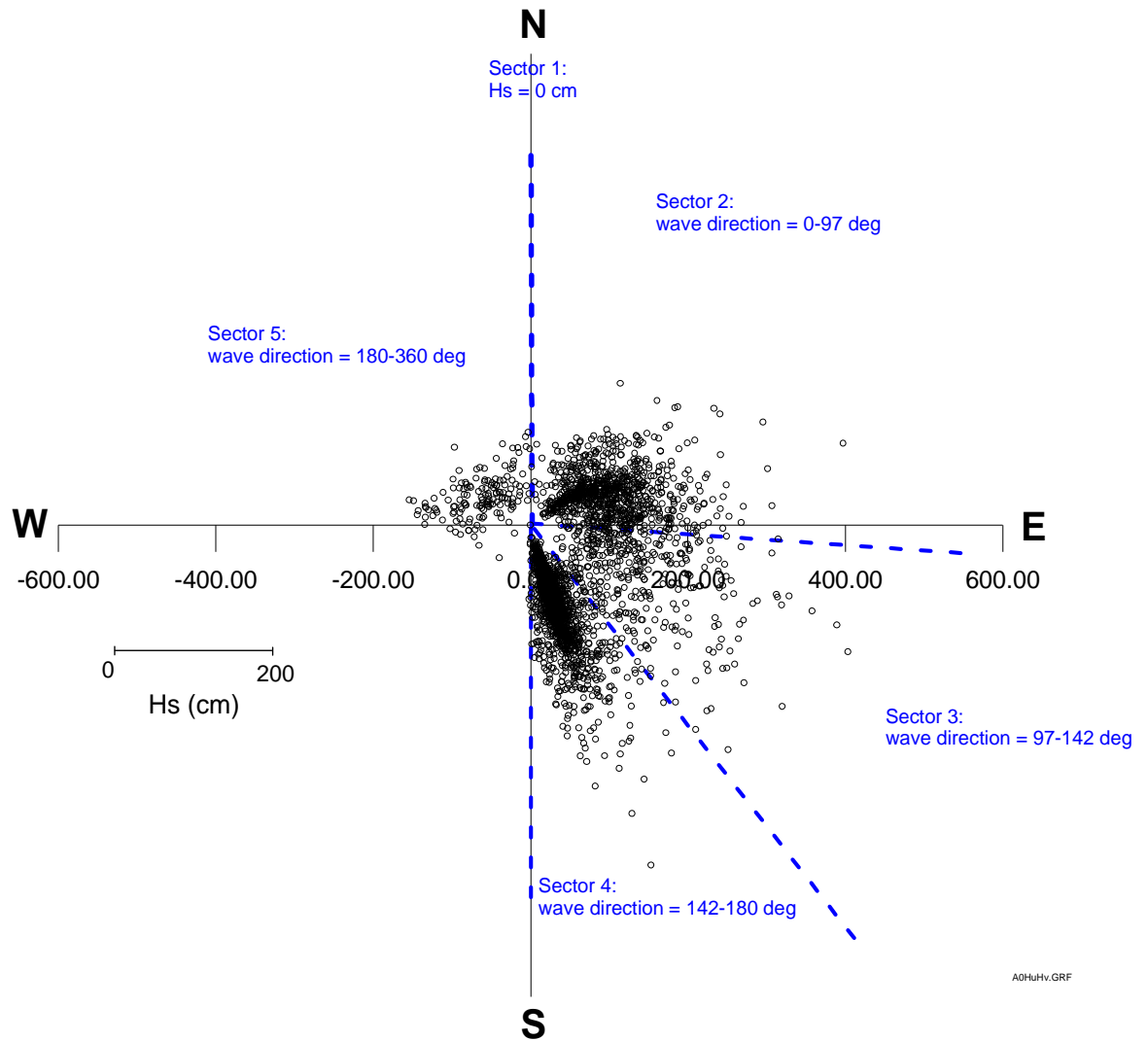


Figure 12.23: Vector plot of hindcast waves at site A0, where the vector magnitude is the significant wave height H_s and the vector direction is D_p , which is the direction that waves propagate from.

Table 12.12: Percentage of total time sediment is resuspended at A0 by 10 years of hindcast waves.

D_s (mm)	Percentage of total time
0.1	55
0.2	41
0.3	33
0.4	27
0.5	23

Table 12.13: Percentage of total time sediment is resuspended at A0 by 10 years of hindcast waves, broken down by wave-direction sector (Fig. 12.23).

Sector				
D _s (mm)	2	3	4	5
0.1	11	7	37	0
0.2	8	6	27	0
0.3	7	6	20	0
0.4	6	5	16	0
0.5	5	5	13	0

Table 12.14: Percent of total time waves are capable of resuspending 0.1-mm fine sands at A0, broken down by season and expressed as percentage of the season duration.

Season			
Summer	Autumn	Winter	Spring
42%	61%	68%	53%

12.5 Comments on long-term sand transport from the disposal mound

12.5.1 Direction of sediment movement

One of the key findings of the sediment transport analysis for sand-sized sediments is that the “net” sediment transport at A0 is very close to the “gross” transport (97+%), implying there is very little sediment transport that would occur in any other direction apart from towards True North. Therefore, there is more surety of the direction of long-term sediment transport for a disposal site at A0, than sites such as A1 closer to the coast, which would be predominantly to the north along the submergent Peninsula Spit.

An indication of where sand-sized sediments (sourced from the disposal mound at A0), could move to can be inferred from the suspended-sediment plume modelling of the disposal over the dredging season (Chapter 11). After being initially deposited on

the disposal mound, sand-sized material, particularly the finer sands (0.1–0.2 mm)¹⁹, can only be re-mobilized again by waves of sufficient height and period and then transported short distances by the near-bed current velocity operating at the time, before settling again. Sediment transport comprises both bedload (sand grains rolling or hopping along the bed) and suspended-load (where the settling velocity provides a strong pull back towards the seabed). So, while much of the sand transport on the shelf occurs relatively close to or on the seabed, the modelling of suspended plumes of sand discussed in Chapter 11 will produce a longer and wider zone of influence because the sediment was released from 5 m below the surface. However, despite these differences for the source location in the water column, the settling of sand-sized material is relatively quick, so the plume-modelling results provide a conservative (overestimate) of the zone of influence, relative to sands re-mobilized from the disposal mound at A0. Figure 12.24 shows zones for various accumulated deposition rates from the disposal plume modelling for both silt and sand sizes (Chapter 11) over a continuous 120-day dredging programme for the 15-m Harbour channel. The dominance of the northward transport is clearly illustrated. The larger deposition rates above 0.4 mm/day, will be where most of the sands deposit (rather than the silts which disperse much further) and therefore are indicative of the long-term (months to year timescales) transport pathway and extent of transported sand that has been sourced and re-mobilized from the seabed off a disposal mound at A0. Some sand particles sourced from the mound at A0 may also reach the longer 0.08 mm/day zone shown on Figure 12.24 if they remain for long periods in suspension or over periods of years, but most sand particles reaching this zone would be sourced from further “downstream” (or to the north) of A0, as resuspension of sand particles occurs ubiquitously on the seabed during moderate to high wave events irrespective of whether they are from the dredged material or “native” sands.

This dominant northward sediment pathway matches very closely with the alignment of the incumbent geomorphological feature (Peninsula Spit), which is outlined by the 30 m depth contour in Figure 12.24, with depths of 25–29 m. This submergent spit, has evolved over the Holocene from the prevailing sediment and hydrodynamic processes that operate in this offshore zone and major sediment sources from the Clutha River and to a much lesser extent the Taieri River (Carter, 1986). Therefore, it will continue to build out to the north and remain detached from the nearshore coastal system.

Given the results from the sediment transport analysis and the above reasoning based on inferences from the plume modelling for sand-sized material and the morphology of the offshore Spit, it is very unlikely that sand-sized material from the disposal mound at A0 would reach the nearshore zone (depths <20 m), other than isolated grains.

¹⁹ which would make up about 40-50% of the sand component of the dredged material

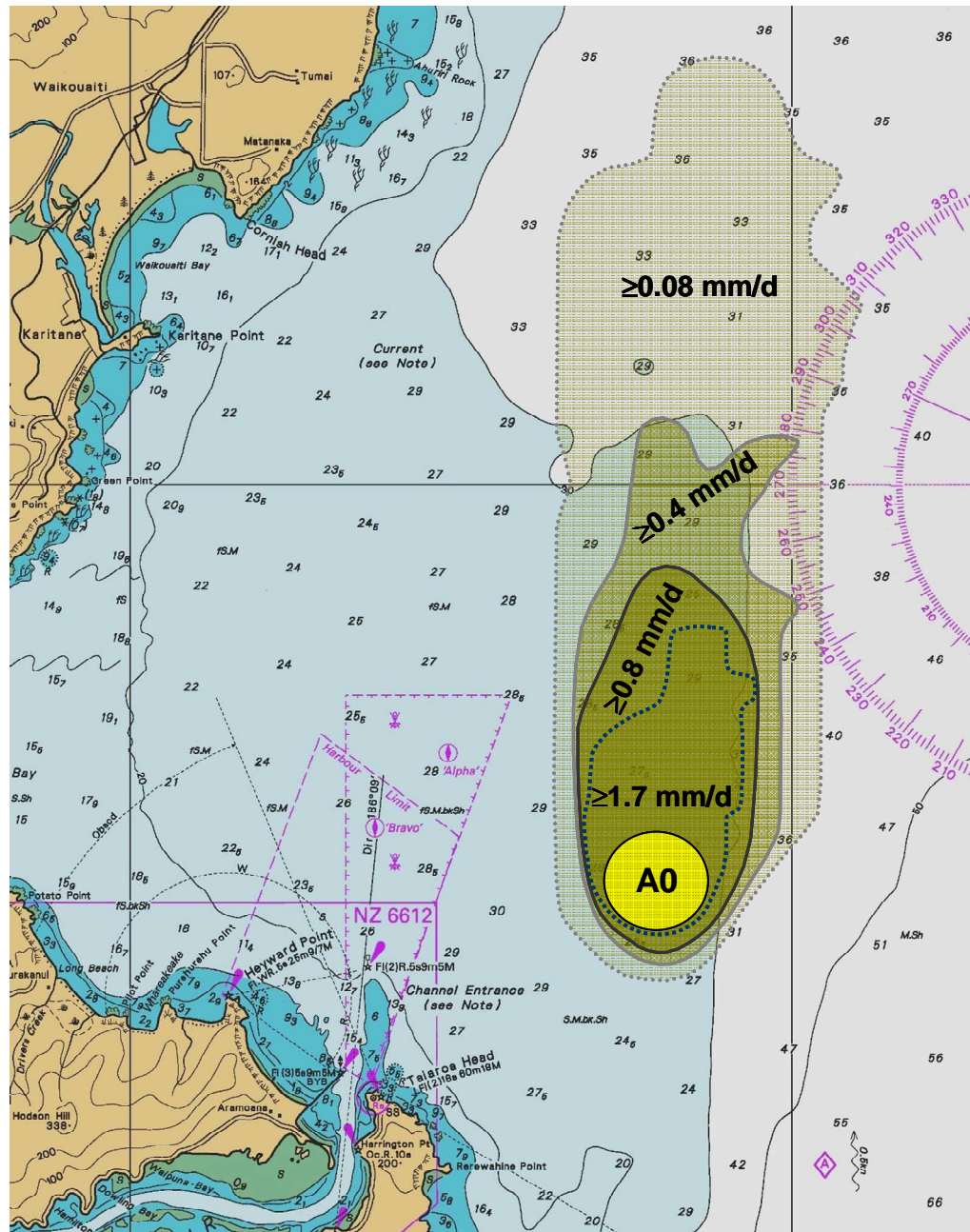


Figure 12.24: Zones within which various average deposition rates (mm per day) are exceeded for all sand/silt fractions from the disposal plume modelling (Chapter 11) over the entire dredging programme (final channel design). The inner zones out to the 0.4 mm/d zone boundary are indicative of the transport pathway and extent of sand transported through the disposal mound at A0. The transport pathway also matches closely with the alignment of the incumbent geomorphological feature (Peninsula Spit) that is marked out by the light-blue 30-m depth contour shading, providing further confidence that the modelled net sediment transport direction is reliable. [Source of background map: Chart NZ661, LINZ].

12.5.2 Transport rates and deflation of the disposal mound

Based on analysis of near-bed currents and wave from the 4-month field monitoring programme at site A1 (30 m depth), currents acting alone are insufficient most of the time to resuspend fine sands with grain sizes of 0.1 mm or more. This applies also to site A0, although there will be a few occurrences when stronger currents are present to mobilize sands independent of waves. Therefore generally sand transport on the seabed is only possible when waves generate near-bed orbital motions of sufficient strength (particularly swell) to resuspend sands from the mound and surrounding seabed, which can then be subsequently carried short distances by the near-bed current until the sands settle again. Based on a 10-year hindcast of the wave climate offshore, waves are capable of suspending 0.1 mm fine sands for 55% of the time at the preferred disposal site A0, reducing to 23% of the time for coarser 0.5 mm sands (from all wave directions). There is also a seasonal variation, with the most energetic season being winter (waves were capable of resuspending fine sand at A0 for 68% of the time) followed by autumn (61%), spring (53%) and summer (42%). These frequencies of sand mobilization will be somewhat higher again at the top of the disposal mound at A0.

A mass of approximately 8×10^6 tonnes of sediment is likely to form the initial mound after the 15-m Harbour channel has been dredged, based on an estimated height of 1.6 m and wet bulk density of 1600 kg/m^3 after some initial consolidation. This compares with the net sediment transport through a 2-km section at A0, which would have been in the range of 4,000 to 92,000 tonnes (based on Rouse and Nielsen models respectively—Table 12.11) for the median sand size (0.2 mm) covering the 4-month 2008 field period, which was more energetic than normal in terms of significant wave height.

Over time periods of months and years, the disposal mound will smooth out and deflate gradually from both consolidation and differential erosion (due to higher local wave–orbital and current velocities over the top of the mound). The evolving shape of the mound is likely to show an elongated “tail” on the northern side of the mound from the prevailing “net” sediment transport to the north, but also a smoothing of the southern side-slope of the mound as the bedload fraction of sand transport from upstream (south) is deposited on the flanks of the mound.

An analysis of potential upper and lower bounds on the deflation of the initial mound was undertaken based on the transport rates determined for the 4-month 2008 field period at A0 and using the mass continuity equation. The two bounds were calculated using the following assumptions (see Fig. 12.25), including the mound being composed of material with a single sand grain size:

- lower bound on deflation period—assumed that the “net” sediment transport onto the mound from the south is zero (i.e., the mound blocks the incoming sediment transport completely) and the outgoing sediment transport away from the mound is at the “net” rate calculated at the height of the initial mound (which was set at 1.6 m high) and a second set of estimates using the rate that would apply at the halfway stage, using both Rouse and Nielsen sediment transport models;
- upper-bound on deflation period—assumed that the “net” sediment transport onto the top of the mound from the south is at the rate calculated for the “upstream” seabed level at A0 (see Table 12.11), which would apply if most of the sand transport from upstream occurs as suspended load. The outgoing sediment transport is at the “net” rate calculated relative to the height of the mound (which was set at 1.6 m high initially, changing to 0.8 m after deflation had reached the halfway stage) using both Rouse and Nielsen sediment transport models.

The ranges of lower- and upper-bound estimates to deflate the entire disposal mound in terms of years are listed in Table 12.15. The differential in local sediment transport rates on the top of the mound (in this case 1.6 m) relative to the surrounding “native” seabed at A0 are around 30% higher for the Rouse model and 37% higher for the Nielsen model, which holds for all five grain sizes. While the estimates of the upper and lower-bound estimates of the mound deflation time vary substantially between the Rouse and Nielsen sediment models, the key result from this overview is that the mound will take many years to fully deflate back to the present seabed level at A0, based on using the median sand size of 0.2 mm (highlighted in Table 12.15).

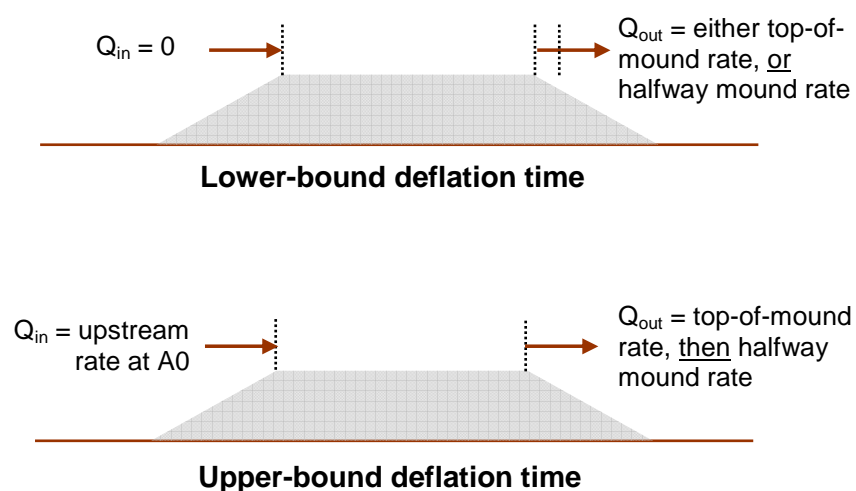


Figure 12.25: Schematic of how the lower- and upper-bound estimates of the disposal mound deflation times were calculated based on various input and output sediment transport rates (Q_{in} and Q_{out}).

Table 12.15a: Lower-bound estimates on mound deflation (years) for the 15-m channel option, with results for the median grain size of the sand component of the dredged material in blue italics.

Grain size (mm)	Deflation based on 1.6 m height (years)		Deflation based on mid 0.8 m height (years)	
	Rouse	Nielsen	Rouse	Nielsen
0.1	39	1	34	1
<i>0.2</i>	<i>580</i>	<i>24</i>	<i>510</i>	<i>21</i>
0.3	1520	115	1340	98
0.4	2900	340	2540	290
0.5	4730	800	4150	680

Table 12.15b: Upper-bound estimates on mound deflation (years) for the 15-m Harbour channel design, with results for the median grain size of the sand component of the dredged material in blue italics.

Grain size (mm)	Deflation based on 1.6 m height initially, then 0.8 m height at half-way stage (years)	
	Rouse	Nielsen
0.1	230	7
<i>0.2</i>	<i>3490</i>	<i>120</i>
0.3	9190	580
0.4	17520	1720
0.5	28330	4010

An optimal time period for placement of dredged material is not obvious since the predominant transport direction to the north is independent of time or season. However, placement of dredged material in autumn or winter would take advantage of a larger wave climate, when compared to the spring and summer, to smooth out the initial mound quicker.

12.6 Comments on long-term silt transport

Modelling the long-term fate of silt-size material (<0.0625 mm), especially the finer fractions (<0.02 mm), is inordinately difficult to achieve because of the computing resources needed to cover the very wide spatial scales and long time scales involved in what is a highly dispersive process due to turbulence, eddies and shear from varying current flow and wind regimes. An indication of the spatial scales that would be involved is shown in Chapter 11 where some of the silt-sized material was still in suspension going through the northern boundary of the hydrodynamic model at Shag Point (35 km north of Taiaroa Head) after just 48 hours of disposal operations.

As discussed in Section 11.4.4, the post-disposal spatial deposition patterns for silt-size classes are only useful to predict an upper-bound on potential environment effects on the benthos as silts will be readily re-mobilised by waves and transported by currents—more so in shallower waters. Initially, deposition of fine silts (Fig. 11.17a, b) would occur over a wide area offshore and to the north mainly (but not Blueskin Bay or Karitane Point area) as expected in a highly dispersive environment with slowly-settling sediments. This contrasts with sandy sediments (Fig. 11.20), where initial deposition occurs well offshore and to the north and north-east of the disposal ground. Initial deposition of silts is low along the limited coastal areas where the suspended-sediment plume edge comes in occasional contact, such as Otago Heads (north of Wickliffe Bay) and the northern coast from Cornish Head northwards (Figs. 11.17–11.18). Where initial deposition is predicted to occur, it would theoretically accumulate to no more than 0.5 mm thick over the course of the dredging programme if no resuspension occurred.

In reality these “deposited” sediments, especially fine and medium silts, will often continue to be re-mobilized by wave activity in shallow coastal waters and further disperse in very low concentrations over a wide area of the Otago shelf, particularly to the north.

The ultimate fate of these widely-dispersed silts in terms of “permanent” deposition is difficult to ascertain, but will be mainly in deeper waters and canyons offshore as exemplified by the deposition of fine terrigenous material from catchment run-off including the Clutha River. There are also preferential natural deposition areas for fine to coarse silts on the shelf such as off Blueskin Bay (Figure 12.26), which possibly arise from the combination of the weak counter-clockwise gyre in outer Blueskin Bay and the loss of momentum in ebb-tide sediment plumes emanating from Otago Harbour towards the north, and hence enhanced settling of coarser silts from the Harbour. Some of the silt material from disposal area A0 could be deposited in this preferential silt zone, but as shown by the disposal plume modelling (Chapter 11), most of the silt material would be dispersed to the north and north-east, with virtually no suspended-sediment plumes sweeping across this preferential silt zone in a 48-hour period after disposal.

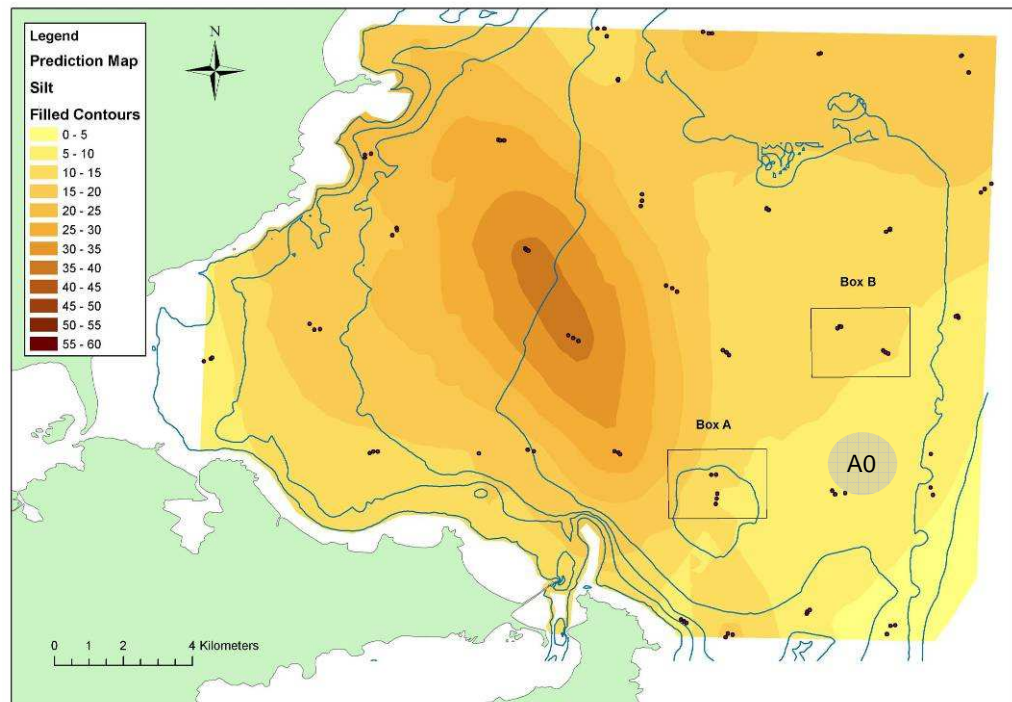


Figure 12.26: Distribution of silt (grain size <0.063 mm) content (%) in the sediments of Blueskin Bay (from Willis et al. 2008). Depth contours are at 5 m intervals from 10 m to 30 m. Box A is disposal area option A1 and Box B is disposal area option A2. The approximate location of the selected disposal area A0 is annotated on the map.

13. Summary and Conclusions

Project Next Generation is an initiative by the Port Otago Ltd. (POL) to expand the capability of Port Chalmers through a substantial channel deepening capital works programme. As part of Project Next Generation, Port Otago Ltd. commissioned NIWA to carry out hydrodynamic, dispersion and sediment transport modelling and MetOcean Solutions to undertake wave modelling to support the assessment of environmental effects likely to occur during and after dredging operations.

An initial design of the dredged channel (e.g., depths, side batter slopes and layout) was developed by POL in June 2008 to handle 8000 TEU size vessels.²⁰ This requires a channel base depth of 15 m below Chart Datum²¹ from Port Chalmers to the commencement of Harington Bend, thereafter progressively deepening until it reaches a 17.5 m (Chart Datum) in the outer approach channel. This deeper section is to allow for vessel motions arising from combinations of waves, swell and currents and the turning manoeuvre around Harington Bend.

Most of the modelling studies in this report are based on this initial dredged channel design. During the wider assessment process after more detailed ship-handling simulations and channel design, POL approved a final design for the dredged channel, which only required minor modifications to the initial design, mainly in the stretch from Harington Bend to the Mole. The initial design, which was used as the basis for the numerical modelling simulations, would have generated around 7.5 Mm³ of dredged sediments (excluding rock). The final channel design adopted by POL would yield a slightly lower volume of around 7.06 Mm³ of dredged sediments (6% less). The slight change in final channel design only affects some of the model simulations already undertaken, namely for assessing changes in the tidal characteristics of Otago Harbour and sediment deposition over the dredging programme. Accordingly, these simulations and analyses were re-run for the final channel design to update the assessments in this Report. Both channel designs are referred to in this study and noted clearly which is used for what purpose.

The dredged material is uncontaminated and would be predominantly sand (64%), with the remainder being silts, clays and a small proportion of rock. Suspended-sediment discharges into the Harbour would occur during dredging from seabed disturbance of the trailing suction head of the dredger and from overflows from the hopper. Dredged material in the hopper would be subsequently released offshore onto

²⁰ Twenty-foot Equivalent Unit (or TEU) is an inexact unit of cargo capacity often used to describe the capacity of container vessels. It is based on the volume of a standard-size 20-foot (~6 m) long shipping container.

²¹ Currently maintained in this channel section at a bed level 13 m below Chart Datum

a circular disposal area nominally 2 km in diameter and in water depths of around 28 m. The resulting sediment mound, comprising mainly sands, is expected to reach between 1.4 and 1.8 m high by the end of the dredging programme, with the final height determined by the proportion of silt/clay material dispersed during discharge and the bulk density of the settled and consolidated sediment in the mound.

As part of this Report, an iterative process was undertaken to determine the most appropriate location for the offshore disposal area that is sufficiently distant from the nearshore area that it minimises the concentrations of suspended sediment reaching the nearshore zone or inner Blueskin Bay area and avoids ecologically-sensitive areas (James et al. 2009). The iterative process resulted in a selection of a disposal area at location A0 (centroid at -45.7358°N , 170.799°E), which is 4 nautical miles (7.3 km) north-east of The Mole and located on the northerly-orientated submarine sand body offshore known as the Peninsula Spit.

The other main decision that was needed to set up the discharges in the suspended-sediment model was the characteristics of the trailing suction hopper dredger (TSHD) to be used. A mid-size vessel of 10,800 m³ hopper capacity was simulated by the model. However, because of the wider, shallower, area that needs dredging on the eastern side of the Turning Basin (Port Chalmers), a small-capacity dredger would also be required in the initial stages of this dredging claim, so a substantially shallower overflow depth was used in sediment plume modelling for this site. The overflow for the second half of this claim, when dredged depths are sufficient, was reset back to the overflow depth for the mid-size TSHD. All other areas of the channel were assumed to be workable by the mid-size TSHD. The Harbour channel dredging claims were coalesced into 5 main source locations and further subdivided into predominantly “sand” and “silt” material.

The focus of the plume modelling was the silt/clay fractions of these claims, with provision in the modelling for a 60-minute overflow discharge when working predominantly “sand” claims and a much shorter 4-minute overflow for “silt” claims. Sediment-plume model runs (inside the Harbour and offshore at the disposal site) were aggregated over the dredging programme to calculate an upper-bound on accumulated deposition thicknesses for sediments discharged during dredging in the channel or discharged offshore after release from the dredge hopper.

This report covers results of the numerical coastal modelling components to support the assessment of effects (AEE) for Project Next Generation, providing clearer understanding and predictions of:

- any significant hydrodynamic effects of the proposed 15-m Harbour channel configuration, particularly changes in velocities, tide heights and tidal phasing within Otago Harbour compared to the present situation;
- the degree of spread (dispersion) and likely concentrations of suspended-sediment plumes and seabed deposition patterns from the dredging operations within the Harbour;
- wave characteristics and patterns for different wind directions within the Lower Harbour to support an assessment of effects on navigation, ship handling, benthic habitats and shoreline change;
- the degree of spread (dispersion) and likely concentrations of suspended-sediment plumes generated during release of dredged material from the bottom of the dredge hopper at an offshore disposal area;
- any significant changes in wave patterns on the Otago shelf arising from a mound at the disposal area and the deepened approach channel to support an assessment of effects on navigation, ship handling, benthic habitats and shoreline change;
- the likely extent of the initial footprint of deposited dredged material in the vicinity of the disposal site (and also subdivided into different sediment size classes);
- the likely occurrence of sediment transport over time, distance travelled and direction of deposited dredged sands away from an offshore disposal mound.

Summaries of results and an overall assessment of the likely or, in most cases, upper-bound changes that would arise from dredging and disposal operations are provided at the end of most of the chapters in this Report. Some of the key conclusions arising from the modelling investigations are briefly outlined below.

Changes in hydrodynamic characteristics of the Harbour (tidal heights, currents, net flow volumes through the entrance and ebb-tide sand bar and waves) would be minor relative to the existing situation. Sediment plume modelling shows that SSC (suspended sediment concentration) will be higher towards the seabed and lower towards the surface, because most of the sediment will be discharged at depth (from the dredger overflow or disturbances by the suction head). This also means there would be only limited opportunities around high tide periods for the deeper layers of the suspended-sediment plumes to disperse onto adjacent intertidal flats. Also

dispersion of the sediment plumes is dominated by material being transported up and down the main channels by tidal currents rather than by more dispersive (spreading) processes that occur, for example, in offshore in deeper waters. Plume modelling, using a conservative approach, indicates that the highest depth-averaged concentrations of SSC (over 100 mg/L) would occur in the main channel, subsidiary side channels and the intertidal banks adjacent to these channels, with some patches over 1000 mg/l in areas immediately adjacent to dredging.

Sediment deposition in the Harbour (excluding the main channels) would be highest on the central intertidal bank that is opposite Port Chalmers and north of Quarantine Island. Discharges from predominantly-silt dredging claims would cause higher deposition thicknesses and rates of deposition than from predominantly-sand claims. Consequently any measures targeted at reducing overflows to a minimum when dredging predominantly-silt areas of the channel would substantially reduce environmental effects arising from deposition of fine sediments. Silts originating from dredging operations inside the Harbour in the long-term would be dispersed further and more thinly throughout the Harbour, eventually finding their way into the main channel system to be exported to the ocean or preferentially settle “permanently” in quiescent areas where wave activity and currents are low or sporadic e.g., the Dunedin basin, behind the railway embankments, sheltered sub-tidal embayments, the lee of groynes or half-tide training walls and in the upper-tide inter-tidal beaches of sheltered embayments. In the Upper Harbour, a guide to where silts could preferentially settle in the long term are those areas that already show a predominance of silt material in seabed samples, as measured by Grove & Probert (1999).

Offshore, the transport and dispersal of suspended sediments from the selected disposal site at A0, following the hopper release, would mostly head to the north. But occasionally the dilute edge of sediment plumes may reach the coast at low concentrations along Otago Heads (during light NNE winds) and north of Cornish Head (Waikouaiti Bay) for strong WSW winds for the near-bed layer or light NNE winds for the surface layer. The modelling shows no sediment deposition would occur within Blueskin Bay or around Karitane Point within 48 hours following disposal at site A0. Finer silt material would be widely dispersed over 10's of kilometres (mainly to the north) within 48 hours of disposal. When it initially settles on the seabed it will be temporary, as silts will be routinely resuspended by waves in waters shallower than 30 m, and more frequently in nearshore waters (<10 m deep). The ultimate fate of these widely-dispersed silts is difficult to ascertain, but is likely to be deposition in much deeper waters and canyons offshore as exemplified by silts exported from the Clutha River.

Long-term sand transport from the disposal area A0 would nearly always be transported slowly to the north along the submarine Peninsula Spit by the prevailing

offshore current. Transport would only occur when wave activity is sufficient to mobilize sands in the region of the disposal mound. This is around 40% of the time on average for the median 0.2 mm sand size and somewhat more often than that on top of the mound and in the most energetic winter season. Deflation of the physical disposal mound (comprising mainly sands) would take at least several years and possibly decades.

The environmental effects from the dredging operations on physical and ecological systems arising from the predicted changes in the hydrodynamics and waves and the sediment dispersal, seabed deposition and transport, both inside the Harbour and offshore, are assessed and discussed in companion technical reports.

14. Acknowledgements

Such a comprehensive study requires the input of several datasets and modelling assistance—the input of the following people or organisations is gratefully acknowledged: a) Allan Sutherland, Port Otago Ltd for wind, tide and bathymetry datasets, culvert/channel measurements and aerial photos; b) Hamish Bowman, Marine Science Dept, University of Otago for provision of S4 current meter data from three deployments in Otago Harbour; c) Andrew Mackay, Otago Regional Council, for provision of LiDAR tiles for the periphery of the Harbour; d) Stuart Hughes of Stuart Hughes Associates Ltd, and Andy Pullar (POL) who provided the analysis of dredging volumes, plume/overflow discharge rates during dredging and turnaround cycles; e) Dr Mark Hadfield, NIWA, who provided outputs from his ocean model of the Otago/Southland area and advice on the characteristics of the Southland Current plus reviewed the report; f) Markus Hanz and Shane Greene, Opus International Consultants, for supplying the sediment grading curves and bulk densities for sediment samples; g) Andrew Swales, NIWA, who generated sediment settling velocities from grain size curves and provided insights into long-term silt distributions in harbours; h) Glen Reeve, NIWA, who carried out some of the plume dispersion model runs and calculated fluxes through the entrance and across the ebb-tide sand bar; i) Kevin McGill, NIWA, who extracted the long-term Taiaroa Head wind dataset; j) McConnell Dowell for the 2007 data from the waverider buoy off Tahuna outfall.

The report benefitted from advice and discussions of results from the project steering group (Lincoln Coe, David O'Malley, Dr Mark James, Dr Phil Mitchell and Dr Martin Single).

15. References

- Barnett, A.G. (1988). Otago Harbour hydrodynamic model study. (*Ed.*) Barnett, A.G. Prepared for the Otago Harbour Board by Barnett Consultants (Hamilton) & DSIR Water Quality Centre [now NIWA (Hamilton office)]. 182 p.
- Bell, R.G.; Hart, C. (2008). Offshore ADCP deployments (Otago Peninsula) for Port of Otago dredging project. NIWA Client Report HAM2008-178 prepared for Port Otago Ltd, 75 p.
- Bowman, H. (2008a). Deployment report, S4 current meter: 1 km north of Quarantine Point, Otago Harbour, May 2008. Dept. of Marine Science, University of Otago, 6 June 2008, 6 p.
- Bowman, H. (2008b). Deployment report, S4 current meter: Raynbirds and Macandrew Bays, Otago Harbour, June - July 2008. Dept. of Marine Science, University of Otago, 12 November 2008, 11 p.
- Carter, L. (1986). A budget for modern-Holocene sediment on the South Otago continental shelf. *New Zealand Journal of Marine and Freshwater Research* 20: 665–676.
- Carter, R.M.; Carter, L.; Williams, J.J.; Landis, C.A. (1985). Modern and relict sedimentation on the South Otago continental shelf, New Zealand. *New Zealand Oceanographic Institute Memoir* 93: 43 p.
- Chiswell, S.M. (1996). Variability in the Southland Current, New Zealand. *New Zealand Journal of Marine and Freshwater Research* 30: 1–17.
- CIRIA (2000). Scoping the assessment of sediment plumes from dredging. *Eds.* John, S.A.; Challinor, S.L.; Simpson, M.; Burt, T.N.; Spearman, J. Construction Industry Research and Information Association (CIRIA) Report C547, London, UK. 188 p.
- Goda, Y. (1970). Numerical experiments on wave statistics with spectral simulation. *Report of Research Institute of Port and Harbour, Japan* 9: 3–57.
- Gorman, R.M.; Bryan, K.R.; Laing, A.K. (2003). Wave hindcast for the New Zealand region: nearshore validation and coastal wave climate. *New Zealand Journal of Marine and Freshwater Research* 37: 567–588.
- Graf, W.H. (1971). *Hydraulics of sediment transport*. McGraw-Hill.

- Grove, S.L.; Probert, P.K. (1999). Sediment macrobenthos of upper Otago Harbour, New Zealand. *New Zealand Journal of Marine and Freshwater Research* 33: 469–480.
- Holthuijsen, L.H.; Booij, N.; Ris, R.C.; Haagsma, I.J.G.; Kieftenburg, A.T.M.M.; Kriezi, E.E.; Zijlema, M. & van der Westhuysen, A.J. (2007). SWAN Cycle III version 40.72 User manual. <http://fluidmechanics.tudelft.nl/swan/index.htm>
- Hume, T.M.; Herdendorf, C.E. (1993). On the use of empirical stability relationships for characterising estuaries. *Journal of Coastal Research* 9(2): 413–422.
- James, M.; Probert, K.; Boyd, R.; Sagar, P. (2009). Biological resources of Otago Harbour and offshore: assessment of effects of proposed dredging by Port Otago Ltd. NIWA Client Report HAM2008-152 prepared for Port Otago Ltd.
- Komar, P.D.; Miller, M.C. (1975). On the comparison between the threshold of sediment motion under waves and unidirectional currents with a discussion on the practical evaluation of the threshold. *Journal of Sedimentary Petrology* 45.
- Murdoch, R.C.; Procter, R.; Jillett, J.B.; Zeldis, J.R. (1990). Evidence for an eddy over the continental shelf in the downstream lee of Otago Peninsula. *Estuarine, Coastal and Shelf Science* 30: 489–507.
- Nielsen, P. (1992). *Coastal bottom boundary layers and sediment transport*. Advanced series on ocean engineering - Volume 4. World Scientific, Singapore.
- Old, C.P. (1998). Otago Harbour tidal jet and channel flow. Technical Report for GRIF Contract POO401. Prepared for Port Otago Ltd.
- Old, C.P.; Vennell, R. (2001). Acoustic Doppler current profiler measurements of the velocity field of an ebb jet. *Journal of Geophysical Research* 106(C4): 7037–7049.
- Oldman, J.W.; Bell, R.G.; Stephens, S.A. (2008). Port of Otago dredging project. NIWA: Preliminary hydrodynamic modelling and scoping further work. NIWA Client Report HAM2007-152 prepared for Port Otago Ltd. 55 p.
- Opus International Consultants (2008). Factual report of geotechnical investigations: Port Otago–Project Next Generation. Opus International Consultants Ltd client report #1230, prepared by Shane Greene for Port Otago Ltd. August 2008. 9 p. + appendices.

- Raudkivi, A.J. (1990). *Loose boundary hydraulics*. 3rd Edition, Pergamon Press, Oxford, UK. [Rouse formulae on p. 166-168; Stokes law on p. 15-27].
- Single, M. et al. (2009). Physical coastal environment of Otago Harbour and offshore: assessment of effects of proposed dredging by Port Otago Ltd. Client Report prepared by Shore Processes and Management Ltd. for Port Otago Ltd.
- Soulsby, R. (1997). *Dynamics of marine sands*. Thomas Telford Publications, London. 249 p.
- Sutton, P.J.H. (2003). The Southland Current: a subantarctic current. *New Zealand Journal of Marine and Freshwater Research* 37: 645-652.
- van Rijn, L.C. (1984). Sediment transport Part II: Suspended load transport. *Journal of Hydraulic Engineering* 110(11): 1613-1641. Published by ASCE, USA.
- Vennell, R. (1999). Acoustic Doppler Current Profiler measurements of tidal currents in Otago Harbour Channel: Port Chalmers to Kilgour Point. Dept. of Marine Science Report, prepared for Port Otago Ltd, June 1999.
- Vennell, R.; Old, C.P. (1999). Acoustic Doppler Current Profiler measurements of tidal currents in Otago Harbour Channel: Landfall Tower to Harington Bend. Dept. of Marine Science Report No. PO-1999-07, prepared for Port Otago Ltd, December 1999.
- Vennell, R.; Old, C.P. (2000). Acoustic Doppler Current Profiler measurements of tidal currents in Otago Harbour Channel: Lower Harbour reaches Beacons 11 to 25. Dept. of Marine Science Report No. PO-2000-02, prepared for Port Otago Ltd, June 2000.
- Walters, R.A.; Goring, D.G.; Bell, R.G. (2001). Ocean tides around New Zealand. *NZ Journal of Marine & Freshwater Research* 35(4): 567-579.
<http://www.royalsociety.org.nz/Site/publish/Journals/nzjmfr/2001/50.aspx>
- Willis, T.J.; Bradley, A.; Handley, S.J.; Paavo, B.; Page, M.J.; James, M. (2008). Benthic offshore surveys of proposed dredge spoil disposal sites off Otago Peninsula. NIWA Client Report NEL2008-024, Project POL08401. 53 p.
- Wilson, G.; Sutherland, A.J. (1991). Numerical modelling of Otago Harbour. In: Coastal Engineering-Climate for Change, (Ed.) Bell, R.G.; Hume, T.M.; Healy,

T.R., Proceedings of the 10th Australasian Conference on Coastal and Ocean Engineering, Auckland. *DSIR Water Quality Centre Publication No. 21*: 481–486.

USACE (2005). Environmental assessment of the Newark Bay area, Appendix 1: Assessment of dredging-induced deposition patterns. New York and New Jersey Harbour Deepening Project. US Army Corps of Engineers, New York District.

Zhang, H-M.; Bates, J.J.; Reynolds, R.W. (2006). Assessment of composite global sampling: Sea surface wind speed. *Geophysical Research Letters* 33, L17714, doi:10.1029/2006GL027086.

16. Appendix I – Wave statistics from full directional wave spectra

Given wave model output in the form of a full directional wave spectrum $S(f, \theta)$ at specified grid locations (Chapter 8) for various wave frequencies f and directions θ , the 1-dimensional wave spectrum is obtained by integrating over all the wave directions:

$$S(f) = \int_0^{2\pi} S(f, \theta) d\theta \quad (1)$$

From the computed spectral energy density $S(f)$, the peak frequency f_p and peak energy $S_p = S(f_p)$ of the spectrum are located. Spectral moments:

$$M_j = \int_0^{\infty} f^j S(f) df \quad (2)$$

are computed, allowing further wave statistics to be defined as follows:

$$\text{significant height} \quad H_s = 4\sqrt{M_0} \quad (3)$$

$$\text{mean period} \quad T_{m1} = M_0 / M_1 \quad (4)$$

$$\text{mean apparent period} \quad T_{m2} = \sqrt{M_0 / M_2} \quad (5)$$

$$\text{mean frequency} \quad f_{mean} = M_1 / M_0 \quad (6)$$

$$\text{mean crest period} \quad T_{cr} = \sqrt{M_2 / M_4} \quad (7)$$

$$\text{spectral width} \quad SW = 1 - \frac{M_2^2}{M_0 M_4} \quad (8)$$

T_{m2} is often used as a spectral approximation of the zero-down-crossing wave period statistic T_z .

Directional moments are:

$$M_c = \int_0^{\infty} \int_0^{2\pi} S(f, \theta) \cos \theta d\theta df \quad (9)$$

$$M_s = \int_0^{\infty} \int_0^{2\pi} S(f, \theta) \sin \theta d\theta df \quad (10)$$

$$\text{The mean direction is } \theta_0 = \arctan\left(\frac{M_s}{M_c}\right) \quad (11)$$

and the directional spread is $\Delta = \sqrt{2 - \frac{2\sqrt{M_c^2 + M_s^2}}{M_0}}$. (12)

The spectral peakedness parameter (Goda, 1970) is given by:

$$Q_p = \frac{2}{M_0^2} \int_0^\infty f S(f)^2 df . \quad (13)$$

17. Appendix II – Offshore sediment transport methodology

17.1 Estimation of sand transport using wave and current field data at site A1

The methodology for assessing the critical (threshold) velocities for initiation of sediment transport at A1 from the ADCP field data is as follows:

- Waves were measured in bursts using an Acoustic Doppler Current Profiler (ADCP) deployed at site A1 during four separate periods in 2008 (18 March – 21 April; 29 April – 26 May; 31 May – 29 June; 4 July – 4 August). In the first deployment the interval between bursts was 1 h, and in the other three deployments it was 2 h. The burst duration was 20 min. The ADCP returned estimates of significant wave height (H_s), peak spectral period at the surface (T_p) and direction of wave travel (D_p) corresponding to the peak wave period. The direction of wave travel is the direction waves propagate from. The wave-orbital speed at the bed (U_w) was calculated using linear wave theory as:

$$U_w = \frac{\pi H_s}{T_p \sinh(kh)} \quad (1)$$

where k is the wavenumber that satisfies the linear-theory dispersion relationship with T_p and water depth h .

- $U_{w,crit}$ is the critical wave-orbital speed for initiation of sediment motion, which was calculated using Komar & Miller (1975):

$$\frac{\rho U_{w,crit}^2}{(\rho_s - \rho)gD_s} = a''(d_w / D_s)^{1/2} \quad (2)$$

which holds for sediment grainsizes smaller than 0.5 mm. Here, $d_w = TU_w / 2\pi$ is the near-bottom semi-excursion of the wave motion, ρ is the fluid density, ρ_s is the sediment density (assumed to be 2.65 g/cm³), g is acceleration due to gravity, and $a'' = 0.21$ (Komar & Miller, 1975).

- Currents were also measured by the ADCP, by sampling in 10 minute bursts at a frequency of 0.77 Hz. (Note that the ADCP is capable of simultaneously running different sampling schedules for waves and currents). U_c is the burst-averaged current speed coinciding with the first ADCP output bin, which was

centred on $z = 2.26$ m, where z is elevation above the bed. Current direction is the direction to which the current sets, referenced to true north.

- $U_{c,crit}$ is the critical current speed for initiation of sediment motion, which was calculated as:

$$U_{c,crit} = \frac{U_{*c,crit}}{\kappa} \ln\left(\frac{z}{Z_0}\right) \quad (3)$$

where κ is von Karman's constant (0.41), Z_0 is the seabed roughness length and $U_{*c,crit}$ is the critical friction velocity. $U_{*c,crit}$ is a skin friction, and therefore the seabed roughness length is related to the bed-sediment grain size D_s as $Z_0 = 2.5D_s / 30$. $U_{*c,crit}$ is related to the critical non-dimensional skin friction for initiation of sediment motion θ_{crit} as:

$$U_{*c,crit}^2 = \frac{\theta_{crit}}{\rho} (\rho_s - \rho) g D_s \quad (4)$$

θ_{crit} is evaluated as a function of sediment grain size using the standard Shields curve for unidirectional, steady flow in, for example, Graf (1971).

- The burst-averaged water depth h was estimated from pressure data recorded by the ADCP. For this estimation, pressure was related to water depth using the hydrostatic equation with an atmospheric pressure of 1 bar, water density of 1000 kg/m^3 and acceleration due to gravity of 9.81 m/s^2 .

Instantaneous depth-integrated suspended-sediment transport was calculated as follows:

$$Q = \int_{z_1}^{z_2} U_c(z) C(z) dz \quad (5)$$

where $U_c(z)$ is the current-speed profile, $C(z)$ is the suspended-sediment concentration profile, and the integration is performed between $z = z_1$ (close to the bed) and $z = z_2$ (far from the bed). Q has units of mass per unit width of seabed perpendicular to the direction of transport per time. Assuming that the waves and currents measured during each burst are representative of conditions during that burst

and up to the start of the next burst, then Φ is the depth-integrated suspended-sediment transport integrated over the duration of the deployment, calculated as:

$$\Phi = \int_{t_1}^{t_2} Q(t) dt \quad (6)$$

where $t = t_1$ is the time corresponding to the start of the deployment, $t = t_2$ is the time corresponding to the end of the deployment, and the timestep is equivalent to the interval between bursts.

- The current-speed profile $U_c(z)$ was calculated from the steady-flow law of the wall by:

$$U_c(z) = (U_{*c} / \kappa) \ln(z / Z_0) \quad (7)$$

Here, $Z_0 = 0.0275$ cm is the roughness length, which was calculated from the law of the wall assuming a seabed drag coefficient $C_{100} = 0.0025$:

$$C_{100} = \left[\frac{\kappa}{\ln(100 / Z_0)} \right]^2 \quad (8)$$

U_{*c} is the steady-flow friction velocity, which was calculated from U_{226} , which is the current speed measured by the ADCP at $z = 226$ cm, as:

$$U_{*c} = (\kappa U_{226}) / \ln(226 / Z_0) \quad (9)$$

- The suspended-sediment concentration profile $C_c(z)$ was calculated in two ways.

The first way was by using the near-bed approximation to the Rouse equation (cited in Raudkivi (1990: p. 166-168), which is predicated on settling flux balanced by pure gradient diffusion and a sediment diffusivity decaying linearly with elevation above the bed:

$$C(z) = C_a \left(\frac{z}{z_a} \right)^{\frac{w_s}{\beta \kappa U_*}} \quad (10)$$

Here, β is the ratio between sediment and momentum diffusivity (assumed to be 1), w_s is the sediment settling velocity (negative one multiplied by the settling speed), and C_a is the suspended-sediment reference concentration

specified at $z = z_a$. For these calculations, w_s is the Stokes settling speed assuming sediment density $\rho_s = 2.65 \text{ g/cm}^3$ and U_* is taken to be U_{*c} , defined previously.

The second way of calculating the suspended-sediment concentration profile was by using the Nielsen (1992) equation, which is based on constant sediment diffusivity (with elevation above the bed):

$$C(z) = C_a e^{-z/l_s} \quad (11)$$

where l_s is the mixing length, given by:

$$l_s = 0.075 \frac{d_w \omega}{w_s} \eta \quad (12)$$

where η is the ripple height (assumed to be 5 cm) and $\omega = 2\pi/T_p$ is the wave radian frequency corresponding to the peak spectral period.

Following Nielsen, the suspended-sediment reference concentration C_a is given by:

$$C_a = 0.005 \rho_s \theta'^3 \quad (13)$$

where θ' is the non-dimensional skin friction, given by:

$$\theta' = \tau' / [(\rho_s - \rho) g D_s] \quad (14)$$

and τ' is the skin friction. Since waves (as opposed to currents) primarily control entrainment of bed sediment, the skin friction is assumed to be purely wave-induced:

$$\tau' = 0.5 \rho f'_w U_w^2 \quad (15)$$

where f'_w is the pure-wave skin-friction wave friction factor:

$$f'_w = \exp[5.213(k_s / d_w)^{0.194} - 5.977] \quad (16)$$

and $k_s = 2.5D_s$ is the flat-bed roughness. Nielsen's reference concentration evaluated in this way is meant to be apply at $z = 0$, but for convenience we assume here it applies at $z = 1$ cm above the bed.

Values for Φ are shown in Table 12.5 (Chapter 12) for each sediment grain size calculated by each of the sediment transport models (Rouse and Nielsen). For these calculations, z_1 was set to 1 cm and z_2 was set to 200 cm, which is the domain where the bulk of the suspended-sediment transport will be located. Also for these calculations, U_c is a scalar only (current speed). This means that Φ is the integral of the scalar instantaneous transport, Q , which can be thought of (loosely) as the “gross” transport. Φ is multiplied by a nominal spoil mound width of 2 km in Table 12.5.

Φ was calculated again, this time treating Q as a vector with direction corresponding to the measured current speed at 2.26 m above the bed. Φ calculated in this way is now a vector itself, with magnitude $MAG[\vec{\Phi}]$ and direction $DIR[\vec{\Phi}]$. This can be thought of (loosely) as the “net” transport. Table 12.6 shows the results, including $MAG[\vec{\Phi}]$ multiplied by a nominal spoil mound width of 2 km (as in Table 12.5).

17.2 Estimation of sand transport using wave and current field data at site A0

Sediment transport at site A0 (the selected disposal site) for the period spanned by the ADCP deployment at site A1 was estimated by applying equations (5) and (6) above.

Wave height, period and direction measured at site A1 by the ADCP were assumed to apply without modification to site A0. However, the conversion of H_s and T_p to wave-orbital speed at the bed (equation 1) was computed with a water depth that was 2.5 m less than the water depth measured by the ADCP at site A1 to account for the shallower depth on top of the submergent Peninsula Spit.

Current speeds and directions at site A0 were predicted by the MIKE-3 (FM) hydrodynamic model (described in Chapter 10) for the entire 2008 field deployment period.

The “gross” and “net” sediment transport at site A0 were calculated in a similar way (as outlined in the previous section) for each sediment grain size using both the Rouse and Nielsen sediment transport models.